MILJÖRIKTIG ANVÄNDNING AV ASKOR 1112

Modelling of leaching and geochemical processes in an aged MSWIBA subbase layer

David Bendz, Pascal Suer, Hans van der Sloot, David Kosson, Peter Flyhammar

värmeforsk

Modelling of leaching and geochemical processes in an aged MSWIBA subbase layer

David Bendz, Pascal Suer. Hans van der Sloot, David Kosson, Peter Flyhammar

Q6-648

VÄRMEFORSK Service AB
101 53 STOCKHOLM · Tel 08-677 25 80
July 2009
ISSN 1653-1248

Acknowledgement

Claes Ribbing and the reference group Ivars Neretnieks, Jon-Petter Gustavsson, Raul Grönholm, Stig-Olov Taberman, Karl-Johan Loorents and Rainer Backman are acknowledged for supporting this study and for providing valuable comments. Cecilia Toomväli and Kristian Hemström are acknowledged for excellent experimental work.

Abstract

The hydraulic modeling of a period of 16 years show that the bottom ash subbase layer endure seasonal wet and dry cycles. Depending on the boundary conditions along the shoulders the capillary potential may drive water either in or out of the road body. The results show that the accumulated LS ratio for the bottom ash subbase layer reached about LS:10 in average with a spatial variability in the sub base layer ranging from LS:1 to LS:50. Geochemical speciation modelling was carried out for major, minor and trace elements in bottom ash aged 16 years under natural conditions. The geochemical model was parameterized with data on HFO, TOC and IC. The governing mineral assembly was selected. Good model fit (compared to pH-stat test data) implies that release of elements could be predicted for a bottom ash under certain environmental conditions if available HFO and TOC are measured.

Summary

In a previous project: *Vändöra Q4-241 (report 964)*, funded by Värmeforsk (Swedish Thermal Engineering Research Institute), the accumulated effects of leaching and aging in a subbase layer of bottom ash in a test road were investigated. The test road were constructed in 1987 in Linköping, Sweden, and was in use until the start of the *Vändöra Q4-241* study in September 2003. The overall objective of the present study is to bring the evaluation of the previous project (*Q4-241)* further by taking advantage of the existing data, perform complementary laboratory experiments on four composite samples reflecting different degree of exposure to atmosphere and leaching. The specific objectives were to investigate: (i) what processes and mineral phases that govern leaching of macro- and trace elements and DOC in the bottom ash after 16 years (1987-2003) of aging under field conditions. (ii) how the hydrologic conditions, infiltration of water and leachate production has evolved with time. The following tests were performed on the composite samples: pH-stat test, column test, Fe/Al oxide extraction and TOC fractioning. Geochemical and hydrological modelling where performed with LeachXS/Orchestra and Hydrus 2-D.

Daily precipitation data from the Swedish Meterological and Hydrological Institute (SMHI) from the Malmslätt (Linköping) measurement station was used in the hydrological modelling of January 1988 to the 1th of september 2003. The hydraulic modeling results show that the bottom ash subbase layer endure seasonal wet and dry cycles. The results confirm that, depending on the boundary conditions along the shoulders the capillary potential may drive moisture either in or out of the road body. The water retention parameters for bottom ash were crucial in the hydraulic modeling and the capillary forces in bottom ash were found to be significant with a water retention curve close to silt. This explains the observed depletion of easily soluble salts in the test road. The results showed that the accumulated LS ratio for the bottom ash subbase layer reached about LS:10 in average with a spatial variability in the sub base layer ranging from LS:1 to LS:50.

The geochemical speciation modeling was carried out for major, minor and trace elements and integrate mineral dissolution/precipitation, iron-oxide adsorption, incorporation in ettringite solid solution, clay interaction and interaction with dissolved and particulate organic matter. The geochemical model was parameterized with data on HFO, TOC and IC. The governing mineral assembly was selected, based on this experience. Iron-oxide sorption was shown to be important for many trace elements (metals as well as oxyanions). The role of organic matter (both dissolved and particulate) is important for elements like Cu, Cr, Cd, Pb (although the major fraction of the available content is associated with the mineral phases). Obviously, proper mineral solubility data are limited for some elements, like Sb, B, Se. The model fit for macroelements was good and for trace elements the match is quite acceptable. The model confirms that Cu, Cr, Pb, and partially Zn, in solution is bound to DOC. The elements Zn, Cd and Ni are present in the solution mainly as free ions. It is important to realize that for ecotoxicity evaluations the free element is of importance and the DOC associated metal is not affecting many organisms. In the solid phase As is entirely associated with iron oxides. Other elements where iron oxides plays an important role are: Pb, Cd and Cu. The elements Cu, Zn and Ni are mainly associated with the solid phase as minerals: malachite (copper hydroxide carbonate) willemite (zinc silicate), nickel silicate and iron chromate.

The result implies that release of elements could be predicted for a bottom ash under certain environmental conditions if available HFO and TOC are measured. The major environmental conditions that needs to be specified are: pH, DOC and DIC of intruding water and degree of exposure to atmosphere.

Keywords: geochemistry, hydrology, model, road, ash

Table of contents

Appendices

1 Introduction

1.1 Background

In a previous Värmeforsk project : *Vändöra Q4-241, (report 964) [4]* the geochemical and geotechnical properties in a 16 year old paved MSWI bottom ash test road in Linköping, Sweden where studied. The objectives of the project were to investigate: (i) the accumulated effects of leaching and aging and (ii) the accumulated effects of load and aging on the geotechnical properties. The project included tests with falling weight deflectometer, triax testing on undisturbed core samples of bottom ash and sampling for chemical analysis. Three trenches were excavated in the test road, samples of the subbase layer and the subgrade were taken in the shaft walls and brought to the laboratory for leaching tests (EN 12457-2) and extraction, respectively. The extraction procedure was used to estimate extractable and chemically available fractions.

Some important observations were made in the *Vändöra study [4]* regarding the leaching process and impact of boundary conditions, which ought to be acknowledged (see also chapter 2). The physical properties of the pavement structure influence the way and the extent to which the construction materials become exposed to water and air. Air contains acid gases (CO_2, SO_2) and strong oxidants (O_2) which may react with alkaline respective reducing mineral phases and influence the chemical environment. The observed patterns of EC and pH and leachable amounts of Cl^-, Ca, DOC, Cu, As and Cr, in addition to exposure to water, where hypothesized to reflect aging, transformation processes and speciation (redox environment). The spatial distribution of leachable content of Cu was found to be closely associated with the leachability of DOC, which in turn, is governed by the content of organic matter (decreases with time due to degradation) and transformation into less soluble forms with time. Further, spatial distribution patterns of mobile elements in the MSWI bottom ash subbase layer confirmed the existence of two major regions, where different transport processes dominate, in a paved road construction with permeable shoulders. The existence of diffusive transport (diffusion an and capillary driven advection) is indicated by gradients in the subbase layer directed towards the road shoulders, where the solutes are carried away by infiltrating water (gravity driven advection). Gradients in pH also evolve as a result of carbon dioxide and oxygen reaction with the solid phase. The data clearly showed pH fronts that propagate from the road shoulders towards the center of road.

1.2 Objective

The overall objective of this study (Q6-648) is to bring the evaluation of the *Vändöra*-data further by taking advantage of the existing data, perform complementary laboratory experiments (pH-stat test, column test, Fe/Al oxide extraction and TOC fractioning) and geochemical and hydrological modelling with Orchestra and Hydrus 2-D.

The specific objectives are to investigate:

- what processes and mineralphases that govern the leaching properties of macro- and trace elements and DOC in the bottom ash after 16 years (1987-2003) of aging under field conditions.
- how the hydrologic conditions, infiltration of water and leachate production has evolved with time. This include also the distribution of water in the bottom ash layer as a function of space and time.
- the evolution of leachate chemistry and mass flux from the road construction with time.

1.3 Description of the research area

The results from leaching tests reflect conditions that in general only are representative on a small spatial scale and a short temporal scale. The aim of predicting leaching processes over a longer period of time under field conditions raises some questions concerning the applicability of the lab test data. A number of parameters may differ if lab and field conditions are compared [36]: temperature, pH, redox conditions, geometry of the material (shape and dimensions), flow field, the area of the solids exposed to water, exposure time and the spatial variability encountered in field-scale. It is important to acknowledge that when residues are used as construction materials they are commonly enclosed in a technical construction, which will govern the exposure to water and atmosphere and the resulting leaching process. The physical properties of the pavement structure influence the way and the extent to which the construction materials become exposed to water and air. Air contains acid gases (CO_2, SO_2) and strong oxidants (O_2) which may react with alkaline and reducing mineral phases which will influence the chemical environment [4].

Fresh MSWI bottom ash is unstable and not in equilibrium with either the atmosphere or the water phase. A number of alteration or aging processes are initiated with exposure of fresh ash to water and atmosphere, such as dissolution and precipitation of minerals of major cations, the slow weathering of glass phases and formation of clay-like minerals, and the formation of carbonates by uptake of carbon dioxide. These processes govern the buffer capacity, the pH conditions and the mobility of heavy metals.

The influence of the degree of exposure to air and the resulting pore gas composition is one likely reason for the different leaching behavior when comparing leaching at different scales and experimental setups. For example, different pH levels were observed when comparing a number of steel slags leaching experiments reported in [16] and [20]. Here, carbonatisation and oxidation of sulphides, governed by the exposure to atmosphere, are important processes that control the development of pH. The experiments were performed with the same material but in different scales and experimental setup: columns (saturated and unsaturated), lysimeters (unsaturated) and lysimeters (unsaturated) at true field conditions (installed underneath an unpaved road).

Water can enter the road body in several ways: it may infiltrate directly through the surface course or at joints, cracks and deformities in the surface course, form surface runoff and infiltrate in the shoulders or it may be stored in depressions at the surface or evaporate [32]. Deformities of the pavement may drain surface runoff water and give rise to large infiltration locally. Dawson and Hill [8] refer to investigations where an infiltration capacity of 1 litre/hour/cm of crack length has been determined. Water may move from the shoulders laterally into the road construction driven by a capillary potential or hydraulic pressure ([6][14][24][34]), vapor pressure and temperature gradients [32]. Wallace [34] demonstrated the significance of the shoulders as water entries to the unbound material layers during transient conditions in a theoretical study. Water may also move into the pavement structure and the embankment directly from surrounding surface or ground water.

Field measurements show that the water content in a pavement structure typically show a seasonal variation (see for ex. [23] and [32]). Depending on the water contents in the shoulders the capillary potential may drive moisture either in or out of the road body. The shoulders of the pavement structure provide an important pathway for vapor and gases out of the pavement structure [23]. Water, as vapour, is typically transported into the pavement structure from the surrounding air in the summer and upward from the underlying soil during winter [19].

If the subgrade has a low permeability a perched water table may develop at the lower boundary of the unbound layers, which will facilitate lateral water movement. Therefore also initial water content, hydraulic conductivity and capillarity of the subgrade are significant for the rate of lateral intrusion. In cold regions the presence of snow along the highway shoulders may prevent the thaw front to progress at the same speed as into the pavement structure. Under such conditions melt water and rain has been observed to infiltrate at the shoulders, flow into the structure and gradually saturate the pavement structure [23].

The general experience from different field studies is that a higher degree of leaching is taking place in unpaved parts of a road construction, such as road shoulders and median strips, than within the pavement structure ([1][4] [15][31][33]).

2 Observations of spatial patterns

2.1 The Linköping test road

The test road was constructed in 1987 in Linköping Sweden [26] and it was almost 16 years old at the time when the samples were taken in 2003. Other studies have been performed on this road in 1998 [1] and later, in 2002 [15]. In two of the test sections MSWI (municipal solid waste incineration) bottom ash was used as subbase below an unbound base course and surface asphalt layers. The bottom ash was poorly separated and contained large pieces of incineration residues (larger than a few decimeters). Mixed heterogeneous shaft masses, containing sand, gravel clay, were used as subgrade. Note that the surface course was sloping towards the inner curve shoulder (which is left in all the cross-section figures that will follow).

The test road has been in a rather bad condition during periods, with longitudinell cracks along the centerline of the road (see Figure 1). A certain infiltration is therefore likely to have taken place.

Figure 1. Longitudinal cracks along the center line of the test road. (Photo: VTI Safwat Said, 1999)

Here some results are presented from the characterization of the bottom ash subbase layer (see description in [26]). The complete set of field data is presented in Bendz et al [4].

2.2 Excavation and sampling (2003)

The field campaign was carried out in September 2003 (*Vändöra Q4-241:[4]).* The unbound base course and asphalt layers were removed and three sample collection trenches were excavated into the road construction in different sections.

Solid samples (approx. 250 ml each) were collected from the subbase layer and the subgrade (embankment) in a check board pattern, se Figure 2. The samples were collected in plastic jars and stored under N_2 atmosphere until pretreatment. A total of 53 samples were taken in the subbase layer and 107 samples were taken in the subgrade layer.

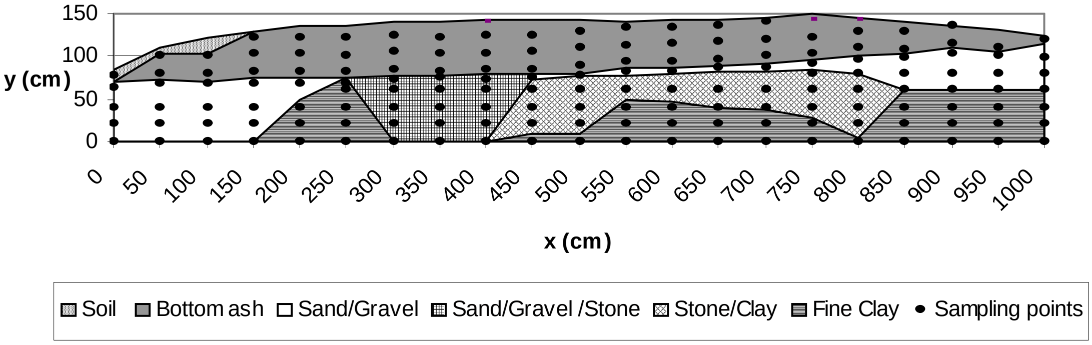

Figure 2. Sampling points

2.3 General about the observed spatial patterns of leachable contents

The spatial distributions of the leachable content (mg/kg) of different elements are presented as contour maps of the shaft wall. Kriging interpolation using default settings in Surfer 7.0 was used to calculate these maps. The spatial distributions of leachable elements are categorized into three groups depending on if the observed patterns reflect leaching, aging (transformation/reaction with time) and redox environment. A subset of data that has been generated in this study is presented below. The complete set of data is present in [4].

Some important observations have been made regarding the leaching process and impact of boundary conditions, which is shown in the subsequent subchapters.

Spatial distribution patterns of mobile elements (leaching controlled by availability), such as Cl^-, in the subbase layer confirm the existence of two major transport processes in a paved road construction with permeable shoulders (see 2.5). The existence of diffusive transport is indicated by gradients in the subbase layer directed towards the road shoulders. These gradients have evolved as result of the exposure of the bottom ash to infiltrating water in the road shoulders.

Gradients may also evolve as a result of carbon dioxide and oxygen reaction with the solid phase. Thanks to that the bottom ash was fresh, at the time of construction of the test road, the effect of diffusion of carbon dioxide and oxygen into the road is clearly seen. The physical properties of the pavement structure influence the way and the extent to which the construction materials become exposed to water and air. Air contains acid gases (CO_2, SO_2) and strong oxidants (O_2) which may react with alkaline respective reducing mineral phases and influence the chemical environment. The observed patterns of EC and pH (see 2.4) and leachable amounts of Cl^-, Ca, DOC, Cu, As and Cr are therefore, in addition to exposure to water, reflecting aging and transformation processes and speciation (redox environment). Ca is transformed into less soluble mineral due to reaction with atmospheric carbon dioxide. The data clearly show pH fronts that propagate from the road shoulders towards the center of road (Figure 4, Figure 12). The spatial distribution of leachable content of Cu is closely associated with the leachability of DOC (Figure 7).

The spatial distribution of the leachability of As and Cr indicate a dependency on varying redox conditions with reducing conditions prevailing in the center of the road and oxidizing conditions in the shoulders of the road (see 2.7). The mobility of these two elements varies with speciation in an opposite way. This manifest itself in a spatial pattern of Cr that shows low leachability in the center of the road body and increasing leachable amounts towards the road shoulders. The spatial distribution of As shows the opposite pattern with high leachable amounts in the center of the road and decreasing figures towards the road shoulders.

2.4 EC and pH

In Figure 3, Figure 4 and Figure 12 the spatial distribution of electrical conductivity and pH in the subbase (bottom ash) and subgrade are presented. In the figures the dashed line marks the location of the boundary between the bottom ash layer and the underlying soil. The location of the former asphalt pavement is indicated in the figures.

The results from the conductivity measurements reveal the existence of horizontal gradients, directed from the center of the road towards the shoulders of the road. This indicates that lateral diffusion and capillary driven advection are governing transport process, from the center of the road to the road shoulders were the dissolved elements are carried away by gravity driven advection with infiltrating water from the surface runoff. The highest conductivity (EC_{max}= 234 mS/m) was found slightly to the right of the center of the road at *x=500–700 cm*. This is likely an effect of that the road surface was inclining towards the inner radius of the curve (which is to the left in the figure).

Thus a larger part of the surface runoff may have infiltrated in the road shoulder along the inner curve which manifest itself in a very low conductivity (EC_{min}= 15 mS/m).

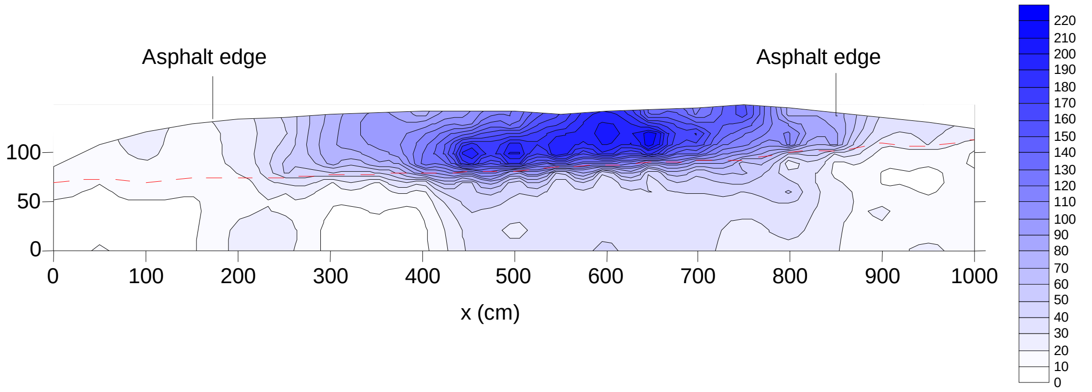

Figure 3. Spatial distribution of electrical conductivity (ISO 11 265). The dashed line marks the boundary between the subbase of bottom ash and the subgrade. The locations of the edges of the former asphalt layer are also shown. The X and Y-axis are graded in centimeters.

The dissolution of carbonate minerals provides the major part of the buffering capacity and controls the evolution of pH [21][27][40]. Leachate that was collected from the test road shortly after construction had a pH of about 11.1 och 11.7 [26], indicating that the bottom ash was fresh, at the time of construction, and that Portlandite was the primary buffering mineral.

In this investigation high pH-values, up to about 9.8, were found in the middle of the road and low values of about 7.5-8 were found along the edges, see Figure 4. Also in this case, the high values are located slightly to the right of the center of the road at *x=500–600 cm*. The spatial pattern indicates that atmospheric carbon dioxide has entered the bottom ash layer laterally by diffusion from the road shoulders. Reaction (carbonization) fronts have evolved and been propagating towards the center of road for 16 years without succeeding to fully carbonize the bottom ash layer.

Metals dissolved at high pH in the center of the road may become trapped as carbonization fronts with neutral pH propagate towards the center. Metals that show a higher solubility with lower pH may go in solution as the conditions change to a lower pH. In this way leaching of heavy metals becomes closely related to the rate of which the reaction front propagates [3][40]. The distribution of pH in the subgrade show a large variation 5.26-8.02 (n=17), which can be explained by the heterogeneous nature of the subgrade (shaft masses).

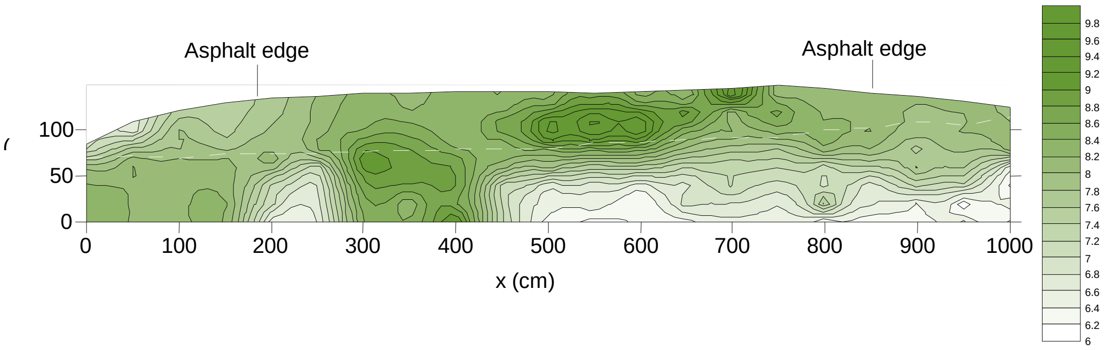

Figure 4. Spatial distribution of pH. The dashed line marks the boundary between subbase of bottom ash and the subgrade. The locations of the edges of the former asphalt layer is also shown. The X and Y-axis are graded in centimeters.

2.5 Patterns governed by leaching

The electrical conductivity represents the content of easily soluble salts and the major cations and anions Cl^- SO_4^{2-}, Ca^{2+}, Na^+ , K^+ och Mg^{2+}. Here the spatial distribution of leachable content of Cl^- is shown. Not suprising, the spatial distribution of Cl^- in Figure 5 correlates well with the electrical conductivity in Figure 3. The highest leachable amounts of Cl^- , about 800 mg/kg , was found in the center of the road at *x=500 cm*. The data indicate that Cl^- has been flushed out in the road shoulders with the lowest value of 20 mg/kg in the road shoulder at the inner curve (left in the figure). By integrating the spatial data, an average leachable amount of Cl^- was determined to be 382 mg/kg.

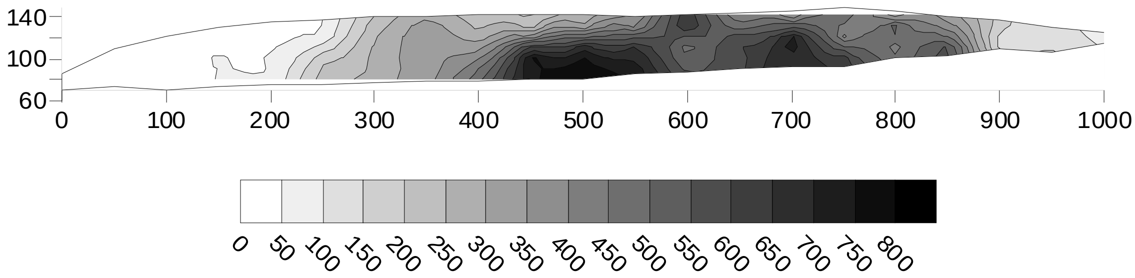

Figure 5. Distribution of leachable content of Cl^- (mg/kg) in the subbase (EN 12457-2). The X and Y-axis are graded in centimeters.

Unfortunately there is no relevant leaching test data for the original ash (at the time when the road was constructed) available. However, in 1996 Fällman [16] carried out a thorough characterization of the leaching behavior of the bottom ash from the same incineration plant in Linköping. In a comparable two-step leaching test, the leachable amount of Cl^- was determined to be 2260 mg/kg at L/S 10. If this figure is assumed to be representative of the leachable amount Cl^- in the ash at the time when the road was constructed in 1987, it can be concluded that the integrated remaining leachable amount of Cl^- of 382 mg/kg represents less than 20 % of the initial amount.

The upper region of the bottom ash at x=400-600 cm, Figure 5 show possible signs of infiltration and certain advective transport of chloride out of the bottom ash may have taken place.

2.6 Patterns influenced by aging

The spatial distribution of leachable Ca , shown in Figure 6, is an effect of leaching, reaction with atmospheric carbon dioxide and formation of less soluble minerals such as calcite. Since the dissolution of carbonate minerals provides the major part of the buffering capacity the observed pattern is correlated with the distribution of pH in Figure 4.

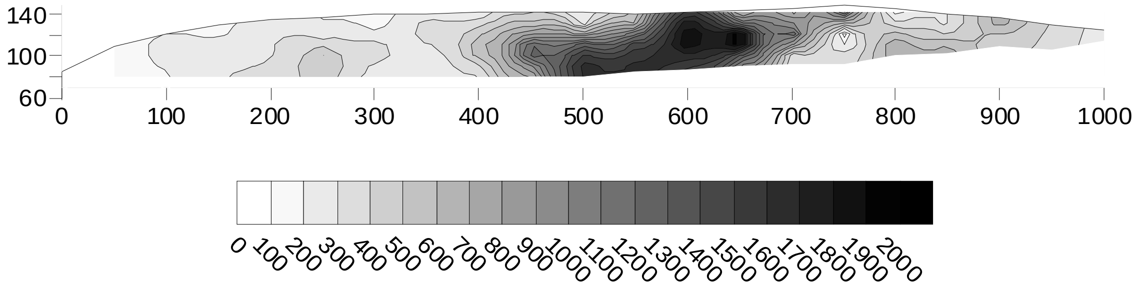

Figure 6. Distribution of leachable content of Ca in the subbase at L/S 10 (EN 12457-2). The X and Y-axis are graded in centimeters.

The spatial distribution of leachable content of DOC is governed by it characteristics (humic, fulvic, and hydrophilic acids) and aging processes. With aging of the bottom ash matrices, the leachable content of DOC may decrease as a result of forming of reactive iron/aluminium surfaces and a pH approaching the neutral range ([11], [17]). This is reflected in high leachable contents in the center of the road, see Figure 7 where the leachable amounts of DOC in the subbase layer have been plotted. The high contents of leachable DOC that can be seen locally at the edges (*x=50 cm* and *x=1000 cm*) are probable due to humus and grass root penetration from the grass covered road shoulder.

It is common knowledge that the leachable contents of Cu is governed by complexation with DOC. In a study by Meima et al. [28] 95-100% of the dissolved Cu in leachate from fresh and weathered bottom ash appeared to be organically bound. Increased leachable contents of Cu can be seen in the center of the road and at the edges, see Figure 8.

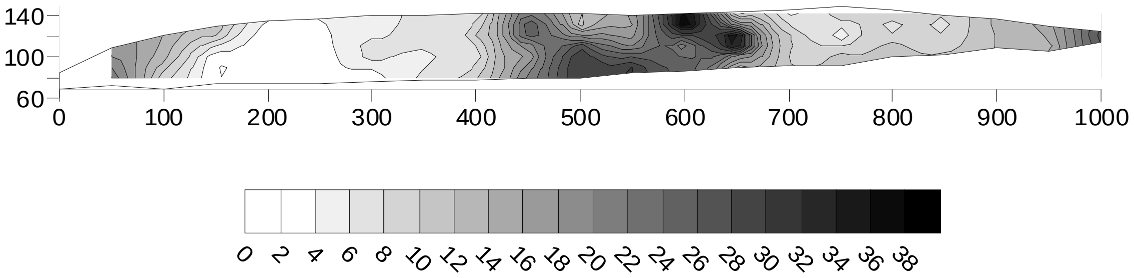

Figure 7. Spatial distribution of leachable (mg/kg) DOC in the subbase (EN 12457-2). The X and Y-axis are graded in centimeters.

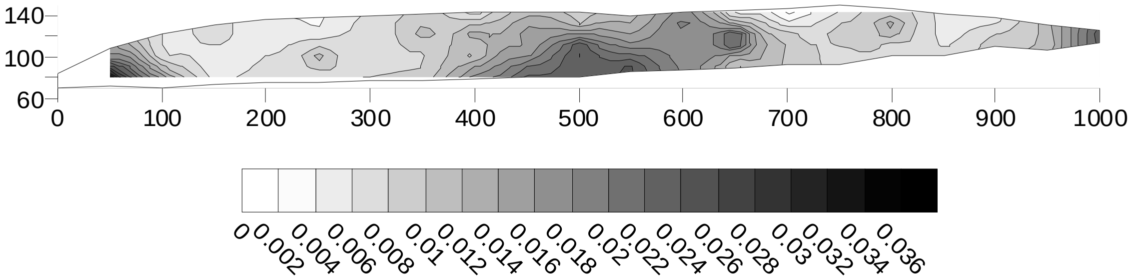

Figure 8. Distribution of leachable amounts (mg/kg) of Cu in the subbase (EN 12457-2). The X and Y axis are marked in centimeters.

The leachable amounts of Cu (mg/kg) where plotted in Figure 9 as a function of DOC (mg/kg) for all sample points (n=53) in the MSWI bottom ash layer. The figure illustrates the positive correlation and confirms the importance of DOC and complexation as a governing process for the leaching behavior of Cu.

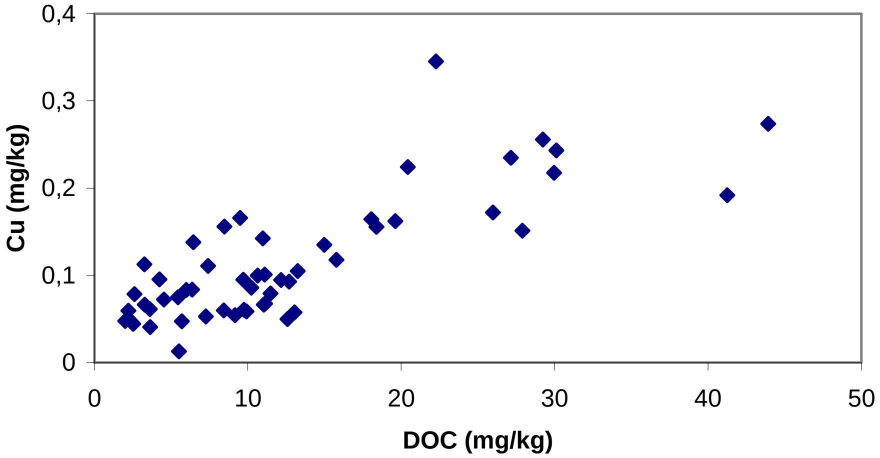

Figure 9. Leachable amount of Cu (mg/kg) *plotted as a function of leachable amount of DOC* (mg/kg) *(EN 12457-2).*

2.7 Patterns influenced by redox conditions

The spatial distribution of the leachability of As and Cr is partly an effect of varying redox conditions. Reducing conditions is probably prevailing in the center of the road and oxidizing conditions in the shoulders of the road.

Arsenic may either be found as arsenite (As(III)) or arsenate (As(V)). The solubility of arsenic is expected to be higher under reducing conditions, where it exist predominately as As(III). In aerobic, pH neutral or weakly acid environments the solubility of arsenic is commonly controlled by iron hydroxides, but also aluminium- and manganoxides. Iron hydroxides are not stable in a reducing environment and the solubility of arsenic is accordingly expected to increase. The spatial distribution of leachable As shown in Figure 10 reflects a possible redox dependency.

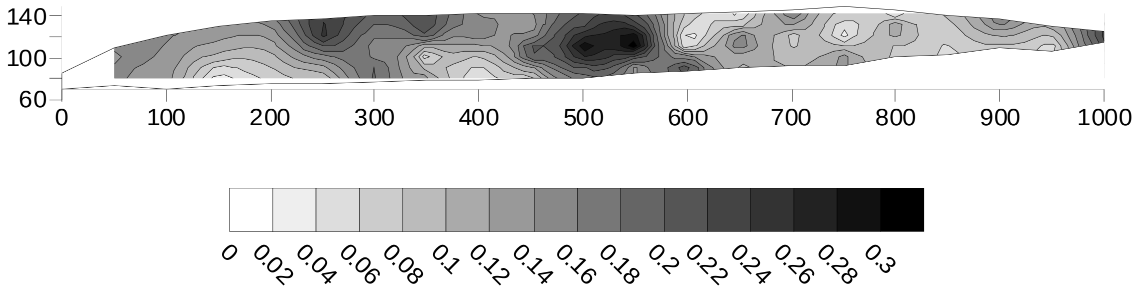

Figure 10. Distribution of leachable amounts (mg/kg) of As in the subbase (EN 12457-2). The X and Y axis are marked in centimeters.

Chromium is highly mobile in an alkaline environment under oxidizing conditions and is present at Cr(VI). In a reducing environment Cr(VI) is reduced to Cr(III) and may precipitate as chromium hydroxide, which limits the mobility. The spatial distribution of leachable Cr reflects redox but also pH as a governing state parameter.

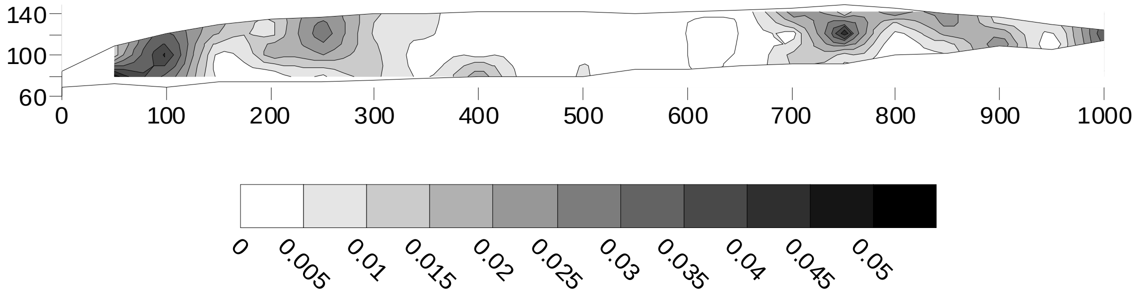

Figure 11. Distribution of leachable amounts (mg/kg) of Cr in the subbase (EN 12457-2). The X and Y axis are marked in centimeters.

3 Methodology

3.1 Laboratory

3.1.1 Pretreatment

All samples were treated according to a standardized procedure (SS-ISO 11464), which is a pretreatment procedure developed for soil samples before physical and chemical analysis. Each sample was dried in 40 ^{o}C. Dry material less than 2 mm was then stored and used for tests and analysis.

The electrical conductivity, pH and moisture content were analyzed for each sample. The pH and the electrical conductivity of the material was measured according to the standards SS-ISO 10 390 and SS-ISO 11 265, respectively. The pH-electrodes were Metrohms ”unitrode”-type and the measuring unit was a MeterLab PHM 290. The conductivity measurements were made with a MeterLab CDM 210.

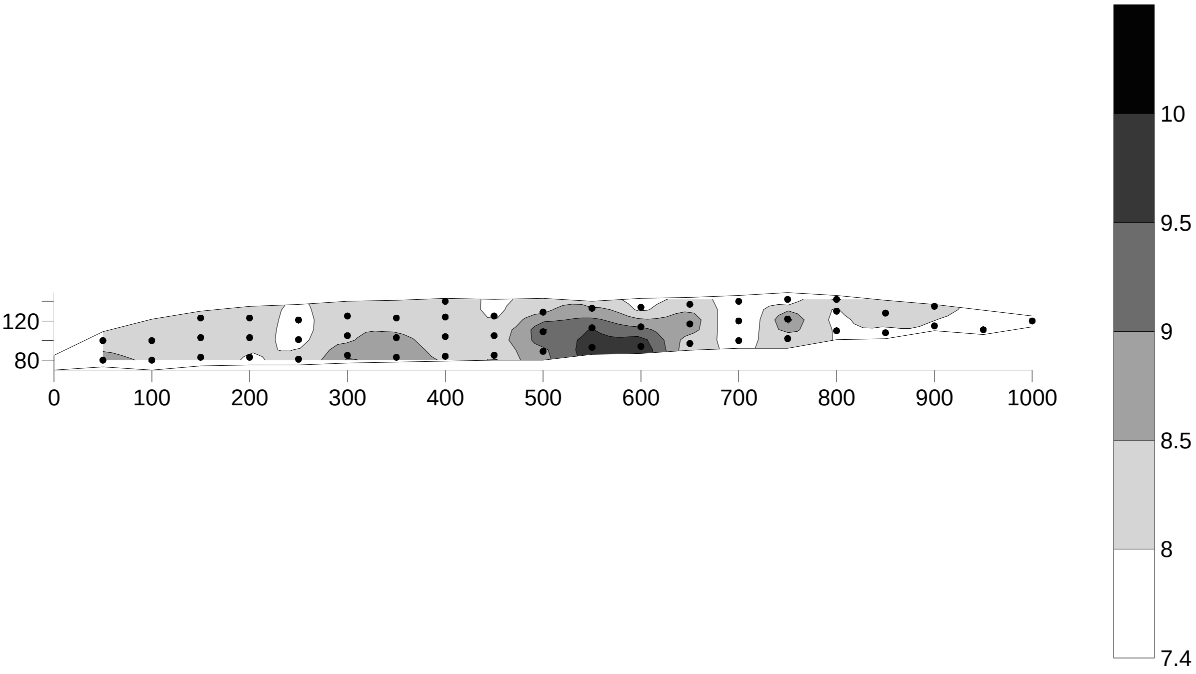

Figure 12. Spatial distribution of pH (EN 12457-2) in a section of the subbase layer of MSW bottom ash. The sampling points are marked as black dots (n=53). The x and y-axis are graded in centimetres.

Batchtests have previously [4] been conducted on all samples (n=53) (see 3.1.2). pH-stat tests and column tests were conducted on four samples created by merging the remaining mass of the samples into four larger samples. This was done by arranging the 53 samples in groups representing different stages of aging as reflected in the pH. In

Figure 13 the data points are arranged in ascending order according to the pH-values (EN 12457-2). The minimum pH-value is 7.4 and the maximum value is 10.0. The sample points and the distribution of pH (EN 12457-2) in the subbase layer are shown in Figure 12 .

Four groups of the data were selected based on the pH-intervals: 8.0-8.5 (n=21), 8.5-9.0 (n=12), 9.0-10.0 (n=4), and marked with different colours in Figure 13.

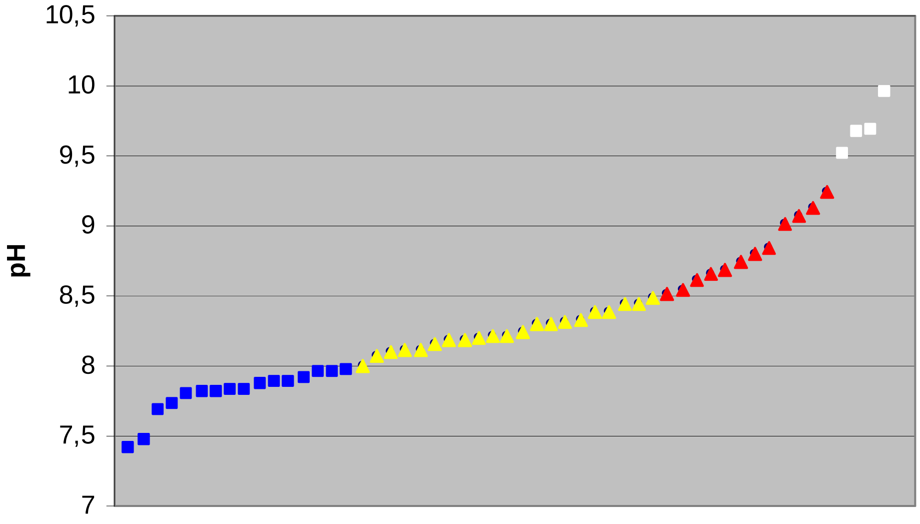

Figure 13. pH-data arranged in ascending order (n=53), The colours indicate the four groups: [pH 7,4-8,0], [pH 8,0-8,5], [pH 8,5-9,5],[pH 9,5-10,0]

In Figure 14-Figure 17 the location of the four groups of samples in the subbase are shown.

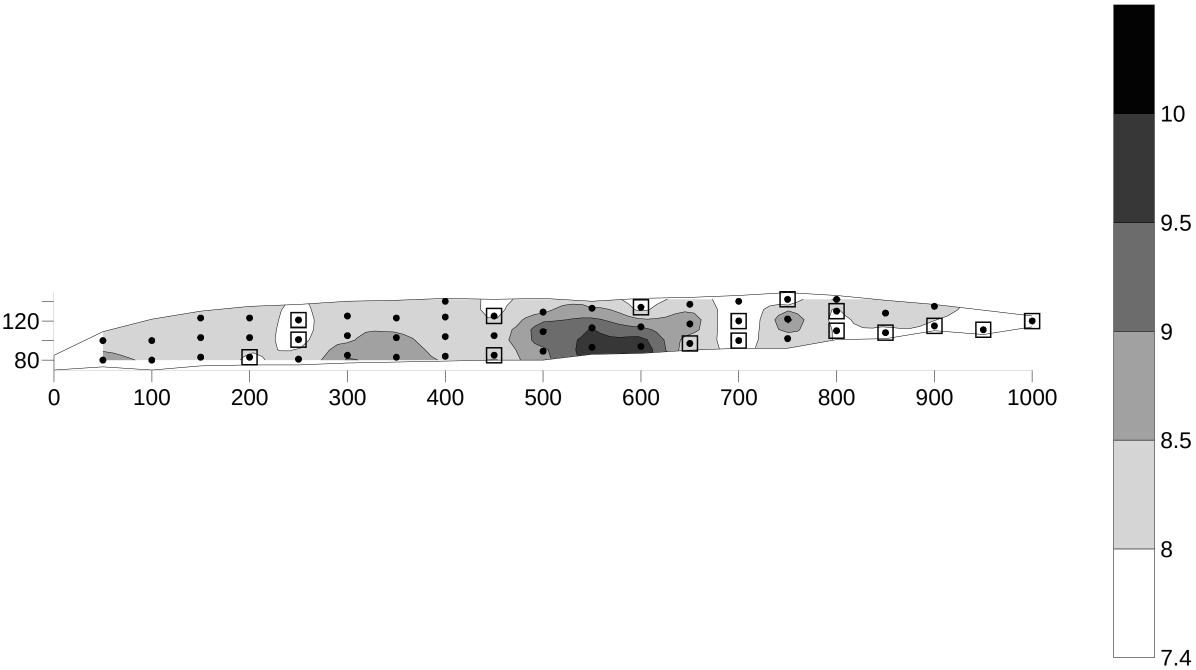

Figure 14. Same as Figure 12, but with the samples in the span 7.4-8.0 marked (group 1).

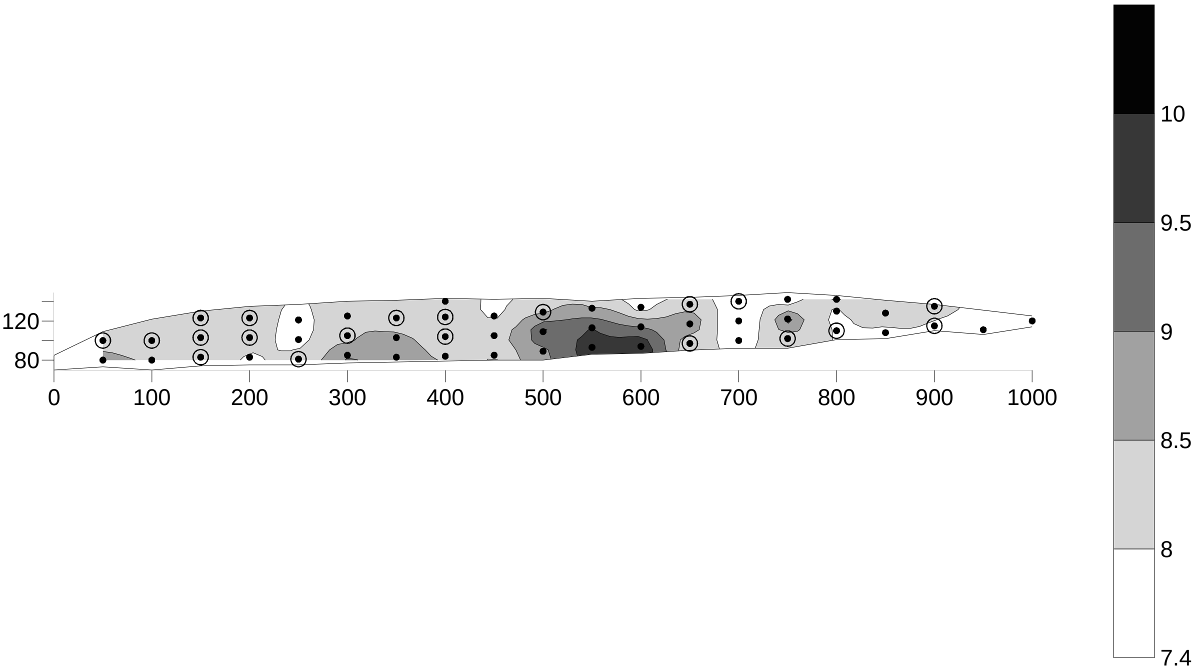

Figure 15. Same as Figure 12, but with the samples in the span 8.0-8.5 marked (group 2).

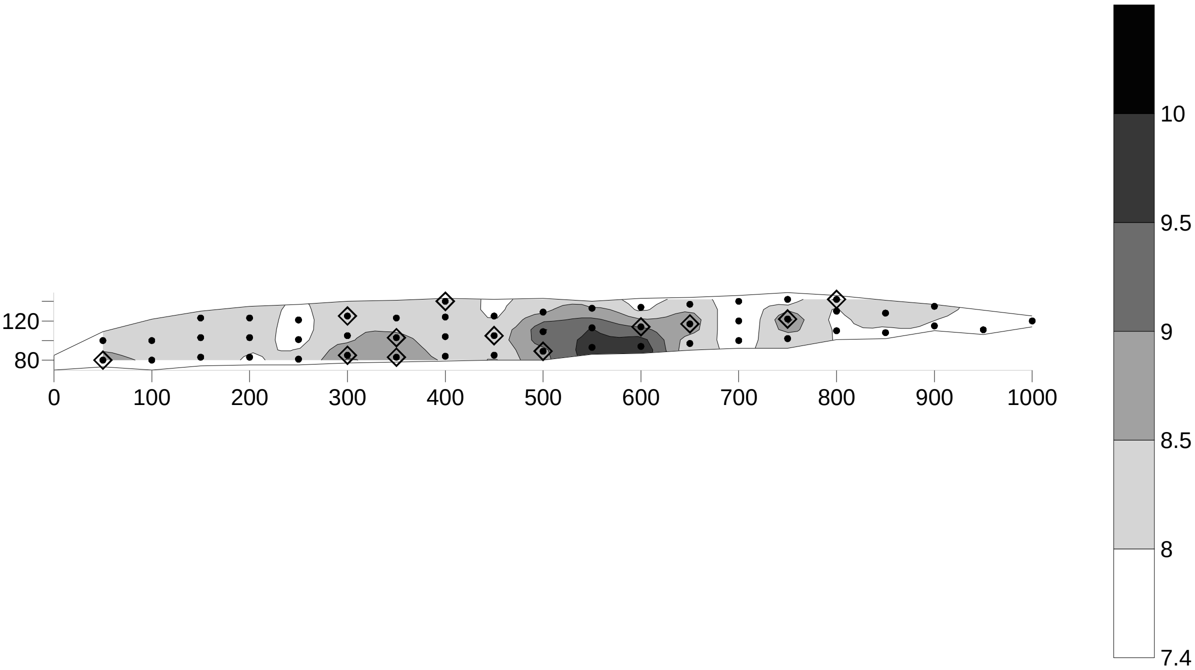

Figure 16. Same as Figure 12, but with the samples in the span 8.5-9.0 marked (group 3).

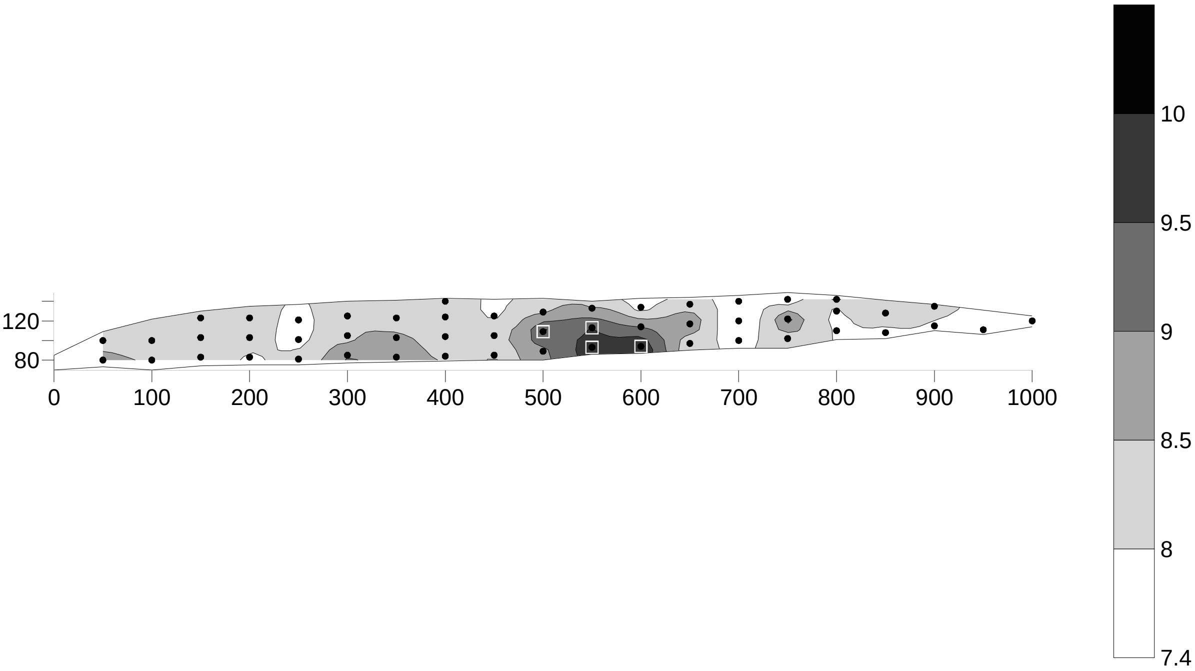

Figure 17. Same as Figure 12, but with the samples in the span 9.0-10.0 marked (group 4).

The four composite samples, the number of subsamples, pH and mass are summarized in table 1

Table 1 The 53 samples merged into four composite samples

Composite sample	pH interval	Number of samples	Mass (g)
1	7.4-8.0	16	1280
2	8.0-8.5	21	1680
3	8.5-9.0	12	960
4	9.0-10.0	4	320

Note that sample 1 and 2 are composed of ash that have been exposed to water and reacted with atmospheric carbon dioxide. Sample 3 are in an intermediate state and sample 4 is still at high pH. The bottom ash was fresh at the time of the construction of the test road with a pH of about 11 (unfortunately no solid data exists here).

3.1.2 Batch tests

One-step batch tests at L/S 10 l/kg were conducted on all 53 samples according to the standard EN 12457-2 with one exception, only 45 gram of material was used. The eluates were filtered through a 0.45 µm filter, stored until analysis, and analyzed with respect to: Al, As, Ba, Ca, Cd, Cl^-, Cr, Cu, Fe, K, Mg, Mn, Mo, Na, Ni, NO_3^-, N, TN, PO_4^{3-}, P, Pb, S, SO_4^{2-}, Si, V, Zn, dissolved organic carbon (DOC) and dissolved inorganic carbon (DIC). The samples were analyzed at the Department of ecology at Lund University and the following equipment was used: TOC analysis equipment by Shimandzu, ionchromatograf Dionex with columns AG14 and AS14A and ICP AEC instrument P-E 3000DV.

3.1.3 pH stat tests and column tests

One-step pH stat tests at L/S 10 l/kg were conducted on the four composite samples according to technical specification SIS-CEN/TS 14997. For sample 1, 2 and 3 pH 2, 4, 5, 6, 7, 8, 10, 11 and 12 were measured. For sample 4, due to the smaller sample size, pH 2, 4, 6, 8, 10 and 12 were measured. The eluates were filtered through a 0.45 µm filter, stored until analysis, and analyzed with respect to: Al, As, B, Ba, Br, Ca, Cd, Co, Cr, Cu, Fe, Hg, I, K, Mg, Mn, Mo, Na, Ni, N, P, Pb, S, Sb, Se, Si, Sr, V, Zn, alkalinity and dissolved inorganic carbon (DIC). The samples were analyzed at ALS Analytica AB.

Percolation tests were conducted on the composite samples 1, 2 and 3 according to technical specification SIS-CEN/TS 14405. The sample amount for sample 4 did not allow for a percolation test. Sampling for sample 1 and 2 was at L/S 0.1, 0.5, 1.0 and 2.0 l/kg (cumulative), and for sample 3 at L/S 0.2, 1.0 and 2.0 l/kg (cumulative). The eluates were filtered through a 0.45 µm filter, stored until analysis, and analyzed with respect to: Al, As, B, Ba, Br, Ca, Cd, Co, Cr, Cu, Fe, Hg, I, K, Mg, Mn, Na, Ni, N, P, Pb, S, Sb, Si, Sr, V, Zn, alkalinity and dissolved inorganic carbon (DIC). The samples were analyzed at ALS Analytica AB. Due to a mistake on behalf of the laboratory DOC, Cl, F and Mo was not analyzed.

3.1.4 TOC, DOC, org fractionation and HFO

The amount of amorphous and crystalline iron (hydr)oxides was estimated by extractions with ascorbine, dithionite and oxalate for amorphous Fe+Al, crystalline Fe, and amorphous Al respectively, following a procedure described in Kostka and Luther [24]. Crystalline Fe was calculated as the difference between ascorbine and dithionite extractions. HFO was calculated as the sum of amorphous Fe+Al, amourphous Al, and a sixth of crystalline Fe, expressed as kg FeOOH for the recalculation from mol to kg.

Four fractions of the solid and organic C in the solid were characterized in a batch procedure derived from the method currently recommended by the International Humic Substances Society. This involved a combination of extraction with 0.1M HCl, with 0.1 M NaOH, centrifugation, filtration, ion exchange, dissolution in 0.1M KOH and analyses of TOC in the extracts [38]. The fractions were humic acids (HA), fulvic acids (FA), hydrophilic acids (Hy) and hydrophobic neutral organic matter (HON), .

3.2 Geochemical modeling

3.2.1 General

Geochemical modeling was done using LeachXS/Orchestra. The degree of saturation in the leachates was calculated for all the minerals in the database. The MINTEQA2 version 4.0 datase [35] was used for the thermodynamic data. Then, a likely mineral assemblage was selected based on previous experience and a calculation of saturation indices. The model prediction of the leachate concentrations were compared with the measured concentrations, and the model of the solid phase were adjusted until the prediction agreed with the measured concentrations.

The following adjustments were made in iteratively to get a satisfactorily fit (listed below in no specific order):

- The mineral assemblage was selected on the basis of their saturation indices in the leachates. By an iterative procedure the mineral assemblage was adjusted to get a satisfactorily fit for all elements.

- Different strategies of modeling the carbonate system were explored. These are described in section 3.2.2 and the results in section 5.6.

The predictive modeling included sorption to solid and dissolved organic matter according to the NICA-Donnan model [22]. The generalized two layer model of Dzombak and Morel [13] was used to model surface complexation and surface precipitation of ions to hydrous ferric oxide (HFO). The same minerals were used for all four samples. Availability of elements differed somewhat, and was taken as the highest emitted amount in the sample's pH stat tests.

Solid humic acid was set to the sum of measured humic and fulvic acid (see chapter 4). Hydrous ferrous oxides (HFO) were set to the measured value (see chapter 4). Clay was set to 1%, because clay is expected to exist in the aged bottom ash. The clay content had very little influence on the predicted leachate concentrations.

By mistake the laboratory, ALS Analytica, did not measure the dissolved organic matter was not measured in the eluates from the pH-stat experiments (see section 3.1.3). Instead, the average of measured concentrations of DOC for the batch tests was used in the model for the interval pH 7-10. Typical distribution of DOC-leaching from fresh bottom ash was combined with the batch test concentrations to derive DOC-values for pH intervals 1-6 and 11-14. The model was not sensitive to selected DOC concentrations: changes in DOC had little effect on the model output, even for elements like Cu.

The final input data for the geochemical model are shown in appendix D.

3.2.2 The carbonate system

The pH-stat tests (SIS-CEN/TS 14997) represent a semi-closed system: interaction with atmosphere is possible at a limited extent. According the technical specification (SIS-CEN/TS 14997) the experimental setup should be closed but allow for release of gas. Carbon dioxide may dissolve into the leachate at high pH and thus increase the carbonate content of the system. Carbon dioxide does escape from the test into the air at low pH, and decreases the carbonate content in the modelled pH-stat test. The carbonate amount in the modeled system primarily affects DIC and Ca concentrations, through the precipitation of calcite. Secondarily, the remaining Ca concentration affects a number of other processes, such as precipitation of other Ca-minerals and cation sorption.

The physical processes governing the carbon dioxide exchange can not be modeled at present. Such model would require precise estimates of the air flow and carbon dioxide contents of the air in the laboratory setup, together with a (kinetically controlled) description of the dissolution of carbon dioxide in the leachate. As an approximation, carbonates were modeled though measured values and a closed system; measured values and where CO_2 (g) were allowed to escape; and with equilibrium with atmospheric carbon dioxide pressure (allowing CO_2 (g) to dissolve into the solution at high pH and escape at low pH). To illustrate the effect of these various ways of modeling the carbonate system, measured concentrations of DIC, Ca and Ba are compared with the concentrations predicted by the various models (see section 5.6).

3.3 Hydrological modeling

3.3.1 Introduction

Daily precipitation data from the Swedish Meterological and Hydrological Institute (SMHI) from the Malmslätt (Linköping) measurement station was used in the modelling. The modelled period was 1th of January 1988 to the 1th of september 2003. The daily data is the registered amount of water recieved from 06.00 (GMT) the actual day to 06.00 (GMT) the next day. Monthly correction factors supplied by SMHI have been used to compensate for losses due to wind and evaporation from the sample containers.

The basic geometry is defined by the surface of the road, the roadshoulders, vertical boundaries down to a horizontal boundary in the subgrade, somewhat arbitrarily defined at z=0 which was the bottom of the excavated shaft. Five domains where defined, the base layer, the subbase layer (bottom ash), the subgrade of sand/gravel/stone, and two separate domains in the subgrade of fine clay (see Figure 2 and Figure 18). The section of the road was measured when the road was excavated in 2003 [4]. The finite element grid of 867 triangular elements and 480 nodes was generated by the HYDRUS/MeshGen2D, and the result is shown in Figure 18.

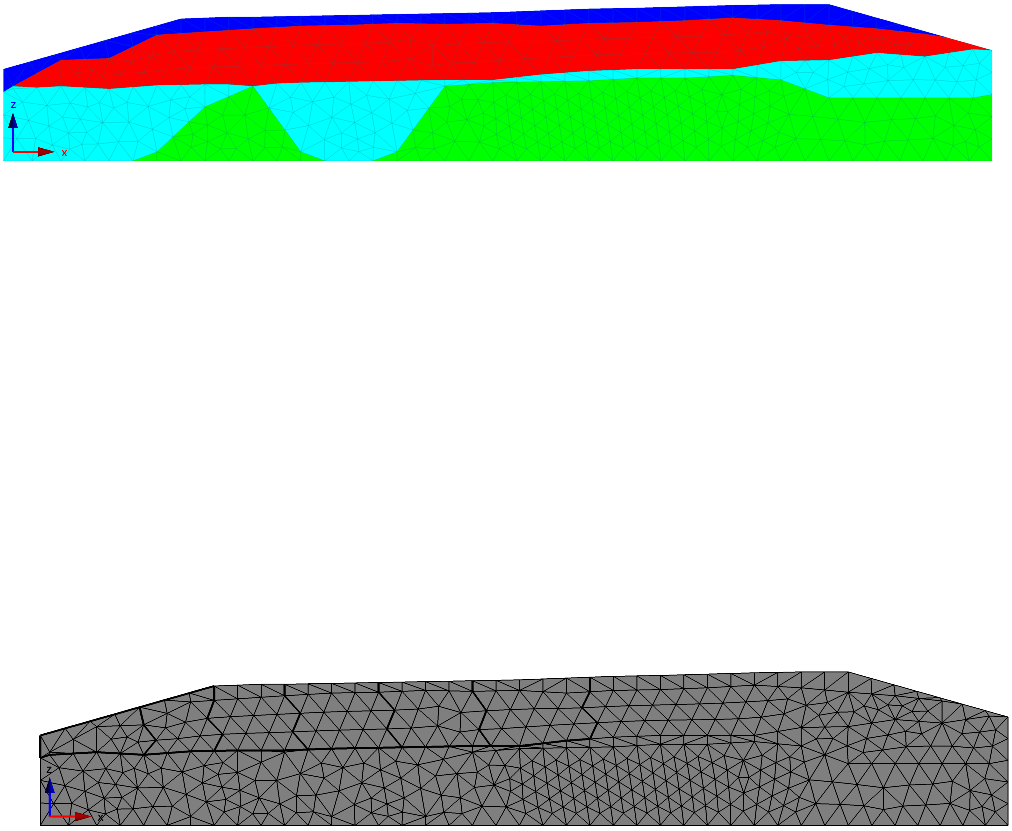

Figure 18. Material domains, finite 2-D elements (n=867) and nodes (n=480). Marin blue is the base layer, red is the subbase layer (bottom ash), light blue is subgrade of sand/gravel/stone, green is subgrade of fine clay (see also Figure 2).

The precipitation on the road surface was assumed to be carried laterally by surface runoff and infiltrate (evenly distributed) together with direct precipitation in the shoulders of the road. The boundary conditions in HYDRUS 2-D were set as follows:

Table 2 Boundary conditions

Boundary	Boundary Condition	Description
Road shoulder	Atmospheric	Allows incorporation of climatic conditions like precipitation, evaporation and transpiration by plants. System-dependent (depend on the solution at the end of each time step). Water input exceeding the infiltration capacity is lost from the system as surface runoff.
Road surface	No flux	Closed boundary
Lower boundary of subgrade	Constant pressure head of zero	

The initial condition of water was set to pressure head = -100 m. Also, as an initial condition: the pore water in the bottom ash subbase layer was spiked with a unit concentration of solute (non-reactive), in order to mimic the transport behaviour of easily soluble constituents in bottom ash.

Evaporation was assumed to take place only at the road shoulders. The evaporation was taken as monthly average values at Malmslätt measurement station calculated by the HBV model for the time period 1961-1990. In HYDRUS, evaporation is given in the atmospheric BC separately.

3.3.2 Input data

The daily precipitation data from the Swedish Meterological and Hydrological Institute (SMHI) from the Malmslätt measurement station for the period 1th of January 1988 to the 1th of september 2003 is shown in Figure 19.

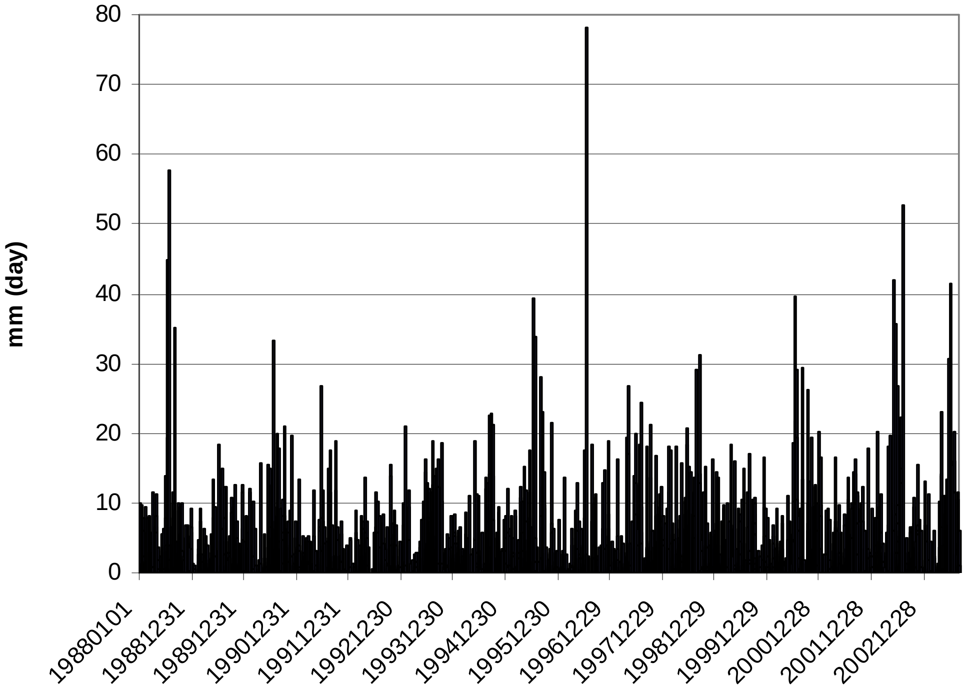

Figure 19. Precipitation Malmslätt measurement station 1th of January 1988 to the 1th of september 2003.

The monthly average potential evaporation data for Malmslätt measurement station for the time period 1961-1990 are given in Table 3.

Table 3 Monthly average potential evaporation data for Malmslätt measurement station

Jan	Feb	Mar	April	May	June	July	Aug	Sept	Oct	Nov	Dec
1	2	6	41	81	79	66	53	32	14	2	0

Specific hydraulic properties were assigned to the different domains, Table 4. The Van Genuchten model [37] was used to describe the water retention properties:

$$\theta(h) = \theta_r + (\theta_s - \theta_r)\left[1 + |\alpha\psi|^n\right]^{-m} \qquad \psi < 0$$

The parameter θ_r and θ_s are the residual and saturated water content (m^3/m^3), respectively, ψ is the capillary suction (m). The α , n and m are material parameters. To obtain a closed form expression for unsaturated hydraulic conductivity Van Genuchten [37] defined :

$$m = 1 - 1/n \quad n > 1$$

For the subgrade and base material, generic material parameters were taken from HYDRUS soil data base. For the bottom ash the water retention data were determined in laboratory at the dry bulk density of 1.3. The parameters α and n were determined by fitting the Van Genuchten [37] model to the data using the RETC software (United states salinity laboratory). The water retention curves and the experimental data (bottom ash) are showed in Figure 20. For a description of the methodology and apparatus for determining the water retention curve, the reader is referred to a previous study by Hemström et al [18].

Table 4 Hydraulic parameters

Domain (see Figure 18)	Description	θr	θs	α	n	Ks
Red	Bottom ash	0,1	0,53	4,0	1,30	5,0
Light blue	Sand[1)]	0,045	0,43	14,5	2,00	7,1
Green	Clay[1)]	0,068	0,38	0,8	1,17	0,048

[1)] HYDRUS 2D Soil database

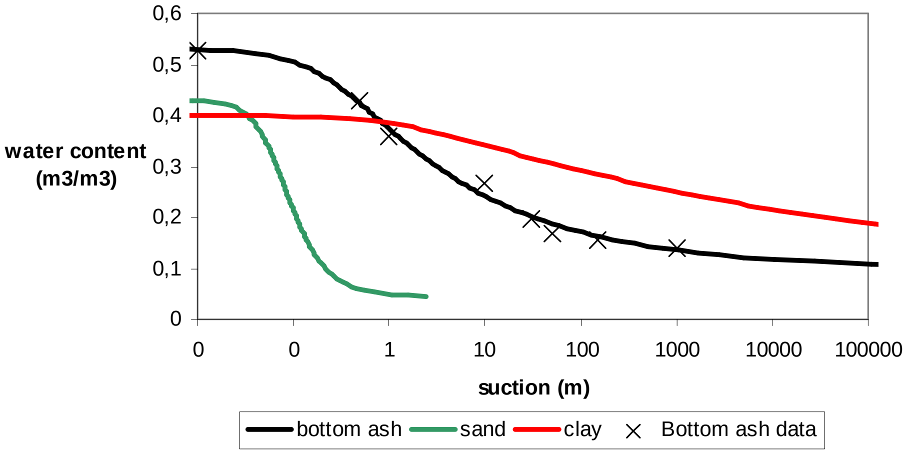

Figure 20. Water retention curves: bottom ash together with the experimental data, sand and clay (HYDRUS 2D soil database).

4 Laboratory characterization - results

4.1 Introduction

In this chapter the experimental data of the four merged samples is presented. Note that samples 1 and 2 have undergone the least degree of aging as reflected by the pH). Sample 3 represent an intermediate state and sample 4 represent regions of the subbase that is still at high pH (section 3.1).

4.2 Direct measurements on ash and extractions

Table 5 shows the result of the analyses of the solid phase. The carbonate content was expected to decrease in the order sample 1>2>3>4, due to aging (carbonatisation). This is in accordance with the experimental data, except that sample 3 had a higher carbonate content.

Table 5: Average content of organic matter and iron and aluminum oxides. Specific data in appendix A.HFO: hydrous ferrous oxide surfaces, SHA: solid humic acid

	HFO kg/kg	TIC %	TOC %	SHA kg OM/kg	DITH extracted Fe g/kg
Sample 1	0.029	0.71	4.03	0.00041	23
Sample 2	0.035	0.63	3.51	0.00030	26
Sample 3	0.039	0.87	5.22	0.00023	24
Sample 4	0.029	0.58	4.56	0.00028	14

Iron and aluminum oxides have been measured using three extractions. The Fe extracted by acetic acid (amorphous Fe, appendix A.1) was slightly lower than the corresponding measurement on fresh bottom ash in [11]. The (amorphous) Al extracted by oxelate was slightly higher. The Fe extracted by DITH, i.e. the crystalline Fe, was considerably higher in the Vändöra samples than the 8.7 g/kg measured by [11] with the same method.

The acid and base neutralizing capacity was measured in the pH-stat tests and is shown in Figure 21. The four composite samples were similar.

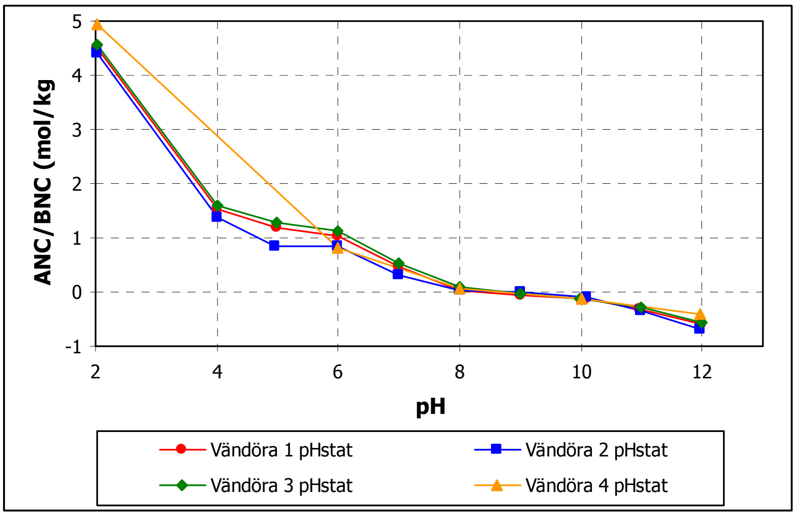

Figure 21. Acid and base neutralizing capacity

4.3 pH stat-leaching data

4.3.1 The data

The complete set of pH stat leaching data is shown in appendix B. A couple of examples focusing on the differences between the four samples are given in this section.

By comparing the EC data it seems that sample 2 had been leached most extensively, as shown by the lowest average EC in the batch tests and the lowest Na emission in the pH-stat and percolation tests. The order of average EC for the composite samples was sample 2 < 1 < 3 << 4. The pH stat leaching data of Na and S followed that order (Figure 22).

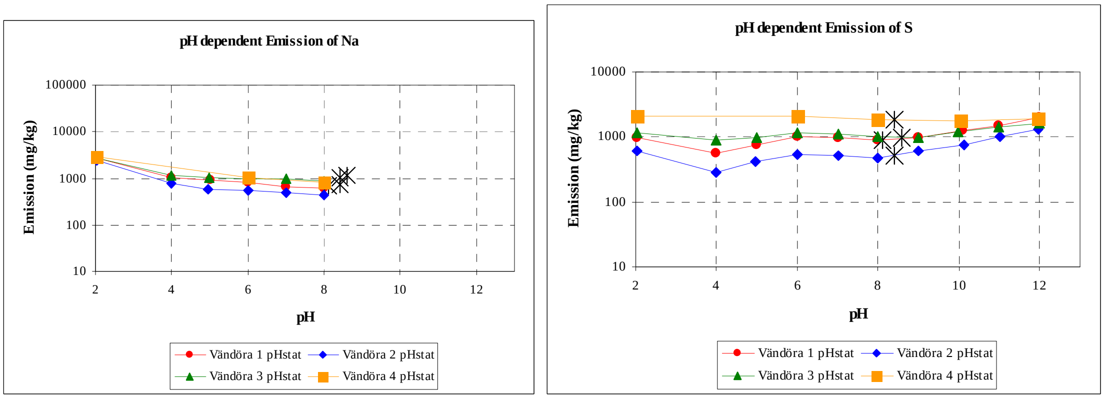

Figure 22. Leached content of Na and S in pH-stat tests. NB Na values at pH>8 not shown since Na (actually NaOH) is added to the test to increase pH. The star symbol represents the pH of the ash.

The spatial distribution of leachable Ca (Figure 6) is an effect of leaching, reaction with atmospheric carbon dioxide and formation of less soluble minerals such as calcite (see section 2.6). With exception of sample 4 (Figure 23), the leaching behaviors of the four samples were found to be similar. The element Sr followed the same pattern.

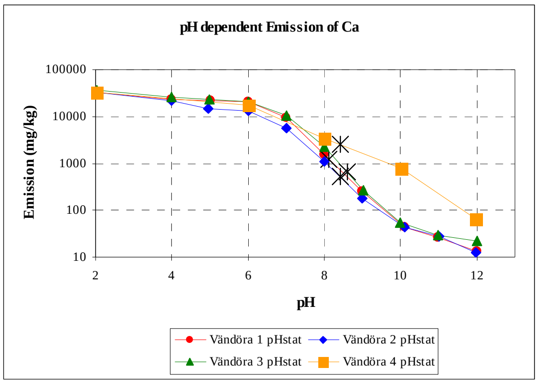

Figure 23. Leached content of Ca in pH-stat tests. The star symbol represents the pH of the ash.

Sample 4 differed from the others also with respect to leaching of Fe and As, with lower availability in the alkaline range (Figure 24).

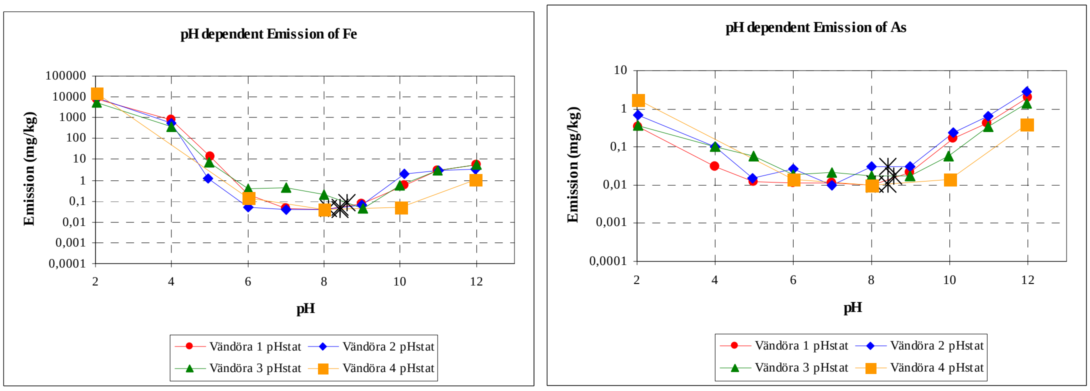

Figure 24. Leached content of Fe and As in pH stat tests. The star symbol represents the pH of the ash.

For other elements no difference in the leaching behavior could be seen if the four samples was compared. The only exception was Sb, here the sample 2 sample showed higher leaching than the other samples.

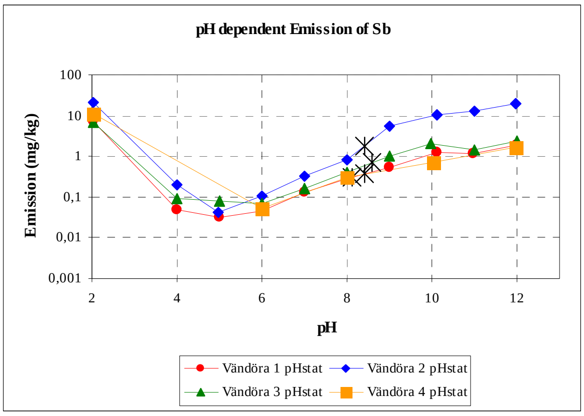

Figure 25. Leached content of Sb in pH stat tests. The star symbol represents the pH of the ash. The star symbol represents the pH of the ash.

4.3.2 The data compared with some international (fresh) ashes

The results from pH-stat and percolation tests have been compared to some Austrian and Dutch bottom ashes from municipal waste incineration. The data was retrieved from LeachXS and shows Dutch and Austrian fresh MSWI bottom ashes in addition to Vändöra The graphs are shown in appendix C, and a selection is shown below. For most elements the Vändöra ash is similar to the Austrian and Dutch bottom ash. However, the release of easily soluble elements, such as Na, was lower for the Vändöra composite samples. This is likely due to the longer exposure of the Vändöra ash to water. The leaching from the 53 batch tests matched the leaching from the 4 composite samples.

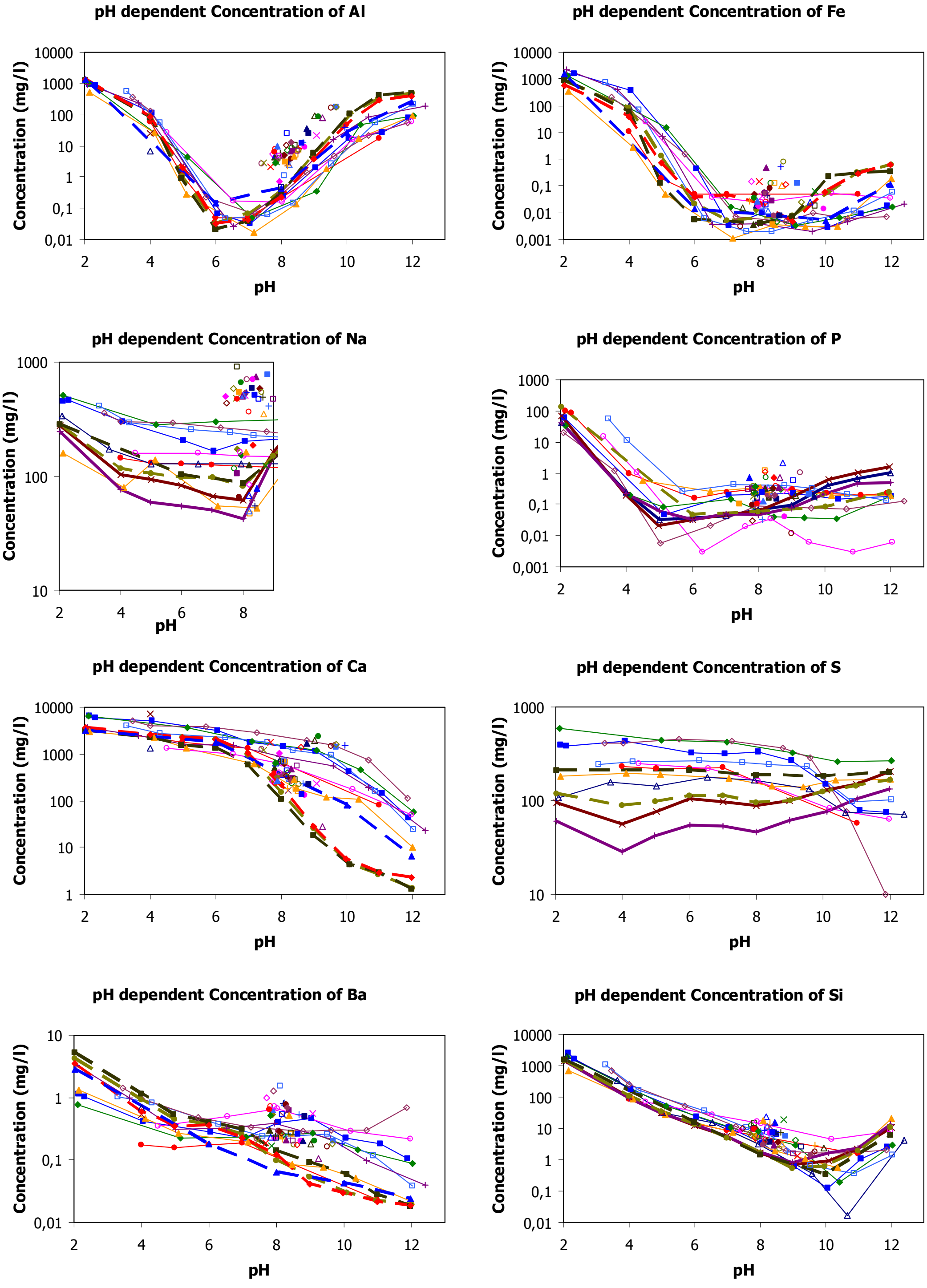

Figure 26. Comparison of leaching of macroelements from Vändöra ash with some bottom ashes from the Leach XS data base. Vändöra composite samples are the bold lines. Na graph truncated since Na is added in the pH-stat test.

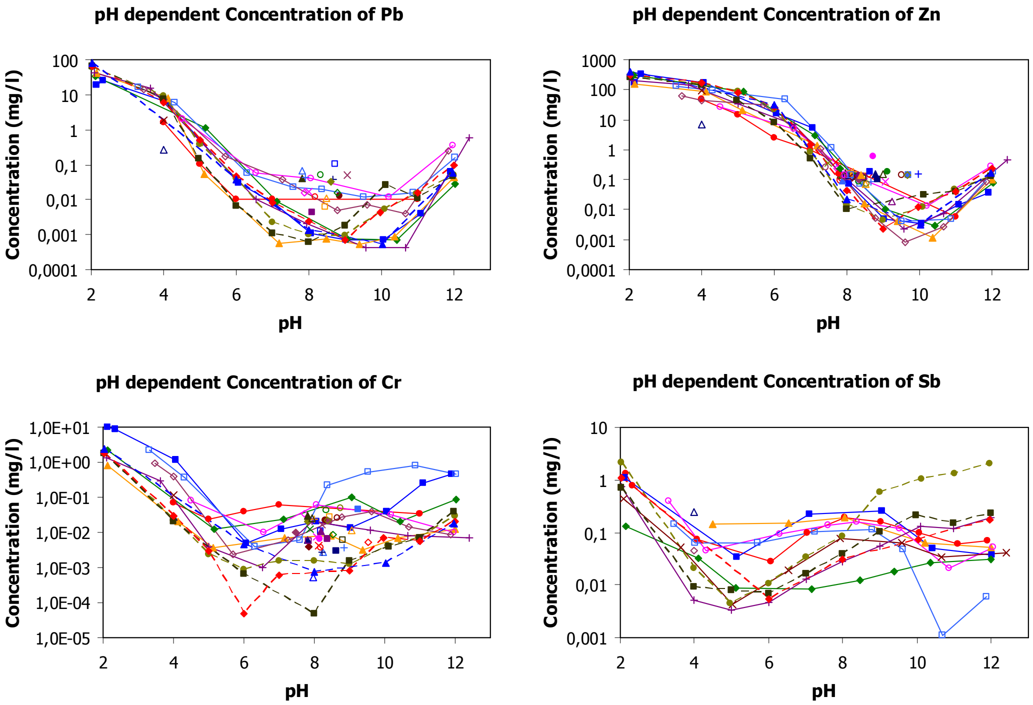
pH dependent Concentration of Pb

pH dependent Concentration of Zn

pH dependent Concentration of Cr

pH dependent Concentration of Sb

Figure 27. Comparison of leaching for selected trace elements from Vändöra ash with some bottom ashes from the Leach XS data base.

5 Geochemical modeling-results

5.1 Reading the graphs

The results from the geochemical modeling are presented in two types of diagrams for each constituent: (i) diagrams showing the model prediction and the experimental concentrations from the pH-stat experiments (ii) Partitioning diagrams showing the phases (minerals, free, DOC, POM, Fe oxide) which the available constituent is associated with.

One example for the constituent Pb is given here as an introduction to the reader. The prediction of the model and the experimental data are presented in Figure 28. The partitioning of the available Pb is presented in Figure 29 and Figure 30. Figure 28 and Figure 30 have a logarithmical y-axis. In Figure 29 a linear y-axis is used.

The model fit diagram, Figure 28, contains four series. The red dots and lines are for the pH-stat tests, the blue for the percolation test. For the composite sample sample 4 no percolation test was possible, so the results of the percolation test for sample 1 are shown. The dots are measured concentrations; the lines predicted (modeled) concentrations. The model is identical for the two tests.

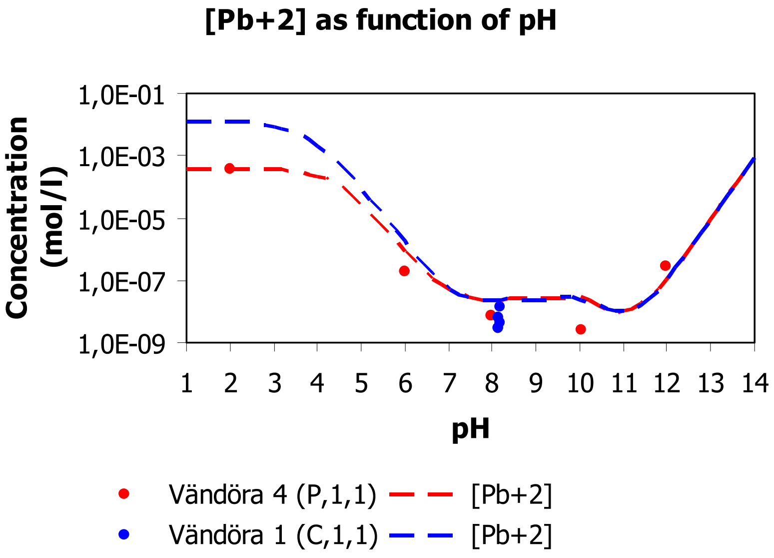

Figure 28. Model prediction and experimental data of Pb in the geochemical model of composite sample 4

The coloured fields in Figure 29 represent the different phases of available Pb as function of pH. Note that the *total content* of Pb in the ash can be higher, but is not involved in the modelling and not shown in the diagrams. The available Pb is divided into a water phase (free and DOC bound) and a solid phase (minerals, POM and FeOxide bound). The free phase is always light blue and includes any inorganic complexes in solution, the DOC-bound phase is always light green. Minerals are represented by varying colours, but some solid phases are fixed. The dark green is always POM-bound. POM refers to particulate organic matter, and shows the amount of Pb that is sorbed to solid organic matter. The red is always FeOxides, and shows the amount of Pb that is associated with iron and aluminum oxides. The white is always ettringite (cannot be seen in this example with Pb), and shows the amount included in ettringite, either as mineral phase or as solid solution.

Figure 29 shows that of available Pb, all is in solution at pH 1-2 (light blue). Between pH 5 and 13, most available Pb was found in the solid phase. At pH under 10 most was associated with iron oxides, at higher pH $Pb(OH)_2$ controlled solubility.

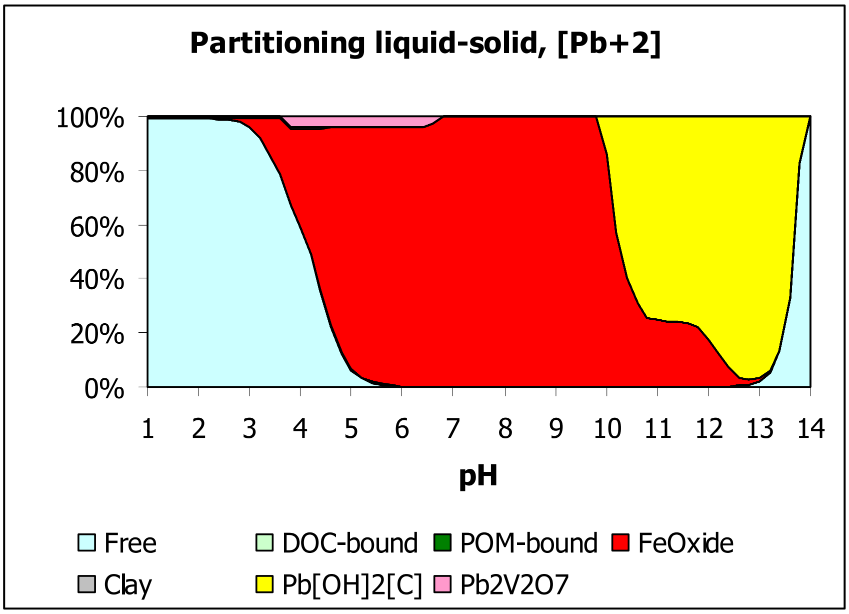

Figure 29. Partitioning of available Pb in the geochemical model of sample 4.: y-axis in % of available Pb.

The y-axis has been changed in Figure 30, but it is otherwise the same as Figure 29. The y-axis is logarithmical, which distorts the surfaces but makes smaller phases visible. See for example the light green (Pb associated with dissolved organic matter) and the dark green (Pb associated with solid organic matter) in Figure 29 and Figure 30, respectively. In addition the y-axis scale shows the concentrations in mol/l. The solid phase concentrations have been expressed as liter water in the system, with the conversion factor of L/S=10l/kg.

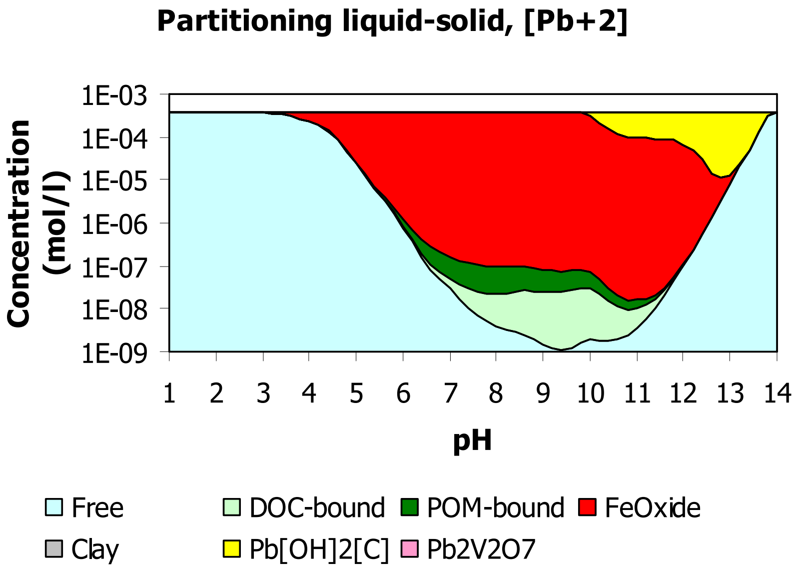

Figure 30. Partitioning of available Pb in the geochemical model of sample 4. y-axis log scale of moles of Pb per liter water in the system.

In the following section a selected number of diagrams showing the results from the geochemical modelling are presented. The complete set of diagrams is presented in appendix F. In addition to the model fit and partitioning diagrams presented in the body of the report, the appendix also includes partinoning in the water phase and in the solid phase, with liniar y-axis. The diagrams may be titled H_2CO_3, VO_2 etc, since these are the primary entities in the model. The diagram do not show only this species of the element, but rather all species of the element in the solution. The chemical formulas of the minerals are listed in appendix E.

5.2 Model fit

The model fit for all elements is shown in appendix F. The performance of the modeling with respect to the macroelements is important as the macroelements influence the trace elements. An example of such influence is how the Ca amount influences the amount of ettringite, and through that the amount of Sr in ettringite solid solution. Another example is that PO_4 may compete with As for places on iron oxide.

The macro-elements were satisfactory described by the model. Some shortcomings exist in the description of easily soluble salts, their behavior is not suited for modeling with mineral and sorption equilibrium. The adverse effect on the trace metals should be negligible. The model also predicted most trace elements satisfactory.

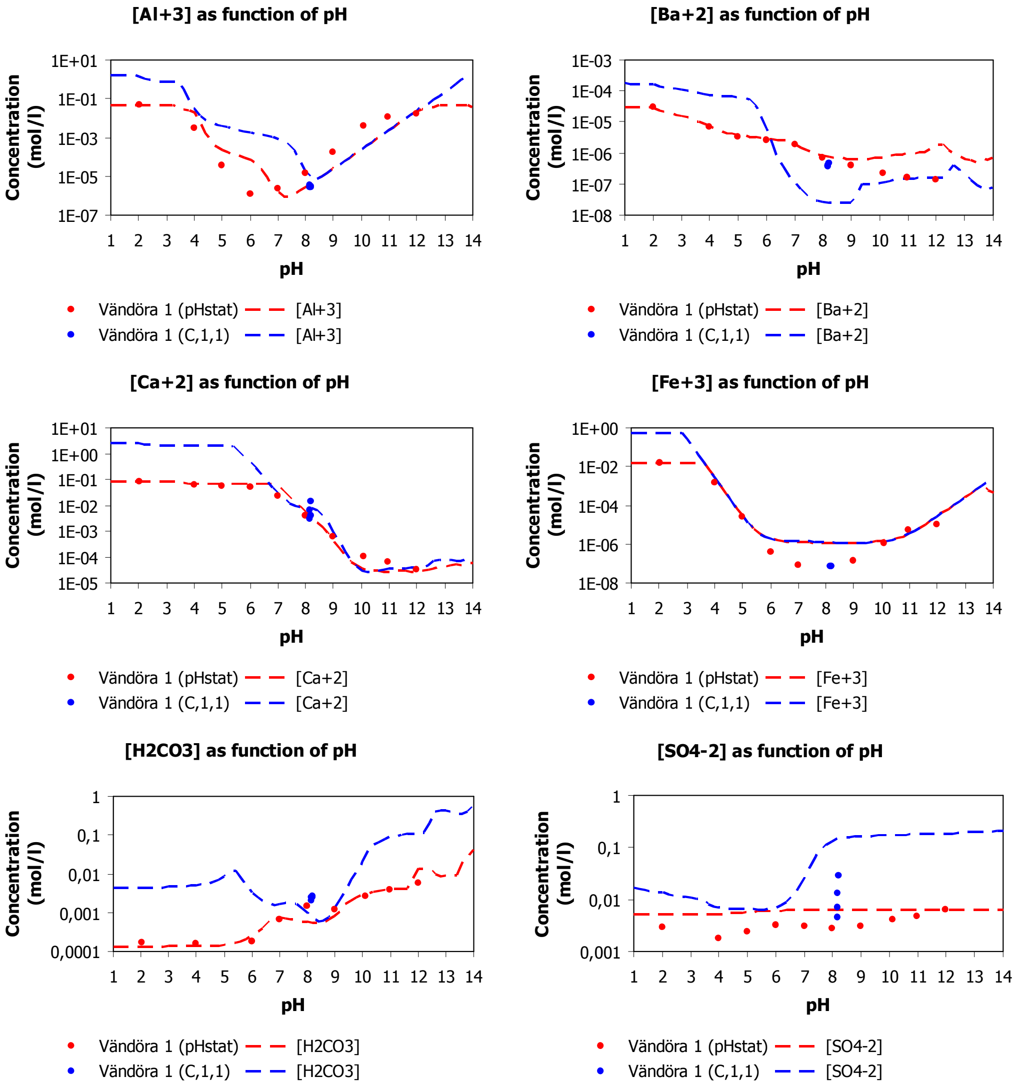

Figure 31. Geochemical model fit for leaching of Al, Ba, Ca, Fe, CO_3 and S for the composite sample sample 1.

5.3 Differences between the four composite samples

The differences between the four composite samples were slight. An almost identical model was applied, and fitted satisfactory for all four samples. The difference was in the content of available carbonate, which also showed in the measurements of TIC on the solid phase.

5.4 Macro elements

Laumontite ($Ca(AlSi_2O_6)_2 \cdot 4H_2O$) was a major control on the leaching of Ca and Al, and calcite ($CaCO_3$) on the leaching of calcium and carbonate.

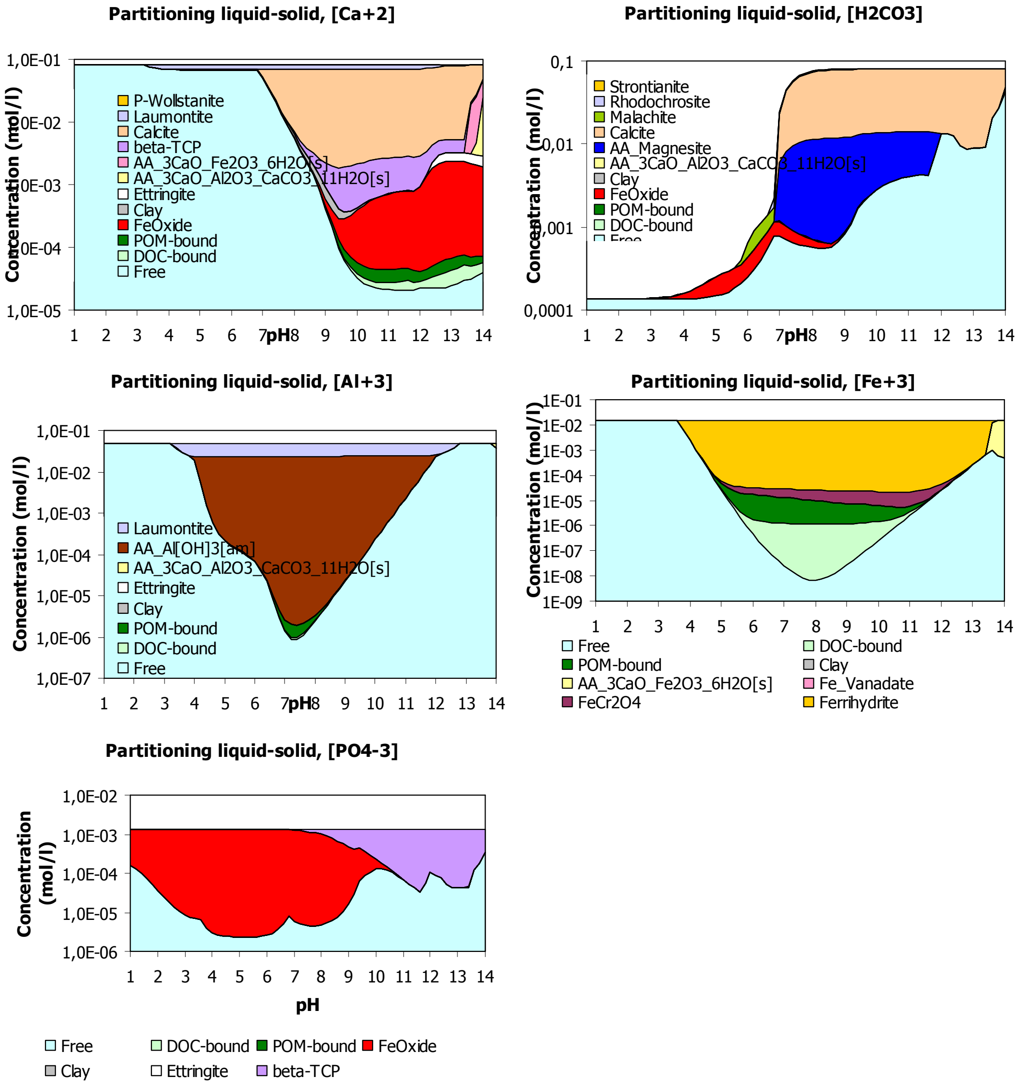

Figure 32. Partitioning of available Ca, CO_3, Al, Fe and P according to the geochemical model for the composite sample sample 1.

5.5 Trace elements

Iron oxides were extremely important for the leaching of trace elements (red fields in Figure 33). At pH ca 8 to 11, many of the trace metals in solution were associated with DOC. At lower pH the effect of DOC was predicted to diminish. Below a short list the distribution of some trace metals at pH around 8:

Pb: Present mainly in the solid phase on iron surfaces, some on organic matter. The solution dominated by DOC bound lead, but the DOC influence is decreasing rapidly with decreasing pH.

Cu: Present mainly in the solid phase, divided between malachite (copper hydroxide carbonate) and iron surfaces. The solution dominated by DOC bound copper, but the DOC influence is decreasing rapidly with decreasing pH.

Zn: Present mainly in the solid phase, in the form of willemite (zinc silicate). The water phase divided equally between free and DOC bound zinc.

As: Present mainly in the solid phase, entirely associated with iron oxides.

Cd: Present mainly in the solid phase, but with pH-decrease much cadmium may be mobilized. The solid phase dominated by iron hydroxides, with some organic bound cadmium. Cadmium in solution mainly free (not bound to DOC).

Ni: Present mainly in the solid phase, but with pH-decrease much nickel may be mobilized. The solid phase dominated by nickel silicate and, at slightly lower pH, iron oxide surfaces. Nickel in solution is mainly free (not bound to DOC).

Cr: Present mainly in the solid phase, as iron chromate. Chromium in solution is present almost entirely bound to DOC.

Mo: Present mainly free in solution, not bound to DOC.

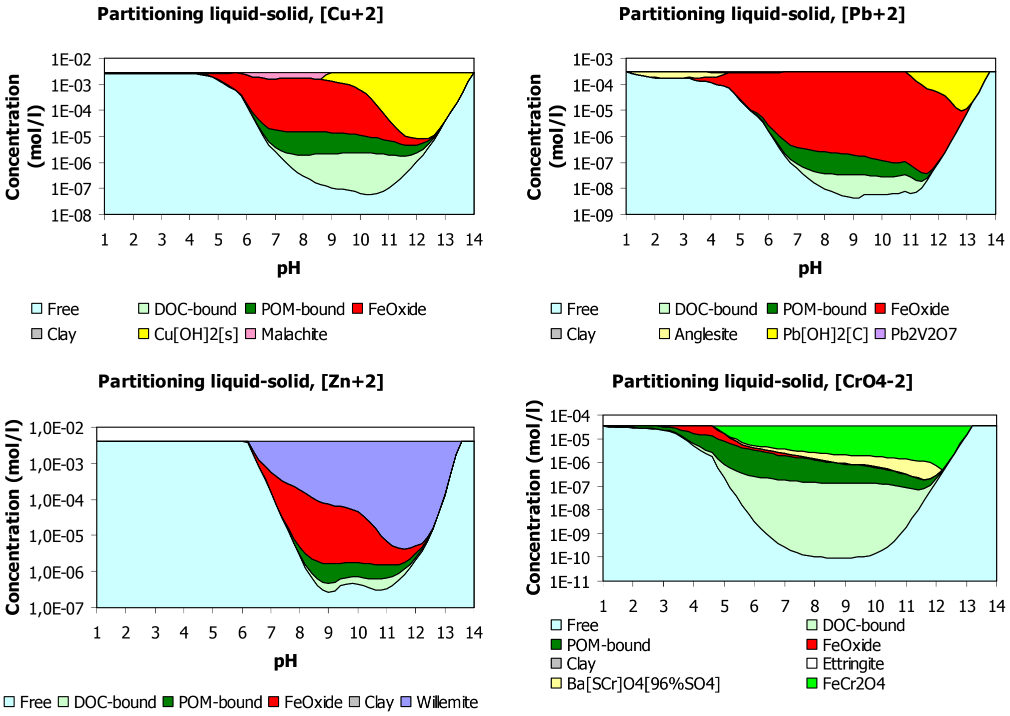

Figure 33. Partitioning of available Cu, Pb, Zn and Cr according to the geochemical model for the composite sample sample 1.

5.5.1 Antimony (Sb)

The geochemical model was not helpful for the explanation of the deviating behaviour of Sb in sample 2 (see chapter 4, Figure 25), Sb was not modeled correctly. This is a general problem for oxyanion modeling: thermodynamic data on the solid solutions that may control leaching is lacking [8]. The measured concentrations were much lower than the modeled concentrations, except at pH 2. The model predicted free Sb for nearly all available Sb. Since the concentration at pH 2 set the availability, this was predicted correctly. However the lower concentrations at pH 4-12 were not successfully predicted.

Ettringite appears as an important host mineral for Sb at high pH. Sorption to iron or aluminum oxides is important as the pH decreases more [28][7], and especially at pH <7 [8]. The otherwise expected mineral around pH 9 is $Ca(Sb(OH)_6)_2$, though the interaction with calcite is not clear either [7]. $Ca(Sb(OH)_6)_2$ was not included in the present geochemical modeling, the solubility constant has been calculated only recently. The effect of the mineral on the geochemical model could prove instructive for the explanation of Sb behavior.

5.6 Modelling carbonate

Various ways of modeling the carbonate system were explored: (i) measured value of carbonate and where CO_2 (g) were allowed to escape at low pH; and (ii) measured value of carbonate with equilibrium with atmospheric carbon dioxide pressure (allowing CO_2 (g) to dissolve into the solution at low pH and escape at high pH) and (iii) by allowing CO_2 (g) adjusted values (increased measured values) of carbonate content to account for the dissolution of CO_2 (g) into the system at high pH.and where CO_2 (g) were allowed to escape at low pH.

To illustrate the effect of these various ways of modeling the carbonate system, measured concentrations of DIC and Ca are compared with the concentrations predicted by the various models, in Figure 34 and Figure 35.

While the modeled concentration of calcium was satisfactorily in the model at equilibrium with atmospheric carbon dioxide, the Ba predictions indicated that the carbonate system was not described correct (Figure 36). The predicted Ba-concentration was to high at high pH when CO_2 equilibrium was used in the model. This was caused by the lower predicted precipitation of ettringite. This was due to that more CO_2 was dissolving into the solution leading to high calcite ($CaCO_3$) precipitation. No calcium was then available for the precipitation of ettringite.

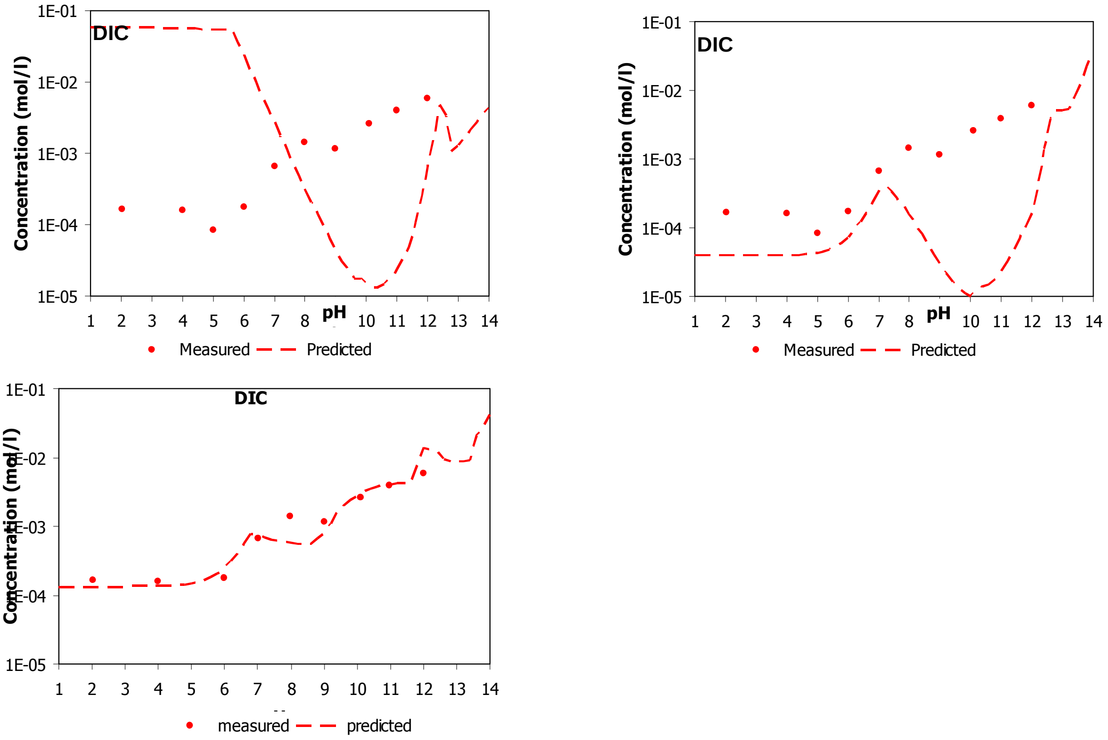

Figure 34. *Model prediction and measured values for DIC in sample 1 for different ways of modeling carbonates. Upper left diagram: measured TIC. Upper right diagram: open system (CO_2 can escape, TIC as measured). Lower diagram: Final model (CO_2 can escape and TIC availability has been adjusted). Open system in equilibrium with CO_2 not shown in the figure.*

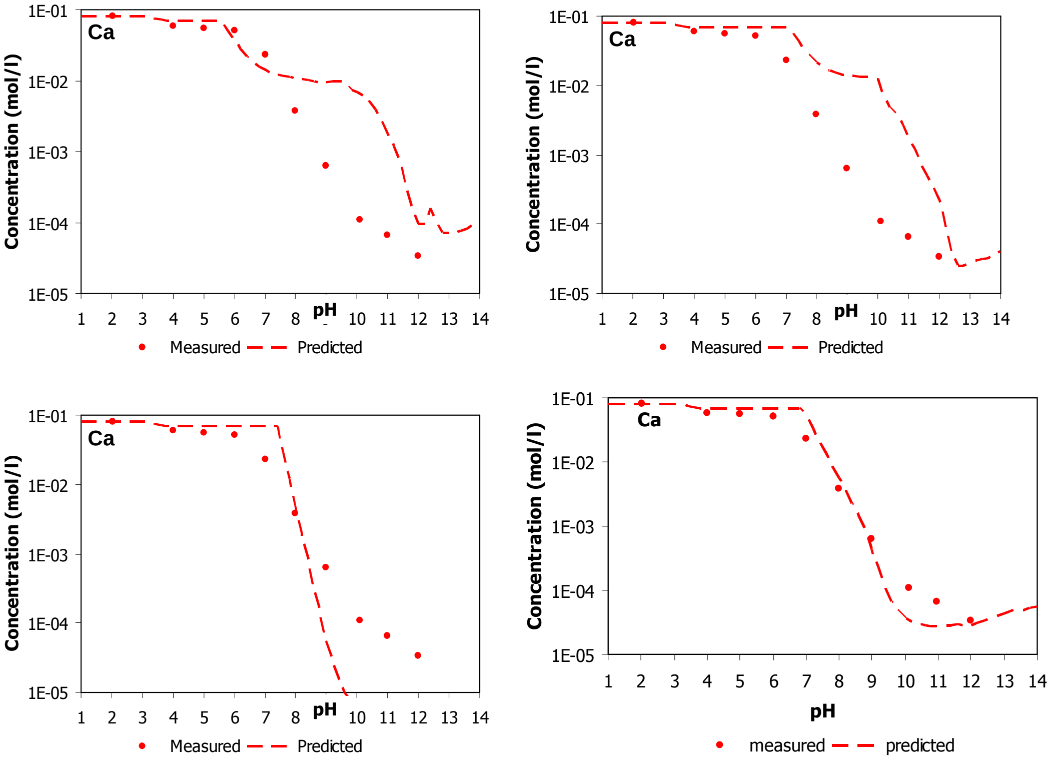

Figure 35. Model prediction and measured values for Ca in sample 1 for different ways of modeling carbonates. Upper left diagram: measured TIC. Upper right diagram: open system (CO_2 can escape). Lower left diagram: Open system in equilibrium with the partial pressure of atmospheric CO_2. Lower right diagram: Final model (CO_2 can escape, TIC adjusted).

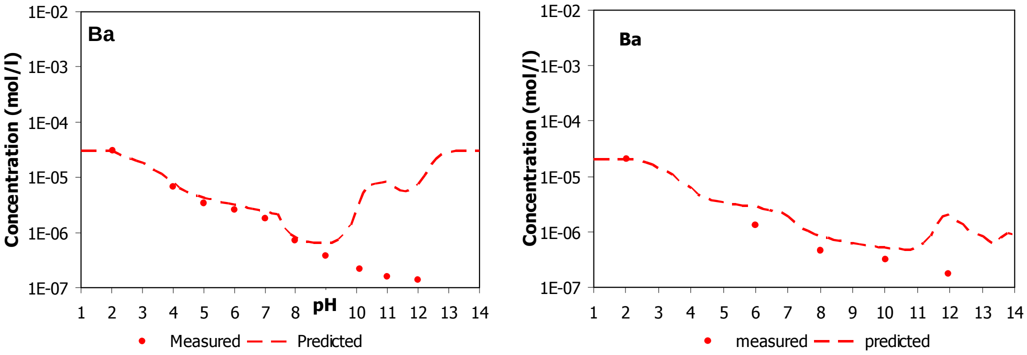

Figure 36. Model prediction and measured values for Ba in sample 1 for different ways of modeling carbonates. Left diagram: open system in equilibrium with atmospheric CO_2. Right diagram: Final model (CO_2 can escape, TIC adjusted).

For the final model the carbonate availability has been used as a fitting parameter, in a system where carbon dioxide is allowed to escape to a gas phase. The carbonate availability was in the model set to measured TIC (see chapter 4), and then slightly increased to provide a better prediction of measured Ca, and (secondary) measured alkalinity.

With this procedure the modeled carbonate content mirror the measured TIC closely (Table 6). Because of the carbonates effect on the other major elements, this was chosen as preferable to adjustments more in concert with physical processes but with less good results.

The model, in accordance with the experimental data, resulted in the highest carbonate content for the composite sample 3. The carbonate content decreased in the order sample 1 > sample 2 > sample 4, as expected and as indicated by pH. The carbonate content in the final model of sample 1 was 0.08 mol/l (TIC fitted). This figure can be compared to the measured TIC: 0.06 mol/l, the model result for an open system in equilibrium with atmospheric carbon dioxide: 0.1 mol/l.

Table 6: Measured and modeled content of carbonates (TIC and available DIC)

Composite sample	measured TIC g/kg	modeled DIC availability g/kg
1	7.1	9.6
2	6.3	9.2
3	8.7	11.0
4	5.8	9.0

6 Hydrological modeling-results

The results from the hydrological modeling are presented as: (i) some snapshots from the years 1988 and 1992 of the spatial distribution of the volumetric water content (m3/m3) (Figure 37-Figure 45), (ii) the accumulated liquid:solid ratios (Figure 46) at the timepoint when the road was excavated in 2003 and (iii) the depletion of solutes as function of time (Figure 47). The initial conditions were set to a uniform capillary pressure of: -100 m. The spatial distribution of the volumetric water content (Figure 37) reflects the different water retention properties of the materials (Figure 20).

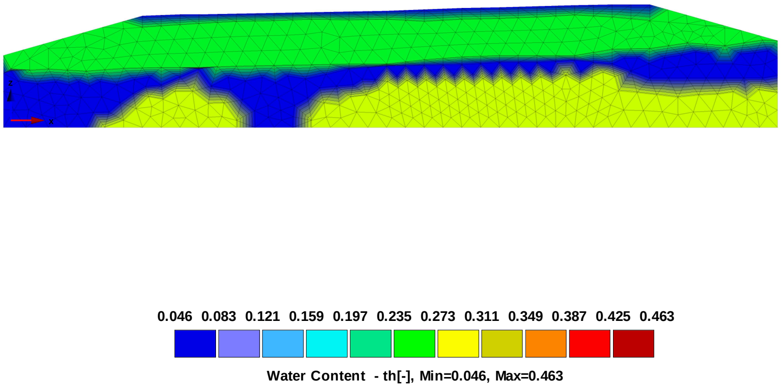

Figure 37. Initial conditions (January 1988)

The distribution of water after 1 month (Figure 38) show water infiltrating in the shoulders and fronts propagating horizontally towards the center of the road, driven by capillary forces. After four months the water fronts had almost reached the center of the road (Figure 39).

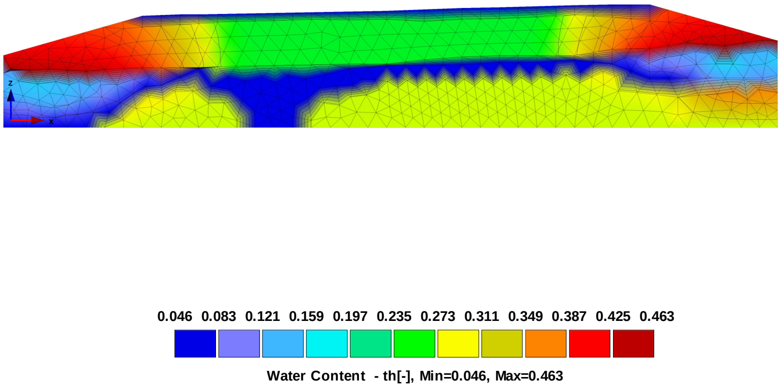

Figure 38. Distribution of water content after 1 month (January 31 1988). Precipitation in January =63 mm.

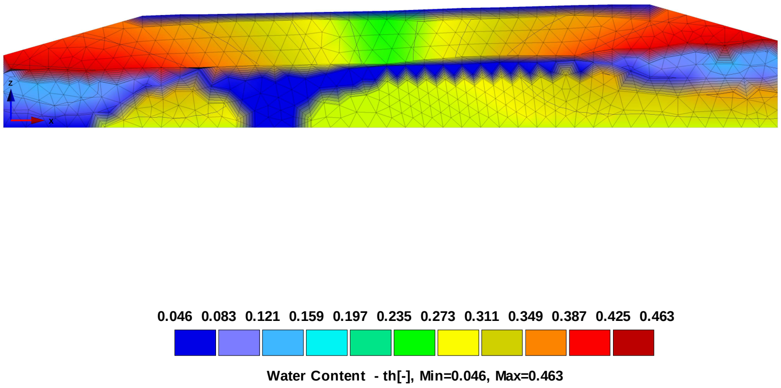

Figure 39. Distribution of water content after 4 months (April 30 1988). Precipitation in April =43 mm.

During the dry summer months the evapotranspiration along the road shoulders effectively transports water out from the road body to the atmosphere and the gradients levels out (Figure 40) before the rain sets in again (Figure 41).

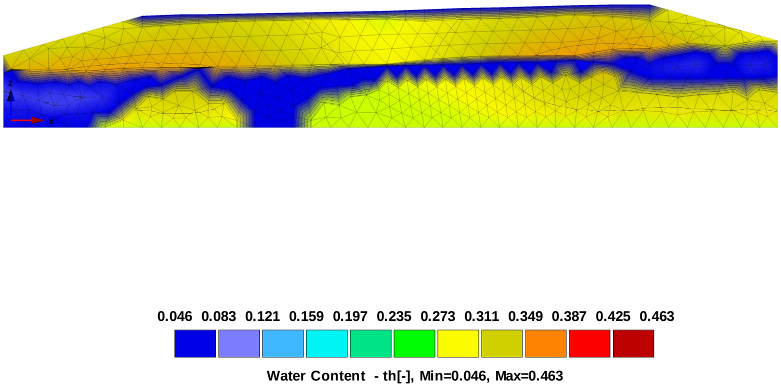

Figure 40. Distribution of water content after 5 months (May 31 1988). Precipitation in May = 14 mm.

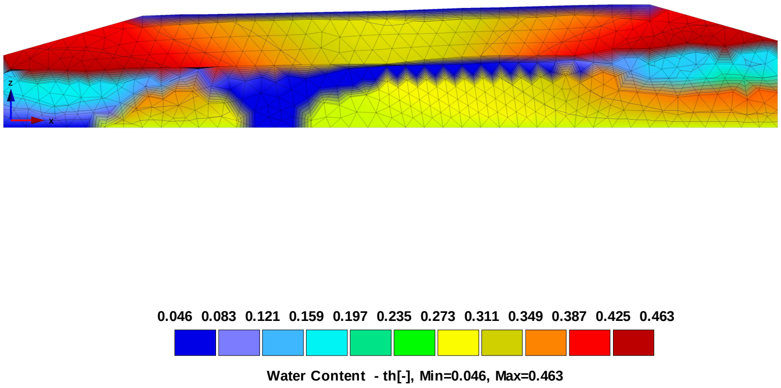

Figure 41. Distribution of water content after 7 months (July 31 1988). Precipitation in July =169 mm.

This phenomenon of seasonal variation of water content in the road body (see for ex. [23] and [32]) is pronounced during dry summers with little precipitation. Four snapshots of the water content during the months April-July in the year 1992 is shown as an example in Figure 42-Figure 45.

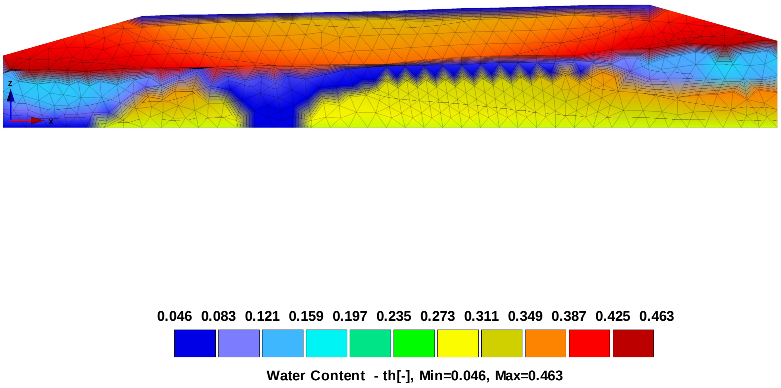

Figure 42. Distribution of water content after 52 months (April 30 1992).Precipitation in April =70 mm.

Figure 42 show the distribution of water content in April 30. In May and June the water content gradient is reversed due to evapotranspiration and very little precipitation, 5 mm and 7 mm respectively (Figure 43, Figure 44). The horizontal outward transport of water by evapotranspiration to the atmosphere is indicated by arrows in the figures below.

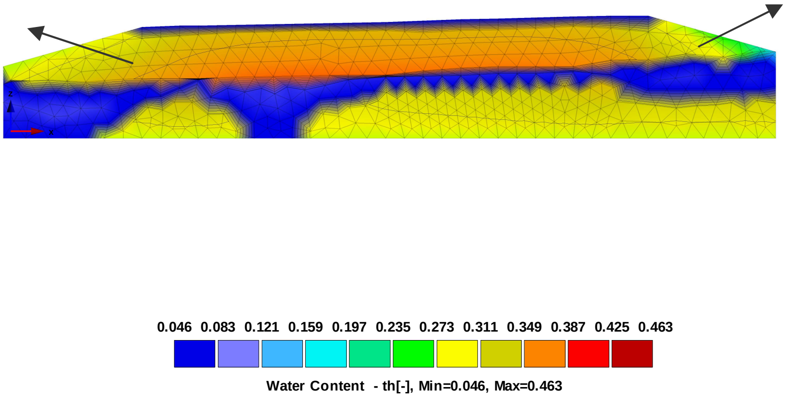

Figure 43. Distribution of water content after 53 months (May 31 1992). Precipitation in May = 5mm.

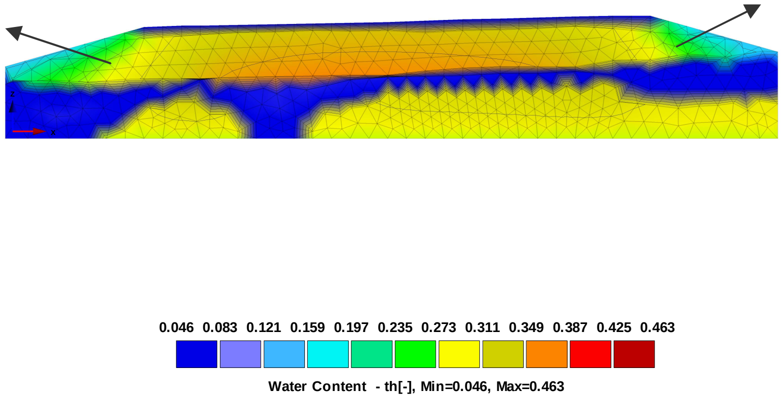

Figure 44. Distribution of water content after 54 months (June 30 1992). Precipitation in June =7 mm.

In July the road receives 56 mm of precipitation, water infiltrates in the shoulders and water fronts move into the road body again (Figure 45).

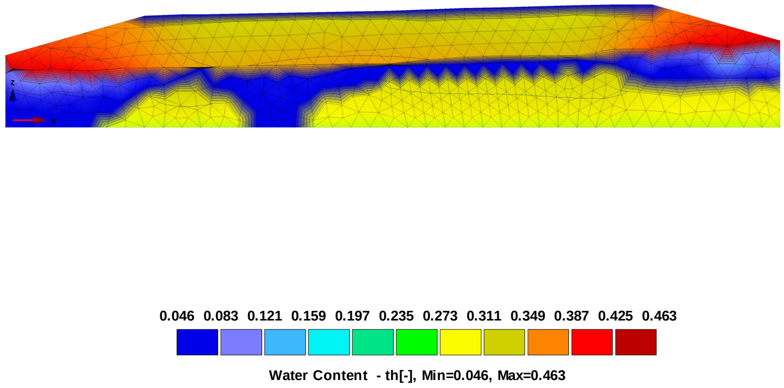

Figure 45. Distribution of water content after 55 months (July 31 1992). Precipitation in July =56 mm

The annual average of precipitation was of about 590 mm during the time period January 1988 to the 1th of september 2003. The road section (10.3 m wide) received an a total of about 94,7 m3/m of water. The modeled accumulated LS ratios in six different domains in the bottom ash subbase layer is shown in Figure 46 together with the time, $T_{1/2}$, to deplete half (massfraction=0.5) of the solute initially present in the porewater in the bottom ash.

In Figure 47 the depletion of the solute in the six domains is plotted as the mass fraction of solute in the pore water as a function of time. As water entered the subbase layer during the first year, solute was displaced from domain 1-3 into domain 4-6 by advection. This is seen in the figure as peaks (massfraction >1).

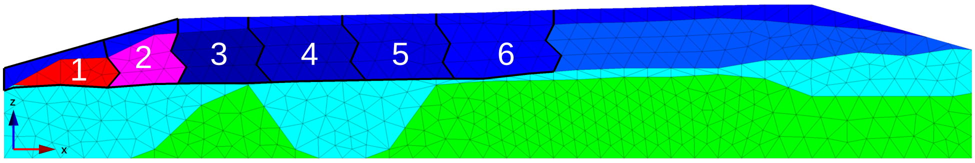

Domain	**1**	**2**	**3**	**4**	**5**	**6**
LS	50	32	10	2	1	1
$T_{1/2}$	1 m	2 m	6 m	2.1 yr	7 yr	8.8 yr

Figure 46. The accumulated LS ratio and the time, $T_{1/2}$, to deplete half (massfraction=0.5) of the solute initially present in the porewater in the bottom ash the for the six domains

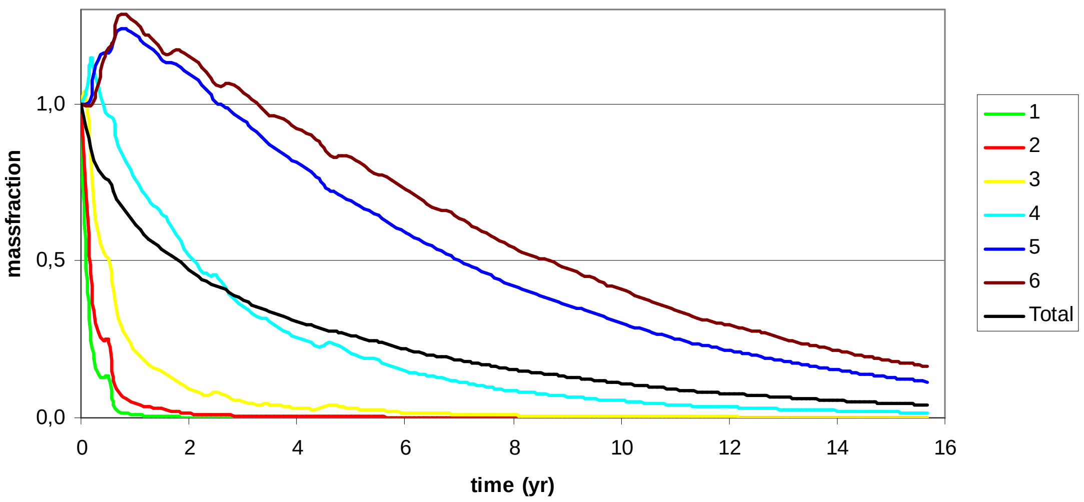

Figure 47. The depletion of solute in the six domains is plotted as mass fraction of solute in the pore water as a function of time. The black line represents the integrated value over the total bottom ash layer.

7 Discussion

7.1 Hydrology

The modeling results show that the bottom ash subbase layer endure seasonal wet and dry cycles. The results confirm that, depending on the boundary conditions along the shoulders the capillary potential may drive moisture either in or out of the road body. The evapotranspiration during dry summer months is effective in driving horizontal transport of water from the subbase to the atmosphere. The water retention parameters are crucial for the modeling of unsaturated flow and transport. The capillary forces in bottom ash were found to be significant with a water retention curve close to silt. The modeling results showed that bottom ash layer had a large capacity in sucking water into the road construction. This explains the observed the depletion of easily soluble salts (see for example Figure 5).

During the time period 1988-2003 the modeling results showed that the accumulated LS ratio for the bottom ash subbase layer reached about 10.1 with a spatial variability of about 1 – 50. The time, $T_{1/2}$, to deplete half (massfraction=0.5) of the solute initially present in the porewater in the bottom ash subbase layer was about 2 year with a spatial variability of about 1 month to 9 years. After 16 years the remaining mass fraction in the pore water was about 5%. This could be compared with the field data showing that the integrated spatial variability of remaining leachable (EN 12457 at LS 10) chloride constituted less than 20 % of the initial amount, see section 2.5.

7.2 Applicability of the geochemical modeling tool

The speciation modeling as carried out here for major, minor and trace elements is quite ambitious, as it integrates mineral dissolution/precipitation, iron-oxide adsorption, incorporation in ettringite solid solution, clay interaction and interaction with dissolved and particulate organic matter. The challenge is to not just be able to predict release behaviour of a single constituent, but to be able to describe release from all major, minor and trace elements simultaneously as good as possible and even match them with prediction at low L/S as obtained from column testing. Obviously, proper mineral solubility data are limited for some elements, like Sb, B, Se. For other trace elements the match is quite acceptable.

It is obvious that iron-oxide sorption is very important for many trace elements (metals as well as oxyanions). Organic matter (both dissolved and particulate) plays an important role for elements like Cu, Cr, Cd, Pb, although the major fraction of the available content is associated with the mineral phases.

For ecotoxicity evaluations the presence of an element as a free ion is crucial and the DOC associated metal is not affecting many organisms. Total dissolved concentrations are thus not a proper measure of impact. The DOC associated forms can, however, travel over much larger distances as they are more mobile than the free elements, which are retained much faster by reactive surfaces in soil.

7.2.1 Minerals that govern leaching

The governing mineral assembly was selected based on experience from modeling leachate composition in fresh bottom ash [41][12][27]. The entire mineral set used in the modeling is shown in appendix D. The minerals that were most relevant to leaching were (see chemical formulas in appendix E.1).

Mineral
AA_3CaO_Al2O3_CaCO3_11H2O[s]
AA_3CaO_Fe2O3_6H2O[s]
AA_Al[OH]3[am]
AA_Brucite: $Mg(OH)_2$
AA_Magnesite: $MgCO_3$
Ba[SCr]O4[96%SO4]
beta-TCP
Calcite: CaCO3
Cu[OH]2[s]
Fe_Vanadate
FeCr2O4
Ferrihydrite: $Fe_5O_3(OH)_9$
Laumontite: $CaAl_2Si_4O_{12}*4H_2O$
Manganite: MnO(OH)
Ni[OH]2[s]
Ni2SiO4
Pb[OH]2[C]
Pb2V2O7
P-Wollstanite: $Ca(SiO_3)$
Rhodochrosite: $MnCO_3$
Strontianite: $SrCO_3$
Willemite: $Zn_2[SiO_4]$
Anglesite: $PbSO_4$
Malachite: $Cu_2[(OH)_2 \vert CO_3]$

7.3 The pH stat test

The pH-stat tests represent a semi-closed system: interaction with atmosphere is possible to a limited extent. According the technical specification (SIS-CEN/TS 14997) the experimental setup should have a lid (not sealed) and allow for release of gas. Carbon dioxide does escape from the test into the air at low pH, and decreases the carbonate content in the system. At high pH carbon dioxide may dissolve into the leachate and increase the carbonate content of the system. The carbonate content primarily affects DIC and Ca concentrations, through the precipitation of calcite.

Secondarily, the remaining Ca concentration affects a number of other processes, such as precipitation of other Ca-minerals and cation sorption.

Since the degree of exchange with atmosphere is not known this is not an optimal situation from a modeling perspective. It would be preferably with either a closed system or an open system in equilibrium with the atmospheric carbon dioxide.

As an approximation, carbonates were modeled by allowing CO_2 (g) to escape at low pH (equilibrium with atmosphere) and use approximate values (increase of the measured values) of carbonate content to account for the dissolution of CO_2 (g) into the system at high pH. The reason for not modeling the system as open at high pH is that it overestimates the influx of pH. In reality the influx of CO_2 (g) is a kinetically controlled process. The physical processes governing the carbon dioxide exchange are not modeled at present.

7.4 Significance and implications of results

This study shows that the release from all major, minor and trace elements can be modeled simultaneously by using a mineral assembly, selected based on experience, and experimental data on available HFO and TOC. Adjustments were made of the measured values of carbonate content to account for the dissolution of CO_2 (g) into the system at high pH (see section 7.3). The bottom ash behaved in a predictable way, similar to fresh ashes except for the difference in own-pH (Figure 26).

This implies that release of elements could be predicted for a bottom ash under certain environmental conditions if available HFO and TOC are measured, and the exchange with carbon dioxide can be quantified. The major environmental conditions that need to be specified are: pH, DOC and DIC of infiltrating water and degree of exposure to atmosphere.

8 Conclusions

- The modeling results show that the bottom ash subbase layer endure seasonal wet and dry cycles. The results confirm that, depending on the boundary conditions along the shoulders the capillary potential may drive moisture either in or out of the road body.
- The water retention parameters for bottom ash are crucial in the hydraulic modeling. The capillary forces in bottom ash were found to be significant with a water retention curve close to silt. This explains the observed depletion of easily soluble salts in the test road.
- During the time period 1988-2003 the hydraulic modeling results showed that the accumulated LS ratio for the bottom ash subbase layer reached about 10.1 with a spatial variability in the sub base layer of about LS:1 – LS:50.
- The general leaching behaviour (as reflected in a pH-stat test) of the Vändöra bottom ash is similar compared to other bottom ashes. The elements and their minerals were well described with Orchestra/LeachXS. The modelling visualised information that was hidden in the pH-stat results
- The release from all major, minor and trace elements can be modeled simultaneously by using a mineral assembly, selected based on experience, and experimental data on available HFO and TOC. This implies that release of elements could be predicted for a bottom ash under certain environmental conditions. The major environmental conditions that needs to be specified are: pH, DOC and DIC of infiltrating water and degree of exposure to atmosphere.
- No difference in acid neutralization capacity could be detected when comparing the four composite samples. Carbonation by reaction with atmospheric CO_2 and leaching of alkalinity seemed to balance each other
- The model confirms that Cu, Cr, Pb, and partially Zn, in solution is bound to DOC. The elements Zn, Cd and Ni are present in the solution mainly as free ions. It is important to realize that for ecotoxicity evaluations the free element is of importance and the DOC associated metal is not affecting many organisms. In the solid phase As is entirely associated with iron oxides. Other elements where iron oxides plays an important role are: Pb, Cd and Cu. The elements Cu, Zn and Ni are mainly associated with the solid phase as minerals: malachite (copper hydroxide carbonate) willemite (zinc silicate), nickel silicate and iron chromate.
- The interpretation of oxyanions (except Cr) was hampered by the lack of thermodynamic data on their interaction with other minerals, f ex ettringite. This problem has been acknowledged and research is in progress to improve the general data. The Orchestra/LeachXS modeling tool is suited to incorporate the data when it becomes available and may then be able to interpret oxyanion leaching.

9 Recommendations and applications

The modeling software HYDRUS 2-D provided a opportunity to look into the hydraulic processes in the road construction and revealed the importance of the water retention properties and capillary transport for the depletion of easily soluble salts in a paved bottom ash road

LeachXS is a powerful tool and allow the user to explore the governing leaching processes. The database functions allow comparison with experimental data from other materials. Here a comparison of leaching data from international ashes showed the striking similarities between bottom ashes from different sources. This function was easy to use once the data were imported, and is at present applicable to leaching test data from batch, percolation, pH-stat, monolitic, lysimeter and field tests. Also, saturation indices were easily calculated and available for a great number of minerals relevant for cement and ash. Both the database function and the saturation indices look suitable for non-expert use. However, predictive modeling and identification of governing processes in LeachXS requires an expert user.

Based on the modeling work in this study it is suggested that the practical execution of pH-stat leaching tests should take into account of interaction with carbon dioxide in the atmosphere to facilitate modeling. The pH-stat experimental setup represents a semi open system, but from a modeling perspective it would be preferable if the system was either closed or open. It is here suggested that one possible option could be to allow CO_2 to escape at pH lower than 8 (fully open system), and a closed the system with nitrogen atmosphere at pH over 9.

A recommendation for future test roads is to ensure that the subgrade is homogenous and the all construction materials are characterized (including hydraulic parameters), so that evaluation of the test road observations is facilitated.

10 Suggestions for continued research

- Integration of geochemical and hydrological modelling and conduct a coupled reaction and transport modeling of the leaching process.

- Carbonate and carbon dioxide dissolution are key parameters in the modeling, and future prediction requires a better description of carbon dioxide interaction with leachates during the pH stat test.

- Some elements (notably Sb) lack thermodynamic data.

- Comparison with ash aged in a different physical field scenarios could give important insight in long term behavior of bottom ash in civil engineering applications.

11 Literature references

[1] Andersson H., M. Arm, M. Carling, B. Schouenborg, Provtagningsmetoder för alternativa material till vägbyggnad – undersökning av rostereldad kolbottenaska, slaggrus och krossad betong (In Swedish), VTI/SGI, 1999.

[2] Arm, M, Suer, P, Arvidsson, H, Lindqvist, J-E, Frogner Kockum, P C, Larsson, L och Toomväli, C, "Förutsägelse av långtidsegenskaper hos restprodukter - Prediction of long-term properties for by-products", Värmeforsk, 2009

[3] Batchelor, B. Leach models for contaminants immobilized by pH dependent mechanisms, Environ. Sci. Technol., 32, 1721-1726, 1998

[4] Bendz, D., Arm M., P. Flyhammar, G. Westberg G., K Sjöstrand, M Lyth and O. Wik, The Vändöra test road, Sweden: A case study of long-term properties of a road constructed with MSWI bottom ash, Q4-241 (In Swedish), 2006.

[5] Bendz, D., P. Flyhammar, M. Elert, J. Hartlén, Leching from residues used in highway constructions – a system anaylsis, in: The Handbook of Environmental Chemistry, Vol. 5, Part F, Springer-Verlag, 293-320, 2004.

[6] Borch-Jensen, J.E., J.J. Linde Jensen, Water in roads (In Danish), The Danish Road Directorate, Report 189, 1986

[7] Cornelis, G, Van Gerven, T och Vandecasteele, C, "Antimony leaching from uncarbonated and carbonated MSWI bottom ash", Journal of Hazardous Materials, vol 137, pp 1284-1292, Oct, 2006

[8] Cornelis, G, Johnson, C A, Van Gerven, T och Vandecasteele, C, "Leaching mechanisms of oxyanionic metalloid and metal species in alkaline solid wastes: A review", Applied Geochemistry, vol 23, pp 955-976, May, 2008

[9] Chrysochoou, M och Dermatas, D, "Application of ettringite on heavy-metal immobilization: A literature review", Protection and restoration of the environment VII, Mykonos, June 2004.

[10] Dawson, A.R., A.R. Hill, Prediction and implication of water regimes in granular basis and sub-bases., Proceedings, International symposium on subdrainage in roadway pavements and subgrades, Granada, Spain, Nov. 11-13, 121- 128, 1998

[11] Dijkstra, J J, Van Zomeren, A, Meeussen, J C L och Comans, R N J, "Effect of accelerated aging of MSWI bottom ash on the leaching mechanisms of copper and molybdenum", Environmental Science & Technology, vol 40, pp 4481-4487, Jul, 2006

[12] Dijkstra, J J, Meeussen, J C L, Van der Sloot, H A och Comans, R N J, "A consistent geochemical modelling approach for the leaching and reactive transport of major and trace elements in MSWI bottom ash", Applied Geochemistry, vol 23, pp 1544-1562, Jun, 2008

[13] Dzombak, D A och Morel, F M M, "Surface complexation modeling: hydrous ferric oxide", Wiley & sons, New York, 1990

[14] Farh, Y., R.J. Freer-Hewish, A.M. Carson, Horizontal infiltration of moisture in road pavements, Proceedings, International symposium on subdrainage in roadway pavements and subgrades, Granada, Spain, Nov. 11-13, 195- 202, 1998

[15] Flyhammar P., D. Bendz, Leaching of different elements from subbase layers of alternative aggregates in pavement constructions, Accepted for publication in Journal of Hazardous Material, 2006.

[16] Fällman, A-M., Characterisation of residues - Release of contaminants from slags and ashes, PhD-thesis, Dept. of Physics and Measurement Technology, Linköping University, Sweden, 1997.

[17] Grøn, C., T.T. Andersen, J.B. Hansen, J. Isaksen S. Klem, L. Nordquist, Udvaskning af organisk stof og kobber fra bundslagg, Center for restprodukter UR-1, DHI, Rapport maj, 2003

[18] Hemström, K., S. Ezziyani, D. Bendz, Vattenretentionsegenskaper hos aska-Implikationer för dimensionering av konstruktioner, Värmeforskrapport Q6-612, 2009.

[19] Huang, Y.H., Pavement Analysis and Design, Prentice Hall, 1993.

[20] Håkansson, K., U. Nilsson, National report for leaching tests for Sweden, ALT-MAT, Contract RO-97-SC.2238, Report WP5.SGI.007, 1999.

[21] Johnson, C.A, S. , Brandenberger, P. Baccini, Acid neutralizing capacity of municipal waste incineration bottom ash, Environ. Sci. Technol., 29, 142-147, 1995

[22] Kinniburg, D G, Van Riemsdijk, W H, Koopal, L K, Korkovec, M, Benedetti, M F och Avena, M J, "Ion binding to natural organic matter: competition, heterogeneity, stoichiometry and thermodynamic consistency", Colloids Surf. , A 151, pp 147-166, 1999

[23] Konrad J.-M., M. Roy, Mechanisms controlling seasonal variations of moisture content in roads, in: International symposium on subdrainage in roadway pavements and subgrades, Granada, 11-13 November, Spain, 259-266, 1998.

[24] Kostka, J.E. and G.W. Luther, Partitioning and speciation of solid phase iron in saltmarsh sediments, Geochim. Cosmochim, Acta 58, 1701-1710, 1994

[25] Krarup, J.A., J.E. Borch Jensen, J.J. Linde Jensen, Water in roads II (In Danish), The Danish Road Directorate, Report 206, 1988

[26] Lundgren T and J. Hartlén; ”Slagg från avfallsförbränning Teknik och Miljö” (In Swedish), REFORSK rapport FoU nr 61, REFORSK, Malmö, 1991

[27] Meima, J.A., R.N.J., Comans, Geochemical modeling of weathering reactions in municipal solid waste incineration ash, Environ. Sci. Technol., 31, 1269-1276, 1997

[28] Meima, J A och Comans, R N J, "Reducing Sb-leaching from municipal solid waste incinerator bottom ash by addition of sorbent minerals", Journal of Geochemical Exploration, vol 62, pp 299-304, 1998

[29] Meima, J.A., A. Van Zomeren, R.N.J. Comans, Complexation of Cu with dissolved organic carbon in municipal soild waste incinerator bottom ash leachates, Environ. Sci. Technol, 33, 1424-1429, 1999.

[30] Piantone, P, Bodenan, F och Chatelet-Snidaro, L, "Mineralogical study of secondary mineral phases from weathered MSWI bottom ash: implications for the modelling and trapping of heavy metals", Applied Geochemistry, vol 19, pp 1891-1904, Dec, 2004

[31] Reid, J.M. Final report. ALT-MAT, Deliverable D3, Vol. 2, Version 2.0, 01-01-08, 2001.

[32] Rimbault G., Description of moisture content and water movement in road pavements and embankments, ALT-MAT, Report No. WP1LCPC.005/WP1.SGI.004, 1999.

[33] Steketee, J.J, Leaching of MSWI bottom ash in laboratory tests, a lyismeter and a field application, WASCON 2003, San Sebestian, 4-6 June, Spain, 197-206, 2003.

[34] Taylor, H F W, "Cement chemistry", Thomas Telford, London, vol pp 1997

[35] USEPA, "MINTEQA2/PRODEFA2, A geochemical assessment model for environmental systems: user manual supplement for version 4.0", National exposure research laboratory, ecosystems research division, Athens, GA, USA, 1999

[36] Van der Sloot, H.A, Developments in evaluating environmental impact from utilization of bulk inert wastes using laboratory leaching tests and field verification, Waste Manage., 16, 65-81, 1996.

[37] Van Genuchten M.T., *A closed form equation for predicting the hydraulic conductivity of unsaturated soils*, Soil Science Society of America Journal, 44, 892-898, 1980

[38] Van Zomeren, A., R.N.J Comans, Measurement of humic and fulvic acid concentrations and dissolution properties by a rapid batch procedure, Environ Sci. Technol., 41, 6755-6761, 2007.

[39] Wallace, K.B., Moisture transients at the pavement edge: analytical studies of the influence of materials and cross-section design, Géotechnique, 27, 4, 497-516, 1977

[40] Yan, J., Bäverman, C., Moreno, L., Neretnieks, I. Neutralising processes of municipal solid waste incineration bottom ash in a flow-through system, Sci. Total Environ., 227, 1-11, 1999

[41] Zevenbergen, C. and R.N.J., Comans., Geochemical factors controlling the mobilization of major elements during weathering of MSWI bottom ash. In: Environmental Aspects of Construction with Waste Materials, Gourmans, J.J.J.M., van der Sloot, H.A. and Aalbers., Th.G., (Eds) Elsevier Science, Netherlands, pp179 – 194. 1994

A Results of analyses on the composite samples (excepting leaching tests)

A.1 Iron and aluminum oxides

		AL mg/kg	FE mg/kg	MN mg/kg	HFO (kg/kg)
sample 1	Amorf Fe+Al	960	1167	238	1,86E-03
	Krist. Fe	5800	23429	556	5,92E-03
	Amorf Al	6401	21159	373	2,11E-02
	Total HFO				**2,89E-02**
sample 2	Amorf Fe+Al	1130	1309	271	2,09E-03
	Krist. Fe	6242	25968	642	6,56E-03
	Amorf Al	7920	24356	507	2,61E-02
	Totaal HFO				**3,47E-02**
sample 3	Amorf Fe+Al	1144	1145	205	1,83E-03
	Krist. Fe	7567	23910	617	6,05E-03
	Amorf Al	9518	33420	630	3,14E-02
	Total HFO				**3,93E-02**
sample 4	Amorf Fe+Al	1413	688	164	1,10E-03
	Krist. Fe	6174	13578	430	3,43E-03
	Amorf Al	7434	17206	899	2,45E-02
	Total HFO				**2,90E-02**

A.2 Total organic matter and carbonate

	Q	TIC %	TOC %
Vandora 1	1	0,65	4,03
	2	0,77	4,03
Vandora 2	1	0,63	3,51
Vandora 3	1	0,87	5,22
Vandora 4	1	0,58	4,56

A.3 Extractable organic matter

	HA (mg/kg d.m.)	FA (mg/kg d.m.)	Hy (mg/kg d.m.)	HON (mg/kg d.m.)	TOC (mg/kg d.m.)
Vandora 1	105	100	172	65	441
Vandora 2	68	83	140	92	382
Vandora 3	32	84	124	31	271
Vandora 4	32	107	167	64	370

B Graphical representation of the pH-stat and percolation test data

Graphs representing most measured elements
for pH static and percolation tests
on the Vändöra test road.
Please note that values below the detection
limit are shown as ½ detection limit, check
original values at need.

pH development as function of L/S

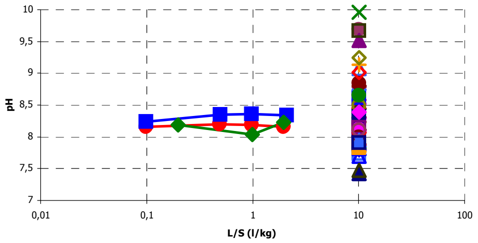

Legend pH dependent Emissions

● Vändöra 1 pHstat

■ Vändöra 2 pHstat

◆ Vändöra 3 pHstat

▲ Vändöra 4 pH stat

Dots: batch test results

Legend Cumulative release

● Vändöra 1 percolation

■ Vändöra 2 percolation

◆ Vändöra 3 percolation

Dots: batch test results

pH dependent Emission of Al

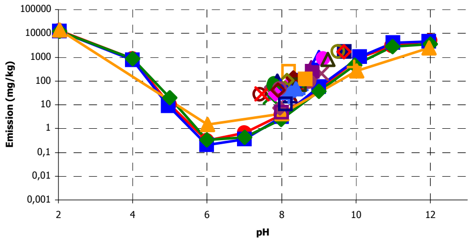

Cumulative release of Al

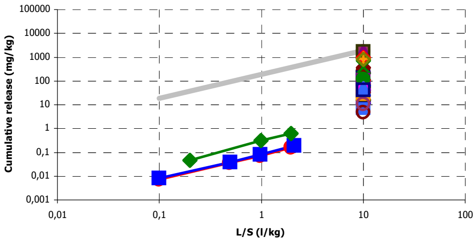

pH dependent Emission of As

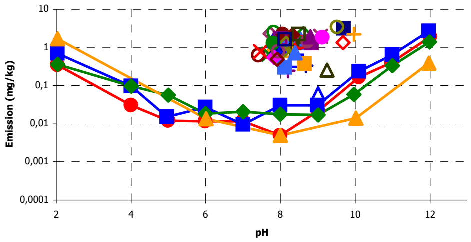

Cumulative release of As

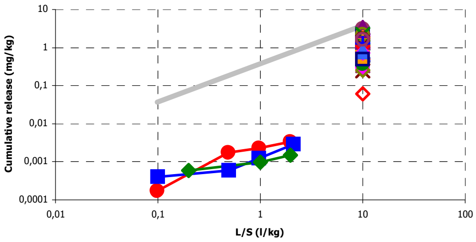

pH dependent Emission of B

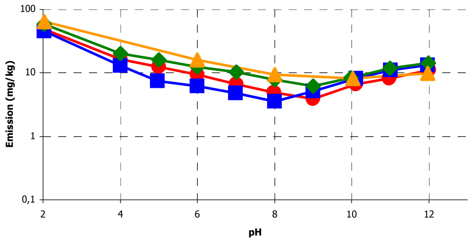

Cumulative release of B

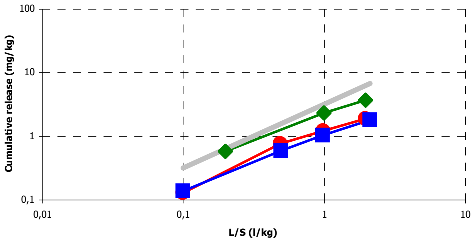

pH dependent Emission of Ba

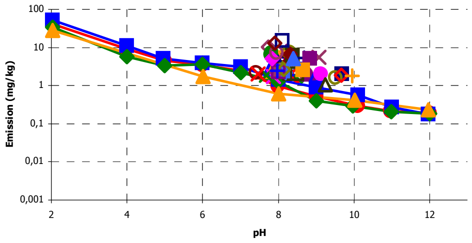

Cumulative release of Ba

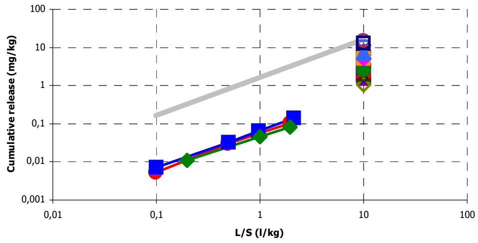

pH dependent Emission of Br

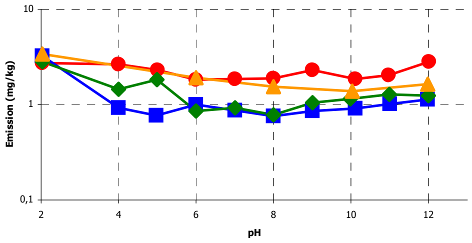

Cumulative release of Br

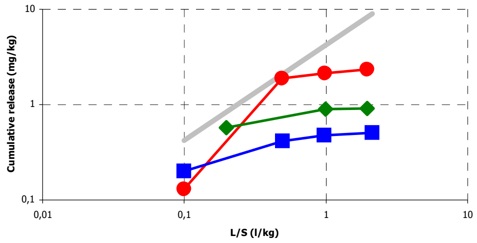

pH dependent Emission of Ca

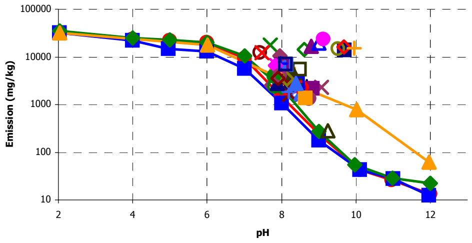

Cumulative release of Ca

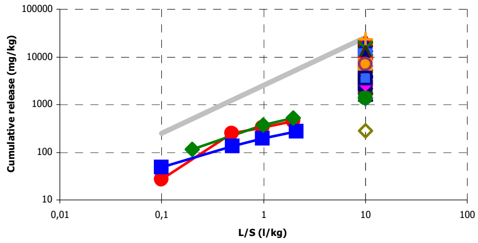

pH dependent Emission of Cd

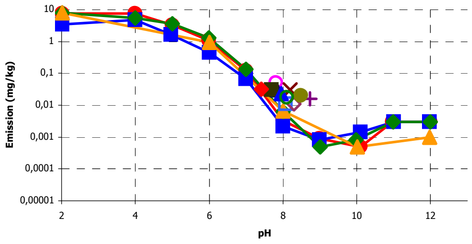

Cumulative release of Cd

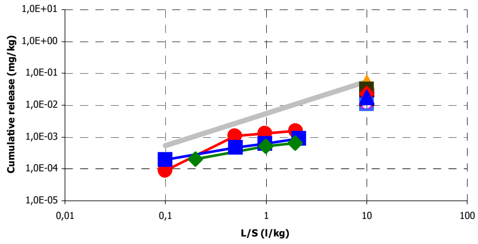

pH dependent Emission of Cl

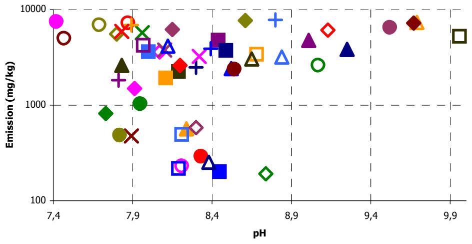

Cumulative release of Cl

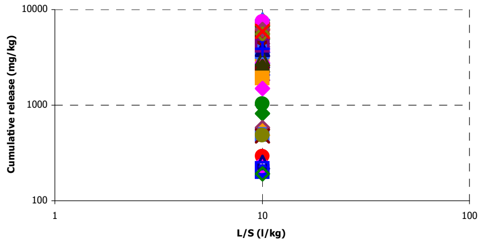

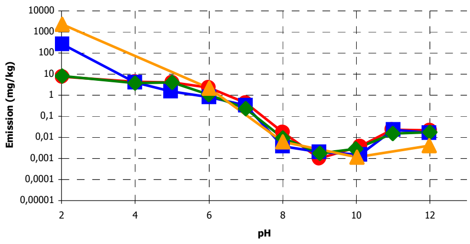
pH dependent Emission of Co

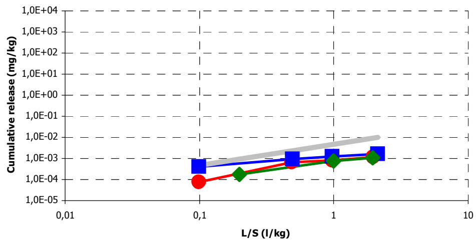
Cumulative release of Co

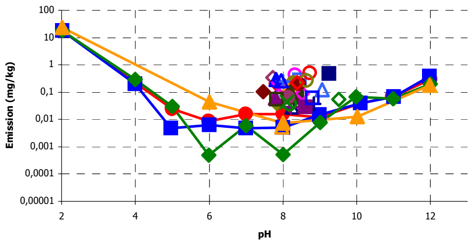
pH dependent Emission of Cr

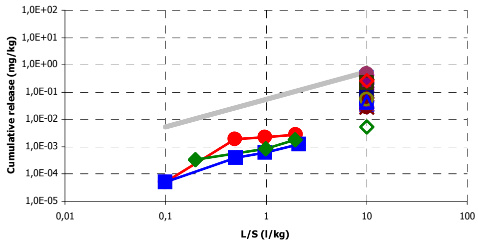
Cumulative release of Cr

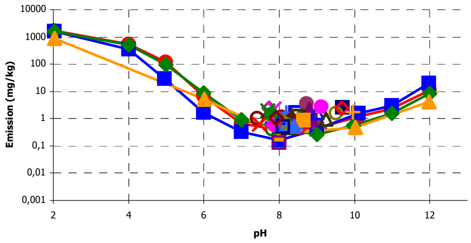
pH dependent Emission of Cu

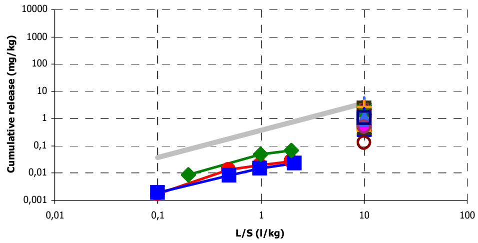
Cumulative release of Cu

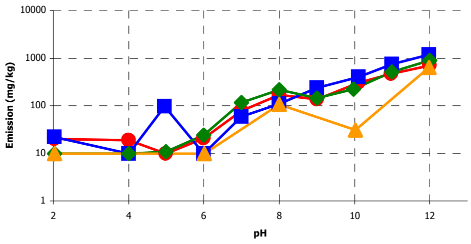
pH dependent Emission of DIC

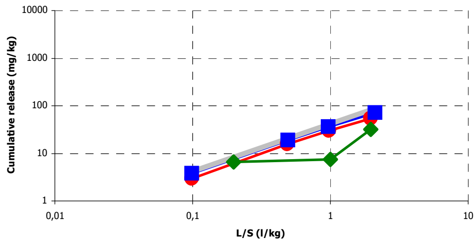
Cumulative release of DIC

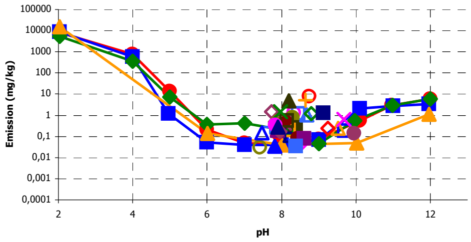
pH dependent Emission of Fe

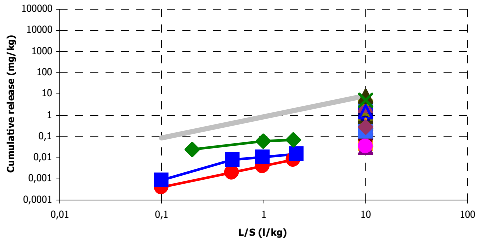
Cumulative release of Fe

pH dependent Emission of Hg

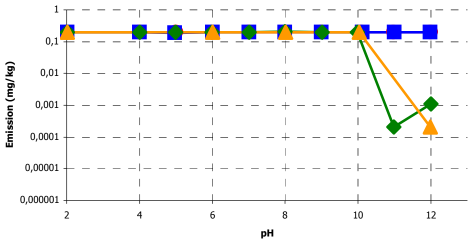

Cumulative release of Hg

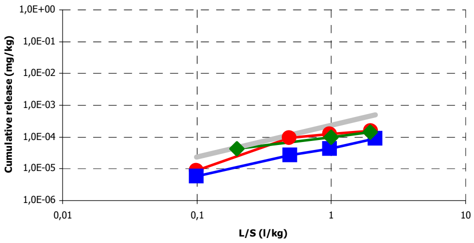

pH dependent Emission of I

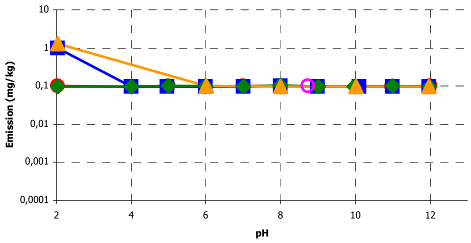

Cumulative release of I

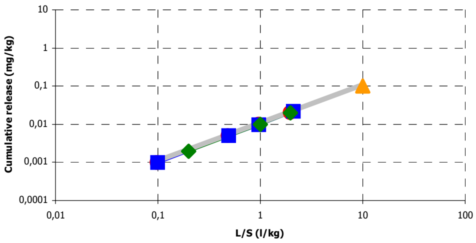

pH dependent Emission of K

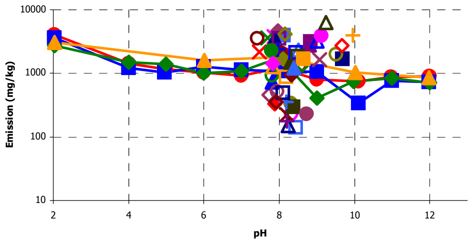

Cumulative release of K

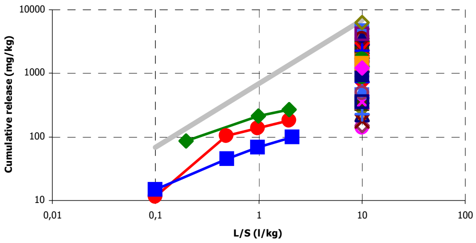

pH dependent Emission of Li

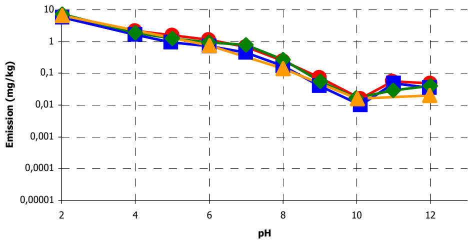

Cumulative release of Li

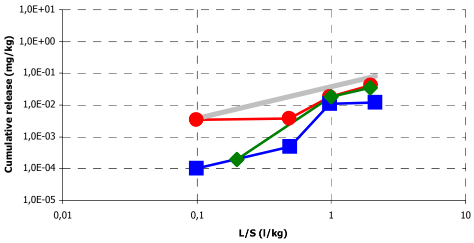

pH dependent Emission of Mg

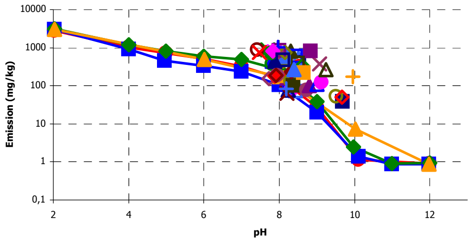

Cumulative release of Mg

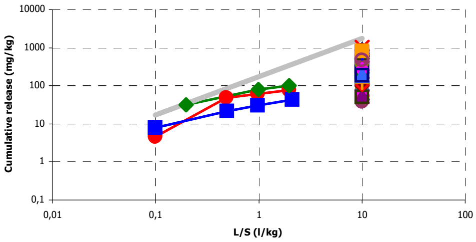

pH dependent Emission of Mn

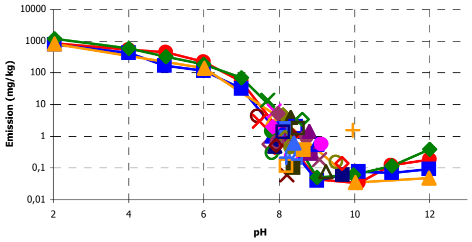

Cumulative release of Mn

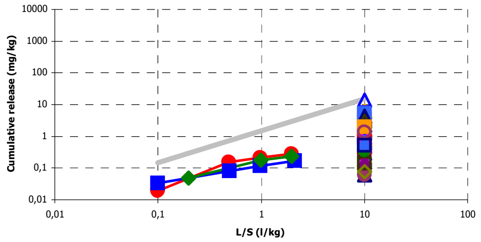

pH dependent Emission of Mo

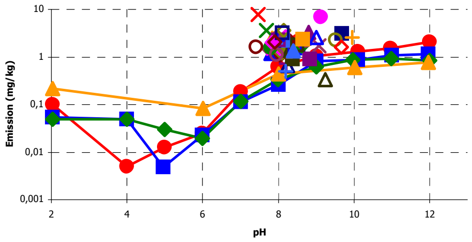

Cumulative release of Mo

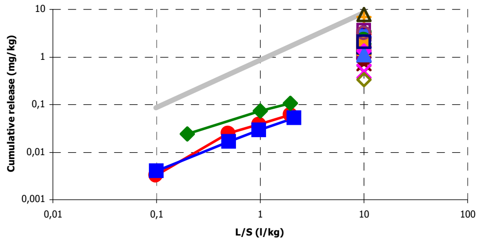

pH dependent Emission of Na

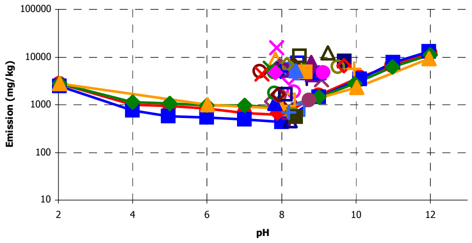

Cumulative release of Na

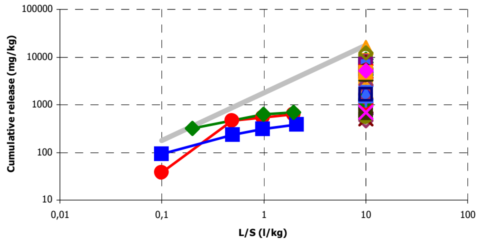

pH dependent Emission of Ni

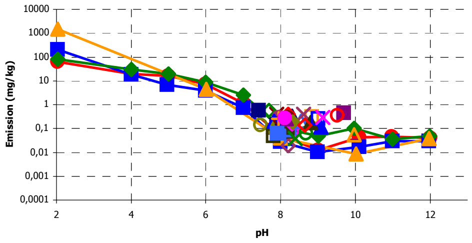

Cumulative release of Ni

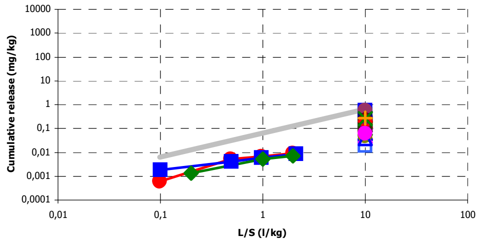

pH dependent Emission of P

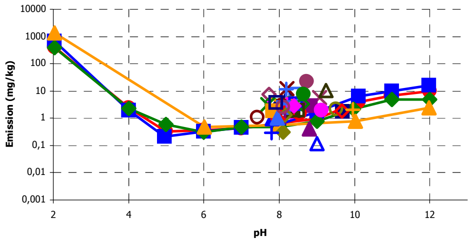

Cumulative release of P

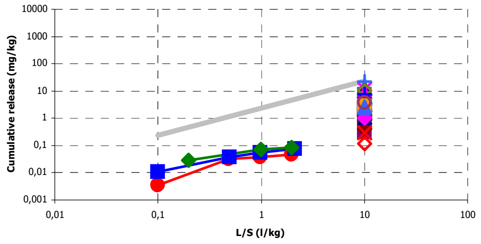

pH dependent Emission of Pb

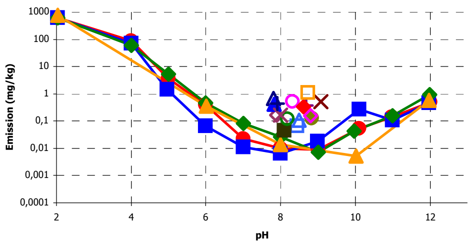

Cumulative release of Pb

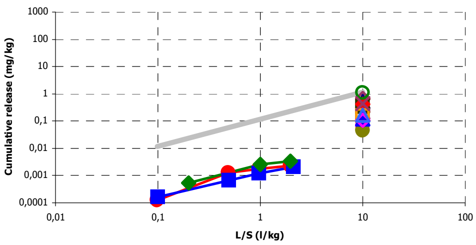

pH dependent Emission of S

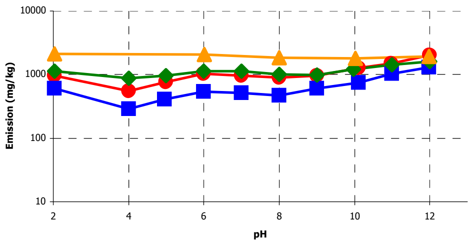

Cumulative release of S

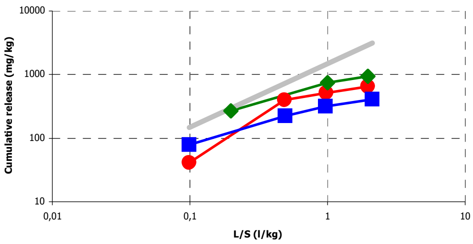

pH dependent Emission of Sb

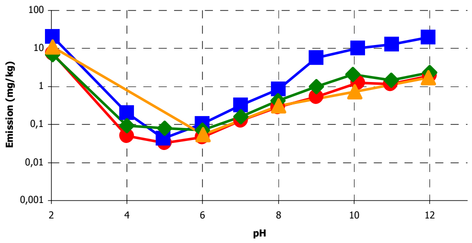

Cumulative release of Sb

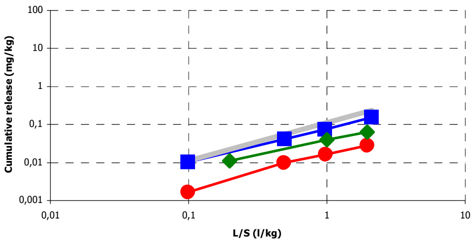

pH dependent Emission of Si

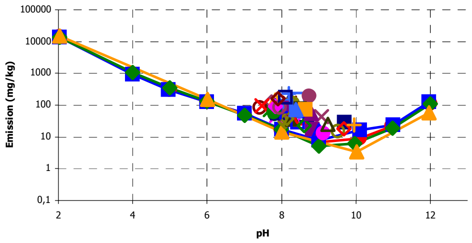

Cumulative release of Si

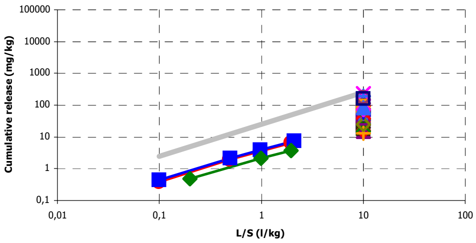

pH dependent Emission of SO4

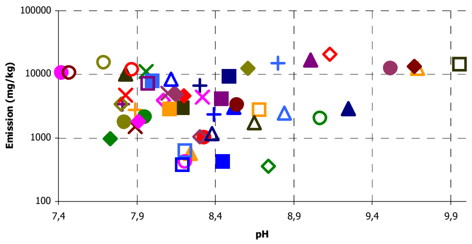

Cumulative release of SO4

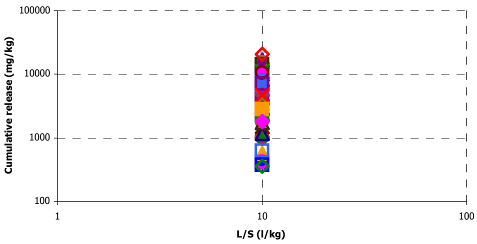

pH dependent Emission of Sr

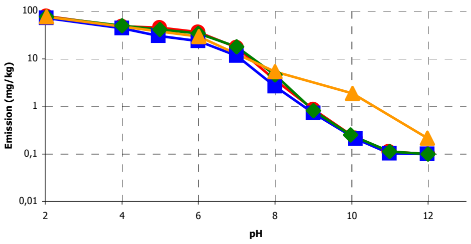

Cumulative release of Sr

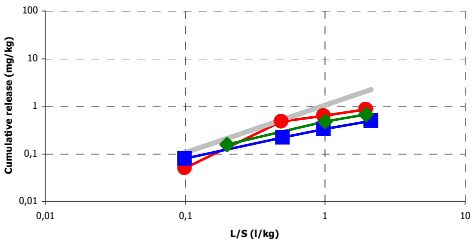

pH dependent Emission of V

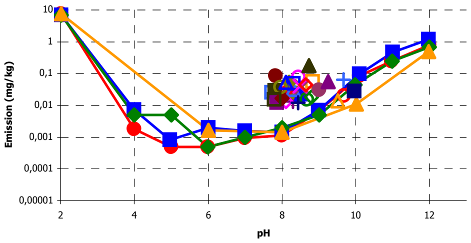

Cumulative release of V

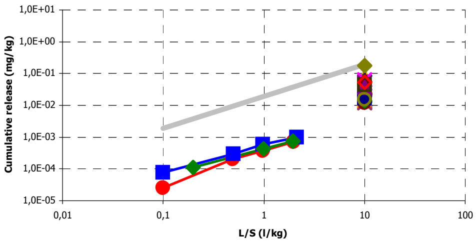

pH dependent Emission of Zn

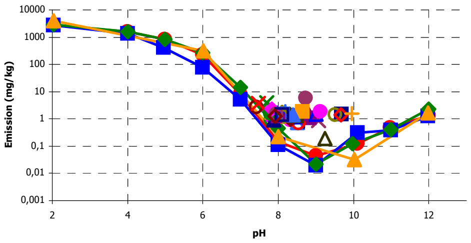

Cumulative release of Zn

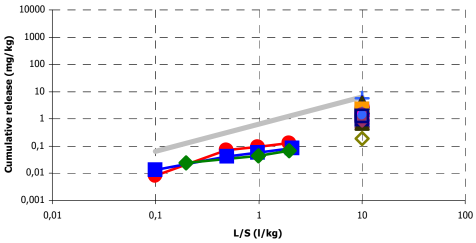

pH dependent Emission of DOC

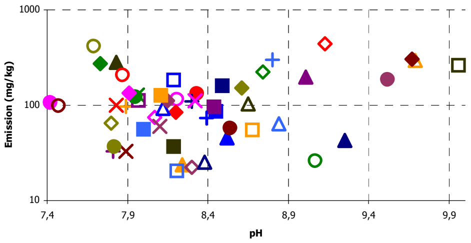

Cumulative release of DOC

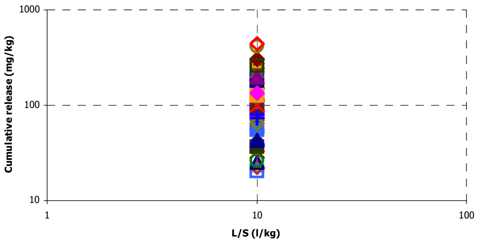

C Comparison of pH stat and percolation data with international ashes

Comparison of data from the four grouped samples from Vändöra, Linköping with some international ashes.
Värmeforsk project Q6-648: Modellering av utlakning och geokemiska processer i förstärkningslager av bottenaska
Authors: David Bendz, Pascal Suer. Hans van der Sloot, David Kosson, Peter Flyhamma

Legend: for clarity, legends are not shown in the graphs.
The legend of the Al-graph, below, is included to give an indication of the included samples
Most of the dots without lines are the 53 batch tests from the road profile in Vändörat

- ● MSWI Bottom ash AU
- ■ MSWI Bottom ash AU
- ◆ MSWI Bottom ash NL 2
- ▲ MSWI Bottom ash NL 2
- ○ MSWI Bottom ash NL 2
- □ MSWI Bottom ash NL
- ◇ MSWI Bottom ash NL 9
- △ MSWI Bottom ash NL 8
- × Vändöra 1 (Column)
- \+ Vändöra 2 (Column)
- ● Vändöra 3 (Column)
- ■ Vändöra field-100-100(B,1,1)
- ◆ Vändöra field-100-80(B,1,1)
- ▲ Vändöra field-1000-120(B,1,1)
- ○ Vändöra field-150-103(B,1,1)
- □ Vändöra field-150-123(B,1,1)
- ◇ Vändöra field-150-83(B,1,1)
- △ Vändöra field-200-103(B,1,1)
- × Vändöra field-200-123(B,1,1)
- \+ Vändöra field-200-83(B,1,1)
- ● Vändöra field-250-101(B,1,1)
- ■ Vändöra field-250-121(B,1,1)
- ◆ Vändöra field-250-81(B,1,1)
- ▲ Vändöra field-300-105(B,1,1)
- ○ Vändöra field-300-125(B,1,1)
- □ Vändöra field-300-85(B,1,1)
- ◇ Vändöra field-350-103(B,1,1)
- △ Vändöra field-350-123(B,1,1)
- × Vändöra field-350-83(B,1,1)
- \+ Vändöra field-400-104(B,1,1)
- ● Vändöra field-400-124(B,1,1)
- ■ Vändöra field-400-140(B,1,1)
- ◆ Vändöra field-400-84(B,1,1)
- ▲ Vändöra field-450-105(B,1,1)
- ○ Vändöra field-450-125(B,1,1)
- □ Vändöra field-450-85(B,1,1)
- ◇ Vändöra field-50-100(B,1,1)
- △ Vändöra field-50-80(B,1,1)
- × Vändöra field-500-109(B,1,1)
- \+ Vändöra field-500-129(B,1,1)
- ● Vändöra field-500-89(B,1,1)
- ■ Vändöra field-550-113(B,1,1)
- ◆ Vändöra field-550-133(B,1,1)
- ▲ Vändöra field-550-93(B,1,1)
- ○ Vändöra field-600-114(B,1,1)
- □ Vändöra field-600-134(B,1,1)
- ◇ Vändöra field-600-94(B,1,1)
- △ Vändöra field-650-117(B,1,1)
- × Vändöra field-650-137(B,1,1)
- \+ Vändöra field-650-97(B,1,1)
- ● Vändöra field-700-100(B,1,1)
- ■ Vändöra field-700-120(B,1,1)
- ◆ Vändöra field-700-140(B,1,1)
- ▲ Vändöra field-750-102(B,1,1)
- ○ Vändöra field-750-122(B,1,1)
- □ Vändöra field-750-142(B,1,1)
- ◇ Vändöra field-800-110(B,1,1)
- △ Vändöra field-800-130(B,1,1)
- × Vändöra field-800-142(B,1,1)
- \+ Vändöra field-850-108(B,1,1)
- ● Vändöra field-850-128(B,1,1)
- ■ Vändöra field-900-115(B,1,1)
- ◆ Vändöra field-900-135(B,1,1)
- ▲ Vändöra field-950-111(B,1,1)
- — slope=1.0

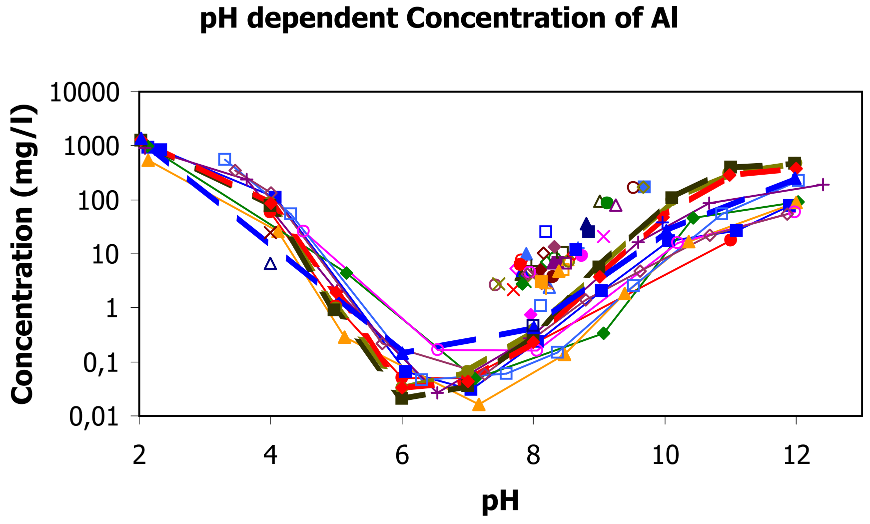
pH dependent Concentration of Al

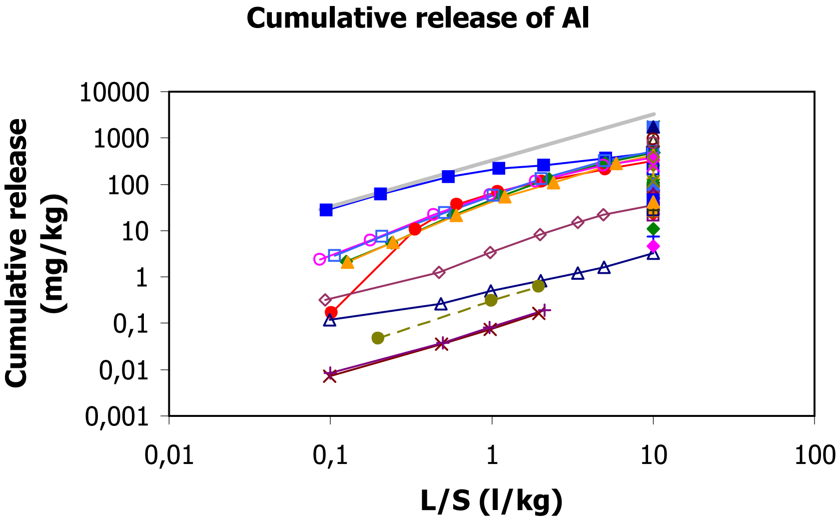
Cumulative release of Al

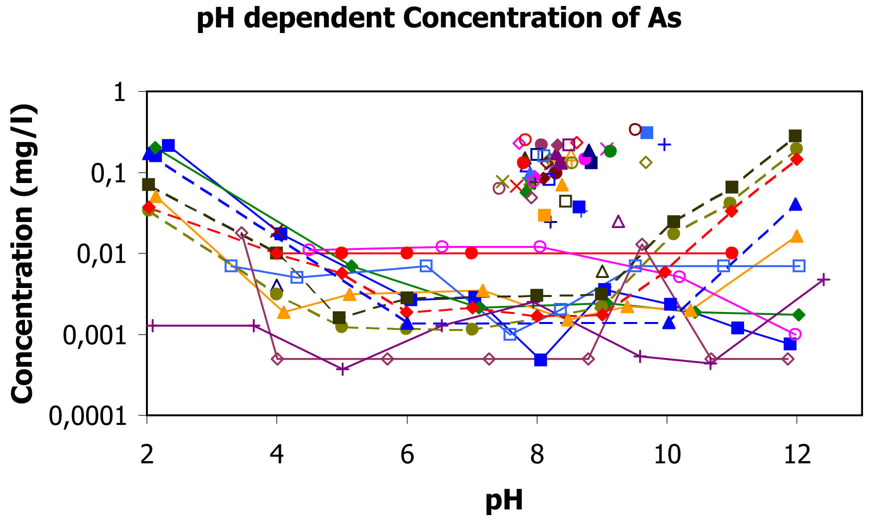
pH dependent Concentration of As

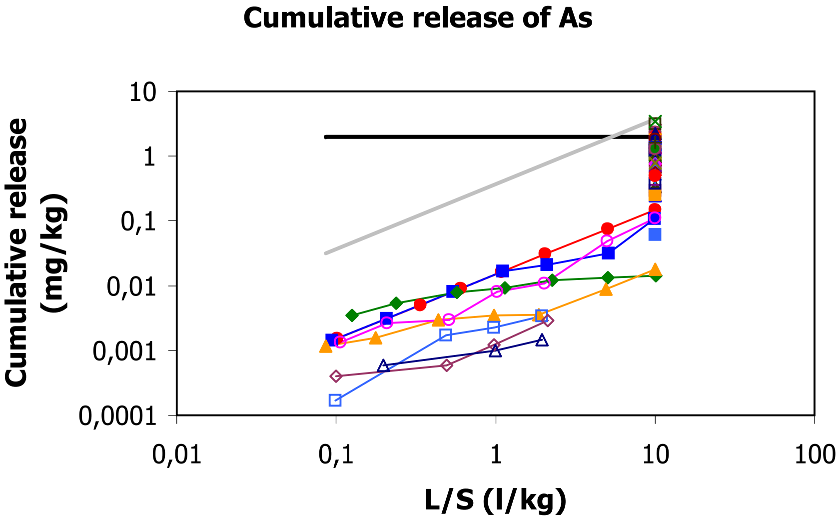
Cumulative release of As

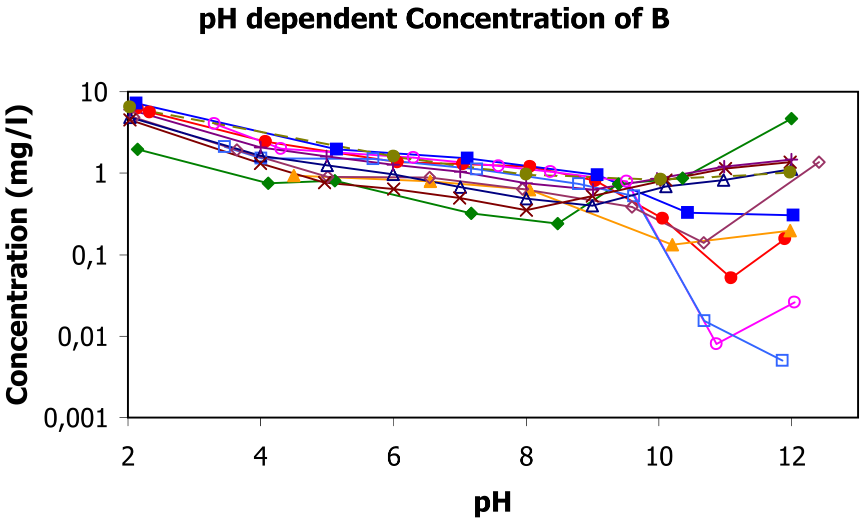
pH dependent Concentration of B
Concentration (mg/l)
10
1
0,1
0,01
0,001
2
4
6
8
10
12
pH

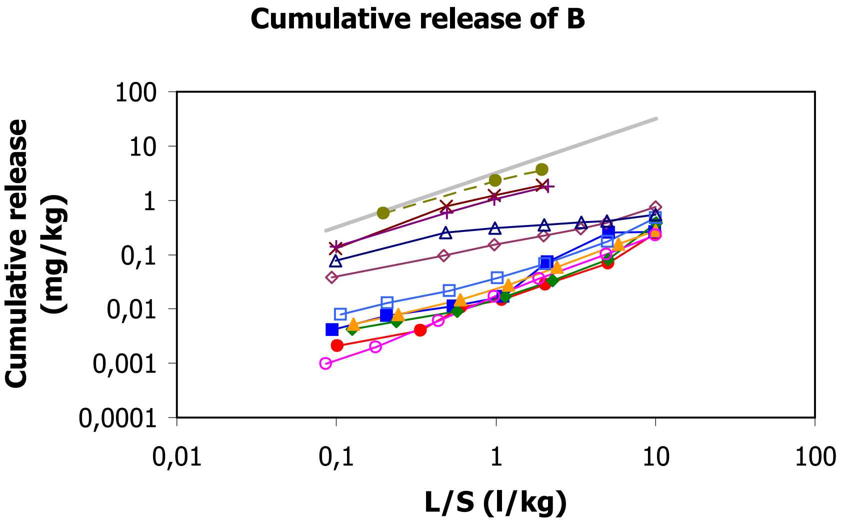
Cumulative release of B
Cumulative release (mg/kg)
100
10
1
0,1
0,01
0,001
0,0001
0,01
0,1
1
10
100
L/S (l/kg)

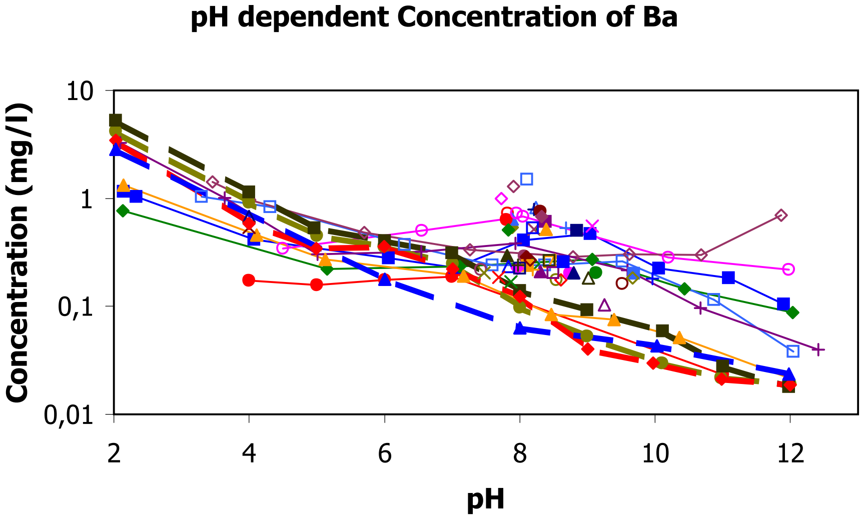
pH dependent Concentration of Ba
Concentration (mg/l)
10
1
0,1
0,01
2
4
6
8
10
12
pH

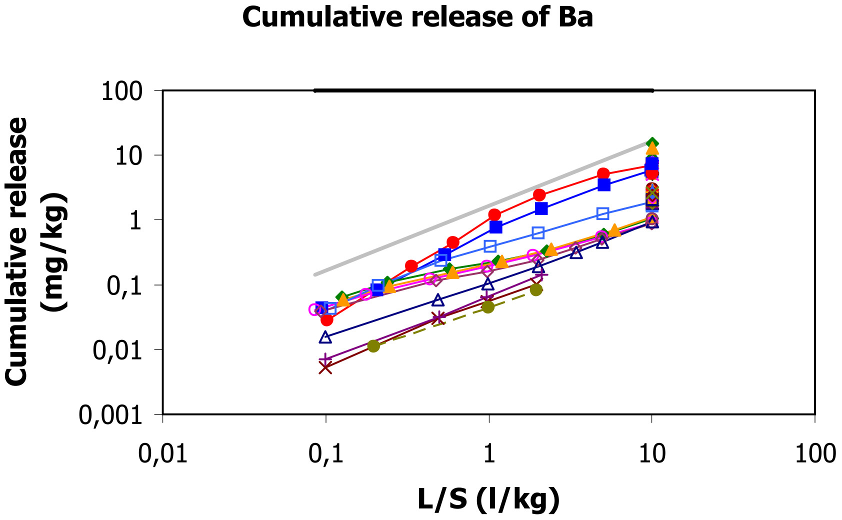
Cumulative release of Ba
Cumulative release (mg/kg)
100
10
1
0,1
0,01
0,001
0,01
0,1
1
10
100
L/S (l/kg)

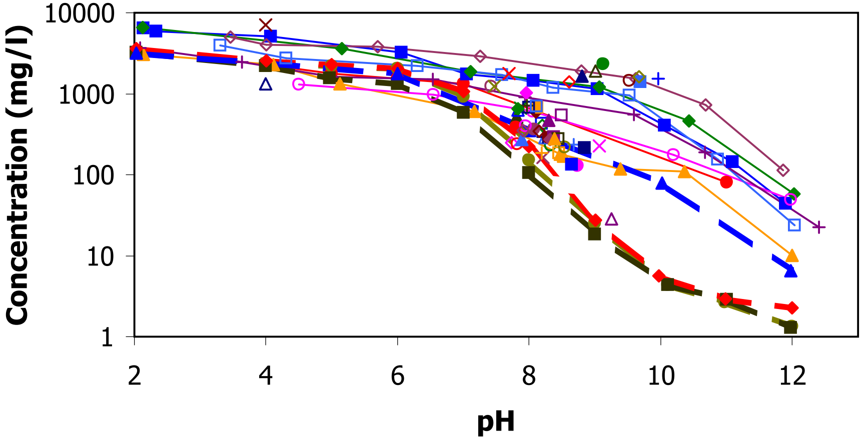
pH dependent Concentration of Ca

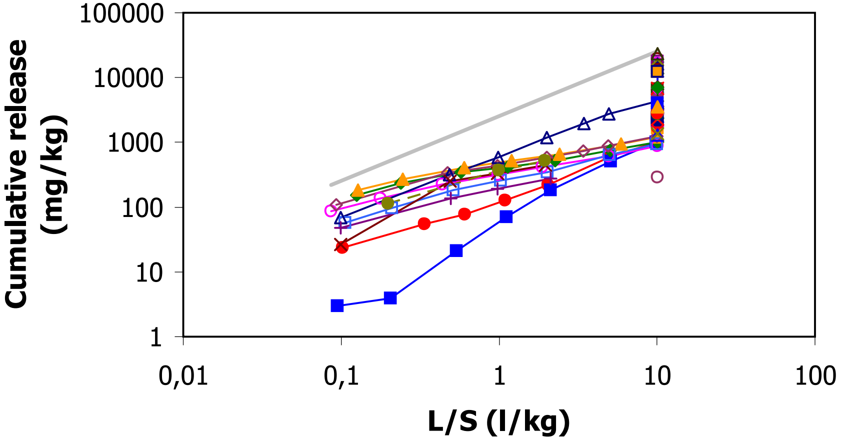
Cumulative release of Ca

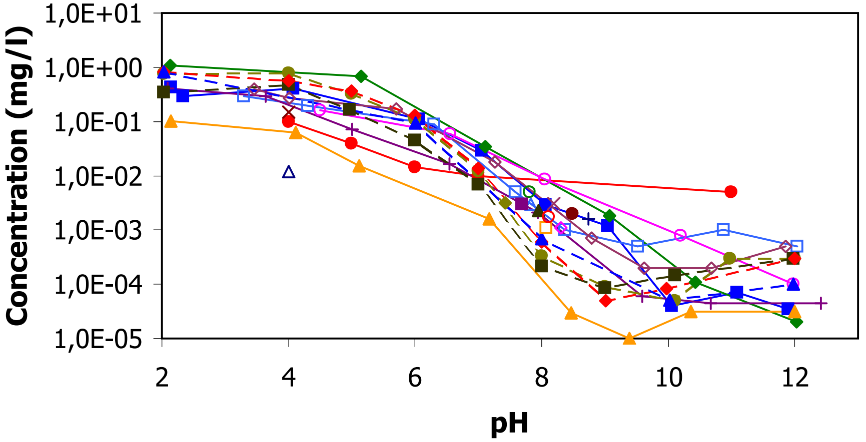
pH dependent Concentration of Cd

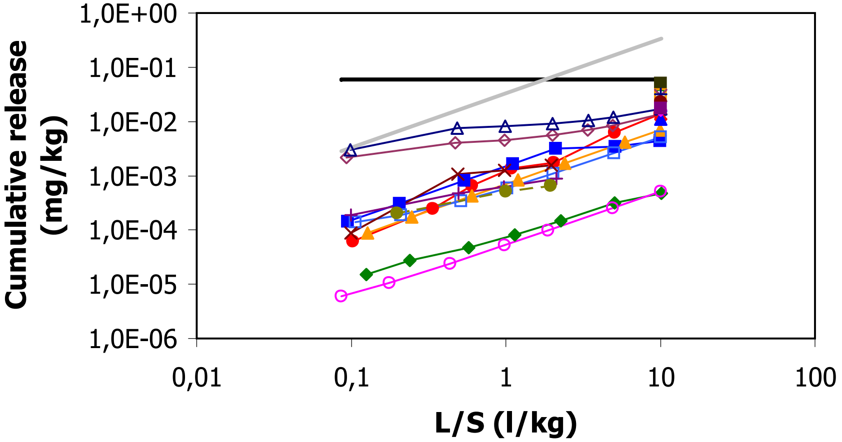
Cumulative release of Cd

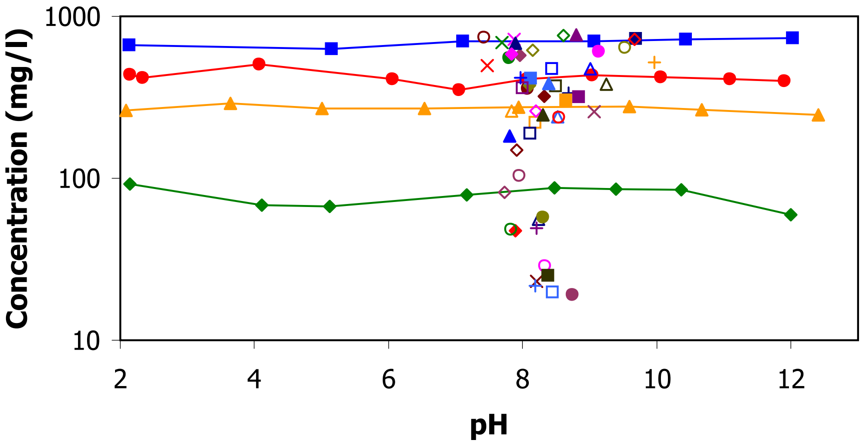
pH dependent Concentration of Cl

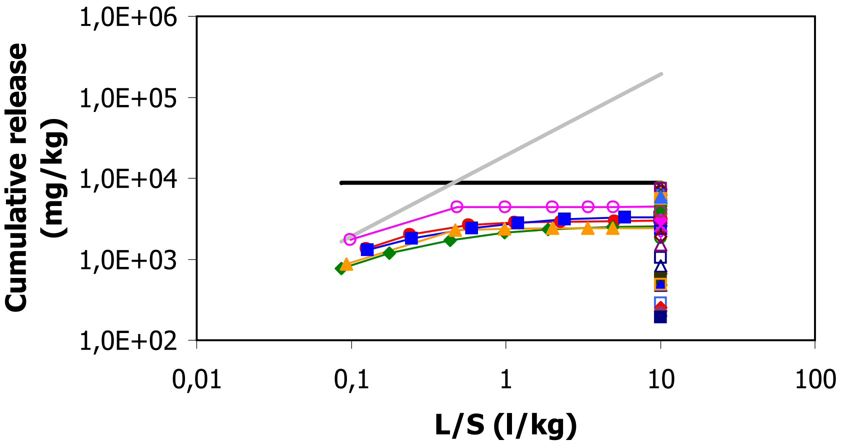
Cumulative release of Cl

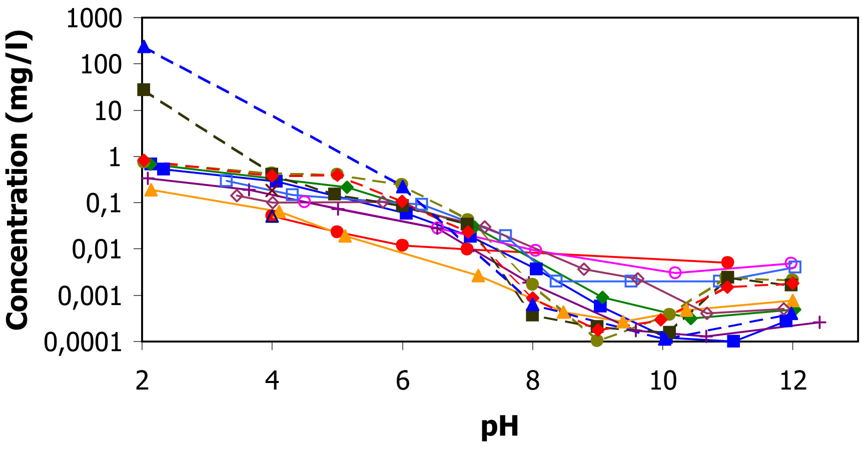
pH dependent Concentration of Co

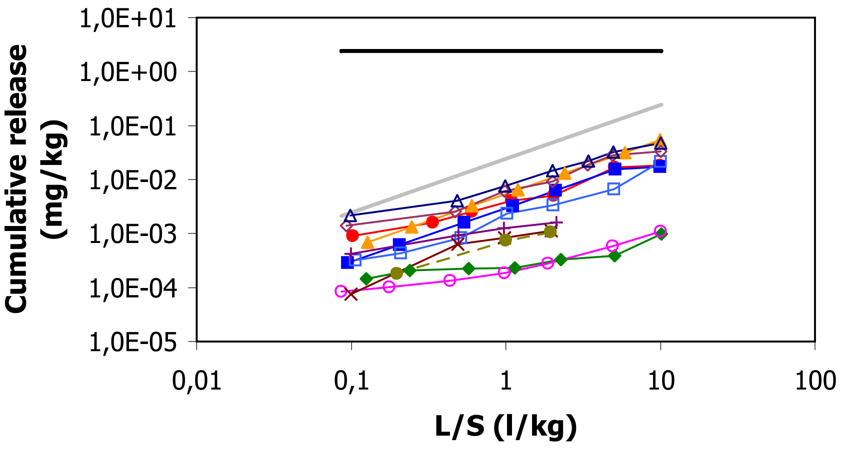
Cumulative release of Co

pH dependent Concentration of Cr

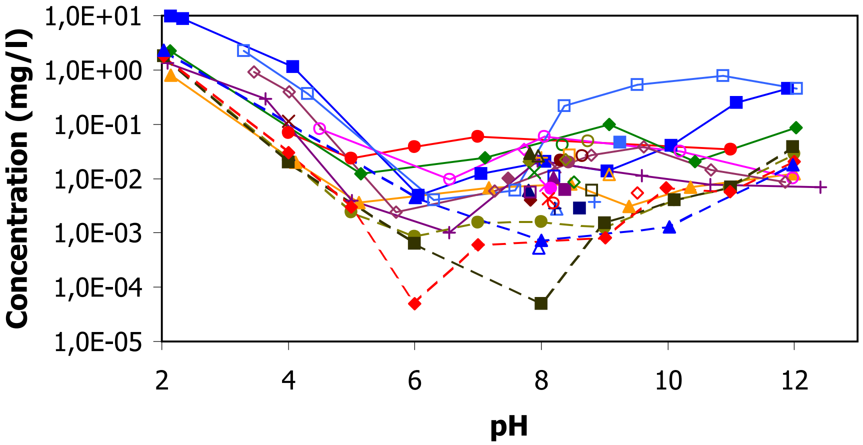

Cumulative release of Cr

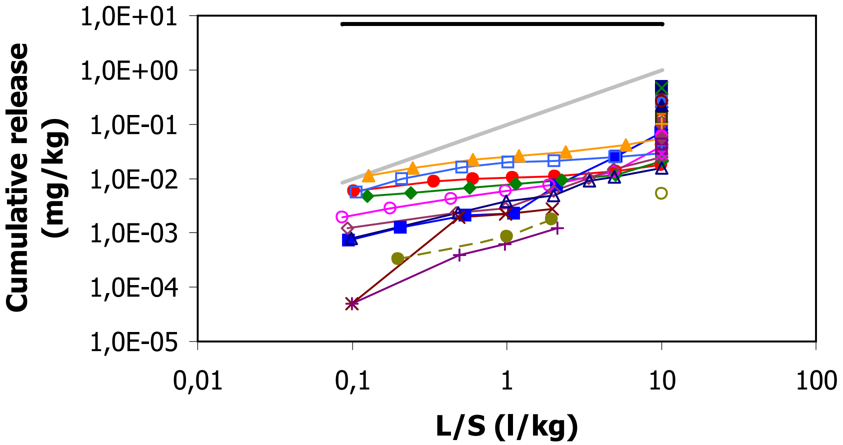

pH dependent Concentration of Cu

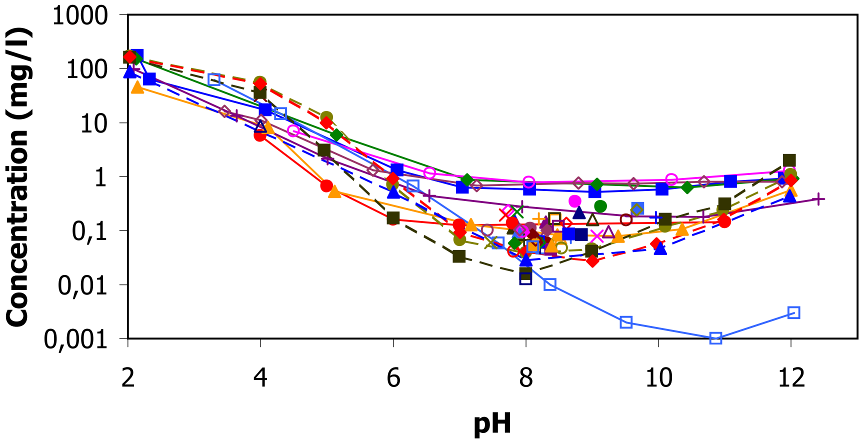

Cumulative release of Cu

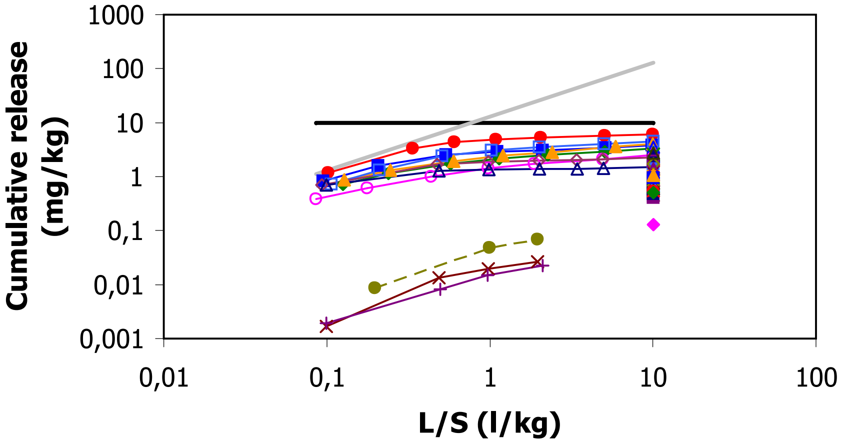

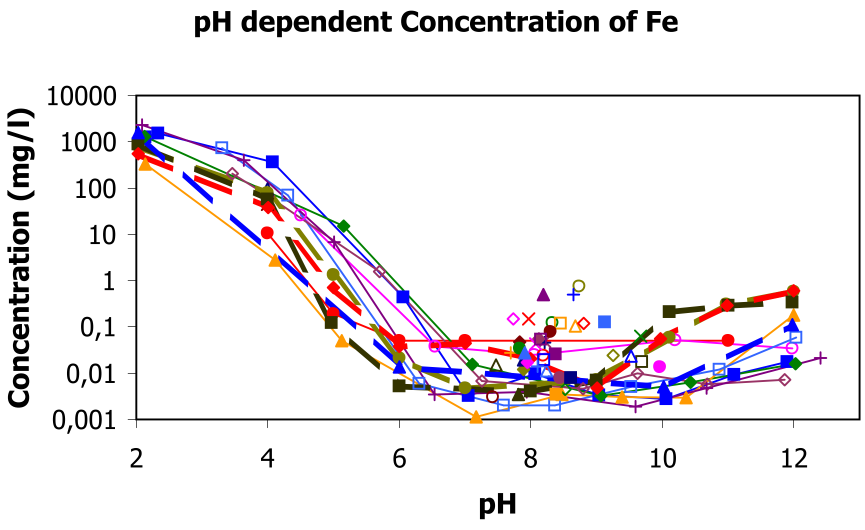
pH dependent Concentration of Fe
Concentration (mg/l)
10000
1000
100
10
1
0,1
0,01
0,001
2
4
6
8
10
12
pH

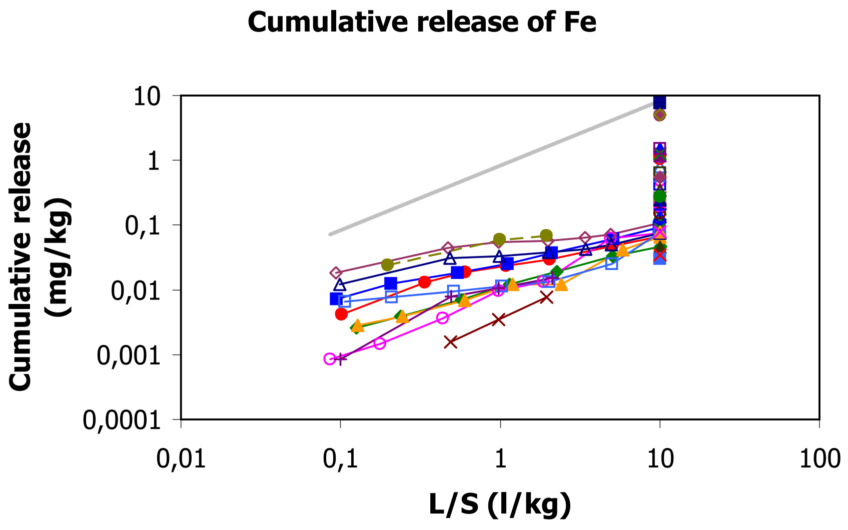
Cumulative release of Fe
Cumulative release (mg/kg)
10
1
0,1
0,01
0,001
0,0001
0,01
0,1
1
10
100
L/S (l/kg)

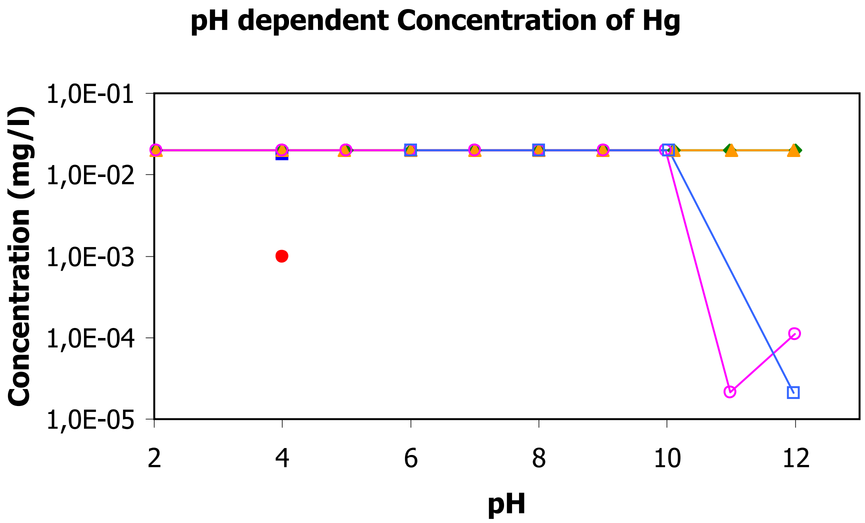
pH dependent Concentration of Hg
Concentration (mg/l)
1,0E-01
1,0E-02
1,0E-03
1,0E-04
1,0E-05
2
4
6
8
10
12
pH

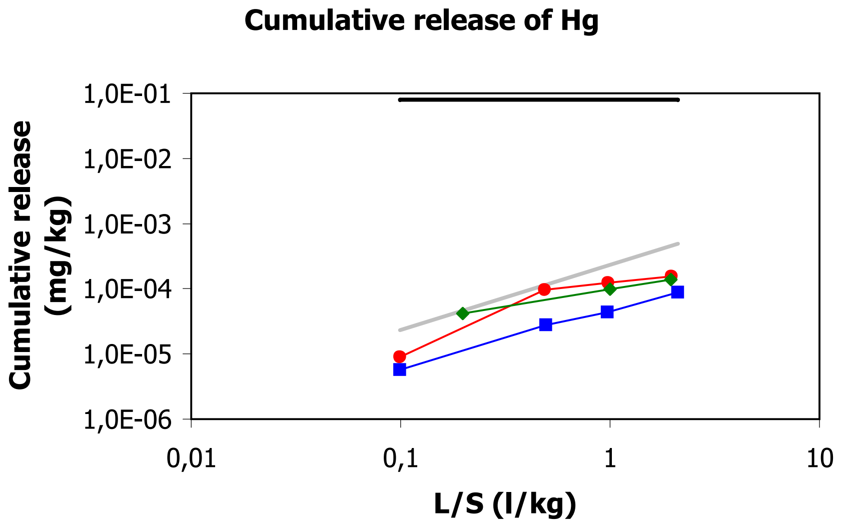
Cumulative release of Hg
Cumulative release (mg/kg)
1,0E-01
1,0E-02
1,0E-03
1,0E-04
1,0E-05
1,0E-06
0,01
0,1
1
10
L/S (l/kg)

pH dependent Concentration of K

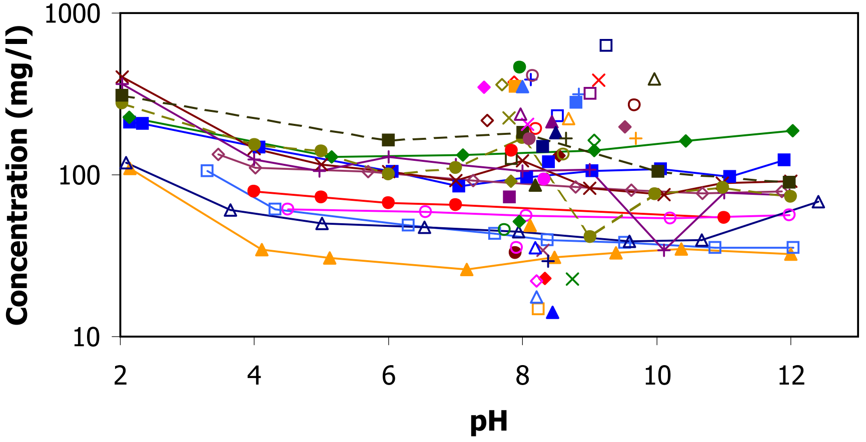

Cumulative release of K

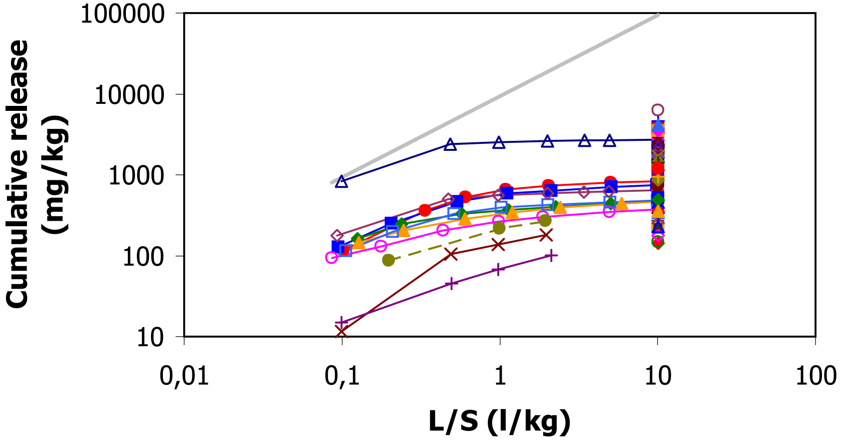

pH dependent Concentration of Mg

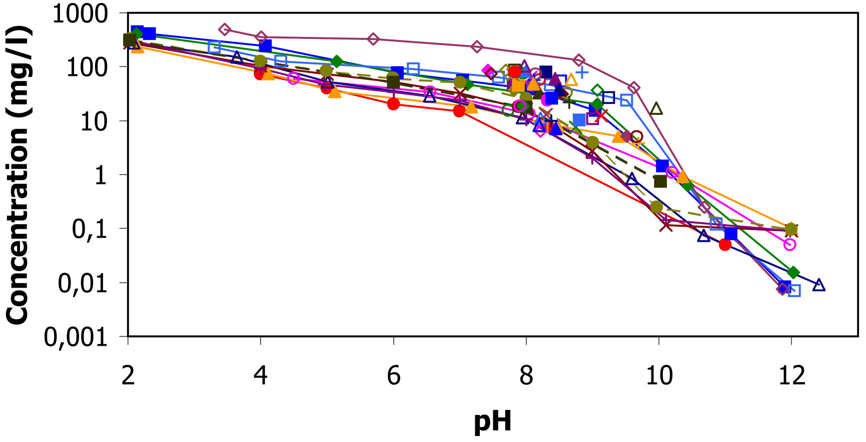

Cumulative release of Mg

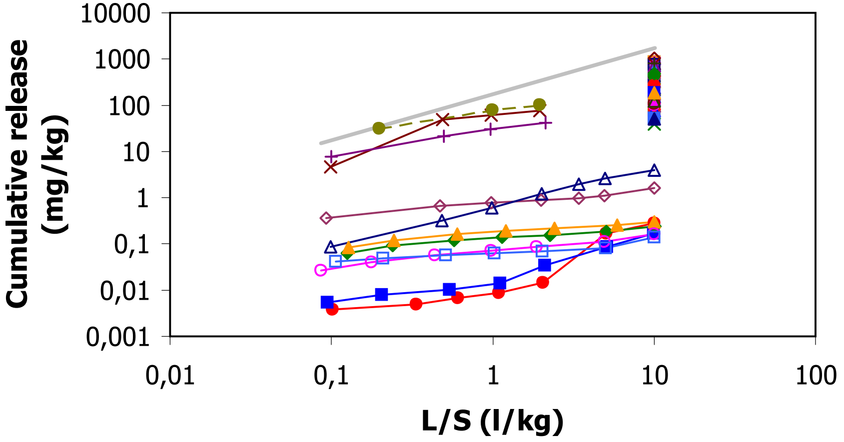

pH dependent Concentration of Mn

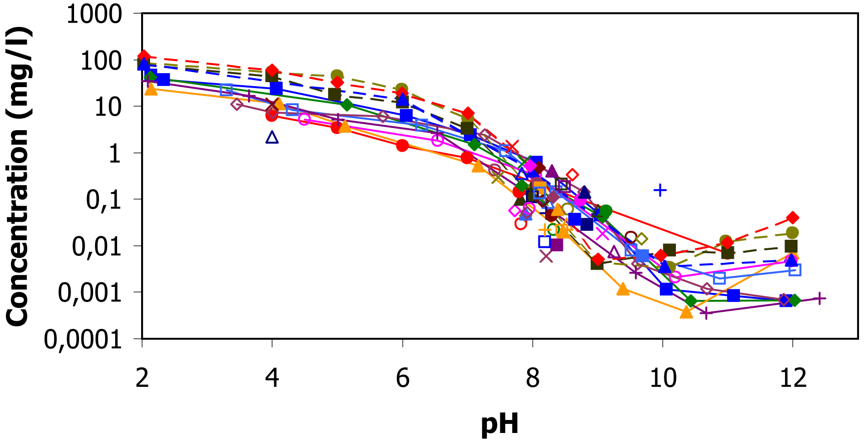

Cumulative release of Mn

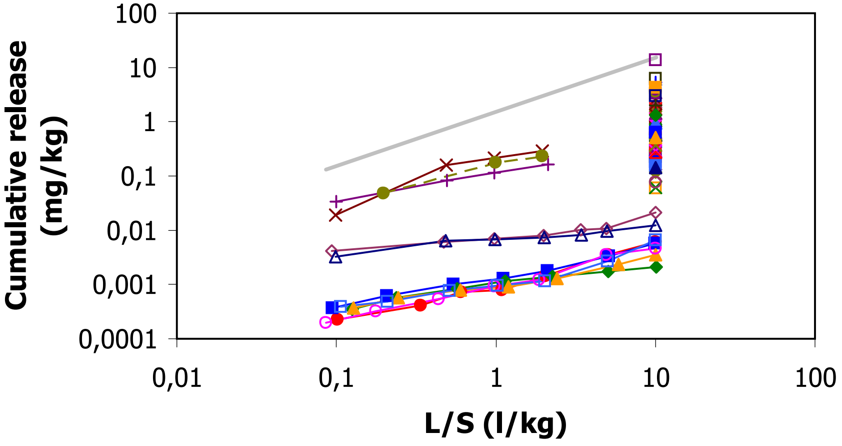

pH dependent Concentration of Mo

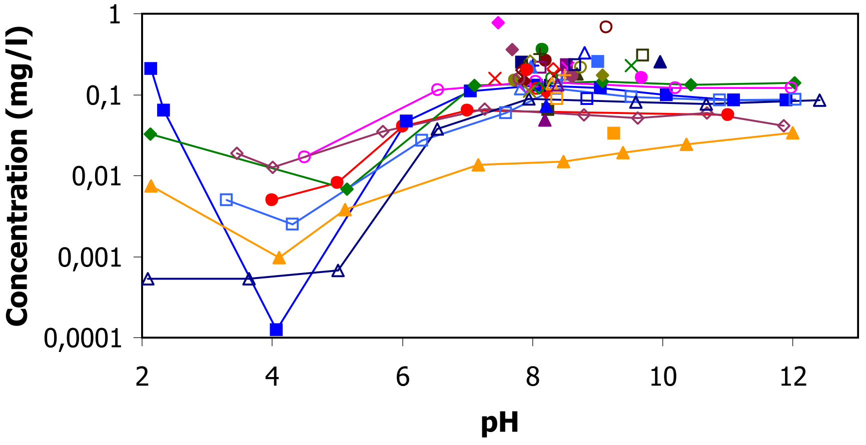

Cumulative release of Mo

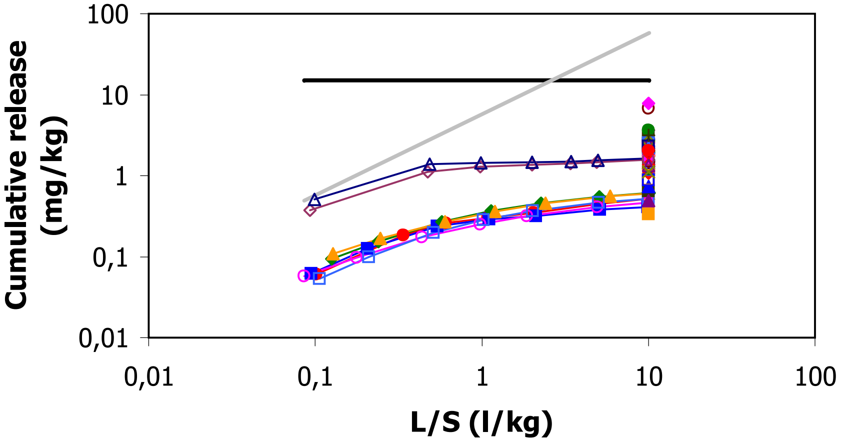

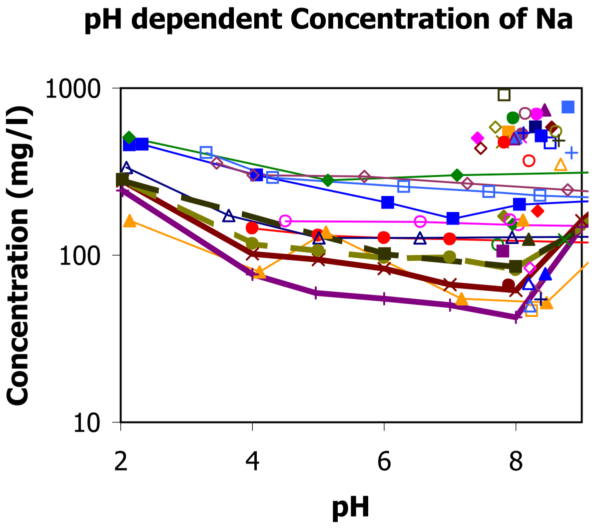
pH dependent Concentration of Na

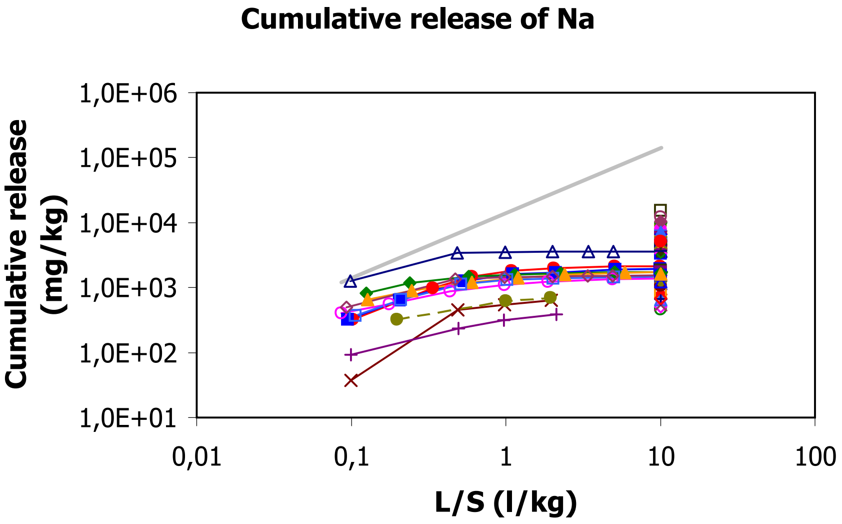
Cumulative release of Na

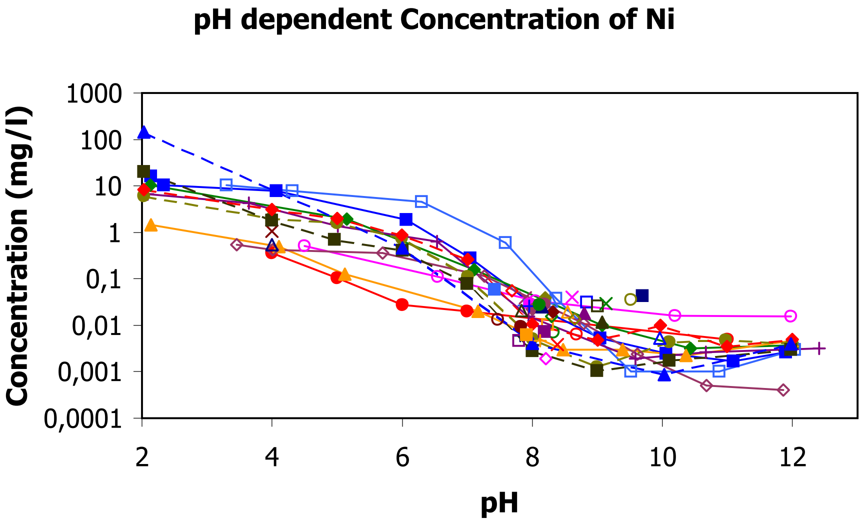
pH dependent Concentration of Ni

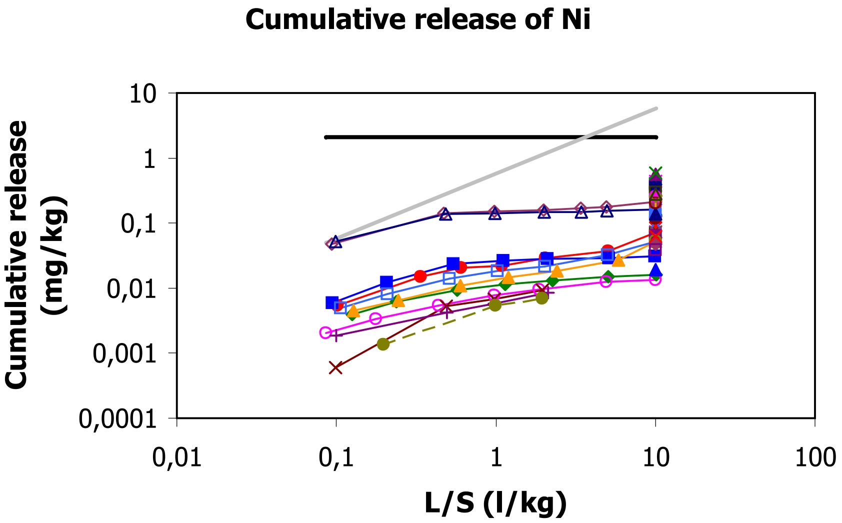
Cumulative release of Ni

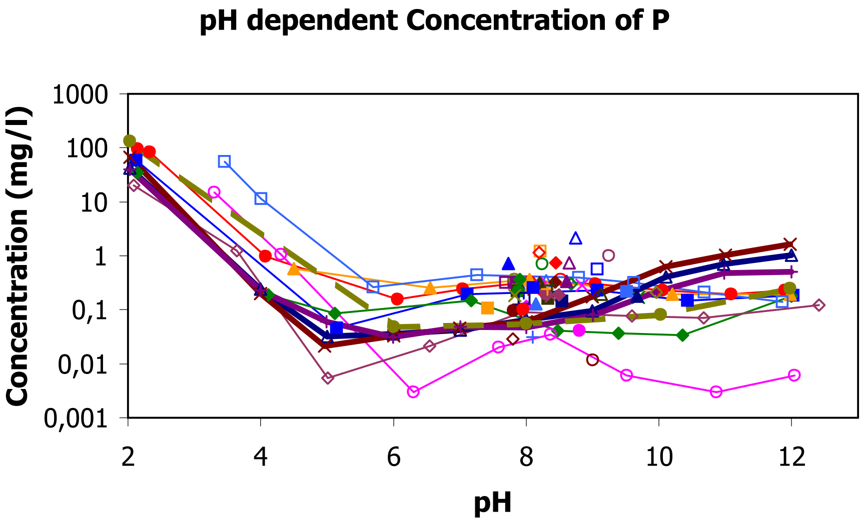
pH dependent Concentration of P

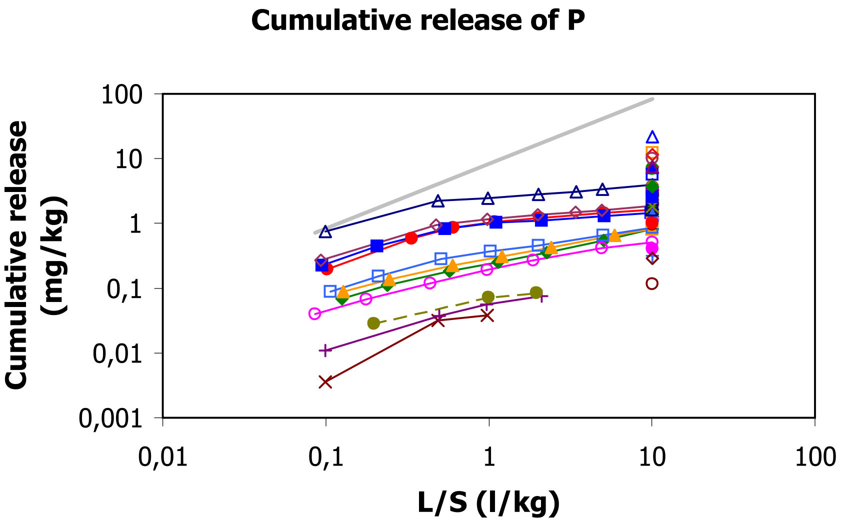
Cumulative release of P

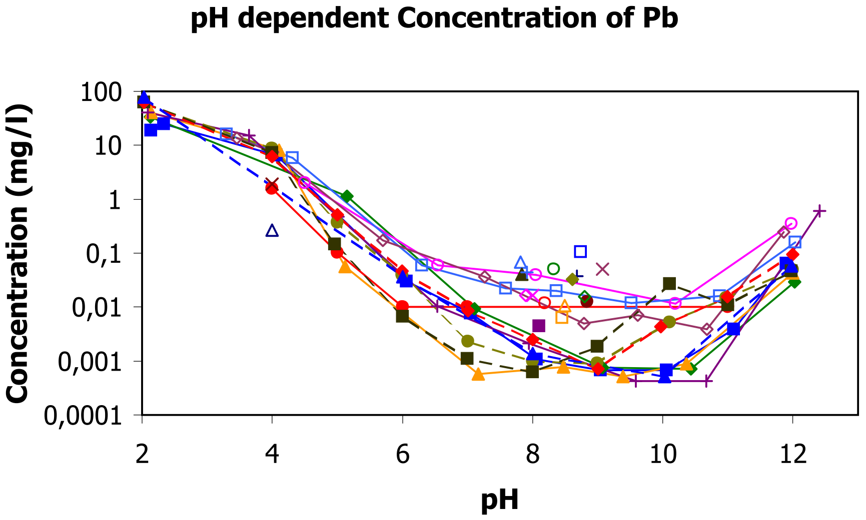
pH dependent Concentration of Pb

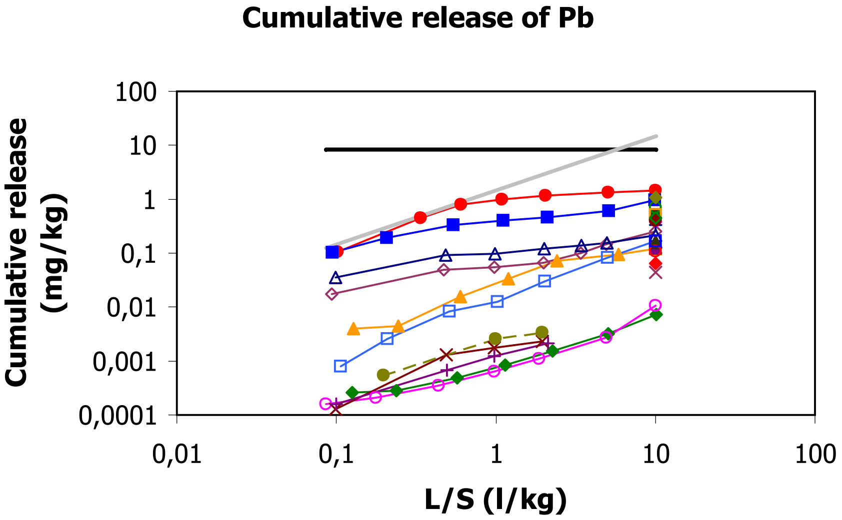
Cumulative release of Pb

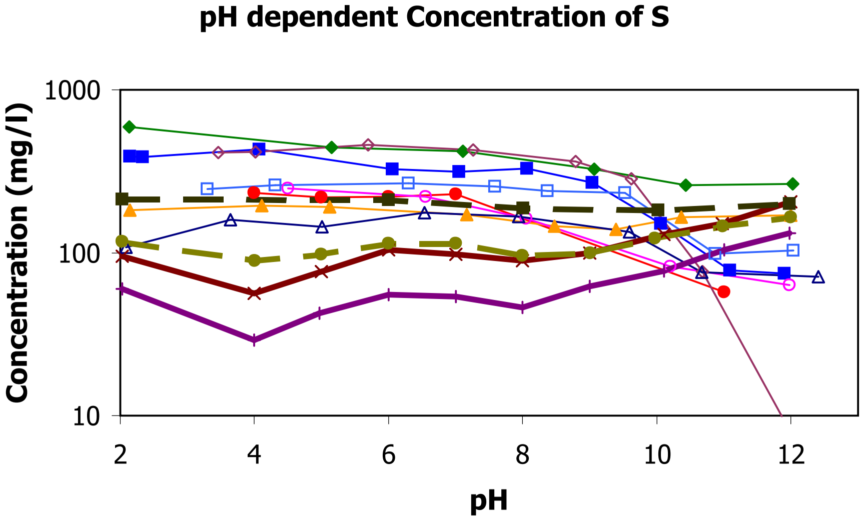
pH dependent Concentration of S

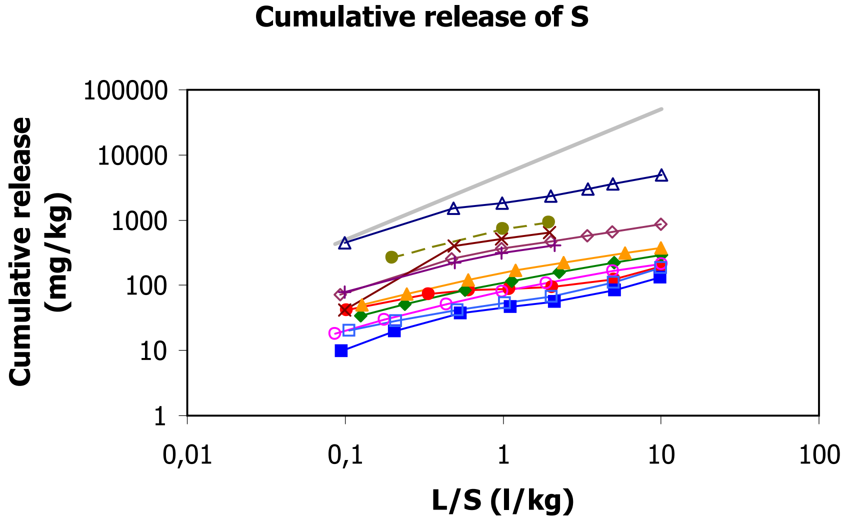
Cumulative release of S

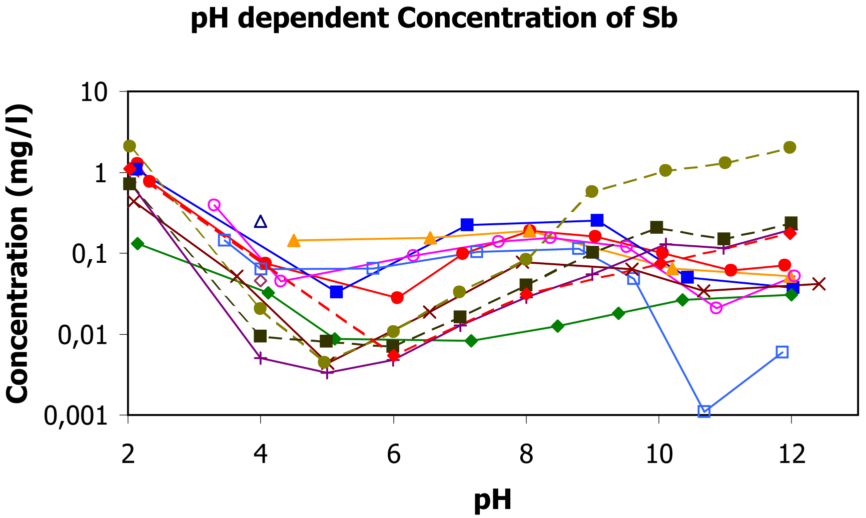
pH dependent Concentration of Sb

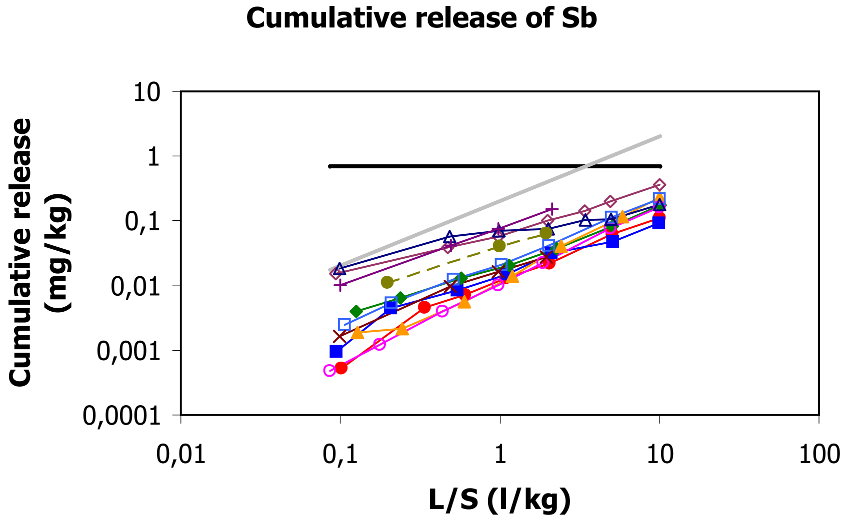
Cumulative release of Sb

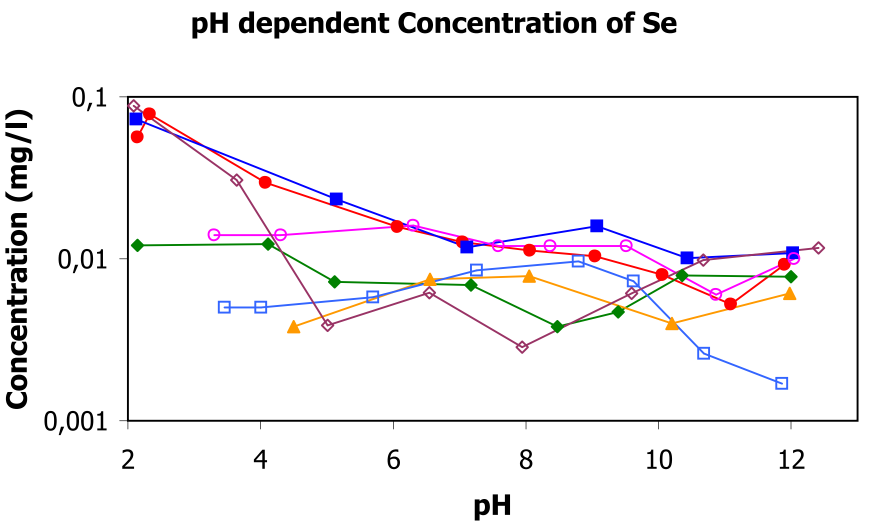
pH dependent Concentration of Se

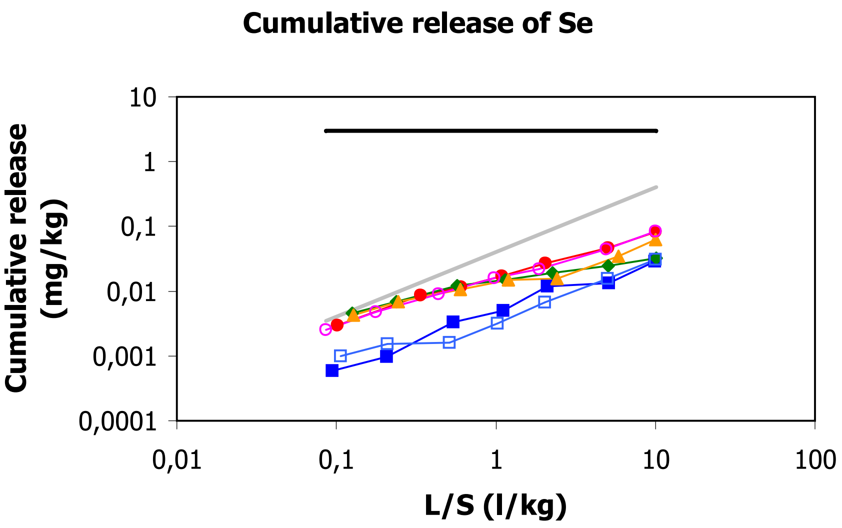
Cumulative release of Se

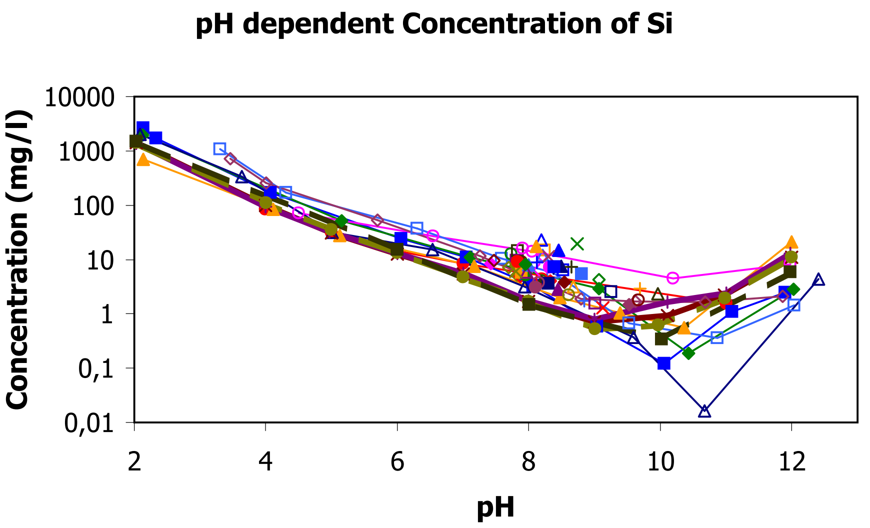
pH dependent Concentration of Si

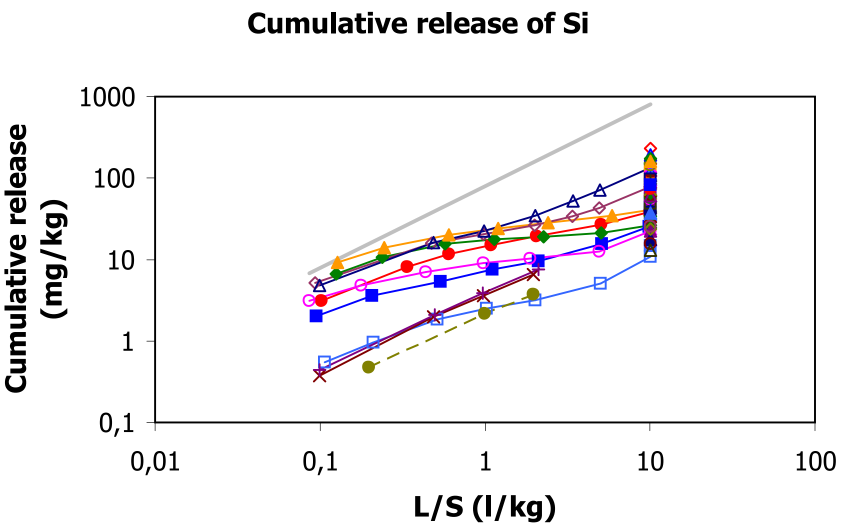
Cumulative release of Si

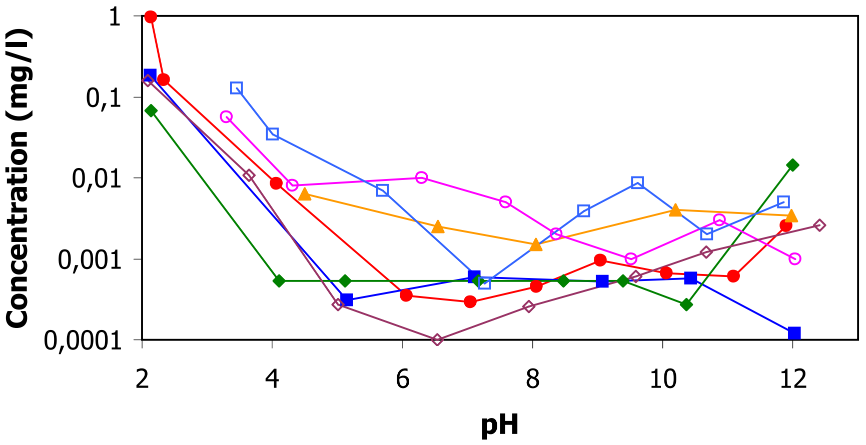
pH dependent Concentration of Sn

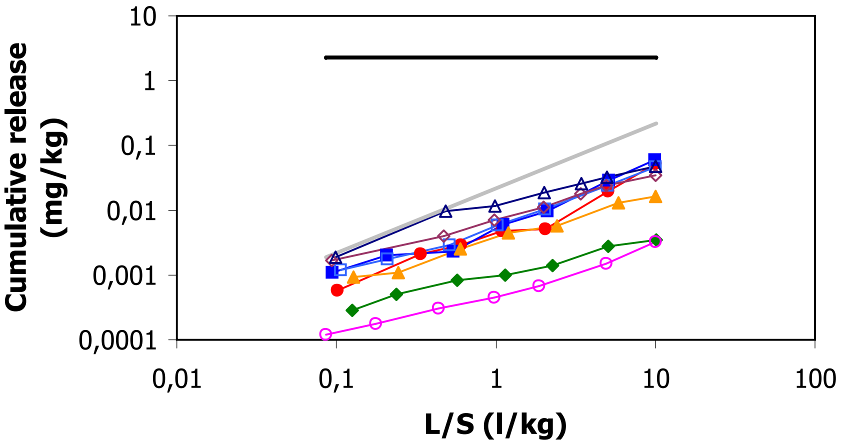
Cumulative release of Sn

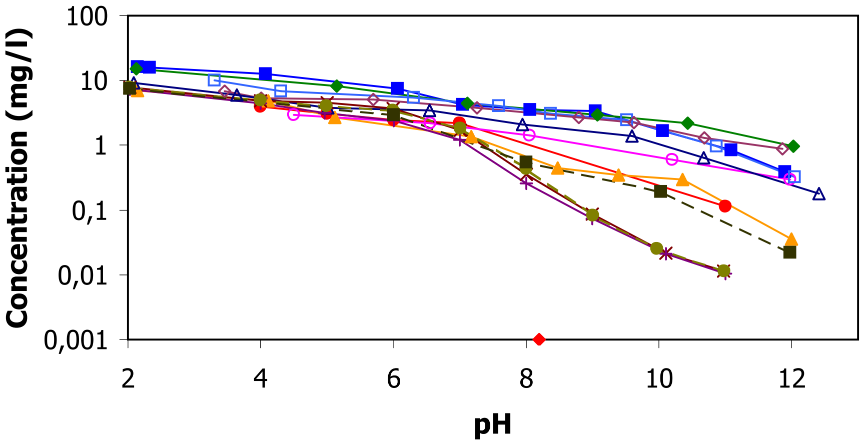
pH dependent Concentration of Sr

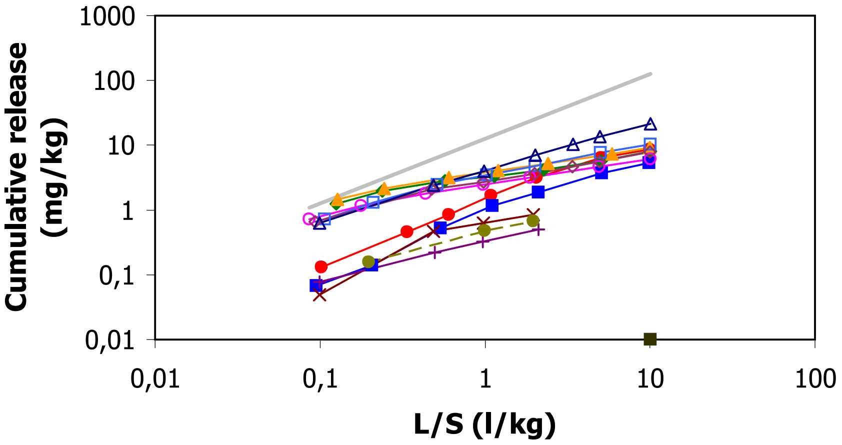
Cumulative release of Sr

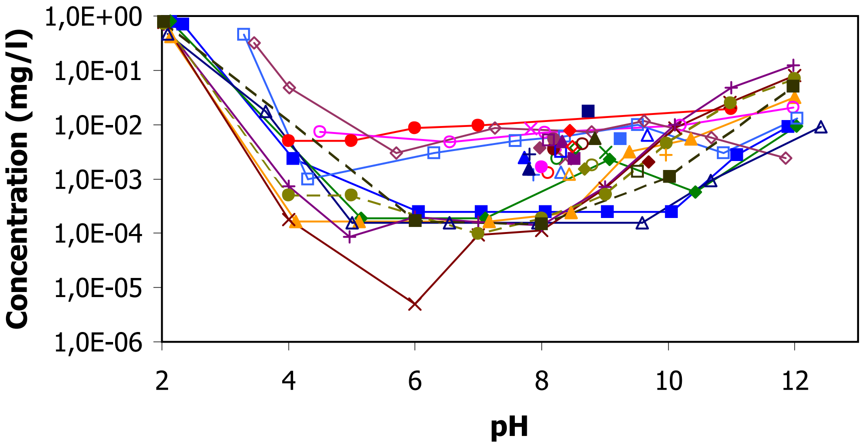

pH dependent Concentration of V

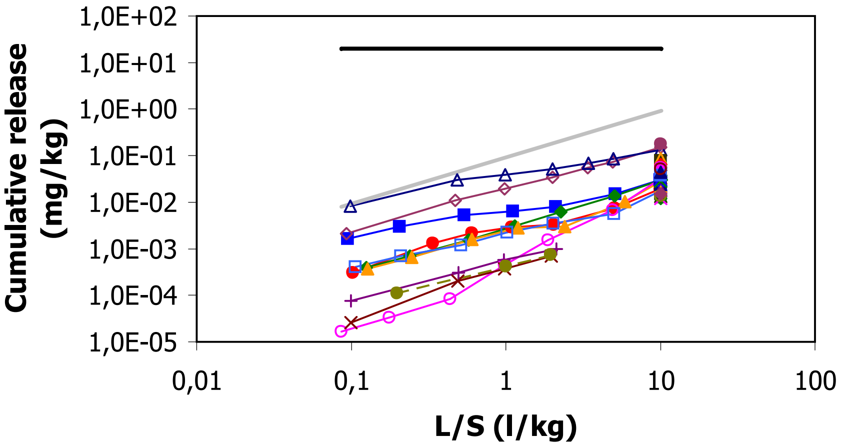

Cumulative release of V

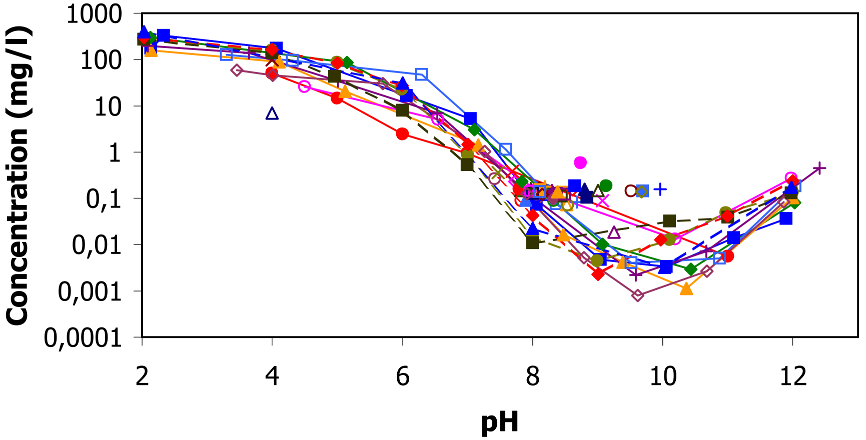

pH dependent Concentration of Zn

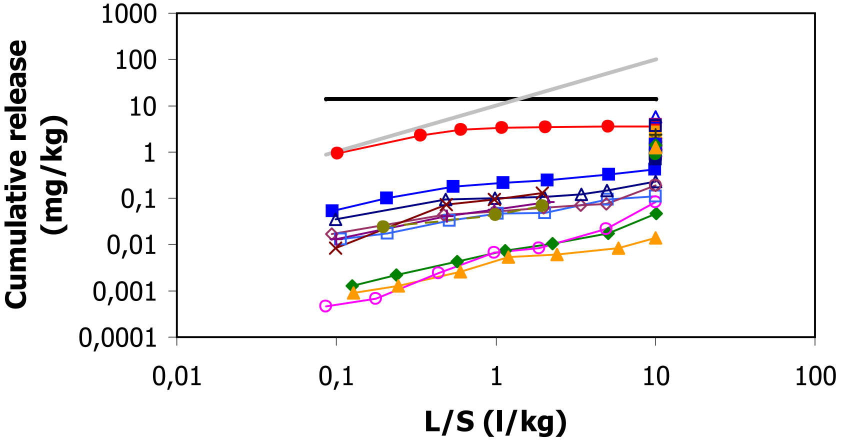

Cumulative release of Zn

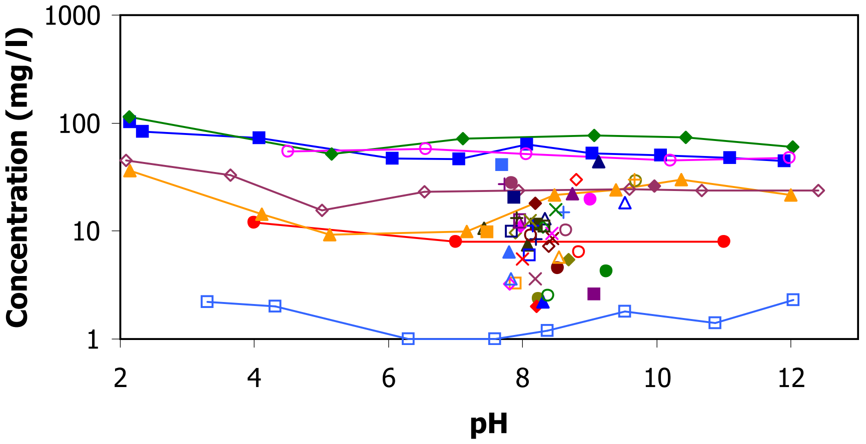
pH dependent Concentration of DOC

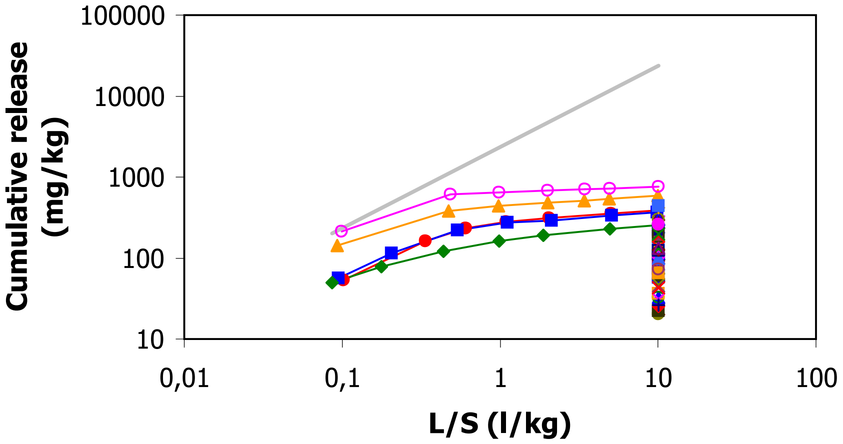
Cumulative release of DOC

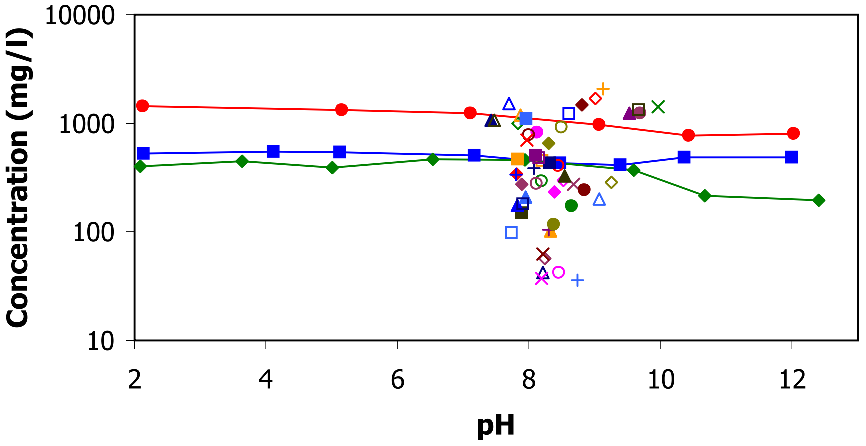
pH dependent Concentration of SO4

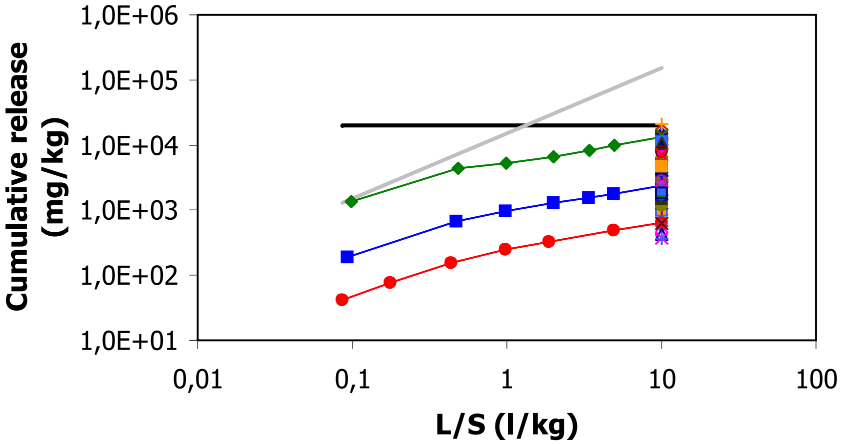
Cumulative release of SO4

D Input for the final geochemical model

D.1

Sample nr	**1**	**2**	**3**	**4**
Sum of pH and pe	13	13	13	13
L/S	9.9	9.8	9.9	9.9
Clay	0.1	0.1	0.1	0.1
HFO kg/kg	0.029	0.035	0.039	0.029
HFO kg/kg measured	**0.029**	**0.035**	**0.039**	**0.029**
SHA kg OM/kg	0.000410	0.000302	0.000233	0.000279
SHA measured kg OM/kg	0.000410	0.000302	0.000233	0.000279
H2CO3 (mg/kg)	9600	9300	11000	8200
TIC measured (mg C/kg)	7100	6300	8700	5800
Gas volume (l)	20	20	20	20
Minerals				
AA_2CaO_Al2O3_8H2O[s]	x	x	x	x
AA_2CaO_Fe2O3_8H2O[s]	x	x	x	x
AA_3CaO_Al2O3[Ca[OH]2]0_5_[CaCO3]0_5_11_5H2O[s]	x	x	x	x
AA_3CaO_Al2O3_CaCO3_11H2O[s]	x	x	x	x
AA_3CaO_Fe2O3_6H2O[s]	x	x	x	x
AA_4CaO_Al2O3_13H2O[s]	x	x	x	x
AA_Al[OH]3[am]	x	x	x	x
AA_Brucite	x	x	x	x
AA_CaO_Al2O3_10H2O[s]	x	x	x	x
AA_Fe[OH]3[am]	x	x	x	x
AA_Gypsum	x	x	x	x
AA_Jennite	x	x	x	x
AA_Magnesite	x	x	x	x
AA_Portlandite	x	x	x	x
AA_Tobermorite-I	x	x	x	x
AA_Tobermorite-II	x	x	x	x
AA_Tricarboaluminate	x	x	x	x
Anglesite	x	x	x	x
Aragonite	x	x	x	x
Ba[SCr]O4[96%SO4]	x	x	x	x
BaSrSO4[50%Ba]	x	x	x	x
beta-TCP	x	x	x	x
Bianchite	x	x	x	x
Ca4Cd[PO4]3OH	x	x	x	x
Calcite	x	x	x	x
Cd[OH]2[A]	x	x	x	x
CdSiO3	x	x	x	x
Celestite	x	x	x	x
Cr[OH]3[A]	x	x	x	x
Cu[OH]2[s]	x	x	x	x
Cu4[OH]6SO4:1.3H2O[c]	x	x	x	x
Dolomite	x	x	x	x
FCO3Apatite	x	x	x	x
Fe_Vanadate	x	x	x	x
FeCr2O4	x	x	x	x
Ferrihydrite	x	x	x	x

Laumontite	x	x	x	x
Magnesite	x	x	x	x
Malachite	x	x	x	x
Manganite	x	x	x	x
Mg3[PO4]2:22H2O[c]	x	x	x	x
Morenosite	x	x	x	x
Ni[OH]2[s]	x	x	x	x
Ni2SiO4	x	x	x	x
NiCO3[s]	x	x	x	x
Otavite	x	x	x	x
Pb[OH]2[C]	x	x	x	x
Pb2V2O7	x	x	x	x
Pb3[VO4]2	x	x	x	x
PbCrO4	x	x	x	x
PbMoO4[c]	x	x	x	x
P-Wollstanite	x	x	x	x
Pyrocroite	x	x	x	x
Pyrolusite	x	x	x	x
Retgersite	x	x	x	x
Rhodochrosite	x	x	x	x
Sb[OH]3[s]	x	x	x	x
Strontianite	x	x	x	x
Struvite	x	x	x	x
Tsumebite	x	x	x	x
Wairakite	x	x	x	x
Willemite	x	x	x	x
Witherite	x	x	x	x
Vivianite	x	x	x	x

D.2 Dissolved organic carbon parameters input to the model

DOC (Dissolved organic carbon)

	1	2	3	4
pH	**[DOC] (kg/l)**	**[DOC] (kg/l)**	**[DOC] (kg/l)**	**[DOC] (kg/l)**
1	2,4E-05	1,8E-05	1,8E-05	1,8E-05
2	1,5E-05	1,1E-05	1,1E-05	1,1E-05
4	1,4E-05	1,1E-05	1,1E-05	
5	1,4E-05	1,1E-05	1,1E-05	
6	1,7E-05	1,2E-05	1,2E-05	1,2E-05
7	1,7E-05	1,3E-05	1,3E-05	
8	1,7E-05	1,3E-05	1,3E-05	1,3E-05
9	1,7E-05	1,3E-05	1,3E-05	
10	1,7E-05	1,3E-05	1,3E-05	1,3E-05
11	1,7E-05	1,3E-05	1,3E-05	
12	2,1E-05	1,6E-05	1,6E-05	1,6E-05
14	2,8E-05	2,1E-05	2,1E-05	2,1E-05

Fraction of DOC that is calculated as dissolved humic acid (DHA)

	1	2	3	4
pH	**DHA fraction**	**DHA fraction**	**DHA fraction**	**DHA fraction**
1	0,35	0,35	0,53	0,53
2	0,23	0,23	0,35	0,35
4	0,15	0,15	0,23	
5	0,15	0,15	0,23	
6	0,10	0,10	0,15	0,15
7	0,12	0,12	0,18	
8	0,15	0,15	0,23	0,23
9	0,19	0,19	0,29	
10	0,30	0,30	0,45	0,45
11	0,37	0,37	0,56	
12	0,40	0,40	0,60	0,60
14	0,40	0,40	0,60	0,60

Resulting amount of DHA, which is used further in the model calculations

Sample	1	2	3	4
pH	**[DHA] (kg/l)**	**[DHA] (kg/l)**	**[DHA] (kg/l)**	**[DHA] (kg/l)**
1	8,2E-06	6,2E-06	9,2E-06	9,2E-06
2	3,5E-06	2,6E-06	3,9E-06	3,9E-06
4	2,1E-06	1,6E-06	2,4E-06	
5	2,1E-06	1,6E-06	2,4E-06	
6	1,7E-06	1,2E-06	1,9E-06	1,9E-06
7	2,1E-06	1,5E-06	2,3E-06	
8	2,6E-06	1,9E-06	2,9E-06	2,9E-06
9	3,2E-06	2,4E-06	3,6E-06	
10	5,1E-06	3,8E-06	5,7E-06	5,7E-06
11	6,4E-06	4,8E-06	7,2E-06	
12	8,2E-06	6,2E-06	9,3E-06	9,3E-06
14	1,1E-05	8,4E-06	1,3E-05	1,3E-05

E Minerals

E.1 Chemical formulas

Minerals	Mineral formulae
AA_2CaO_Al2O3_8H2O[s]	
AA_2CaO_Fe2O3_8H2O[s]	
AA_3CaO_Al2O3[Ca[OH]2]0_5_[CaCO3]0_5_11_5H2O[s]	
AA_3CaO_Al2O3_CaCO3_11H2O[s]	
AA_3CaO_Fe2O3_6H2O[s]	
AA_4CaO_Al2O3_13H2O[s]	
AA_Al[OH]3[am]	
AA_Brucite	$Mg(OH)_2$
AA_CaO_Al2O3_10H2O[s]	
AA_Fe[OH]3[am]	
AA_Gypsum	$CaSO_4*2H_2O$
AA_Jennite	$Ca_9H_2Si_6O_{18}(OH)_8 *6H_2O$
AA_Magnesite	$MgCO_3$
AA_Portlandite	$Ca(OH)_2$
AA_Tobermorite-I	$Ca_5Si_6(O,OH)_{18} *5H_2O$
AA_Tobermorite-II	
AA_Tricarboaluminate	
Anglesite	$PbSO_4$
Aragonite	$CaCO_3$
Ba[SCr]O4[96%SO4]	
BaSrSO4[50%Ba]	
beta-TCP	
Bianchite	$(Zn, Fe)SO_4*6H_2O$
Ca4Cd[PO4]3OH	
Calcite	$CaCO_3$
Cd[OH]2[A]	
CdSiO3	
Celestite	$SrSO_4$
Cr[OH]3[A]	
Cu[OH]2[s]	
Cu4[OH]6SO4:1.3H2O[c]	
Dolomite	$CaMg(CO_3)_2$
FCO3Apatite	$Ca_5[F,CO_3,PO_4)_3$
Fe_Vanadate	
FeCr2O4	
Ferrihydrite	$Fe_5O_3(OH)_9$
Laumontite	$CaAl_2Si_4O_{12}*4H_2O$
Magnesite	$MgCO_3$
Malachite	$Cu_2[(OH)_2 \vert CO_3]$
Manganite	$MnO(OH)$
Mg3[PO4]2:22H2O[c]	
Morenosite	$NiSO_4 *7H_2O$
Ni[OH]2[s]	
Ni2SiO4	
NiCO3[s]	

Otavite	$CdCO_3$
Pb[OH]2[C]	
Pb2V2O7	
Pb3[VO4]2	
PbCrO4	
PbMoO4[c]	
P-Wollstanite	wollastonite: $Ca(SiO_3)$
Pyrochroite	$Mn(OH)_2$
Pyrolusite	MnO_2
Retgersite	$NiSO_4*6H_2O$
Rhodochrosite	$MnCO_3$
Sb[OH]3[s]	
Strontianite	$SrCO_3$
Struvite	$NH_4MgPO_4*6H_2O$
Tsumebite	$Pb_2Cu[OH\vert SO_4\vert PO_4]$
Wairakite	$Ca[Al_2Si_4O_{12}]*2H_2O$
Willemite	$Zn_2[SiO_4]$
Witherite	$BaCO_3$
Vivianite	$Fe_3(PO_4)_2*8H_2O$

F Result geochemical modelling sample 1

[Al+3] as function of pH

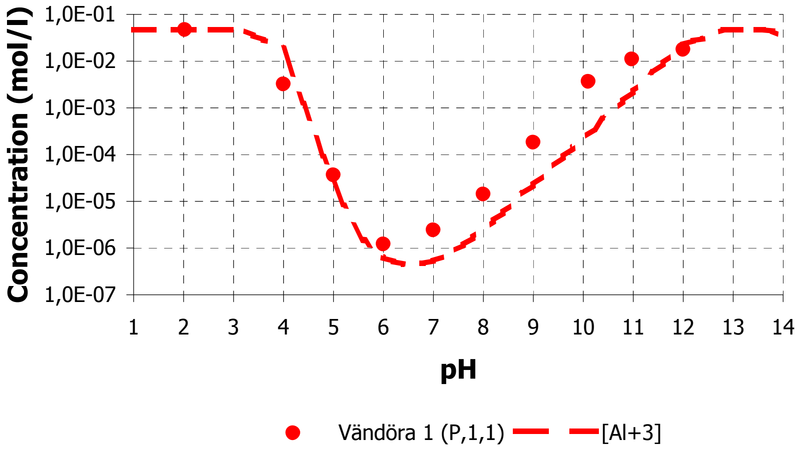

[Ba+2] as function of pH

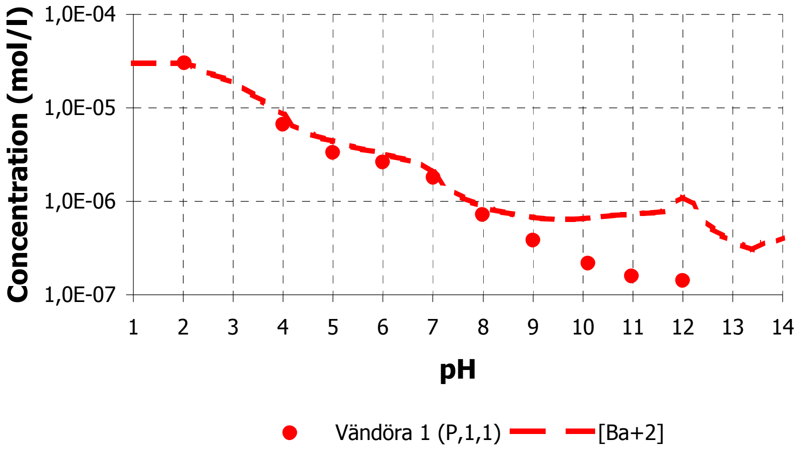

[H2CO3] as function of pH

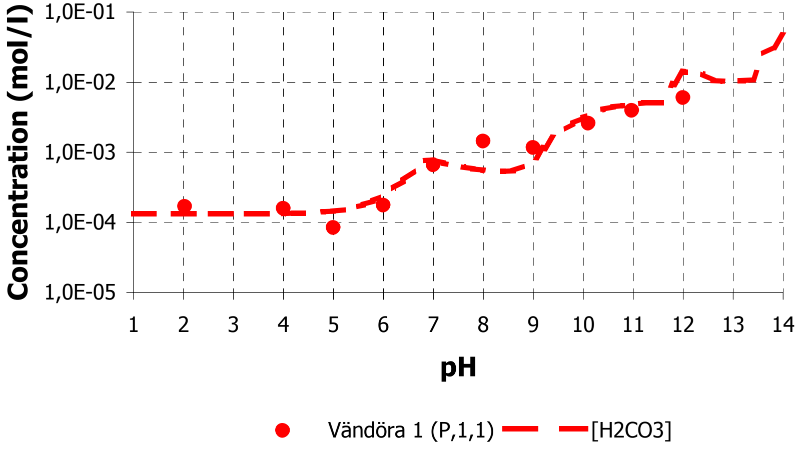

[Mg+2] as function of pH

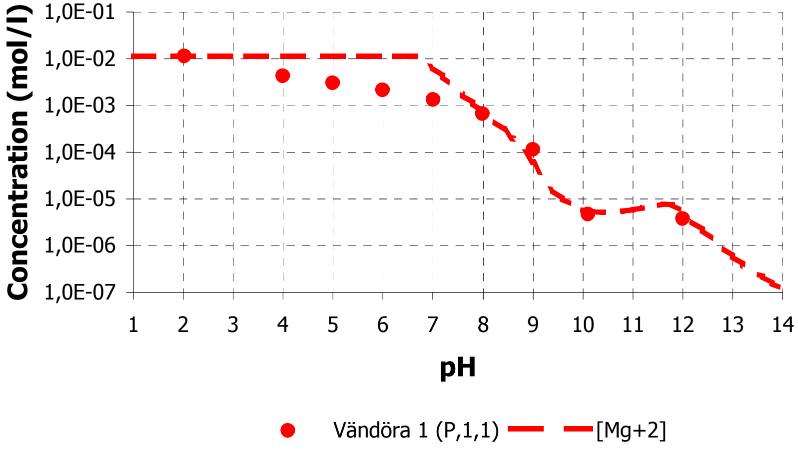

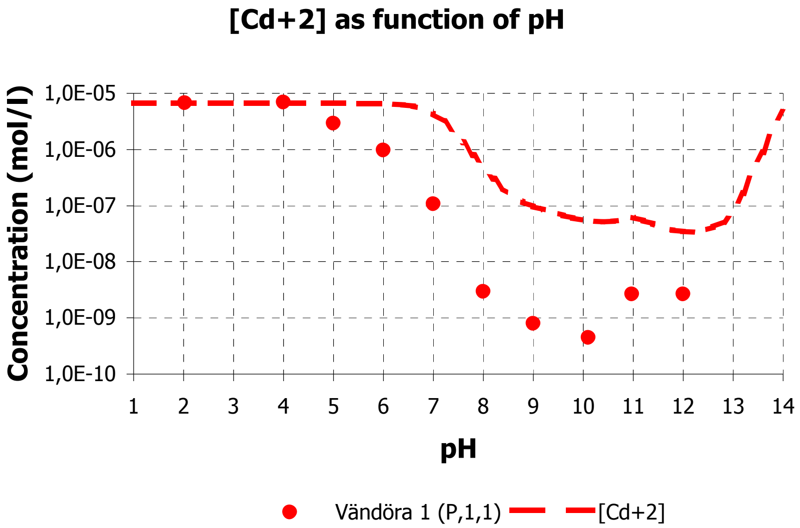

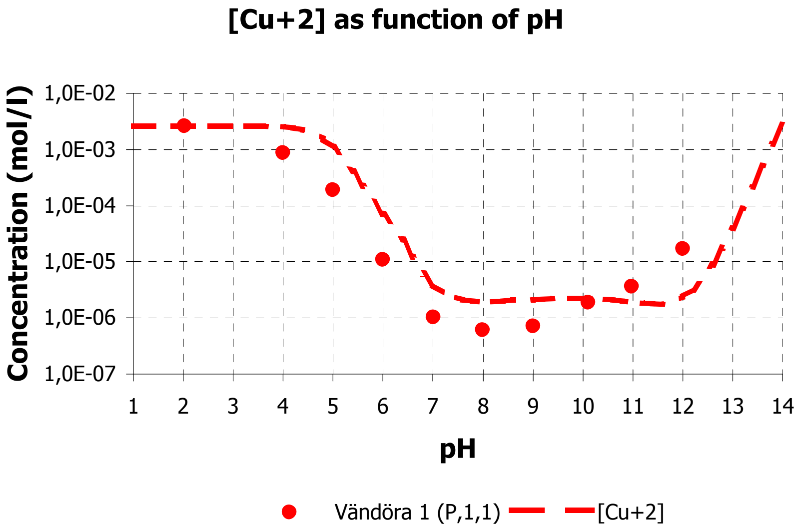

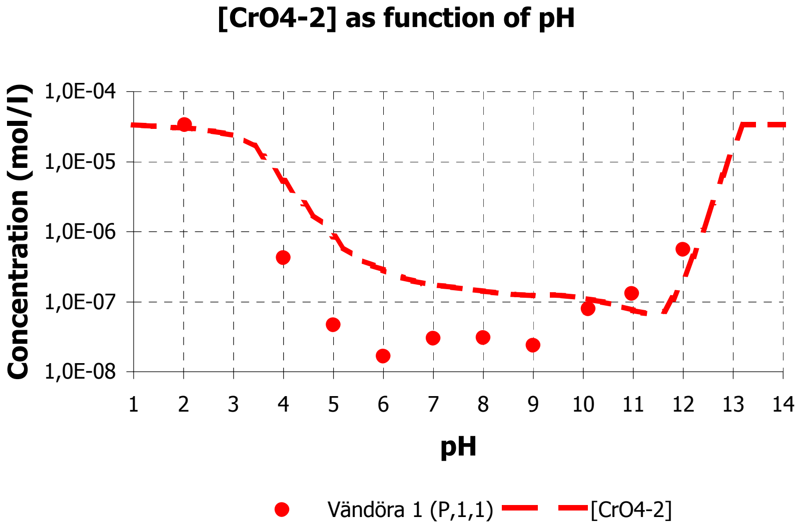

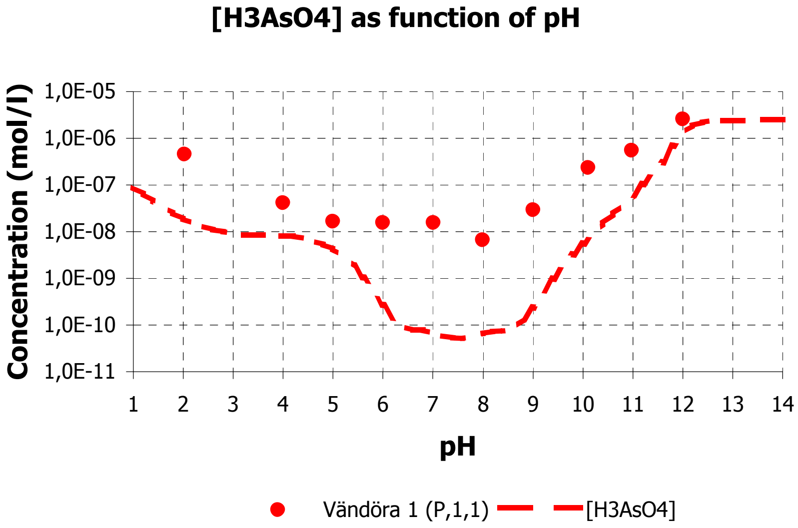

[Br-] as function of pH

[Cl-] as function of pH

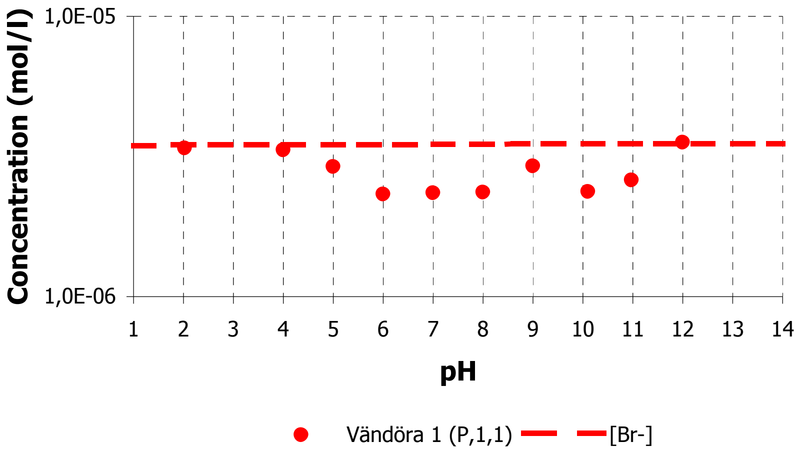

[Br-] as function of pH

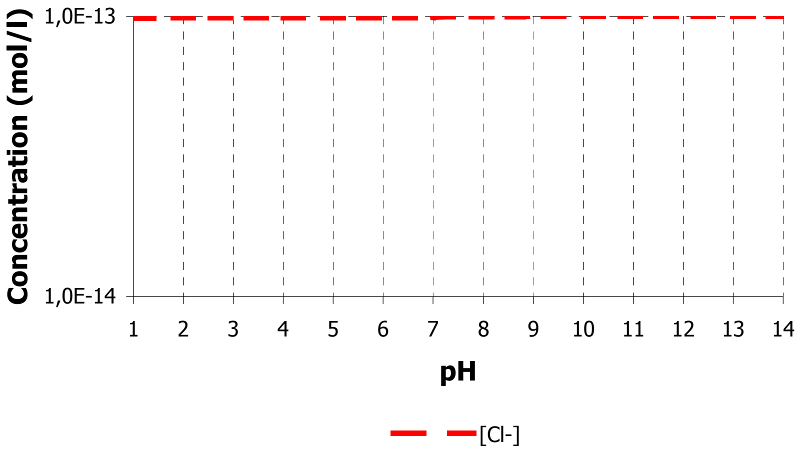

[Cl-] as function of pH

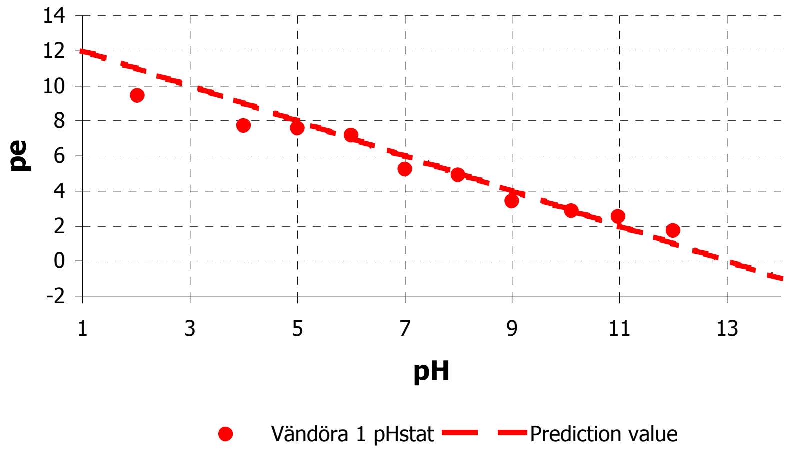

Vändöra 1 ecn-090406: pe as function of pH

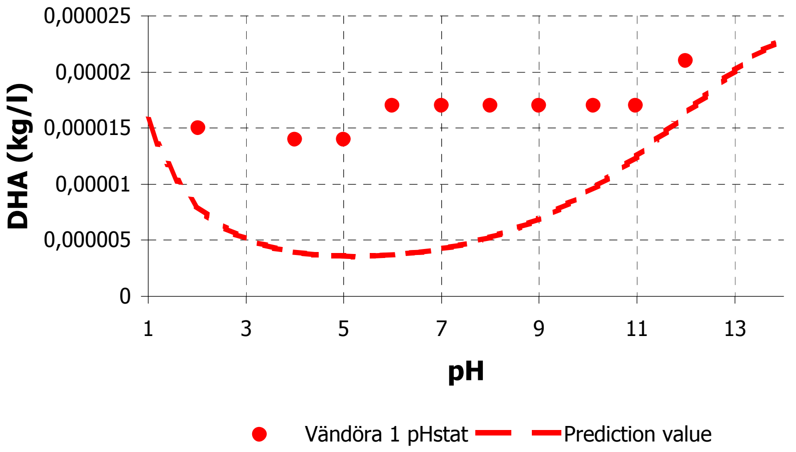

Vändöra 1 ecn-090406: DHA as function of pH

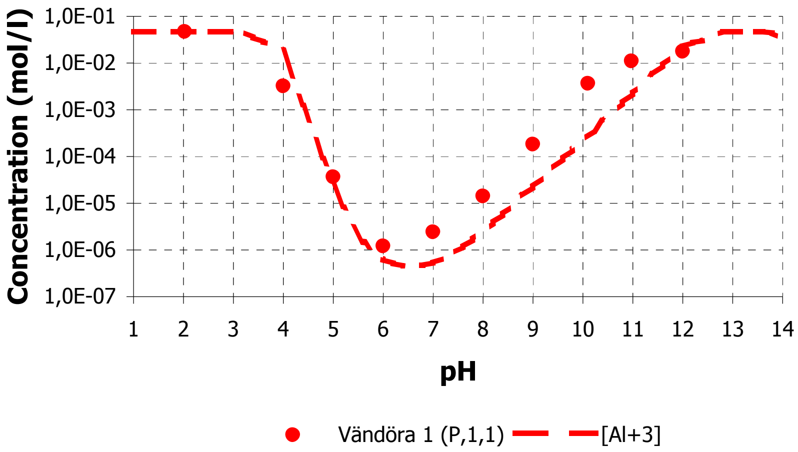
[Al+3] as function of pH

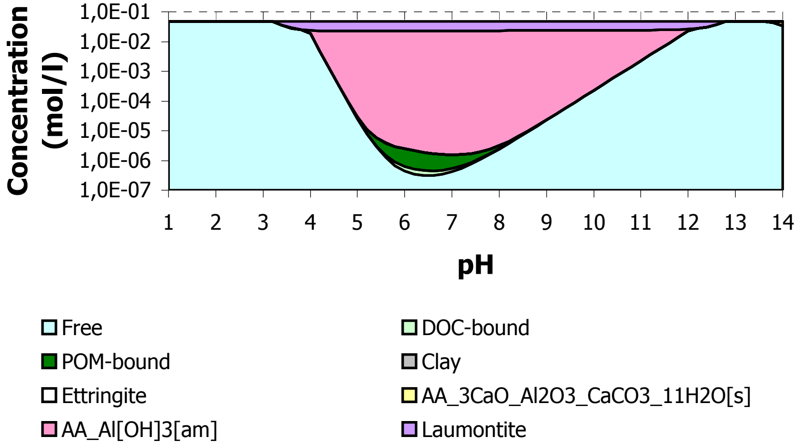
Partitioning liquid-solid, [Al+3]

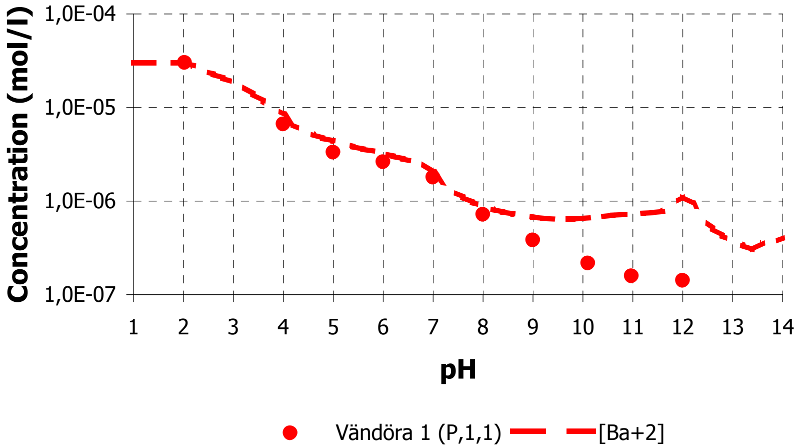
[Ba+2] as function of pH

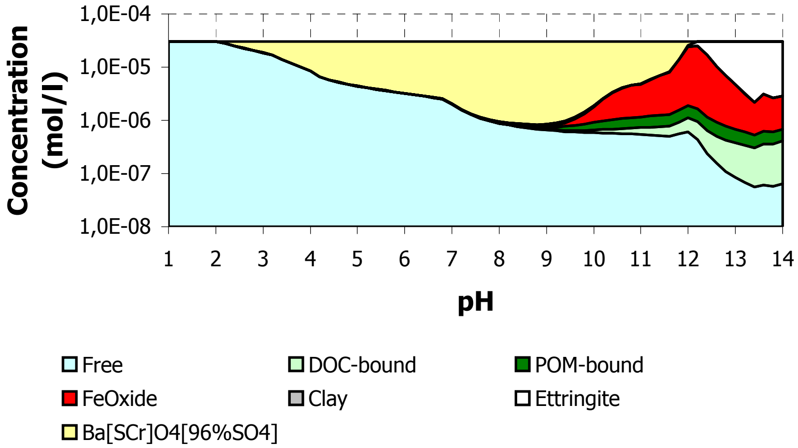
Partitioning liquid-solid, [Ba+2]

[Ca+2] as function of pH

Partitioning liquid-solid, [Ca+2]

[Ca+2] as function of pH

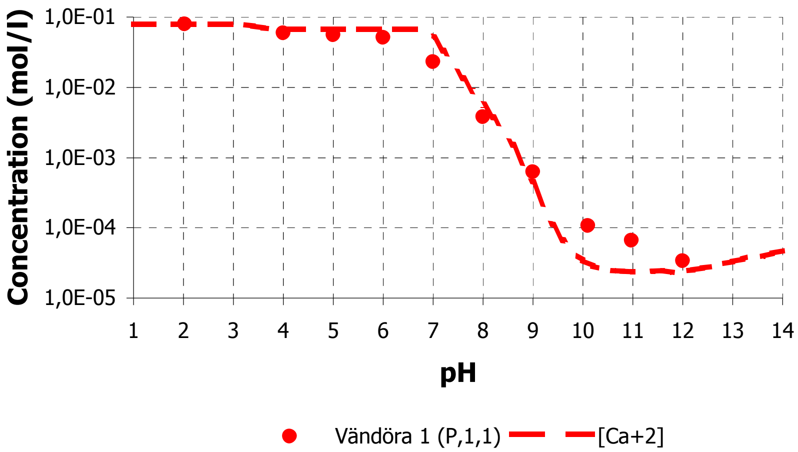

Partitioning liquid-solid, [Ca+2]

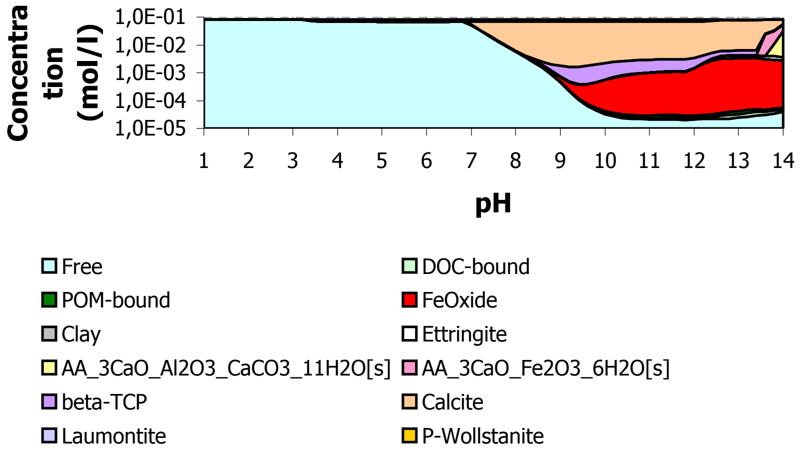

[Fe+3] as function of pH

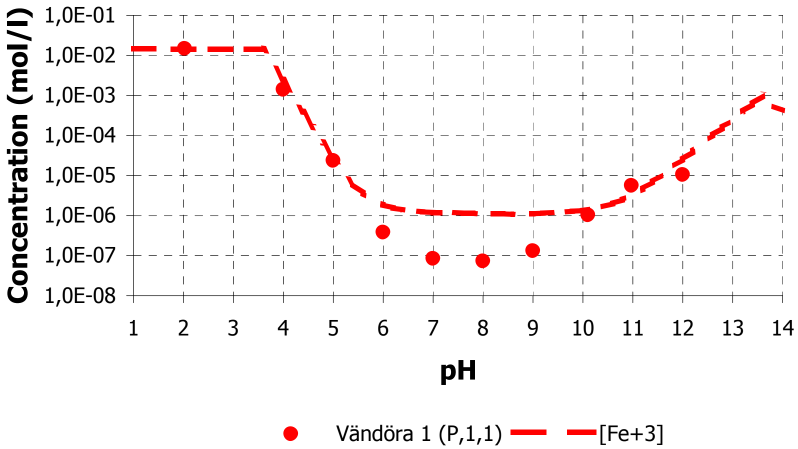

Partitioning liquid-solid, [Fe+3]

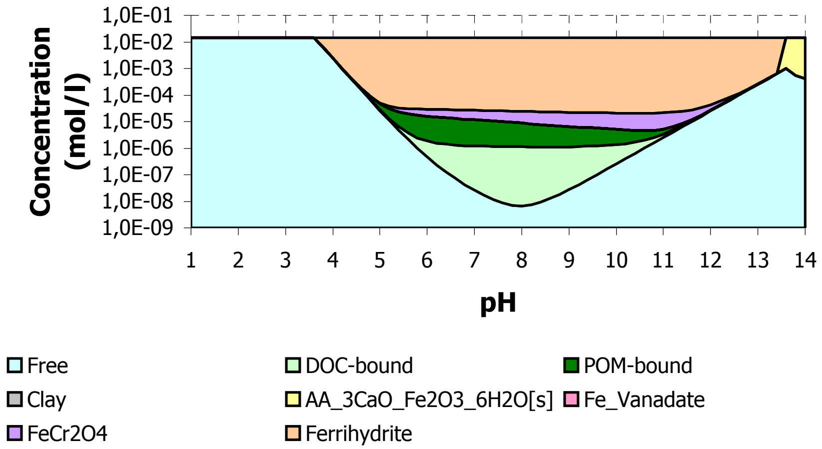

[H4SiO4] as function of pH

Partitioning liquid-solid, [H4SiO4]

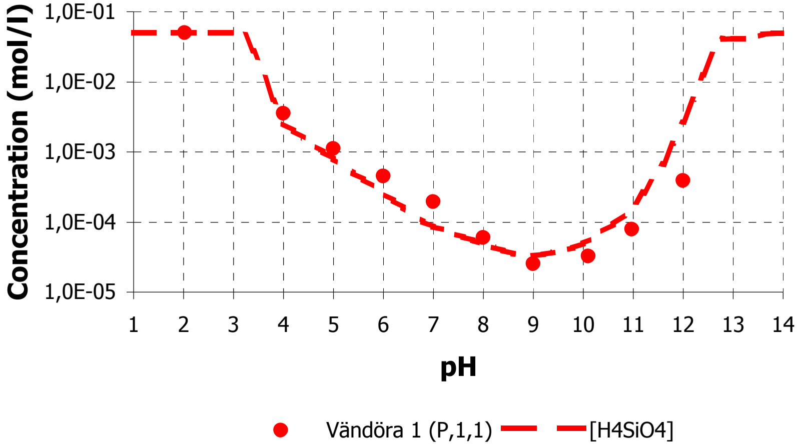
[H4SiO4] as function of pH

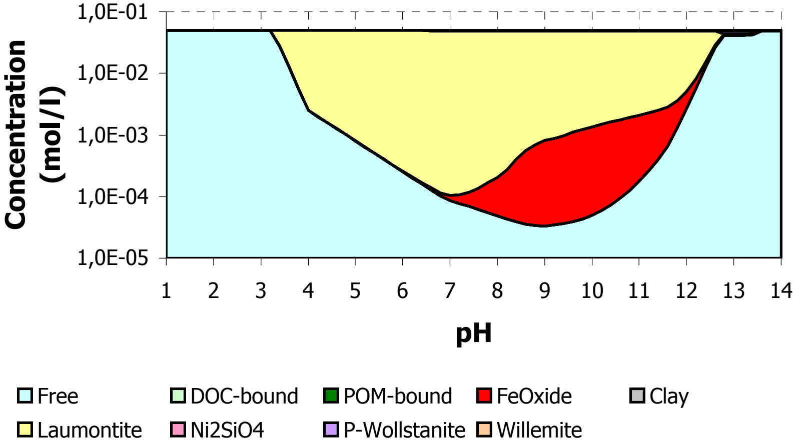
Partitioning liquid-solid, [H4SiO4]

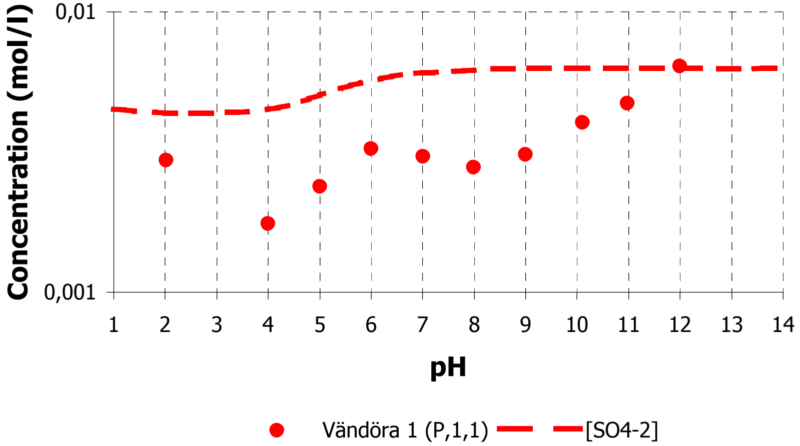
[SO4-2] as function of pH

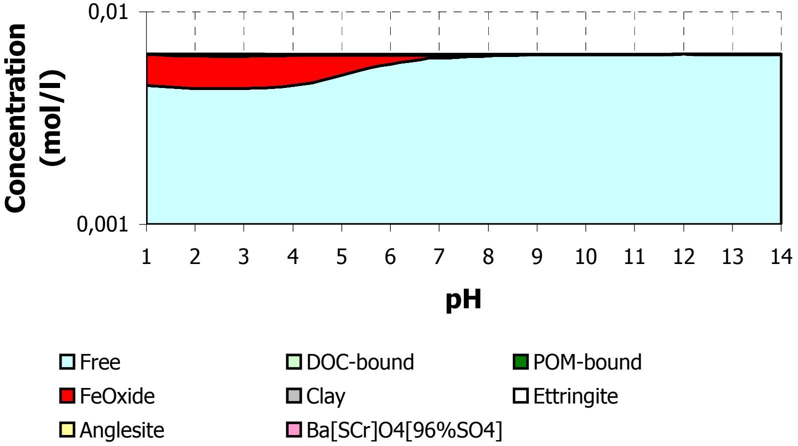
Partitioning liquid-solid, [SO4-2]

[H2CO3] as function of pH

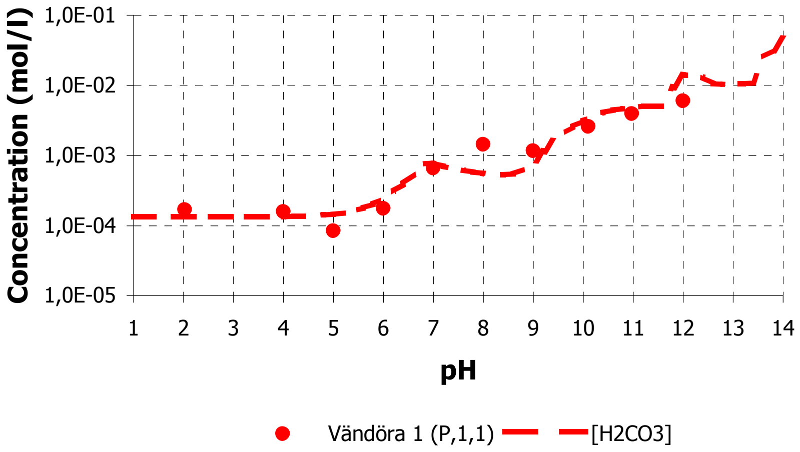

Partitioning liquid-solid, [H2CO3]

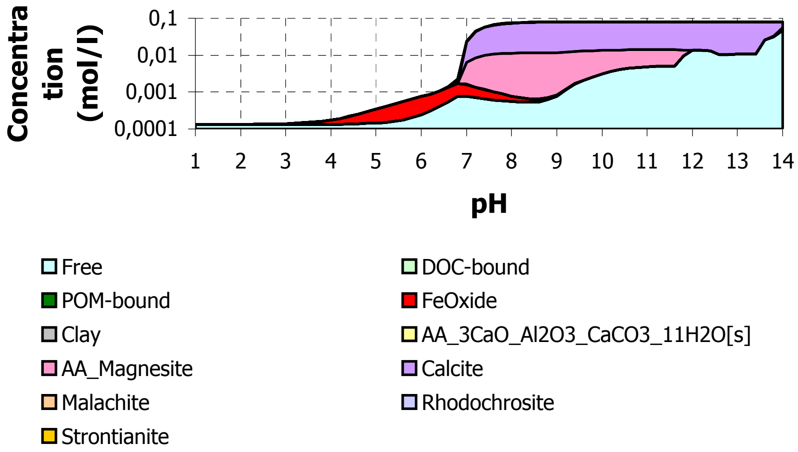

[Mg+2] as function of pH

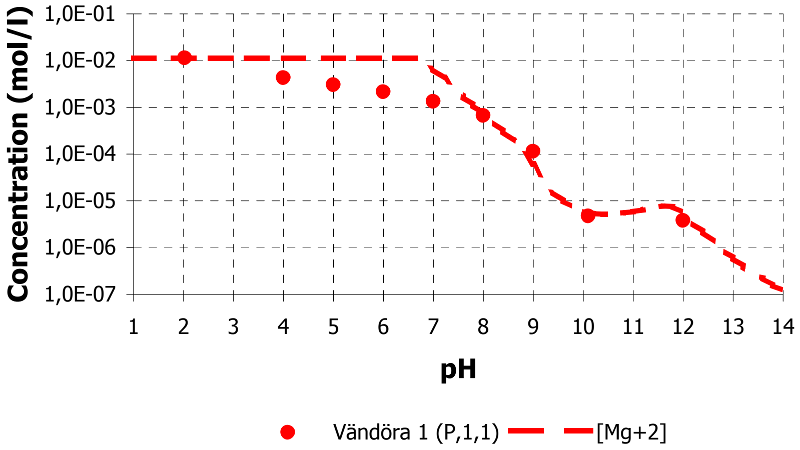

Partitioning liquid-solid, [Mg+2]

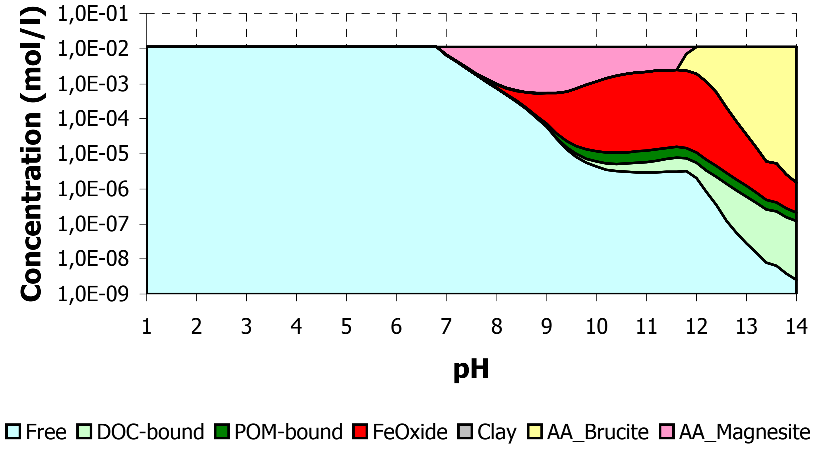

[PO4-3] as function of pH

Partitioning liquid-solid, [PO4-3]

[PO4-3] as function of pH

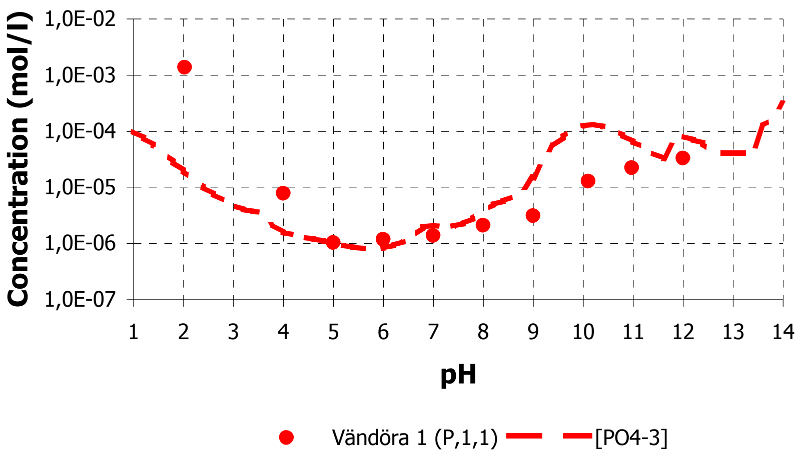

Partitioning liquid-solid, [PO4-3]

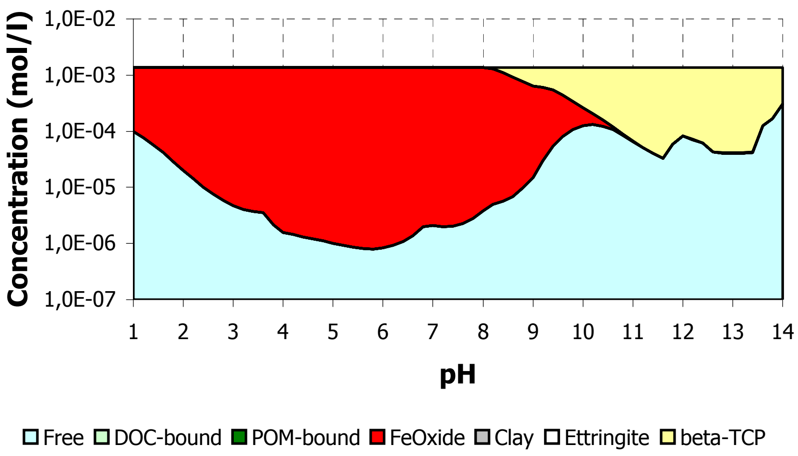

[Sr+2] as function of pH

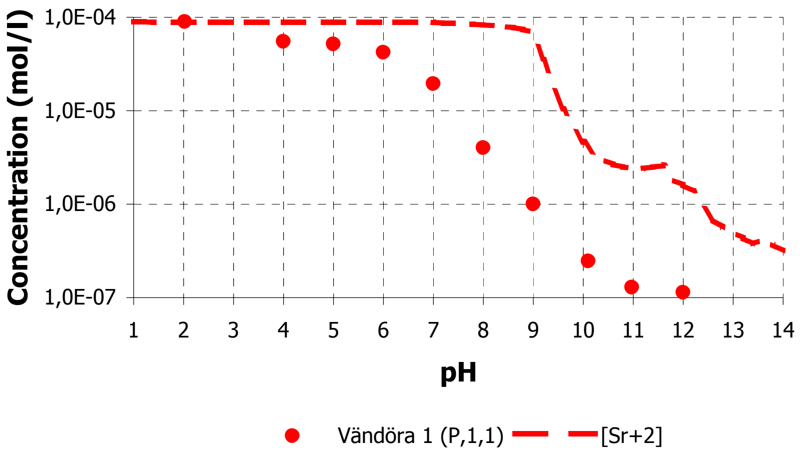

Partitioning liquid-solid, [Sr+2]

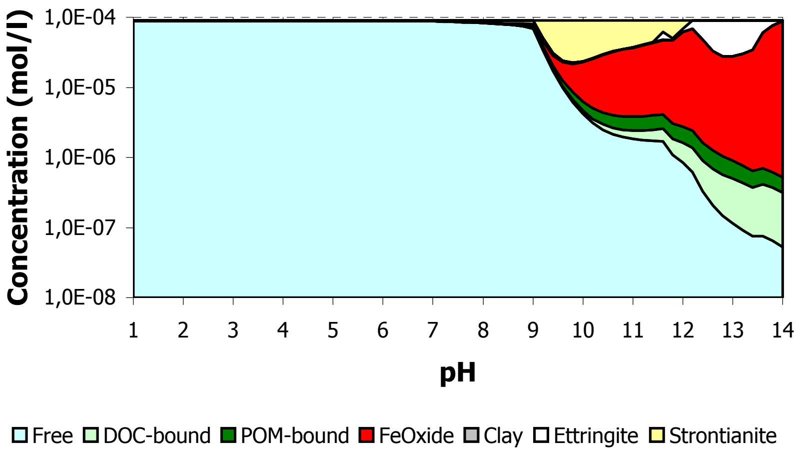

[Cd+2] as function of pH

Partitioning liquid-solid, [Cd+2]

[Cd+2] as function of pH

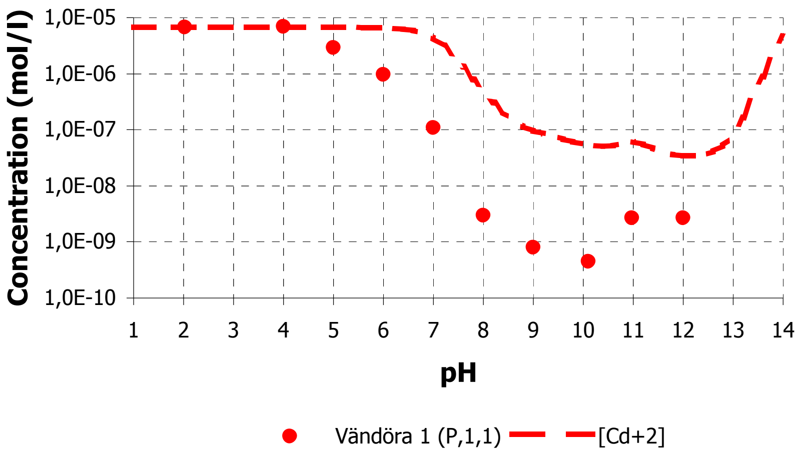

Partitioning liquid-solid, [Cd+2]

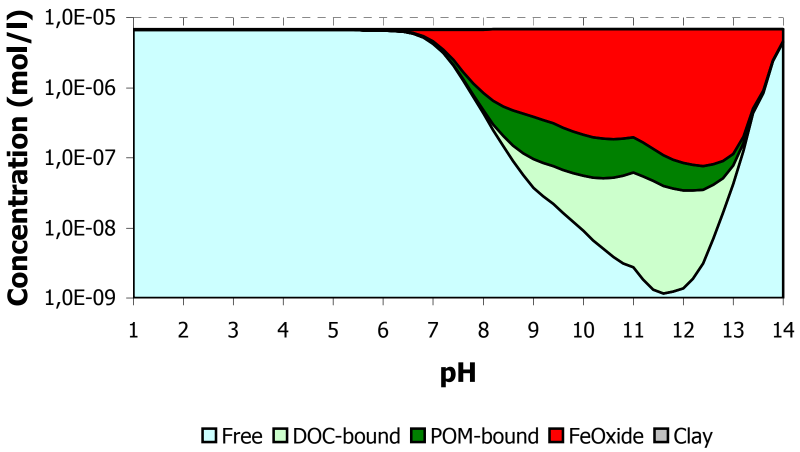

[Cu+2] as function of pH

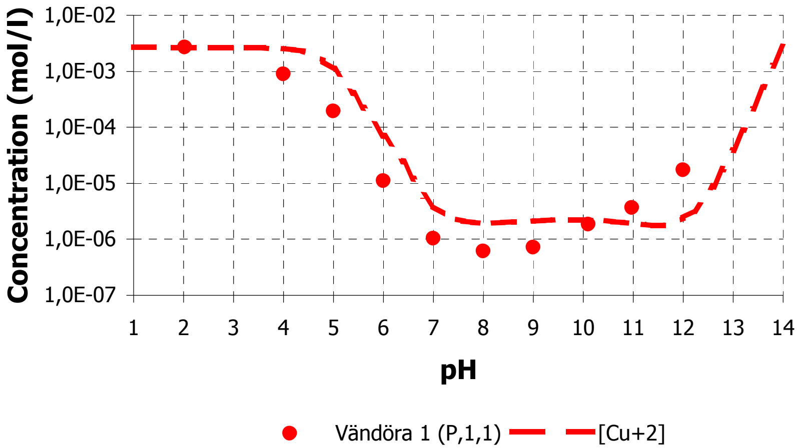

Partitioning liquid-solid, [Cu+2]

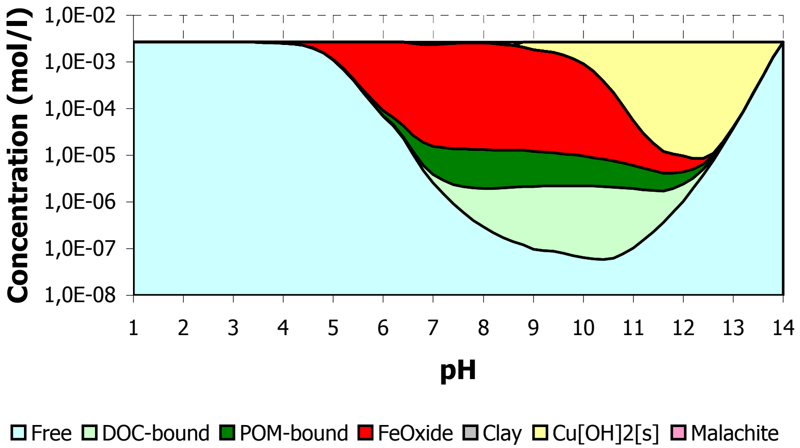

[Mn+2] as function of pH

Partitioning liquid-solid, [Mn+2]

[Mn+2] as function of pH

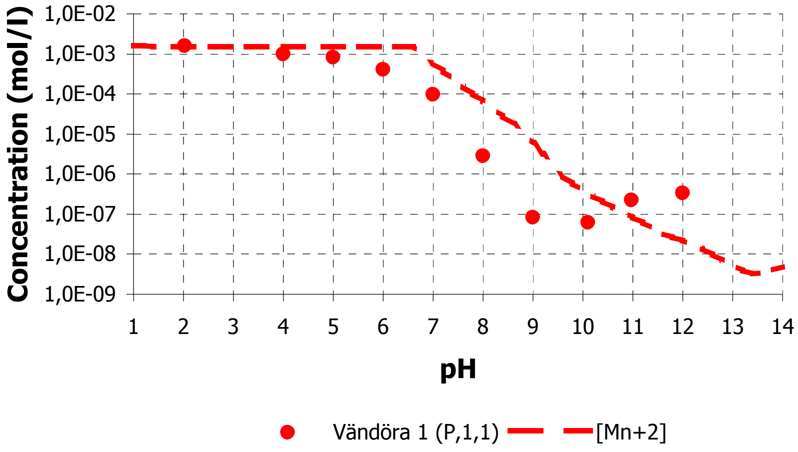

Partitioning liquid-solid, [Mn+2]

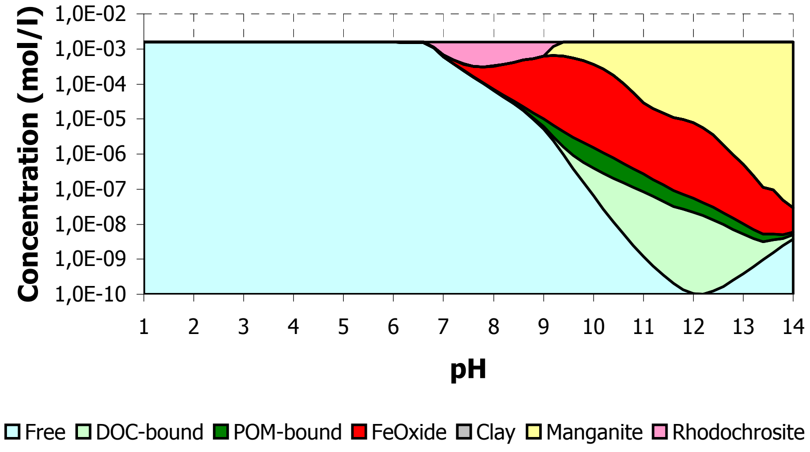

[Ni+2] as function of pH

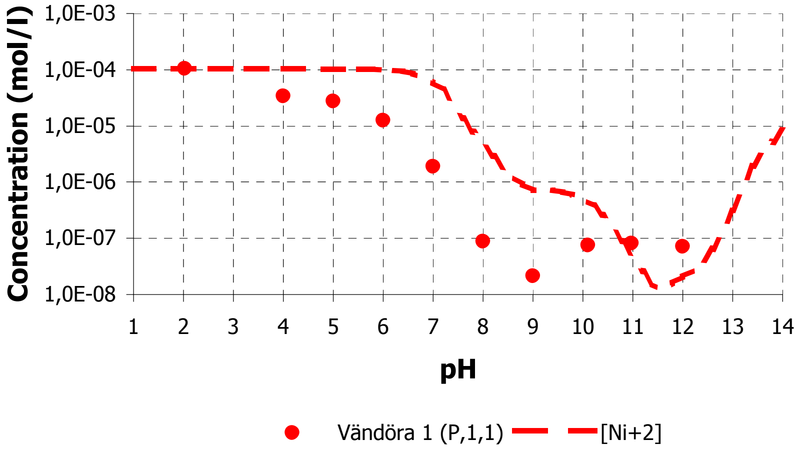

Partitioning liquid-solid, [Ni+2]

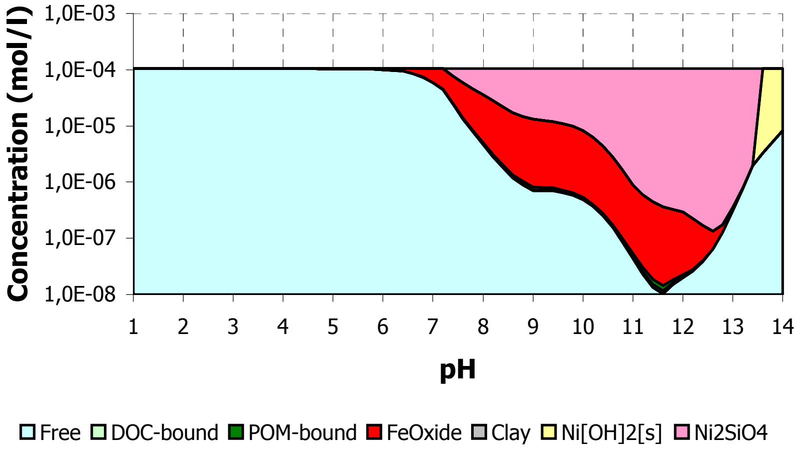

[Pb+2] as function of pH

Partitioning liquid-solid, [Pb+2]

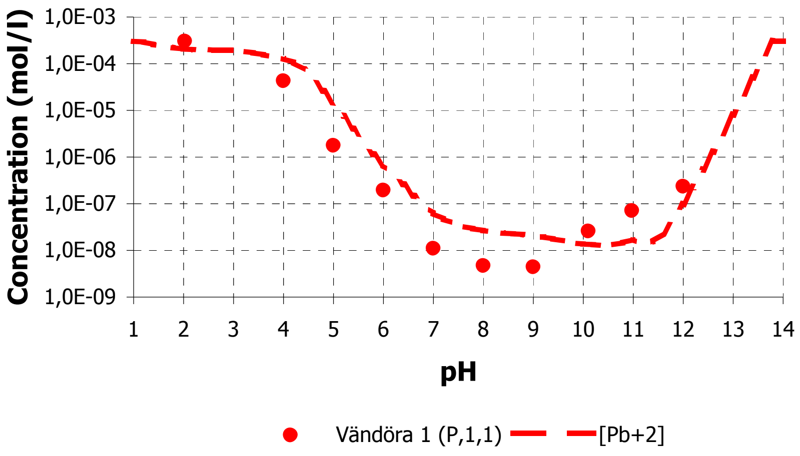
[Pb+2] as function of pH

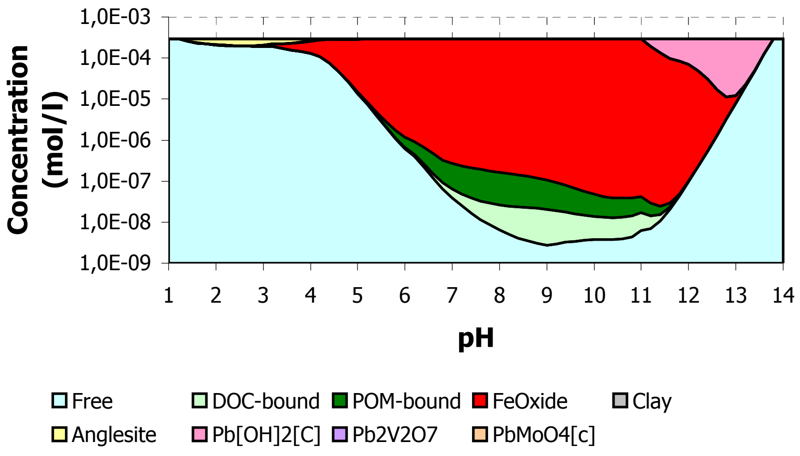
Partitioning liquid-solid, [Pb+2]

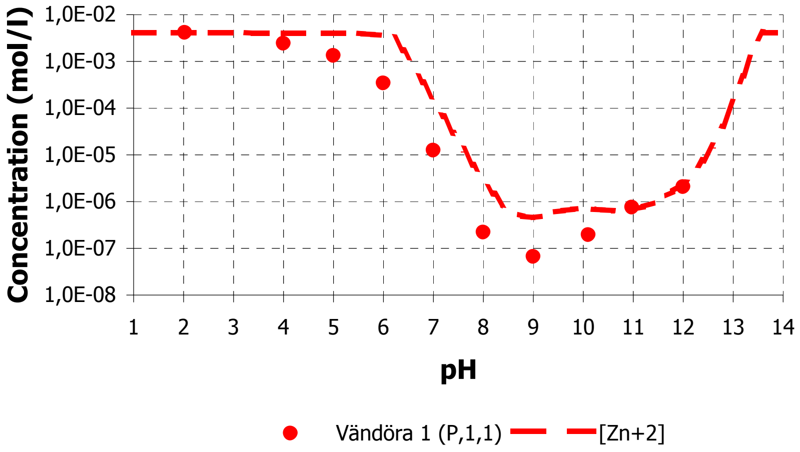
[Zn+2] as function of pH

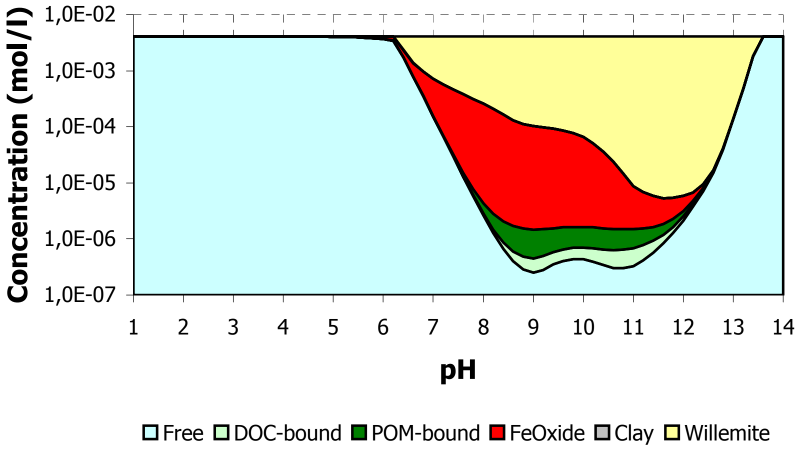
Partitioning liquid-solid, [Zn+2]

[CrO4-2] as function of pH

Partitioning liquid-solid, [CrO4-2]

[CrO4-2] as function of pH

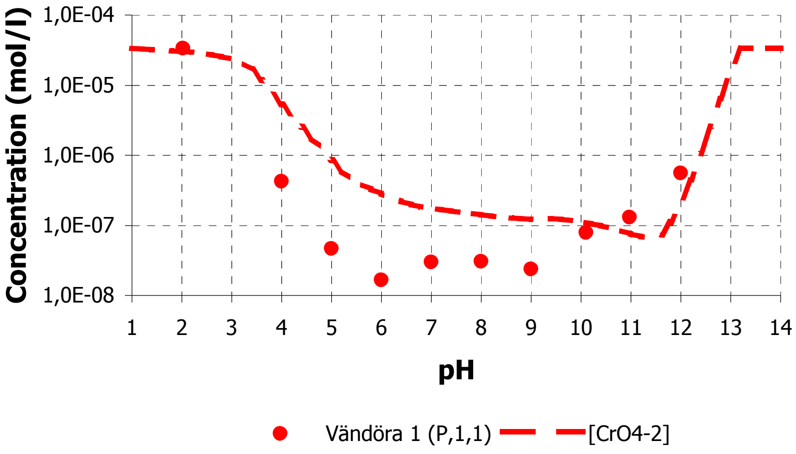

Partitioning liquid-solid, [CrO4-2]

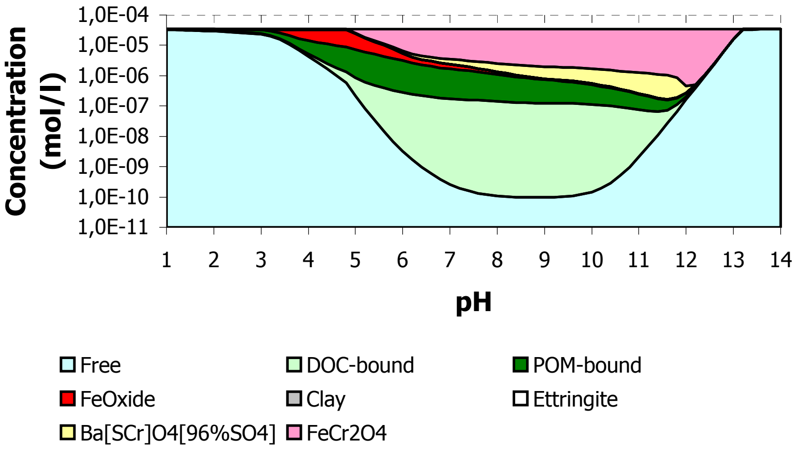

[H3AsO4] as function of pH

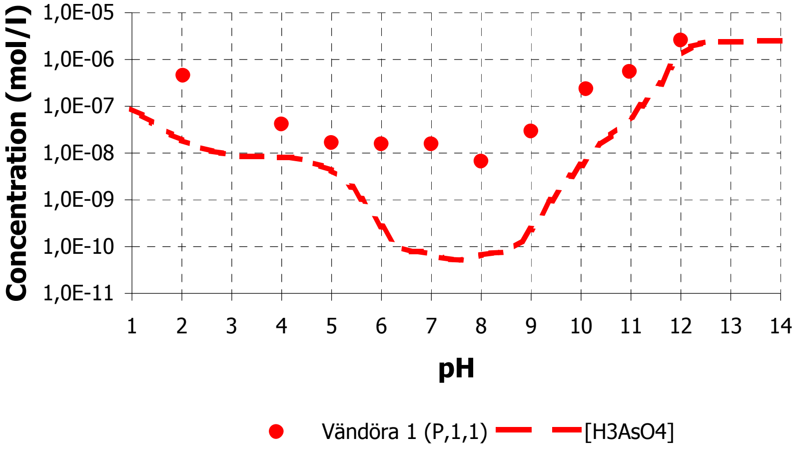

Partitioning liquid-solid, [H3AsO4]

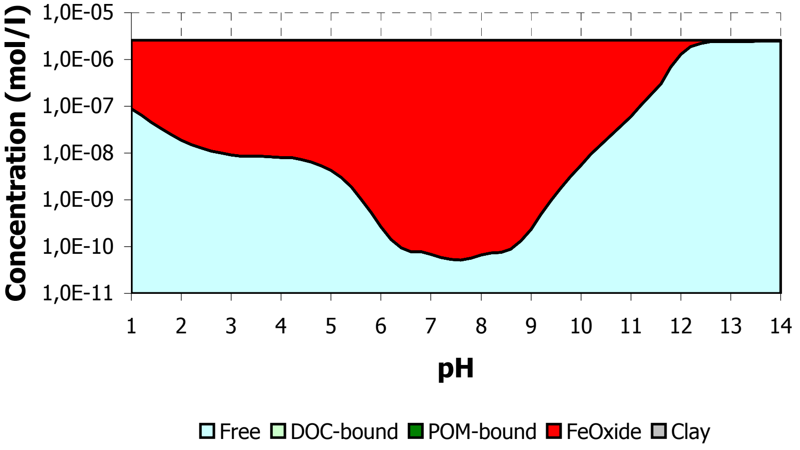

[H3BO3] as function of pH

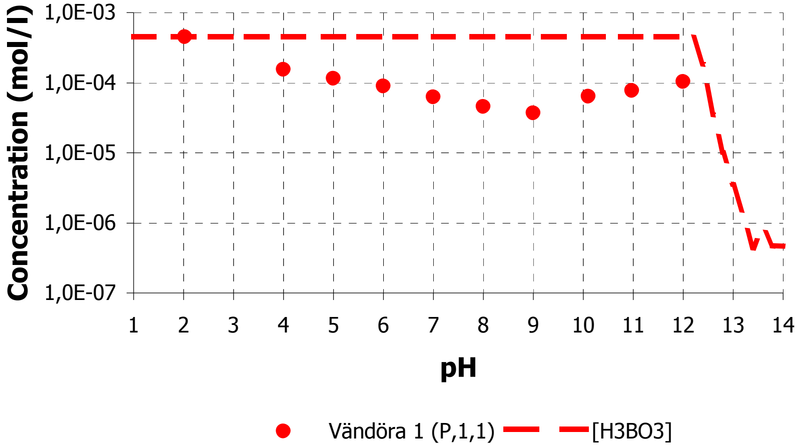

Partitioning liquid-solid, [H3BO3]

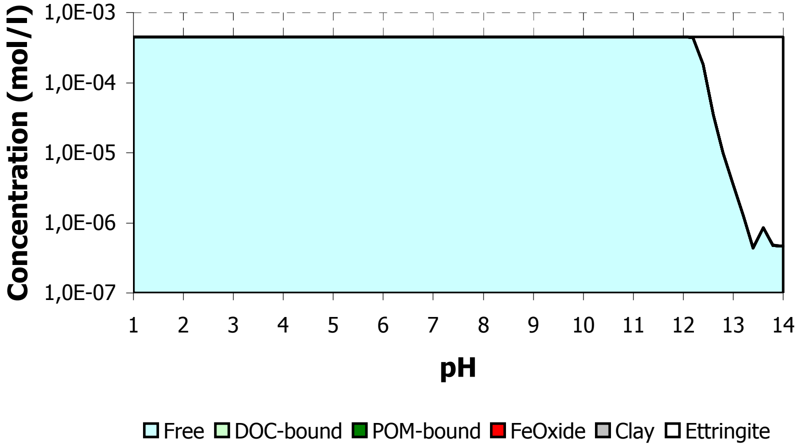

[MoO4-2] as function of pH

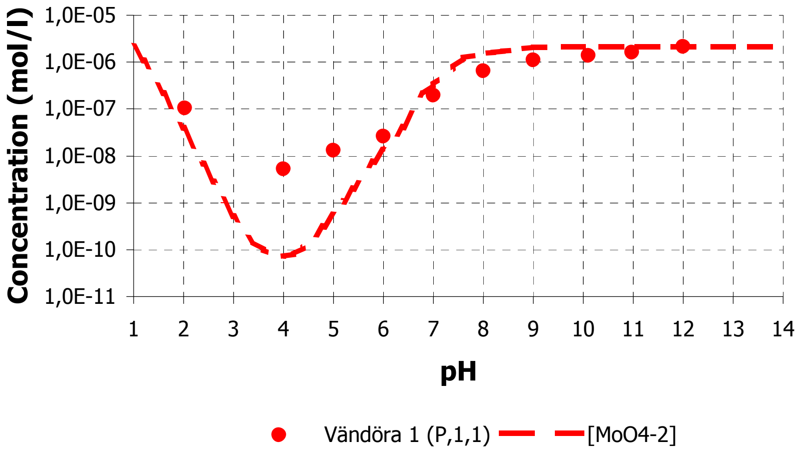

Partitioning liquid-solid, [MoO4-2]

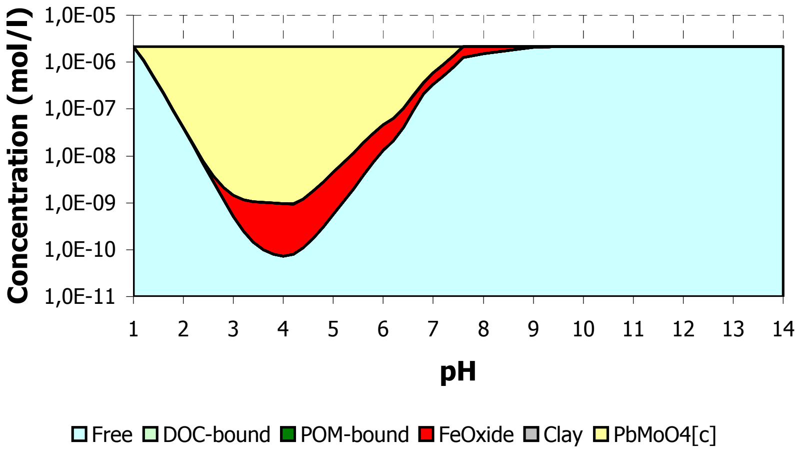

[Sb[OH]6-] as function of pH

Partitioning liquid-solid, [Sb[OH]6-]

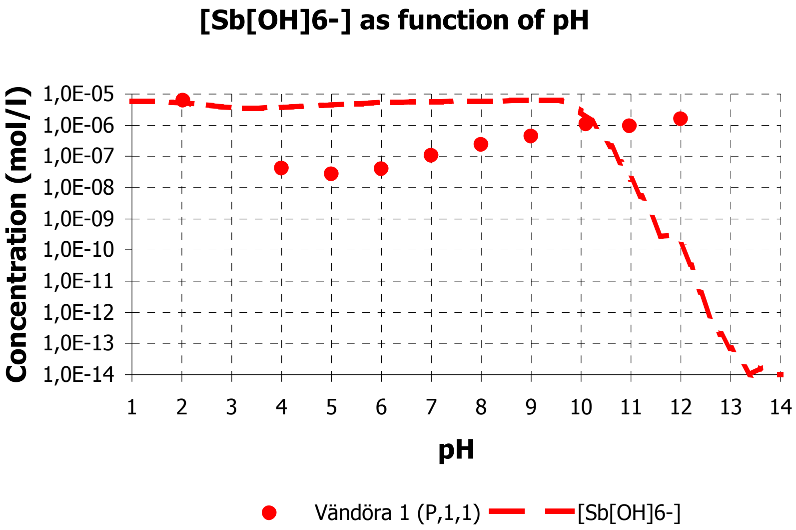

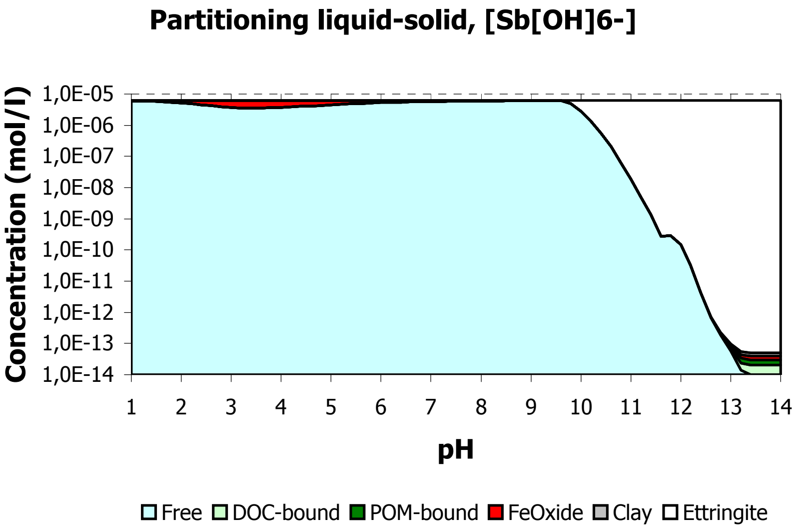

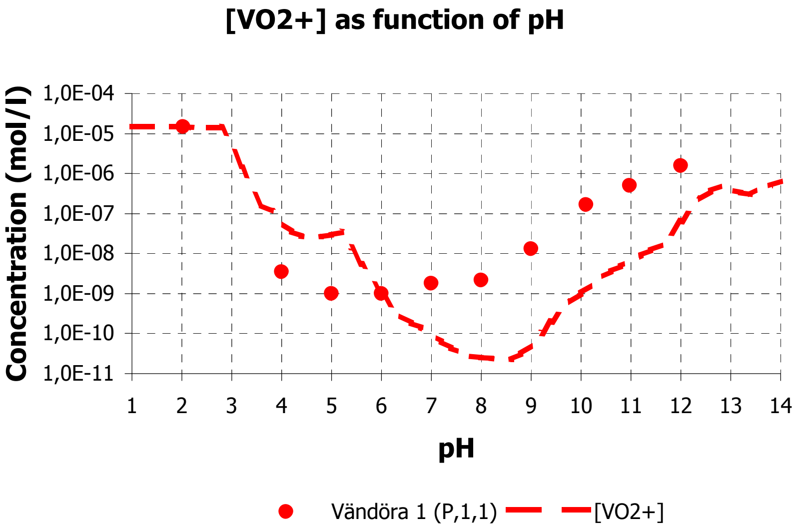

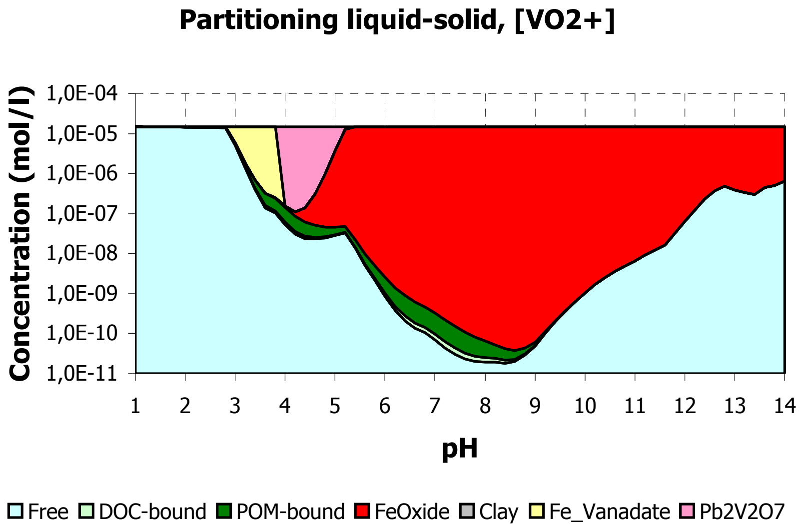

[Br-] as function of pH

Partitioning liquid-solid, [Br-]

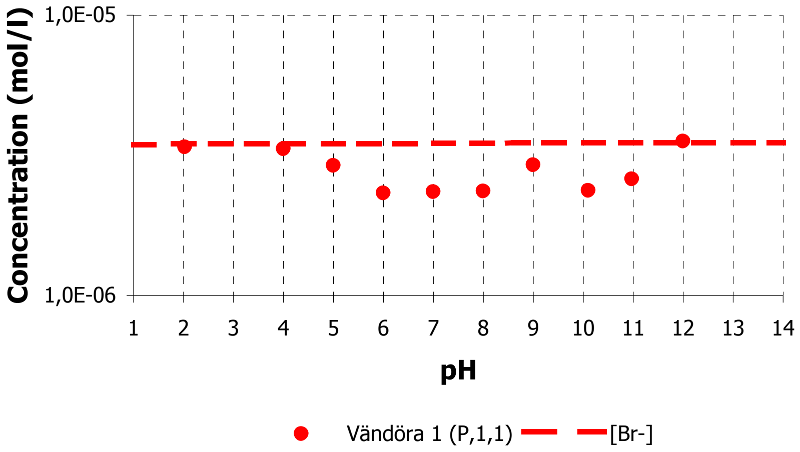

[Br-] as function of pH

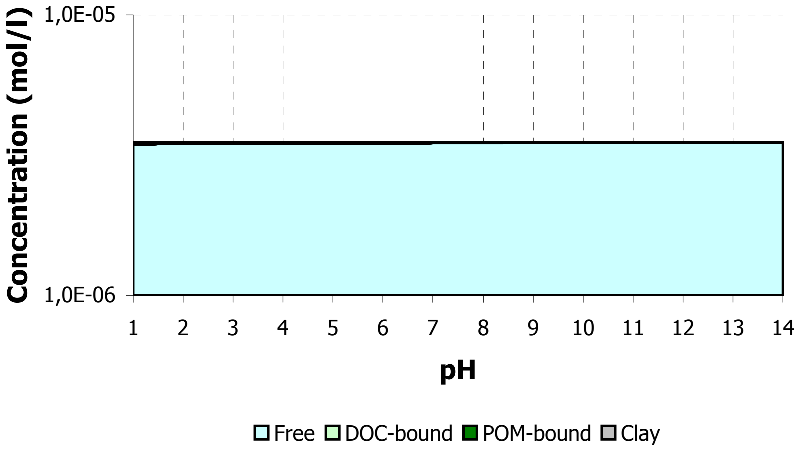

Partitioning liquid-solid, [Br-]

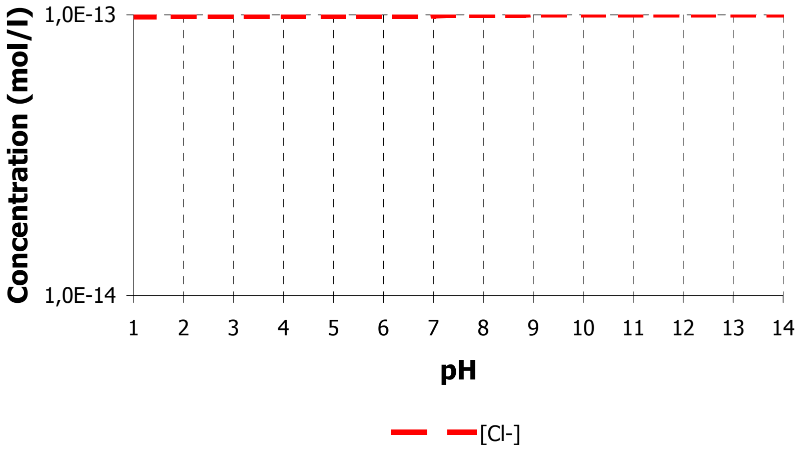

[Cl-] as function of pH

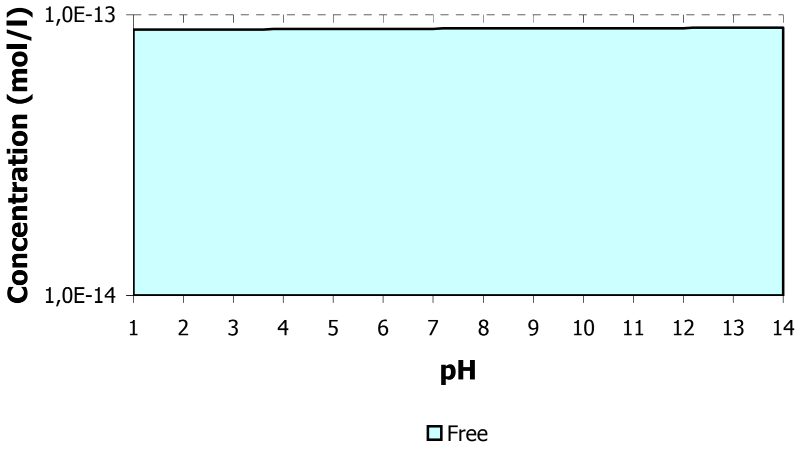

Partitioning liquid-solid, [Cl-]

[F-] as function of pH

Partitioning liquid-solid, [F-]

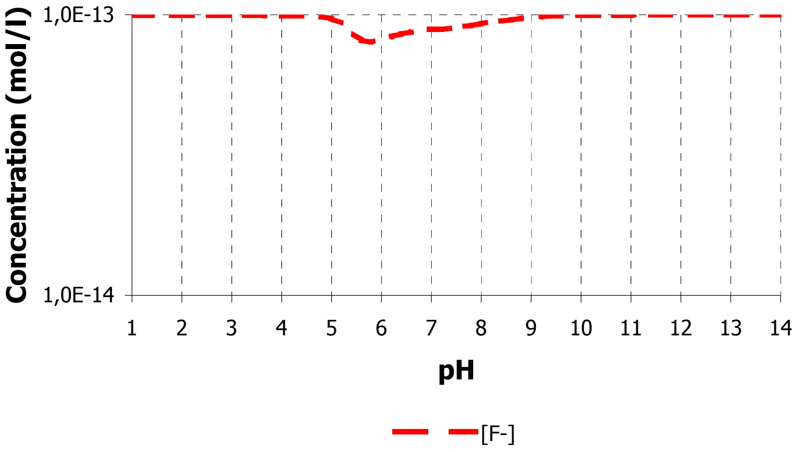

[F-] as function of pH

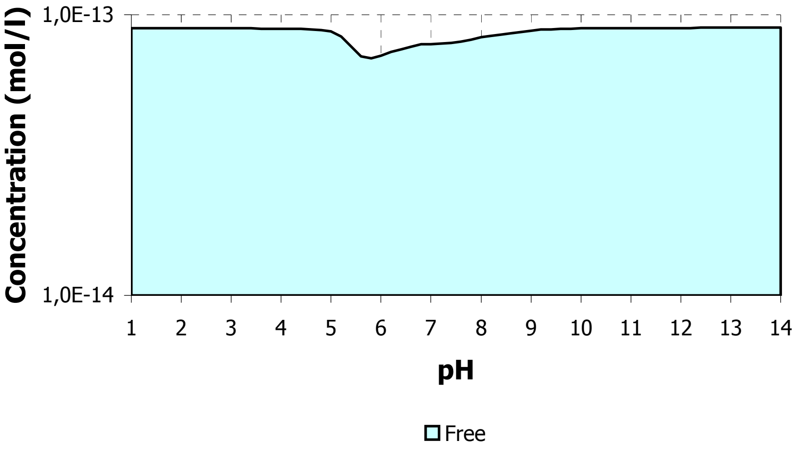

Partitioning liquid-solid, [F-]

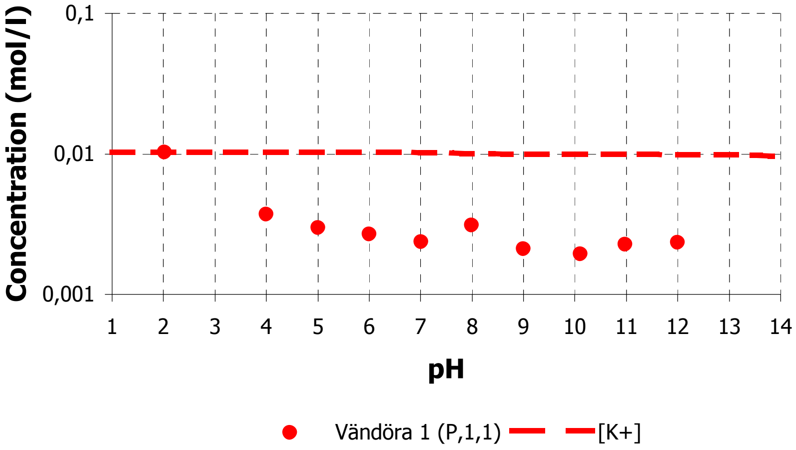

[K+] as function of pH

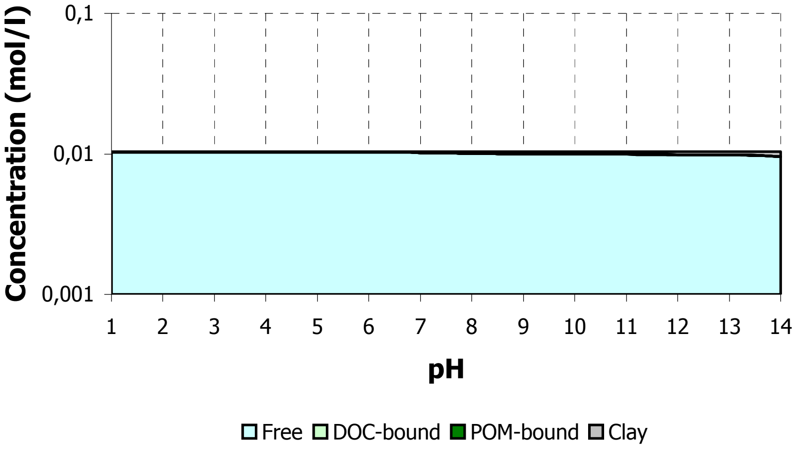

Partitioning liquid-solid, [K+]

[Li+] as function of pH

Partitioning liquid-solid, [Li+]

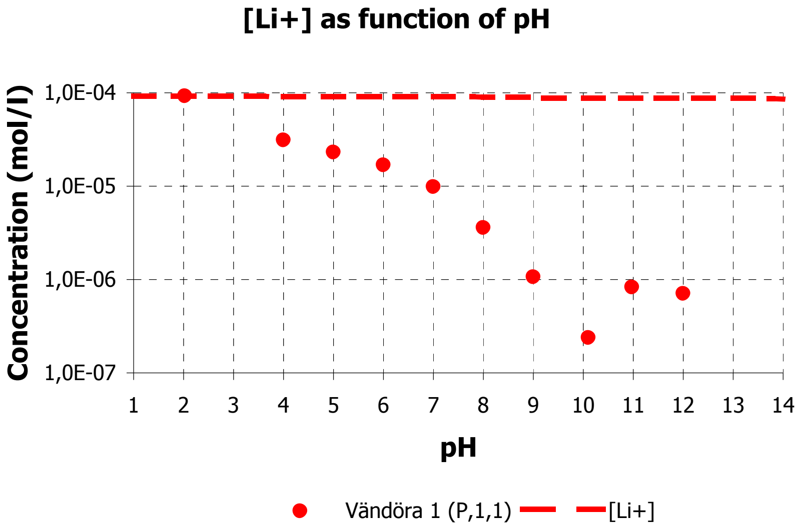
[Li+] as function of pH

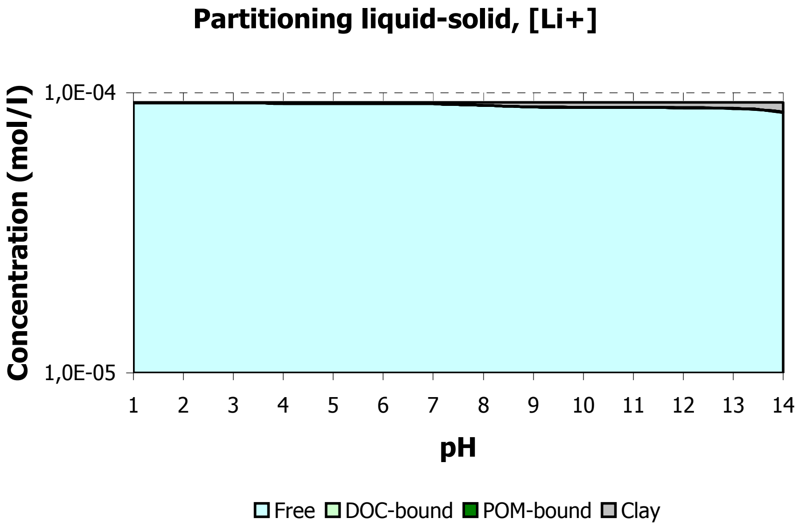
Partitioning liquid-solid, [Li+]

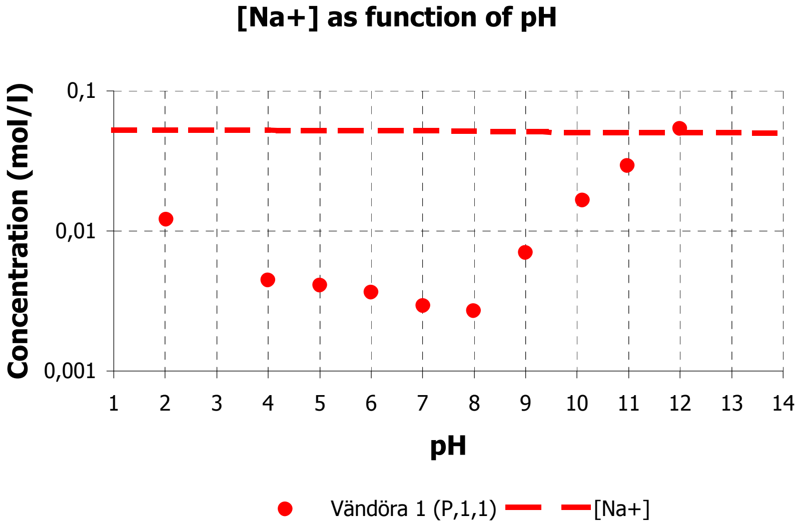
[Na+] as function of pH

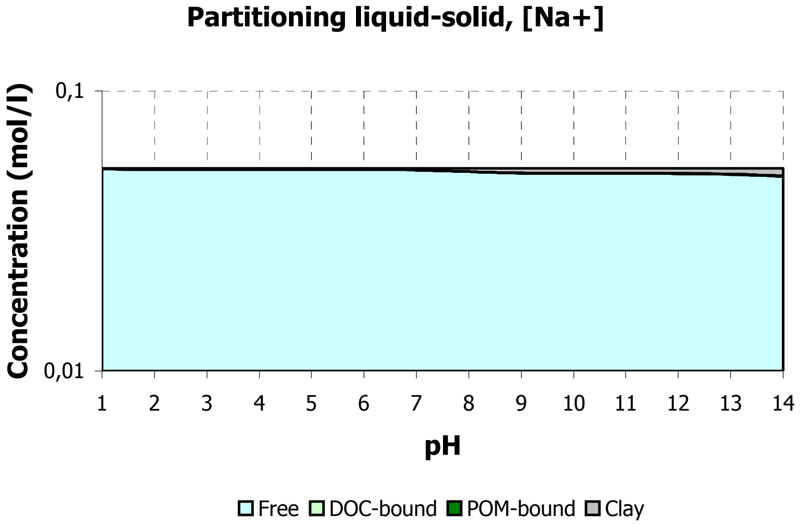
Partitioning liquid-solid, [Na+]

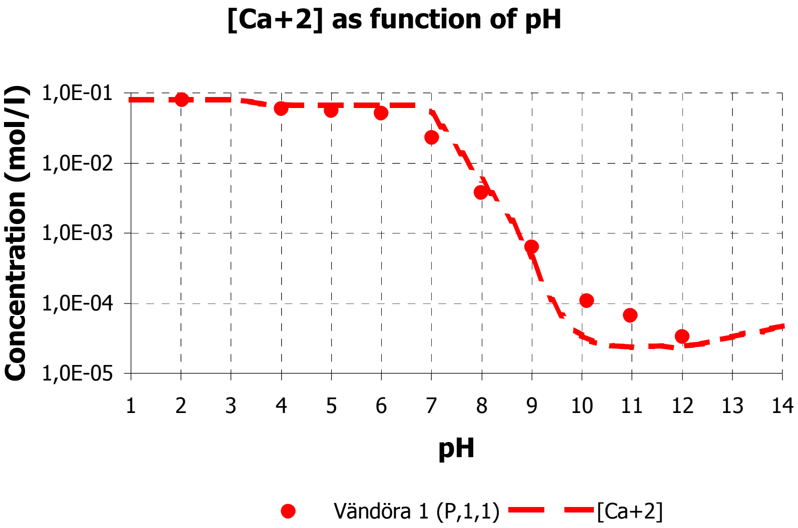
[Ca+2] as function of pH

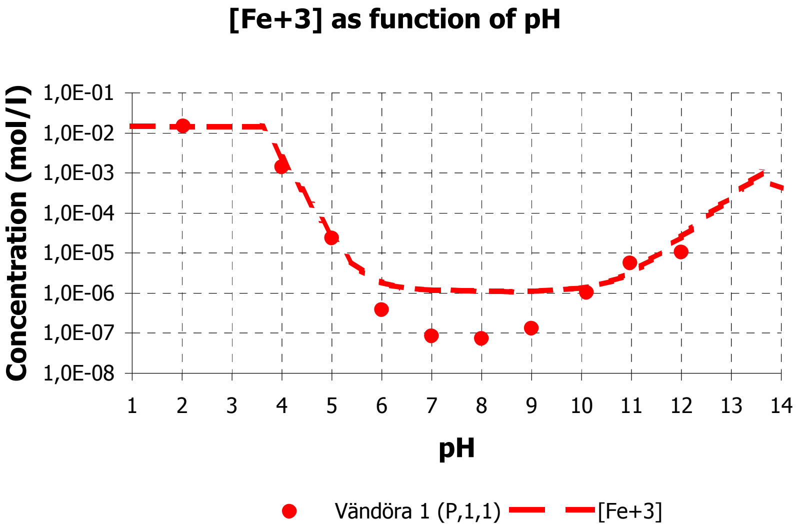
[Fe+3] as function of pH

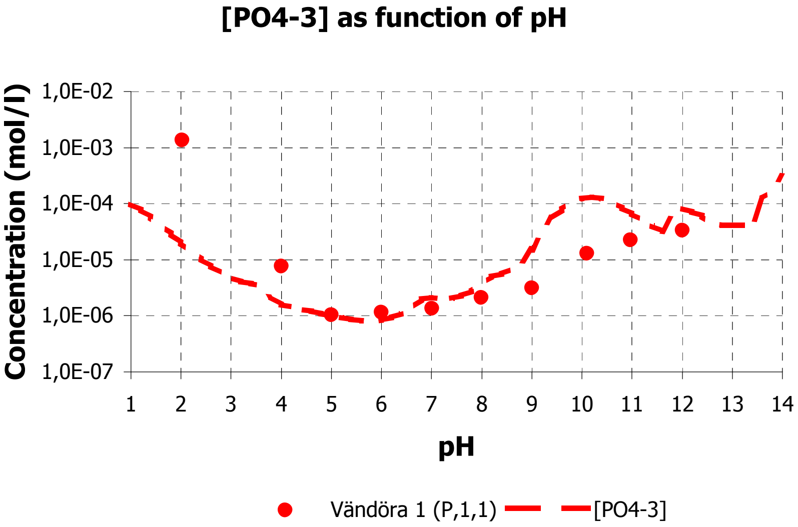
[PO4-3] as function of pH

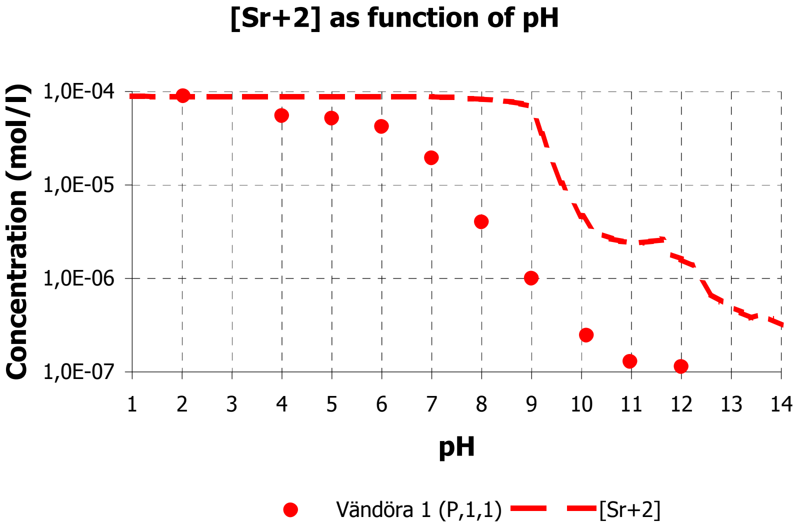
[Sr+2] as function of pH

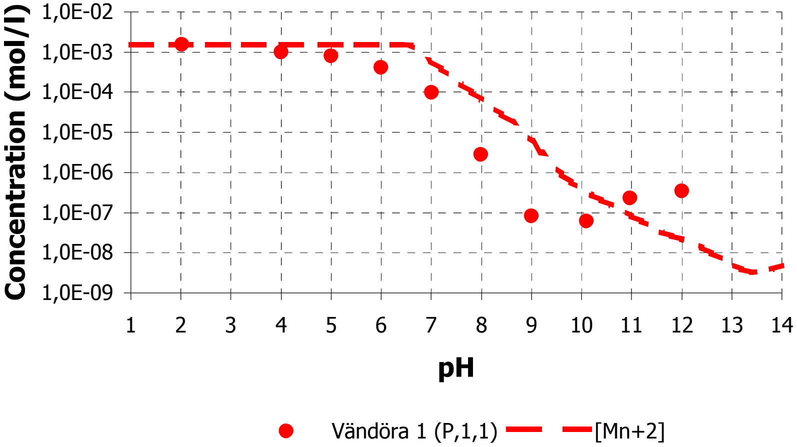
[Mn+2] as function of pH

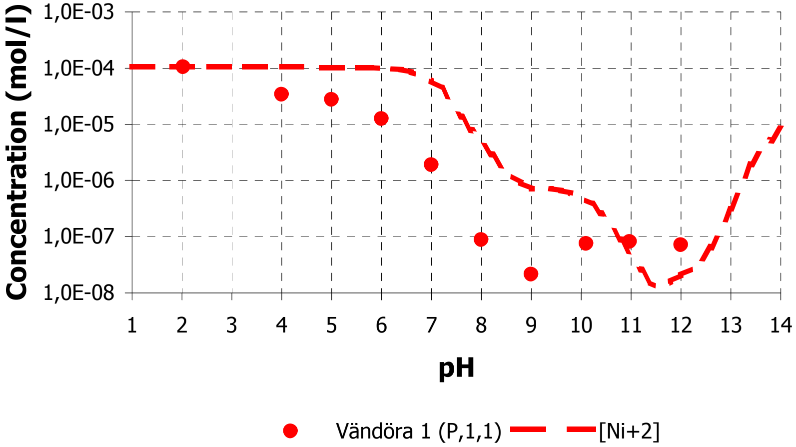
[Ni+2] as function of pH

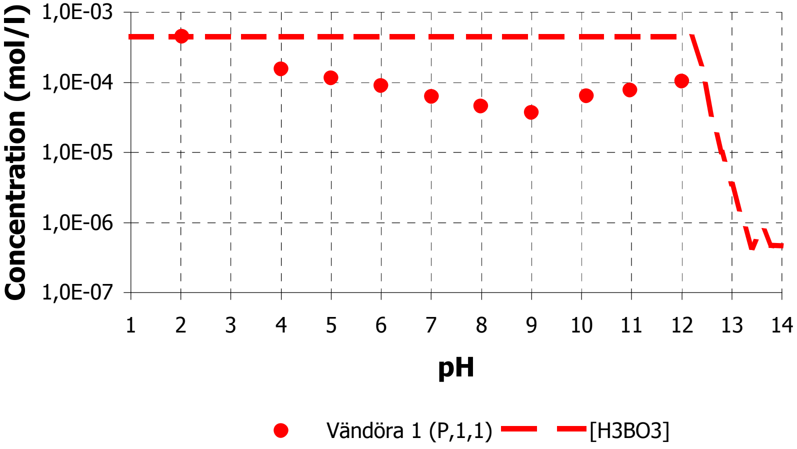
[H3BO3] as function of pH

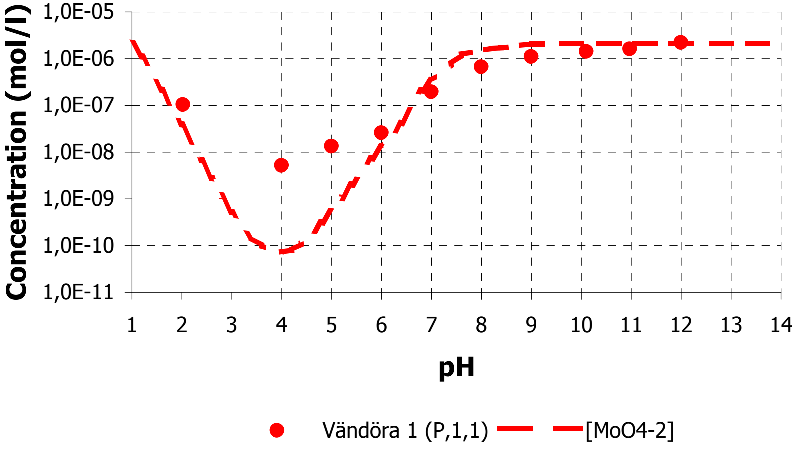
[MoO4-2] as function of pH

[F-] as function of pH

[K+] as function of pH

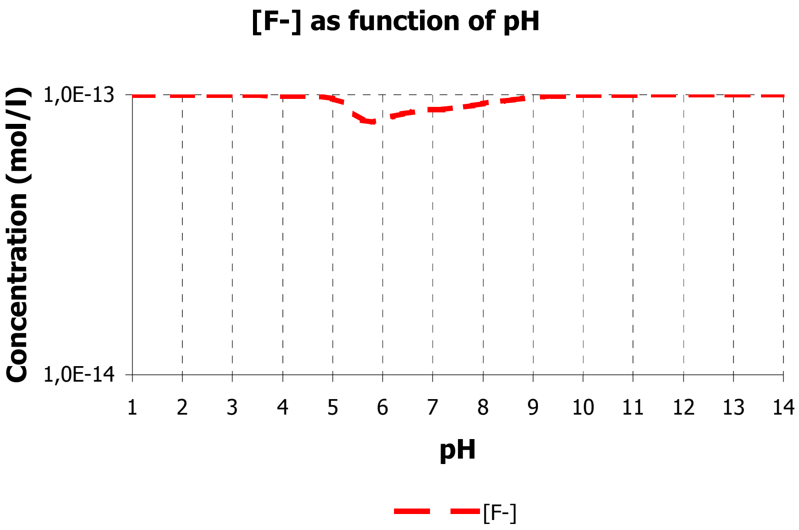
[F-] as function of pH
Concentration (mol/l)
1,0E-13
1,0E-14
1
2
3
4
5
6
7
8
9
10
11
12
13
14
pH
[F-]

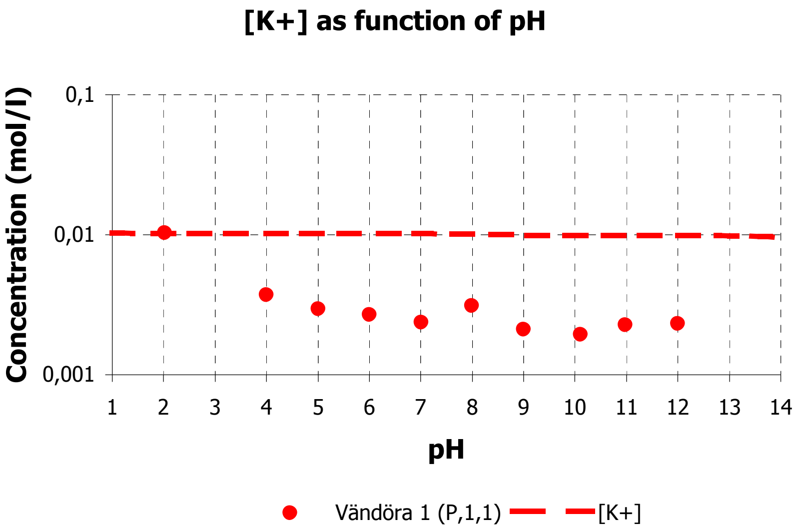
[K+] as function of pH
Concentration (mol/l)
0,1
0,01
0,001
1
2
3
4
5
6
7
8
9
10
11
12
13
14
pH
Vändöra 1 (P,1,1)
[K+]

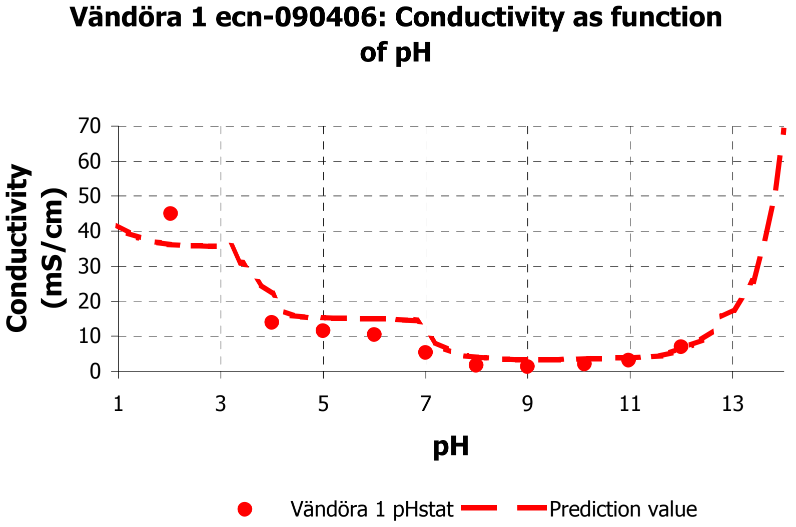
Vändöra 1 ecn-090406: Conductivity as function of pH
Conductivity (mS/cm)
70
60
50
40
30
20
10
0
1
3
5
7
9
11
13
pH
Vändöra 1 pHstat
Prediction value

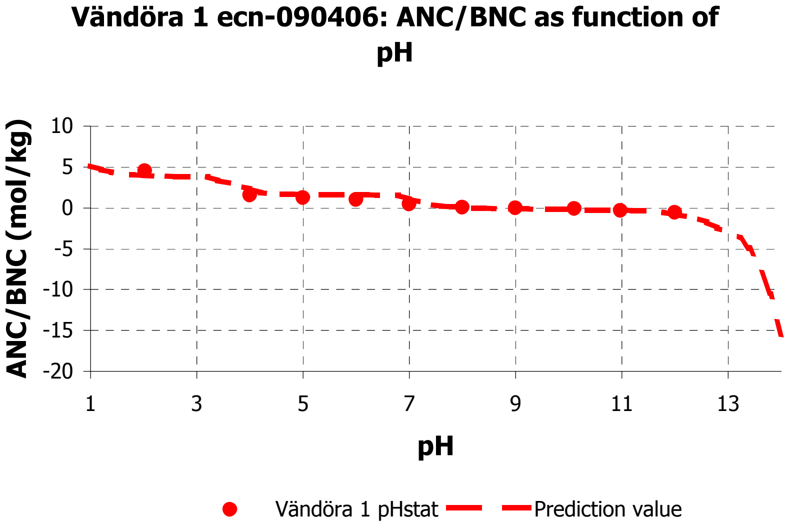
Vändöra 1 ecn-090406: ANC/BNC as function of pH
ANC/BNC (mol/kg)
10
5
0
-5
-10
-15
-20
1
3
5
7
9
11
13
pH
Vändöra 1 pHstat
Prediction value

Al+3 fractionation in solution

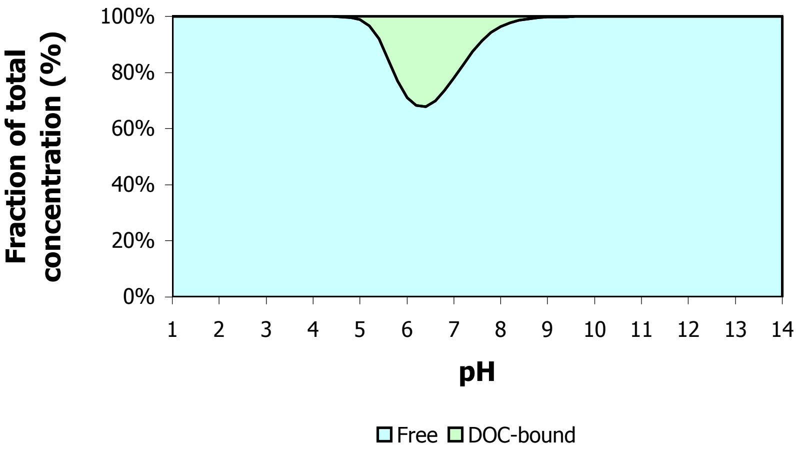

Al+3 fractionation in the solid phase

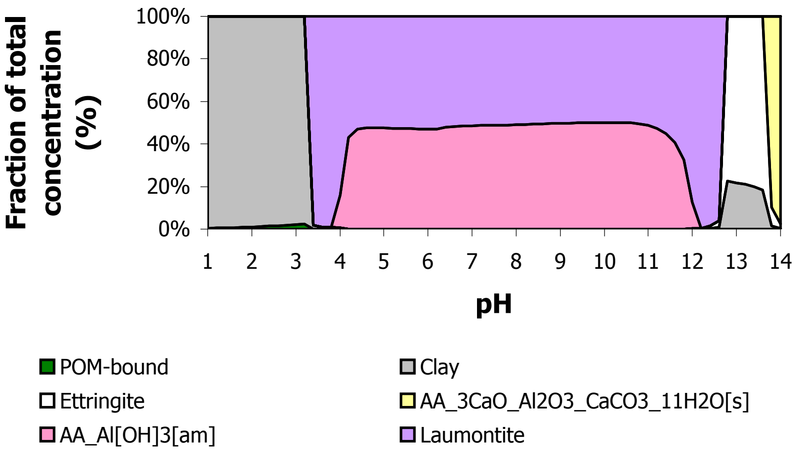

Ba+2 fractionation in solution

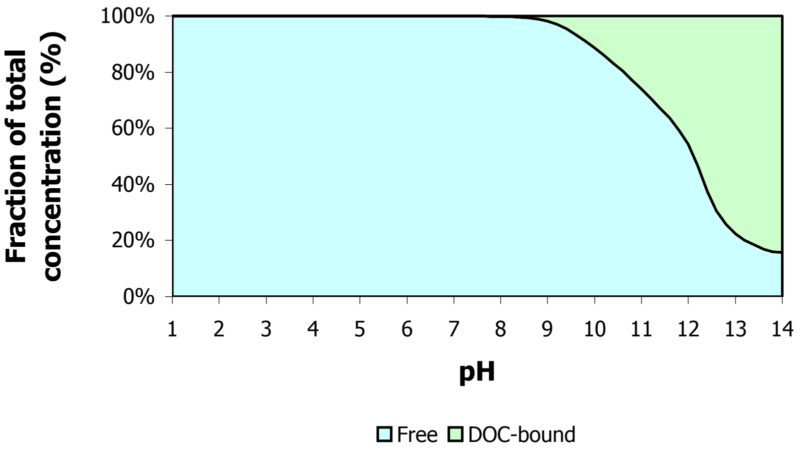

Ba+2 fractionation in the solid phase

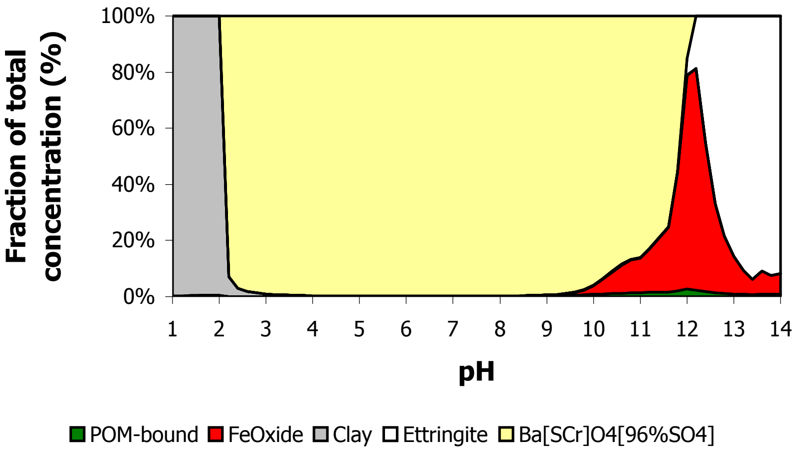

Ca+2 fractionation in solution

Ca+2 fractionation in the solid phase

Ca+2 fractionation in solution

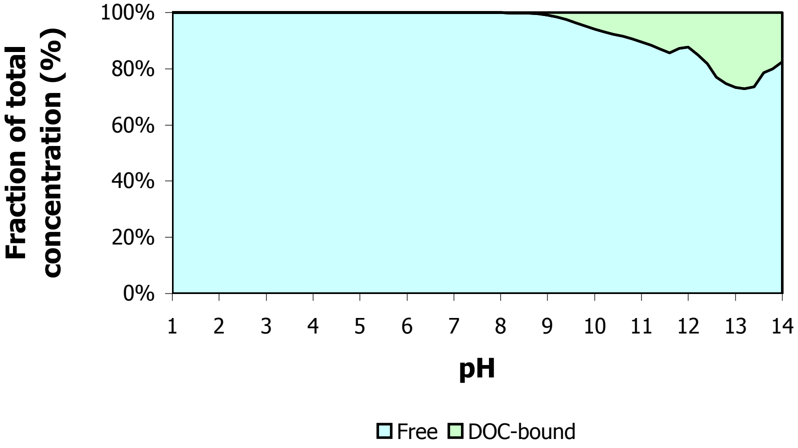

Ca+2 fractionation in the solid phase

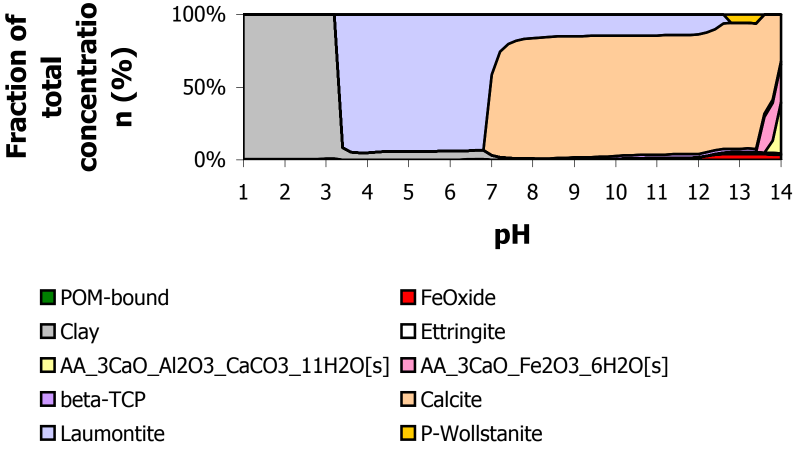

Fe+3 fractionation in solution

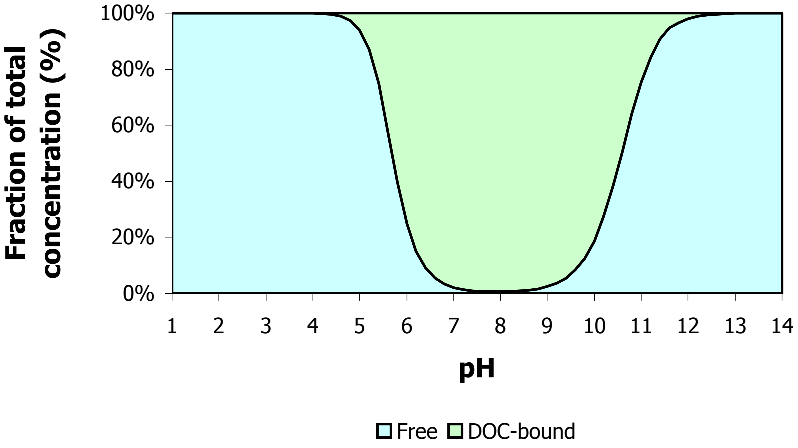

Fe+3 fractionation in the solid phase

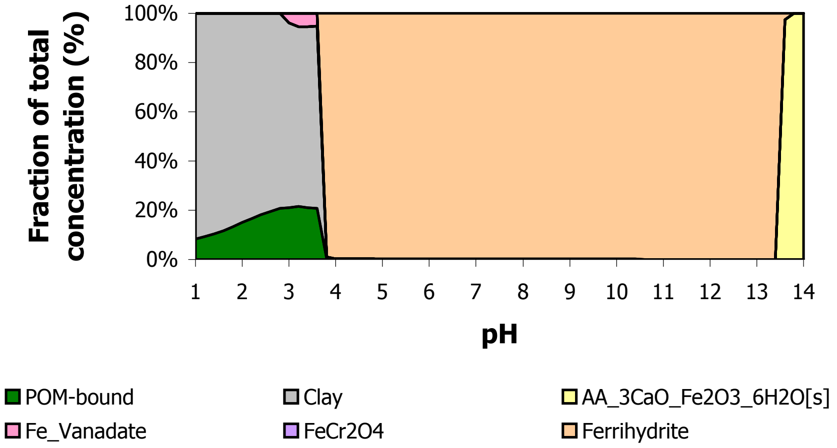

H4SiO4 fractionation in solution

H4SiO4 fractionation in the solid phase

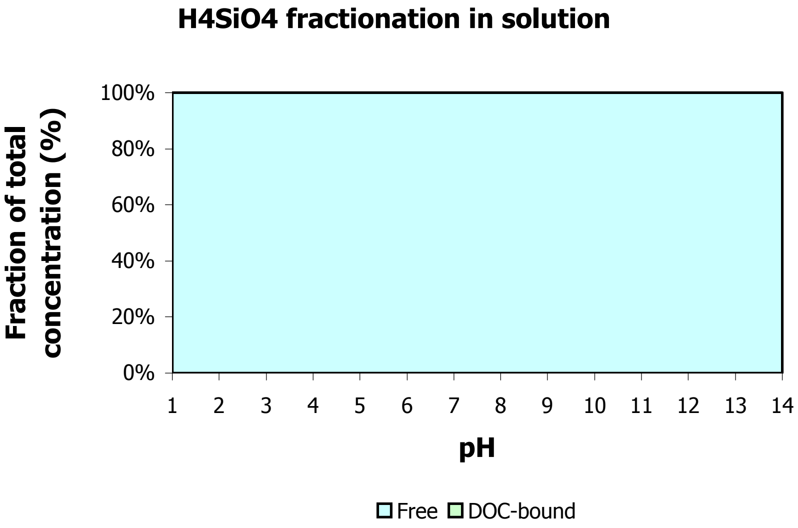
H4SiO4 fractionation in solution

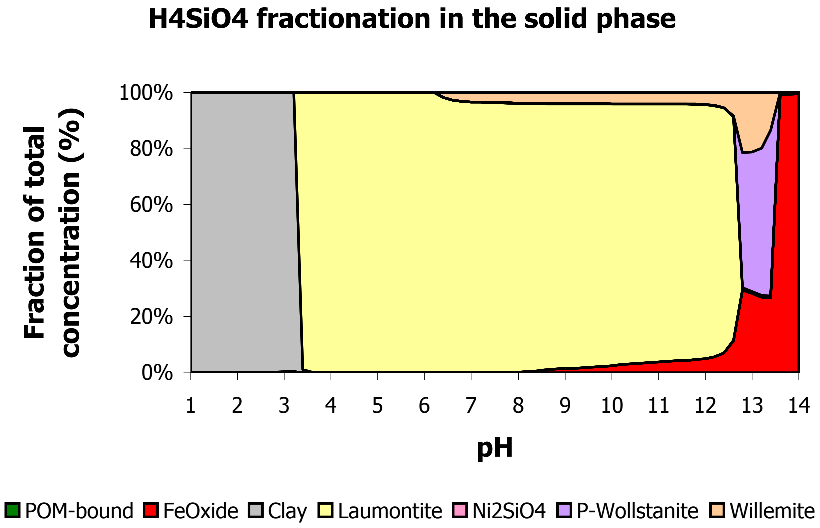
H4SiO4 fractionation in the solid phase

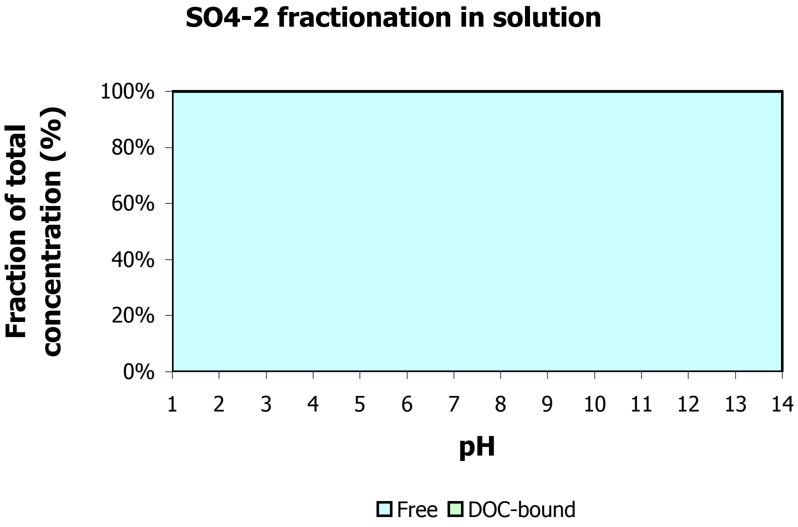
SO4-2 fractionation in solution

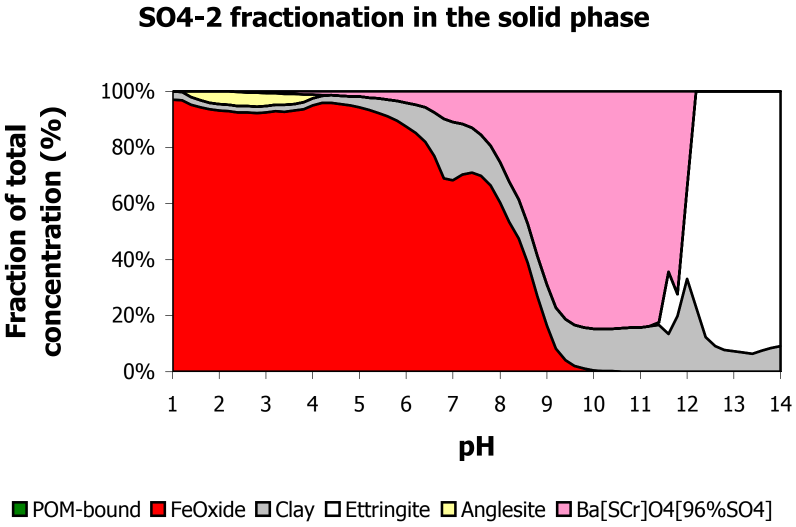
SO4-2 fractionation in the solid phase

H2CO3 fractionation in solution

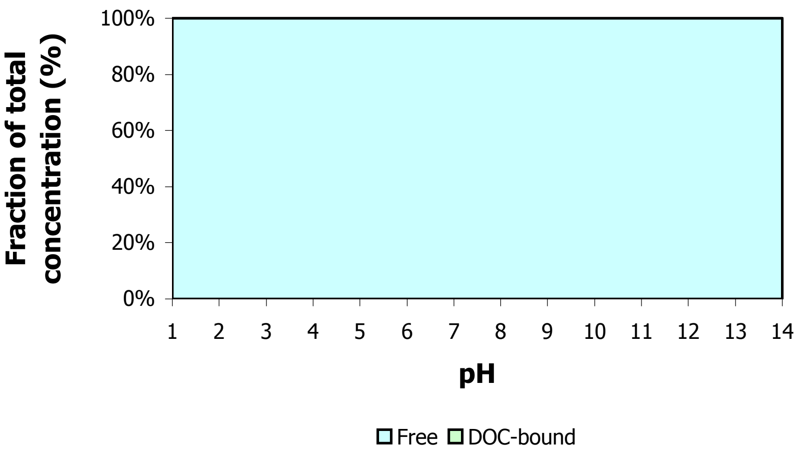

H2CO3 fractionation in the solid phase

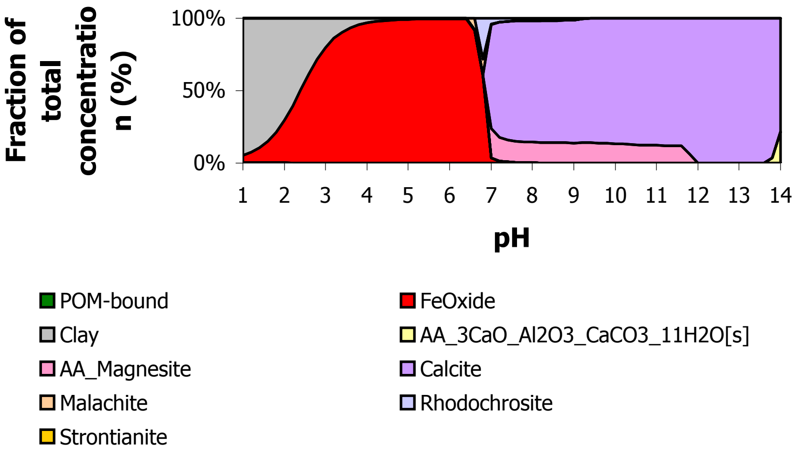

Mg+2 fractionation in solution

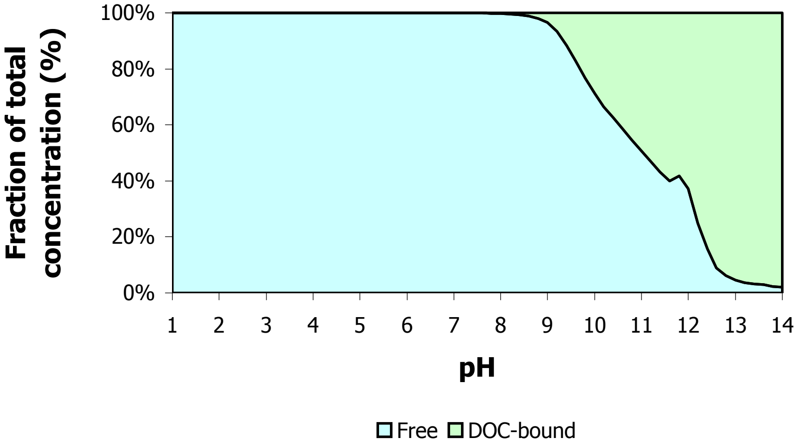

Mg+2 fractionation in the solid phase

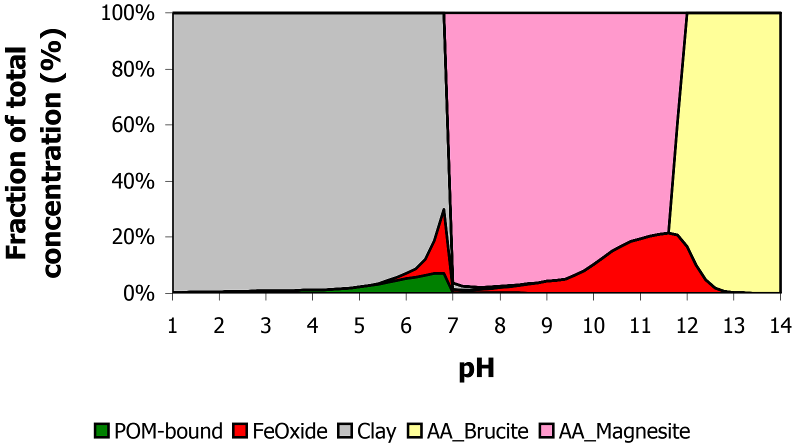

PO4-3 fractionation in solution

PO4-3 fractionation in the solid phase

PO4-3 fractionation in solution

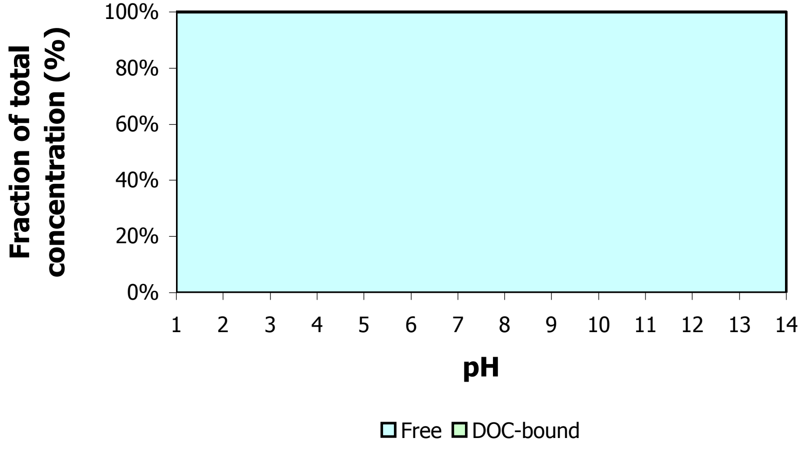

PO4-3 fractionation in the solid phase

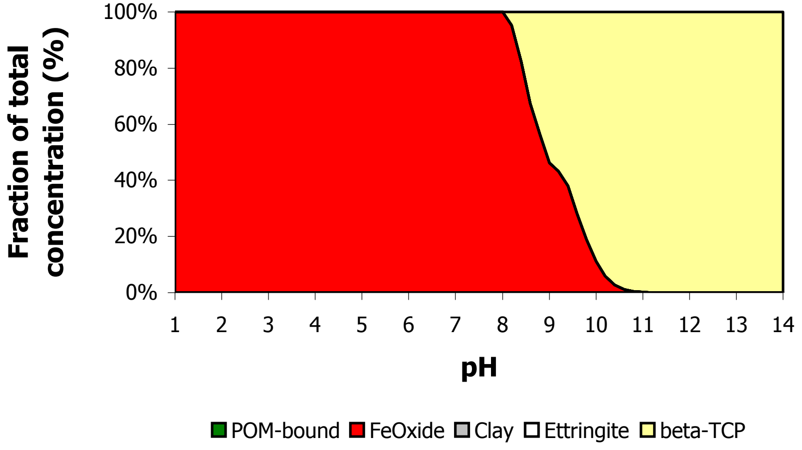

Sr+2 fractionation in solution

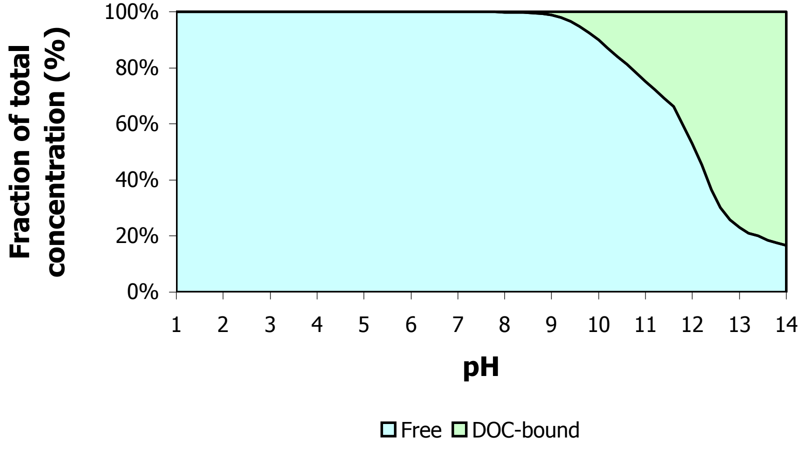

Sr+2 fractionation in the solid phase

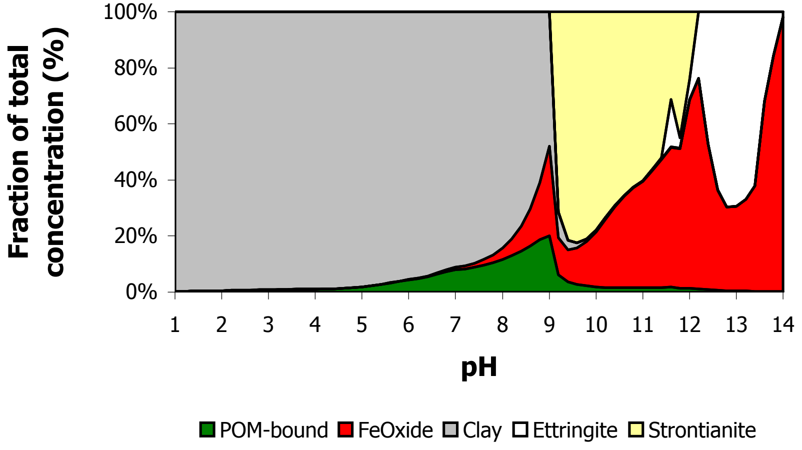

Cd+2 fractionation in solution

Cd+2 fractionation in the solid phase

Cd+2 fractionation in solution

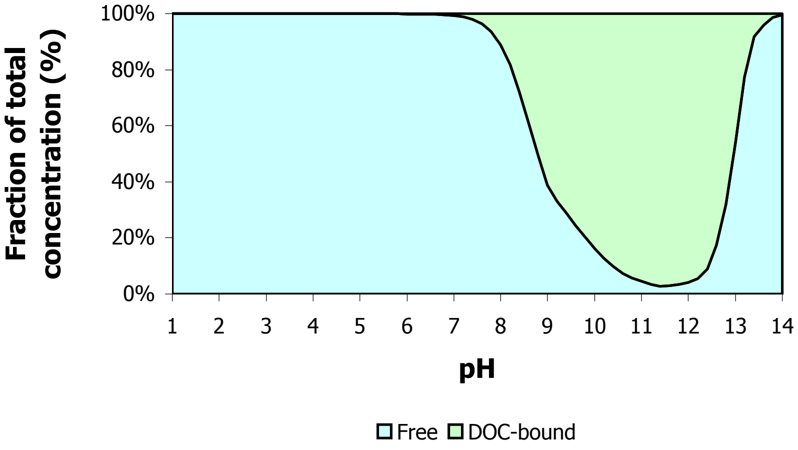

Cd+2 fractionation in the solid phase

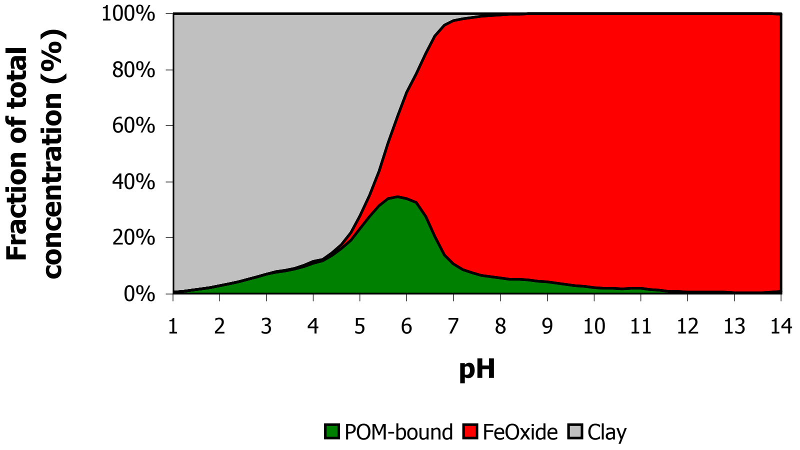

Cu+2 fractionation in solution

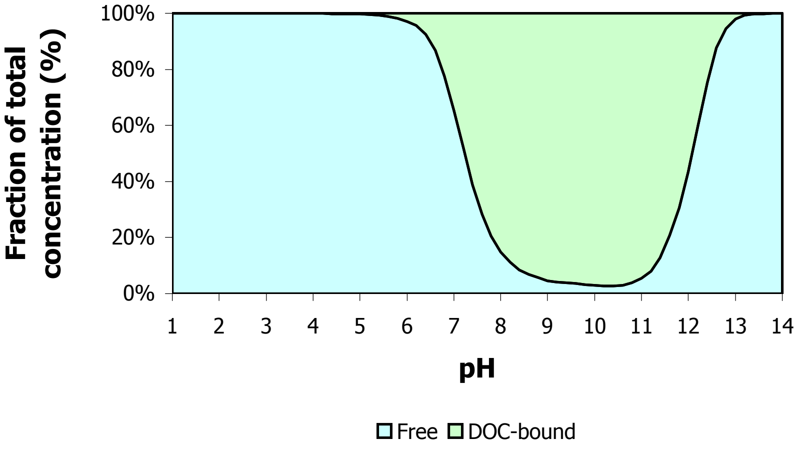

Cu+2 fractionation in the solid phase

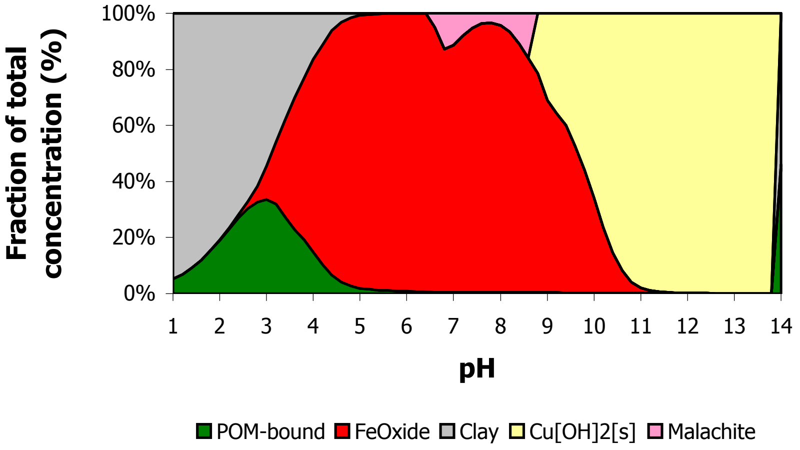

Mn+2 fractionation in solution

Mn+2 fractionation in the solid phase

Mn+2 fractionation in solution

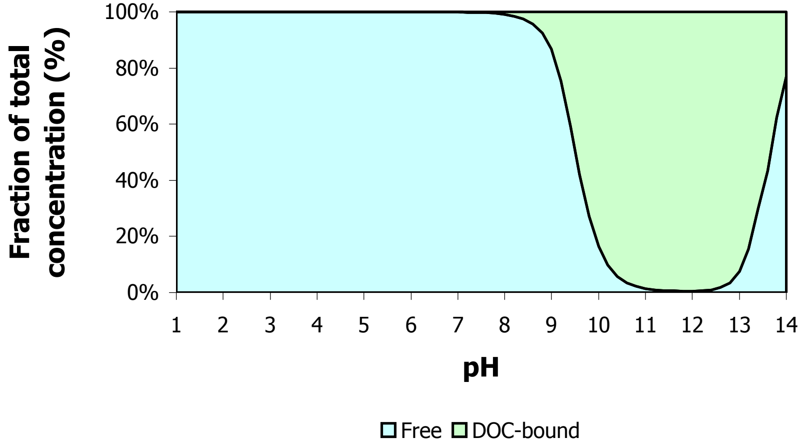

Mn+2 fractionation in the solid phase

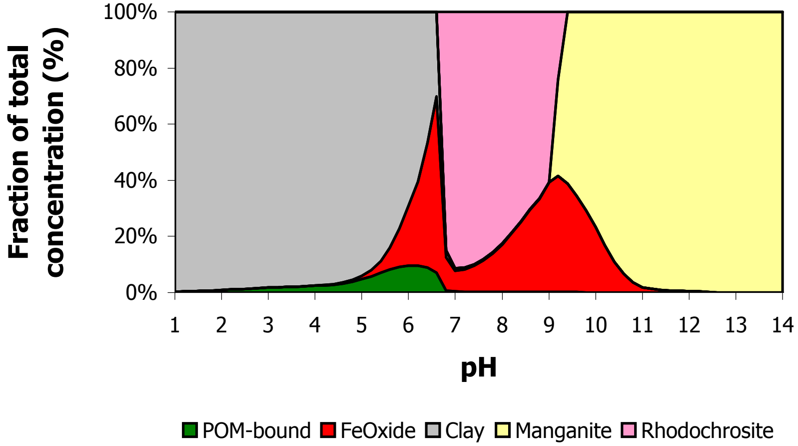

Ni+2 fractionation in solution

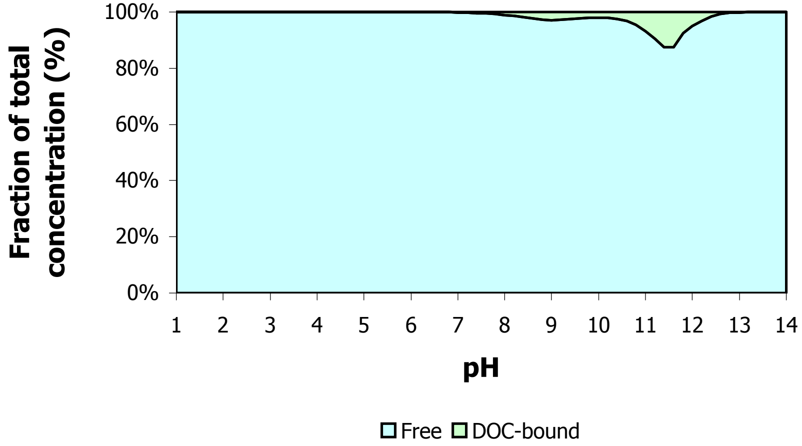

Ni+2 fractionation in the solid phase

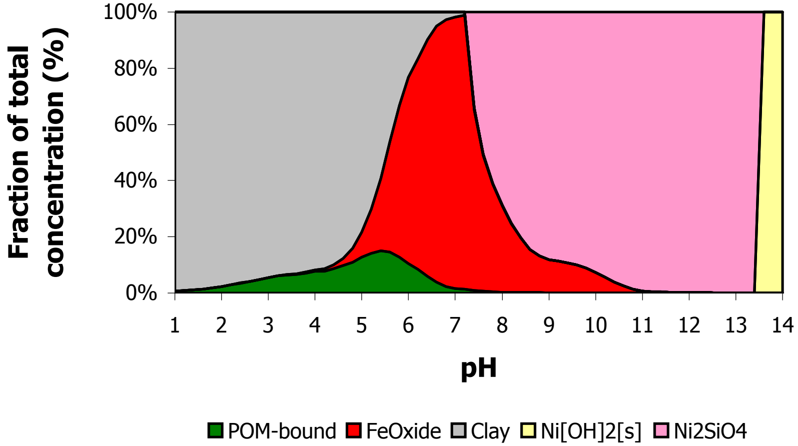

Pb+2 fractionation in solution

Pb+2 fractionation in the solid phase

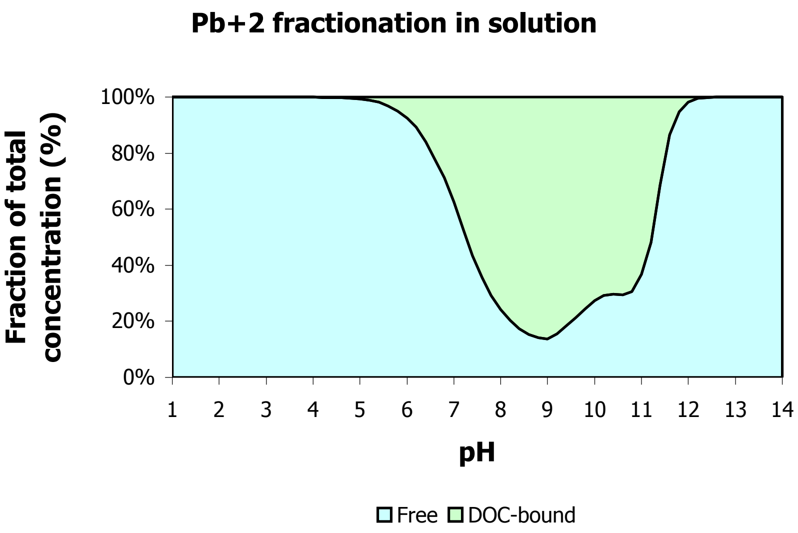
Pb+2 fractionation in solution

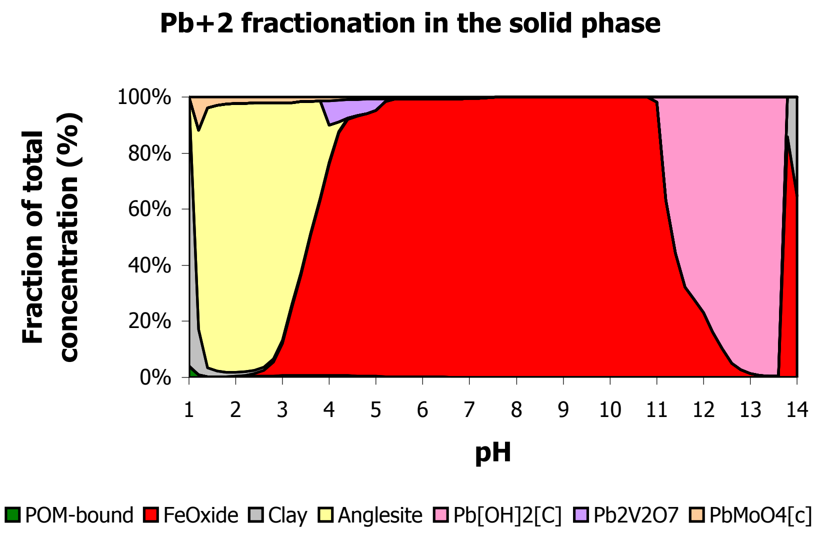
Pb+2 fractionation in the solid phase

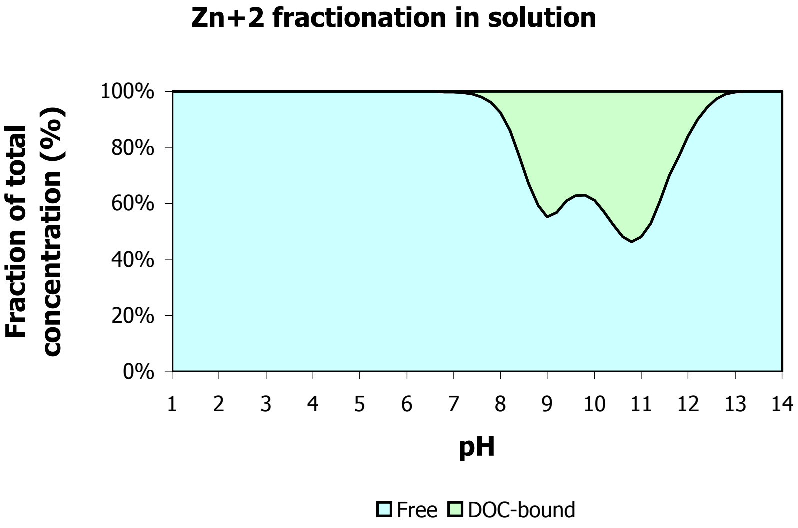
Zn+2 fractionation in solution

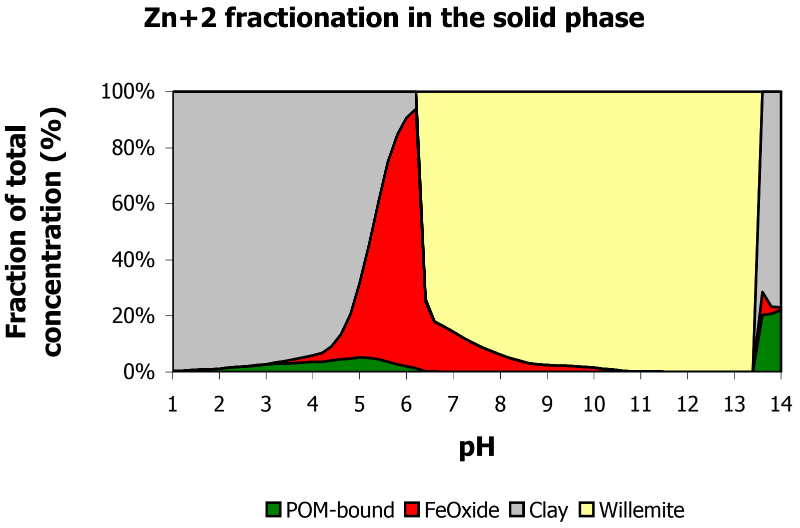
Zn+2 fractionation in the solid phase

CrO4-2 fractionation in solution

CrO4-2 fractionation in the solid phase

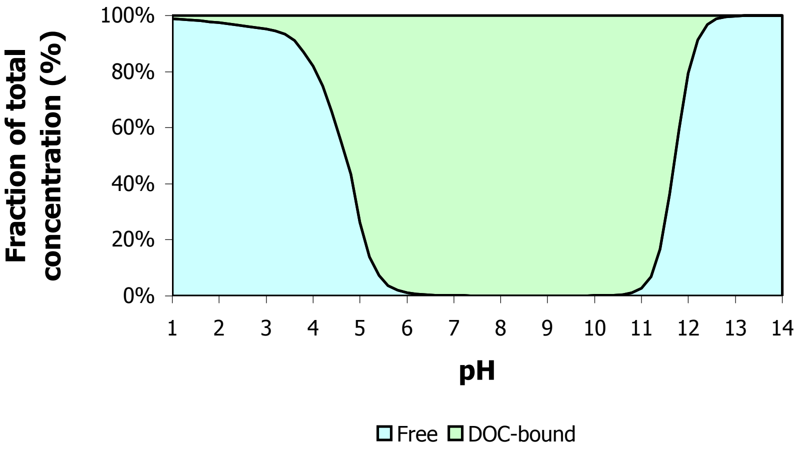
CrO4-2 fractionation in solution

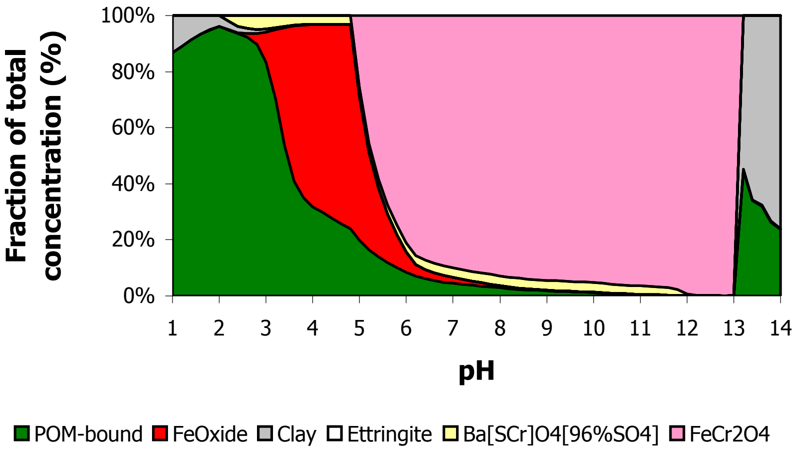
CrO4-2 fractionation in the solid phase

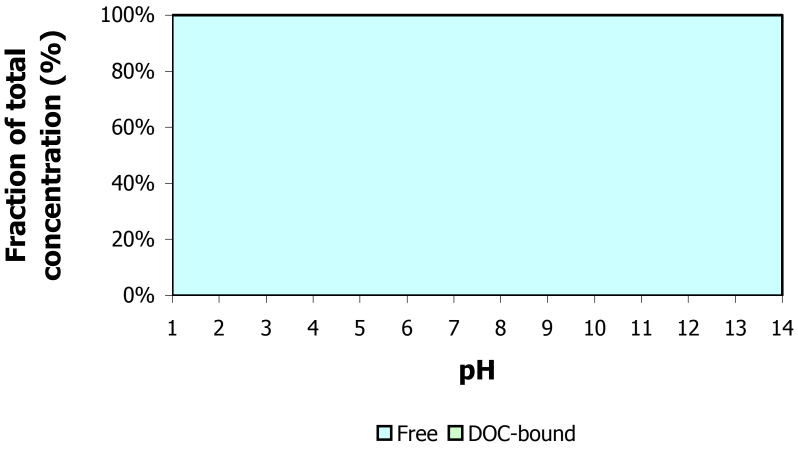
H3AsO4 fractionation in solution

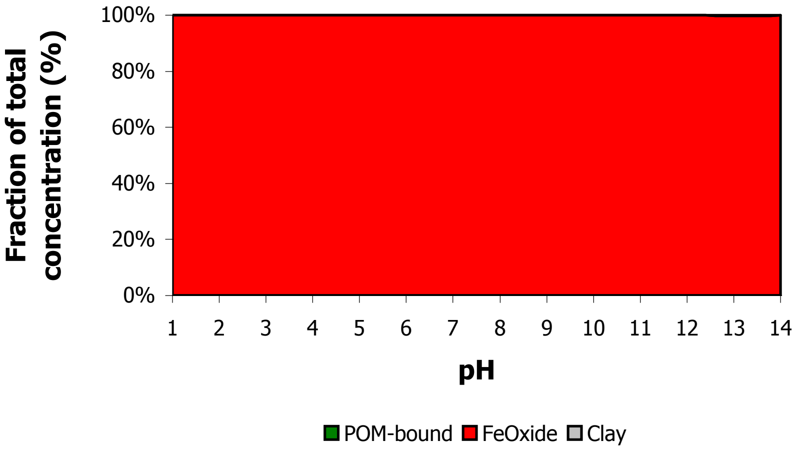
H3AsO4 fractionation in the solid phase

H3BO3 fractionation in solution

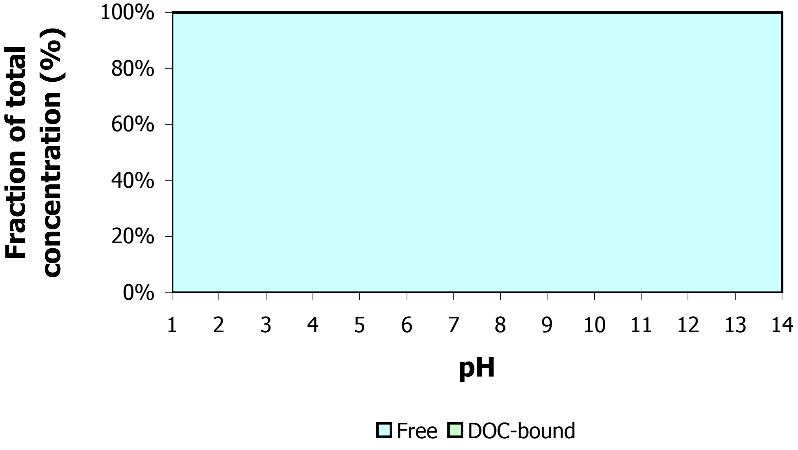

H3BO3 fractionation in the solid phase

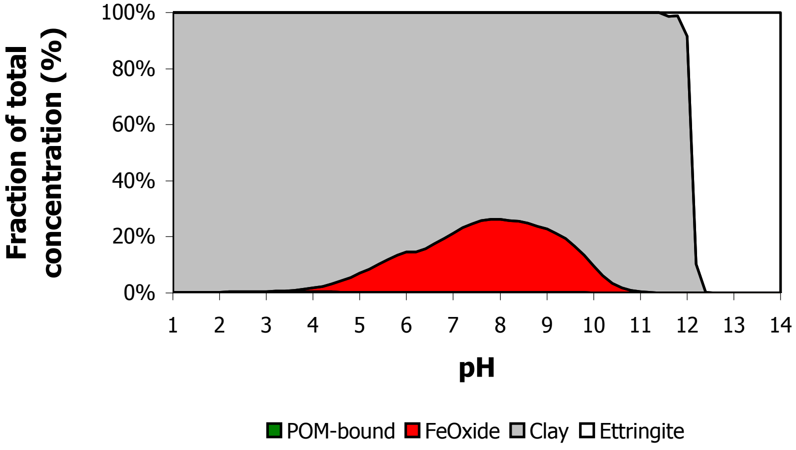

MoO4-2 fractionation in solution

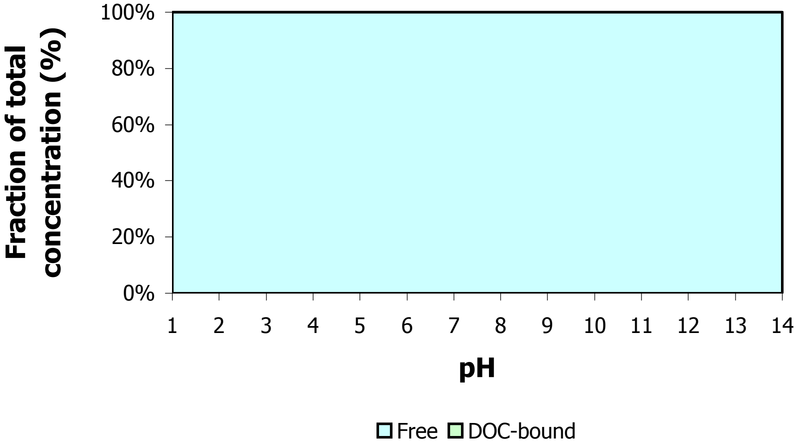

MoO4-2 fractionation in the solid phase

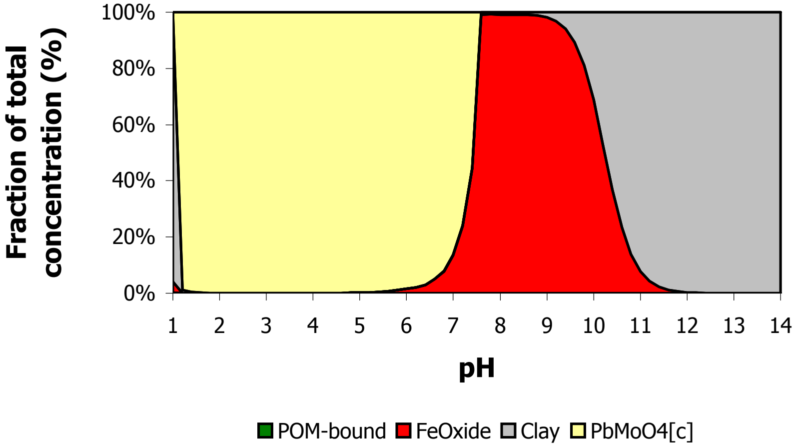

Sb[OH]6- fractionation in solution

Sb[OH]6- fractionation in the solid phase

Sb[OH]6- fractionation in solution

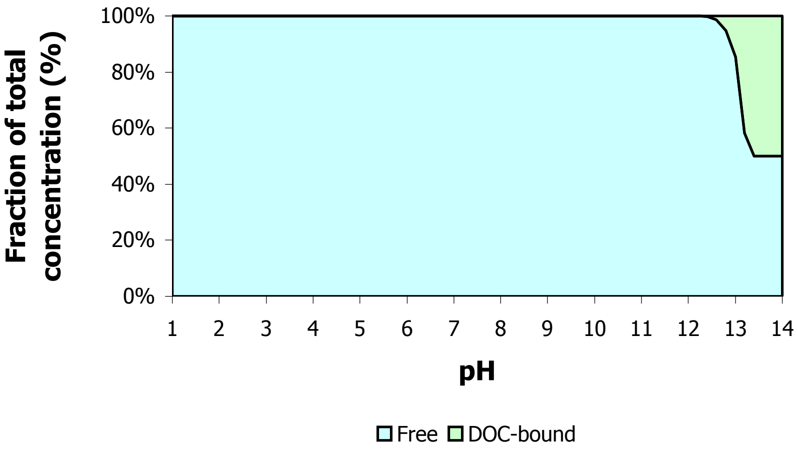

Sb[OH]6- fractionation in the solid phase

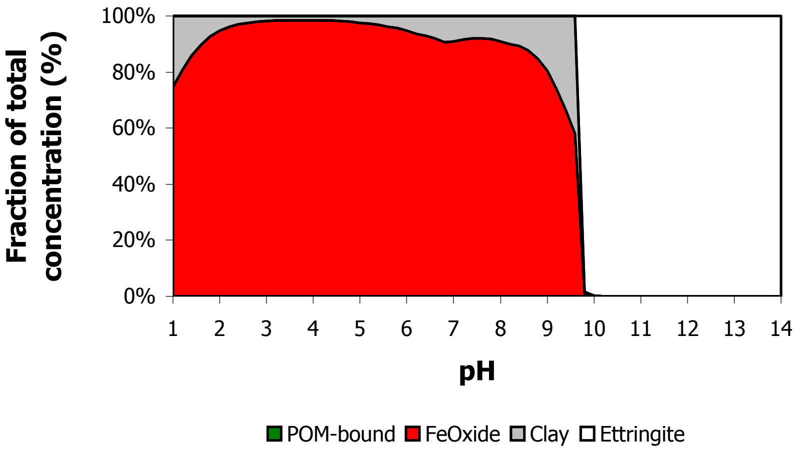

VO2+ fractionation in solution

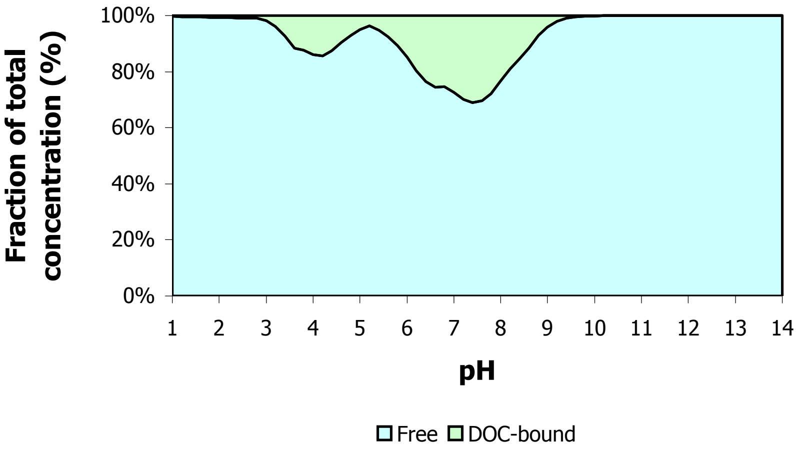

VO2+ fractionation in the solid phase

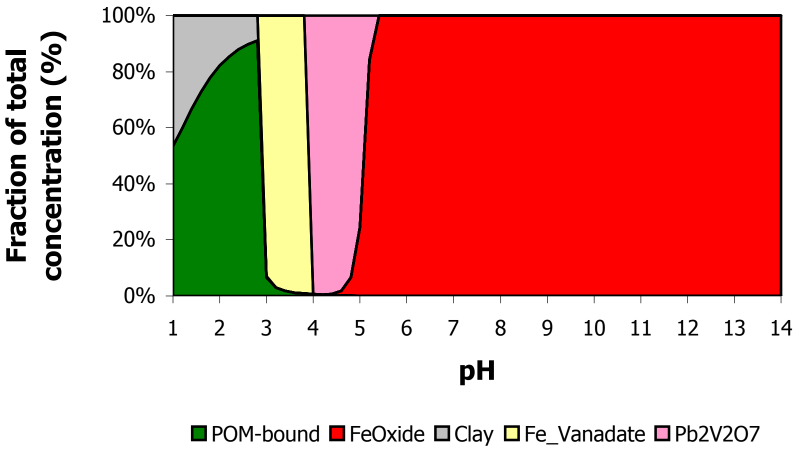

Br- fractionation in solution

Br- fractionation in the solid phase

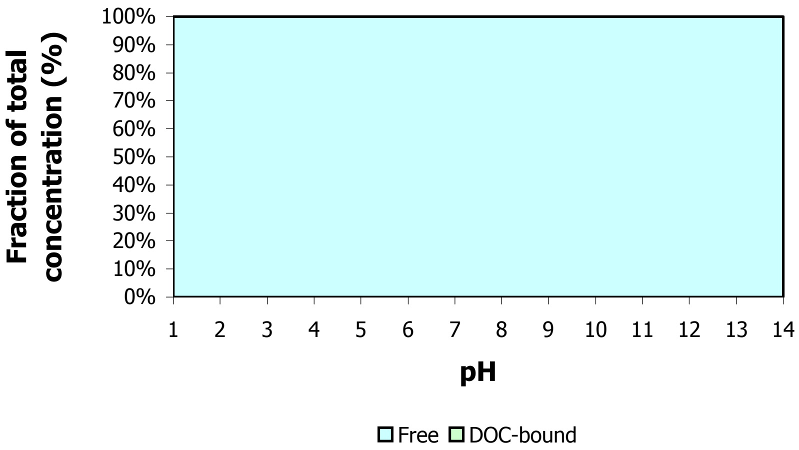
Br- fractionation in solution

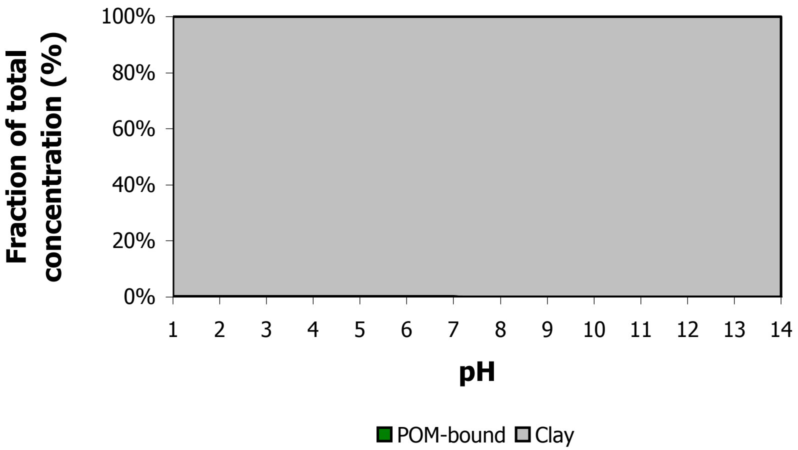
Br- fractionation in the solid phase

K+ fractionation in solution

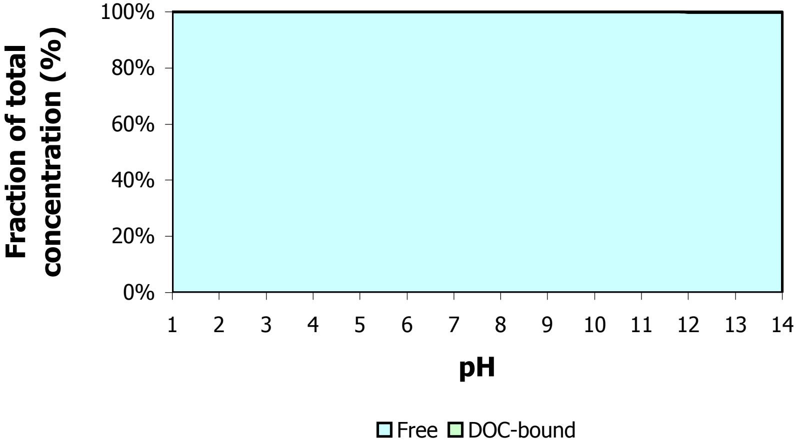

K+ fractionation in the solid phase

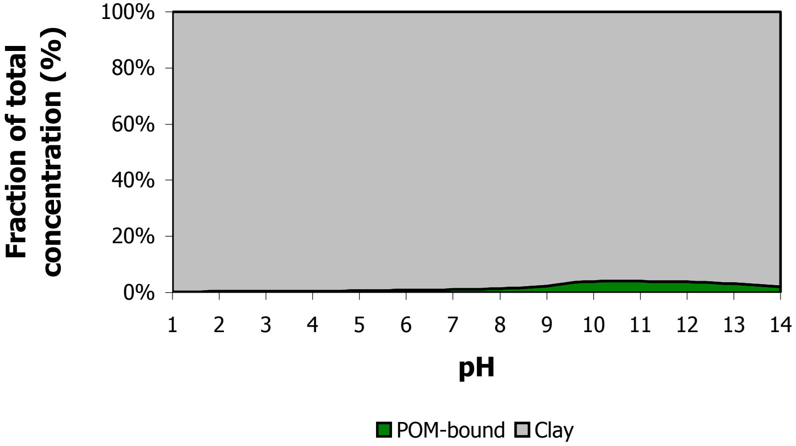

Li+ fractionation in solution

Li+ fractionation in the solid phase

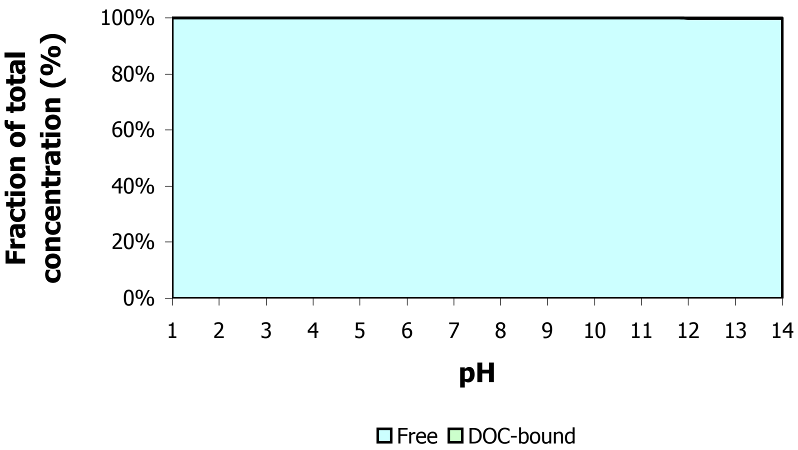
Li+ fractionation in solution

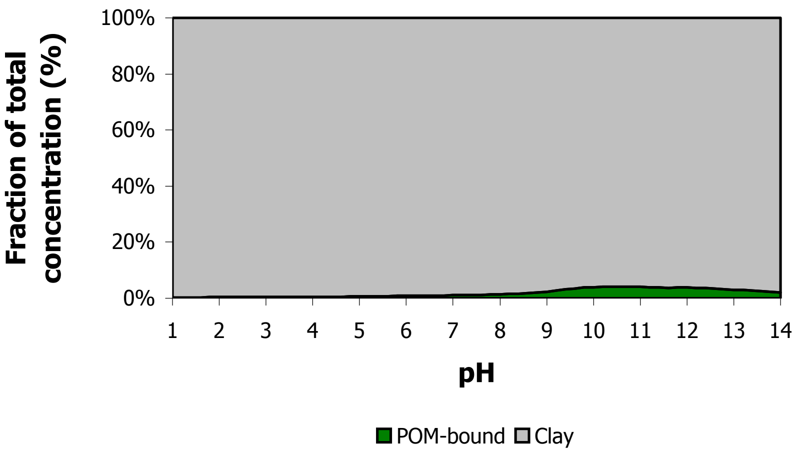
Li+ fractionation in the solid phase

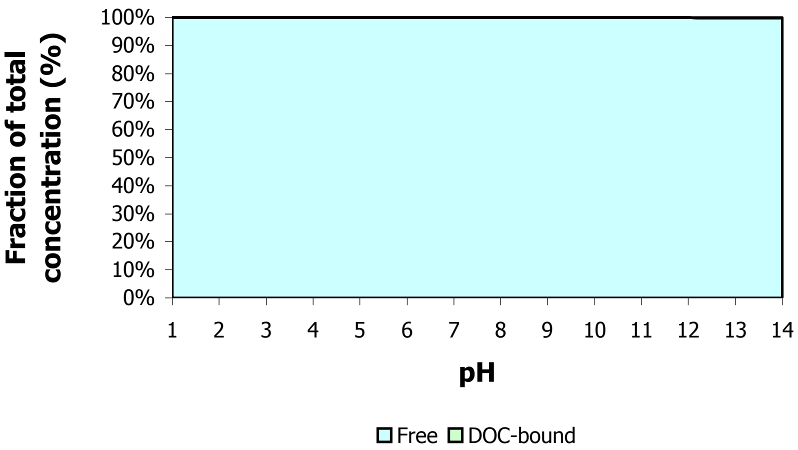
Na+ fractionation in solution

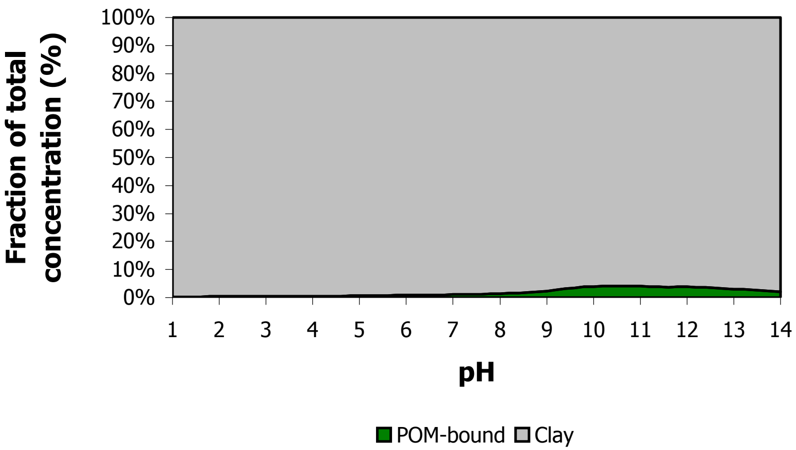
Na+ fractionation in the solid phase

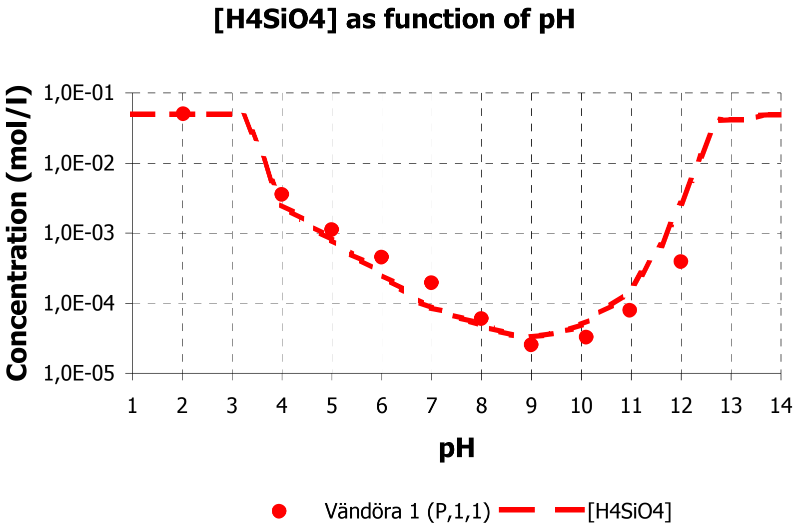
[H4SiO4] as function of pH
Concentration (mol/l)
1,0E-01
1,0E-02
1,0E-03
1,0E-04
1,0E-05
1
2
3
4
5
6
7
8
9
10
11
12
13
14
pH
Vändöra 1 (P,1,1)
[H4SiO4]

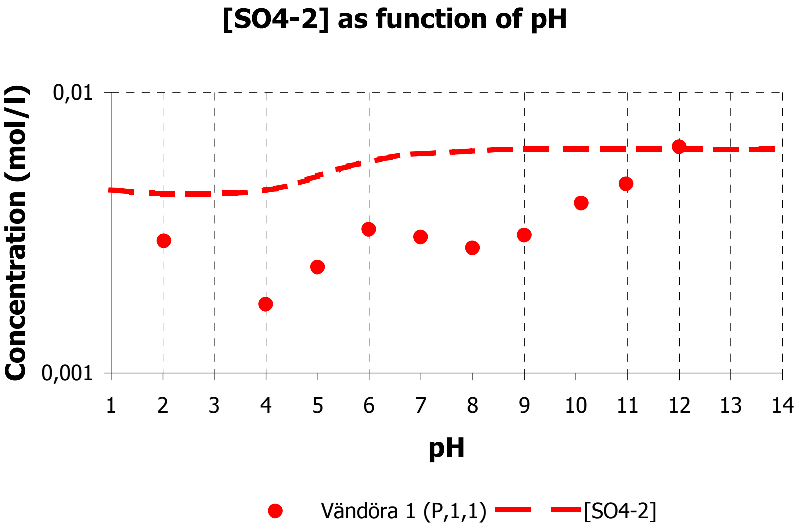
[SO4-2] as function of pH
Concentration (mol/l)
0,01
0,001
1
2
3
4
5
6
7
8
9
10
11
12
13
14
pH
Vändöra 1 (P,1,1)
[SO4-2]

[Pb+2] as function of pH

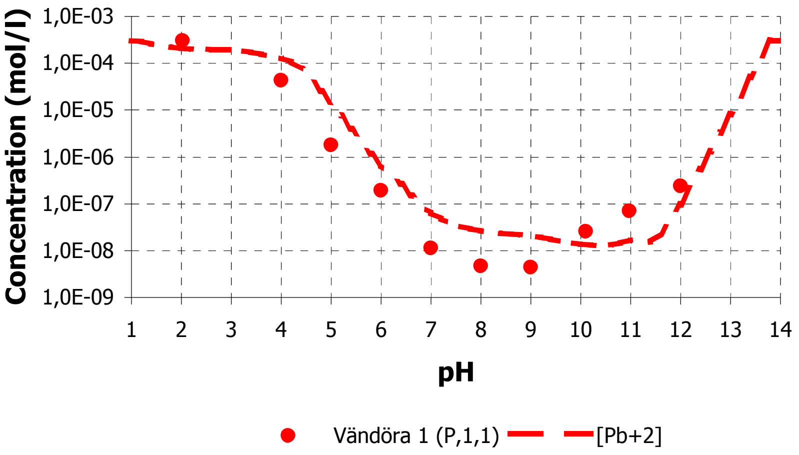

[Zn+2] as function of pH

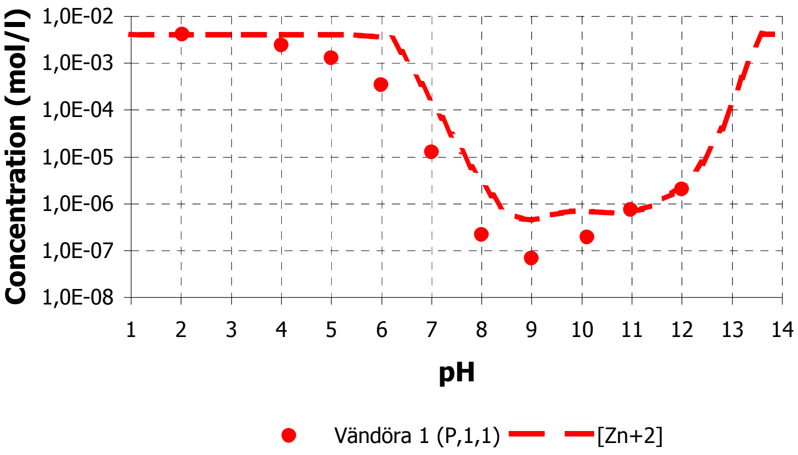

[Sb[OH]6-] as function of pH

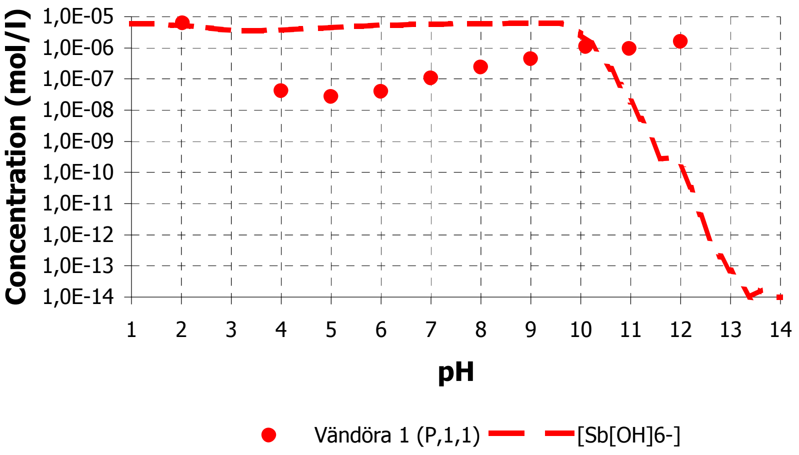

[VO2+] as function of pH

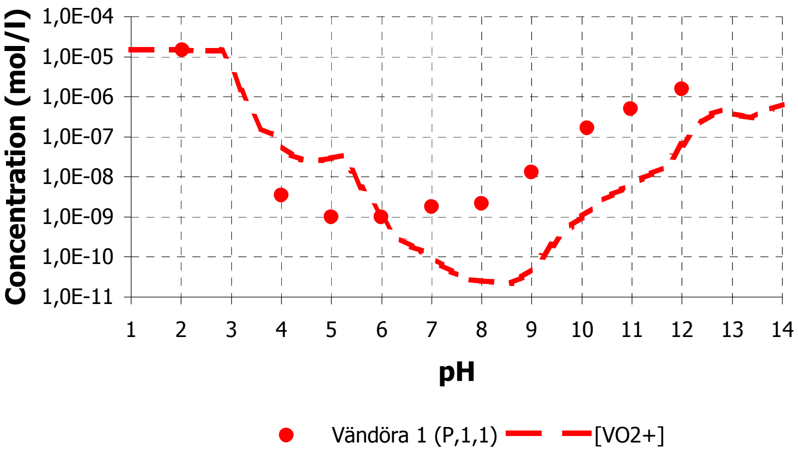

[Li+] as function of pH

[Na+] as function of pH

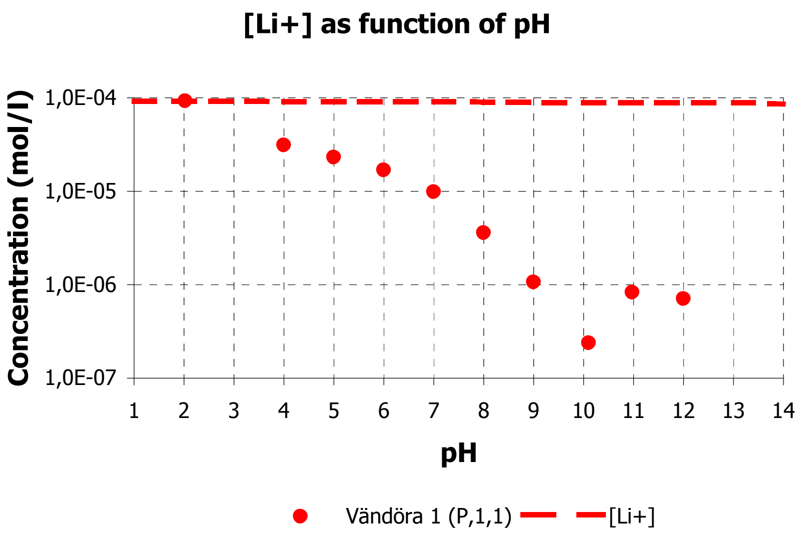
[Li+] as function of pH
Concentration (mol/l)
1,0E-04
1,0E-05
1,0E-06
1,0E-07
1
2
3
4
5
6
7
8
9
10
11
12
13
14
pH
Vändöra 1 (P,1,1)
[Li+]

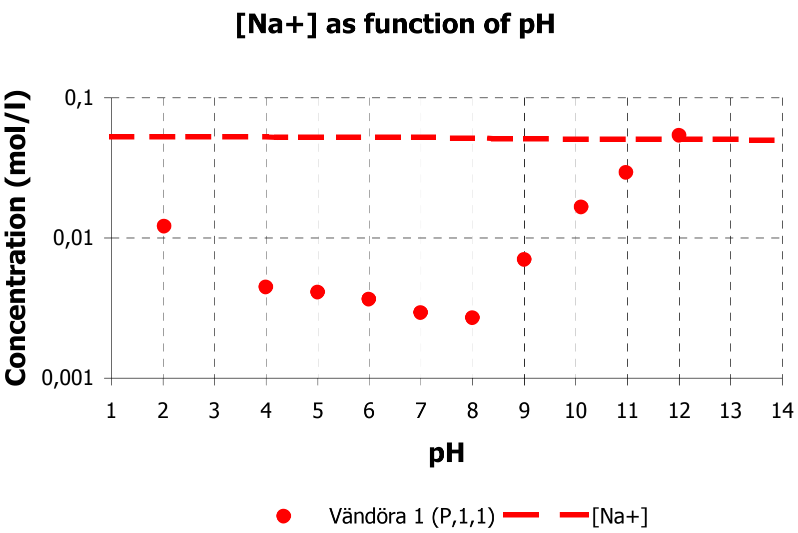
[Na+] as function of pH
Concentration (mol/l)
0,1
0,01
0,001
1
2
3
4
5
6
7
8
9
10
11
12
13
14
pH
Vändöra 1 (P,1,1)
[Na+]

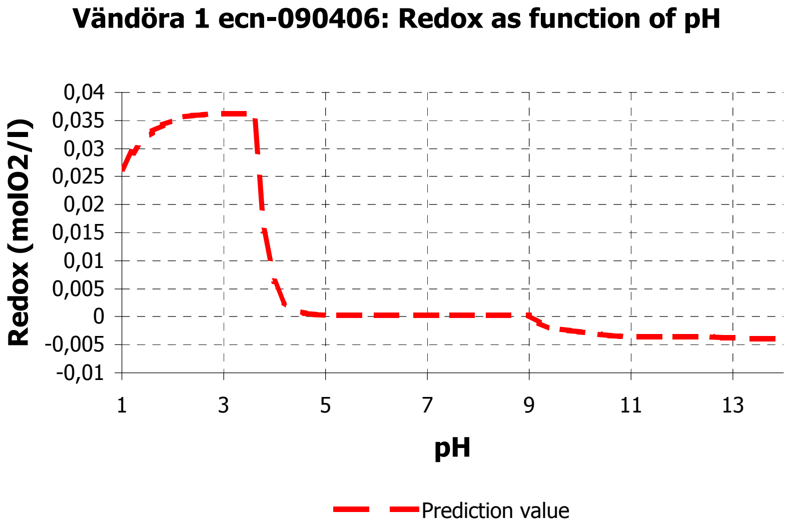
Vändöra 1 ecn-090406: Redox as function of pH
Redox (molO2/l)
0,04
0,035
0,03
0,025
0,02
0,015
0,01
0,005
0
-0,005
-0,01
1
3
5
7
9
11
13
pH
Prediction value

G Result geochemical modelling sample 2

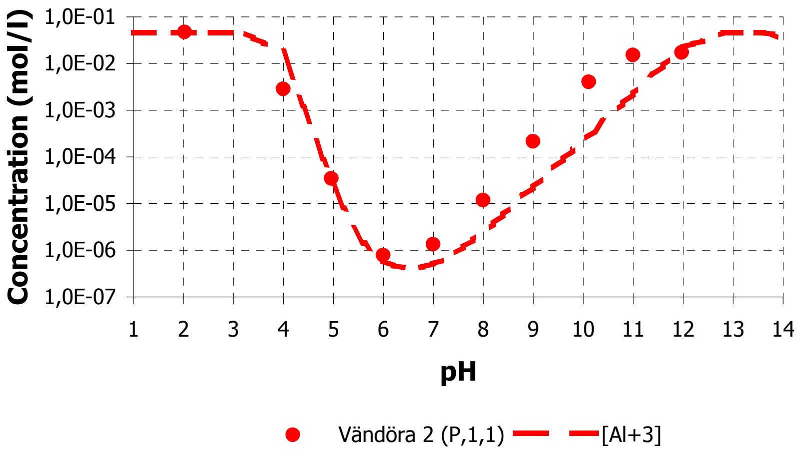

[Al+3] as function of pH

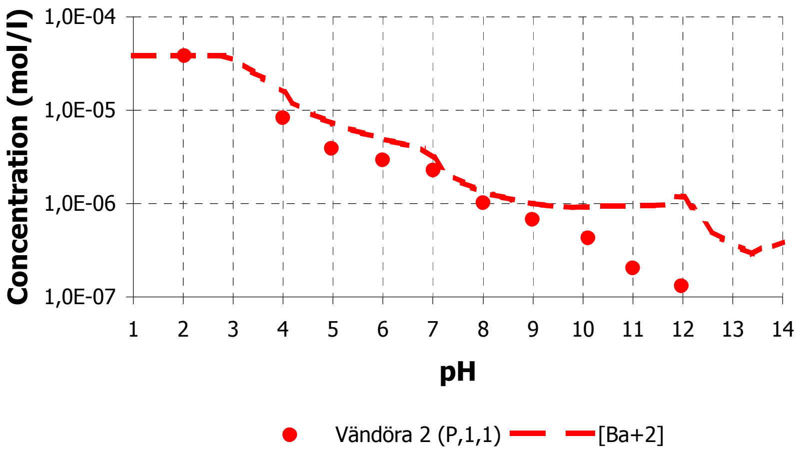

[Ba+2] as function of pH

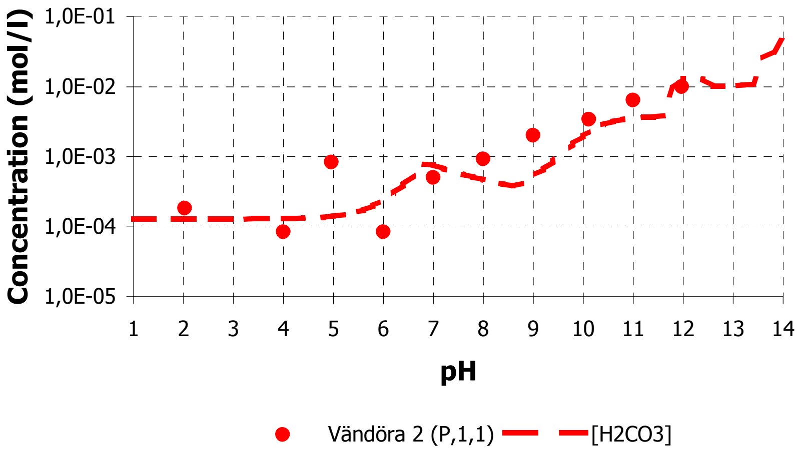

[H2CO3] as function of pH

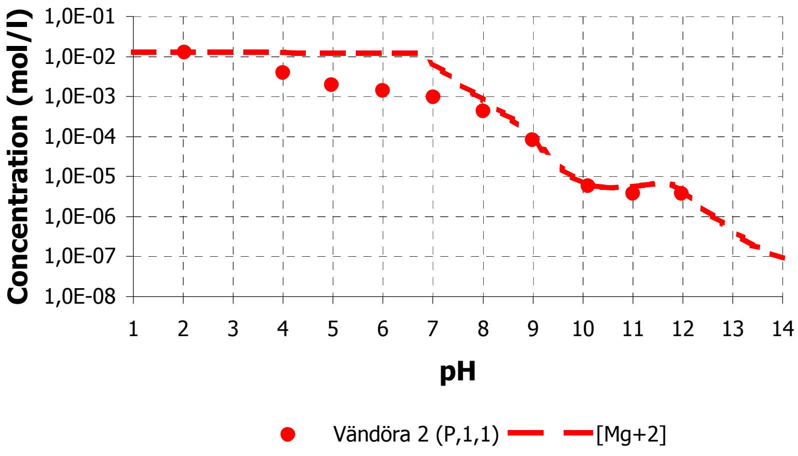

[Mg+2] as function of pH

[Cd+2] as function of pH

[Cu+2] as function of pH

[Cd+2] as function of pH

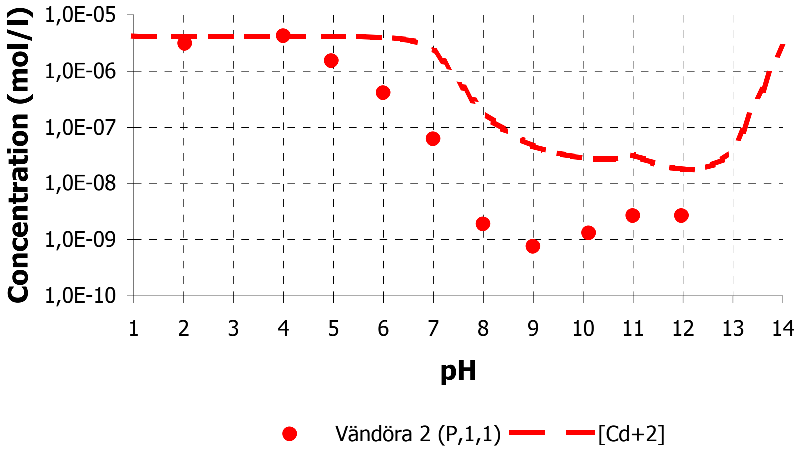

[Cu+2] as function of pH

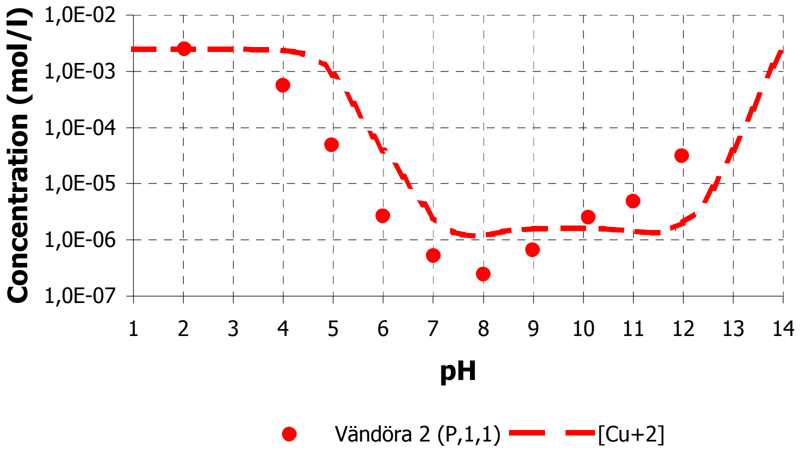

[CrO4-2] as function of pH

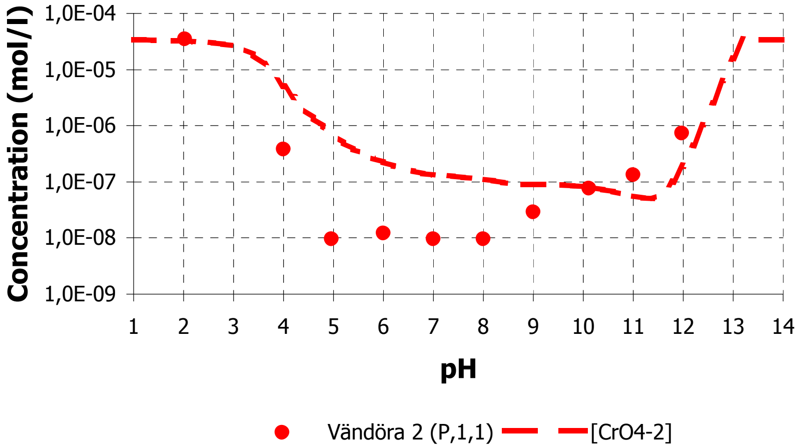

[H3AsO4] as function of pH

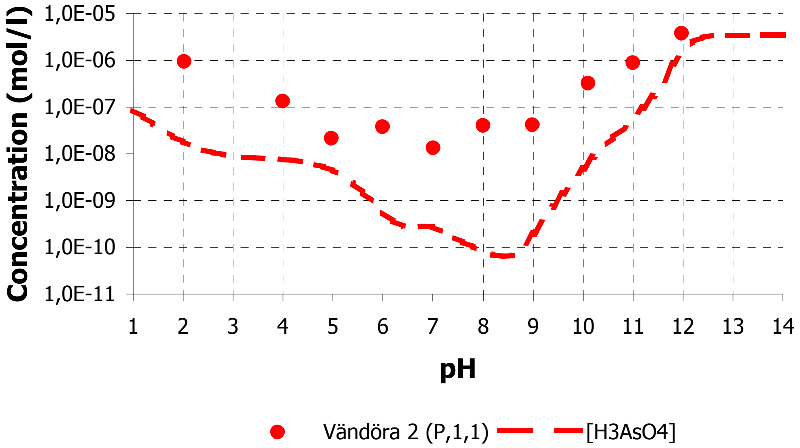

[Br-] as function of pH

[Cl-] as function of pH

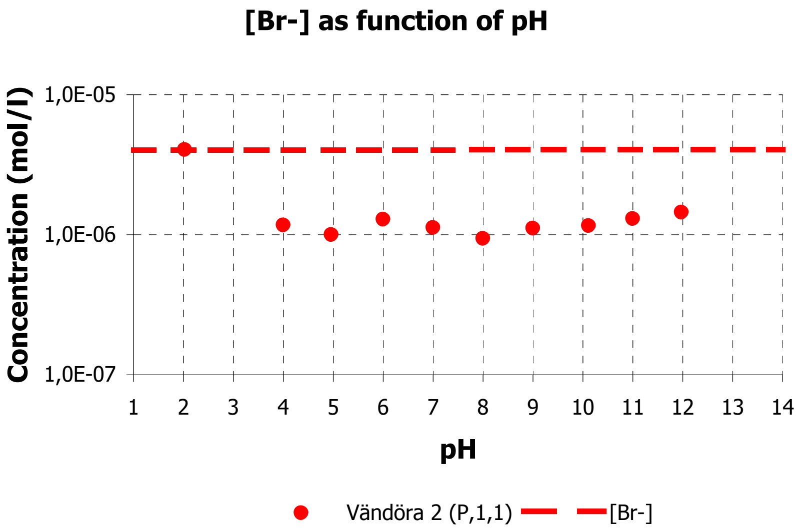

[Br-] as function of pH

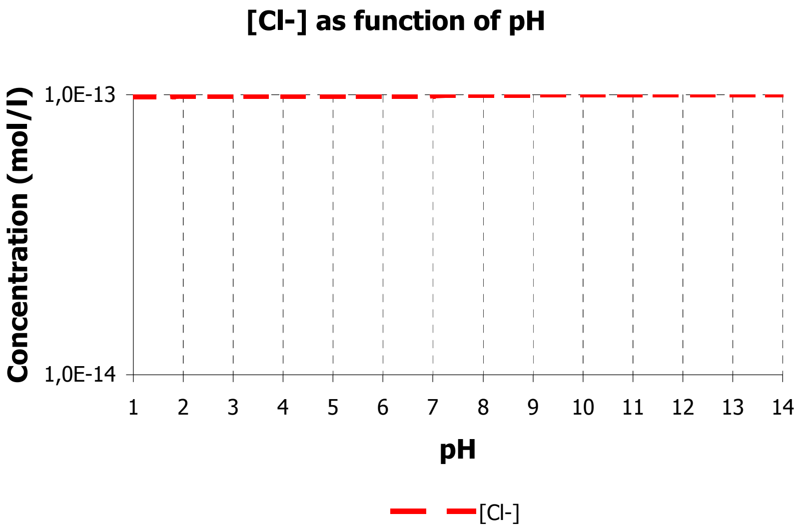

[Cl-] as function of pH

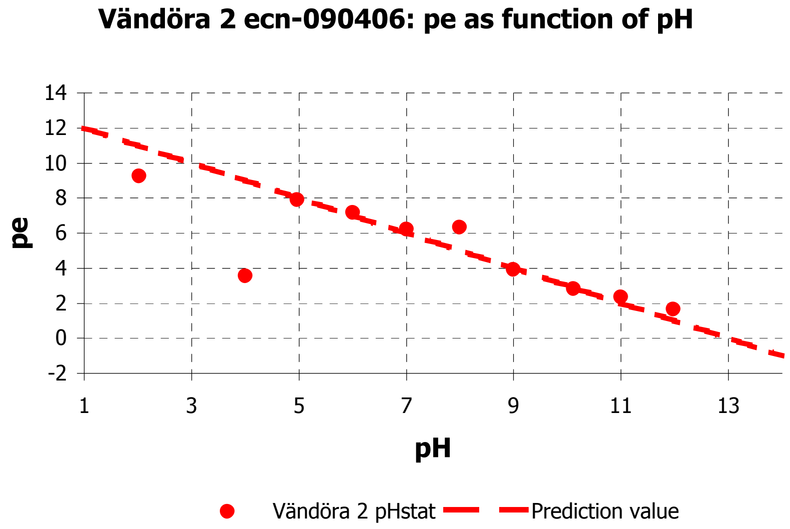

Vändöra 2 ecn-090406: pe as function of pH

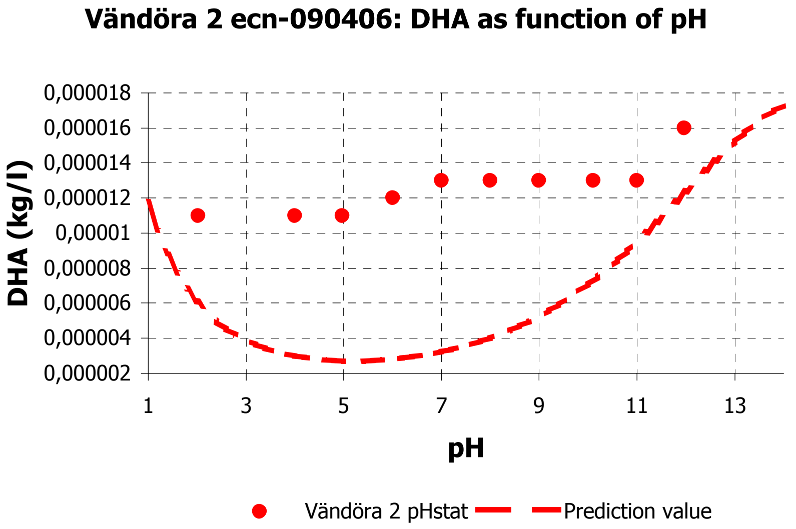

Vändöra 2 ecn-090406: DHA as function of pH

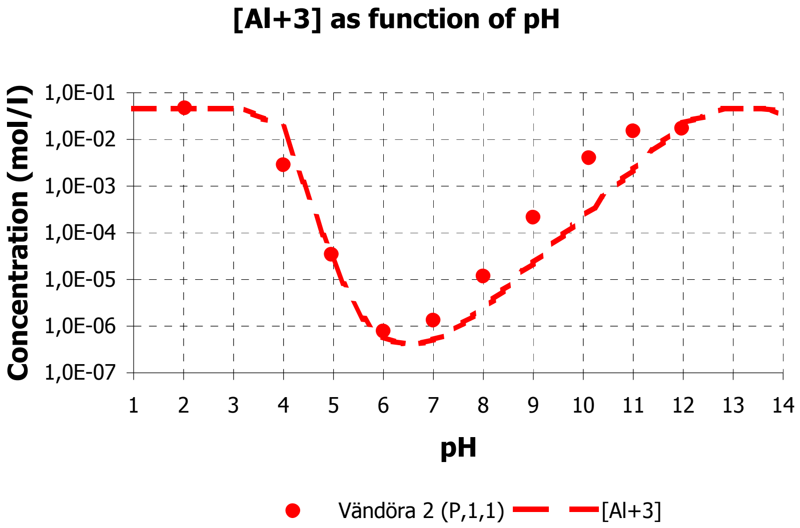
[Al+3] as function of pH

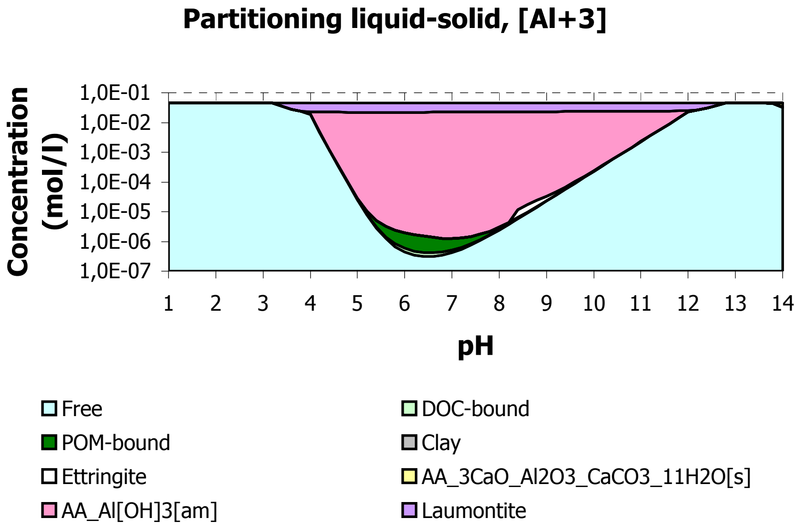
Partitioning liquid-solid, [Al+3]

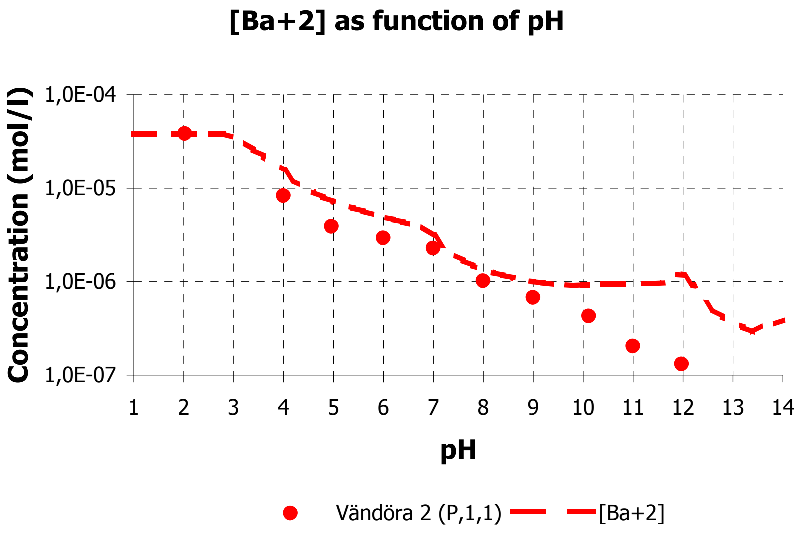
[Ba+2] as function of pH

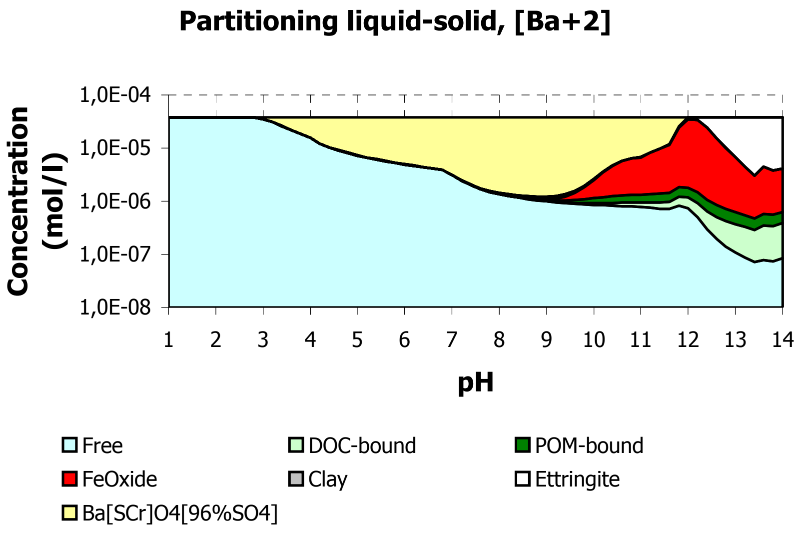
Partitioning liquid-solid, [Ba+2]

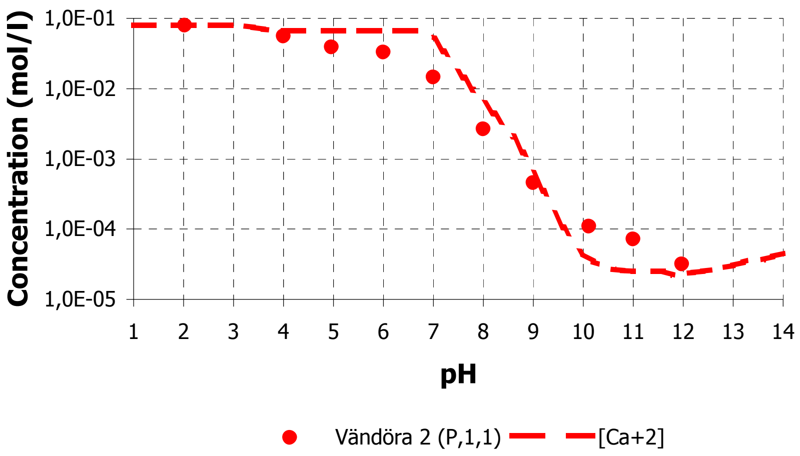

[Ca+2] as function of pH

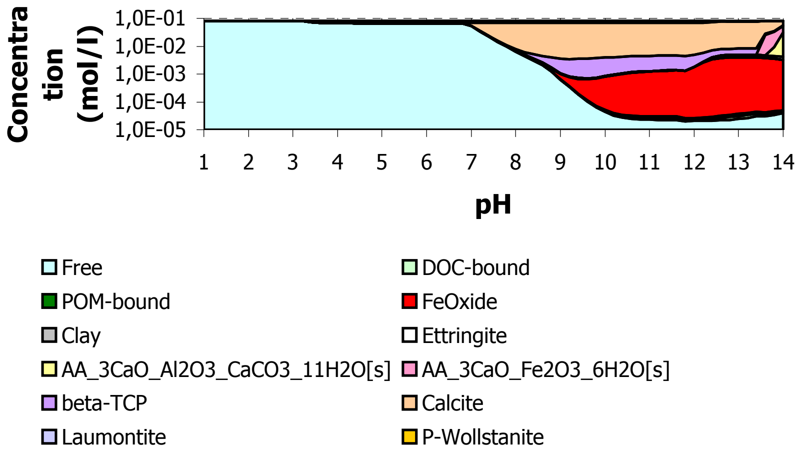

Partitioning liquid-solid, [Ca+2]

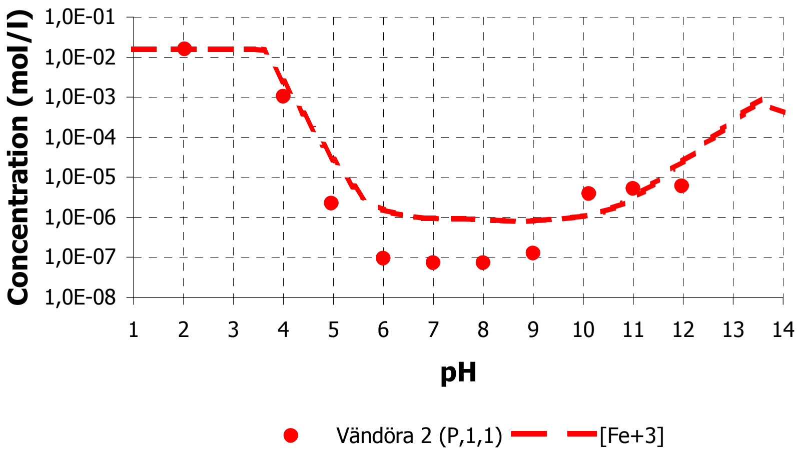

[Fe+3] as function of pH

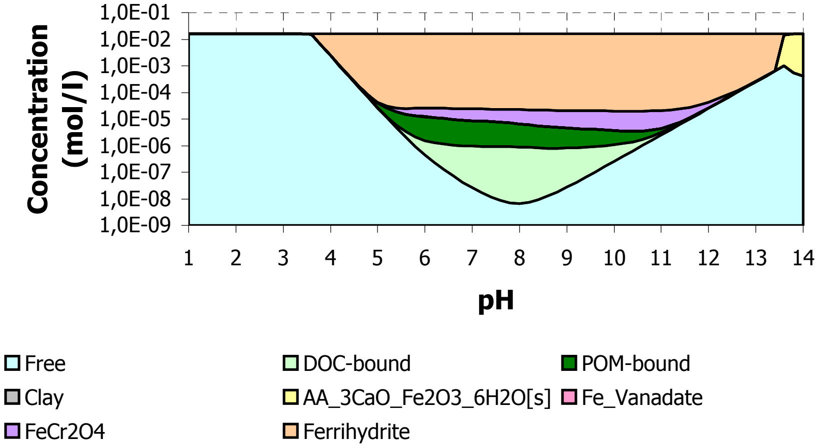

Partitioning liquid-solid, [Fe+3]

[H4SiO4] as function of pH

Partitioning liquid-solid, [H4SiO4]

[H4SiO4] as function of pH

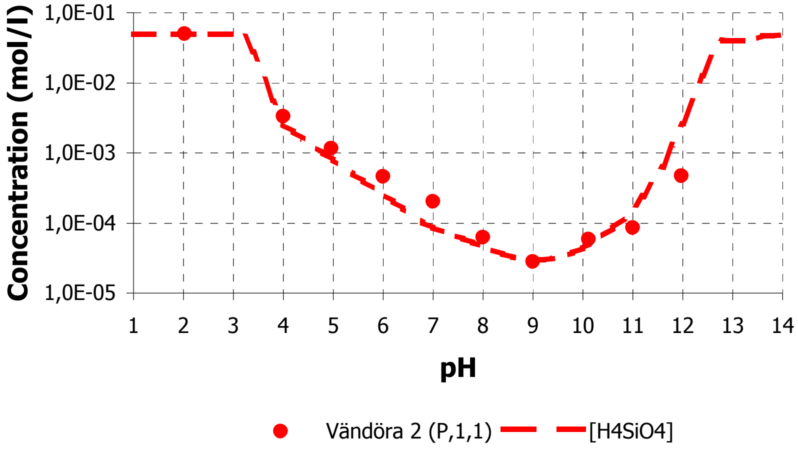

Partitioning liquid-solid, [H4SiO4]

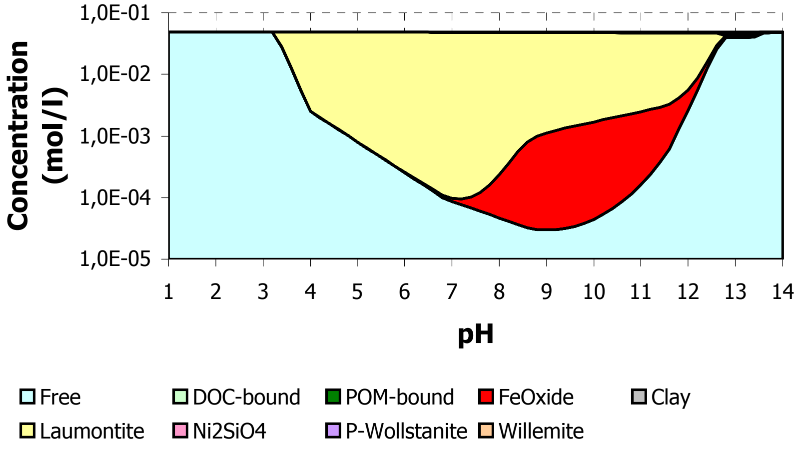

[SO4-2] as function of pH

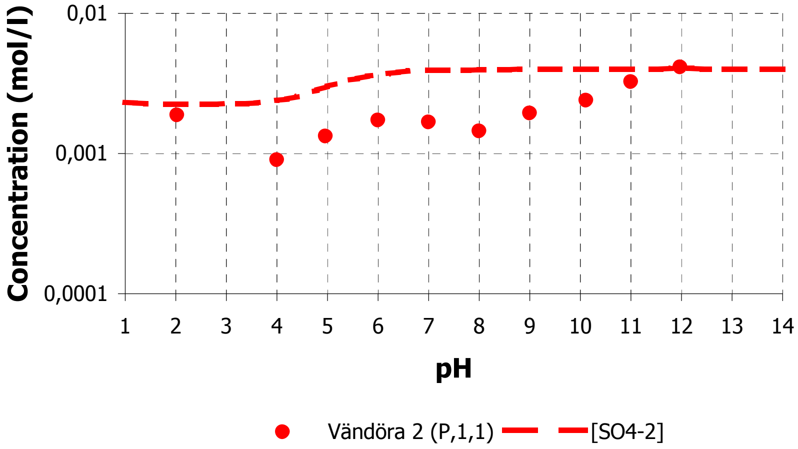

Partitioning liquid-solid, [SO4-2]

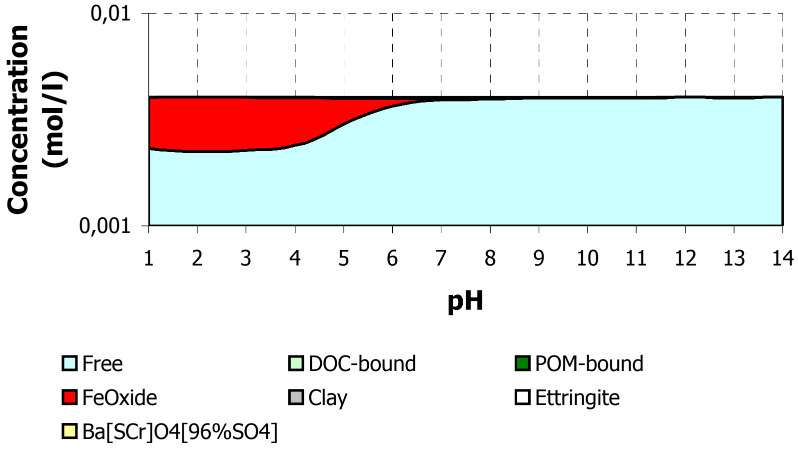

[H2CO3] as function of pH

Partitioning liquid-solid, [H2CO3]

[H2CO3] as function of pH

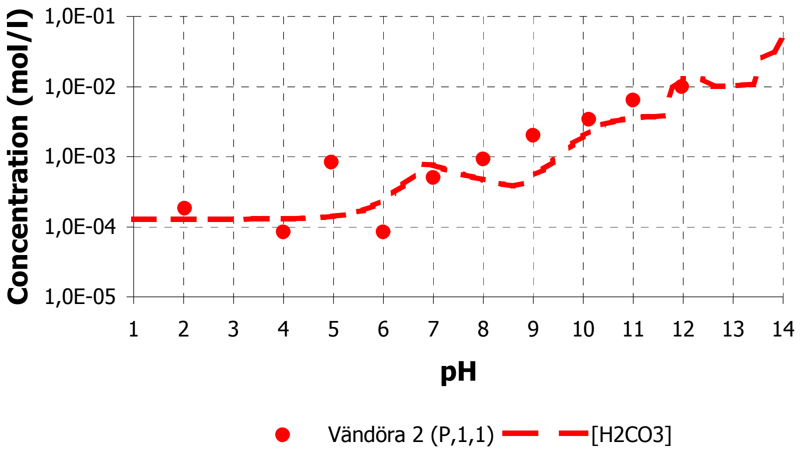

Partitioning liquid-solid, [H2CO3]

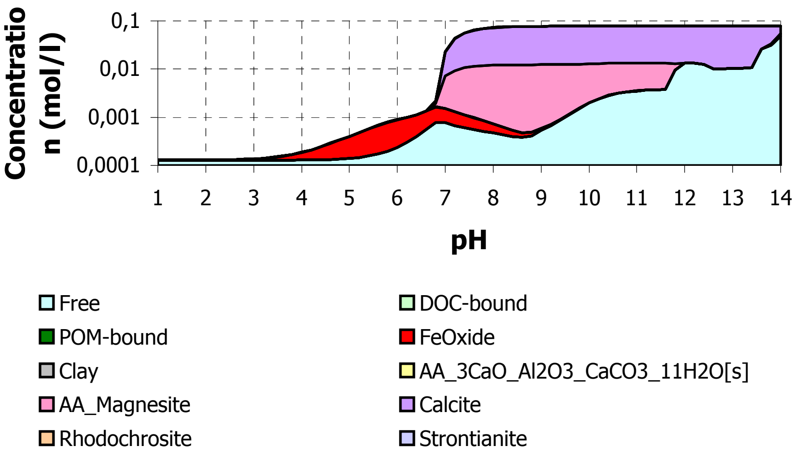

[Mg+2] as function of pH

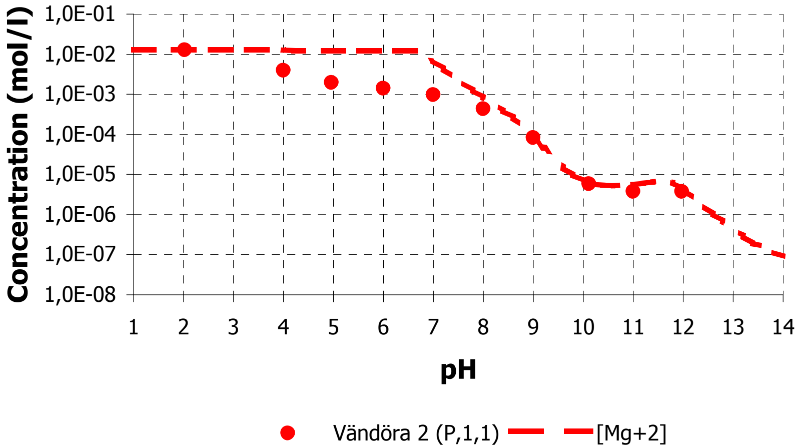

Partitioning liquid-solid, [Mg+2]

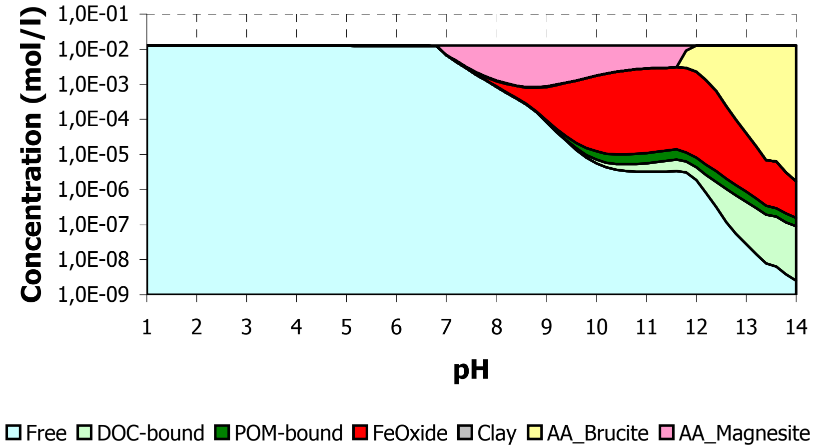

[PO4-3] as function of pH

Partitioning liquid-solid, [PO4-3]

[PO4-3] as function of pH

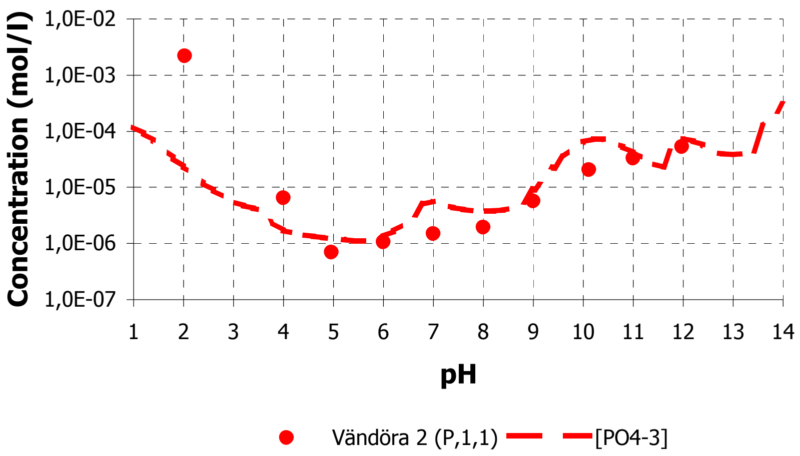

Partitioning liquid-solid, [PO4-3]

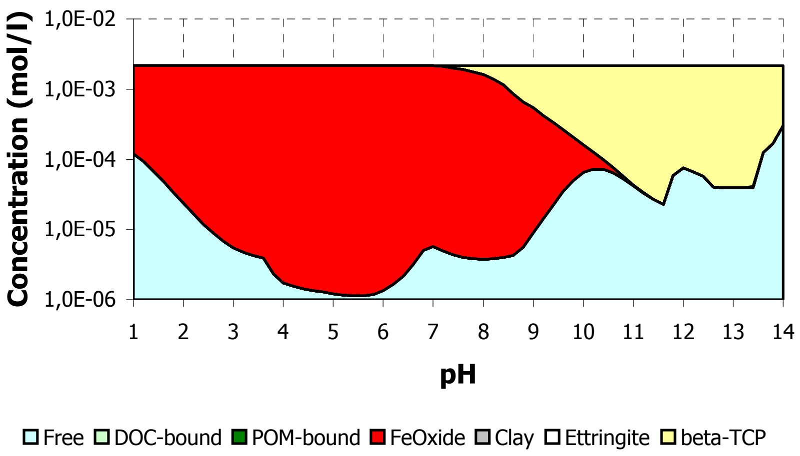

[Sr+2] as function of pH

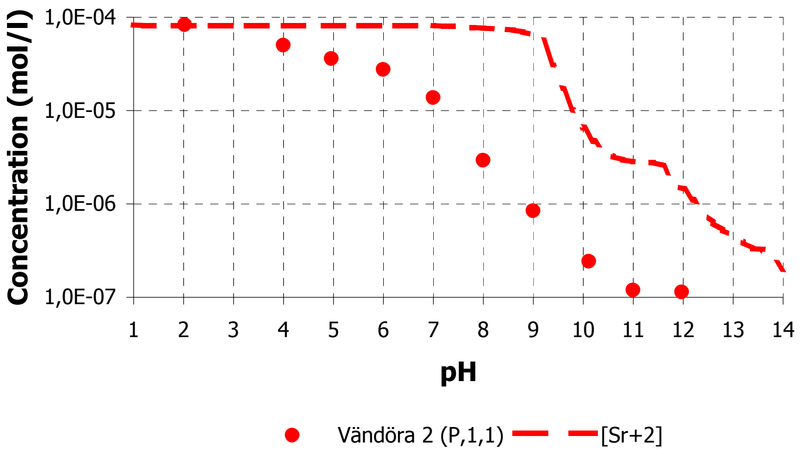

Partitioning liquid-solid, [Sr+2]

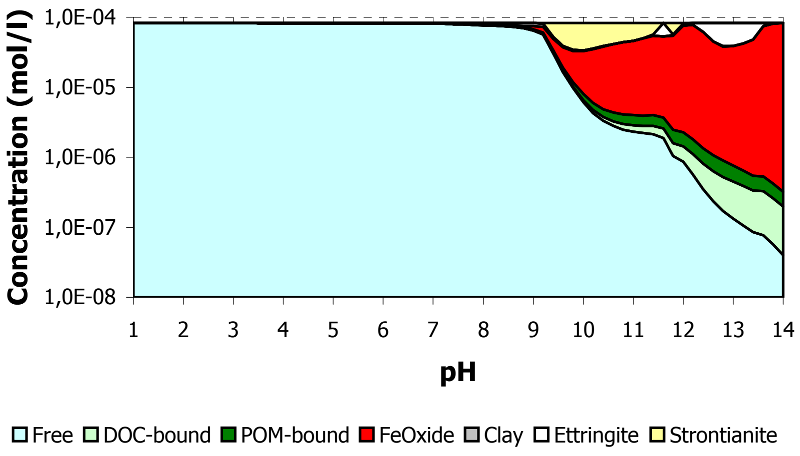

[Cd+2] as function of pH

Partitioning liquid-solid, [Cd+2]

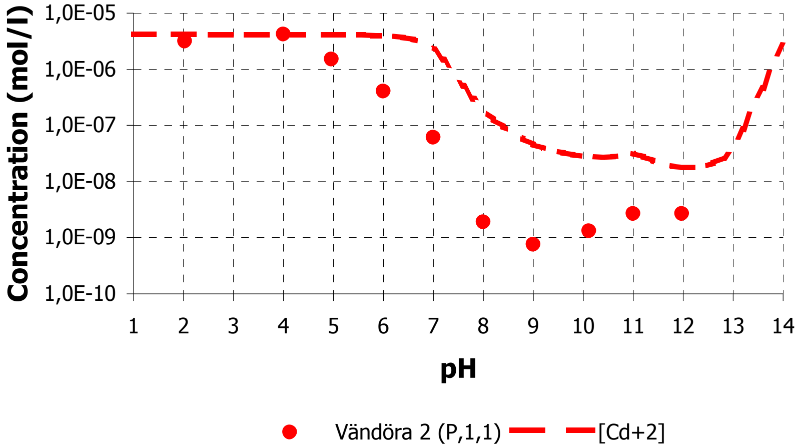
[Cd+2] as function of pH

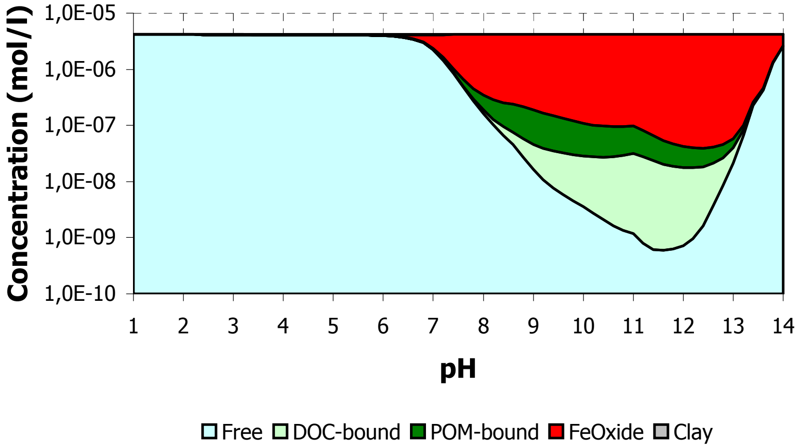
Partitioning liquid-solid, [Cd+2]

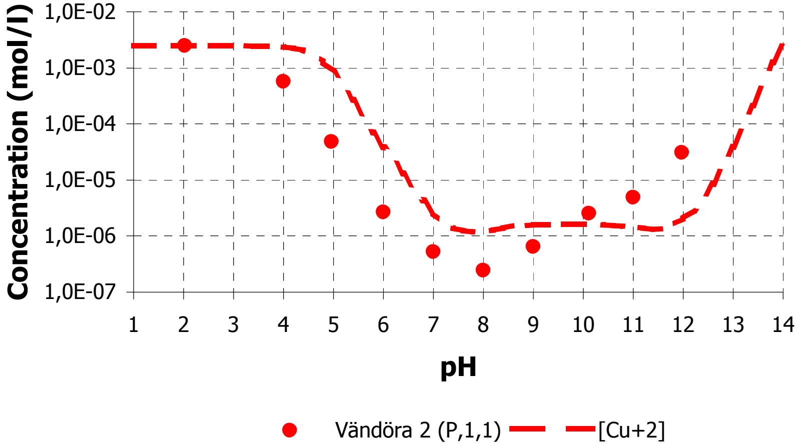
[Cu+2] as function of pH

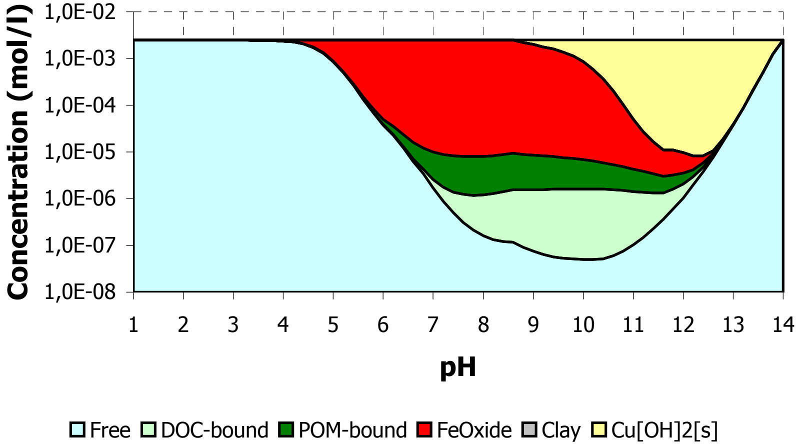
Partitioning liquid-solid, [Cu+2]

[Mn+2] as function of pH

Partitioning liquid-solid, [Mn+2]

[Mn+2] as function of pH

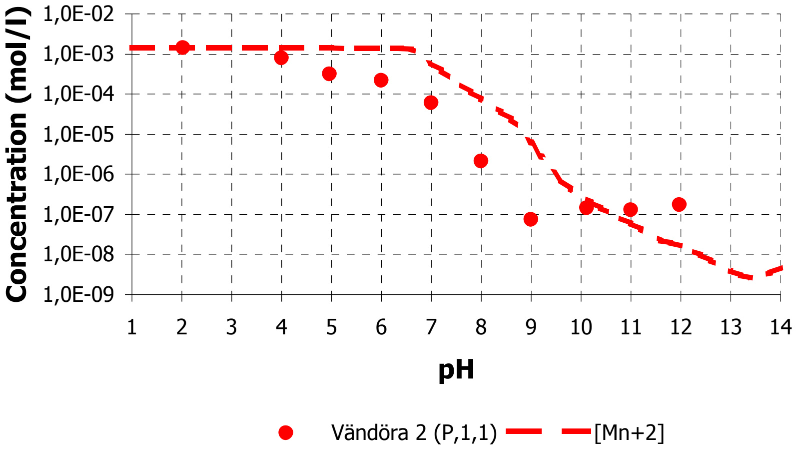

Partitioning liquid-solid, [Mn+2]

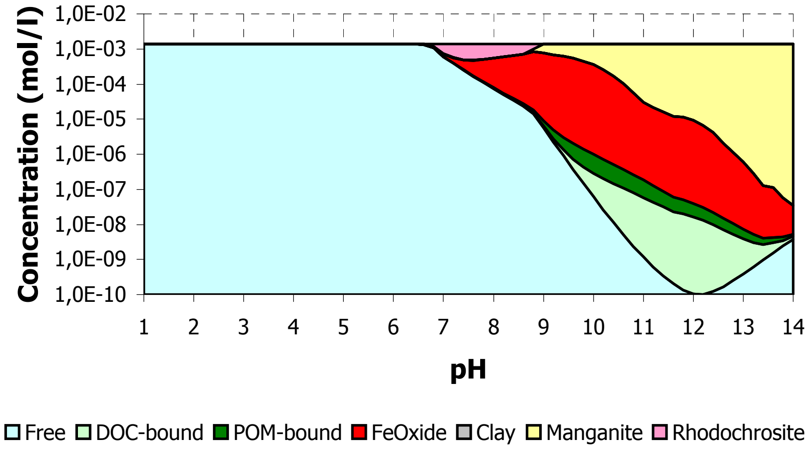

[Ni+2] as function of pH

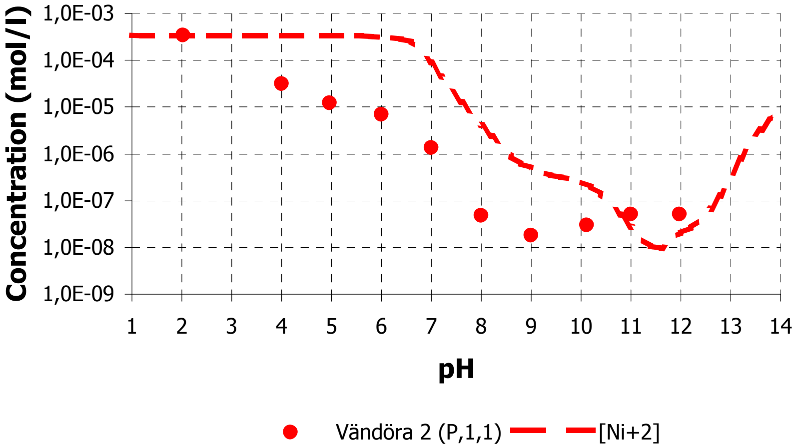

Partitioning liquid-solid, [Ni+2]

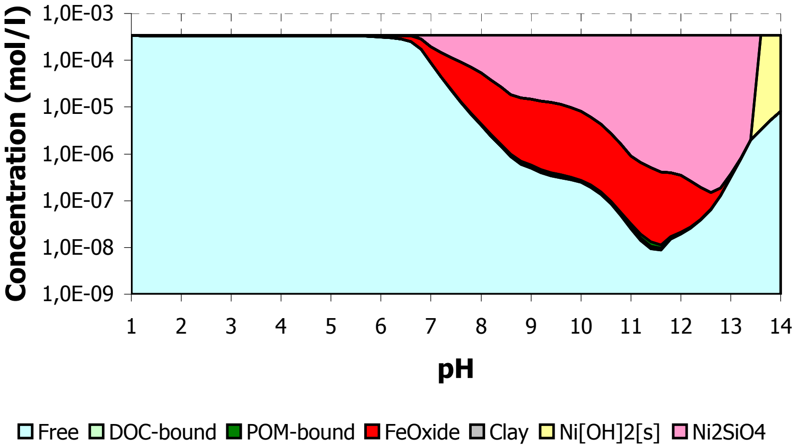

[Pb+2] as function of pH

Partitioning liquid-solid, [Pb+2]

[Pb+2] as function of pH

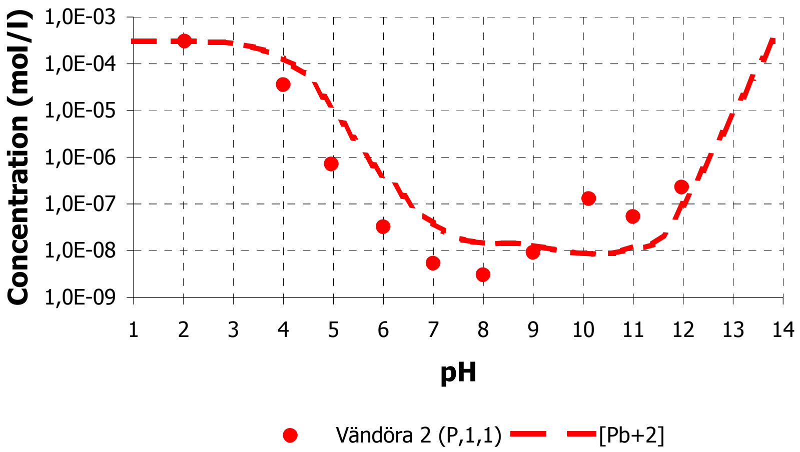

Partitioning liquid-solid, [Pb+2]

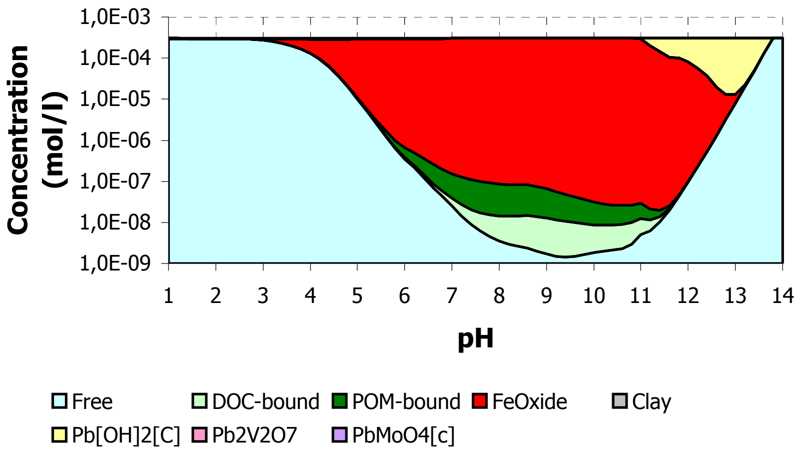

[Zn+2] as function of pH

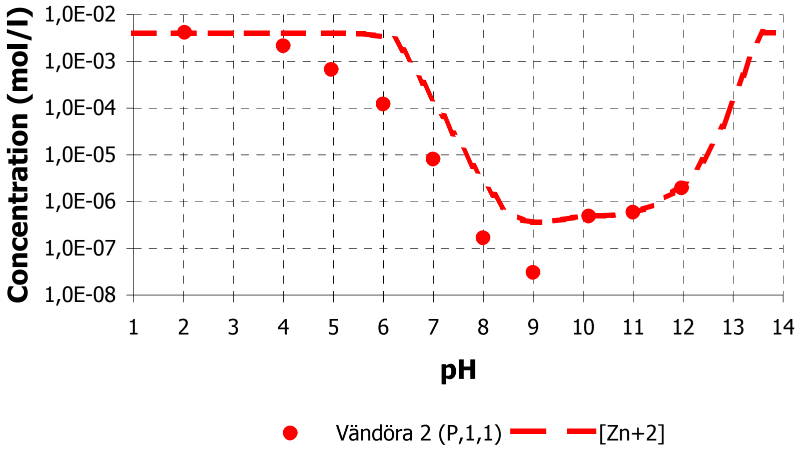

Partitioning liquid-solid, [Zn+2]

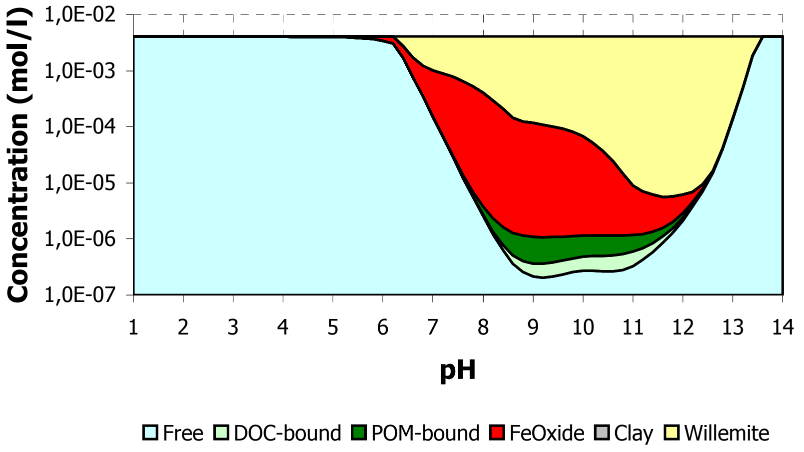

[CrO4-2] as function of pH

Partitioning liquid-solid, [CrO4-2]

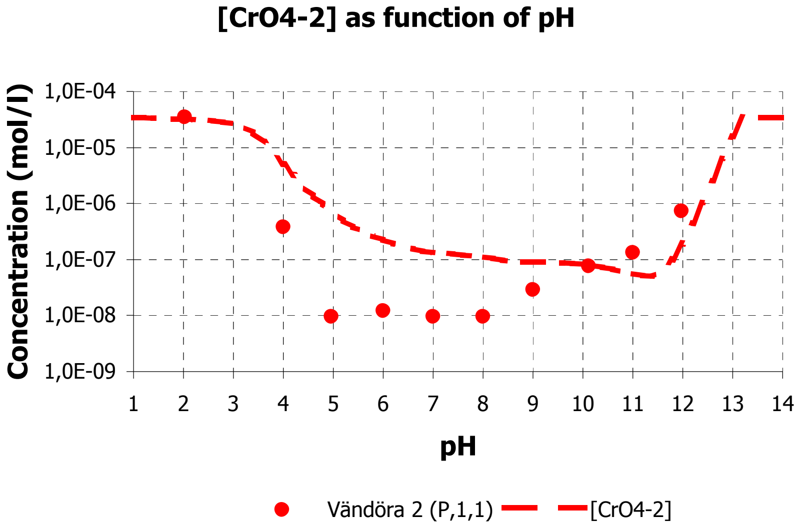
[CrO4-2] as function of pH
Concentration (mol/l)
1,0E-04
1,0E-05
1,0E-06
1,0E-07
1,0E-08
1,0E-09
1 2 3 4 5 6 7 8 9 10 11 12 13 14
pH
● Vändöra 2 (P,1,1)
[CrO4-2]

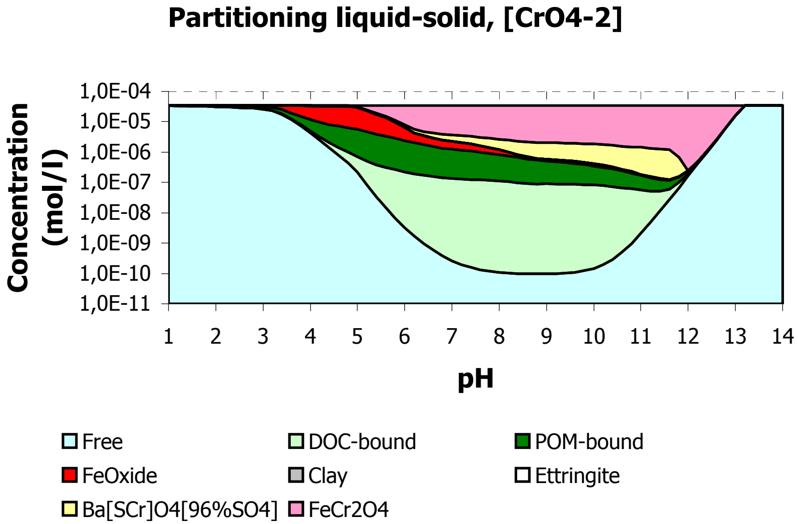
Partitioning liquid-solid, [CrO4-2]
Concentration (mol/l)
1,0E-04
1,0E-05
1,0E-06
1,0E-07
1,0E-08
1,0E-09
1,0E-10
1,0E-11
1 2 3 4 5 6 7 8 9 10 11 12 13 14
pH
Free
DOC-bound
POM-bound
FeOxide
Clay
Ettringite
Ba[SCr]O4[96%SO4]
FeCr2O4

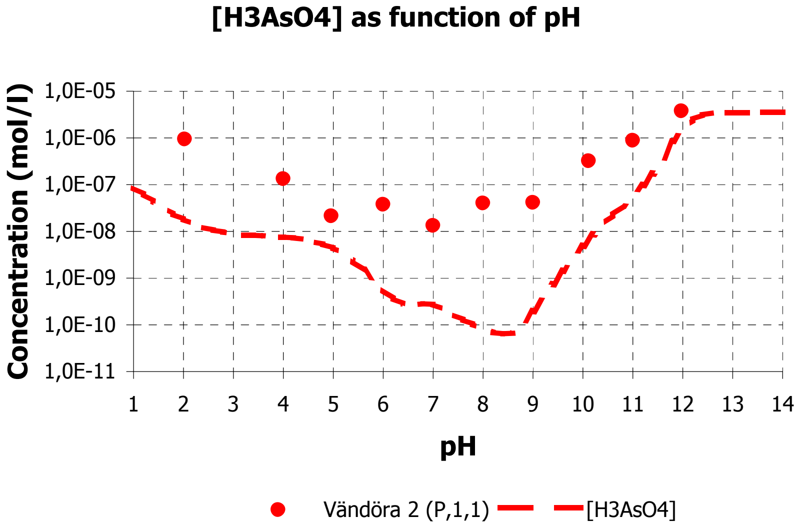
[H3AsO4] as function of pH
Concentration (mol/l)
1,0E-05
1,0E-06
1,0E-07
1,0E-08
1,0E-09
1,0E-10
1,0E-11
1 2 3 4 5 6 7 8 9 10 11 12 13 14
pH
● Vändöra 2 (P,1,1)
[H3AsO4]

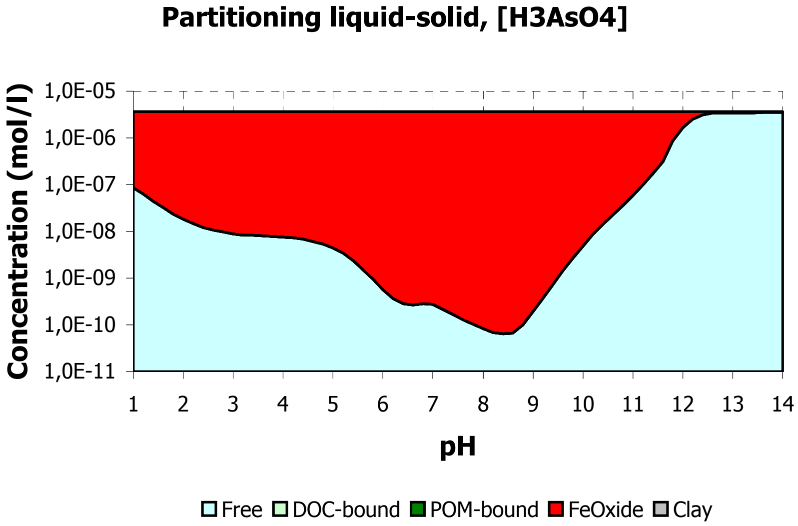
Partitioning liquid-solid, [H3AsO4]
Concentration (mol/l)
1,0E-05
1,0E-06
1,0E-07
1,0E-08
1,0E-09
1,0E-10
1,0E-11
1 2 3 4 5 6 7 8 9 10 11 12 13 14
pH
Free
DOC-bound
POM-bound
FeOxide
Clay

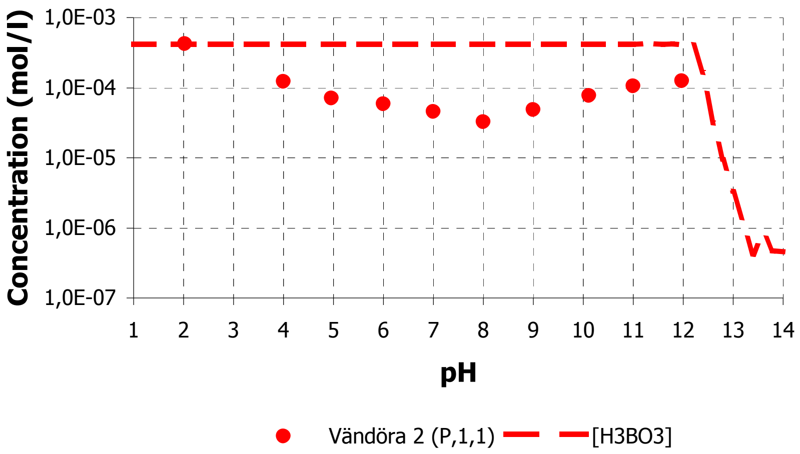
[H3BO3] as function of pH

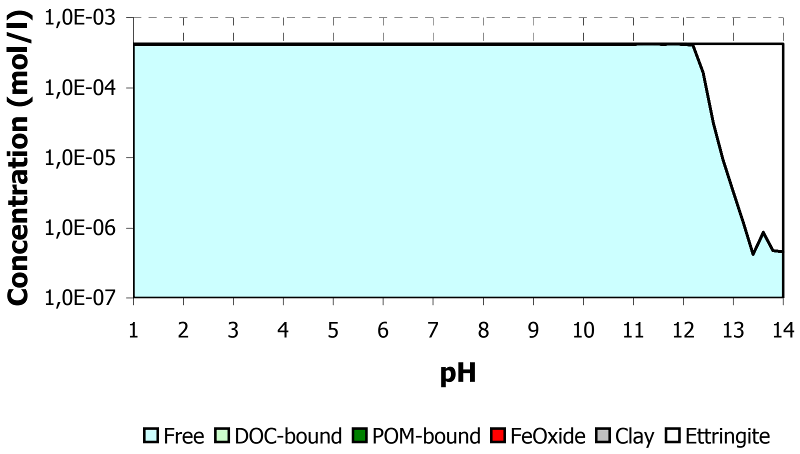
Partitioning liquid-solid, [H3BO3]

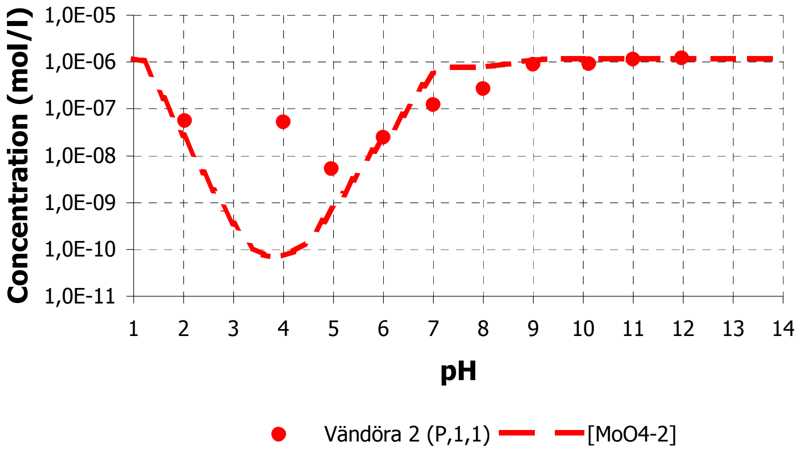
[MoO4-2] as function of pH

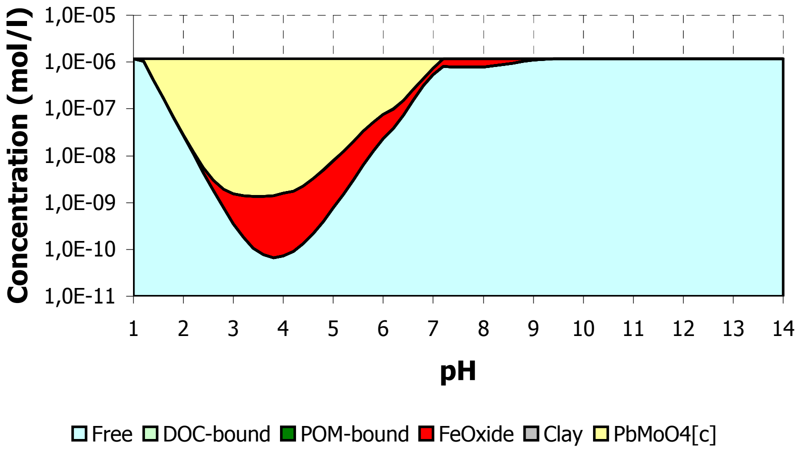
Partitioning liquid-solid, [MoO4-2]

[Sb[OH]6-] as function of pH

Partitioning liquid-solid, [Sb[OH]6-]

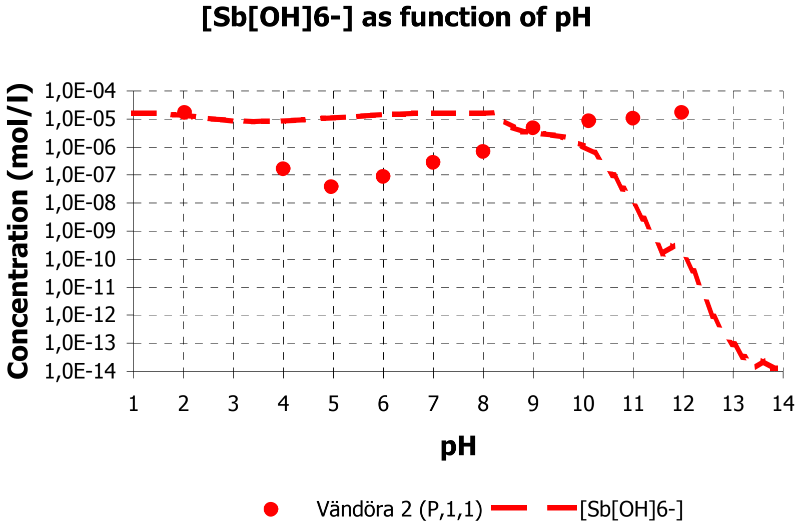
[Sb[OH]6-] as function of pH

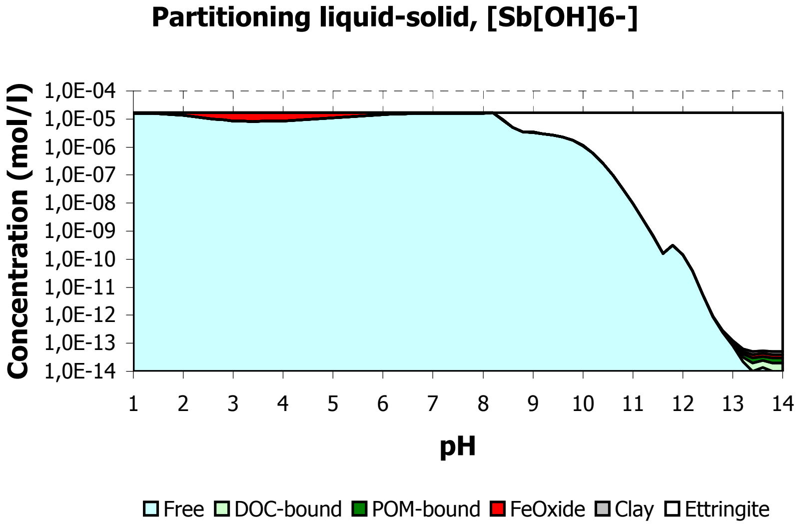
Partitioning liquid-solid, [Sb[OH]6-]

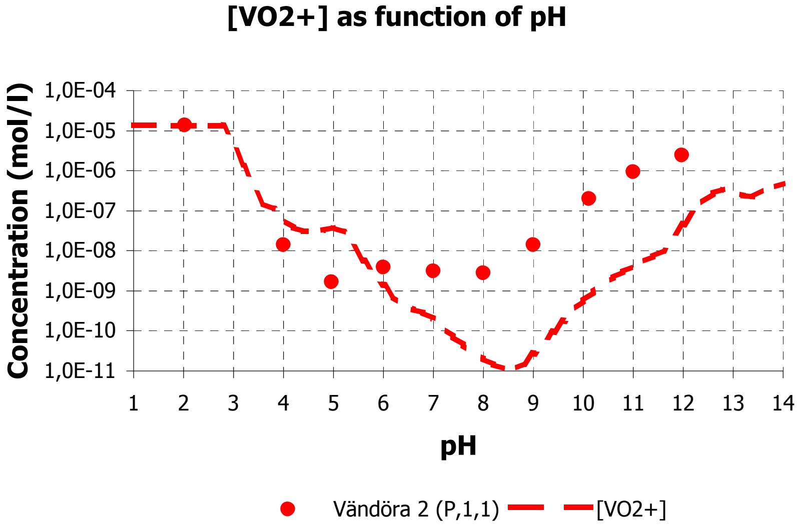
[VO2+] as function of pH

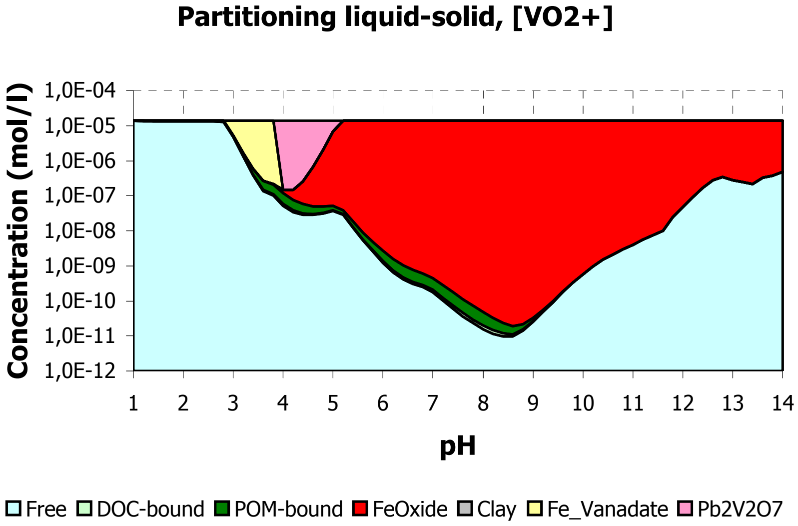
Partitioning liquid-solid, [VO2+]

[Br-] as function of pH

Partitioning liquid-solid, [Br-]

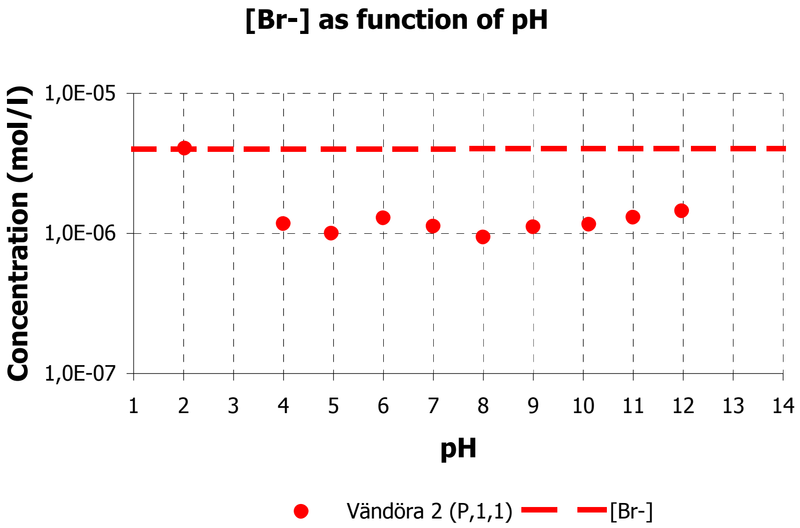

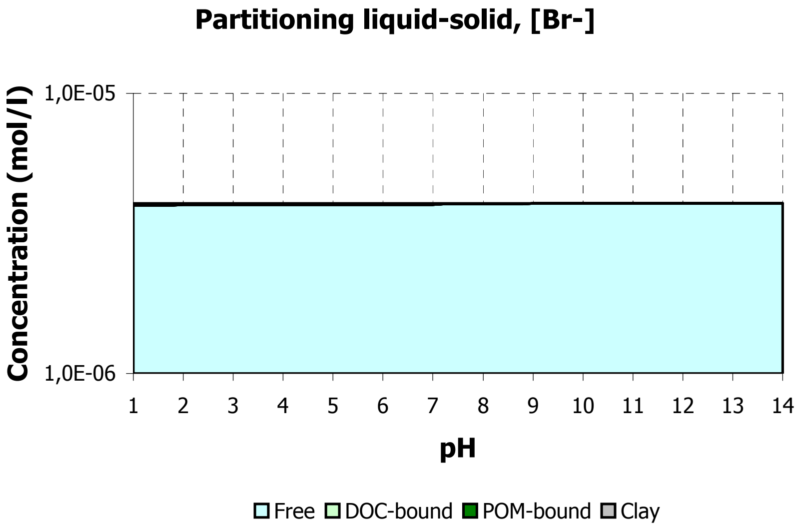

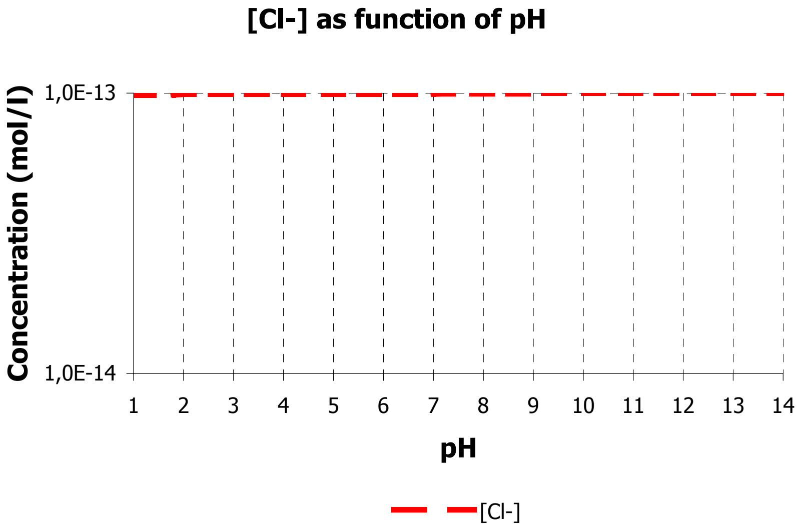

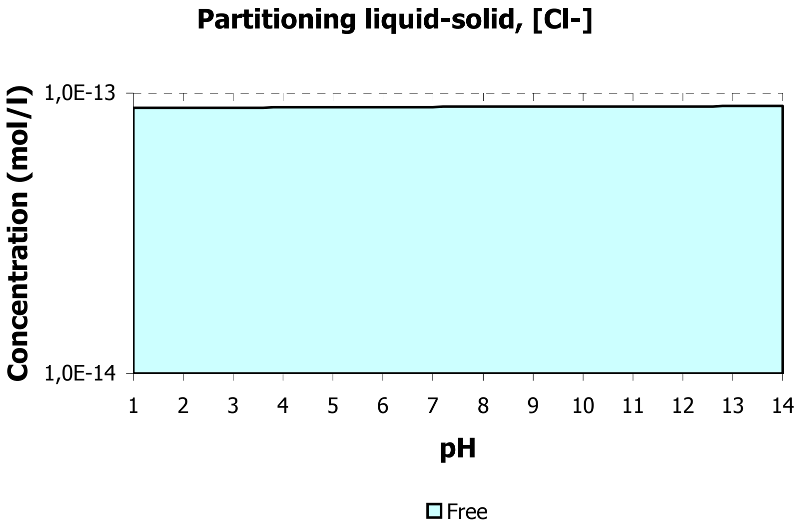

[F-] as function of pH

Partitioning liquid-solid, [F-]

[F-] as function of pH

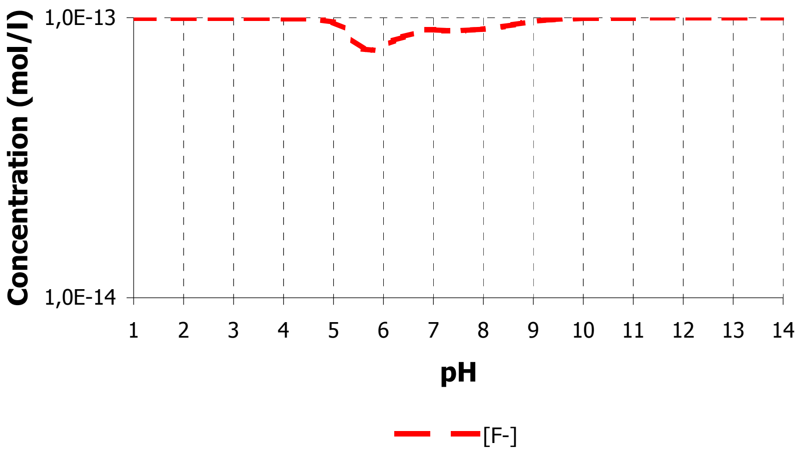

Partitioning liquid-solid, [F-]

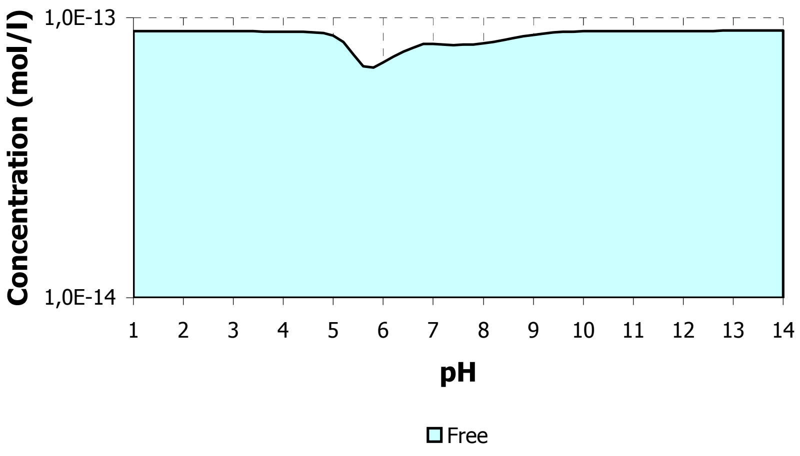

[K+] as function of pH

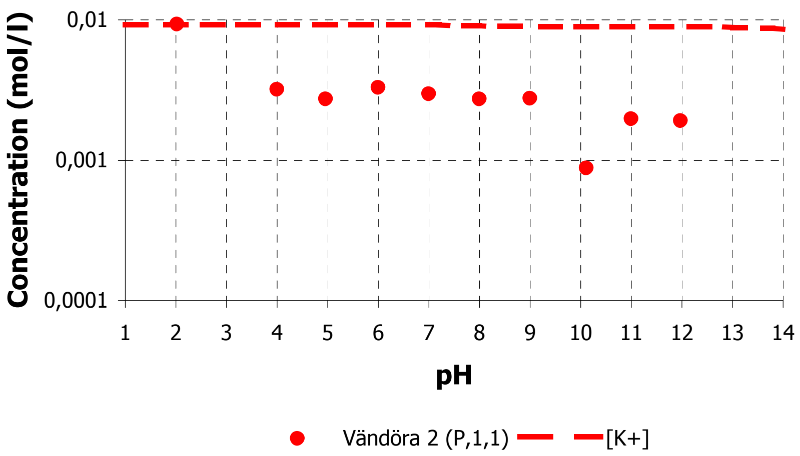

Partitioning liquid-solid, [K+]

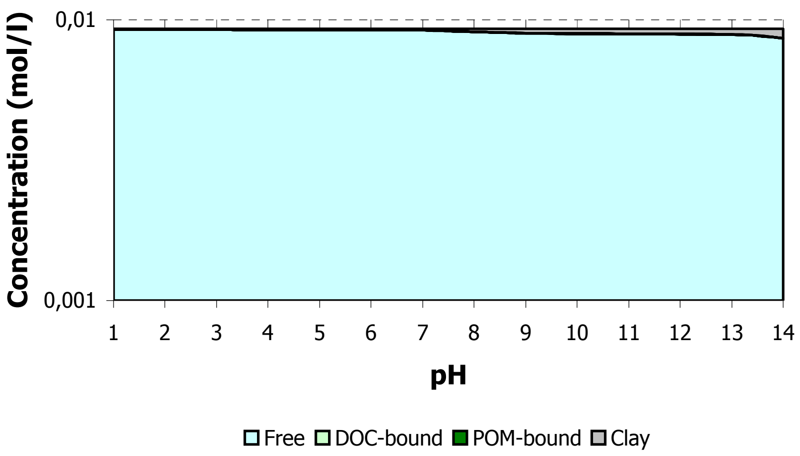

[Li+] as function of pH

Partitioning liquid-solid, [Li+]

[Li+] as function of pH

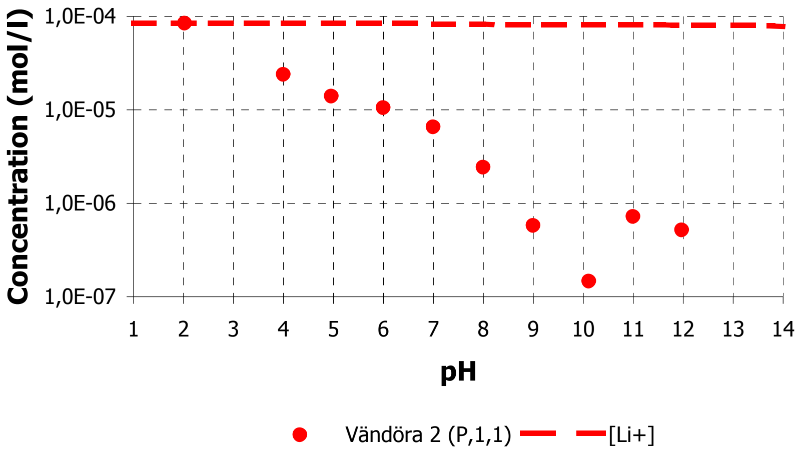

Partitioning liquid-solid, [Li+]

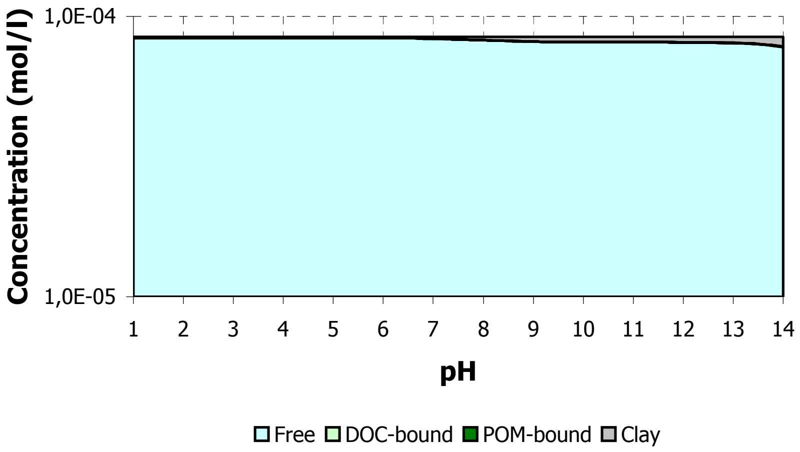

[Na+] as function of pH

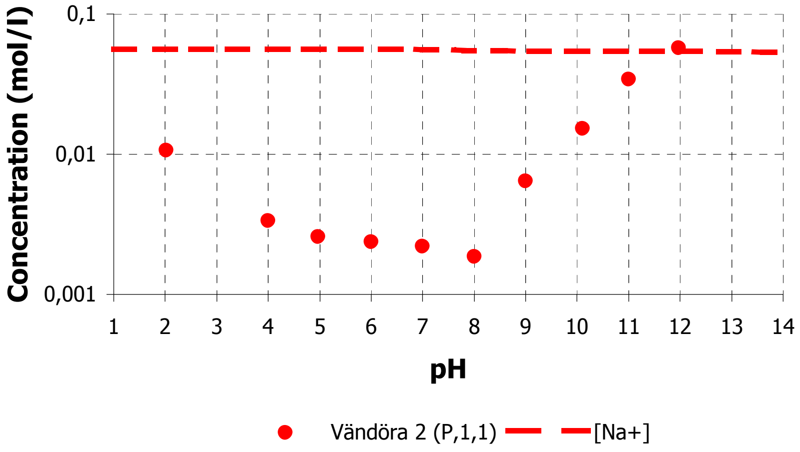

Partitioning liquid-solid, [Na+]

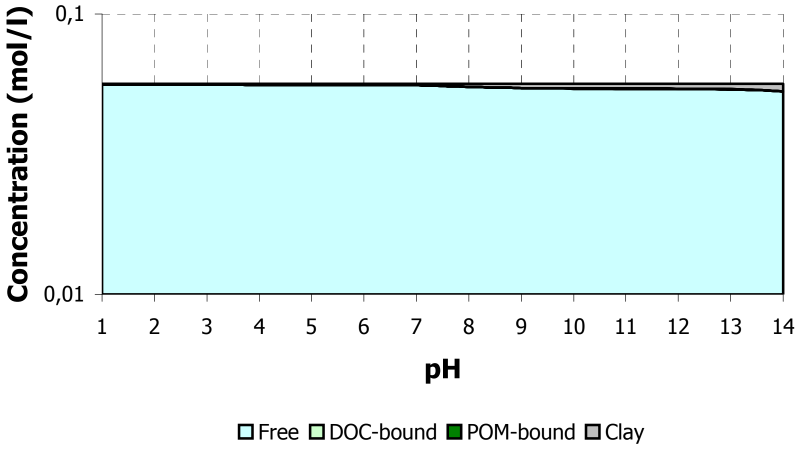

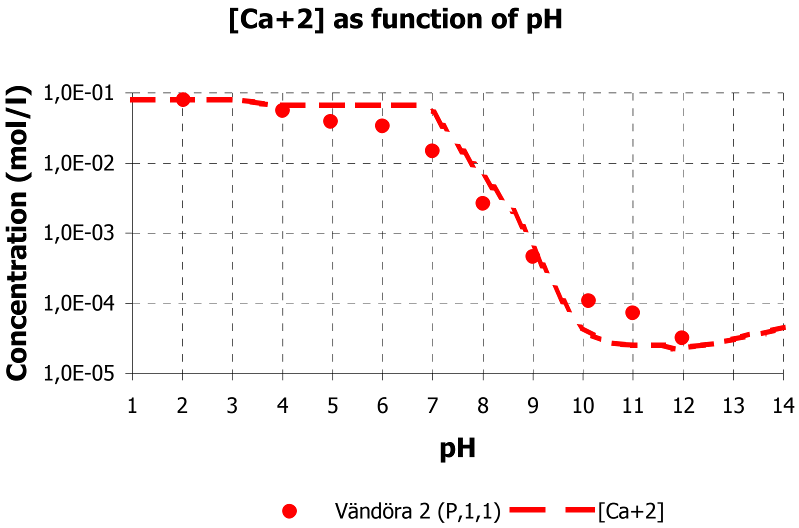

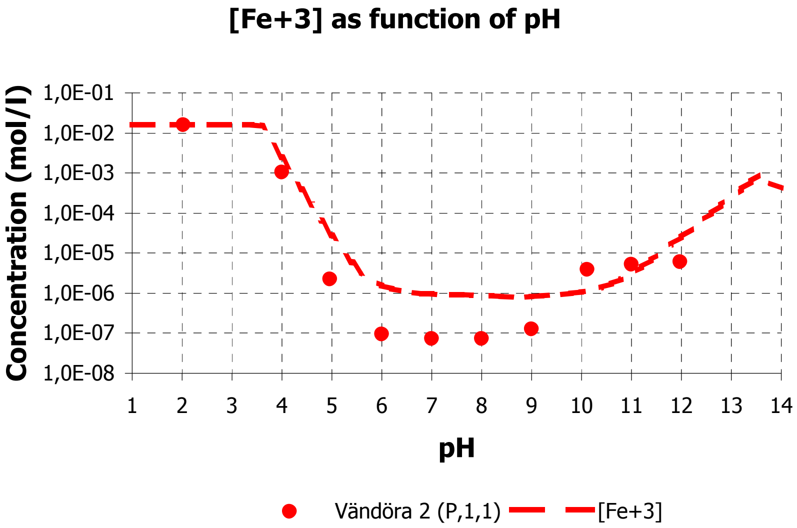

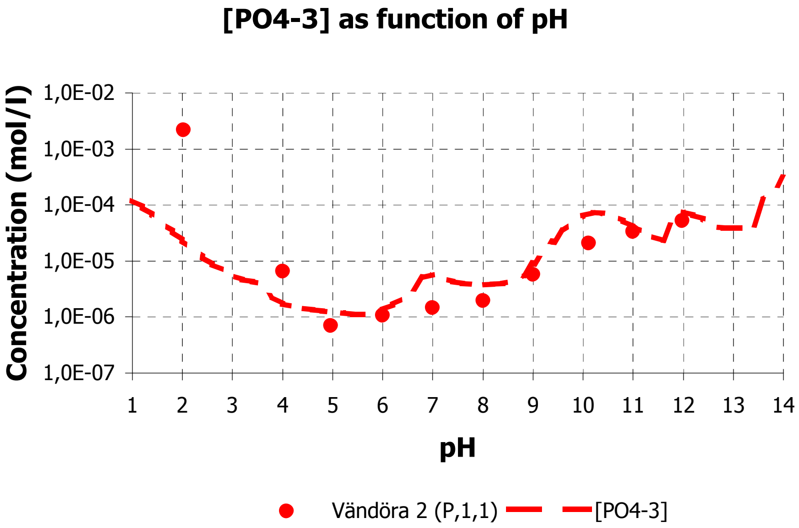

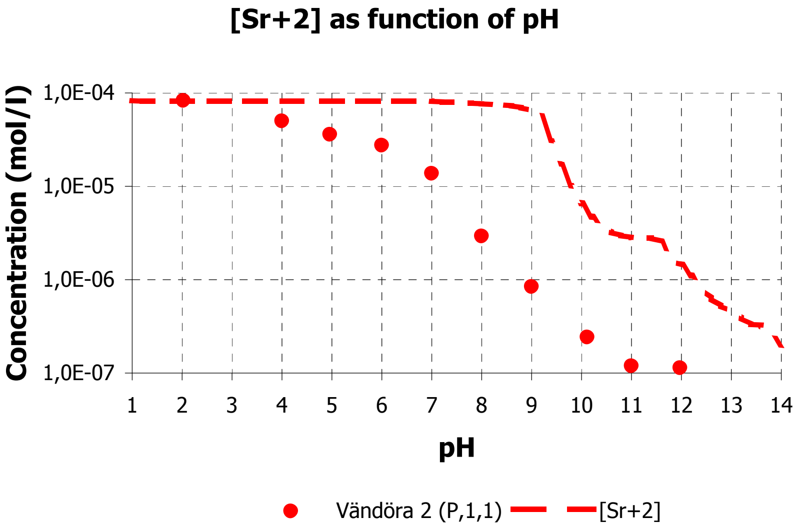

[Mn+2] as function of pH

[Ni+2] as function of pH

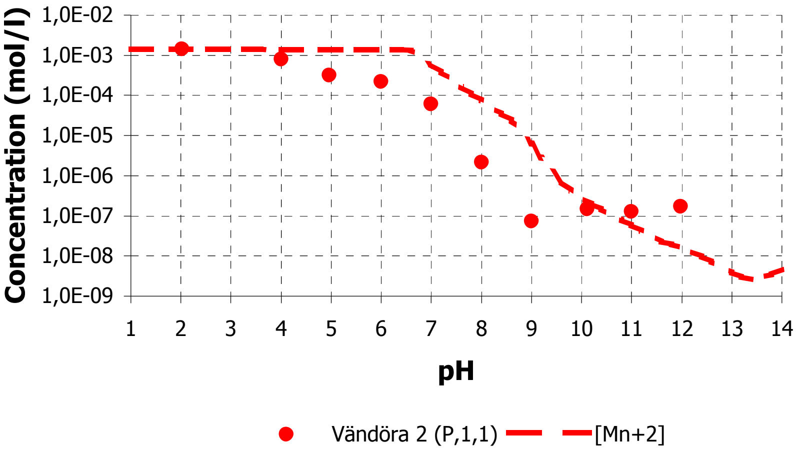
[Mn+2] as function of pH

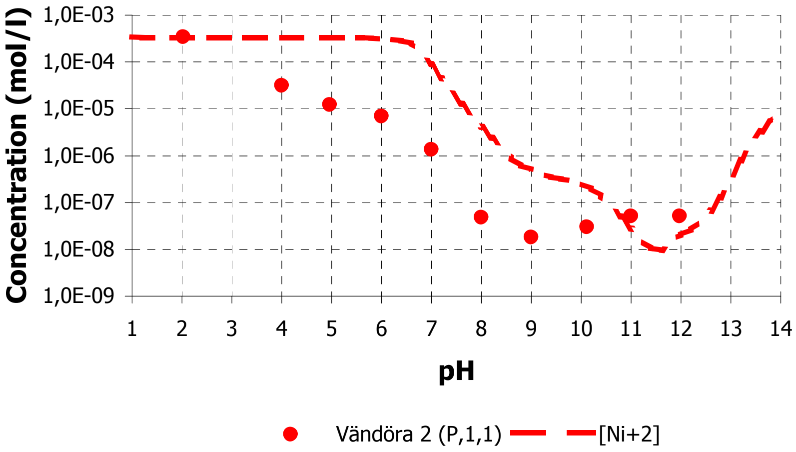
[Ni+2] as function of pH

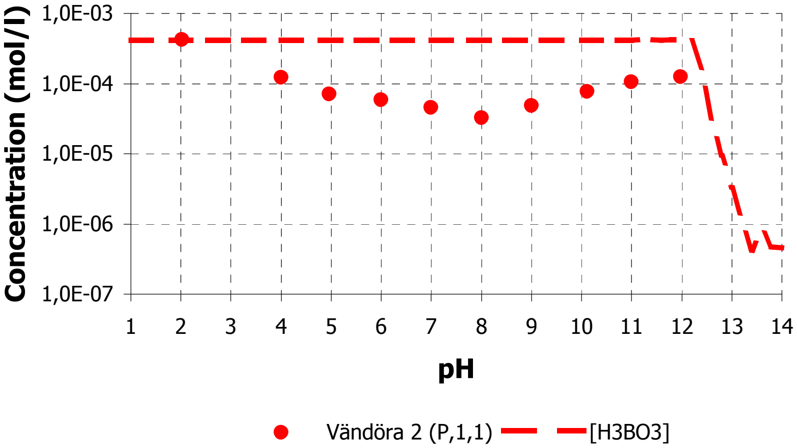
[H3BO3] as function of pH

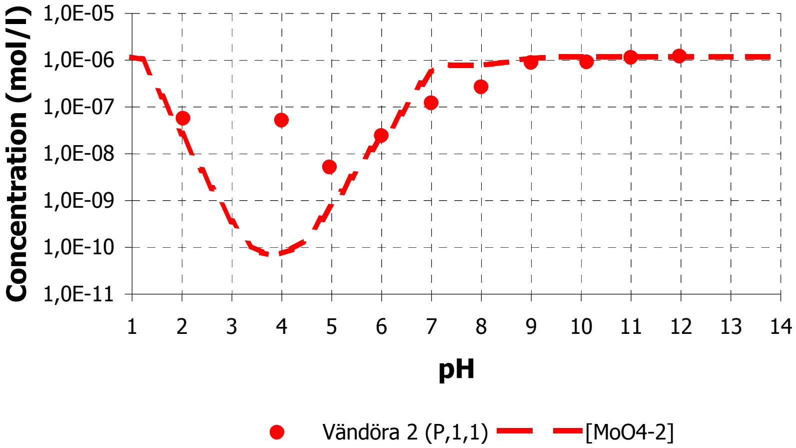
[MoO4-2] as function of pH

[F-] as function of pH

[K+] as function of pH

[F-] as function of pH

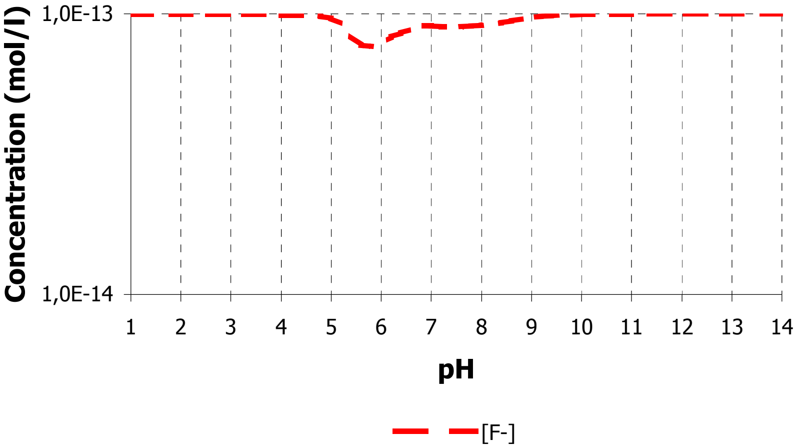

[K+] as function of pH

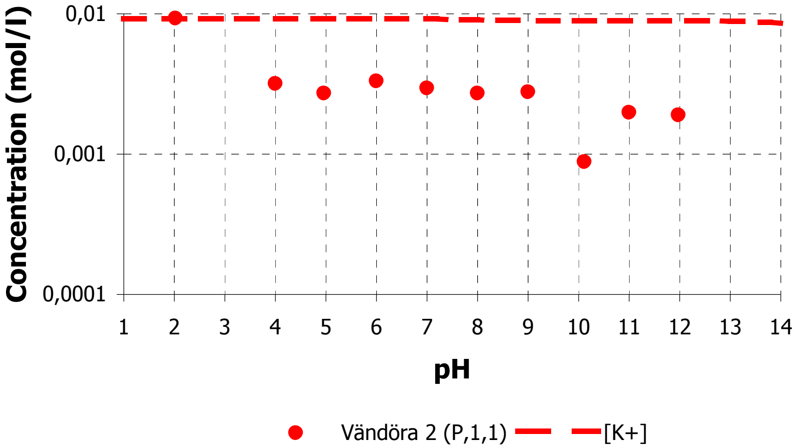

Vändöra 2 ecn-090406: Conductivity as function of pH

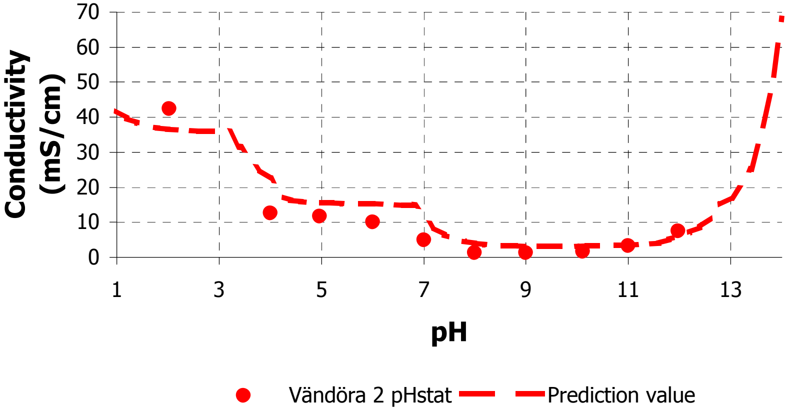

Vändöra 2 ecn-090406: ANC/BNC as function of pH

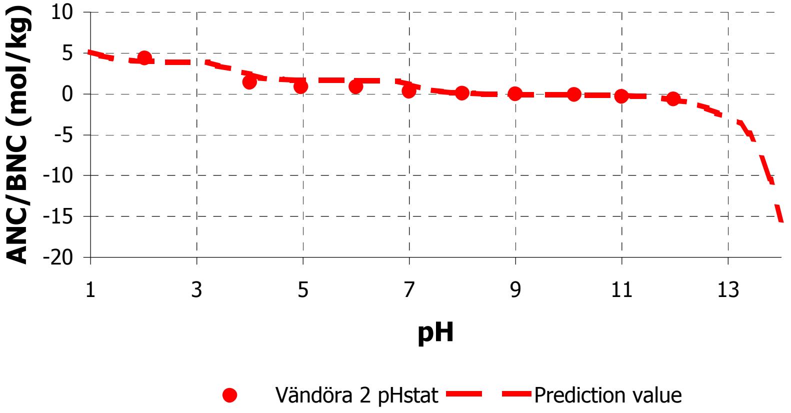

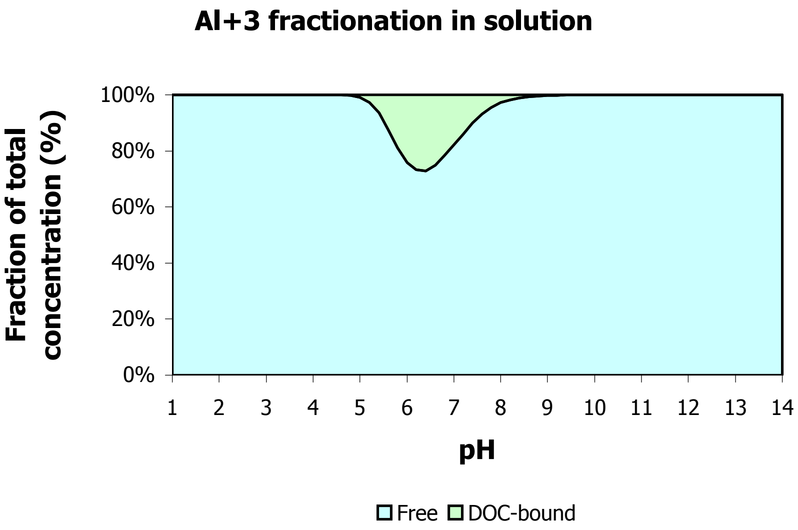
Al+3 fractionation in solution

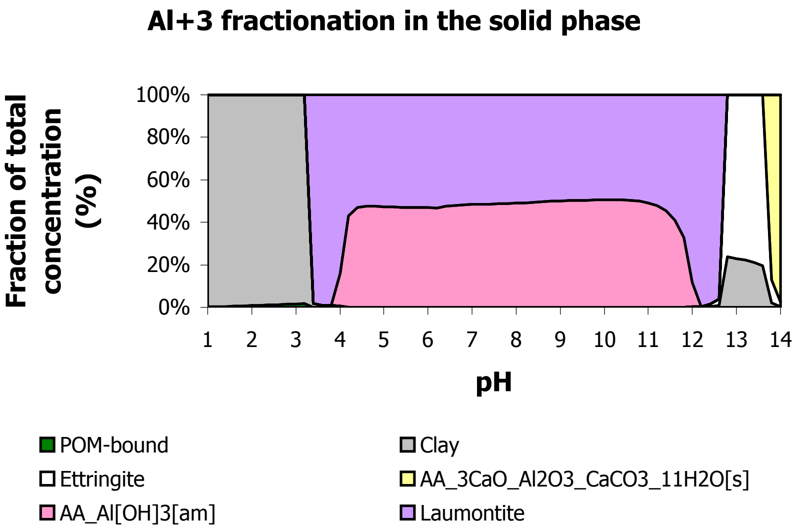
Al+3 fractionation in the solid phase

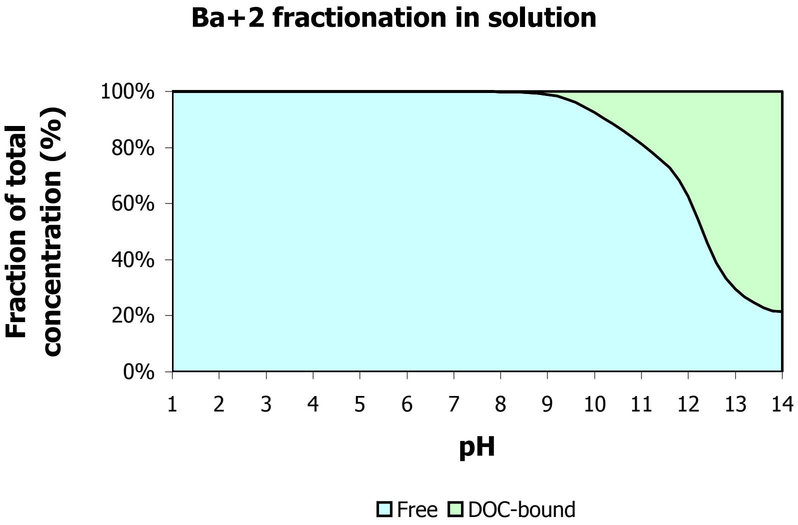
Ba+2 fractionation in solution

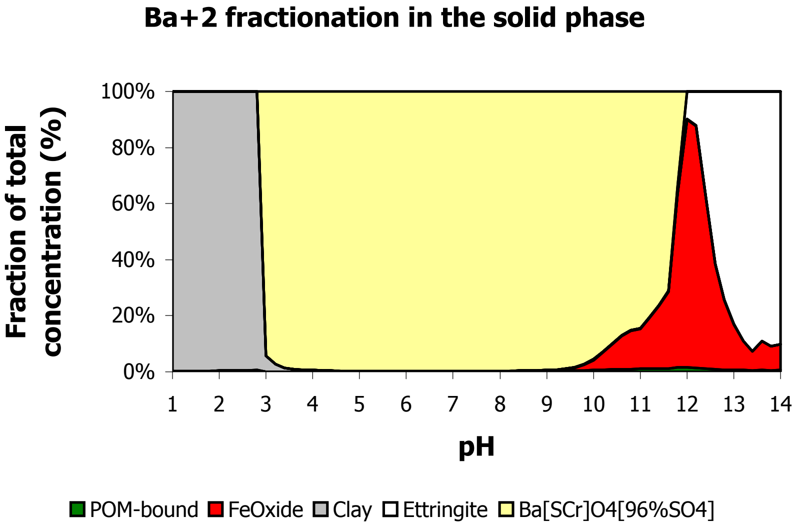
Ba+2 fractionation in the solid phase

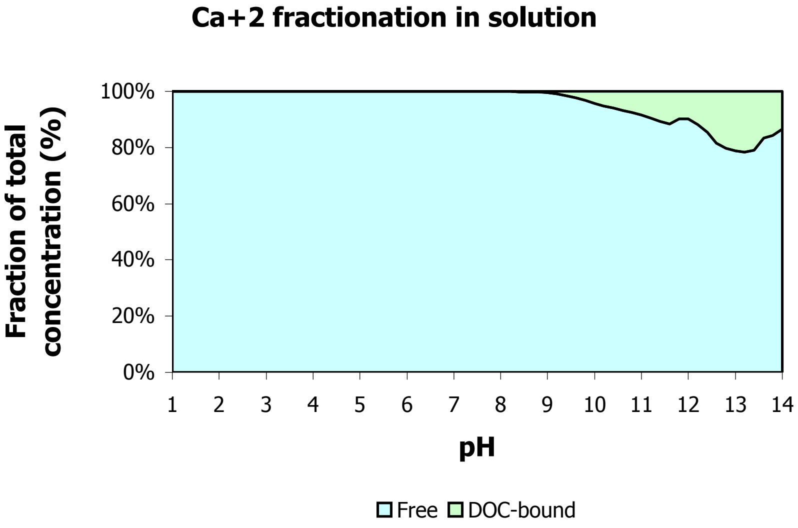

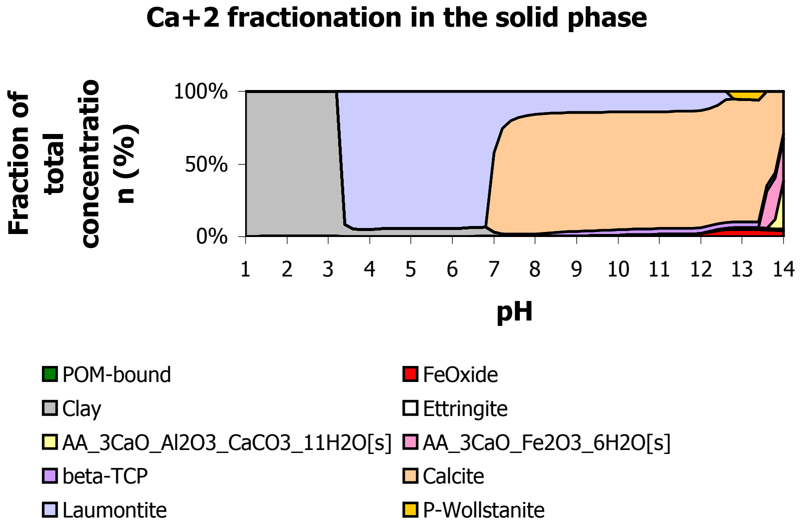

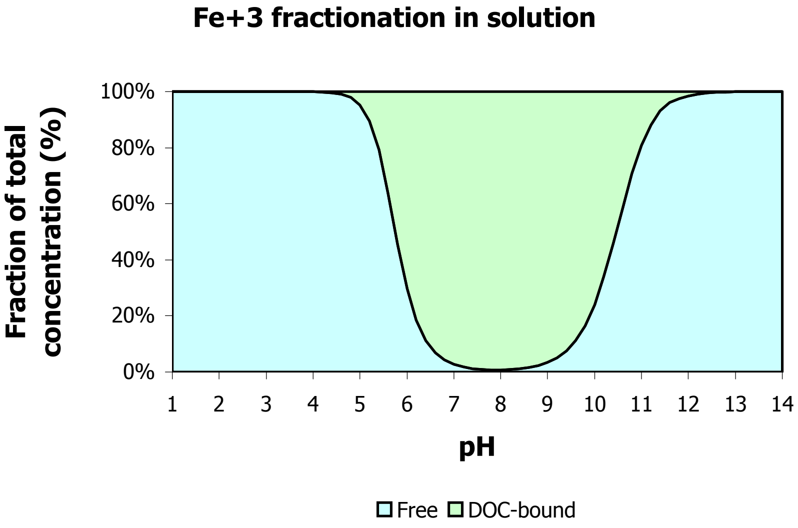

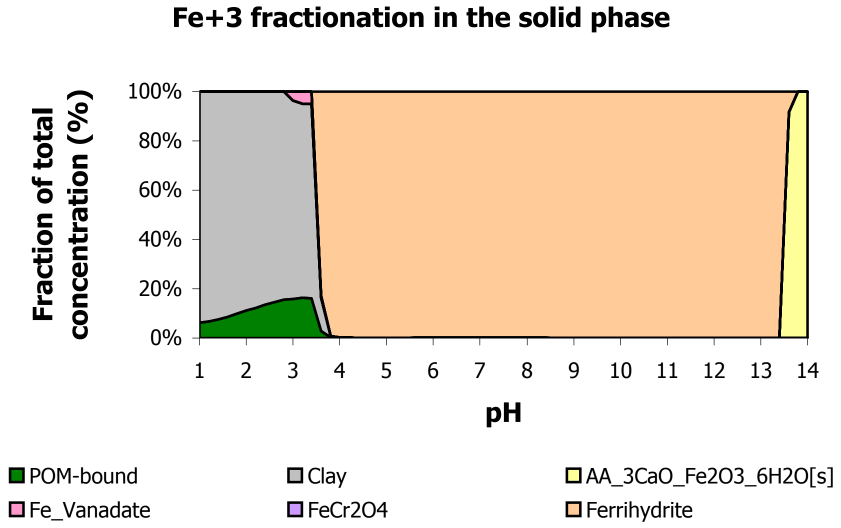

H4SiO4 fractionation in solution

H4SiO4 fractionation in the solid phase

H4SiO4 fractionation in solution

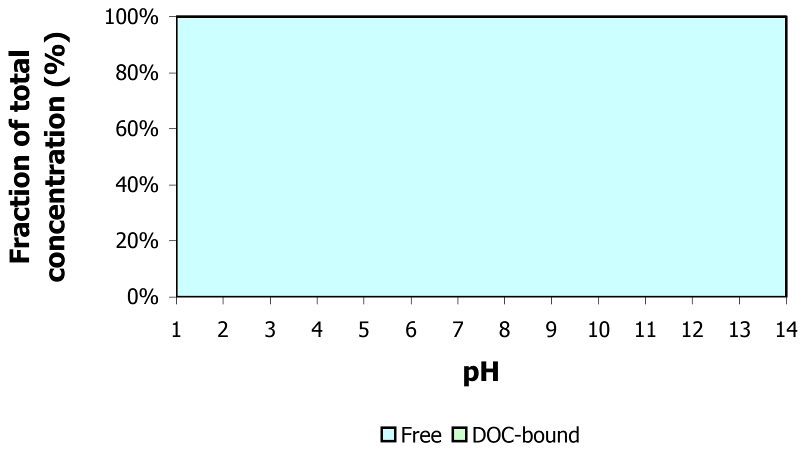

H4SiO4 fractionation in the solid phase

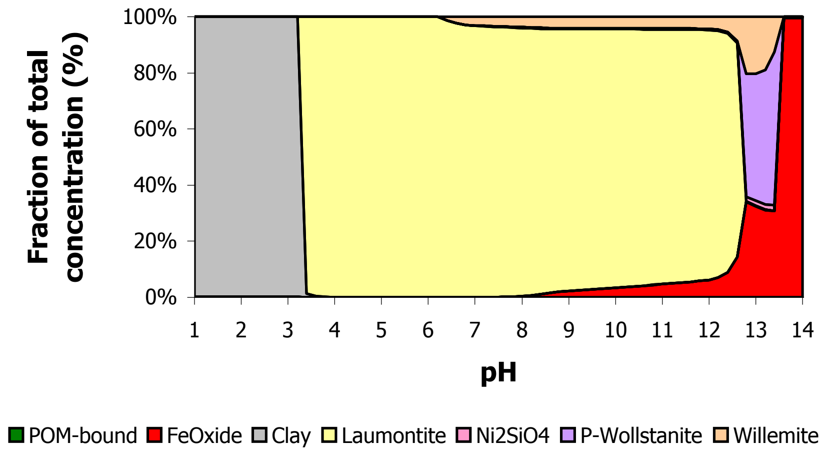

SO4-2 fractionation in solution

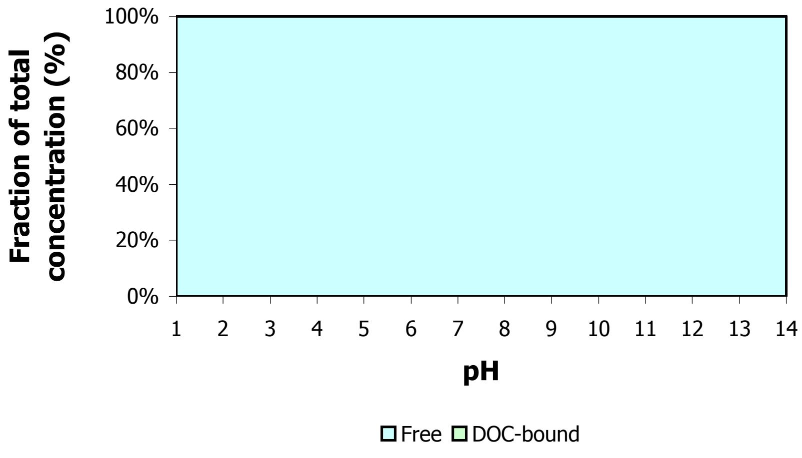

SO4-2 fractionation in the solid phase

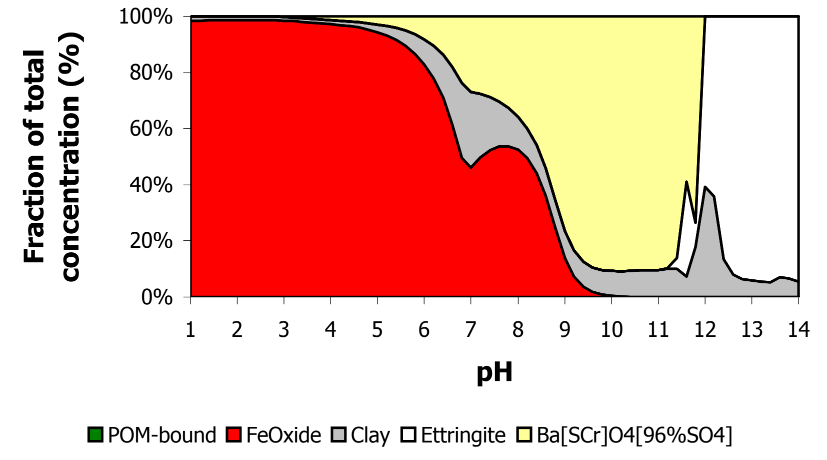

H2CO3 fractionation in solution

H2CO3 fractionation in the solid phase

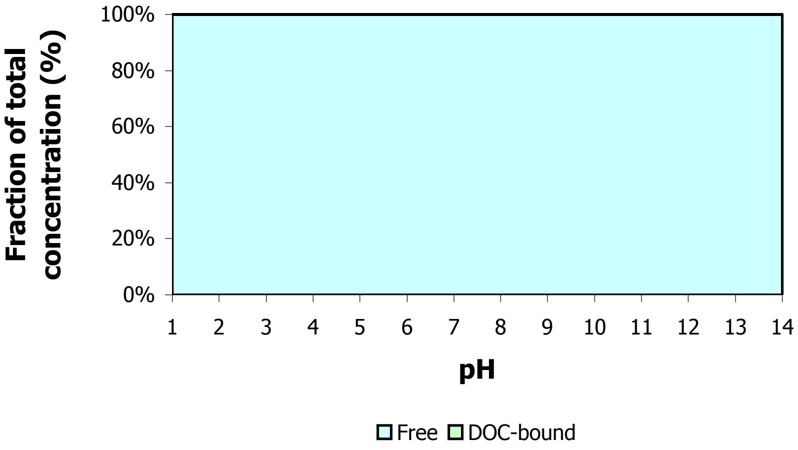
H2CO3 fractionation in solution

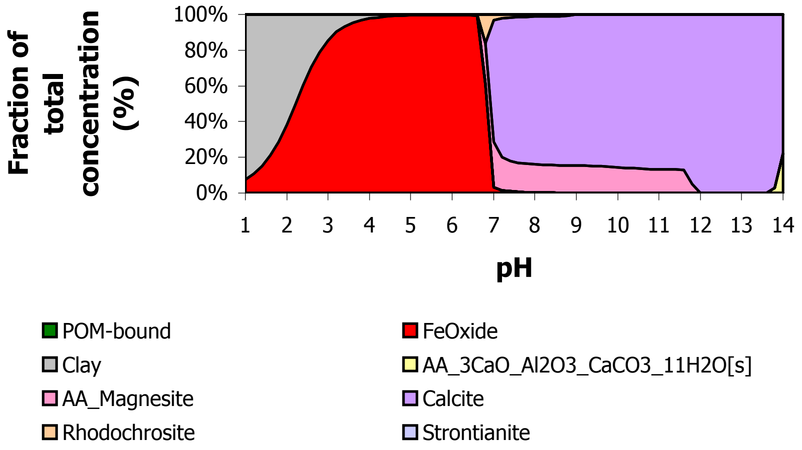
H2CO3 fractionation in the solid phase

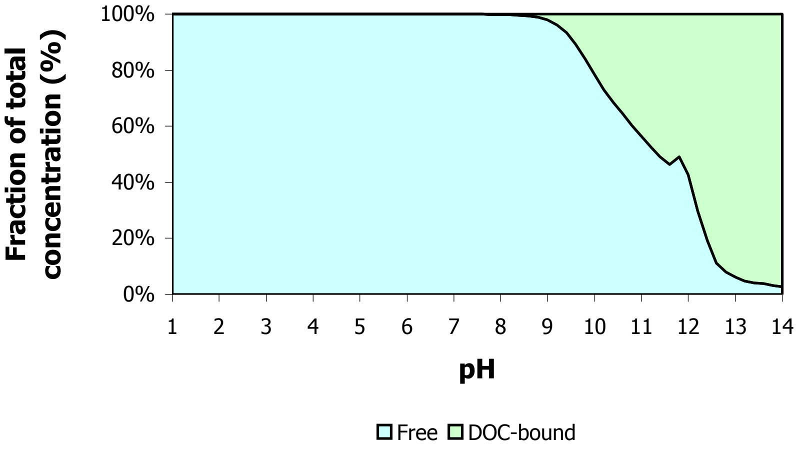
Mg+2 fractionation in solution

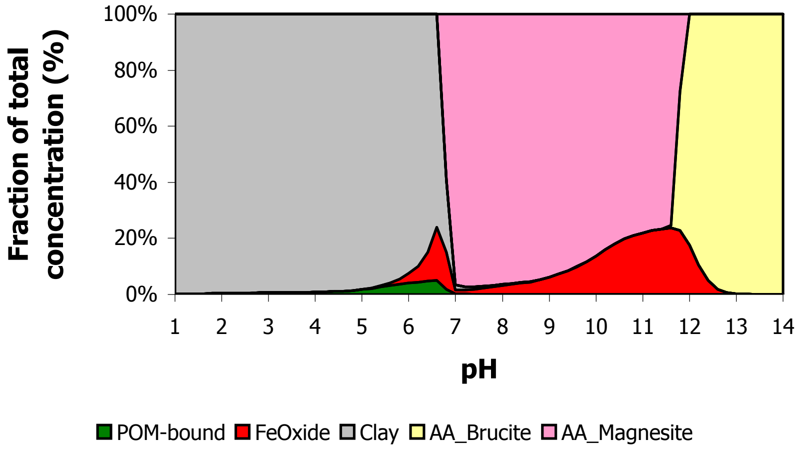
Mg+2 fractionation in the solid phase

PO4-3 fractionation in solution

PO4-3 fractionation in the solid phase

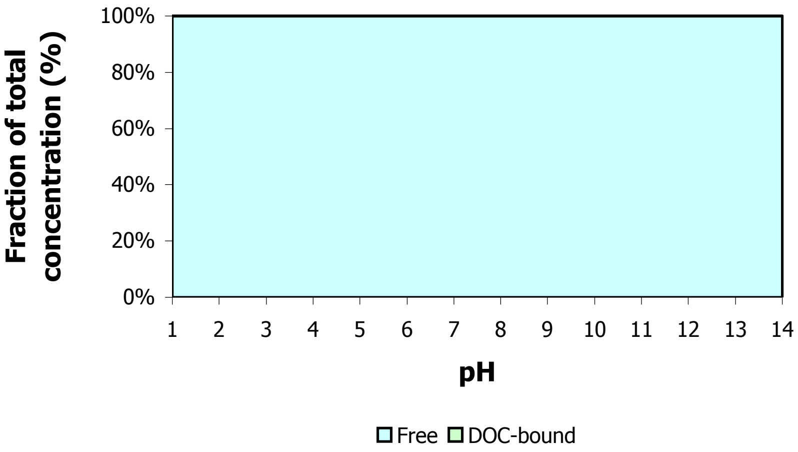
PO4-3 fractionation in solution

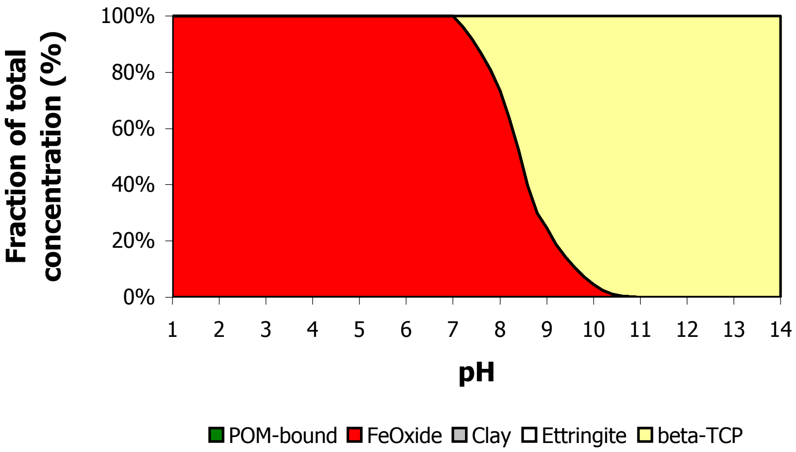
PO4-3 fractionation in the solid phase

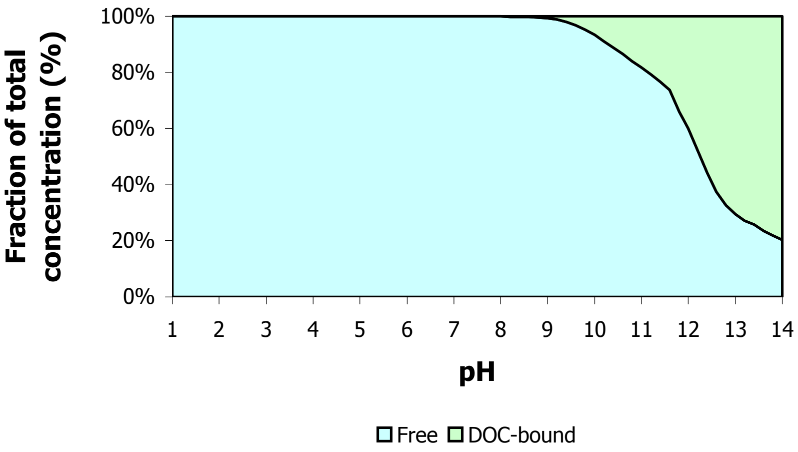
Sr+2 fractionation in solution

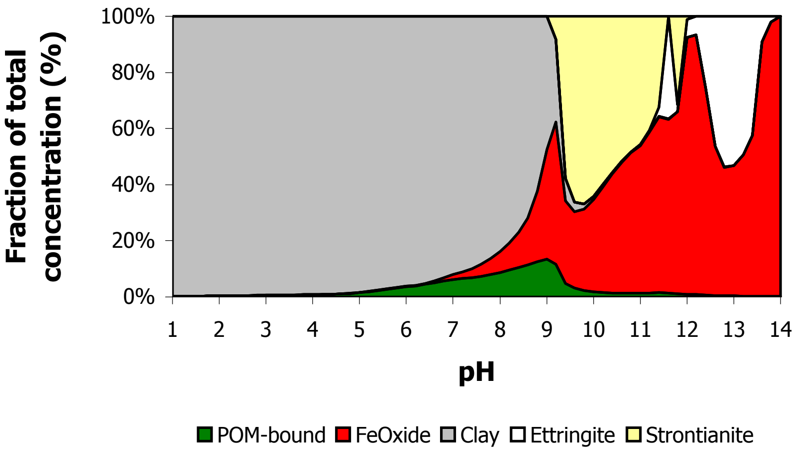
Sr+2 fractionation in the solid phase

Cd+2 fractionation in solution

Cd+2 fractionation in the solid phase

Cd+2 fractionation in solution

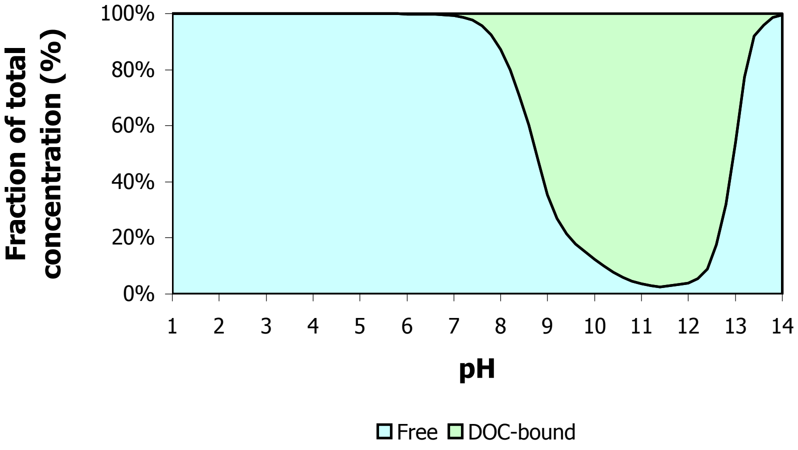

Cd+2 fractionation in the solid phase

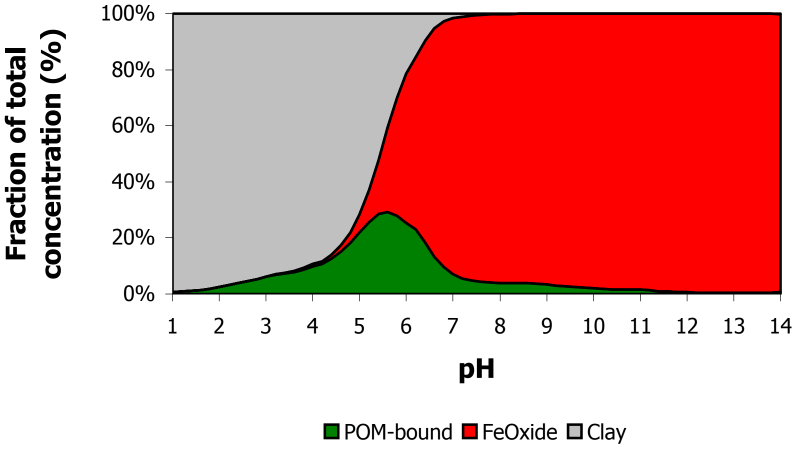

Cu+2 fractionation in solution

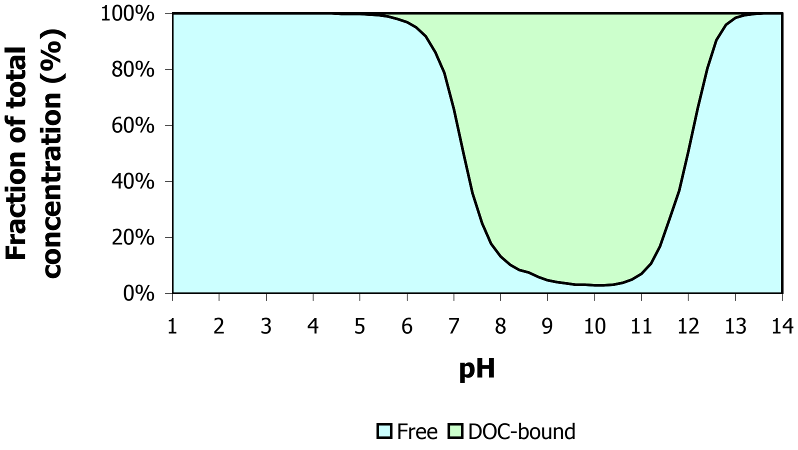

Cu+2 fractionation in the solid phase

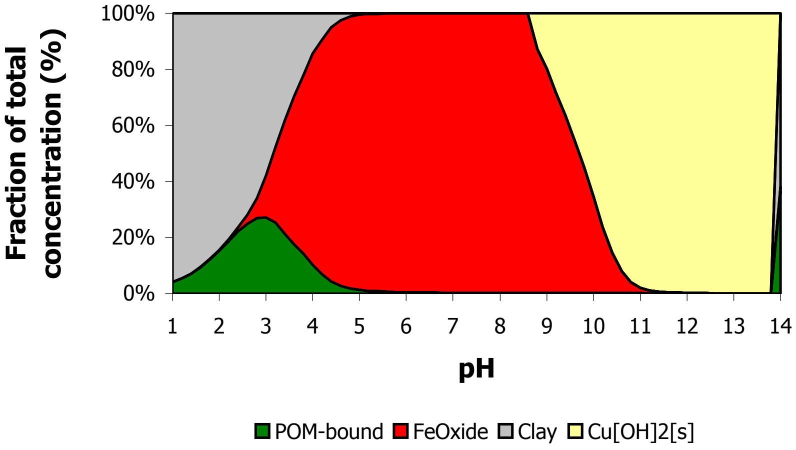

Mn+2 fractionation in solution

Mn+2 fractionation in the solid phase

Mn+2 fractionation in solution

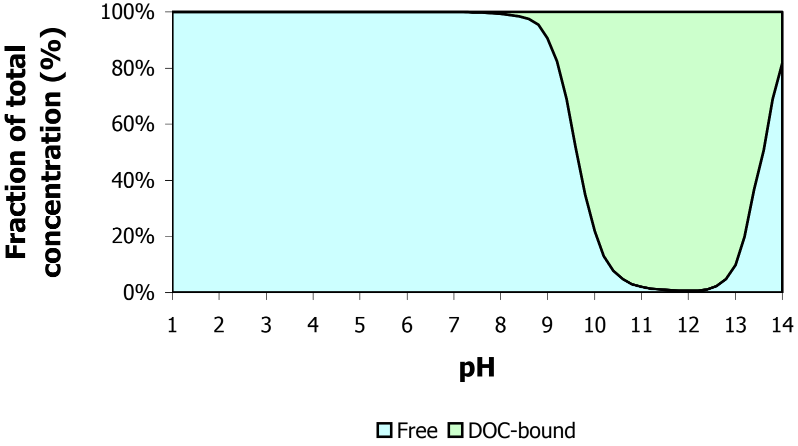

Mn+2 fractionation in the solid phase

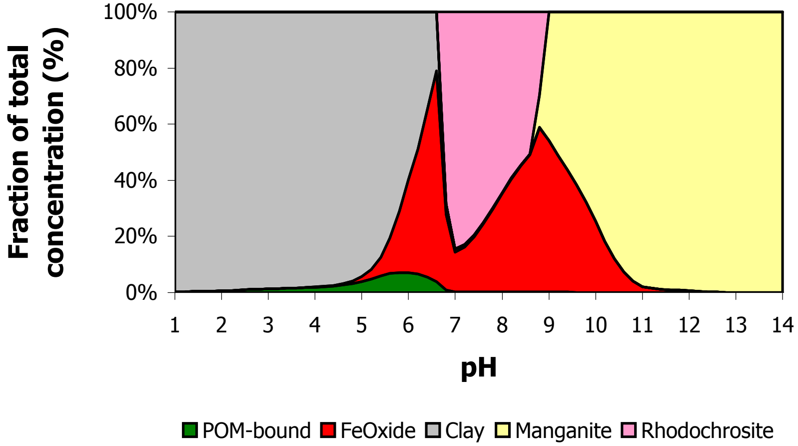

Ni+2 fractionation in solution

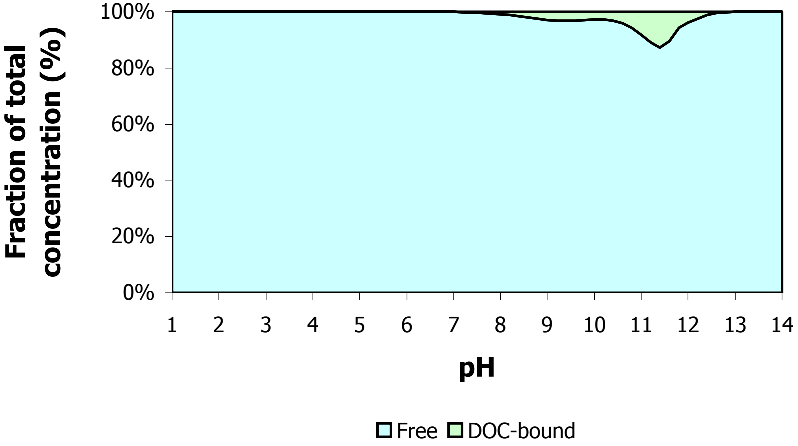

Ni+2 fractionation in the solid phase

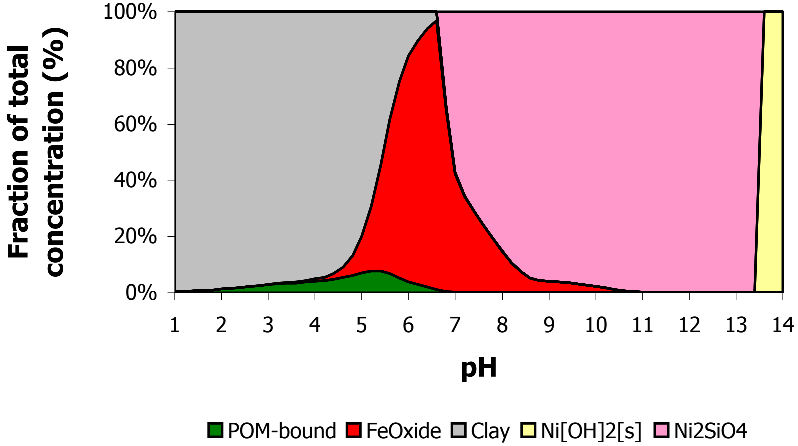

Pb+2 fractionation in solution

Pb+2 fractionation in the solid phase

Pb+2 fractionation in solution

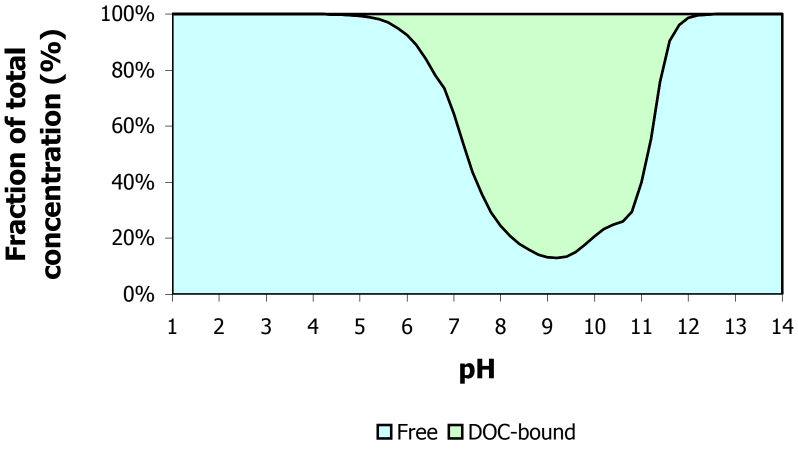

Pb+2 fractionation in the solid phase

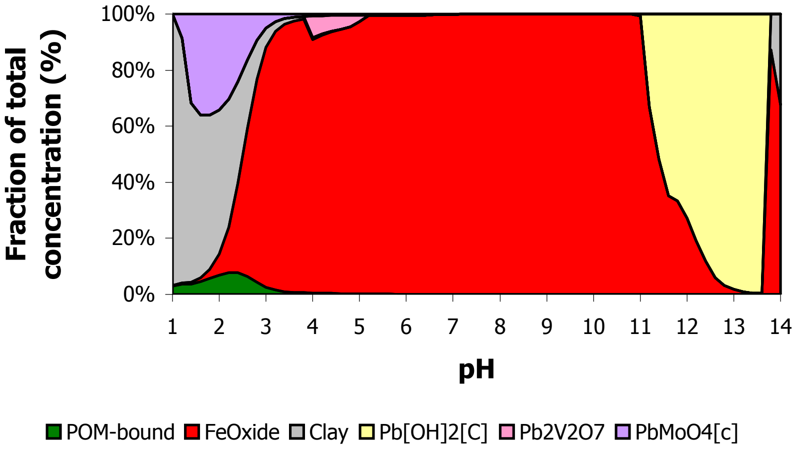

Zn+2 fractionation in solution

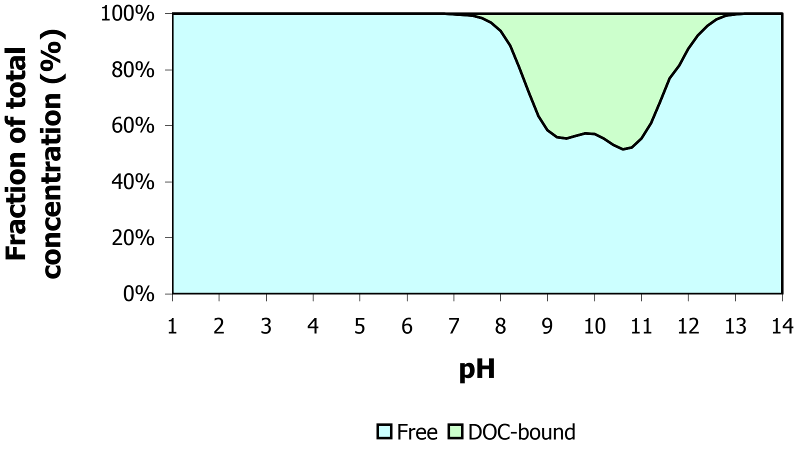

Zn+2 fractionation in the solid phase

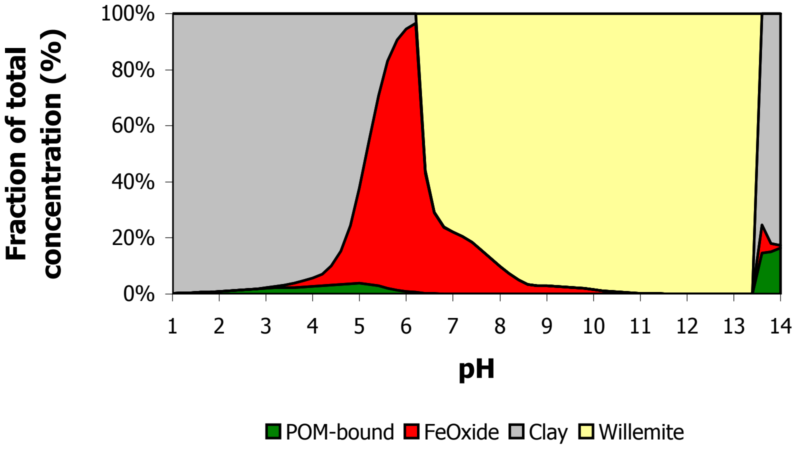

CrO4-2 fractionation in solution

CrO4-2 fractionation in the solid phase

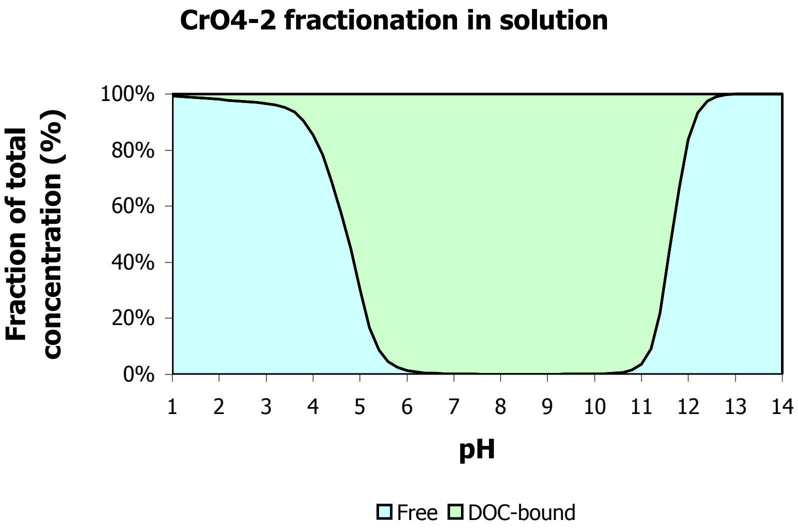
CrO4-2 fractionation in solution

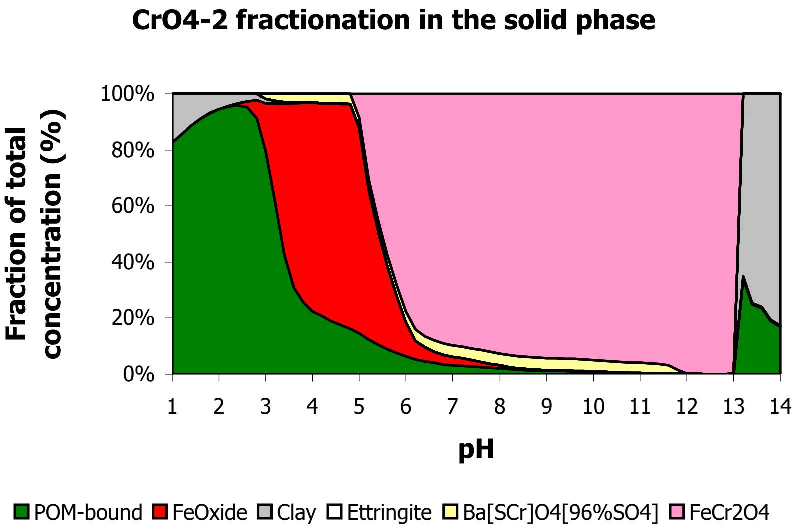
CrO4-2 fractionation in the solid phase

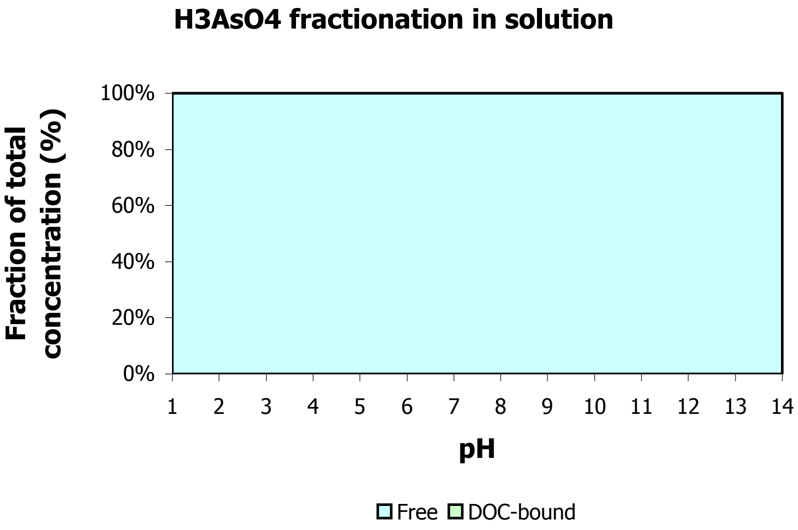
H3AsO4 fractionation in solution

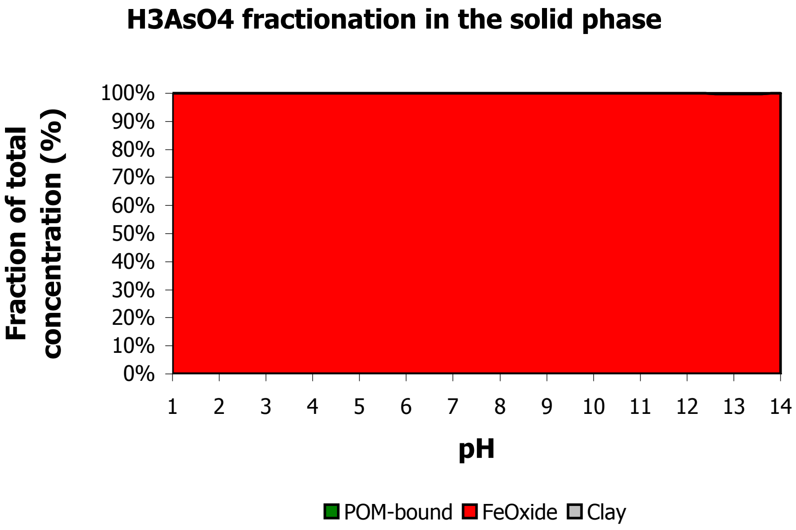
H3AsO4 fractionation in the solid phase

H3BO3 fractionation in solution

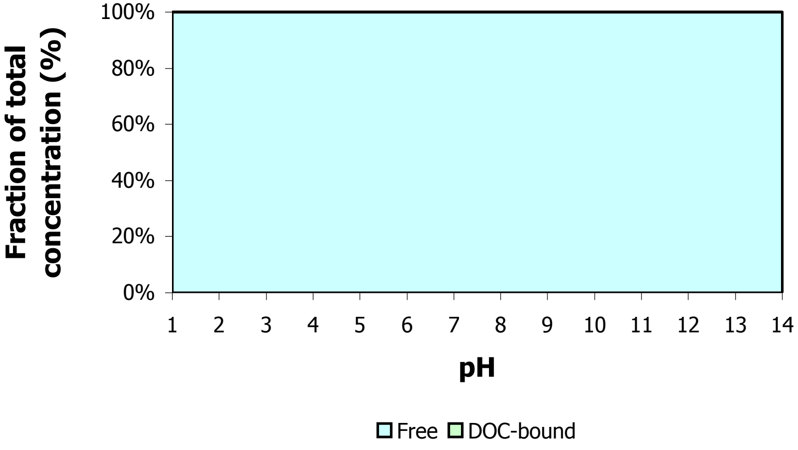

H3BO3 fractionation in the solid phase

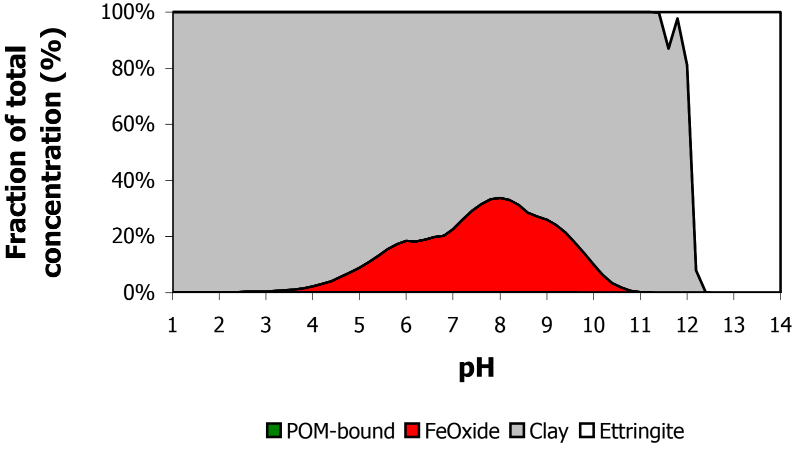

MoO4-2 fractionation in solution

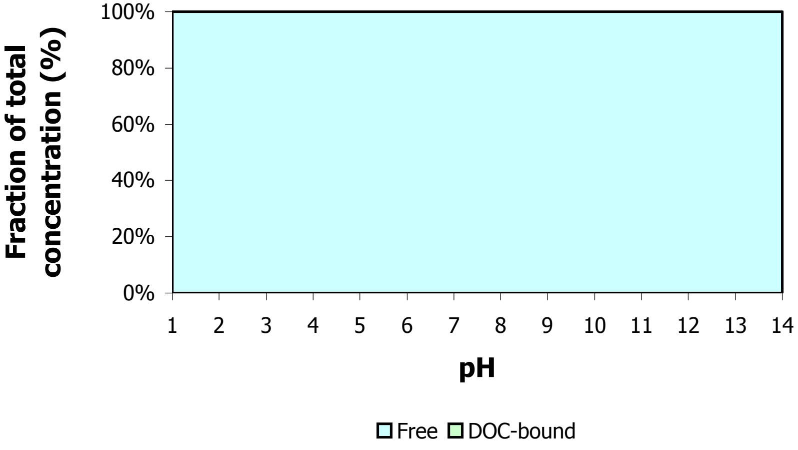

MoO4-2 fractionation in the solid phase

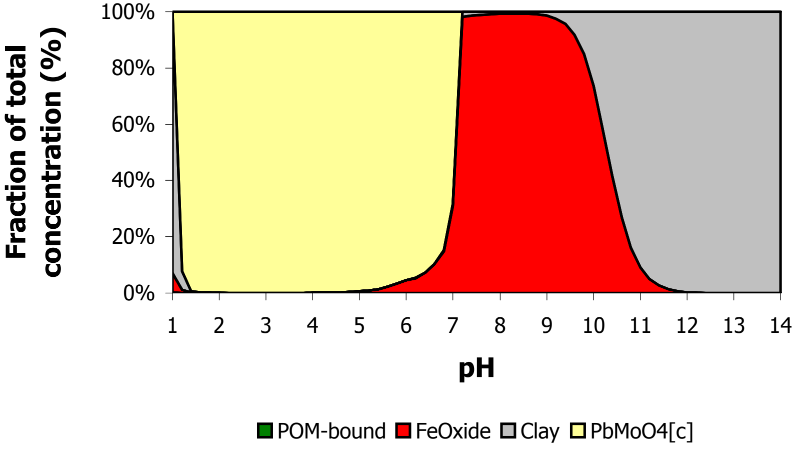

Sb[OH]6- fractionation in solution

Sb[OH]6- fractionation in the solid phase

Sb[OH]6- fractionation in solution

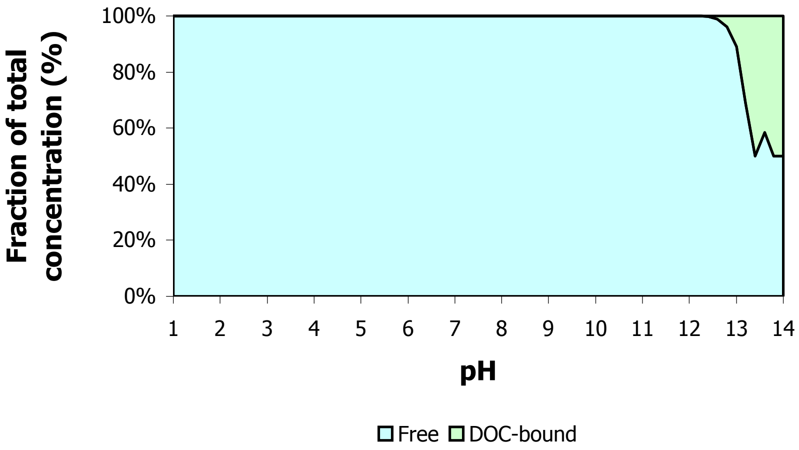

Sb[OH]6- fractionation in the solid phase

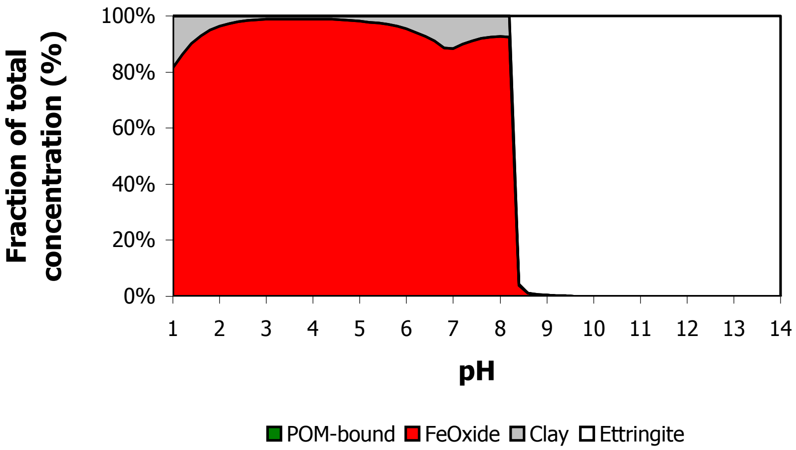

VO2+ fractionation in solution

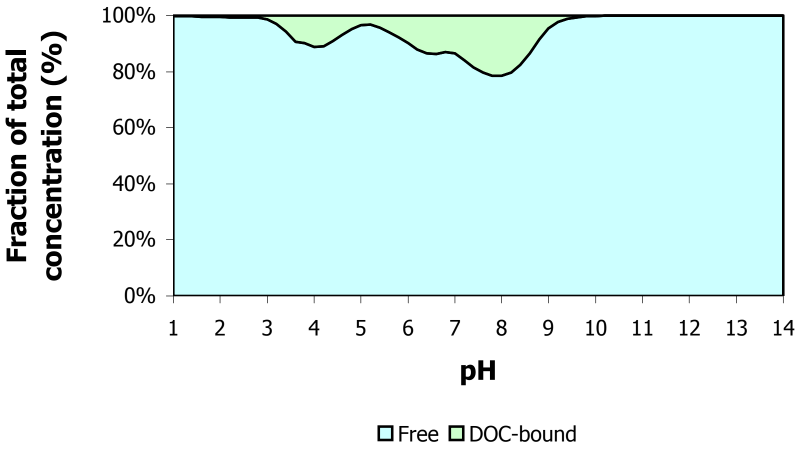

VO2+ fractionation in the solid phase

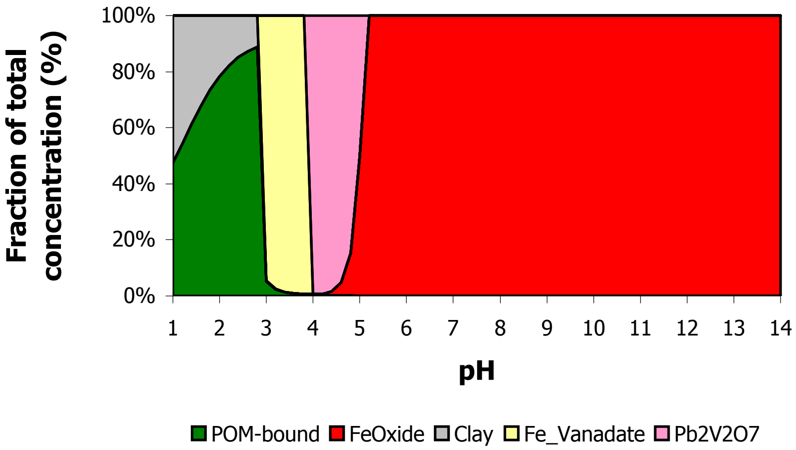

Br- fractionation in solution

Br- fractionation in the solid phase

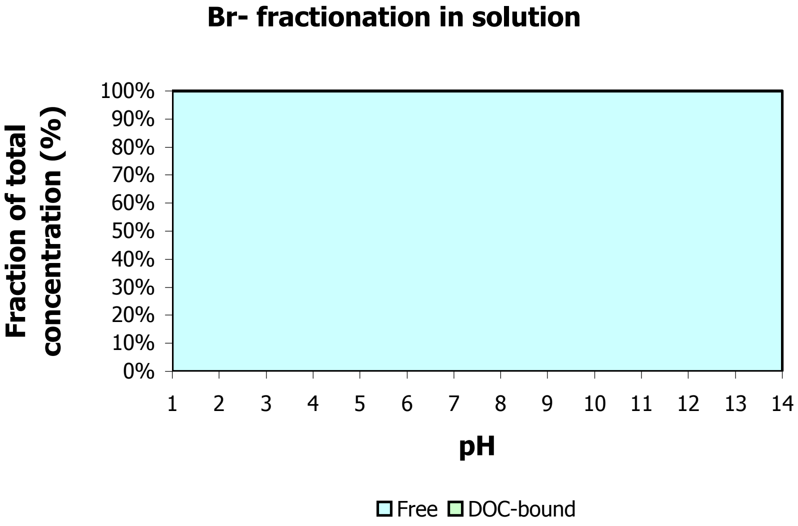
Br- fractionation in solution

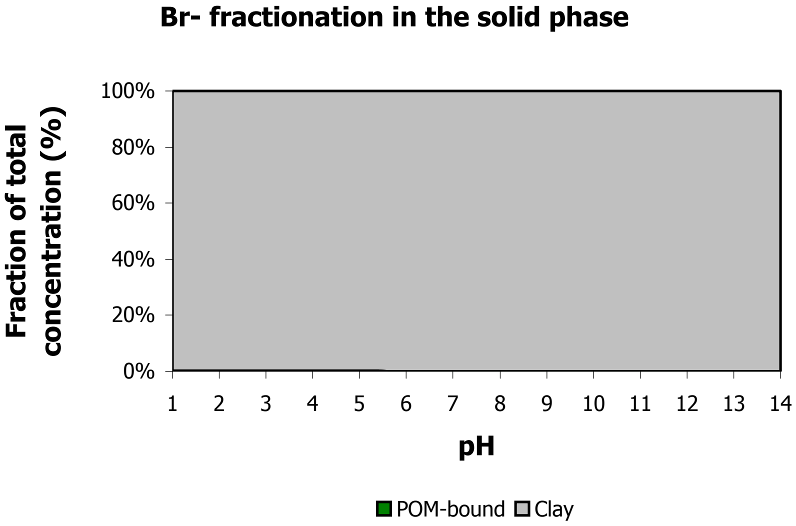
Br- fractionation in the solid phase

K+ fractionation in solution

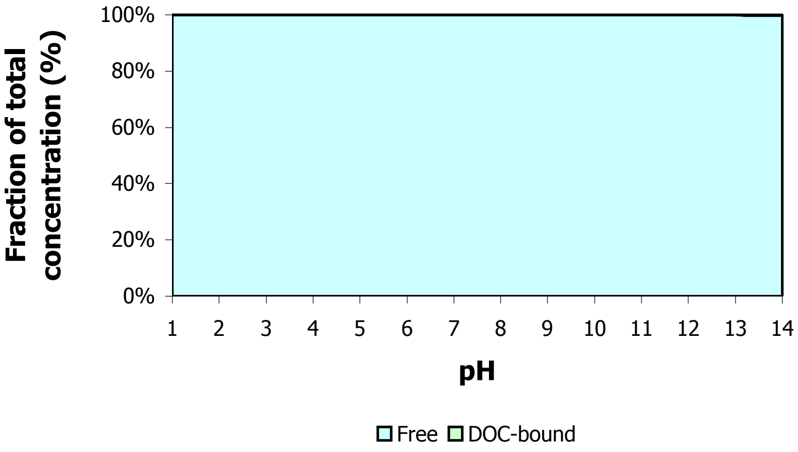

K+ fractionation in the solid phase

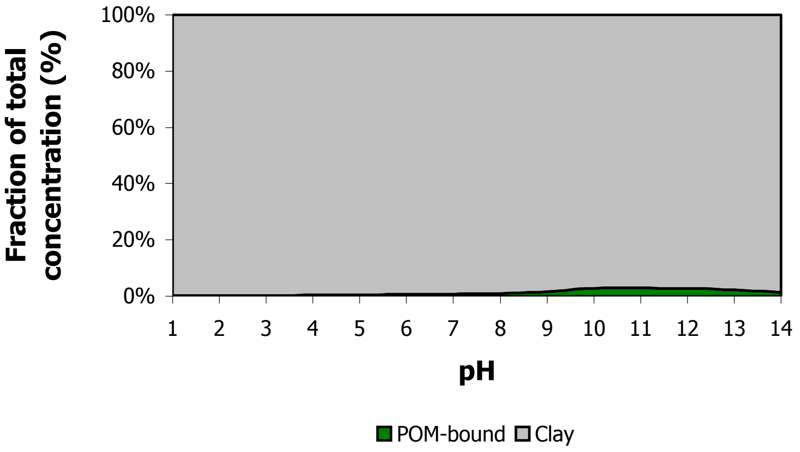

Li+ fractionation in solution

Li+ fractionation in the solid phase

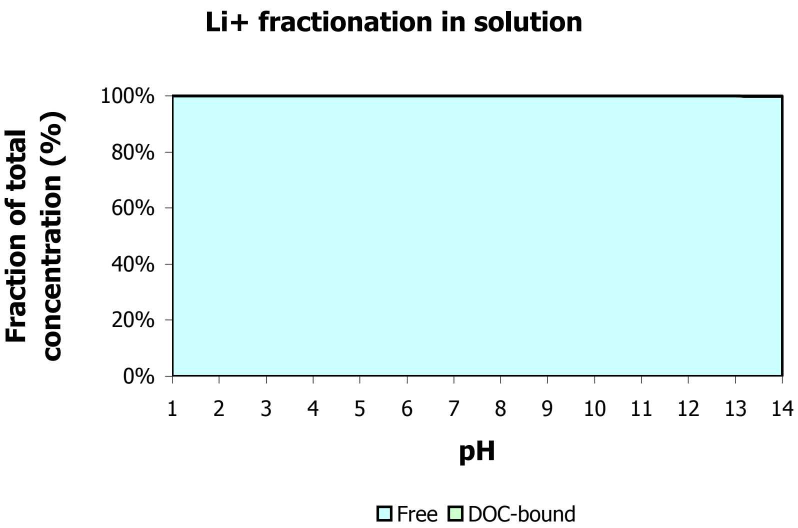
Li+ fractionation in solution
Fraction of total concentration (%)
100%
80%
60%
40%
20%
0%
1 2 3 4 5 6 7 8 9 10 11 12 13 14
pH
Free
DOC-bound

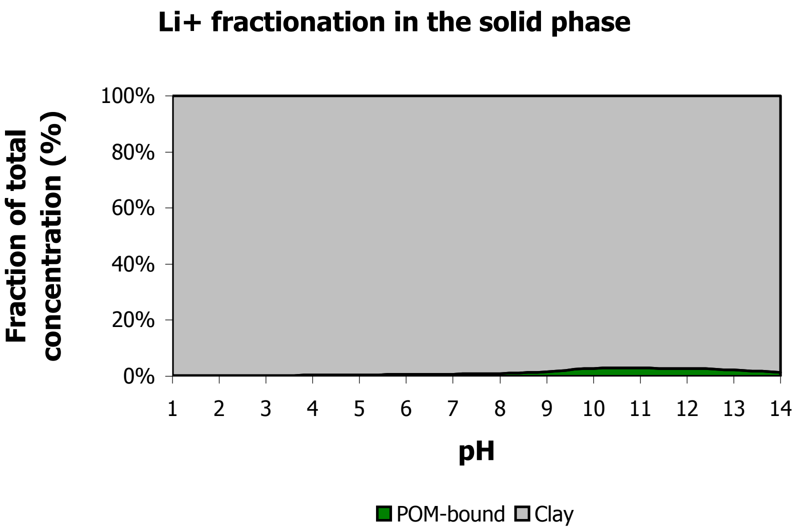
Li+ fractionation in the solid phase
Fraction of total concentration (%)
100%
80%
60%
40%
20%
0%
1 2 3 4 5 6 7 8 9 10 11 12 13 14
pH
POM-bound
Clay

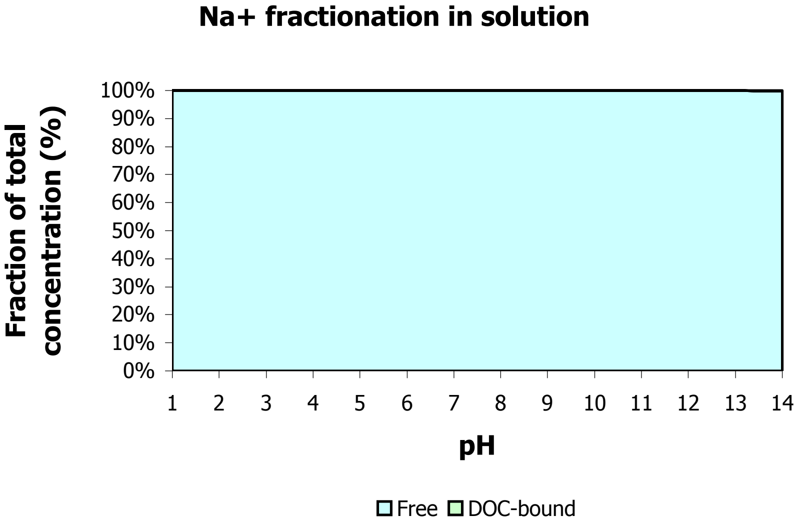
Na+ fractionation in solution
Fraction of total concentration (%)
100%
90%
80%
70%
60%
50%
40%
30%
20%
10%
0%
1 2 3 4 5 6 7 8 9 10 11 12 13 14
pH
Free
DOC-bound

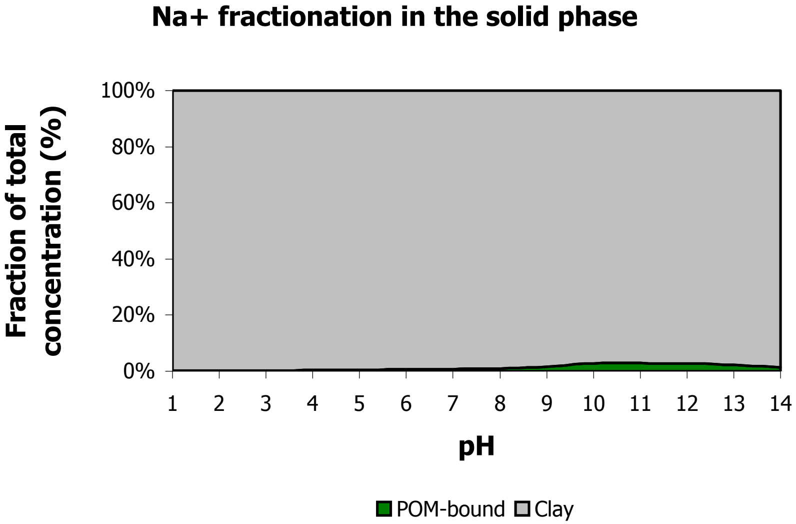
Na+ fractionation in the solid phase
Fraction of total concentration (%)
100%
80%
60%
40%
20%
0%
1 2 3 4 5 6 7 8 9 10 11 12 13 14
pH
POM-bound
Clay

[H4SiO4] as function of pH

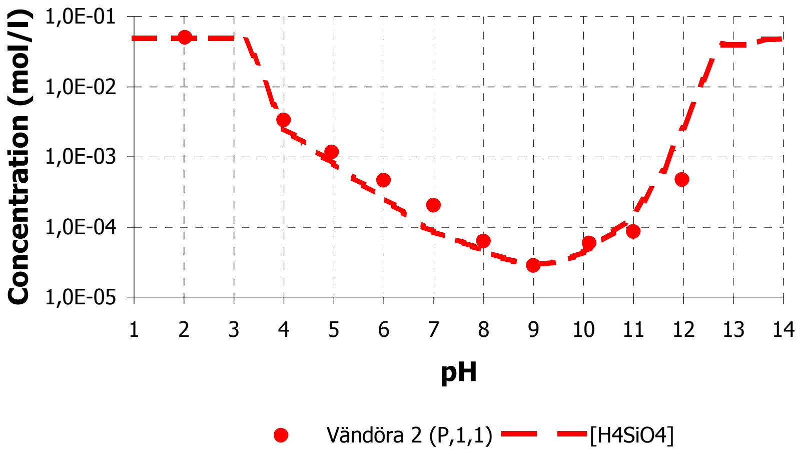

[SO4-2] as function of pH

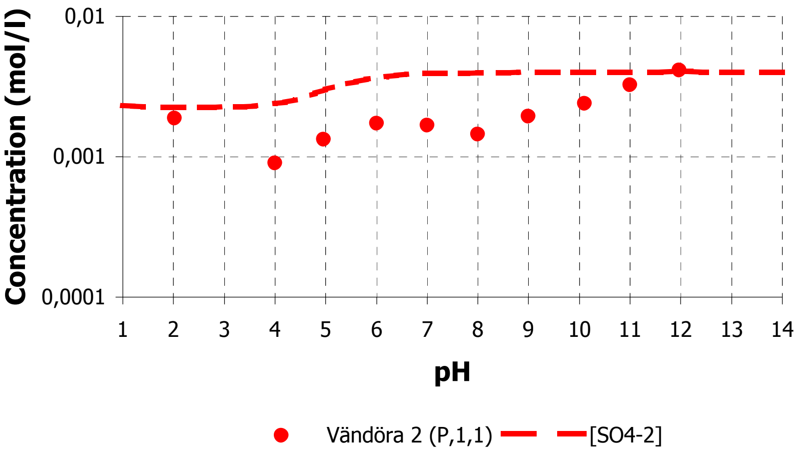

[Pb+2] as function of pH

[Zn+2] as function of pH

[Pb+2] as function of pH

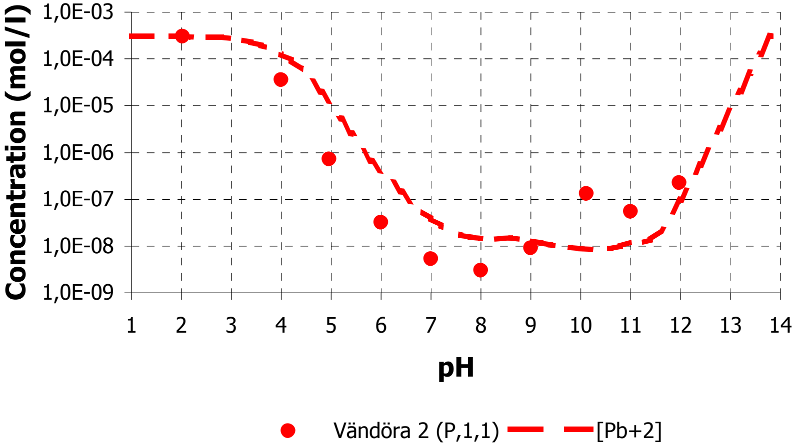

[Zn+2] as function of pH

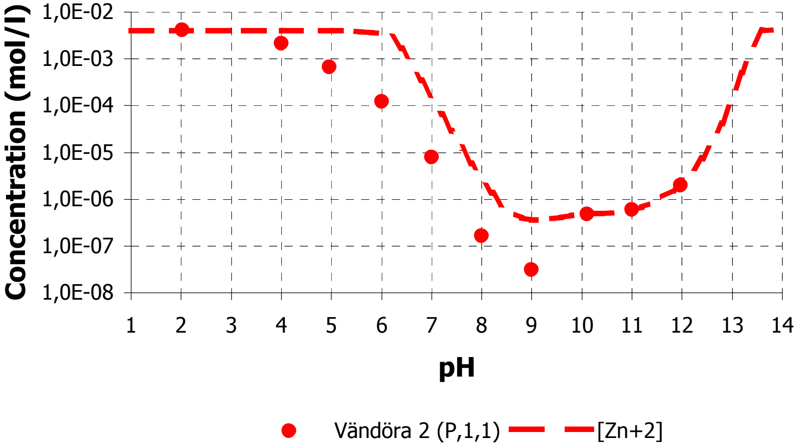

[Sb[OH]6-] as function of pH

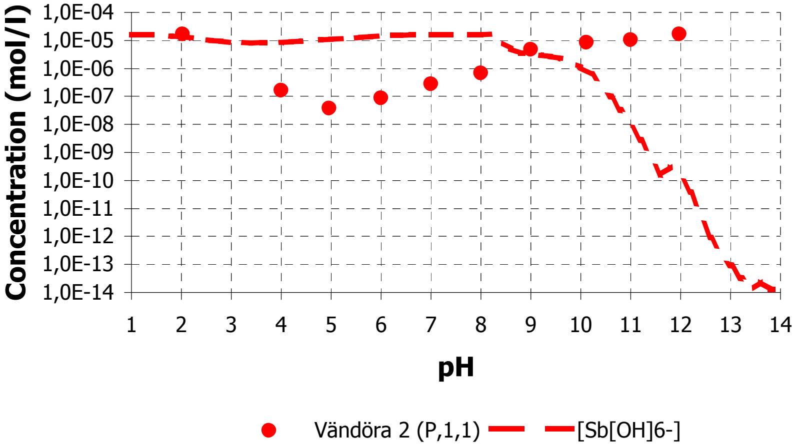

[VO2+] as function of pH

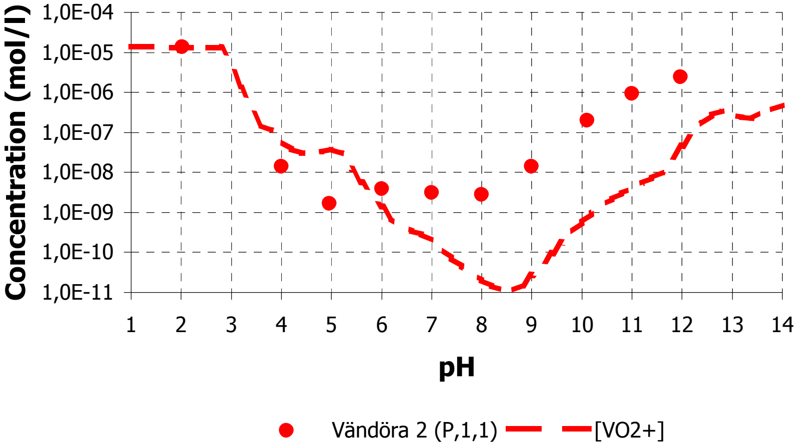

[Li+] as function of pH

[Na+] as function of pH

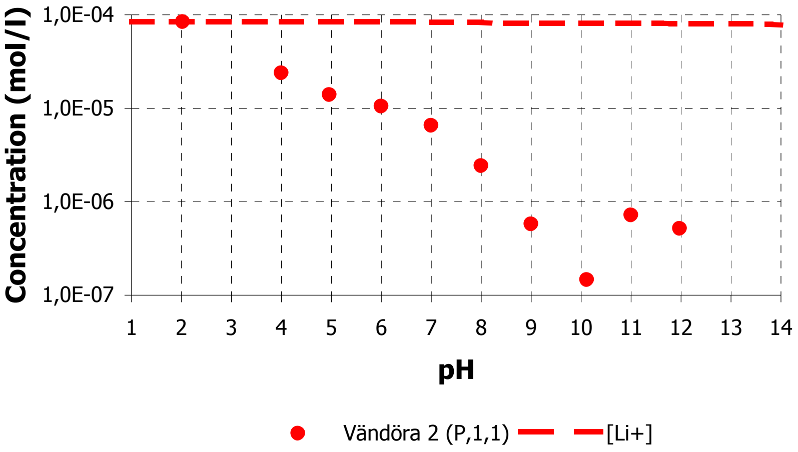

[Li+] as function of pH

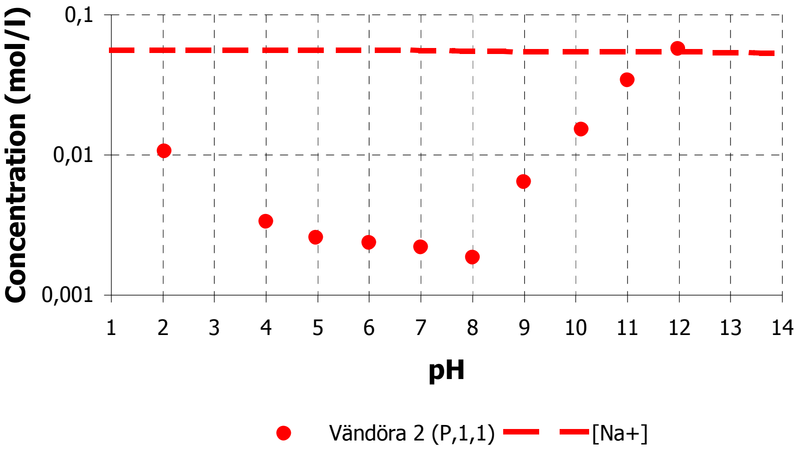

[Na+] as function of pH

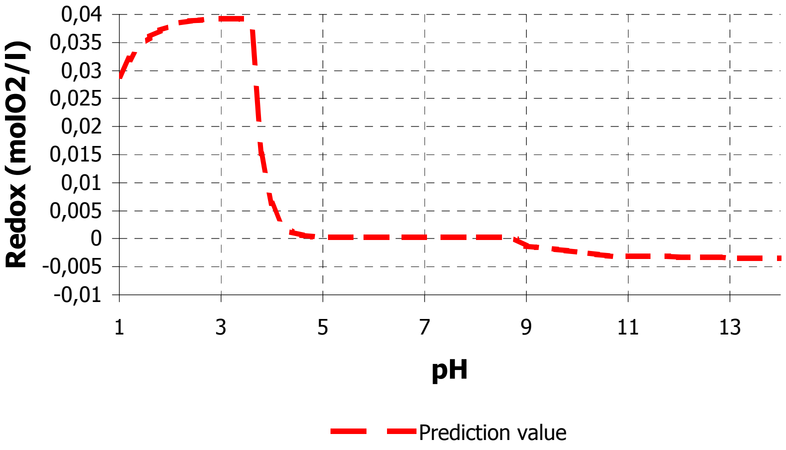

Vändöra 2 ecn-090406: Redox as function of pH

H Result geochemical modelling sample 3

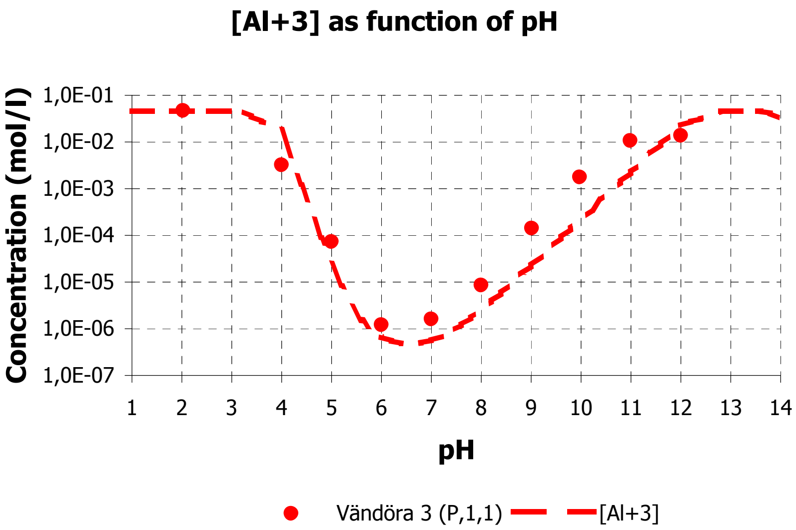
[Al+3] as function of pH
Concentration (mol/l)
1,0E-01
1,0E-02
1,0E-03
1,0E-04
1,0E-05
1,0E-06
1,0E-07
1 2 3 4 5 6 7 8 9 10 11 12 13 14
pH
Vändöra 3 (P,1,1)
[Al+3]

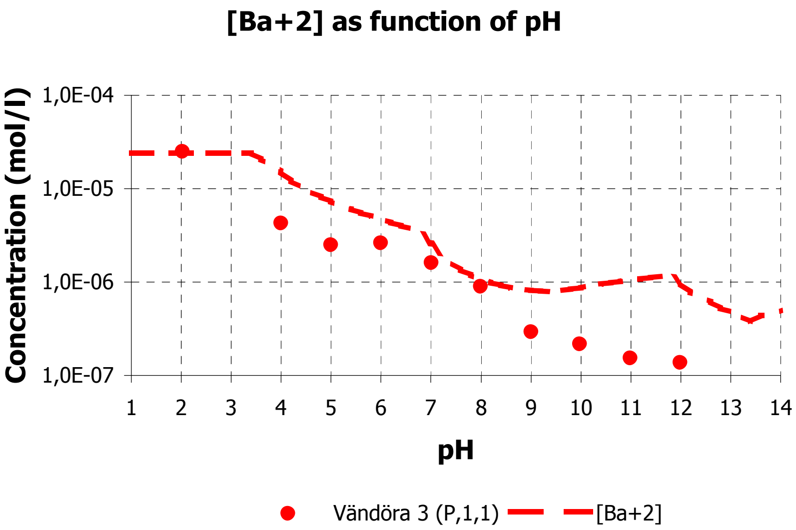
[Ba+2] as function of pH
Concentration (mol/l)
1,0E-04
1,0E-05
1,0E-06
1,0E-07
1 2 3 4 5 6 7 8 9 10 11 12 13 14
pH
Vändöra 3 (P,1,1)
[Ba+2]

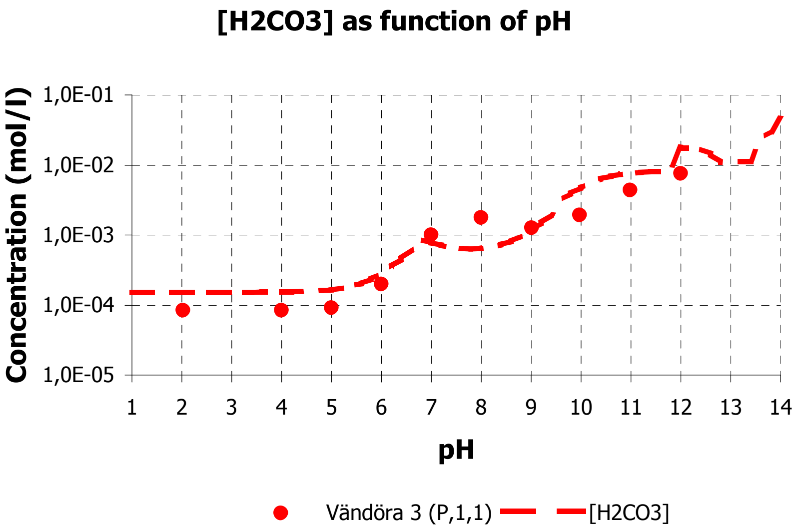
[H2CO3] as function of pH
Concentration (mol/l)
1,0E-01
1,0E-02
1,0E-03
1,0E-04
1,0E-05
1 2 3 4 5 6 7 8 9 10 11 12 13 14
pH
Vändöra 3 (P,1,1)
[H2CO3]

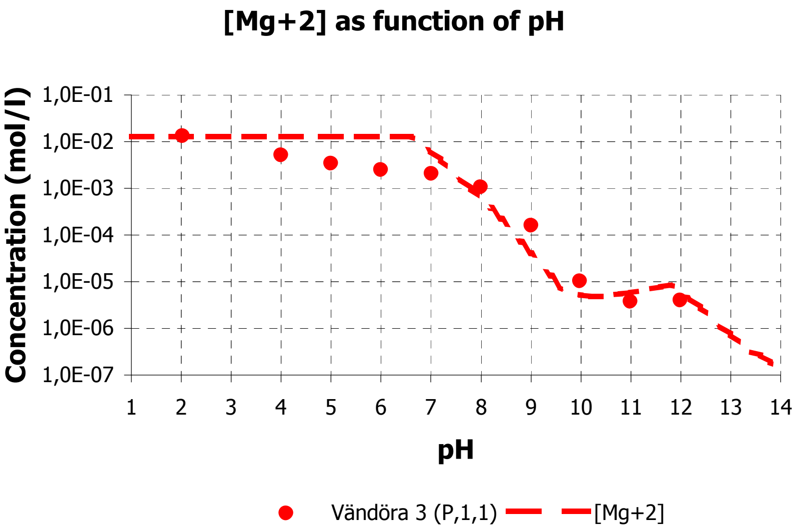
[Mg+2] as function of pH
Concentration (mol/l)
1,0E-01
1,0E-02
1,0E-03
1,0E-04
1,0E-05
1,0E-06
1,0E-07
1 2 3 4 5 6 7 8 9 10 11 12 13 14
pH
Vändöra 3 (P,1,1)
[Mg+2]

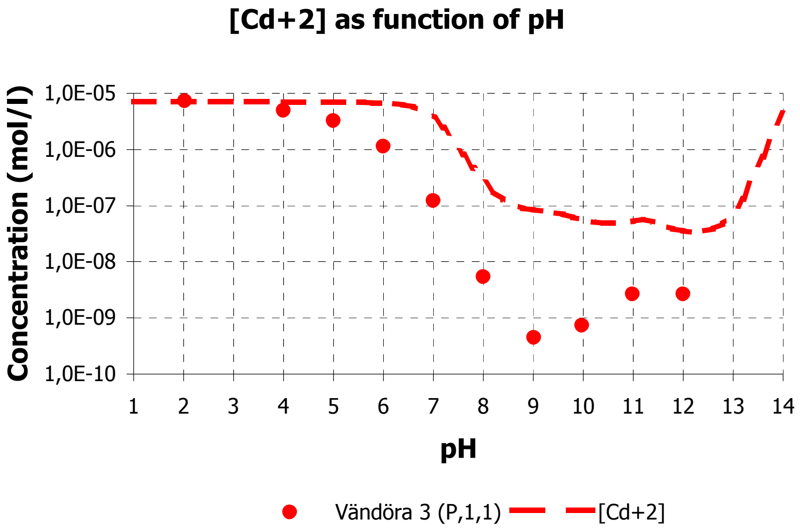
[Cd+2] as function of pH

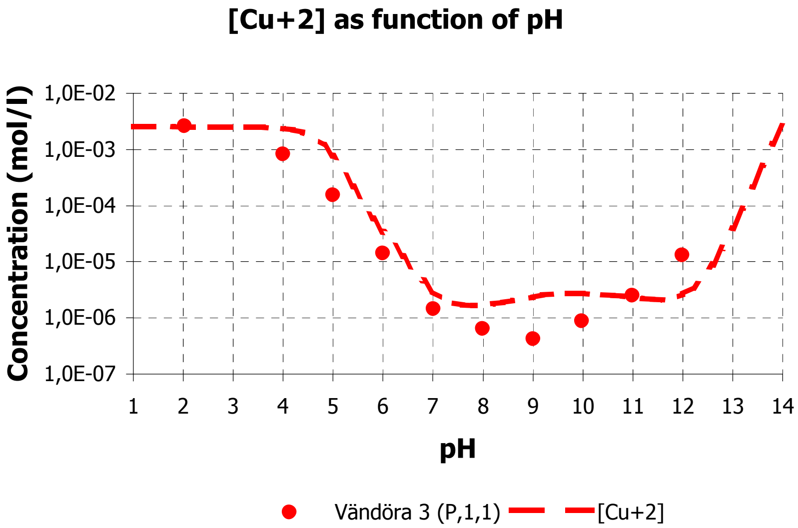
[Cu+2] as function of pH

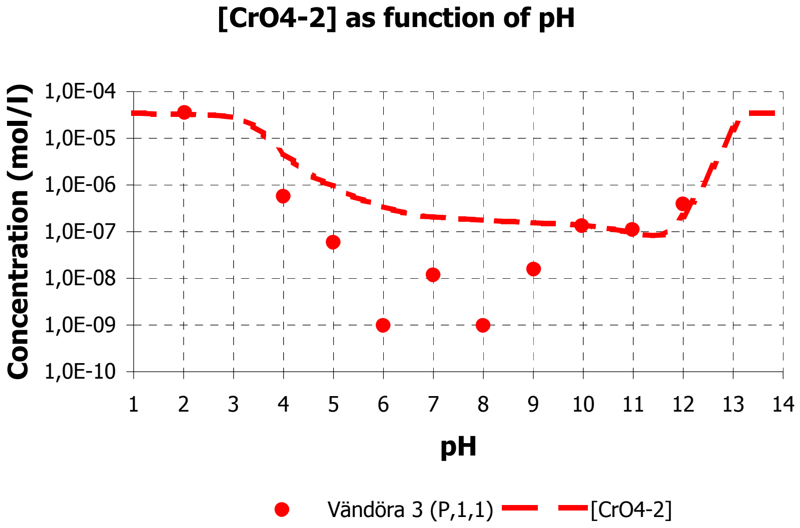
[CrO4-2] as function of pH

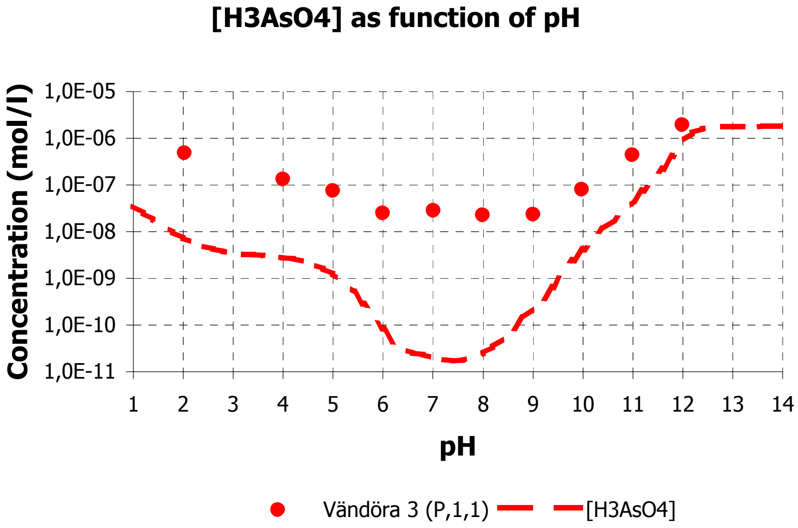
[H3AsO4] as function of pH

[Br-] as function of pH

[Cl-] as function of pH

[Br-] as function of pH

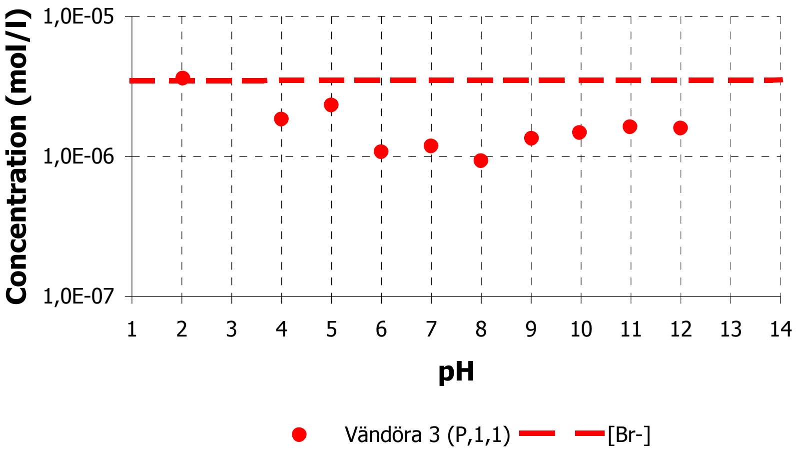

[Cl-] as function of pH

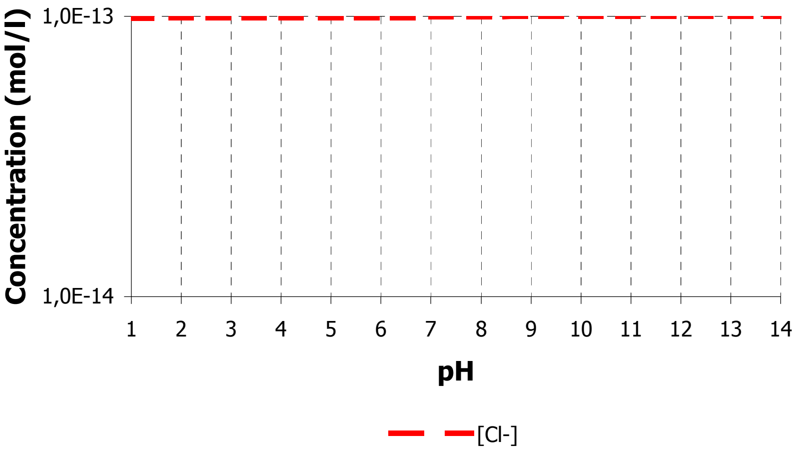

Vändöra 3 ecn-090406: pe as function of pH

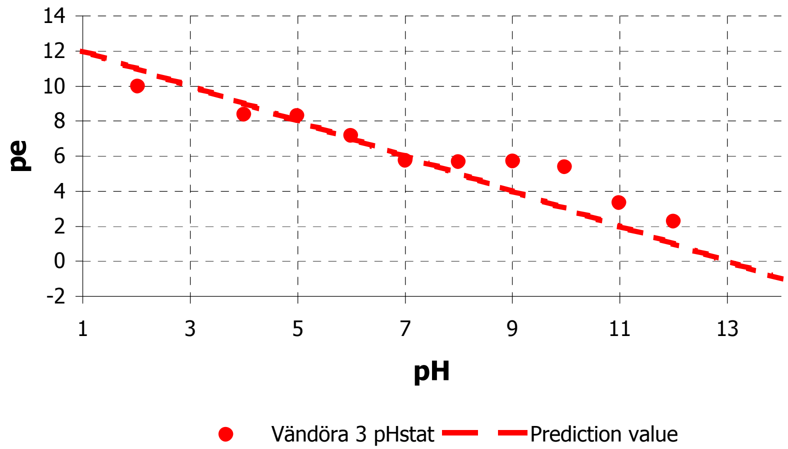

Vändöra 3 ecn-090406: DHA as function of pH

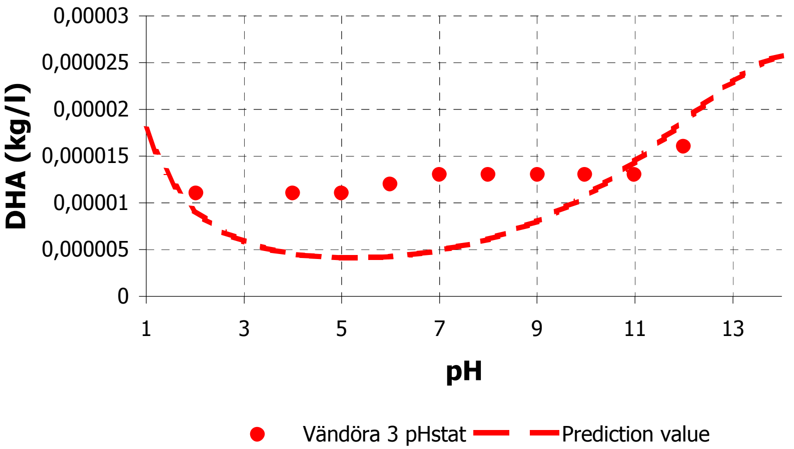

[Al+3] as function of pH

Partitioning liquid-solid, [Al+3]

[Al+3] as function of pH

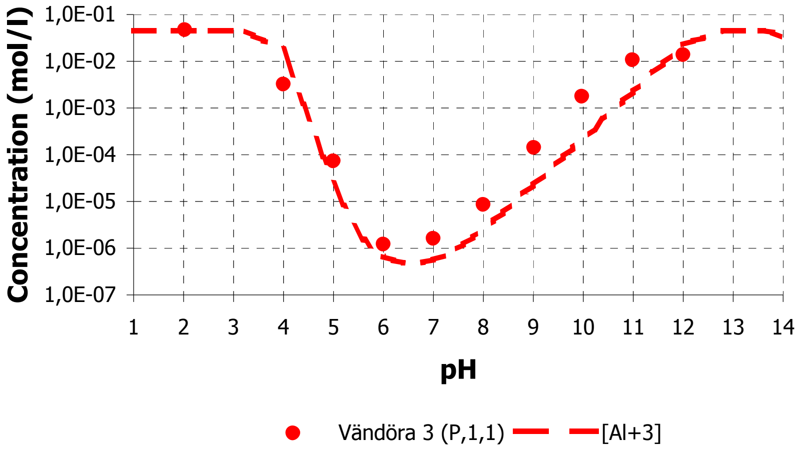

Partitioning liquid-solid, [Al+3]

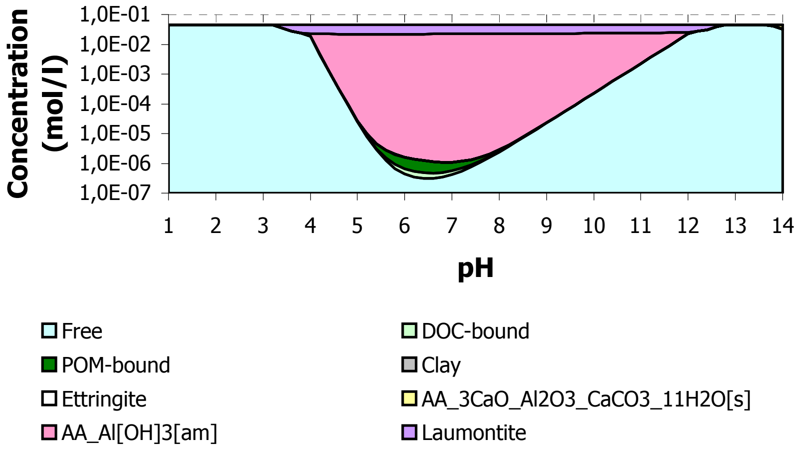

[Ba+2] as function of pH

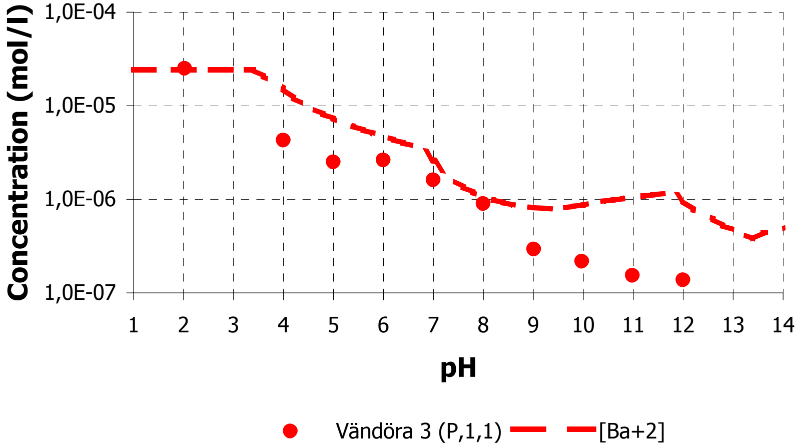

Partitioning liquid-solid, [Ba+2]

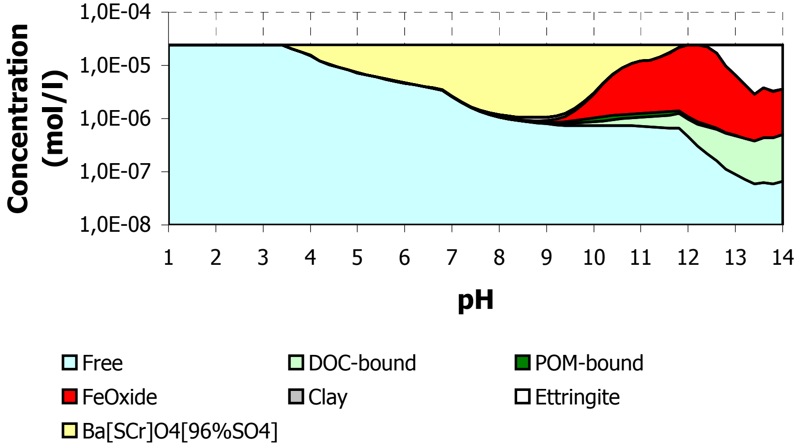

[Ca+2] as function of pH

Partitioning liquid-solid, [Ca+2]

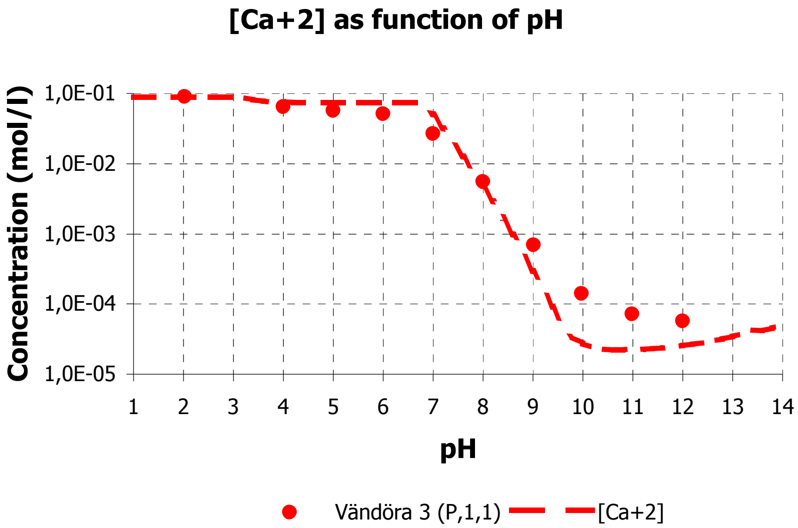
[Ca+2] as function of pH

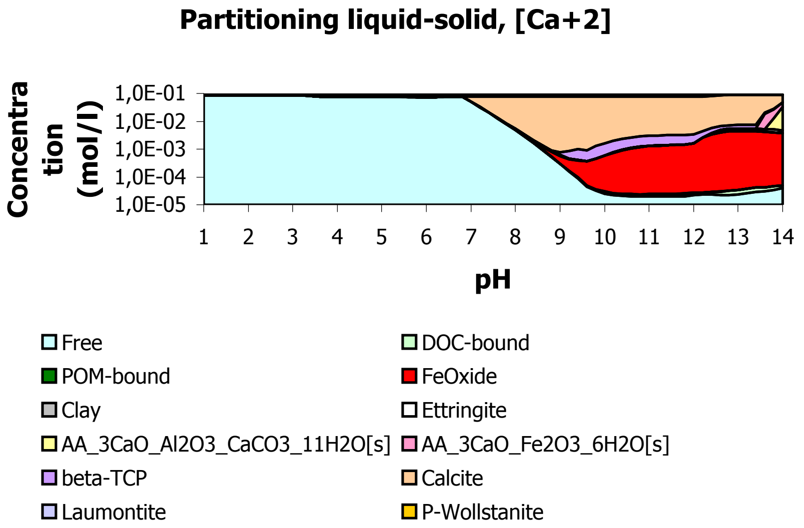
Partitioning liquid-solid, [Ca+2]

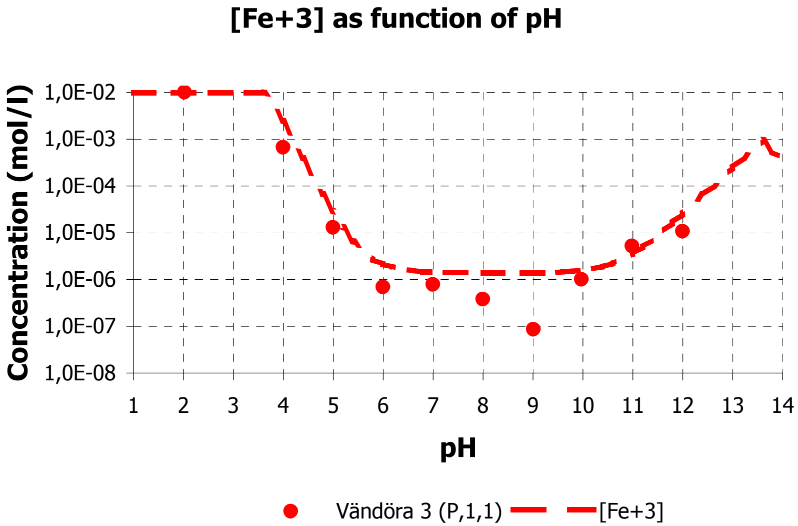
[Fe+3] as function of pH

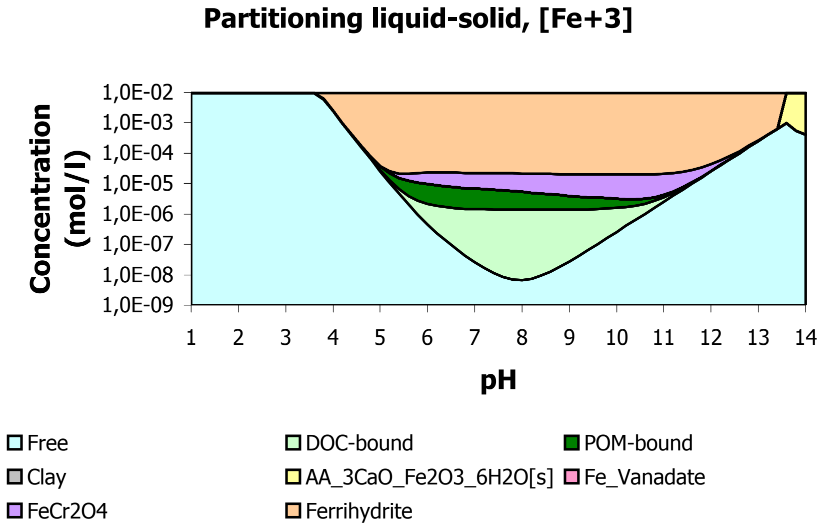
Partitioning liquid-solid, [Fe+3]

[H4SiO4] as function of pH

Partitioning liquid-solid, [H4SiO4]

[H4SiO4] as function of pH

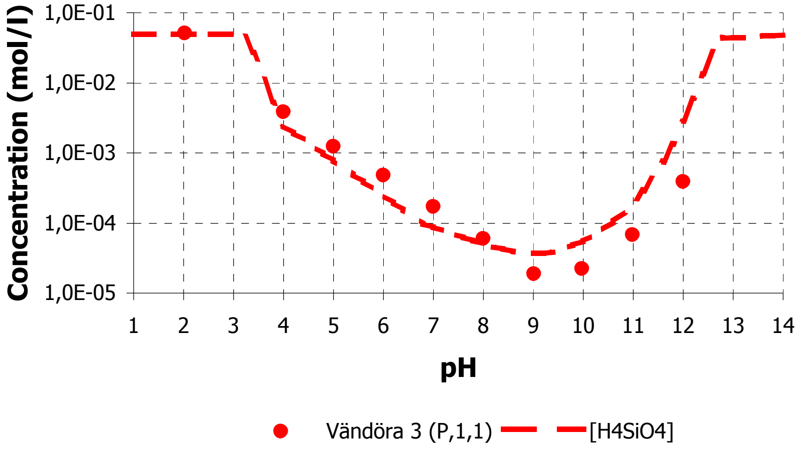

Partitioning liquid-solid, [H4SiO4]

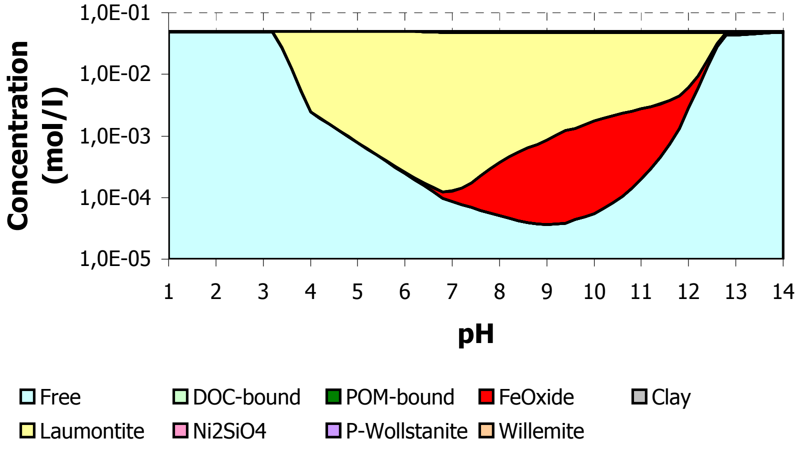

[SO4-2] as function of pH

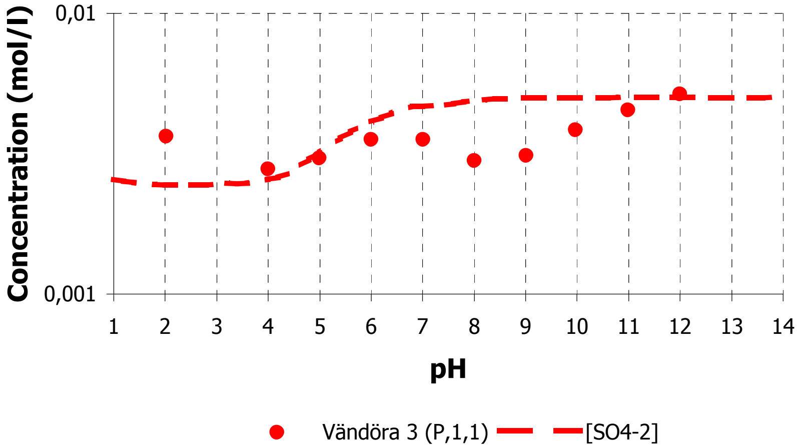

Partitioning liquid-solid, [SO4-2]

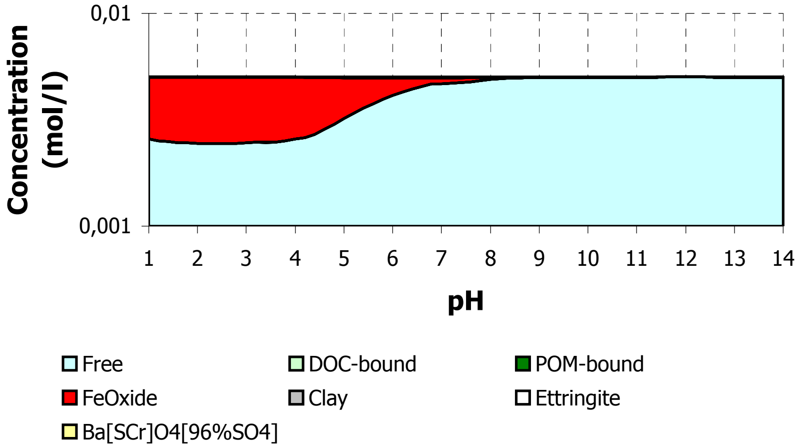

[H2CO3] as function of pH

Partitioning liquid-solid, [H2CO3]

[H2CO3] as function of pH

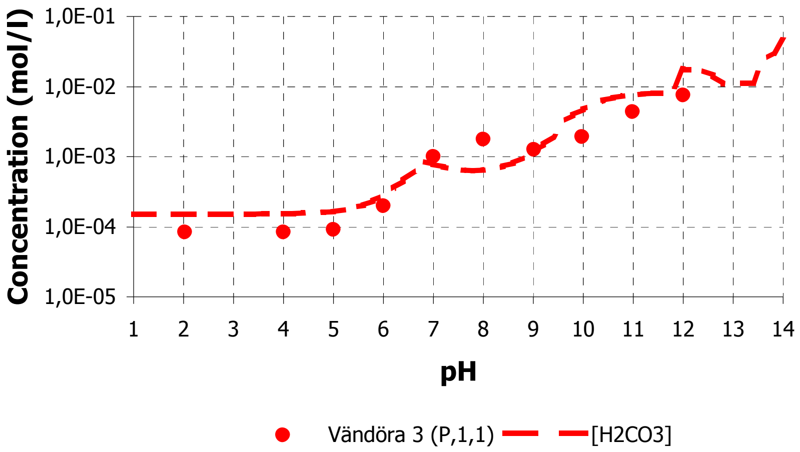

Partitioning liquid-solid, [H2CO3]

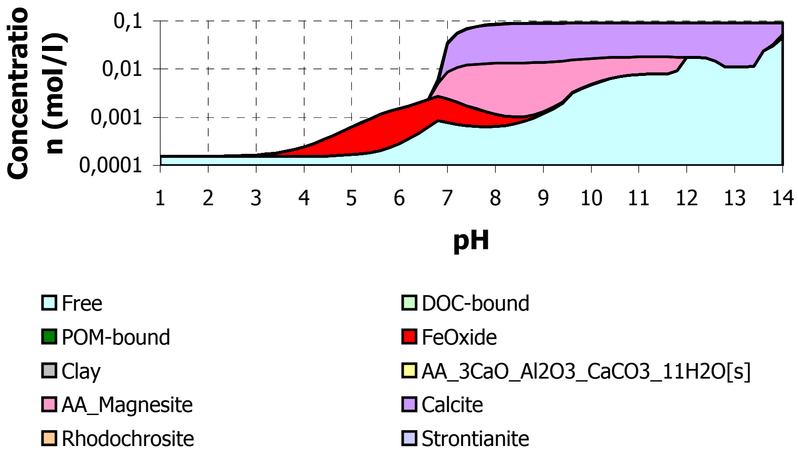

[Mg+2] as function of pH

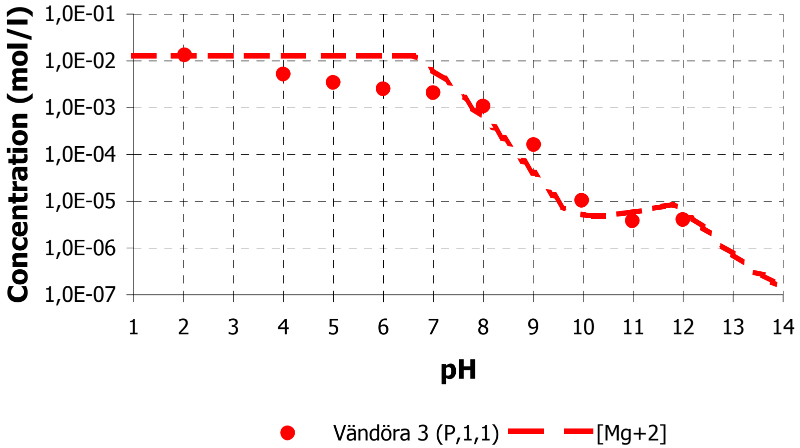

Partitioning liquid-solid, [Mg+2]

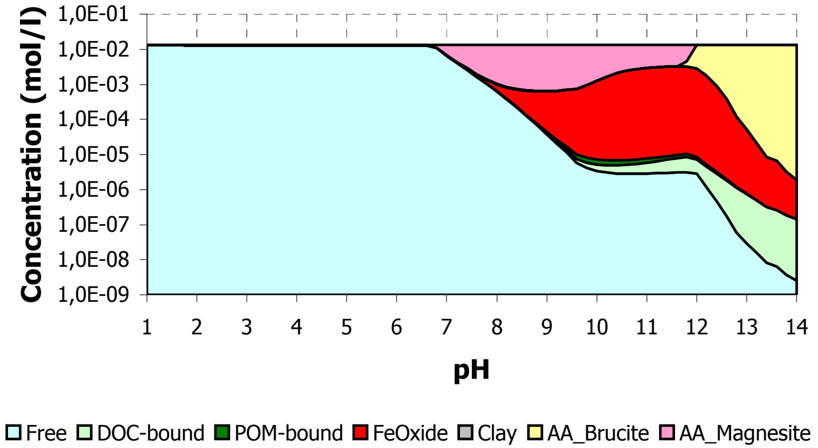

[PO4-3] as function of pH

Partitioning liquid-solid, [PO4-3]

[PO4-3] as function of pH

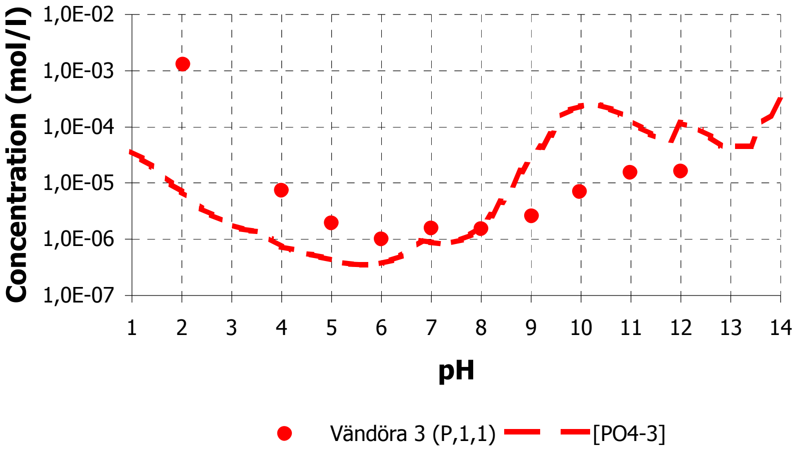

Partitioning liquid-solid, [PO4-3]

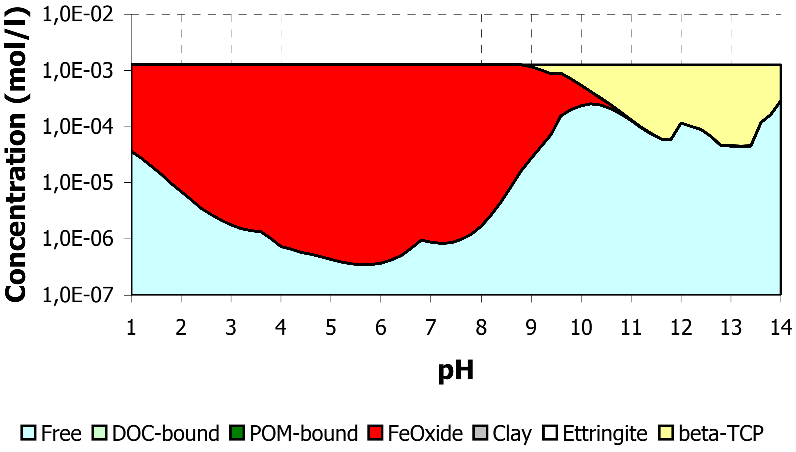

[Sr+2] as function of pH

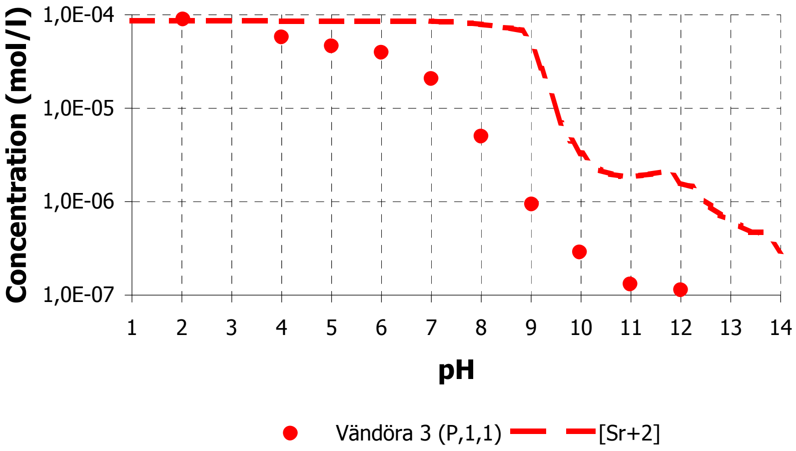

Partitioning liquid-solid, [Sr+2]

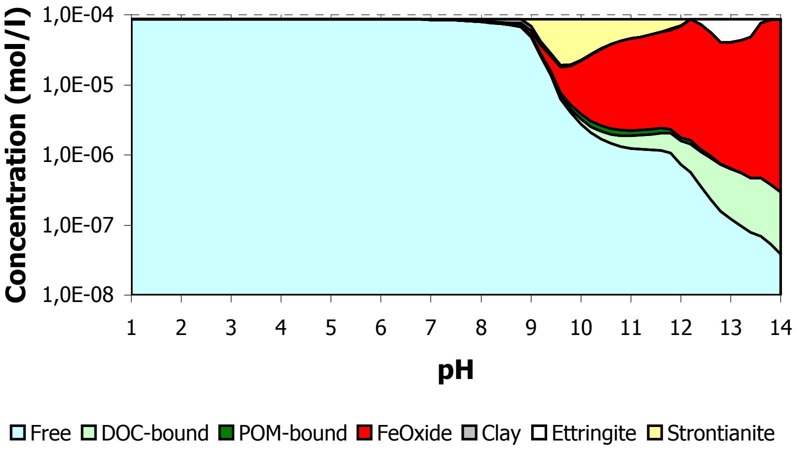

[Cd+2] as function of pH

Partitioning liquid-solid, [Cd+2]

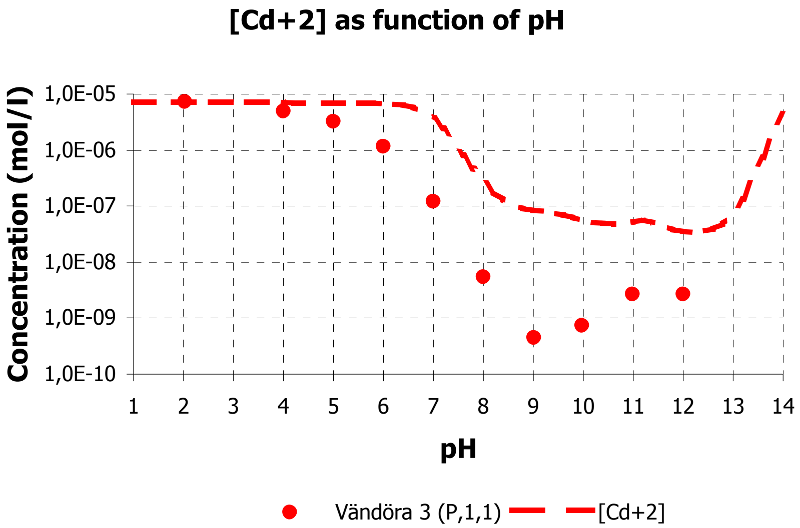
[Cd+2] as function of pH

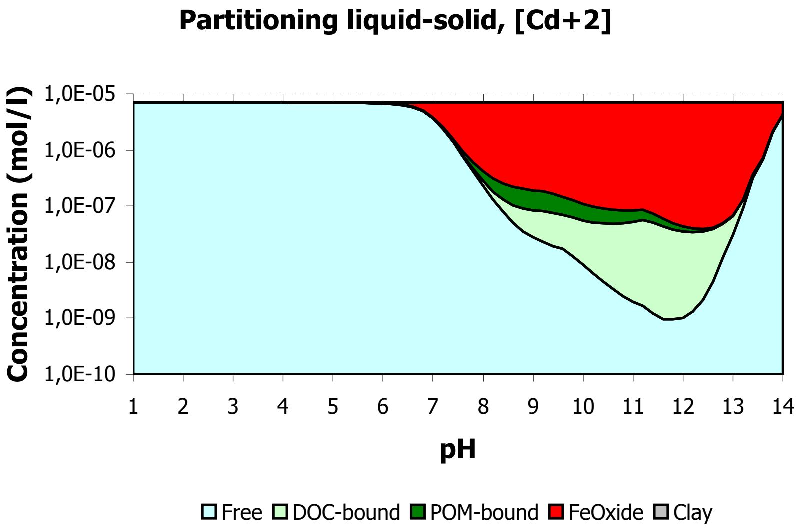
Partitioning liquid-solid, [Cd+2]

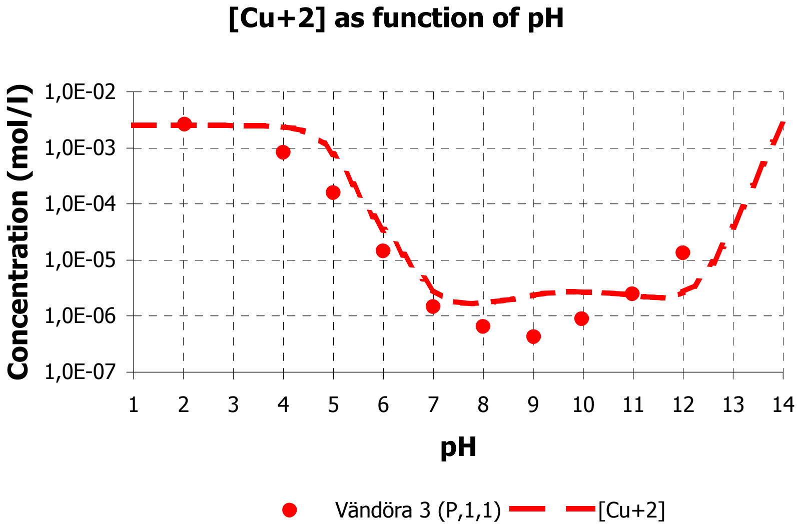
[Cu+2] as function of pH

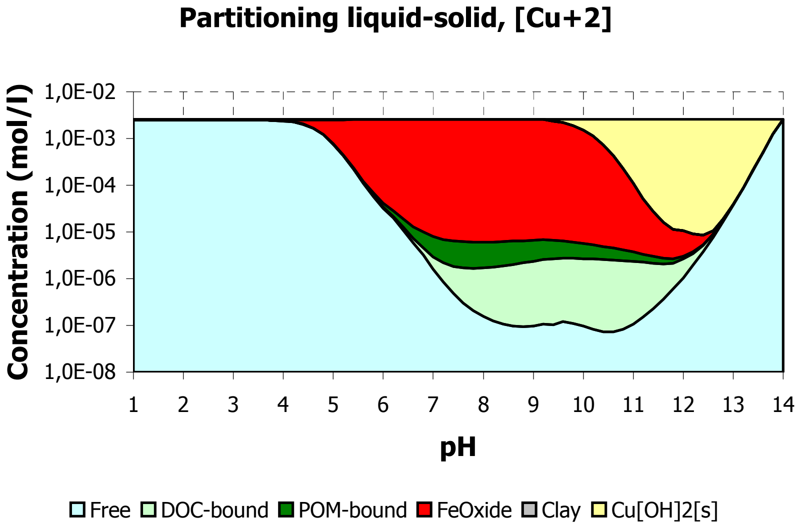
Partitioning liquid-solid, [Cu+2]

[Mn+2] as function of pH

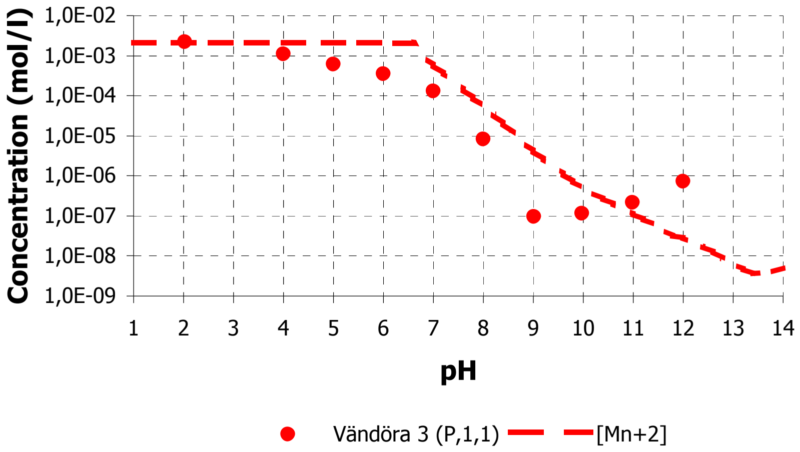

Partitioning liquid-solid, [Mn+2]

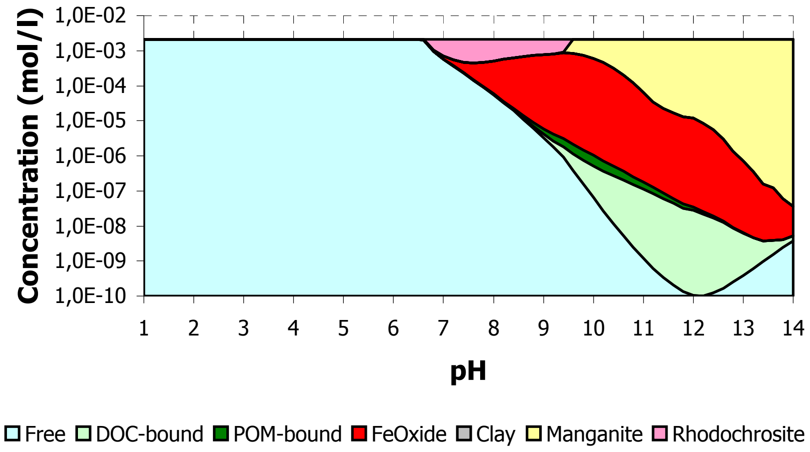

[Ni+2] as function of pH

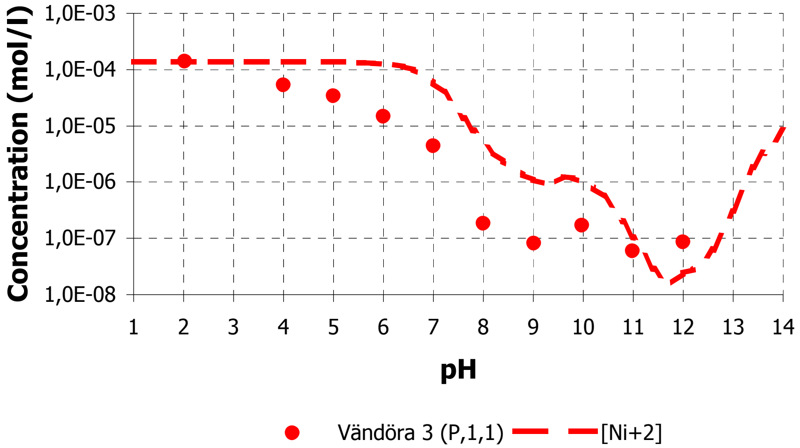

Partitioning liquid-solid, [Ni+2]

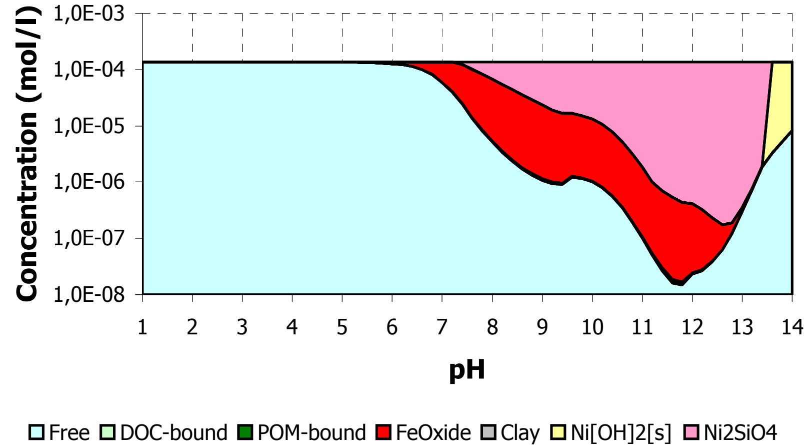

[Pb+2] as function of pH

Partitioning liquid-solid, [Pb+2]

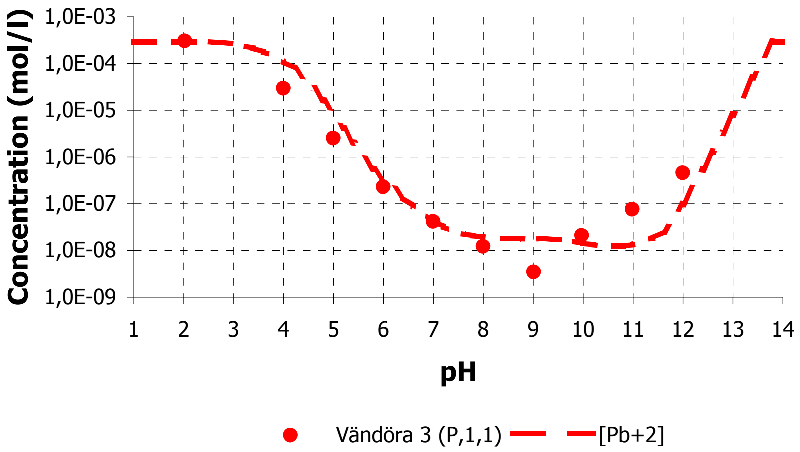

[Pb+2] as function of pH

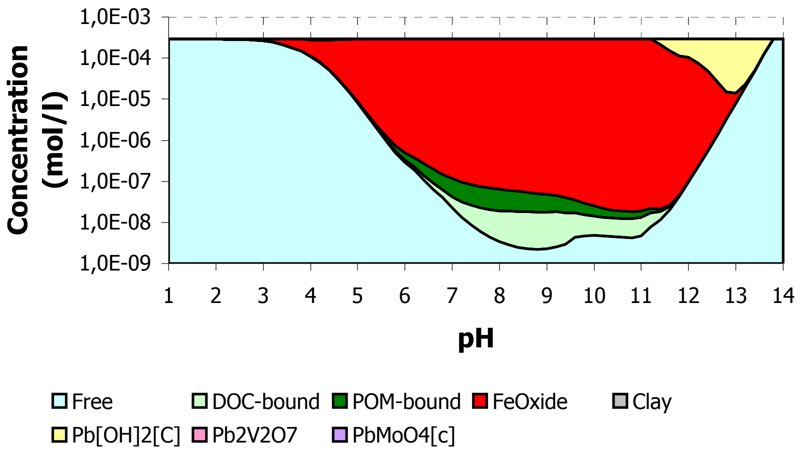

Partitioning liquid-solid, [Pb+2]

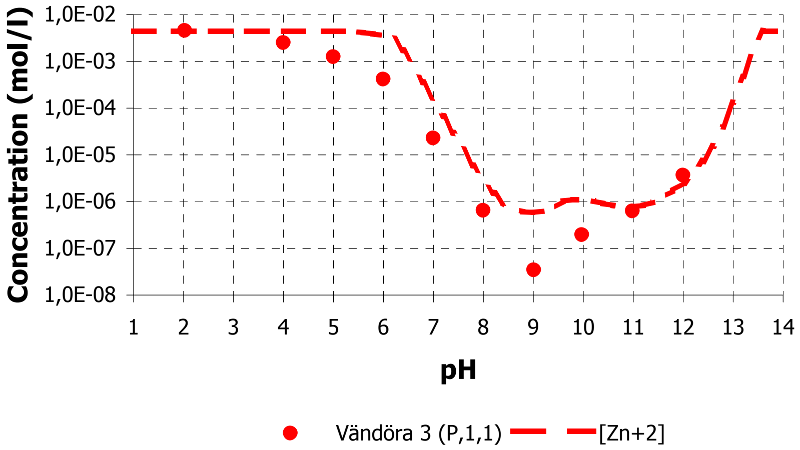

[Zn+2] as function of pH

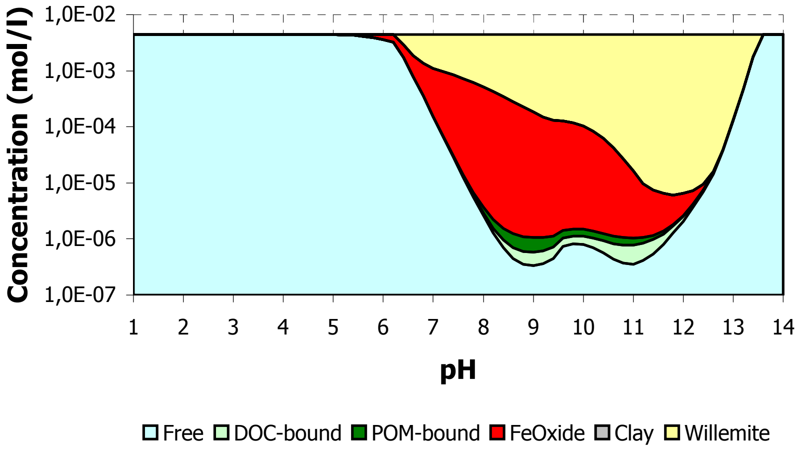

Partitioning liquid-solid, [Zn+2]

[CrO4-2] as function of pH

Partitioning liquid-solid, [CrO4-2]

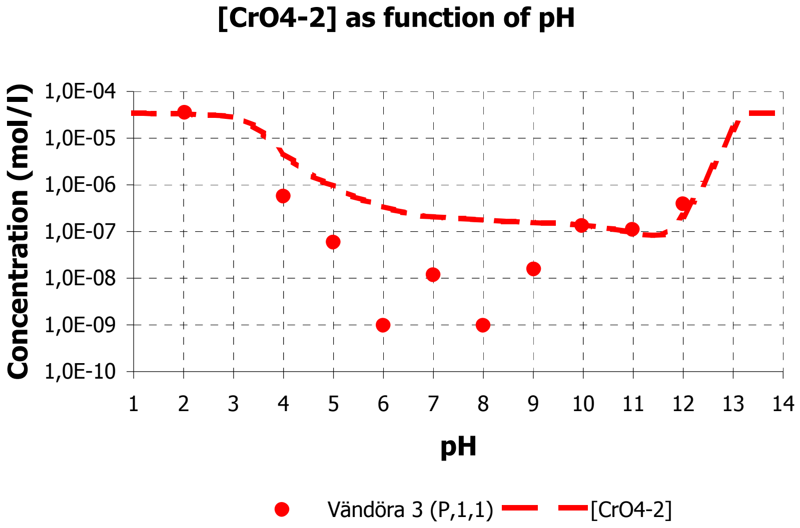
[CrO4-2] as function of pH

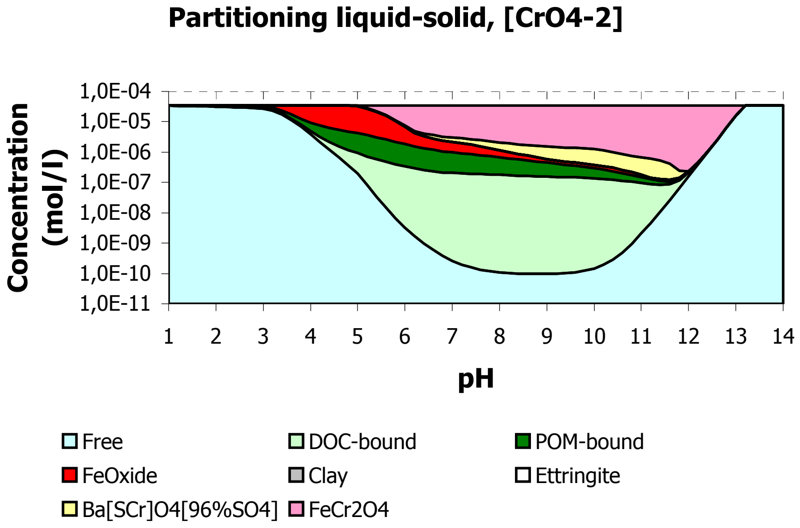
Partitioning liquid-solid, [CrO4-2]

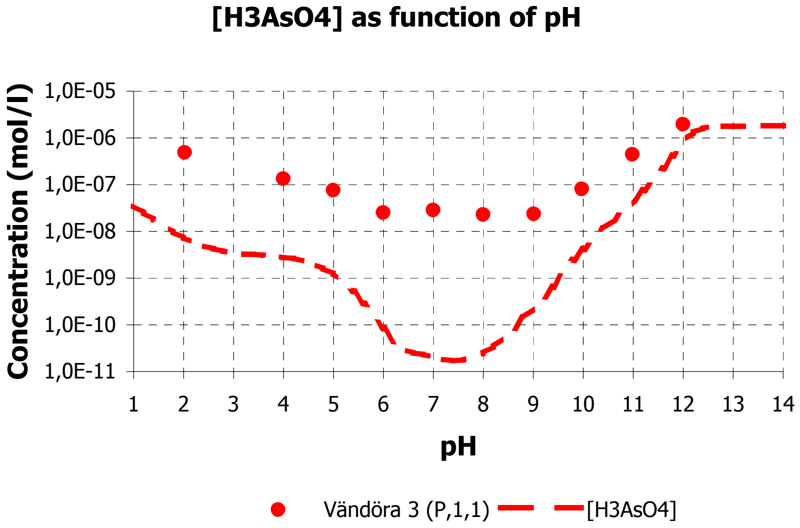
[H3AsO4] as function of pH

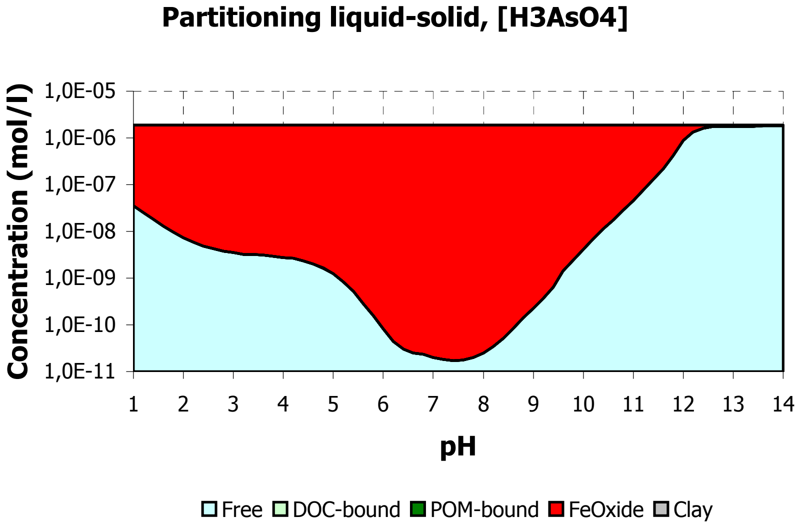
Partitioning liquid-solid, [H3AsO4]

[H3BO3] as function of pH

Partitioning liquid-solid, [H3BO3]

[H3BO3] as function of pH

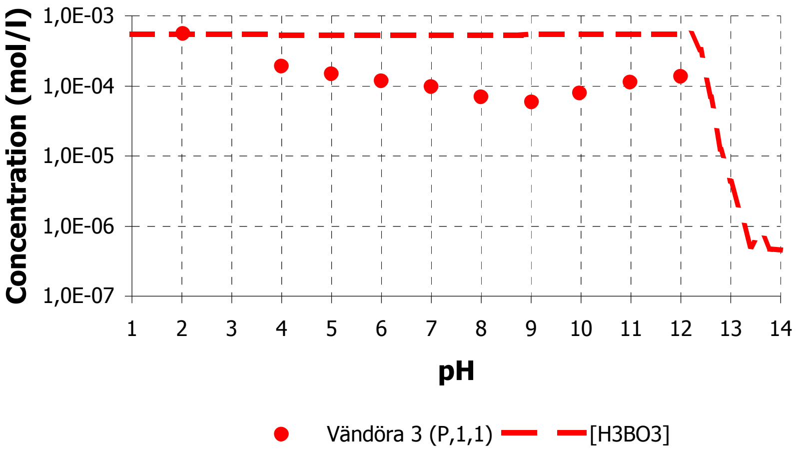

Partitioning liquid-solid, [H3BO3]

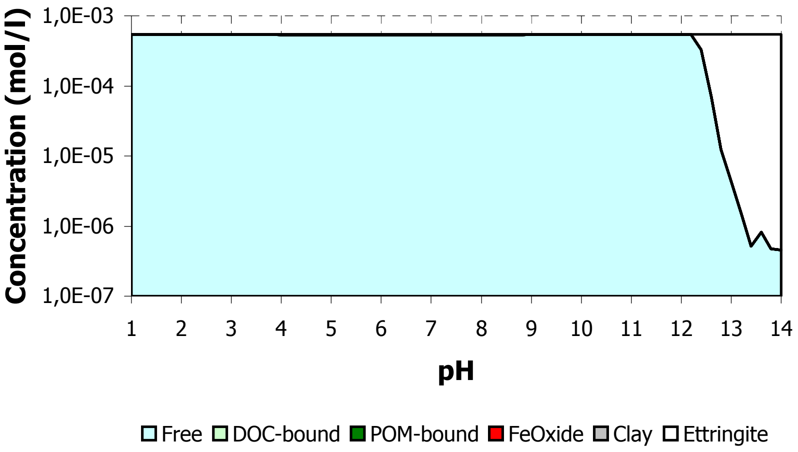

[MoO4-2] as function of pH

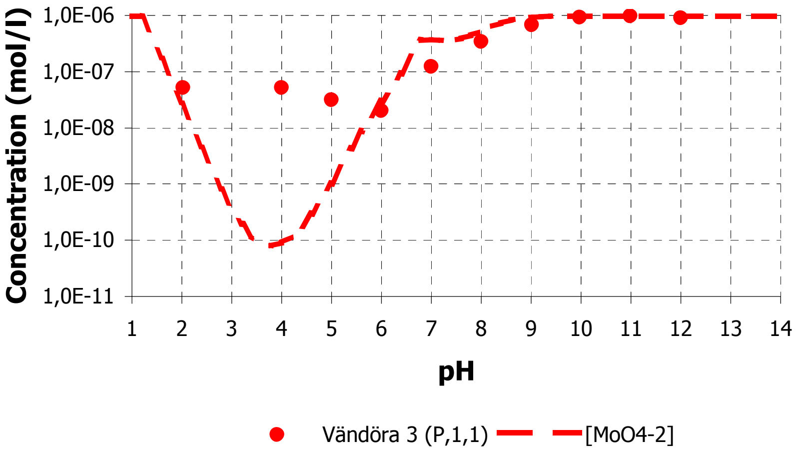

Partitioning liquid-solid, [MoO4-2]

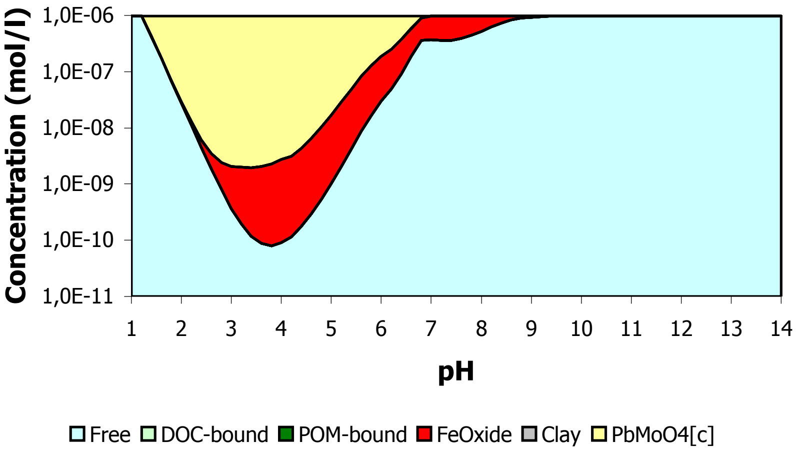

[Sb[OH]6-] as function of pH

Partitioning liquid-solid, [Sb[OH]6-]

[Sb[OH]6-] as function of pH

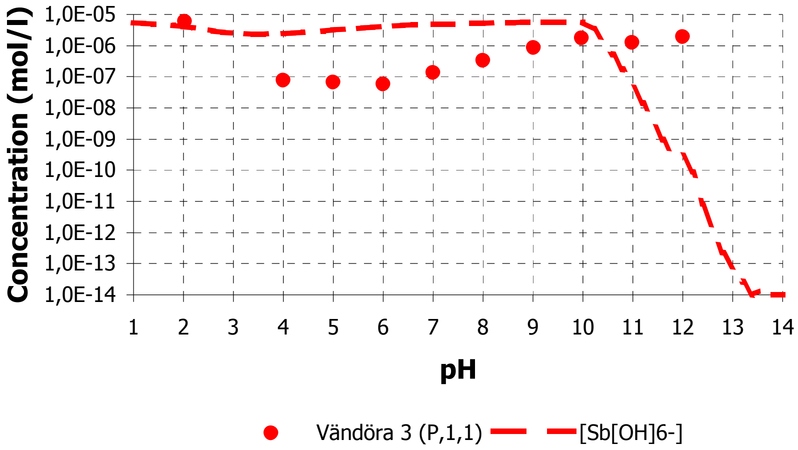

Partitioning liquid-solid, [Sb[OH]6-]

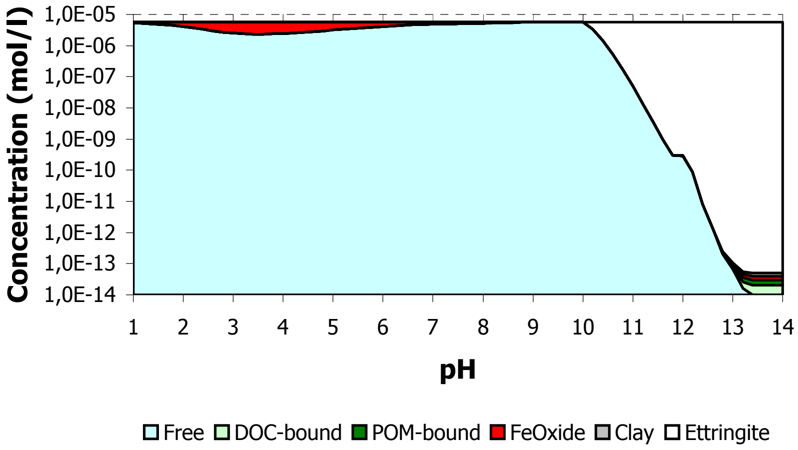

[VO2+] as function of pH

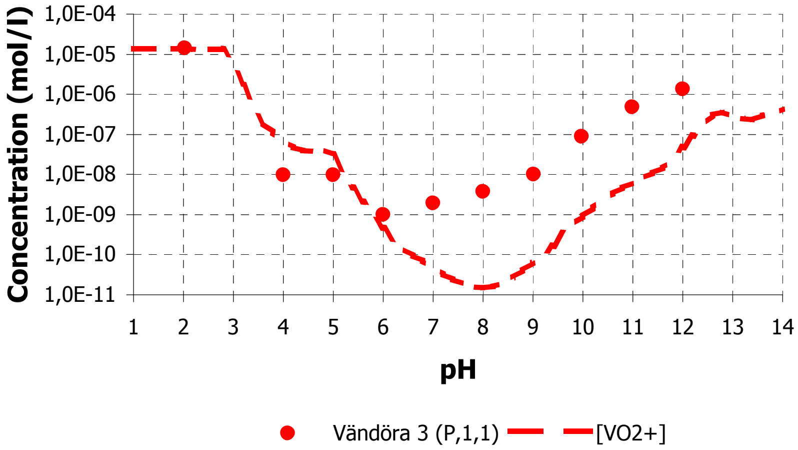

Partitioning liquid-solid, [VO2+]

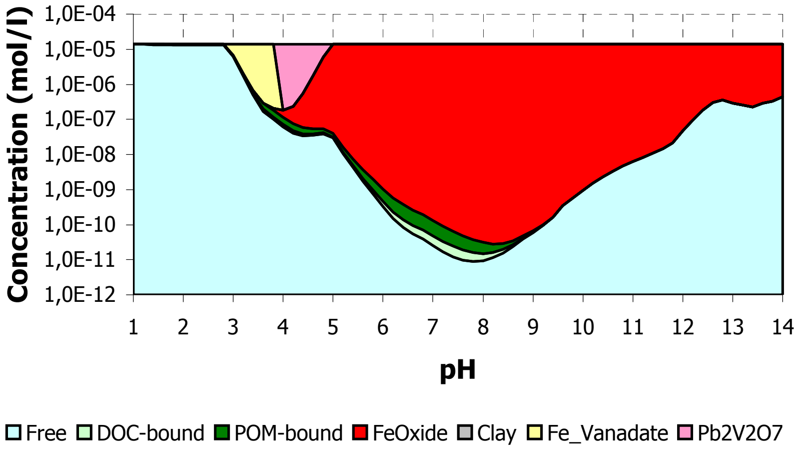

[Br-] as function of pH

Partitioning liquid-solid, [Br-]

[Br-] as function of pH

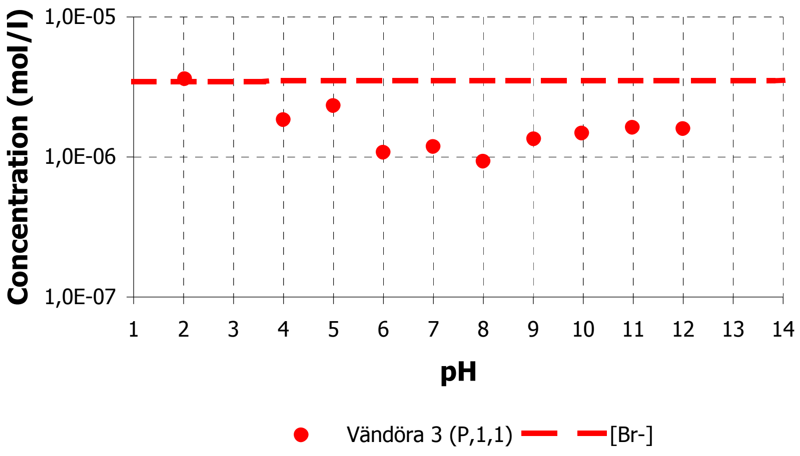

Partitioning liquid-solid, [Br-]

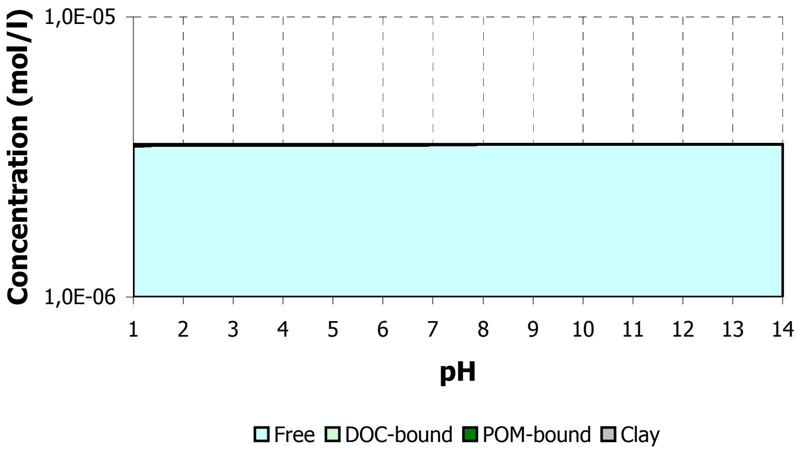

[Cl-] as function of pH

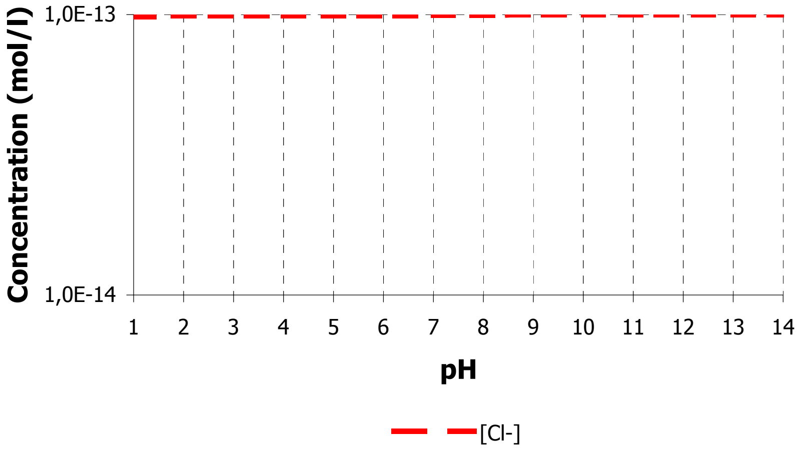

Partitioning liquid-solid, [Cl-]

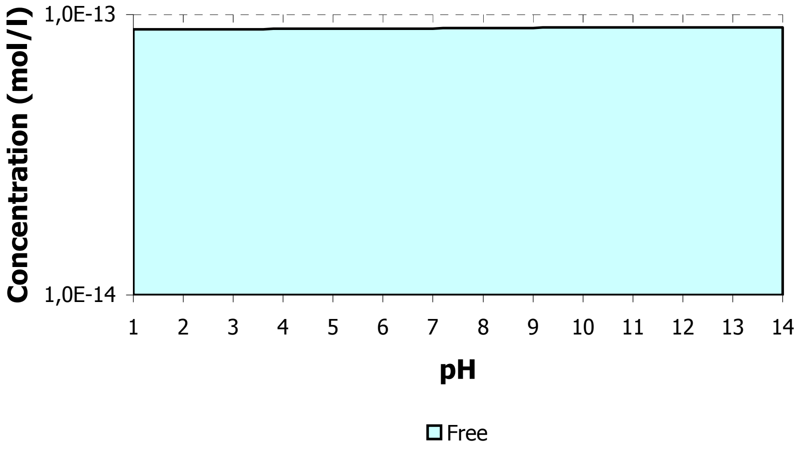

[F-] as function of pH

Partitioning liquid-solid, [F-]

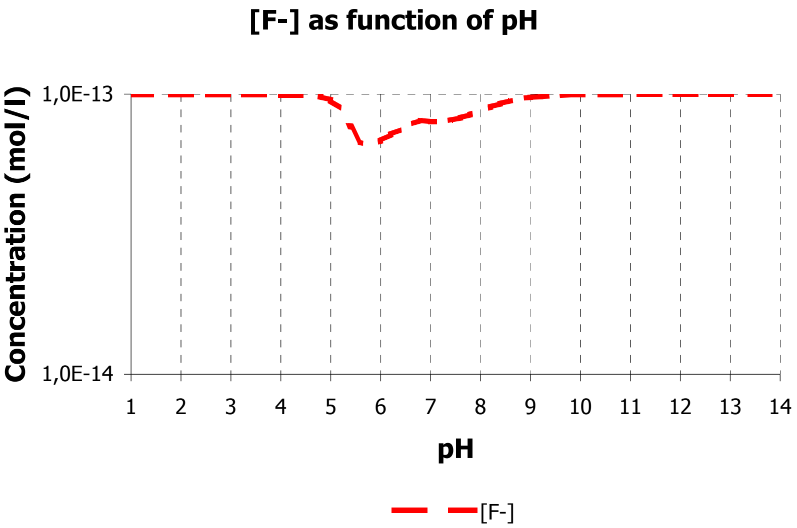

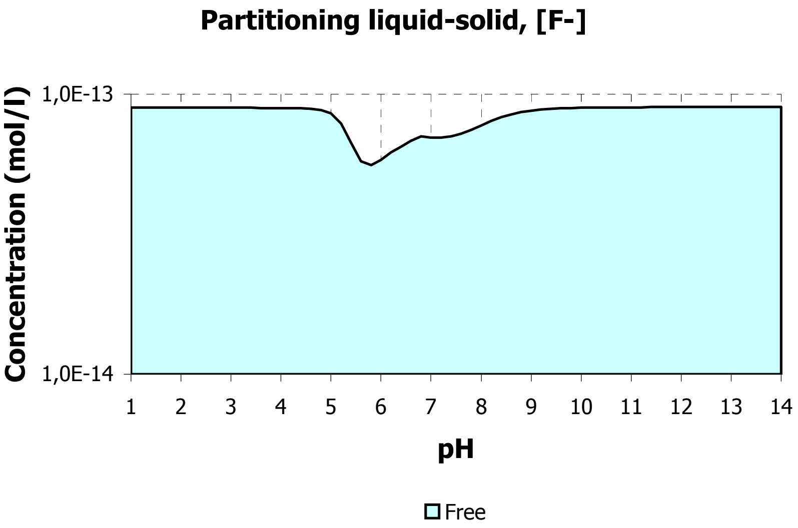

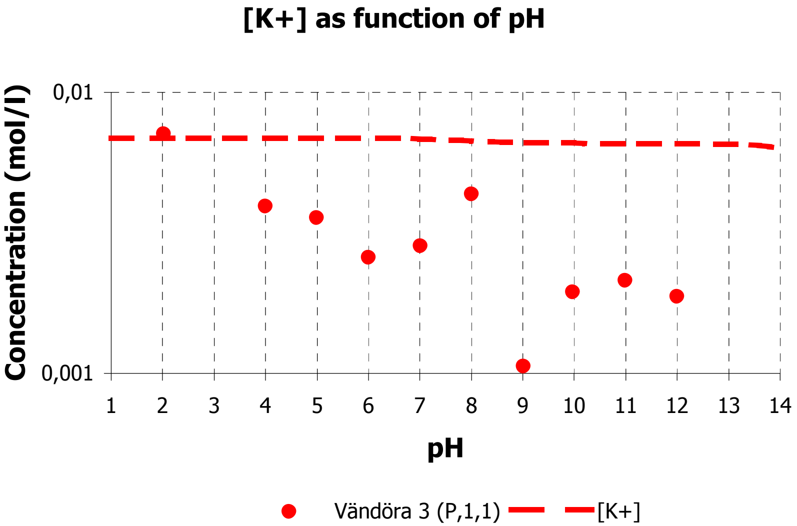

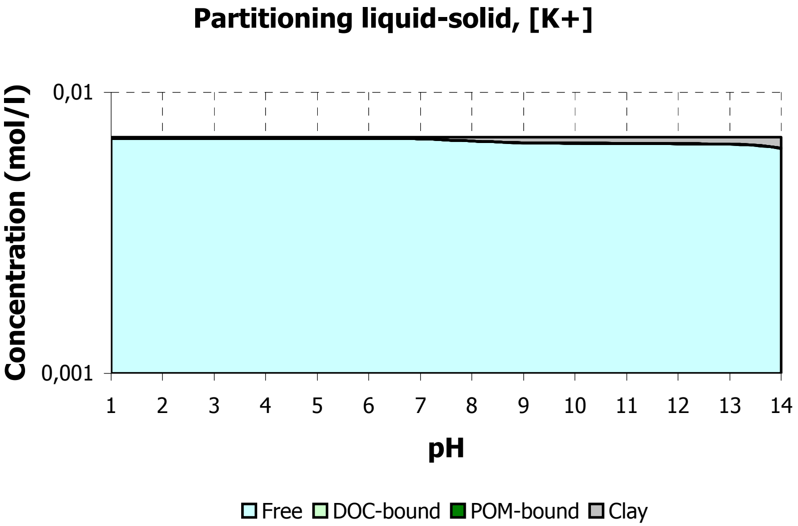

[Li+] as function of pH

Partitioning liquid-solid, [Li+]

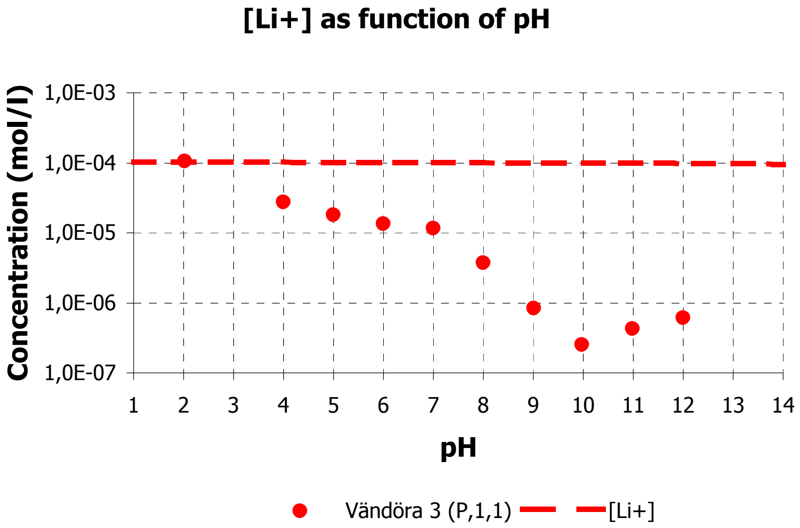
[Li+] as function of pH
Concentration (mol/l)
1,0E-03
1,0E-04
1,0E-05
1,0E-06
1,0E-07
1
2
3
4
5
6
7
8
9
10
11
12
13
14
pH
Vändöra 3 (P,1,1)
[Li+]

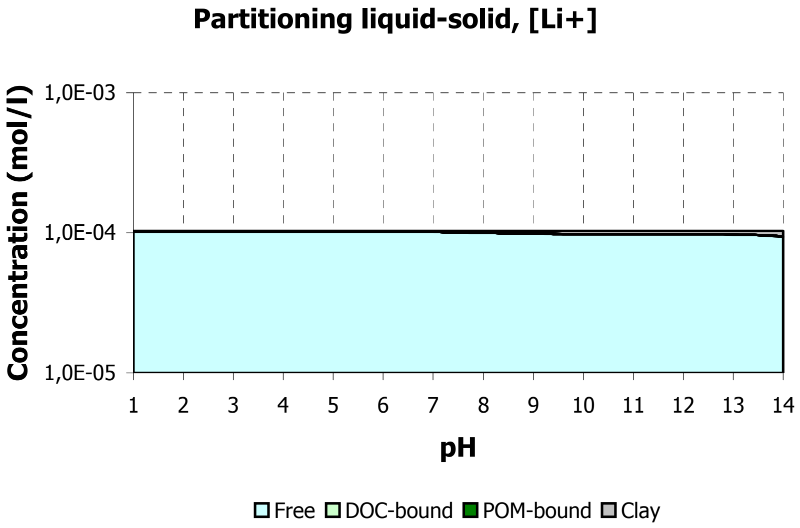
Partitioning liquid-solid, [Li+]
Concentration (mol/l)
1,0E-03
1,0E-04
1,0E-05
1
2
3
4
5
6
7
8
9
10
11
12
13
14
pH
Free
DOC-bound
POM-bound
Clay

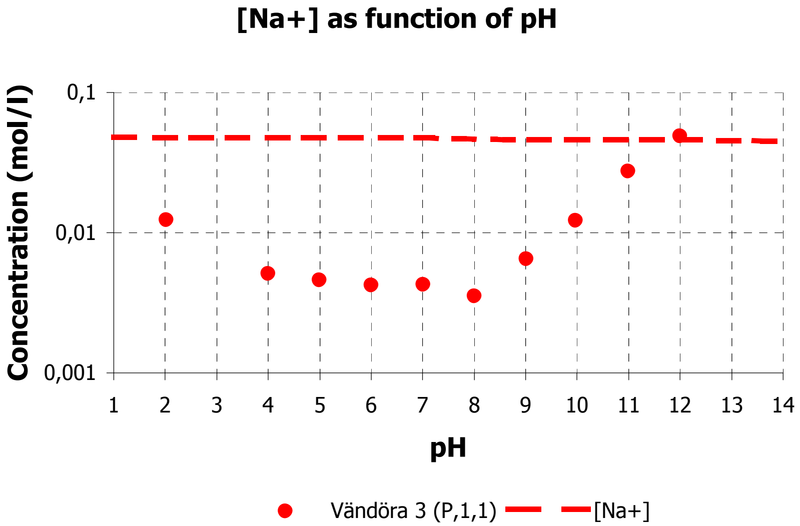
[Na+] as function of pH
Concentration (mol/l)
0,1
0,01
0,001
1
2
3
4
5
6
7
8
9
10
11
12
13
14
pH
Vändöra 3 (P,1,1)
[Na+]

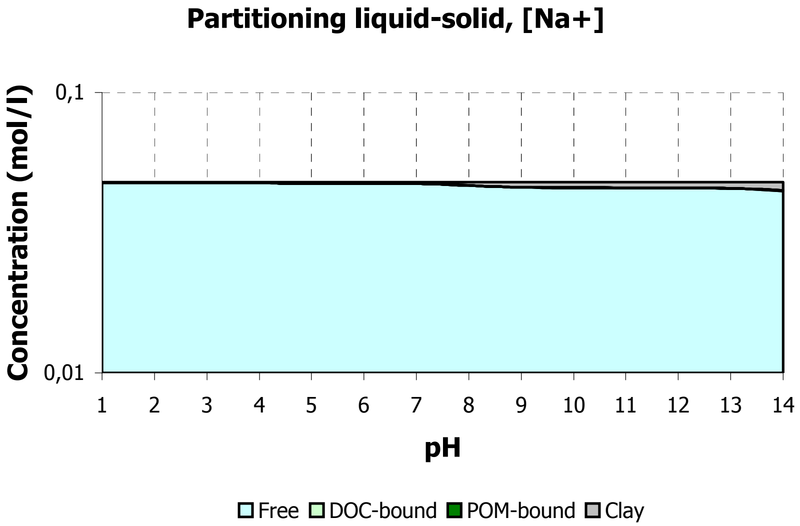
Partitioning liquid-solid, [Na+]
Concentration (mol/l)
0,1
0,01
1
2
3
4
5
6
7
8
9
10
11
12
13
14
pH
Free
DOC-bound
POM-bound
Clay

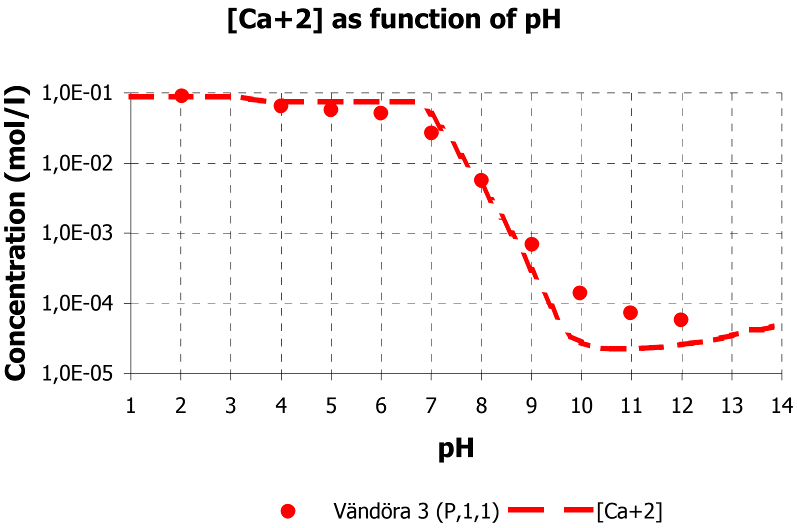
[Ca+2] as function of pH
Concentration (mol/l)
1,0E-01
1,0E-02
1,0E-03
1,0E-04
1,0E-05
1 2 3 4 5 6 7 8 9 10 11 12 13 14
pH
Vändöra 3 (P,1,1)
[Ca+2]

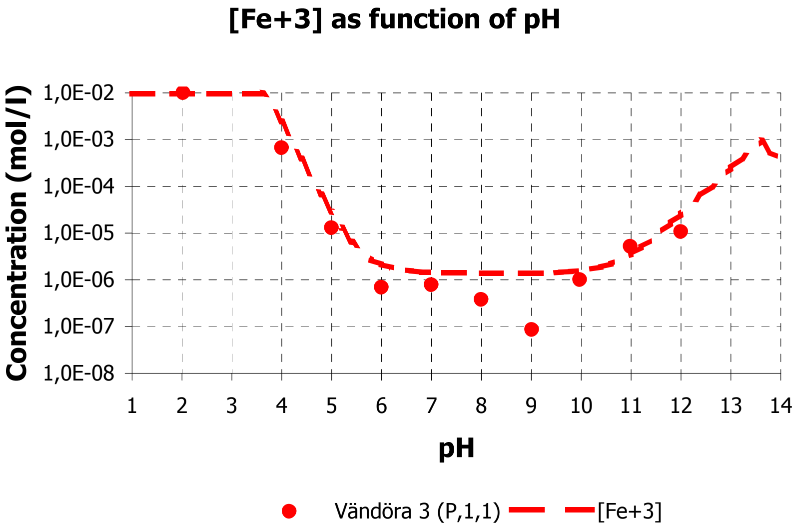
[Fe+3] as function of pH
Concentration (mol/l)
1,0E-02
1,0E-03
1,0E-04
1,0E-05
1,0E-06
1,0E-07
1,0E-08
1 2 3 4 5 6 7 8 9 10 11 12 13 14
pH
Vändöra 3 (P,1,1)
[Fe+3]

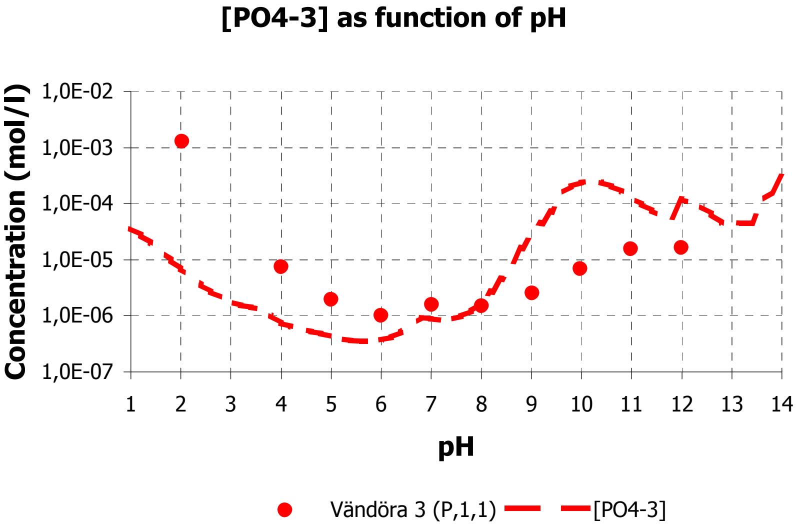
[PO4-3] as function of pH
Concentration (mol/l)
1,0E-02
1,0E-03
1,0E-04
1,0E-05
1,0E-06
1,0E-07
1 2 3 4 5 6 7 8 9 10 11 12 13 14
pH
Vändöra 3 (P,1,1)
[PO4-3]

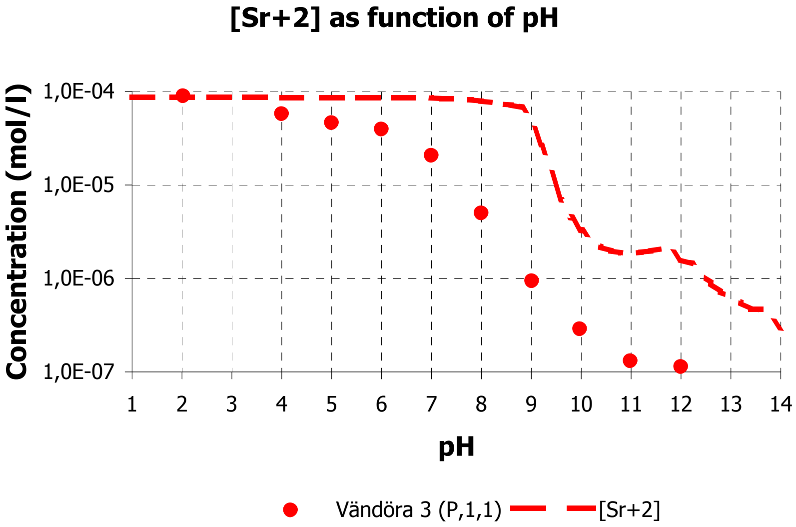
[Sr+2] as function of pH
Concentration (mol/l)
1,0E-04
1,0E-05
1,0E-06
1,0E-07
1 2 3 4 5 6 7 8 9 10 11 12 13 14
pH
Vändöra 3 (P,1,1)
[Sr+2]

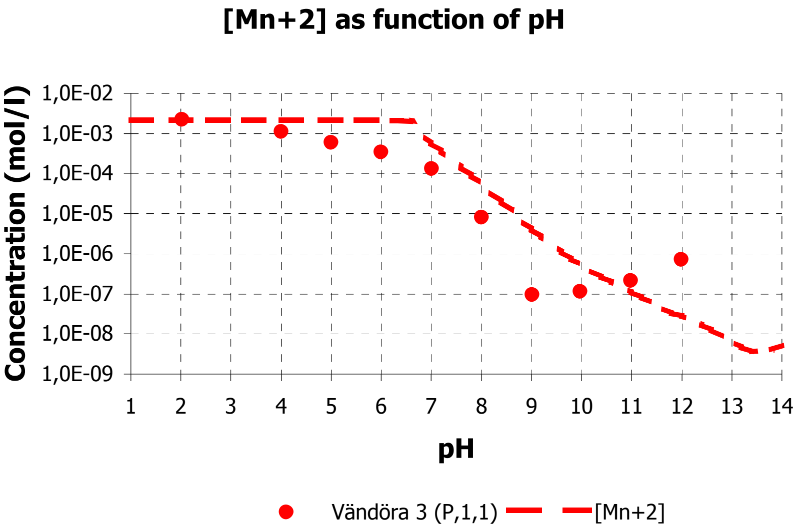
[Mn+2] as function of pH

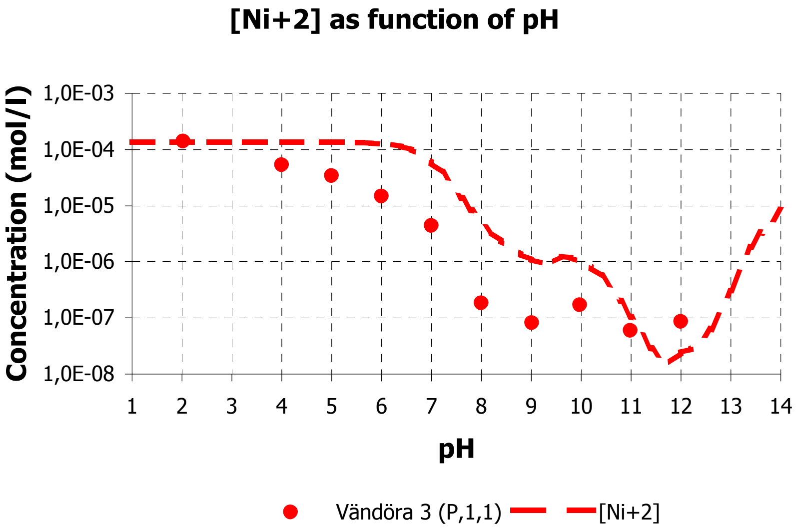
[Ni+2] as function of pH

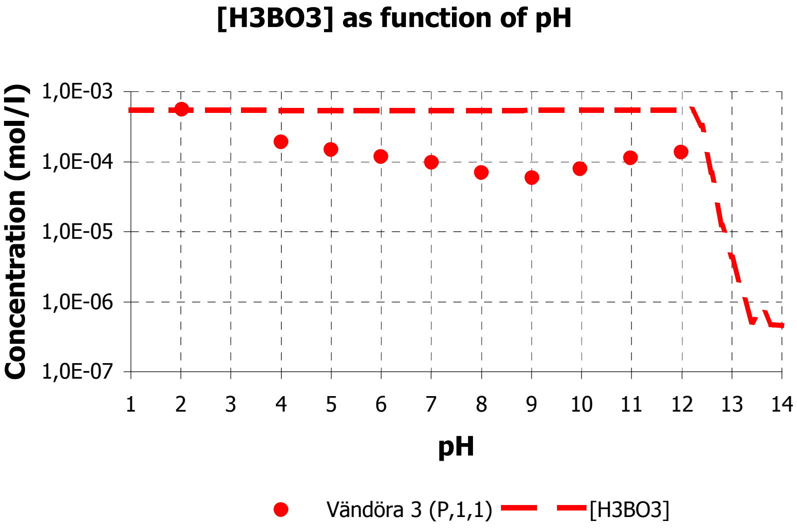
[H3BO3] as function of pH

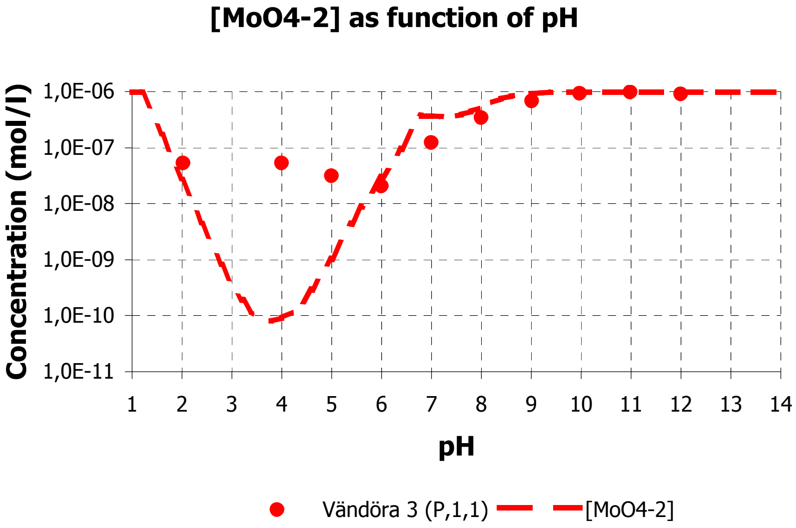
[MoO4-2] as function of pH

[F-] as function of pH

[K+] as function of pH

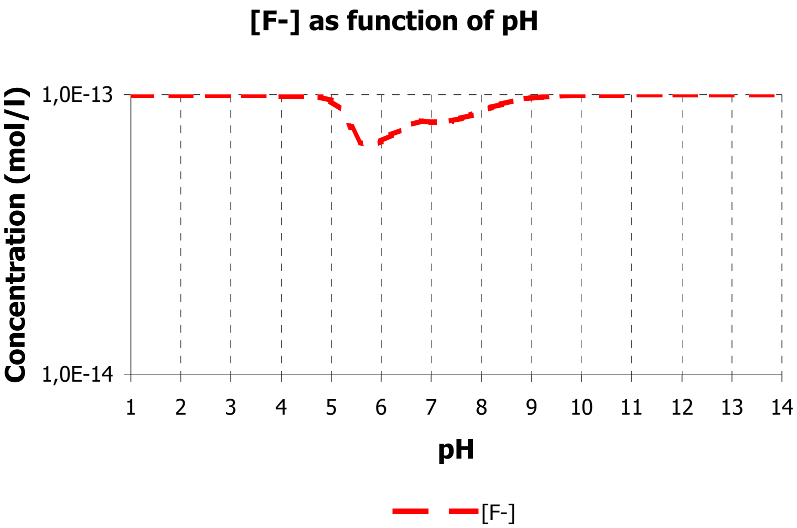

[F-] as function of pH

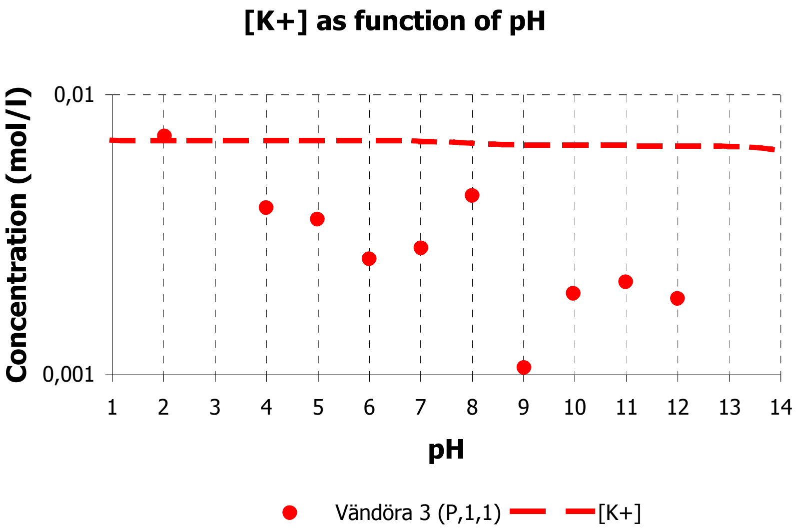

[K+] as function of pH

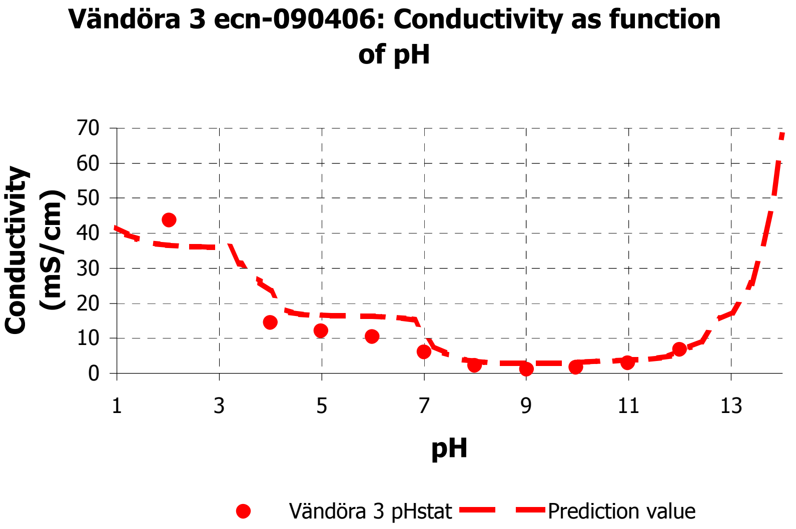

Vändöra 3 ecn-090406: Conductivity as function of pH

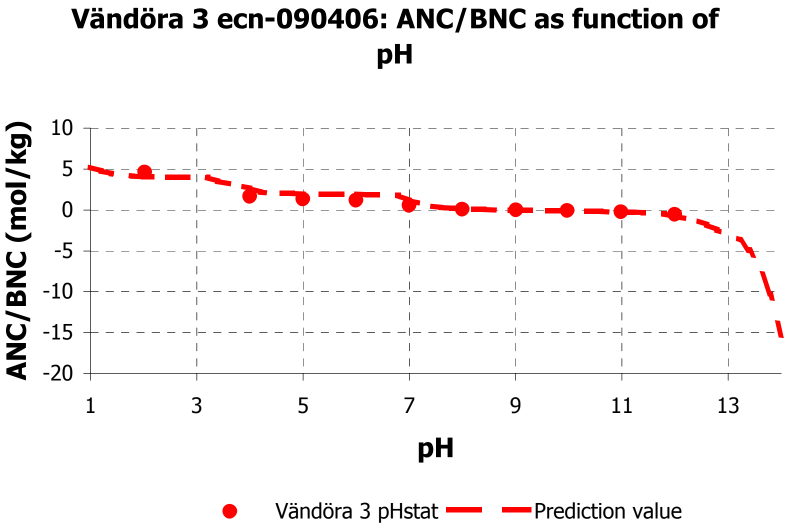

Vändöra 3 ecn-090406: ANC/BNC as function of pH

Al+3 fractionation in solution

Al+3 fractionation in the solid phase

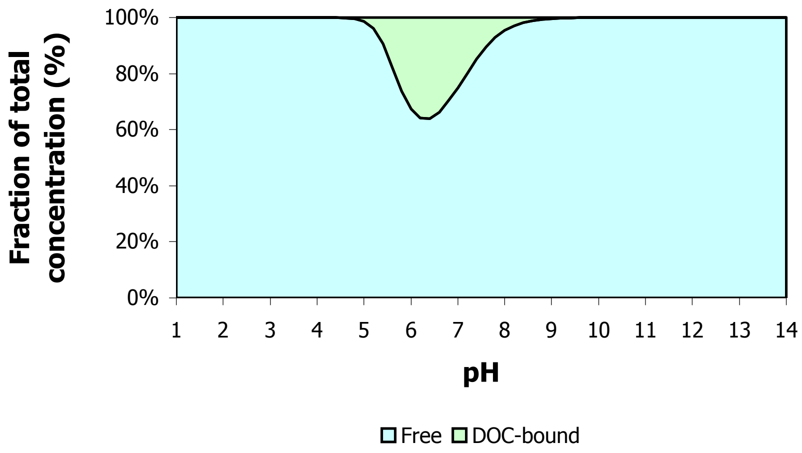

Al+3 fractionation in solution

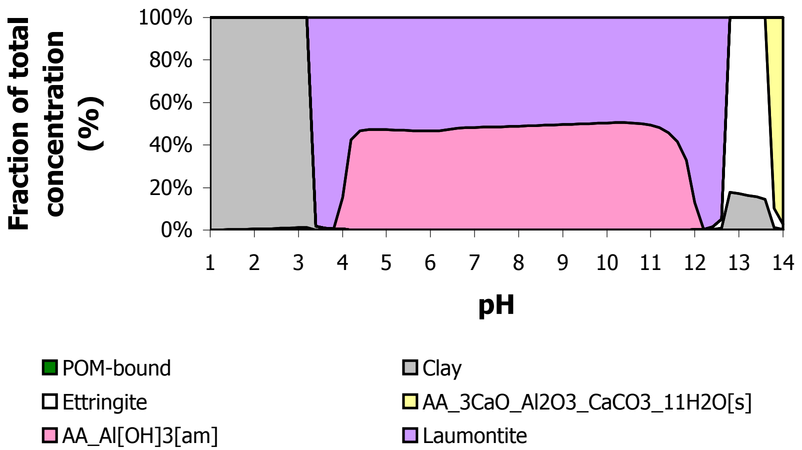

Al+3 fractionation in the solid phase

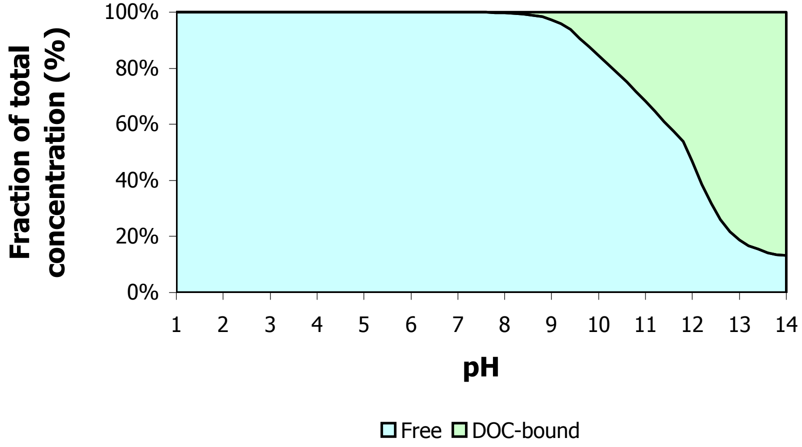

Ba+2 fractionation in solution

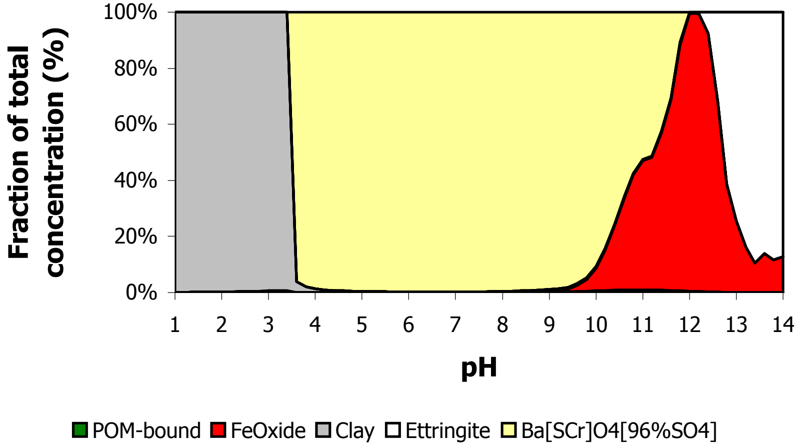

Ba+2 fractionation in the solid phase

Ca+2 fractionation in solution

Ca+2 fractionation in the solid phase

Ca+2 fractionation in solution

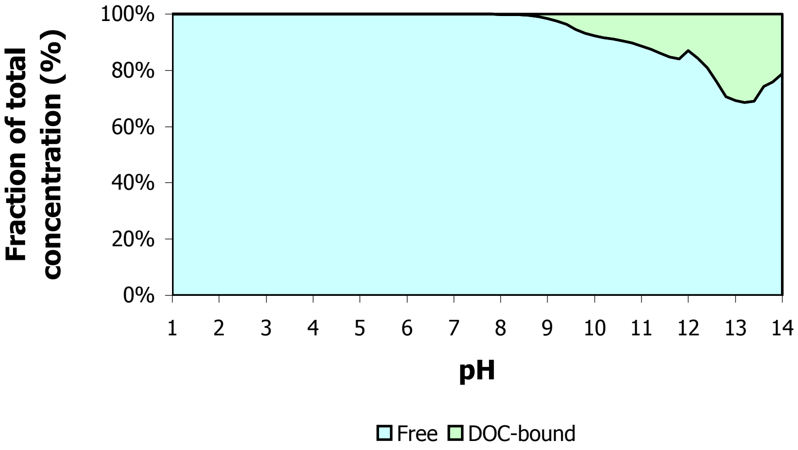

Ca+2 fractionation in the solid phase

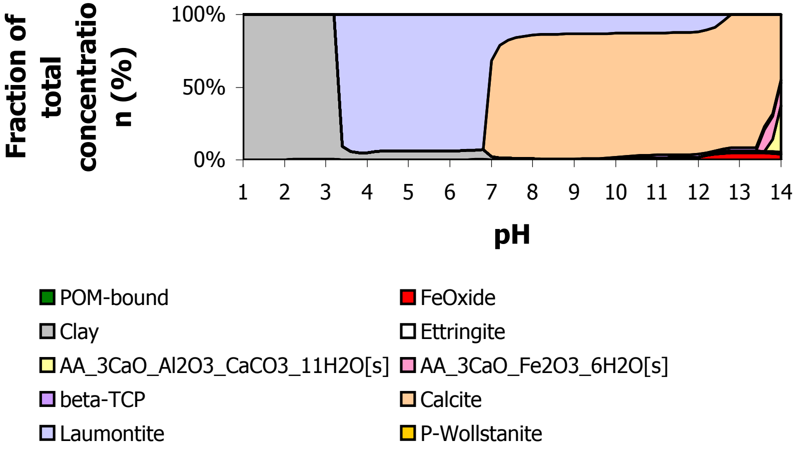

Fe+3 fractionation in solution

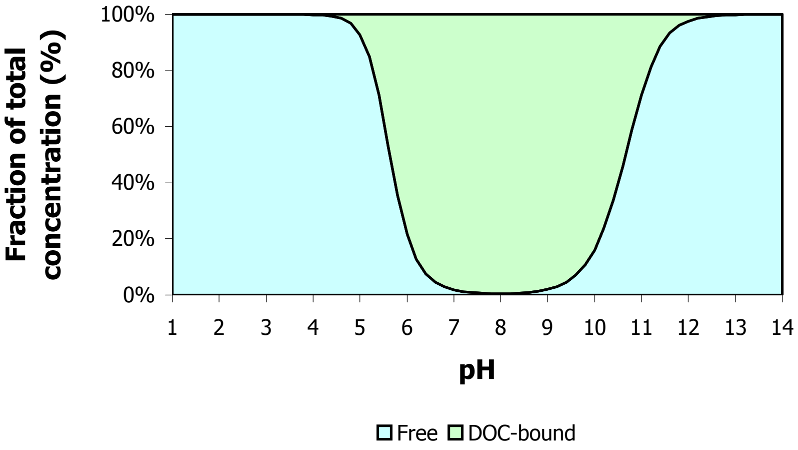

Fe+3 fractionation in the solid phase

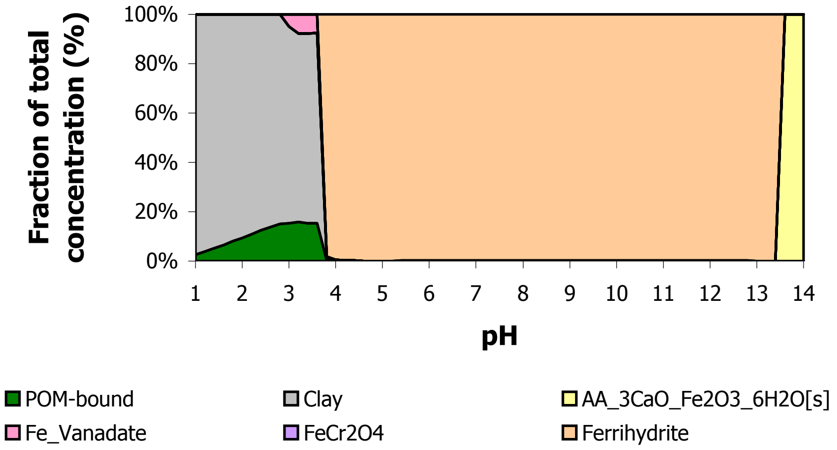

H4SiO4 fractionation in solution

H4SiO4 fractionation in the solid phase

H4SiO4 fractionation in solution

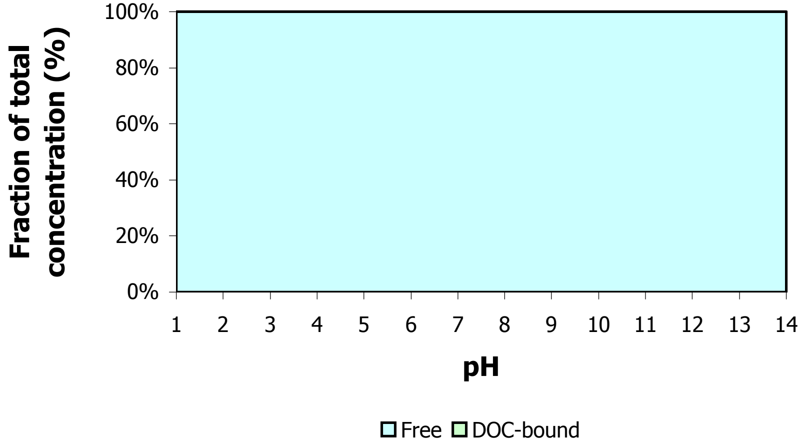

H4SiO4 fractionation in the solid phase

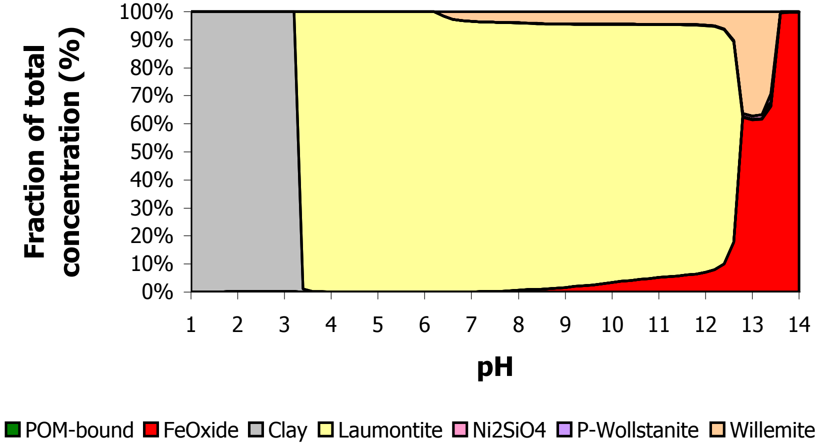

SO4-2 fractionation in solution

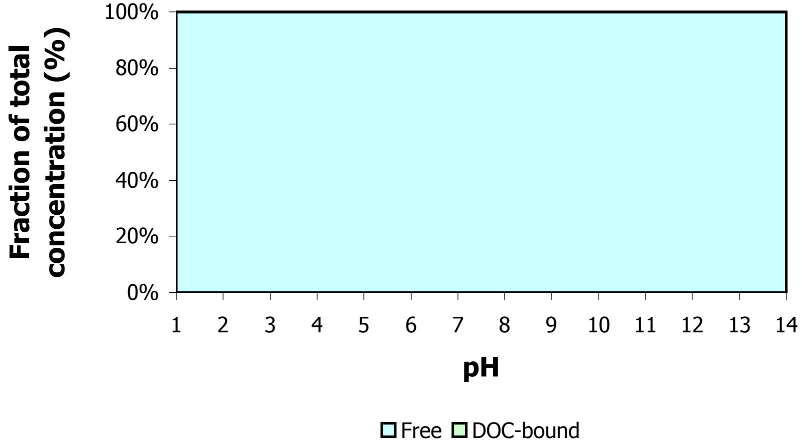

SO4-2 fractionation in the solid phase

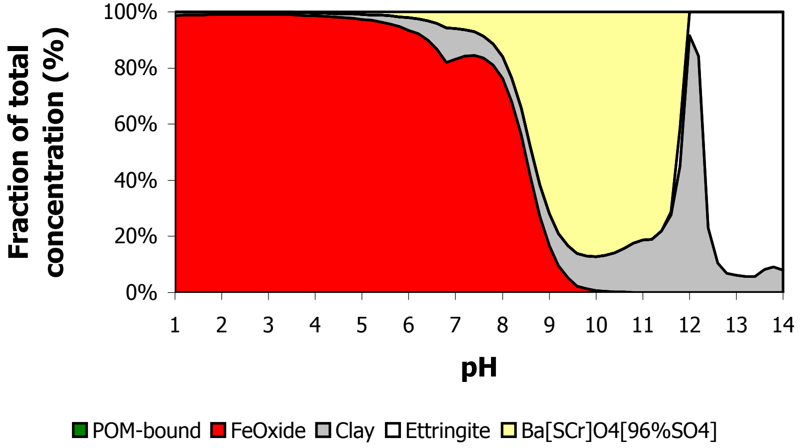

H2CO3 fractionation in solution

H2CO3 fractionation in the solid phase

H2CO3 fractionation in solution

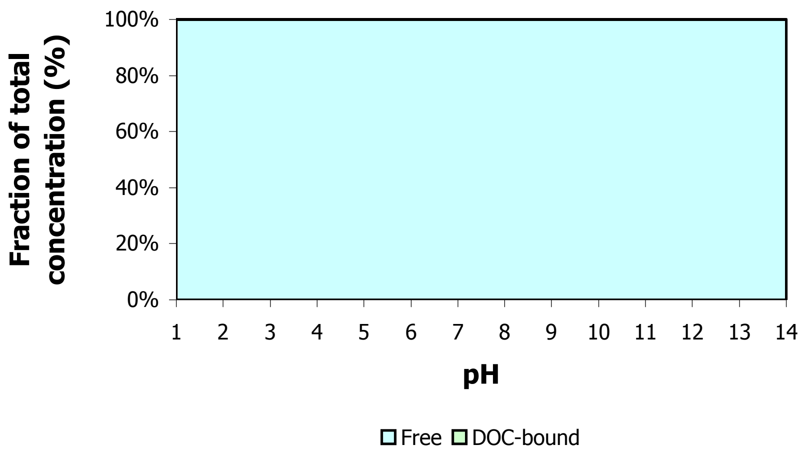

H2CO3 fractionation in the solid phase

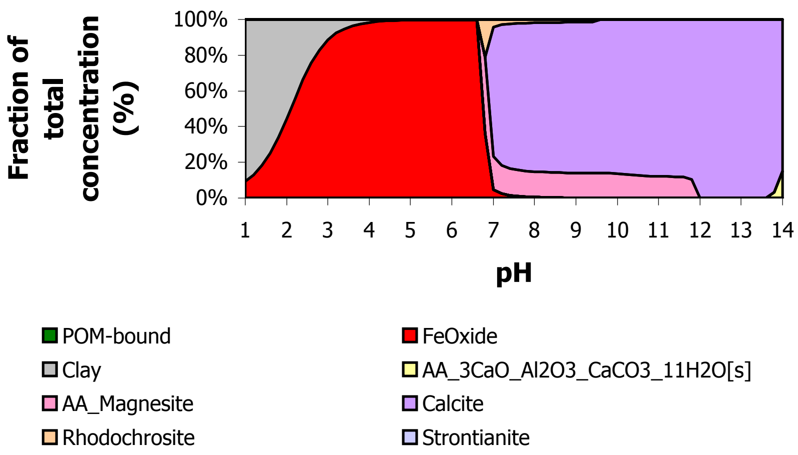

Mg+2 fractionation in solution

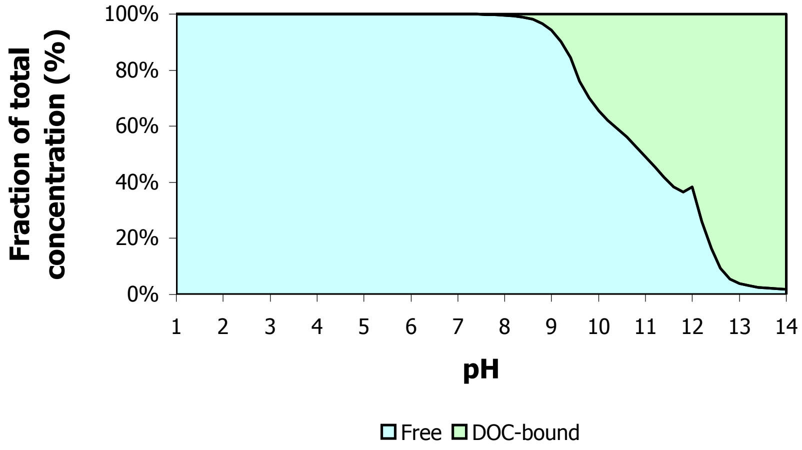

Mg+2 fractionation in the solid phase

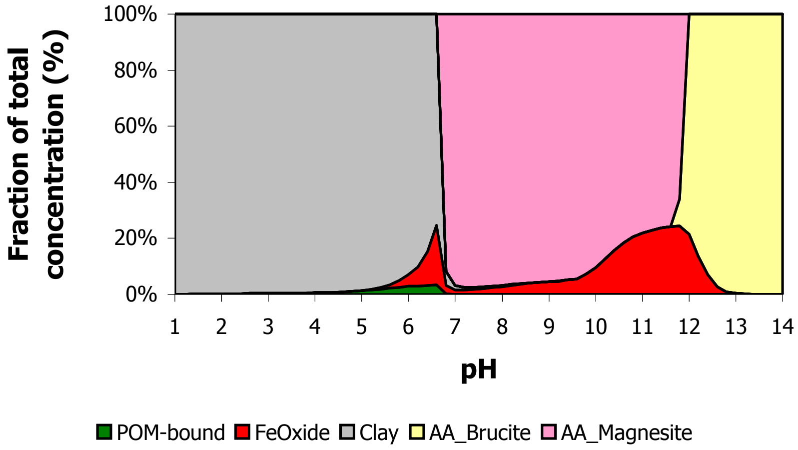

PO4-3 fractionation in solution

PO4-3 fractionation in the solid phase

PO4-3 fractionation in solution

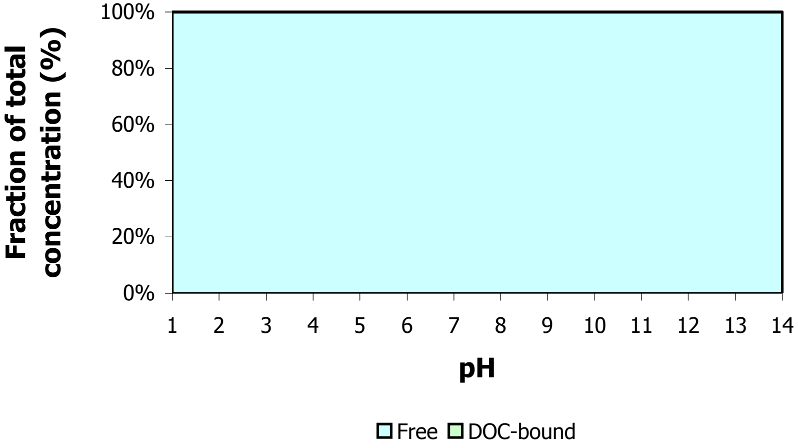

PO4-3 fractionation in the solid phase

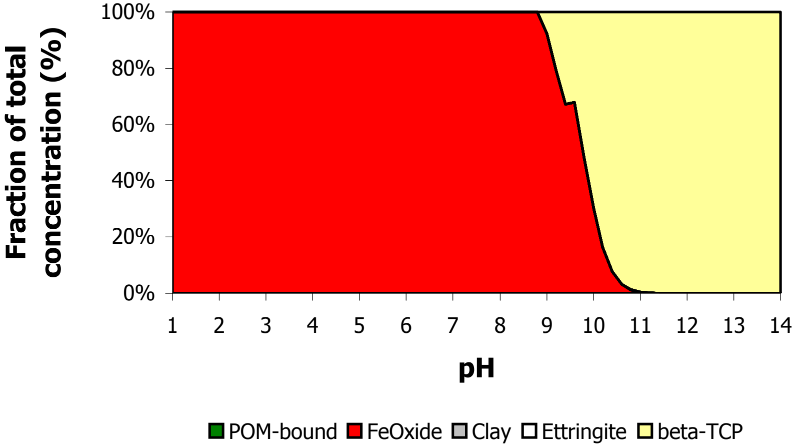

Sr+2 fractionation in solution

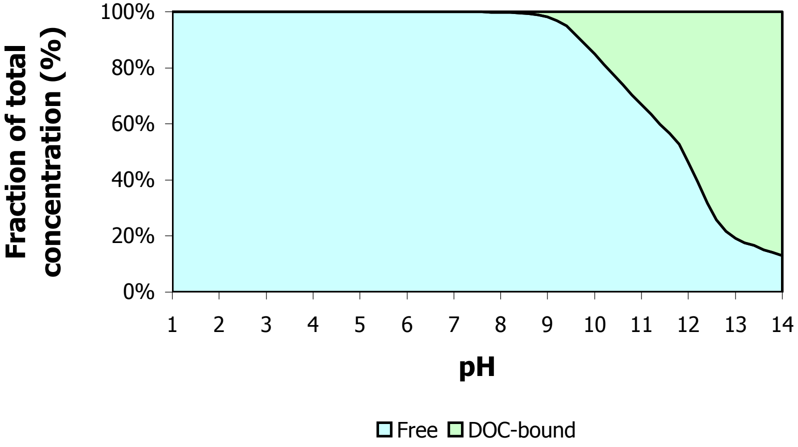

Sr+2 fractionation in the solid phase

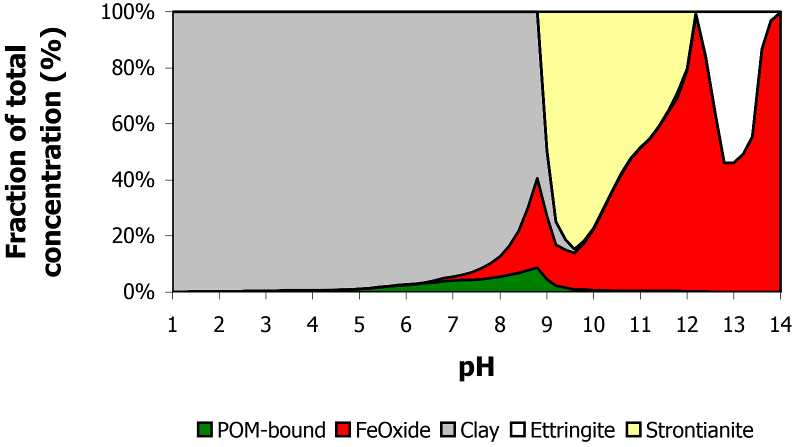

Cd+2 fractionation in solution

Cd+2 fractionation in the solid phase

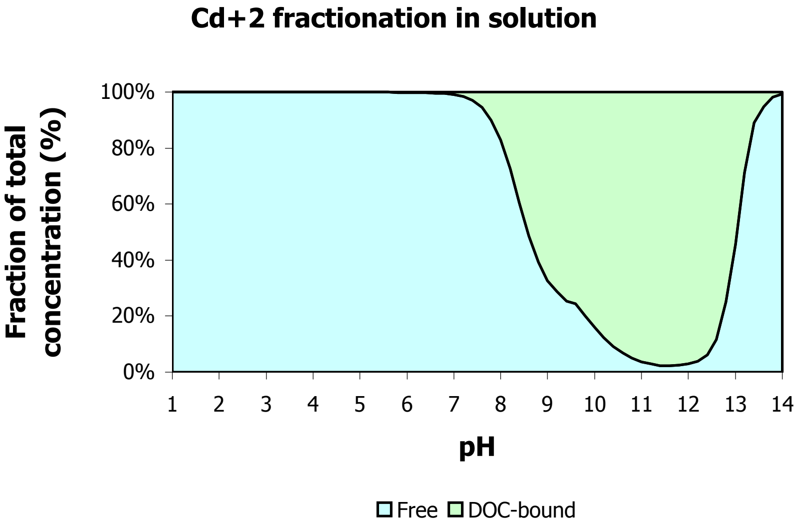
Cd+2 fractionation in solution
Fraction of total concentration (%)
100%
80%
60%
40%
20%
0%
1
2
3
4
5
6
7
8
9
10
11
12
13
14
pH
Free
DOC-bound

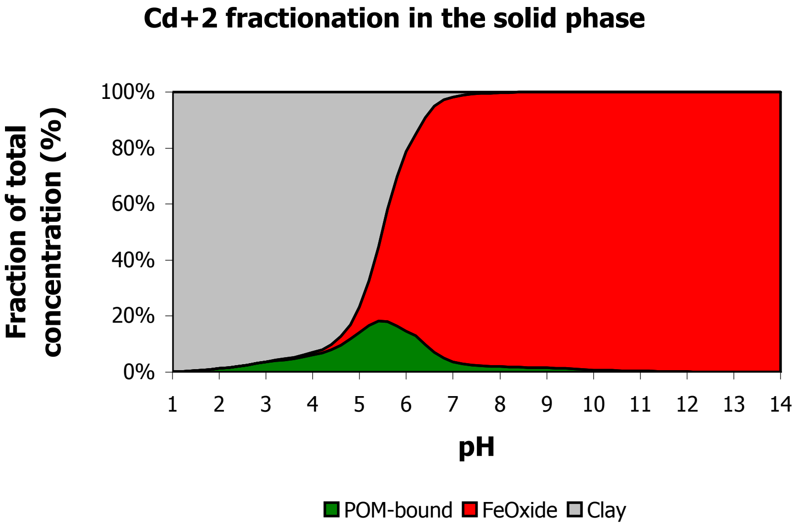
Cd+2 fractionation in the solid phase
Fraction of total concentration (%)
100%
80%
60%
40%
20%
0%
1
2
3
4
5
6
7
8
9
10
11
12
13
14
pH
POM-bound
FeOxide
Clay

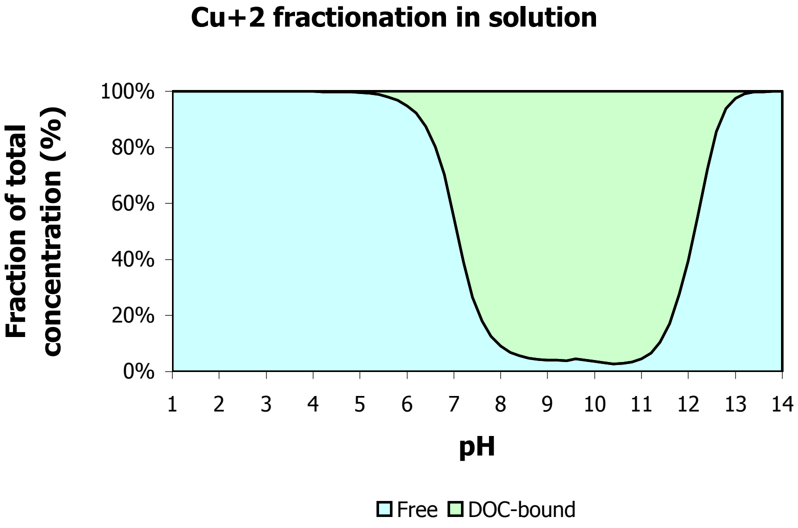
Cu+2 fractionation in solution
Fraction of total concentration (%)
100%
80%
60%
40%
20%
0%
1
2
3
4
5
6
7
8
9
10
11
12
13
14
pH
Free
DOC-bound

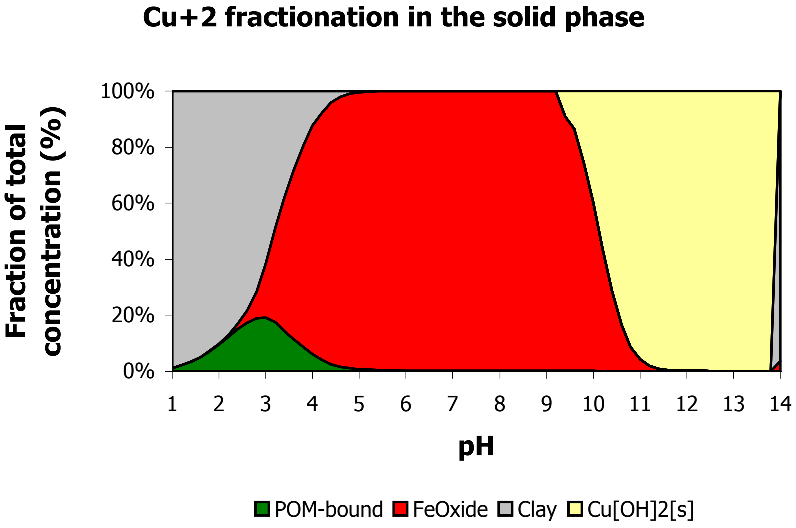
Cu+2 fractionation in the solid phase
Fraction of total concentration (%)
100%
80%
60%
40%
20%
0%
1
2
3
4
5
6
7
8
9
10
11
12
13
14
pH
POM-bound
FeOxide
Clay
Cu[OH]2[s]

Mn+2 fractionation in solution

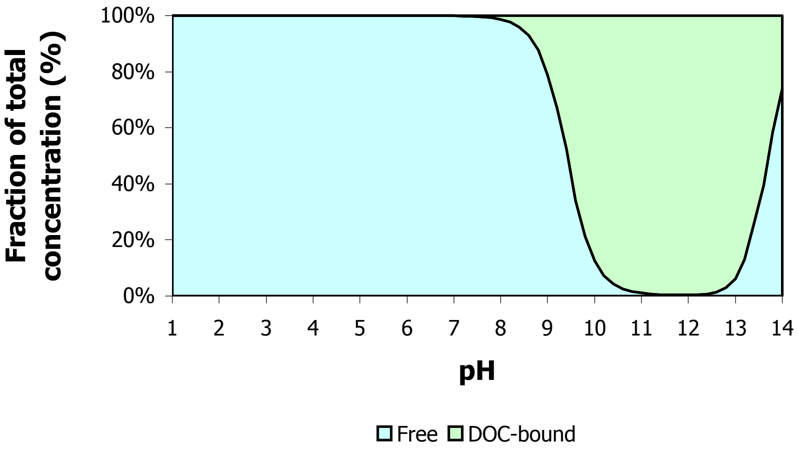

Mn+2 fractionation in the solid phase

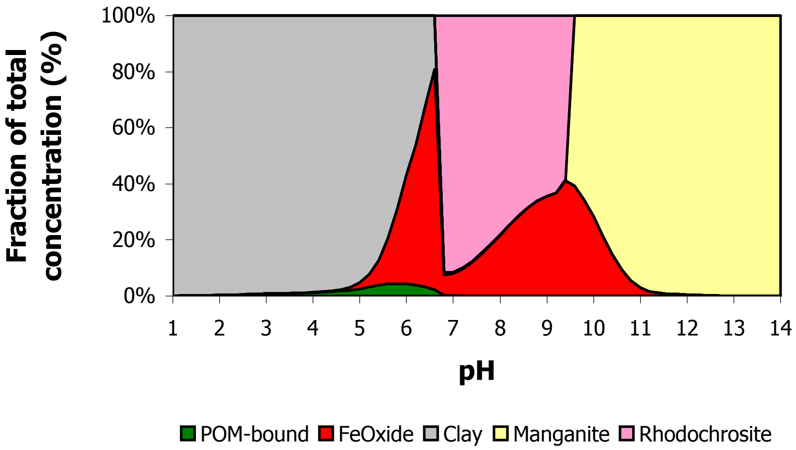

Ni+2 fractionation in solution

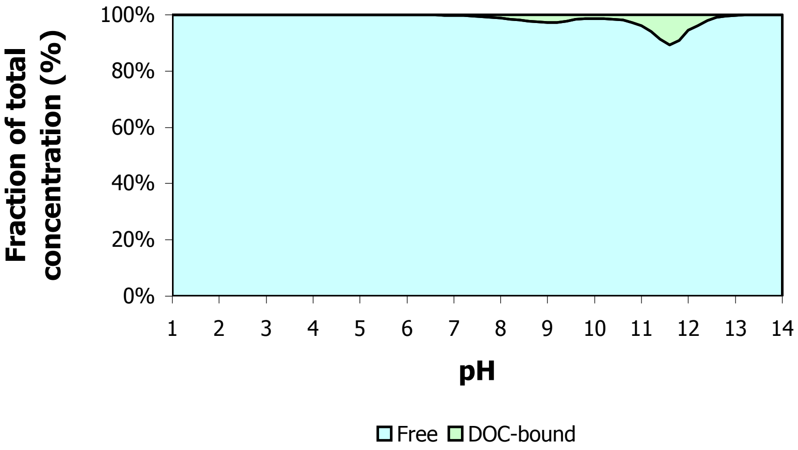

Ni+2 fractionation in the solid phase

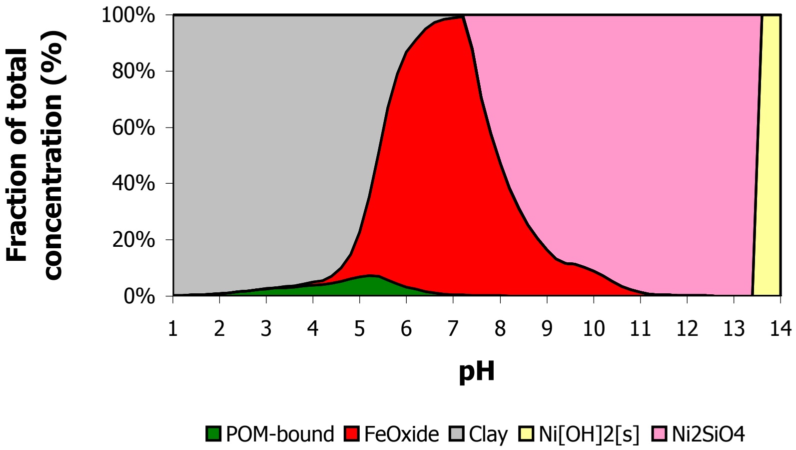

Pb+2 fractionation in solution

Pb+2 fractionation in the solid phase

Pb+2 fractionation in solution

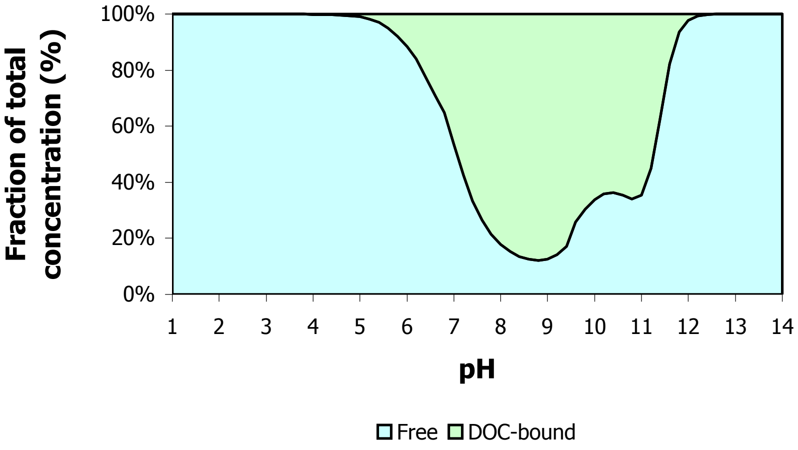

Pb+2 fractionation in the solid phase

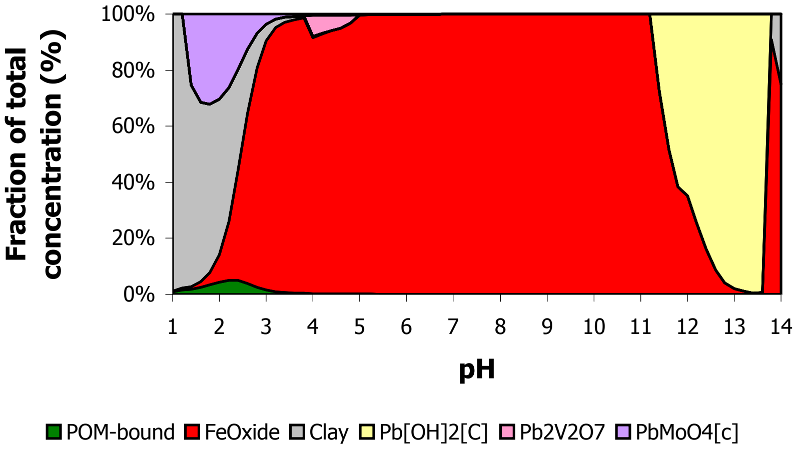

Zn+2 fractionation in solution

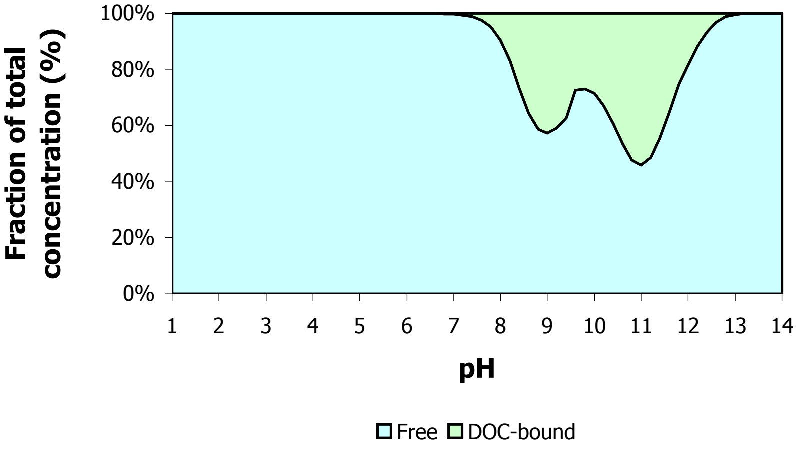

Zn+2 fractionation in the solid phase

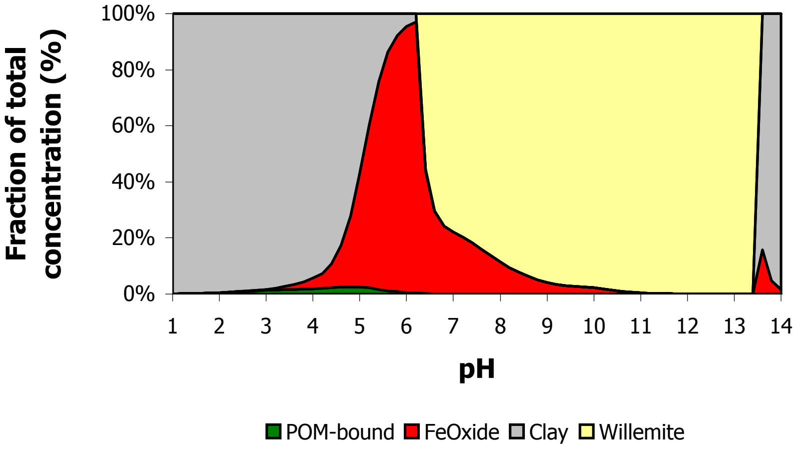

CrO4-2 fractionation in solution

CrO4-2 fractionation in the solid phase

CrO4-2 fractionation in solution

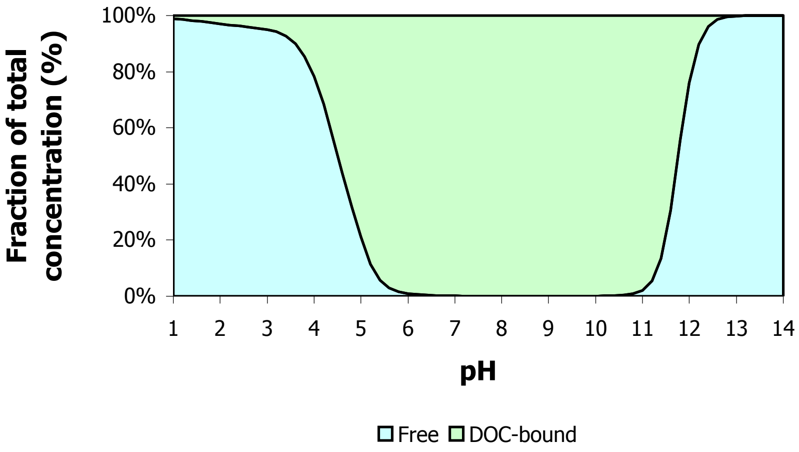

CrO4-2 fractionation in the solid phase

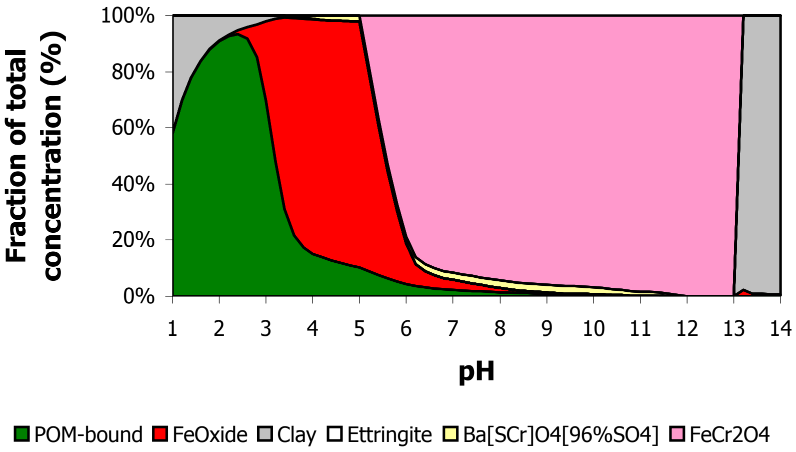

H3AsO4 fractionation in solution

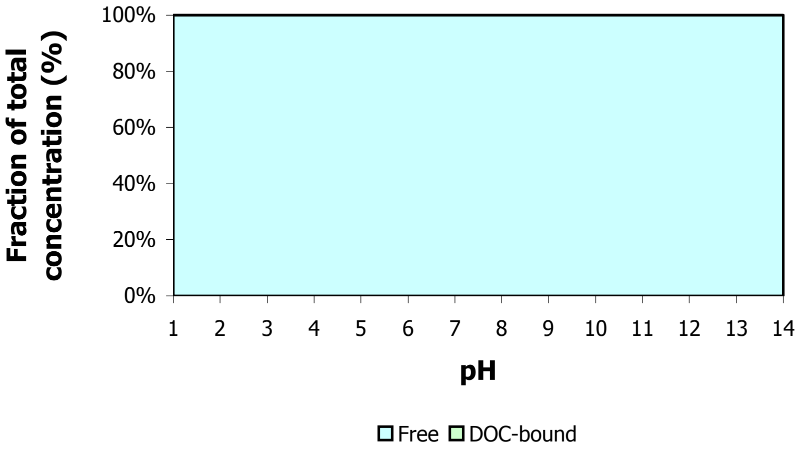

H3AsO4 fractionation in the solid phase

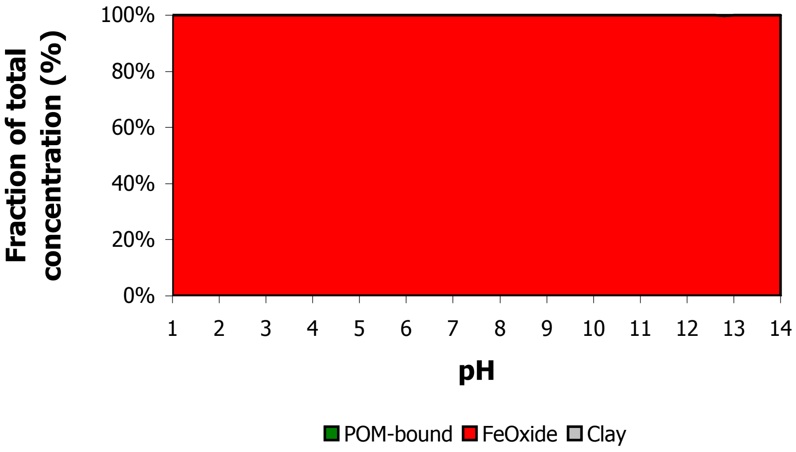

H3BO3 fractionation in solution

H3BO3 fractionation in the solid phase

H3BO3 fractionation in solution

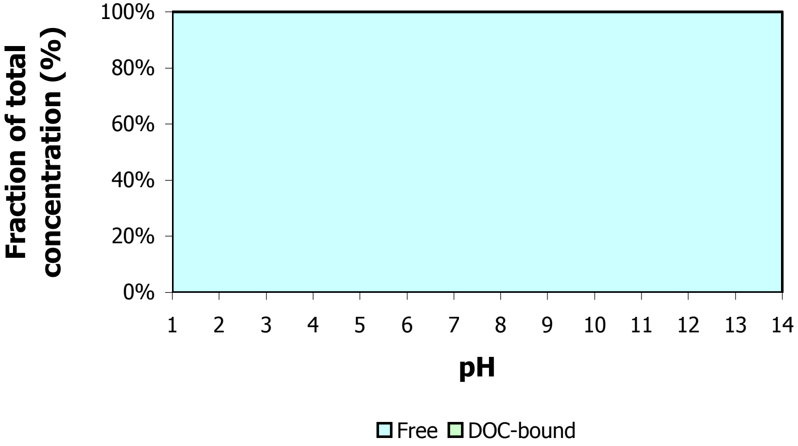

H3BO3 fractionation in the solid phase

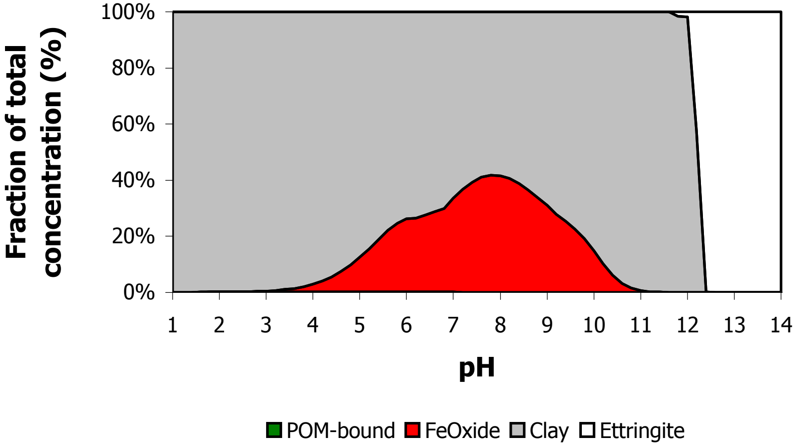

MoO4-2 fractionation in solution

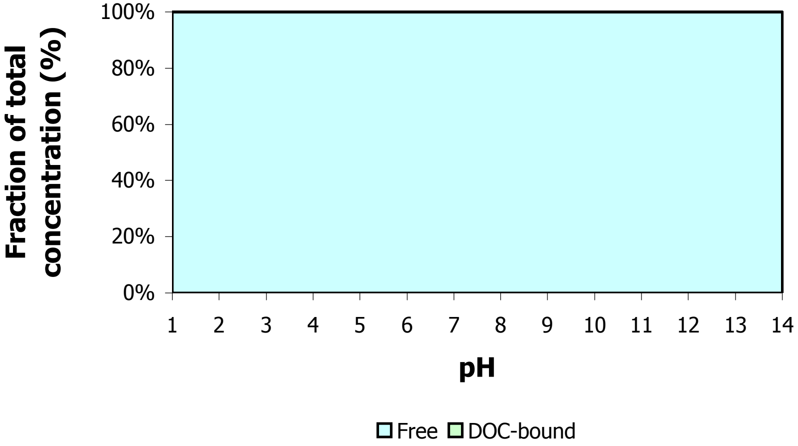

MoO4-2 fractionation in the solid phase

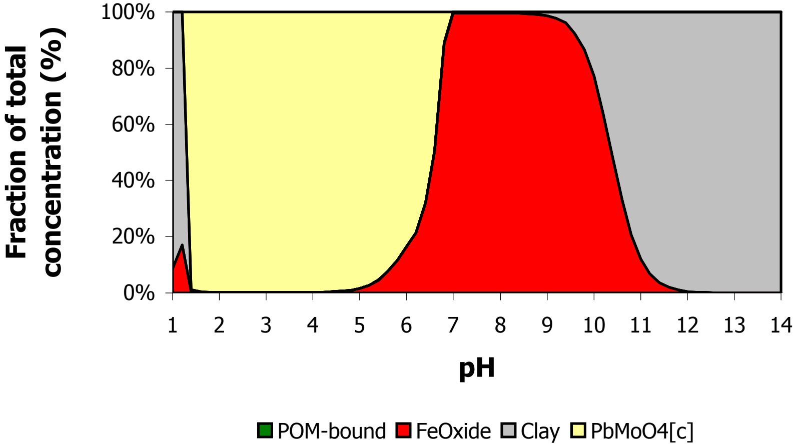

Sb[OH]6- fractionation in solution

Sb[OH]6- fractionation in the solid phase

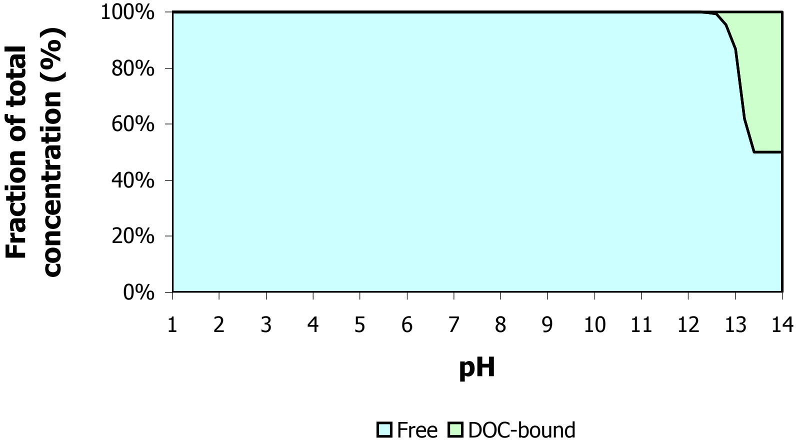

Sb[OH]6- fractionation in solution

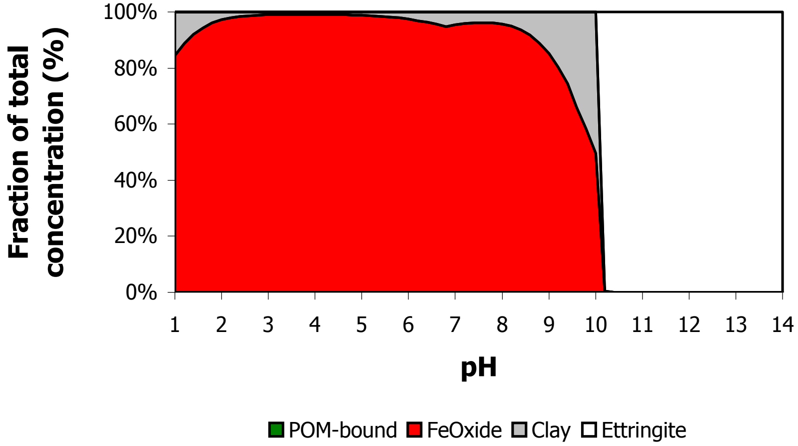

Sb[OH]6- fractionation in the solid phase

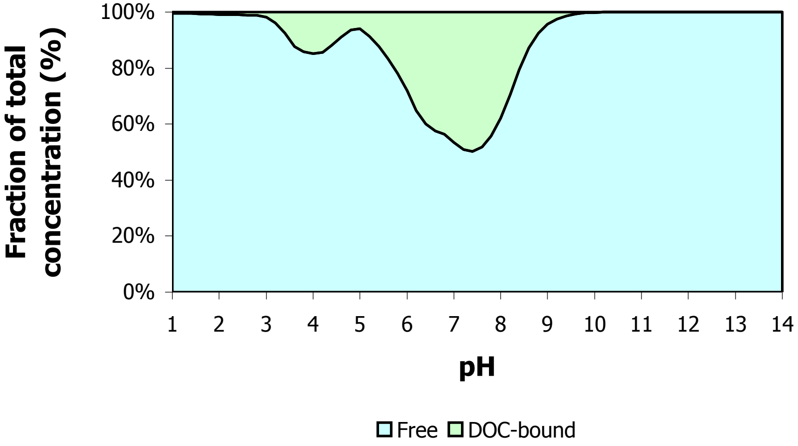

VO2+ fractionation in solution

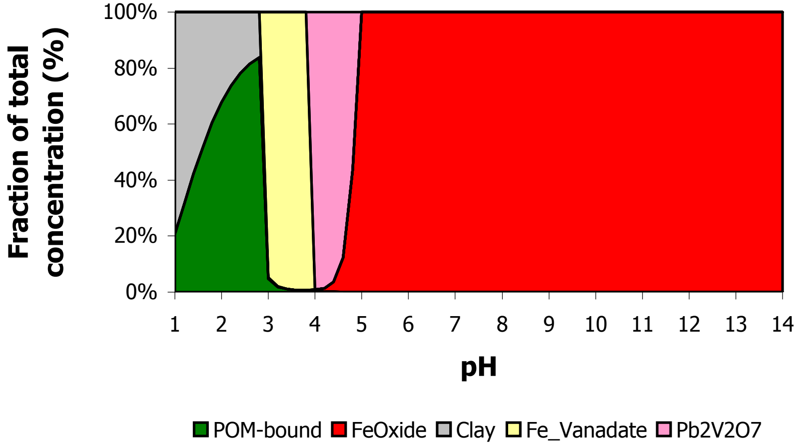

VO2+ fractionation in the solid phase

Br- fractionation in solution

Br- fractionation in the solid phase

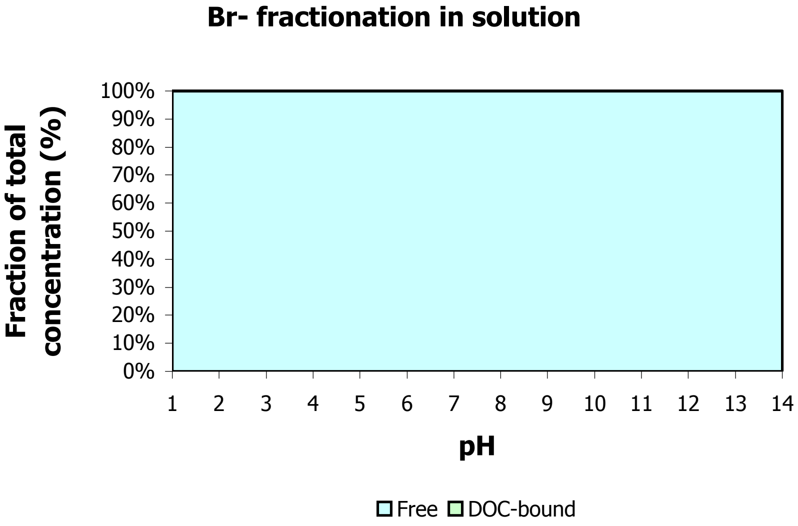
Br- fractionation in solution
Fraction of total concentration (%)
100%
90%
80%
70%
60%
50%
40%
30%
20%
10%
0%
1 2 3 4 5 6 7 8 9 10 11 12 13 14
pH
Free
DOC-bound

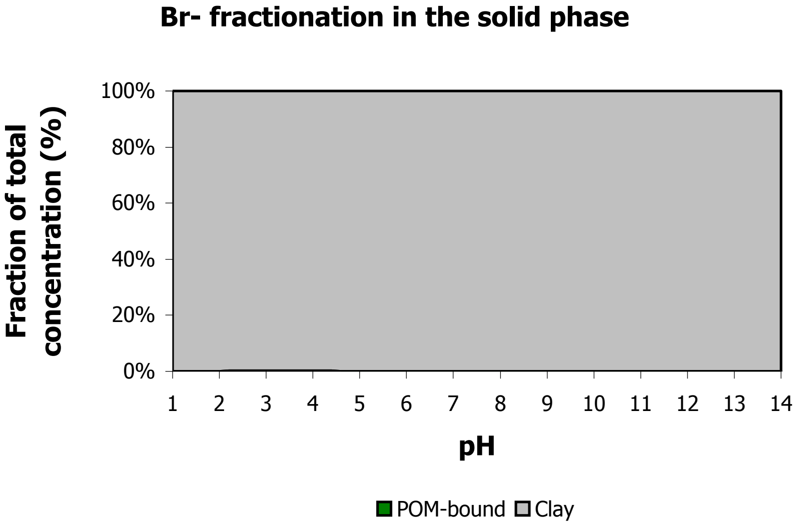
Br- fractionation in the solid phase
Fraction of total concentration (%)
100%
80%
60%
40%
20%
0%
1 2 3 4 5 6 7 8 9 10 11 12 13 14
pH
POM-bound
Clay

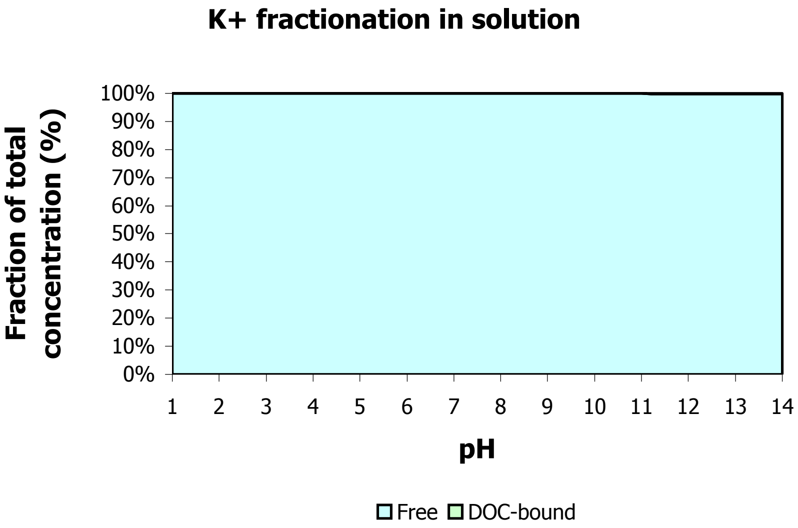

K+ fractionation in solution

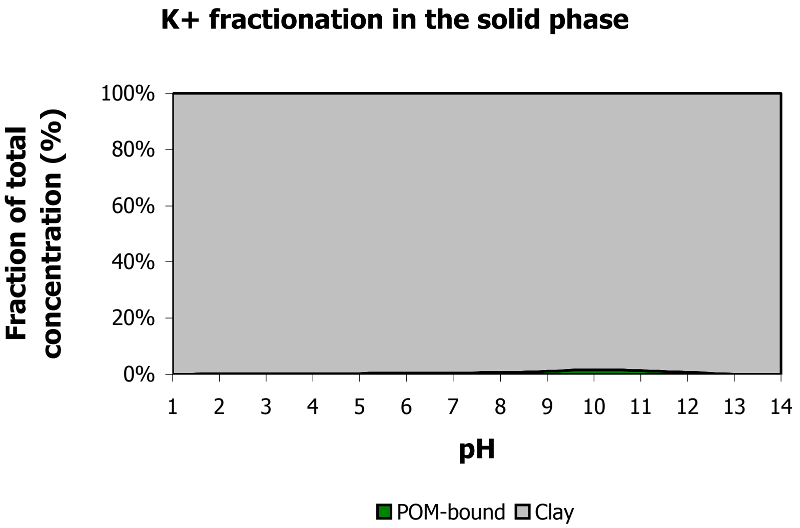

K+ fractionation in the solid phase

Li+ fractionation in solution

Li+ fractionation in the solid phase

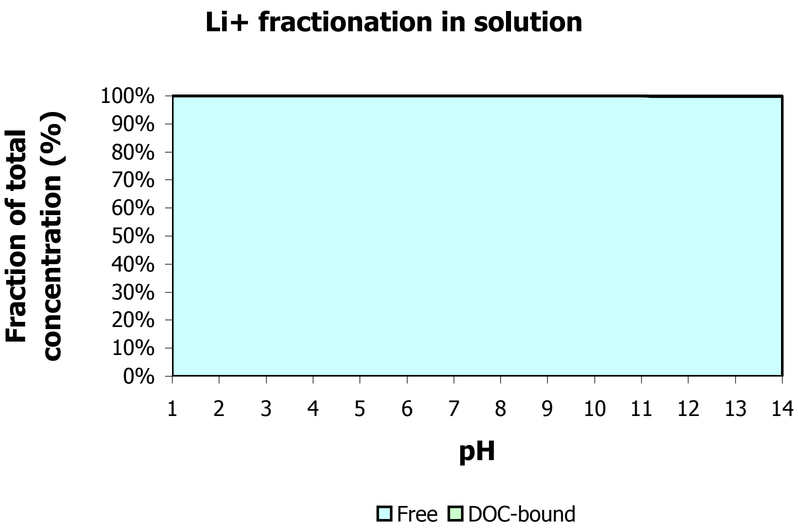
Li+ fractionation in solution

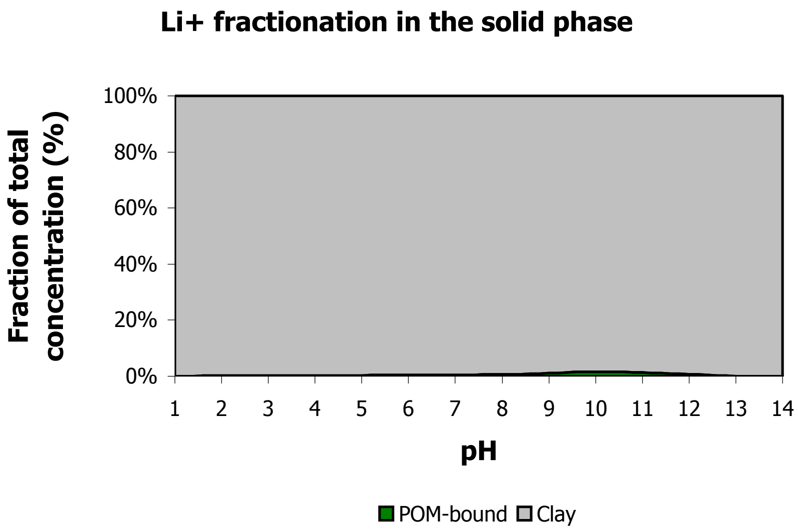
Li+ fractionation in the solid phase

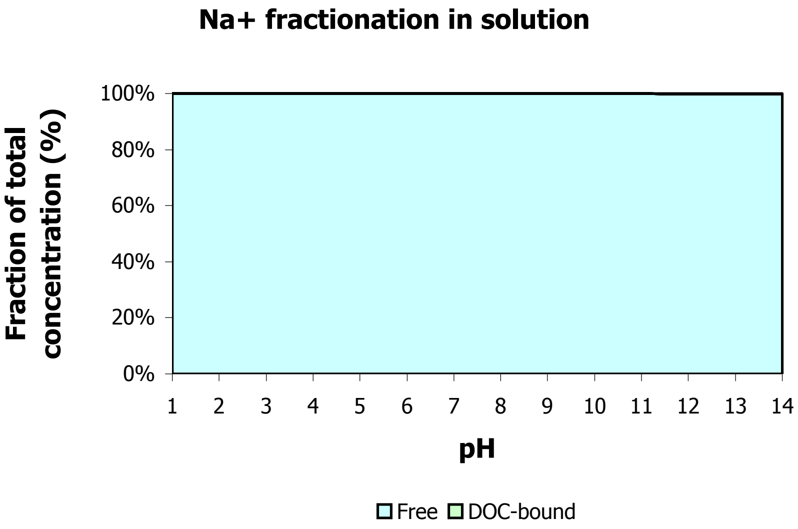
Na+ fractionation in solution

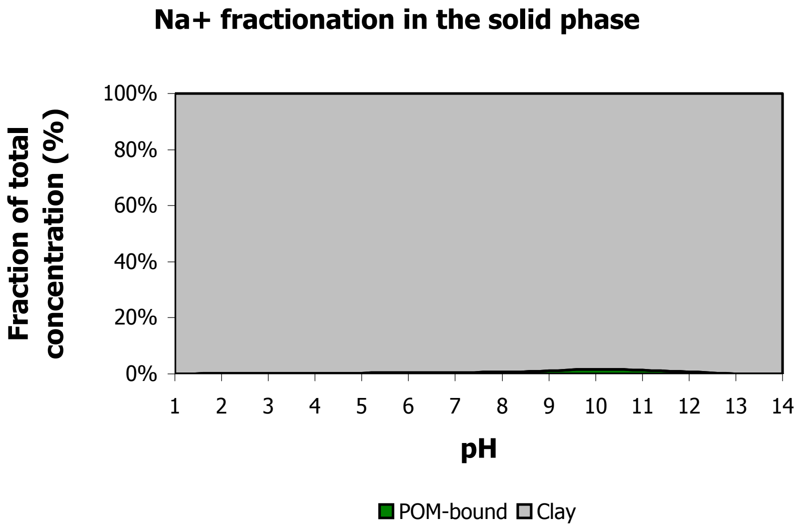
Na+ fractionation in the solid phase

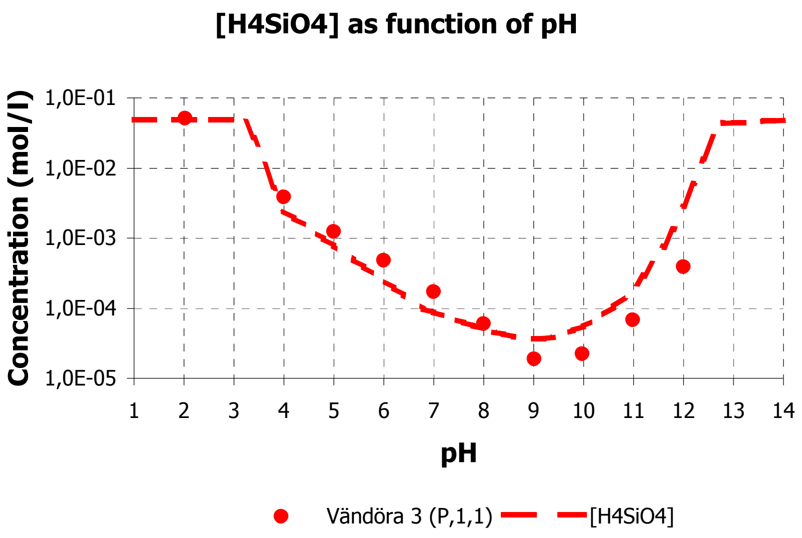
[H4SiO4] as function of pH
Concentration (mol/l)
1,0E-01
1,0E-02
1,0E-03
1,0E-04
1,0E-05
1
2
3
4
5
6
7
8
9
10
11
12
13
14
pH
Vändöra 3 (P,1,1)
[H4SiO4]

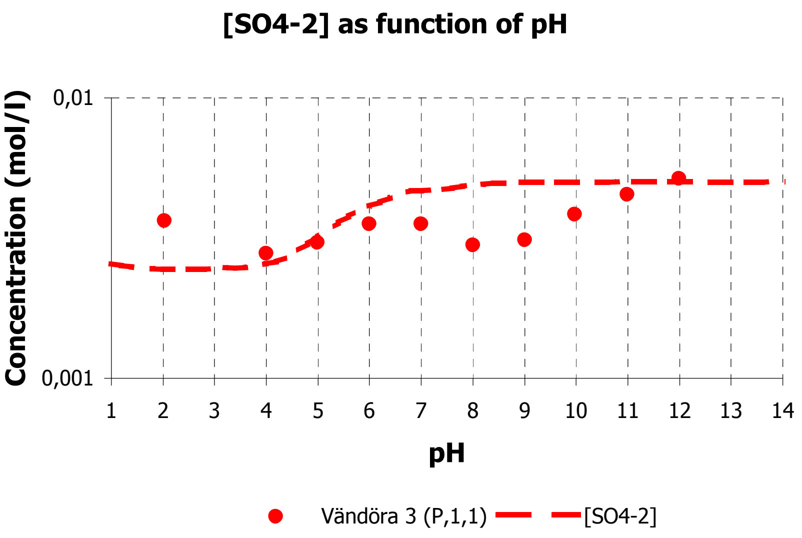
[SO4-2] as function of pH
Concentration (mol/l)
0,01
0,001
1
2
3
4
5
6
7
8
9
10
11
12
13
14
pH
Vändöra 3 (P,1,1)
[SO4-2]

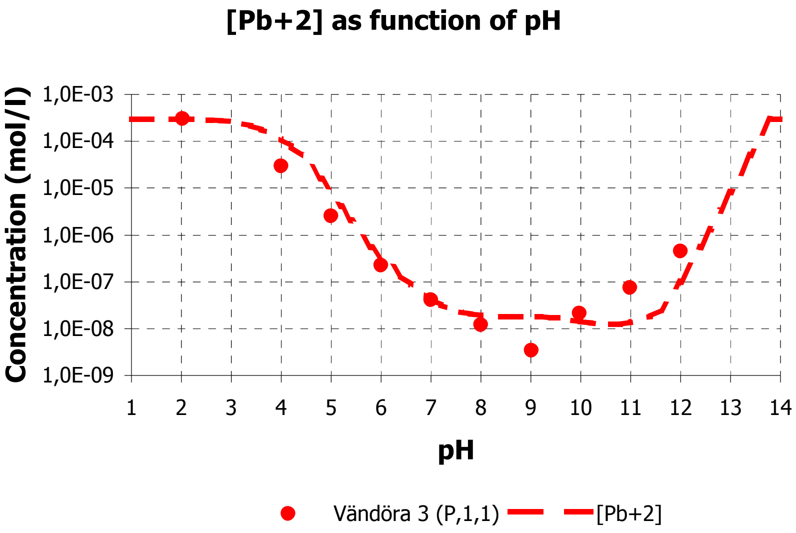

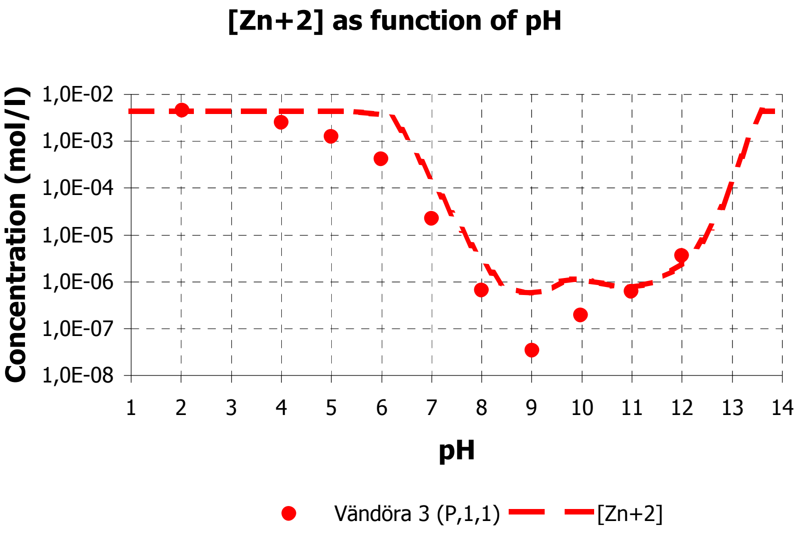

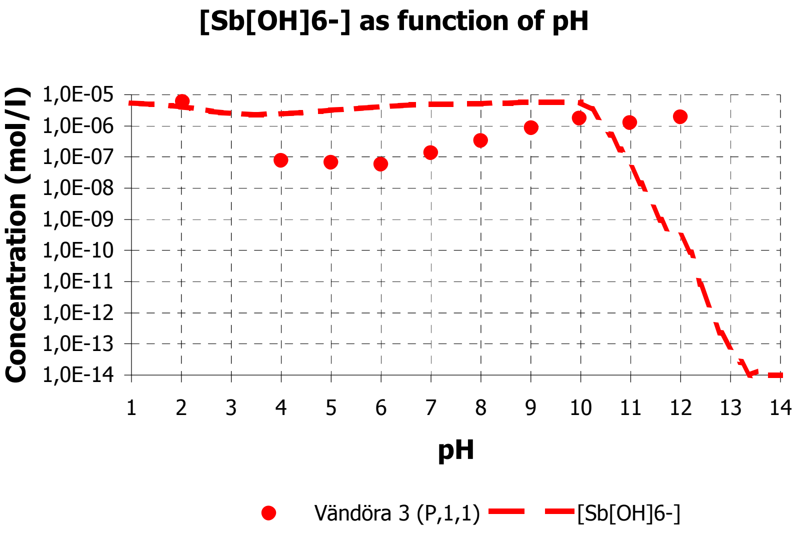

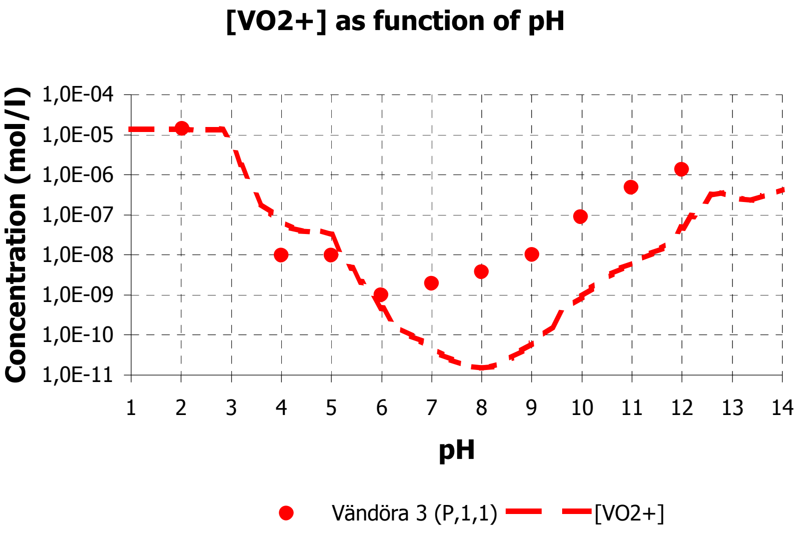

[Li+] as function of pH

[Na+] as function of pH

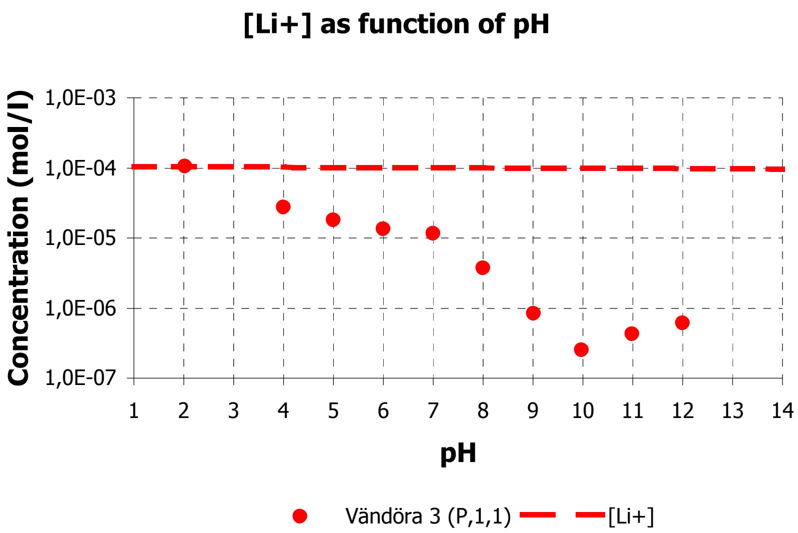

[Li+] as function of pH

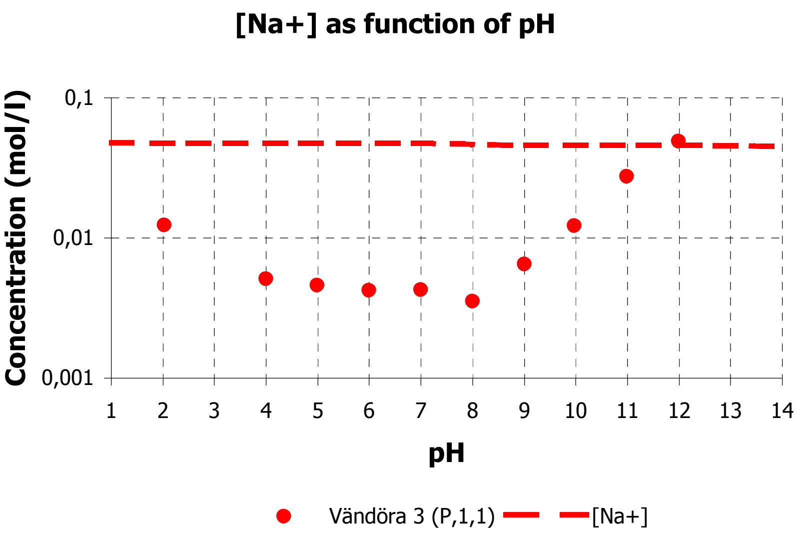

[Na+] as function of pH

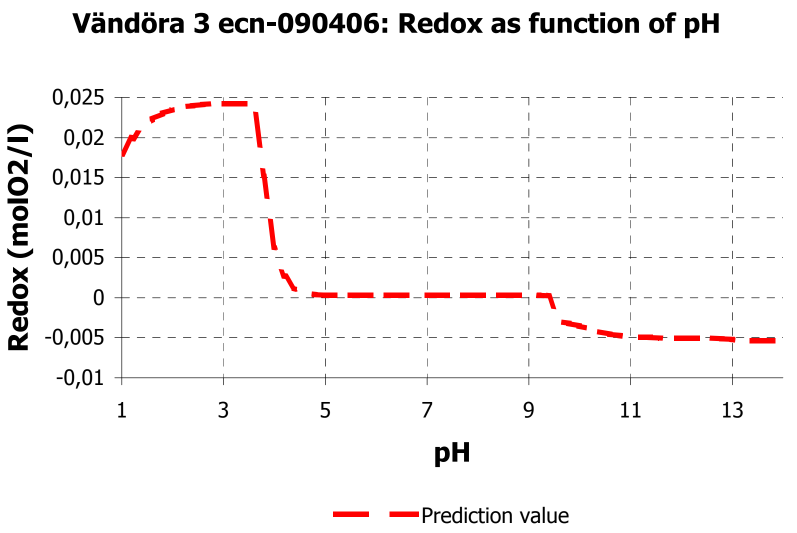

Vändöra 3 ecn-090406: Redox as function of pH

I Result geochemical modelling sample 4

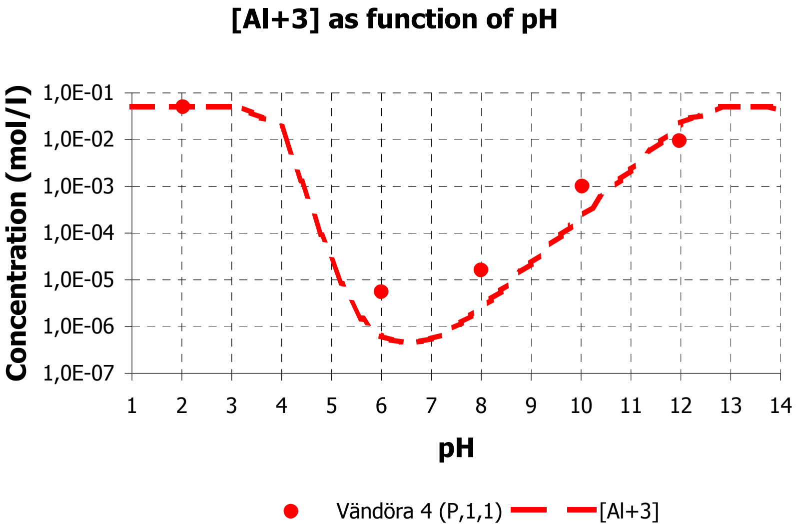
[Al+3] as function of pH
Concentration (mol/l)
1,0E-01
1,0E-02
1,0E-03
1,0E-04
1,0E-05
1,0E-06
1,0E-07
1 2 3 4 5 6 7 8 9 10 11 12 13 14
pH
Vändöra 4 (P,1,1)
[Al+3]

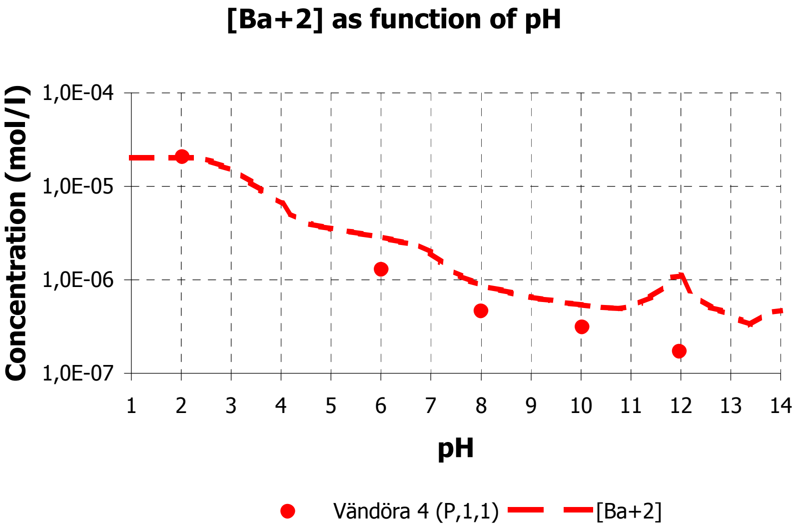
[Ba+2] as function of pH
Concentration (mol/l)
1,0E-04
1,0E-05
1,0E-06
1,0E-07
1 2 3 4 5 6 7 8 9 10 11 12 13 14
pH
Vändöra 4 (P,1,1)
[Ba+2]

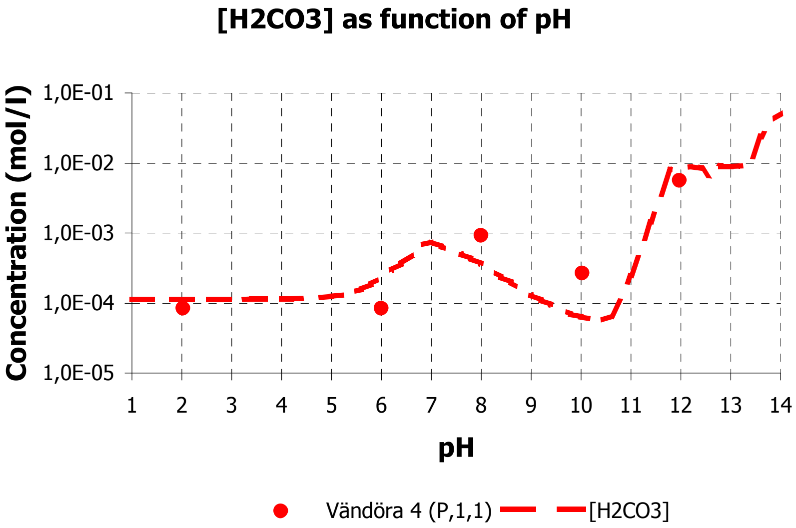
[H2CO3] as function of pH
Concentration (mol/l)
1,0E-01
1,0E-02
1,0E-03
1,0E-04
1,0E-05
1 2 3 4 5 6 7 8 9 10 11 12 13 14
pH
Vändöra 4 (P,1,1)
[H2CO3]

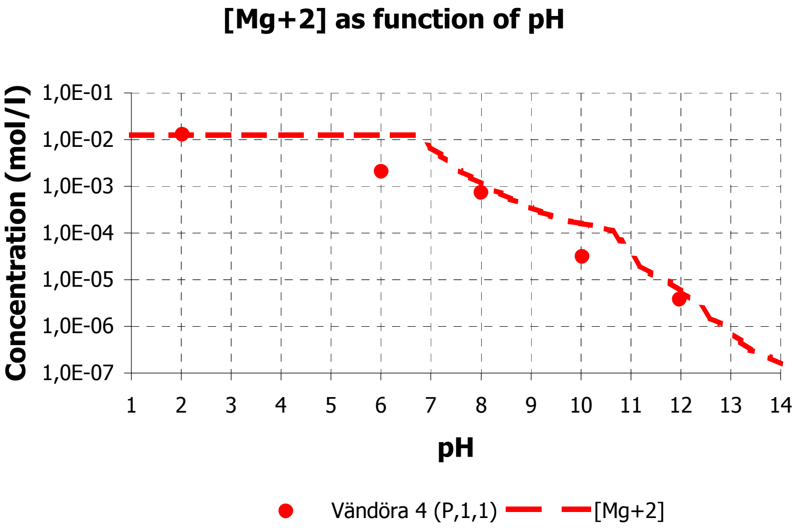
[Mg+2] as function of pH
Concentration (mol/l)
1,0E-01
1,0E-02
1,0E-03
1,0E-04
1,0E-05
1,0E-06
1,0E-07
1 2 3 4 5 6 7 8 9 10 11 12 13 14
pH
Vändöra 4 (P,1,1)
[Mg+2]

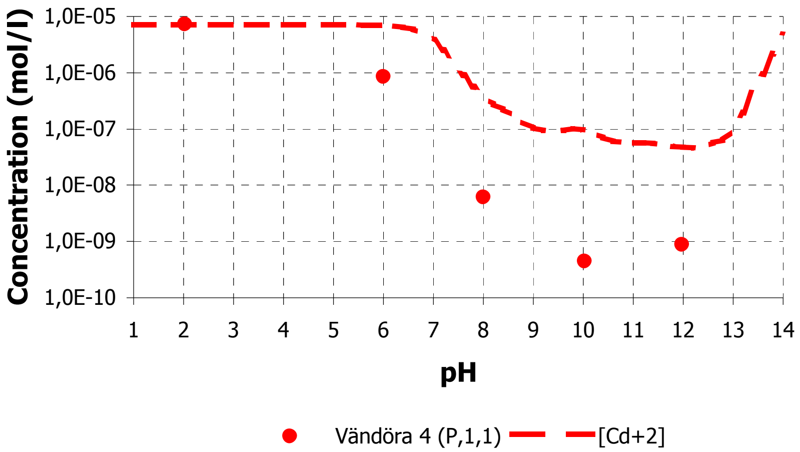
[Cd+2] as function of pH

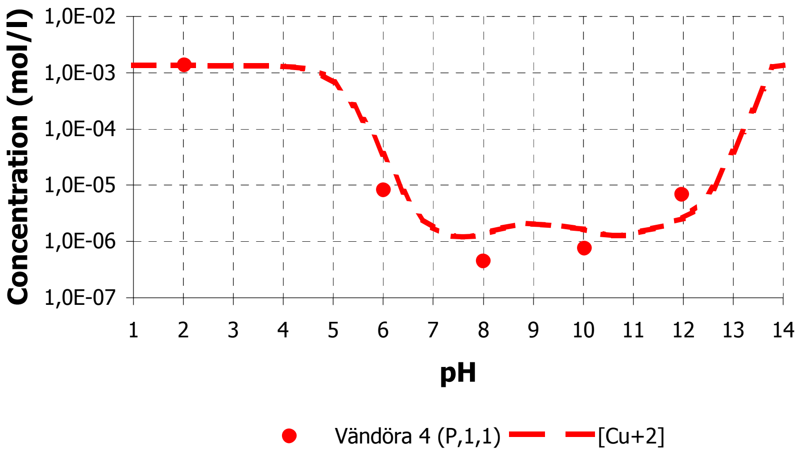
[Cu+2] as function of pH

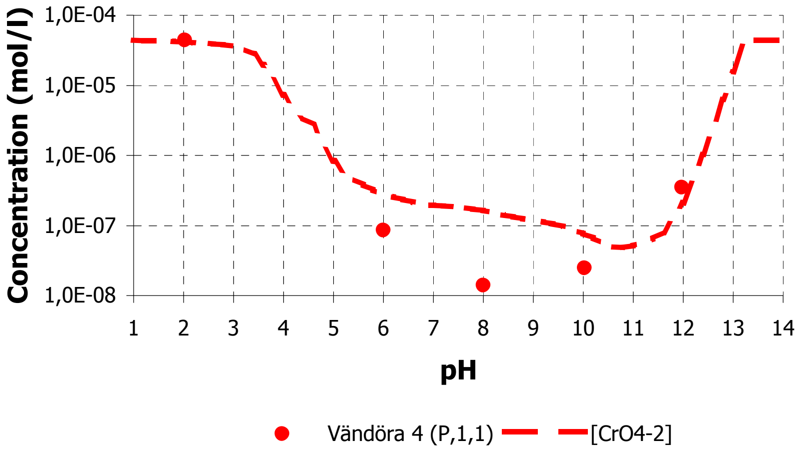
[CrO4-2] as function of pH

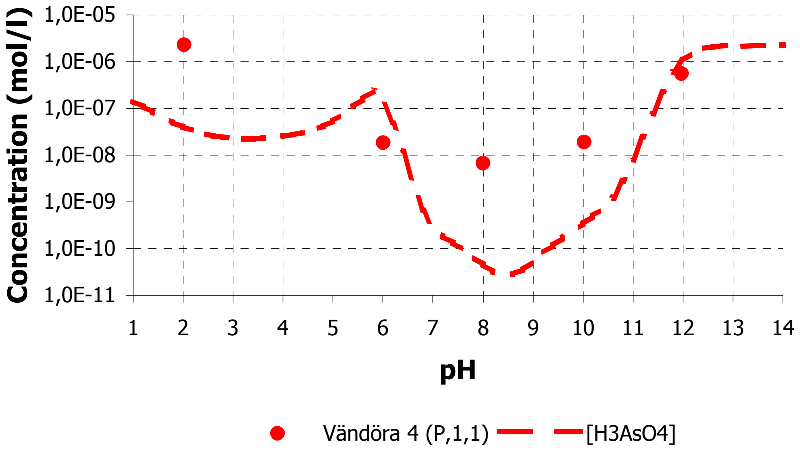
[H3AsO4] as function of pH

[Br-] as function of pH

[Cl-] as function of pH

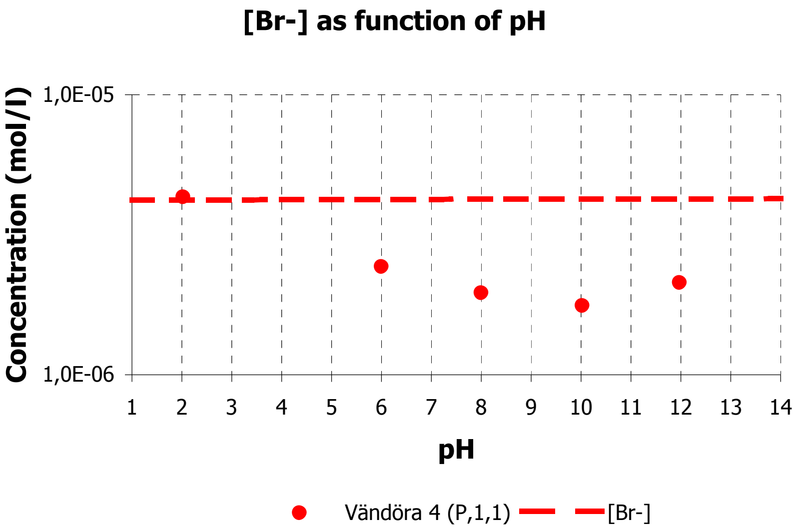
[Br-] as function of pH

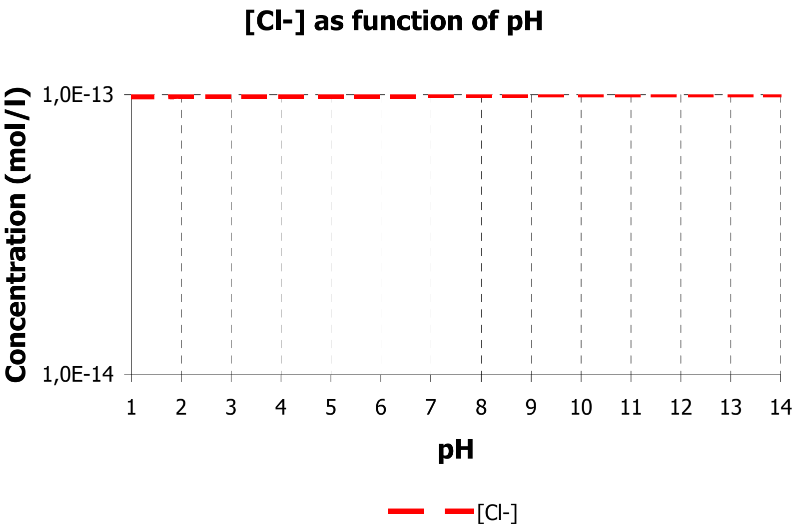
[Cl-] as function of pH

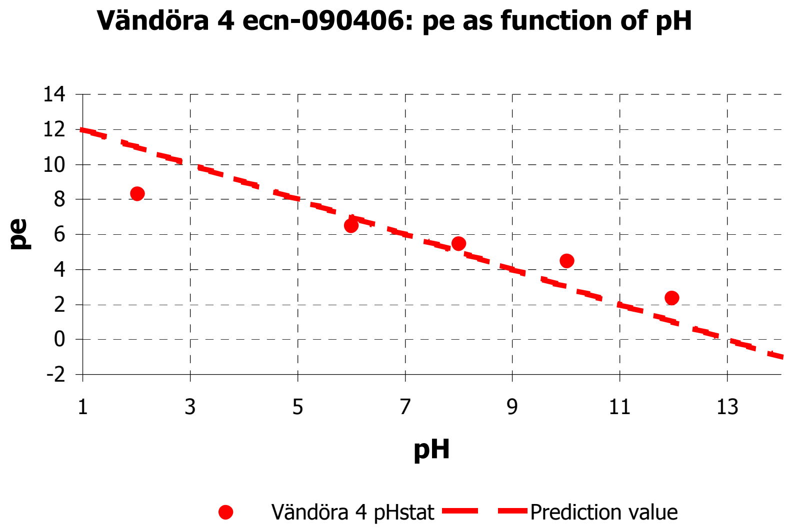
Vändöra 4 ecn-090406: pe as function of pH

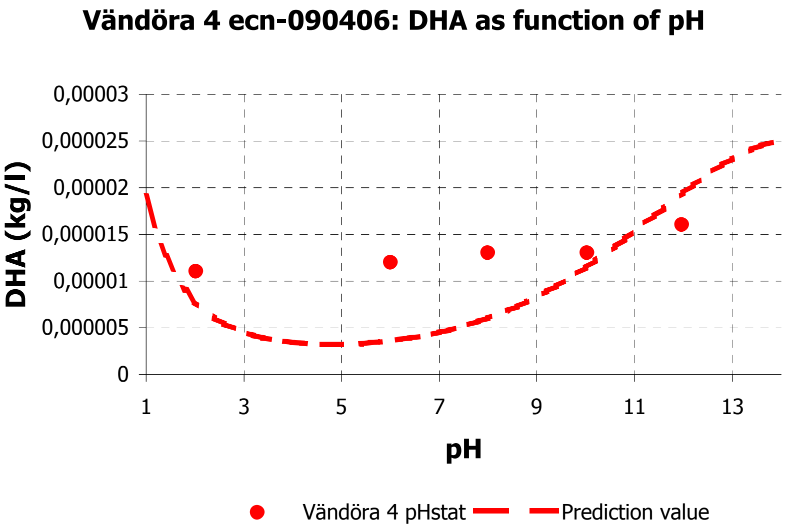
Vändöra 4 ecn-090406: DHA as function of pH

[Al+3] as function of pH

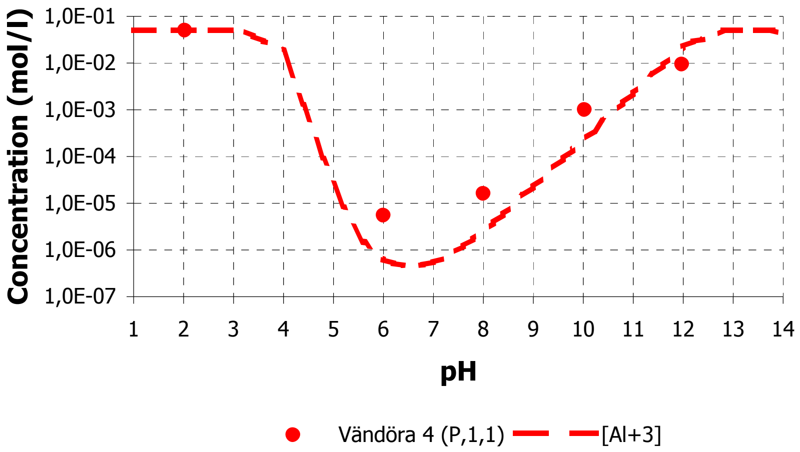

Partitioning liquid-solid, [Al+3]

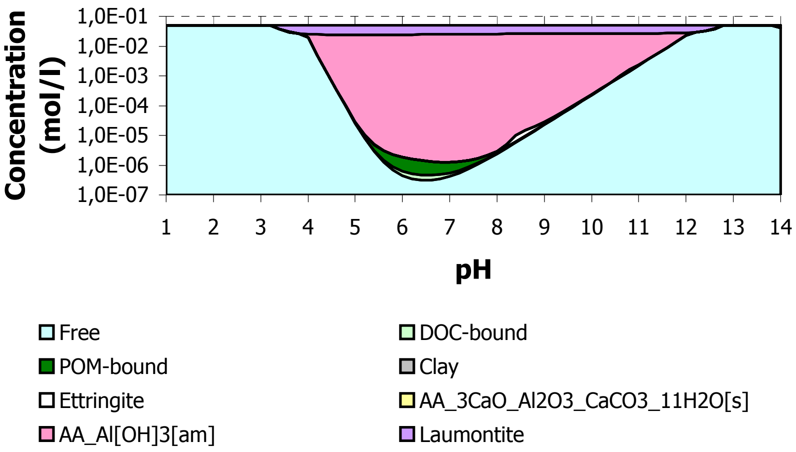

[Ba+2] as function of pH

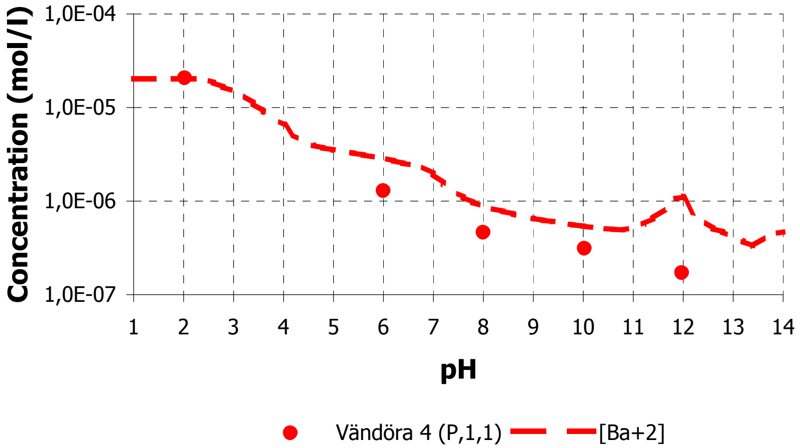

Partitioning liquid-solid, [Ba+2]

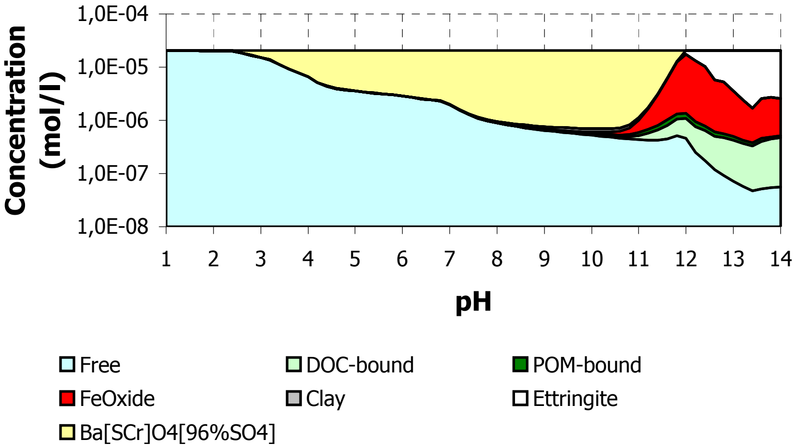

[Ca+2] as function of pH

Partitioning liquid-solid, [Ca+2]

[Ca+2] as function of pH

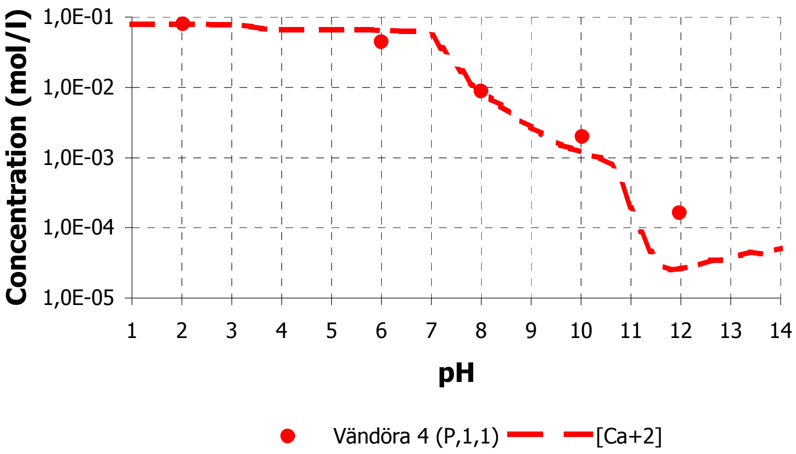

Partitioning liquid-solid, [Ca+2]

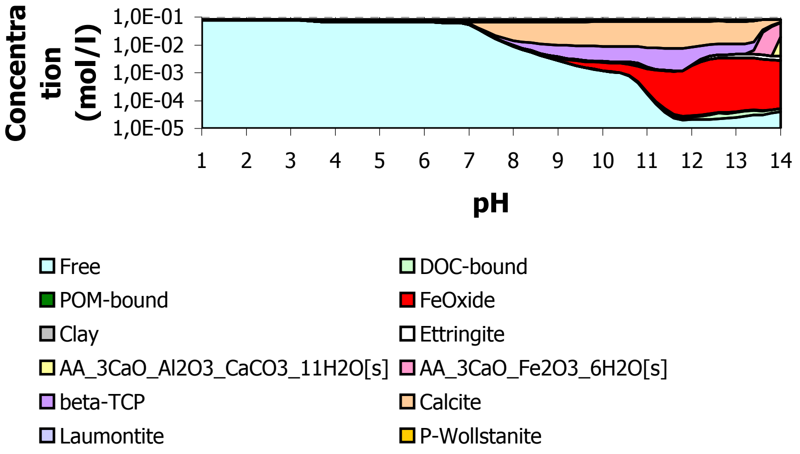

[Fe+3] as function of pH

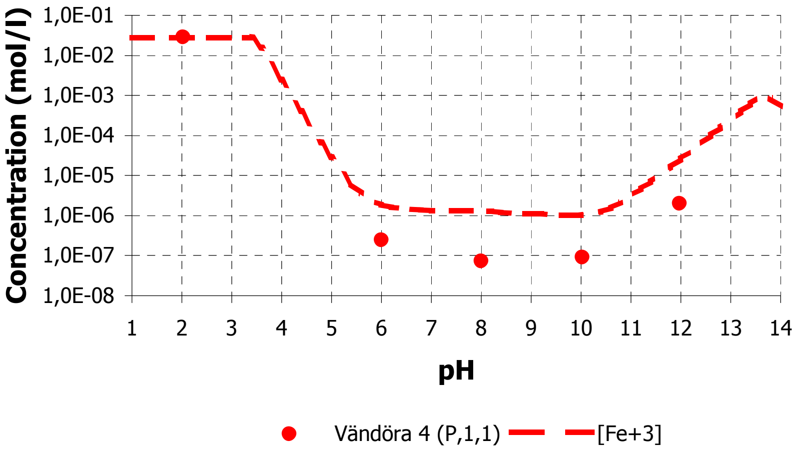

Partitioning liquid-solid, [Fe+3]

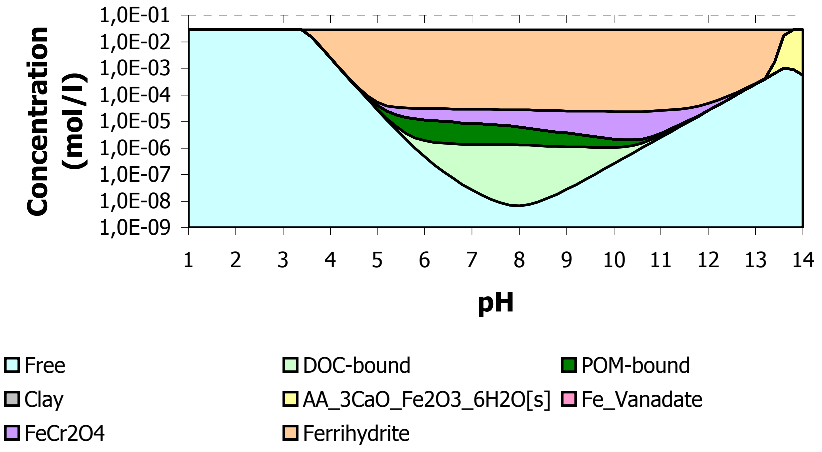

[H4SiO4] as function of pH

Partitioning liquid-solid, [H4SiO4]

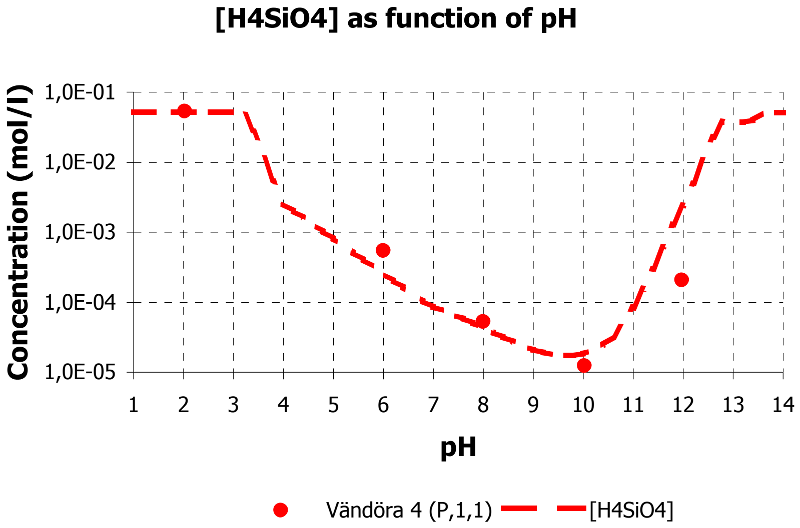
[H4SiO4] as function of pH

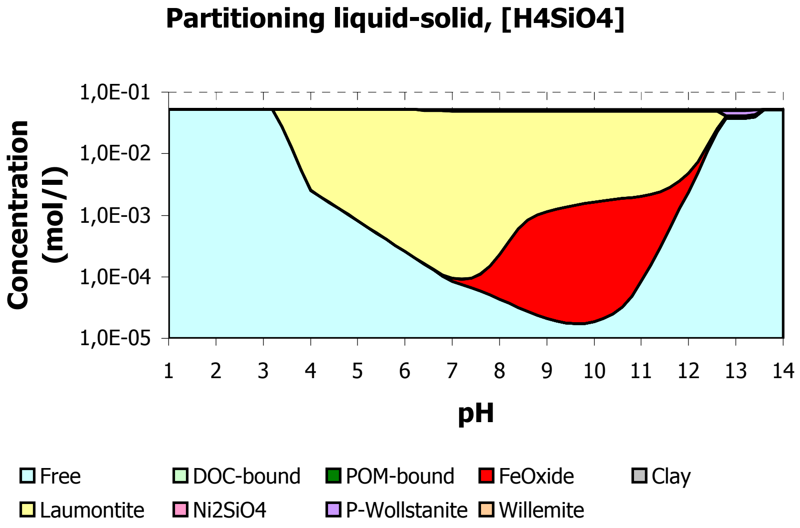
Partitioning liquid-solid, [H4SiO4]

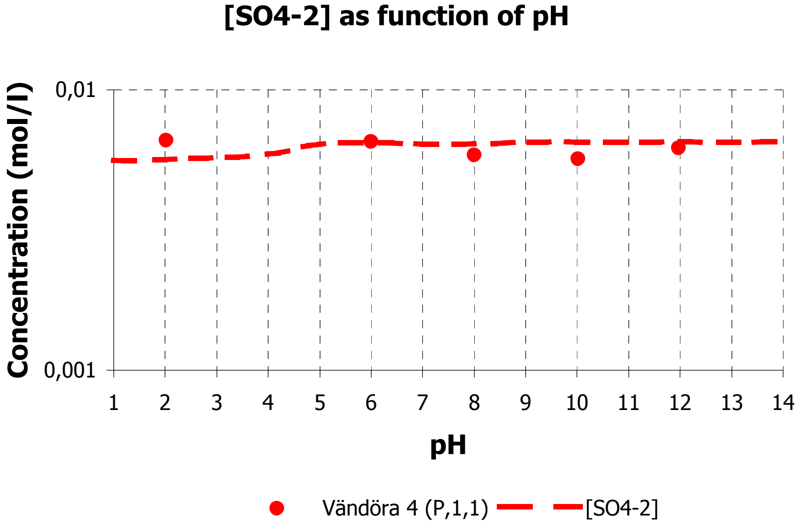
[SO4-2] as function of pH

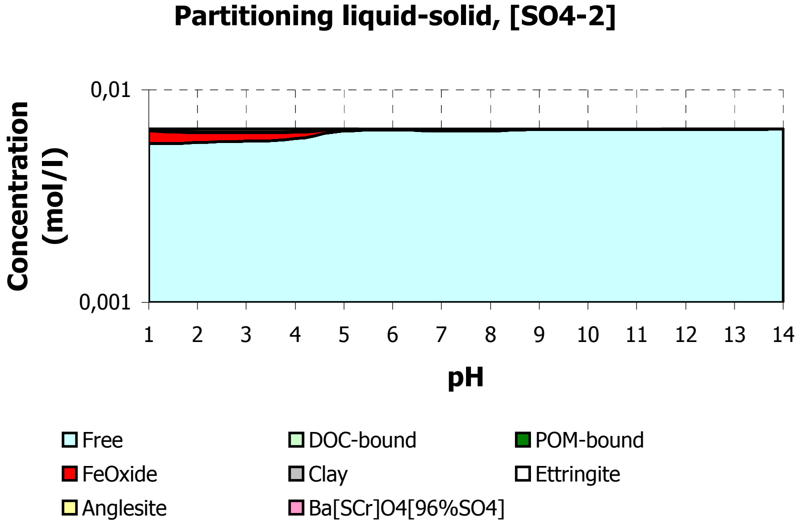
Partitioning liquid-solid, [SO4-2]

[H2CO3] as function of pH

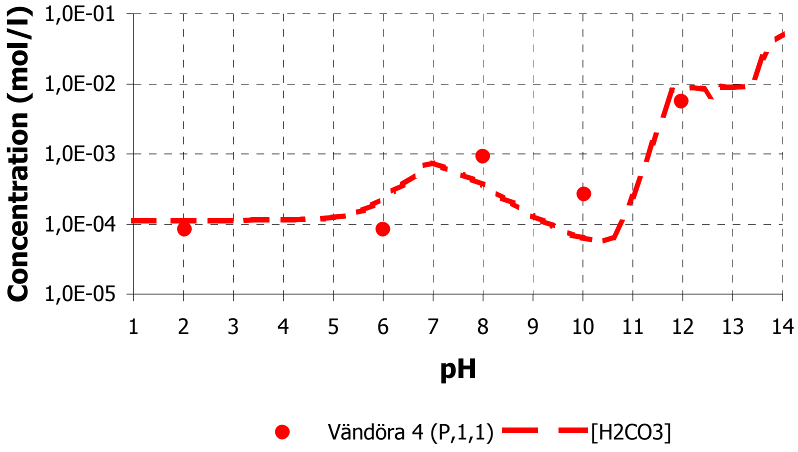

Partitioning liquid-solid, [H2CO3]

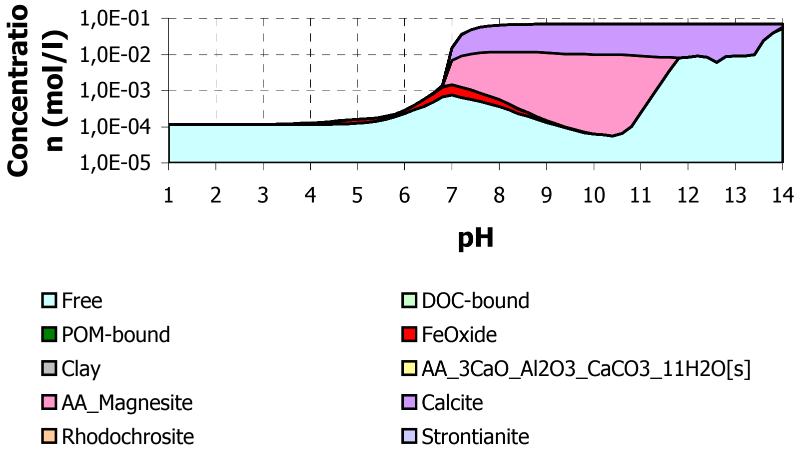

[Mg+2] as function of pH

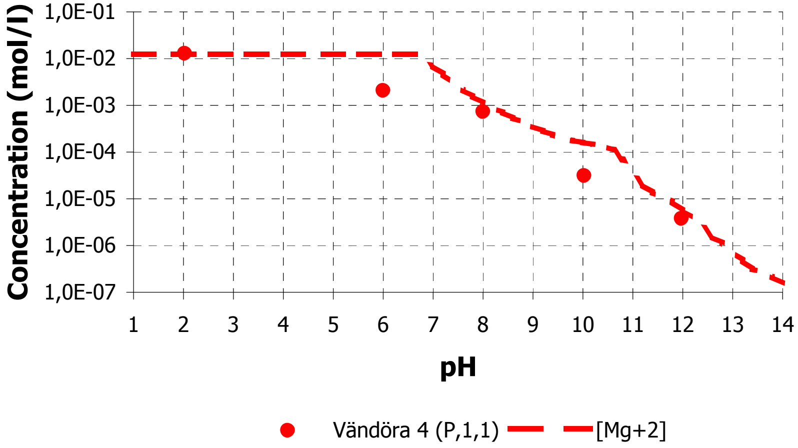

Partitioning liquid-solid, [Mg+2]

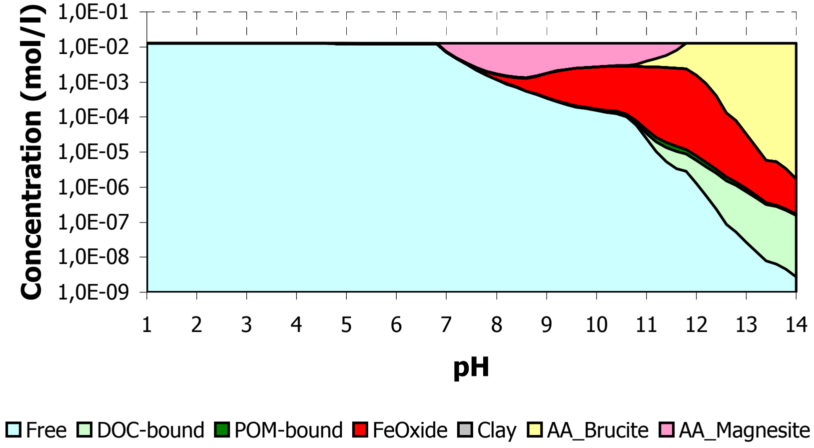

[PO4-3] as function of pH

Partitioning liquid-solid, [PO4-3]

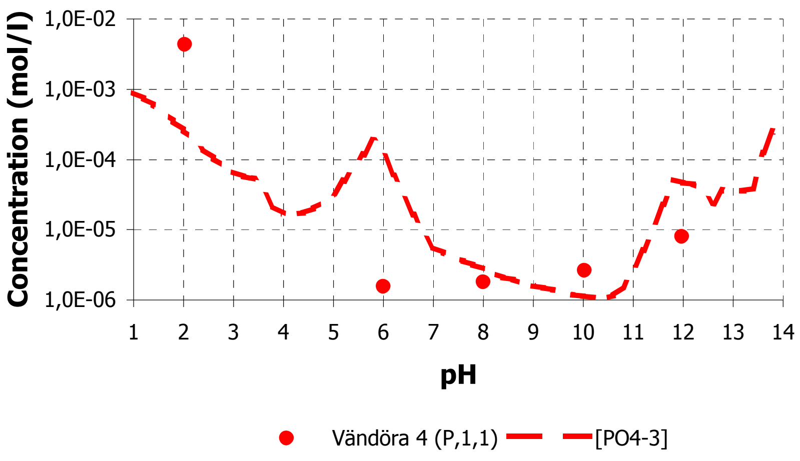

[PO4-3] as function of pH

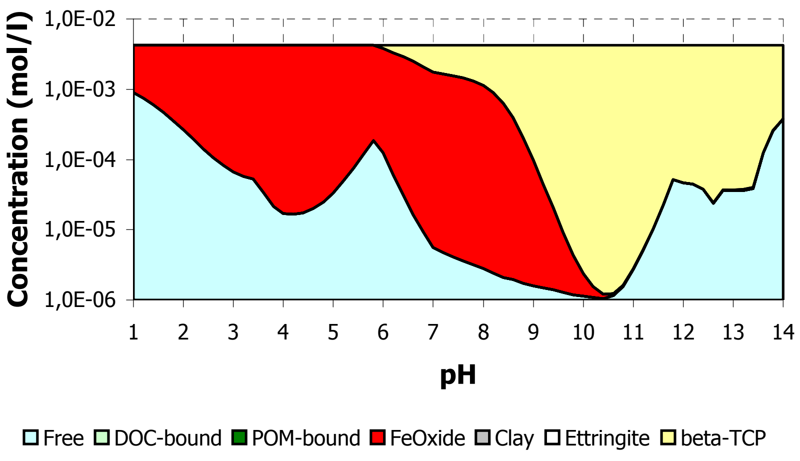

Partitioning liquid-solid, [PO4-3]

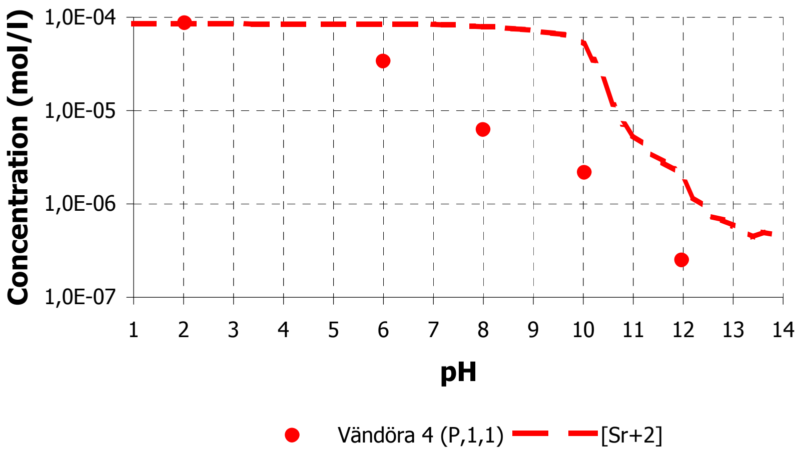

[Sr+2] as function of pH

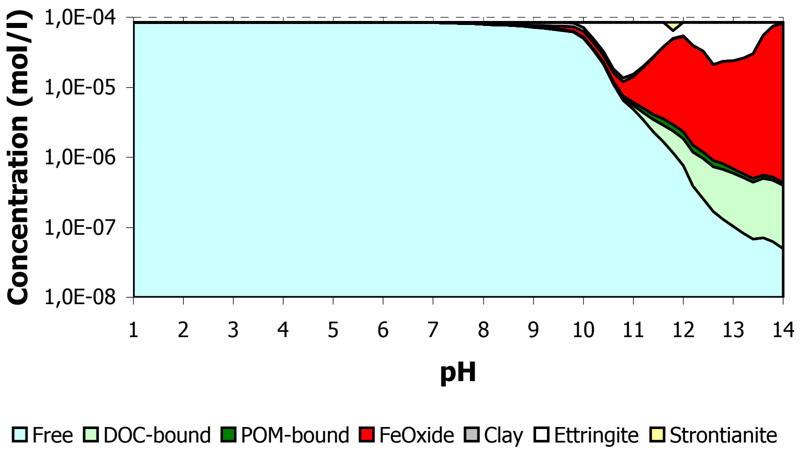

Partitioning liquid-solid, [Sr+2]

[Cd+2] as function of pH

Partitioning liquid-solid, [Cd+2]

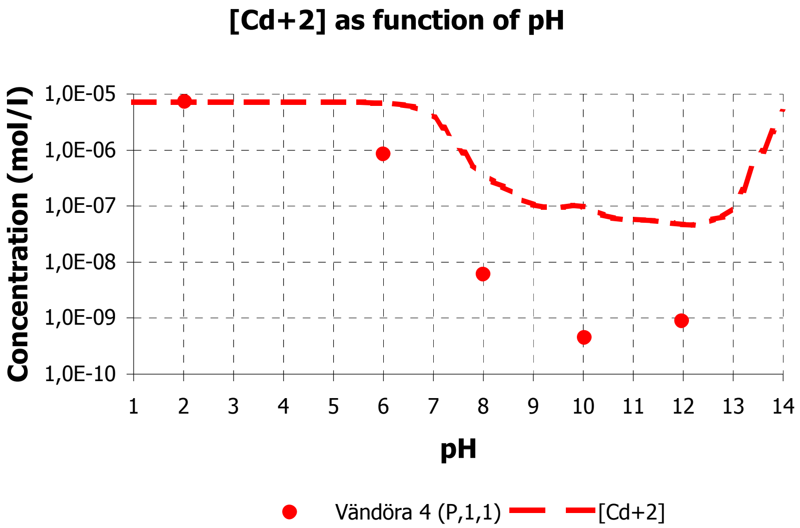
[Cd+2] as function of pH

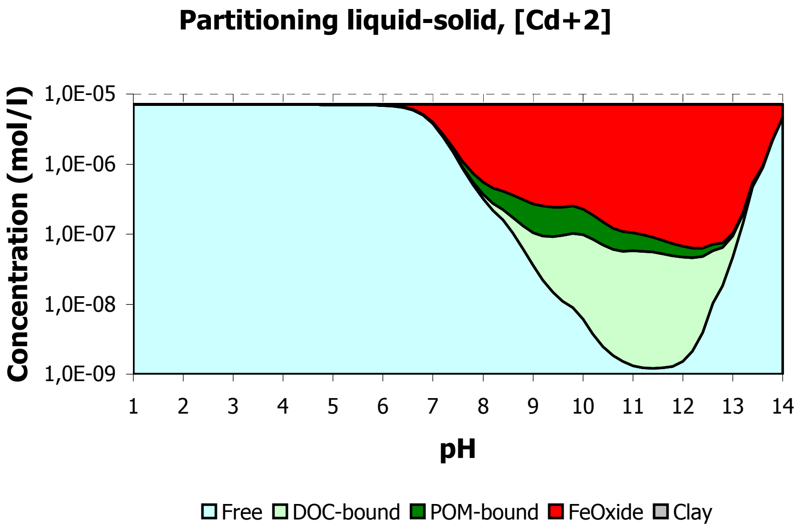
Partitioning liquid-solid, [Cd+2]

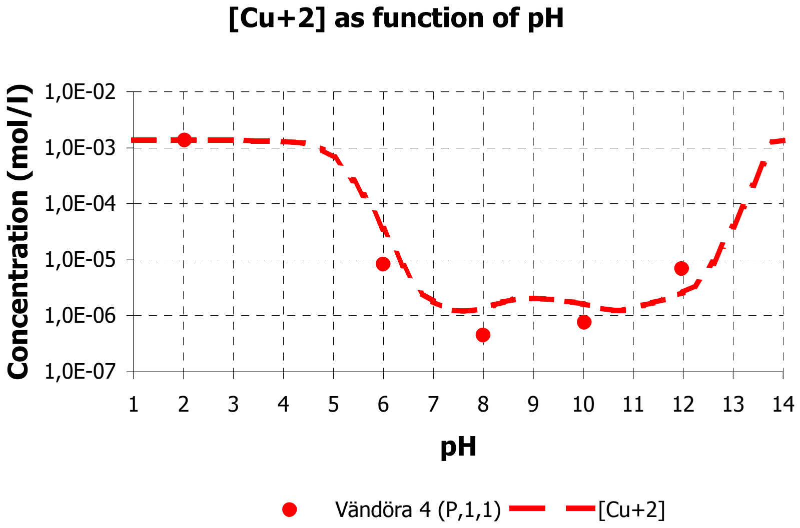
[Cu+2] as function of pH

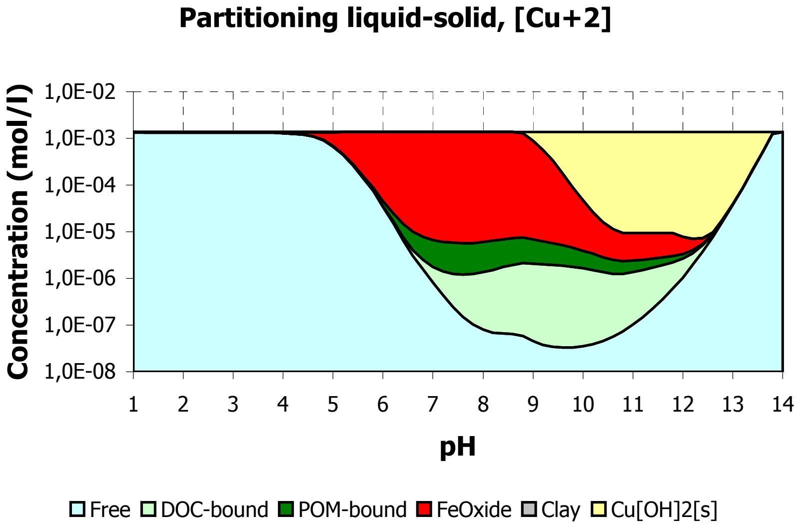
Partitioning liquid-solid, [Cu+2]

[Mn+2] as function of pH

Partitioning liquid-solid, [Mn+2]

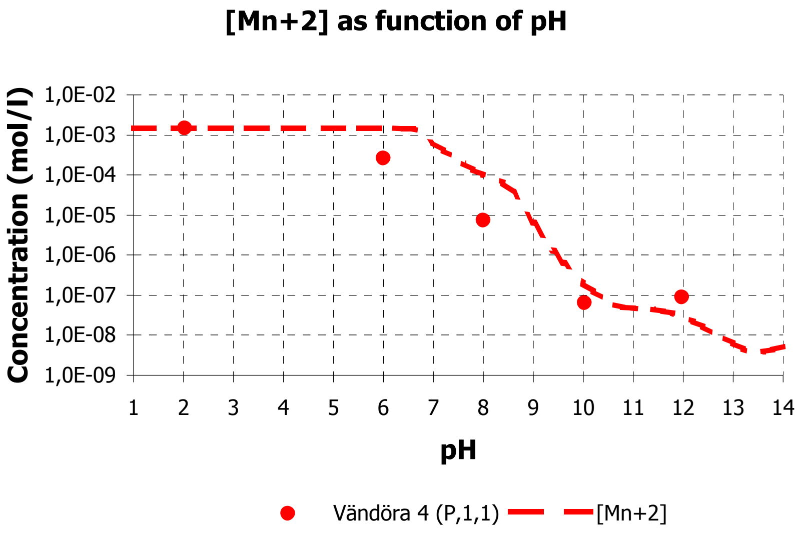
[Mn+2] as function of pH

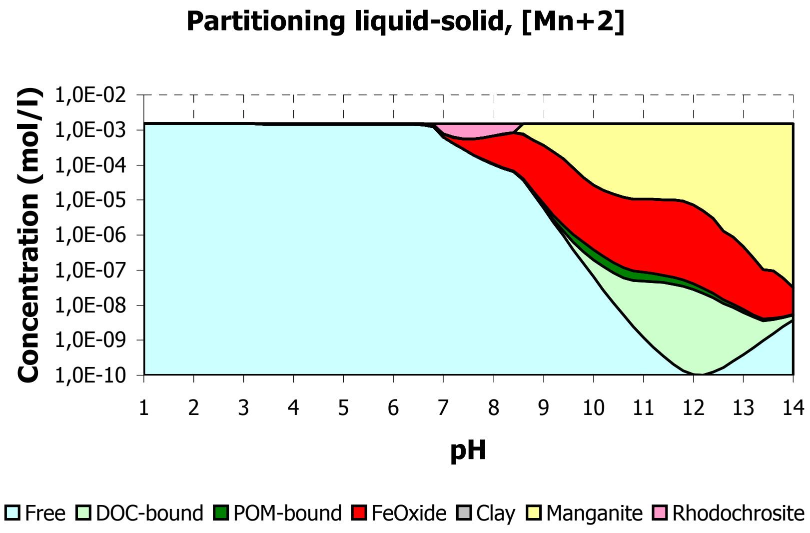
Partitioning liquid-solid, [Mn+2]

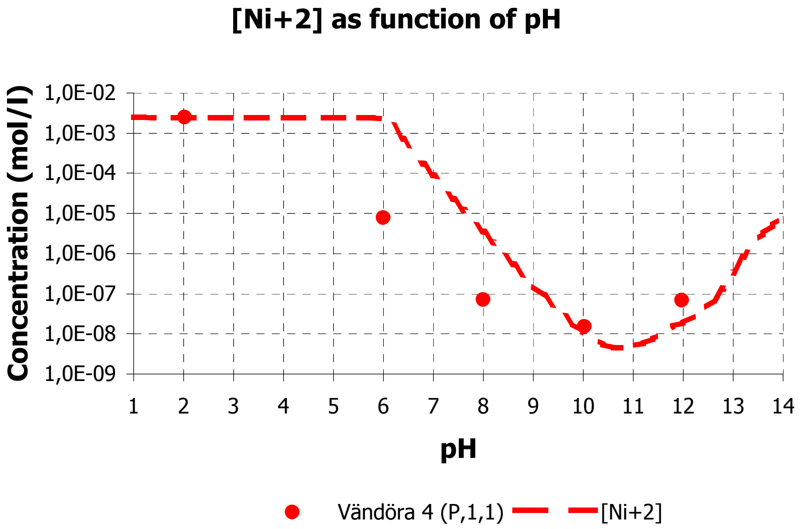
[Ni+2] as function of pH

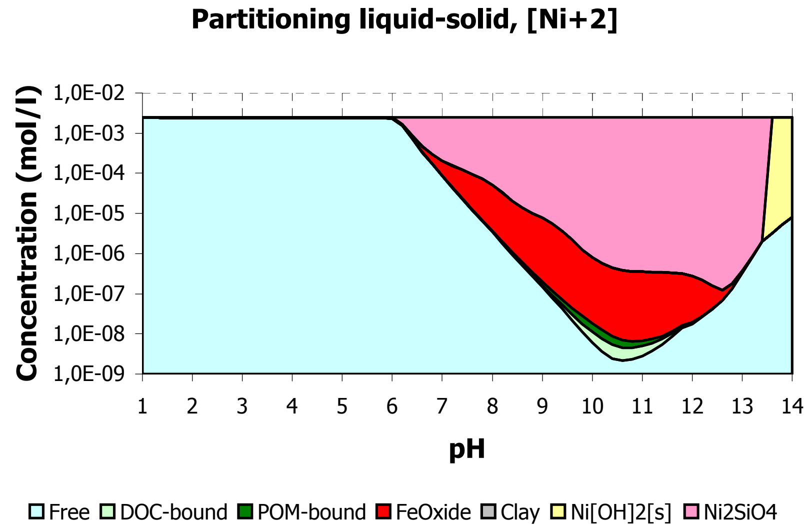
Partitioning liquid-solid, [Ni+2]

[Pb+2] as function of pH

Partitioning liquid-solid, [Pb+2]

[Pb+2] as function of pH

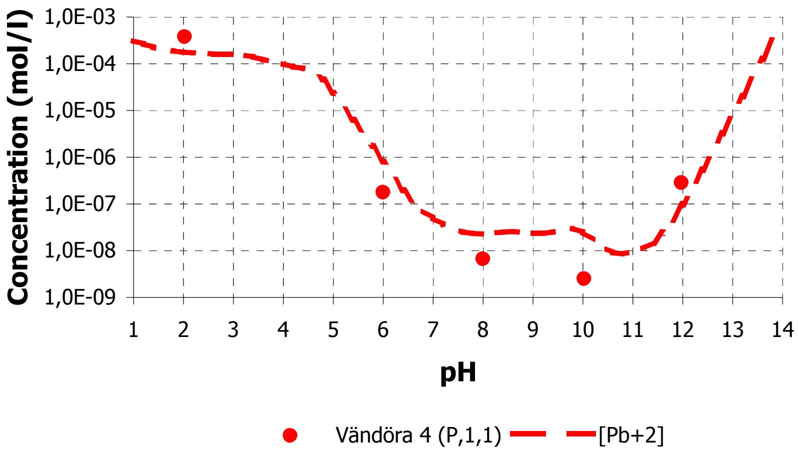

Partitioning liquid-solid, [Pb+2]

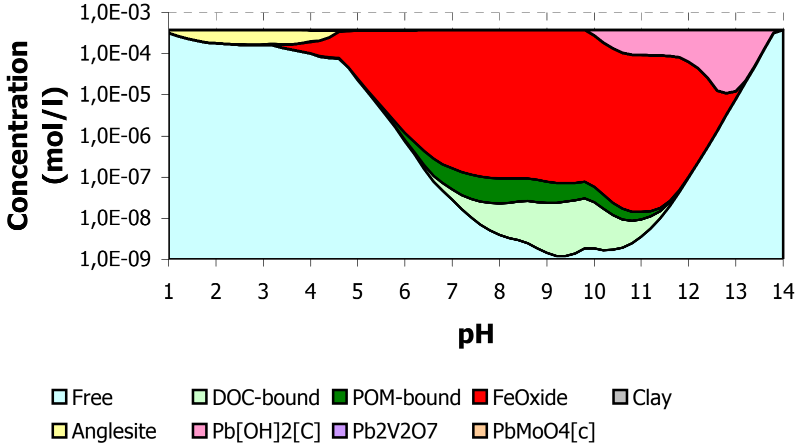

[Zn+2] as function of pH

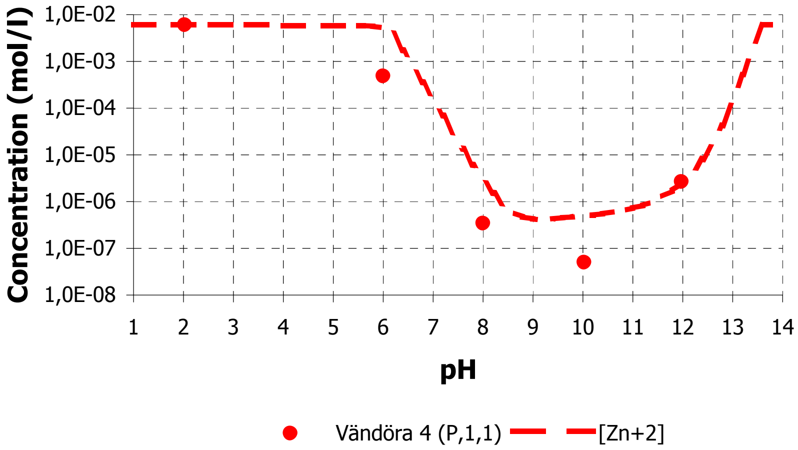

Partitioning liquid-solid, [Zn+2]

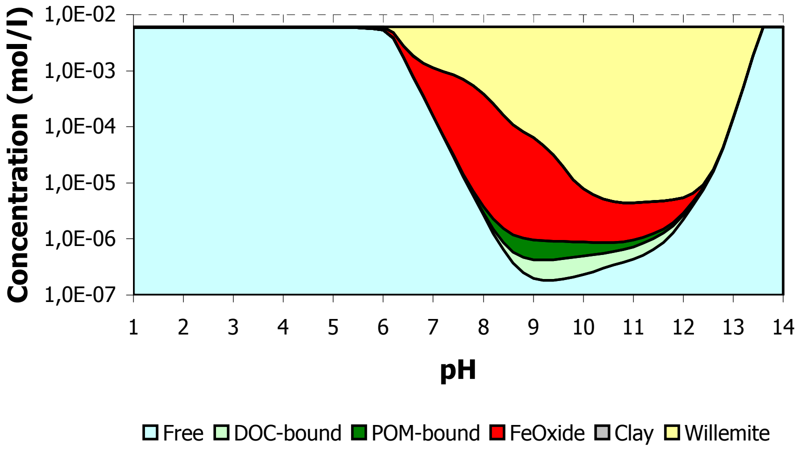

[CrO4-2] as function of pH

Partitioning liquid-solid, [CrO4-2]

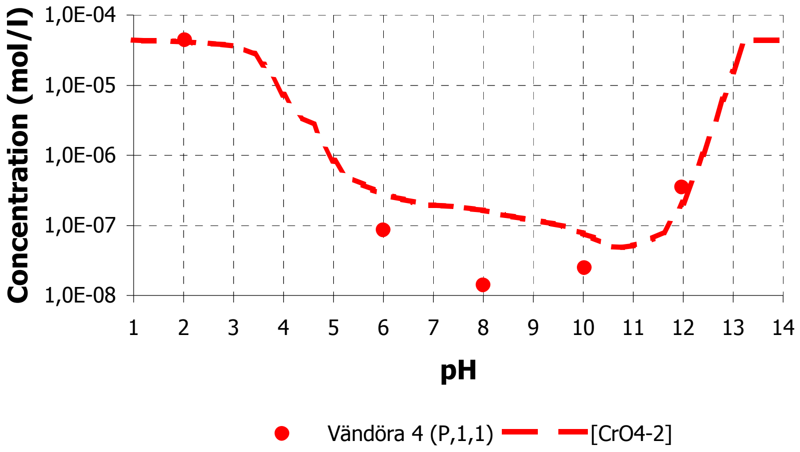
[CrO4-2] as function of pH

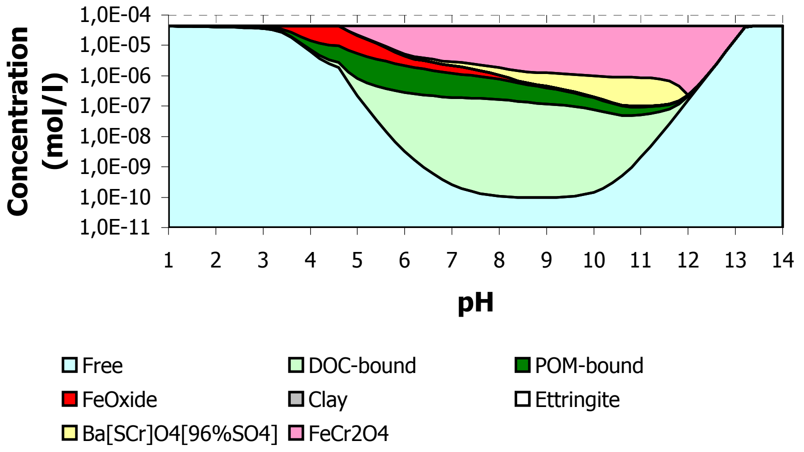
Partitioning liquid-solid, [CrO4-2]

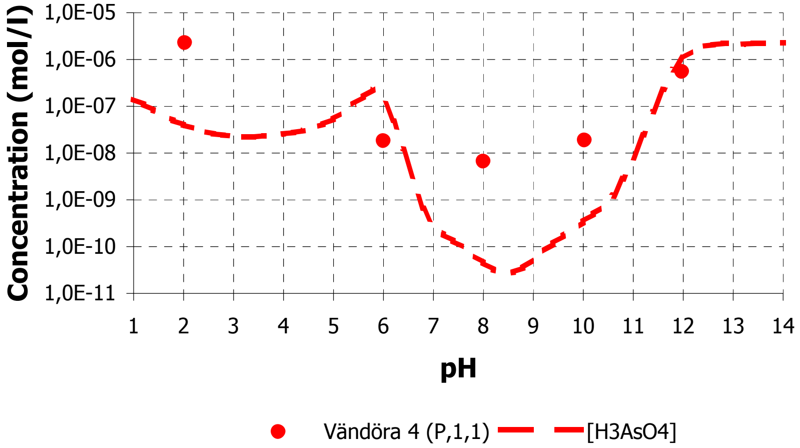
[H3AsO4] as function of pH

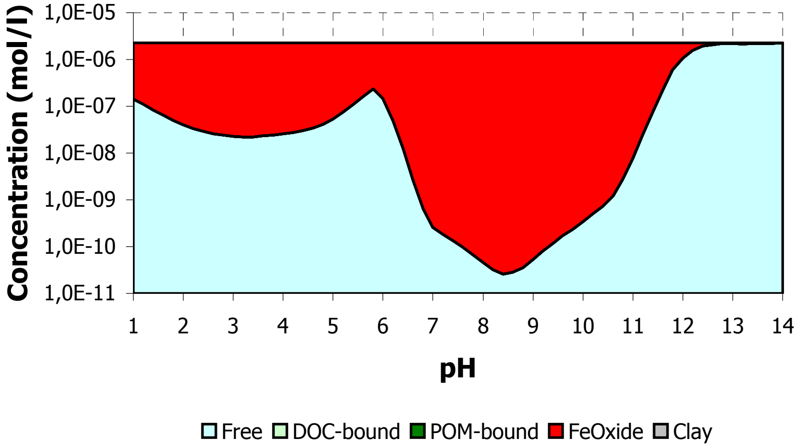
Partitioning liquid-solid, [H3AsO4]

[H3BO3] as function of pH

Partitioning liquid-solid, [H3BO3]

[H3BO3] as function of pH

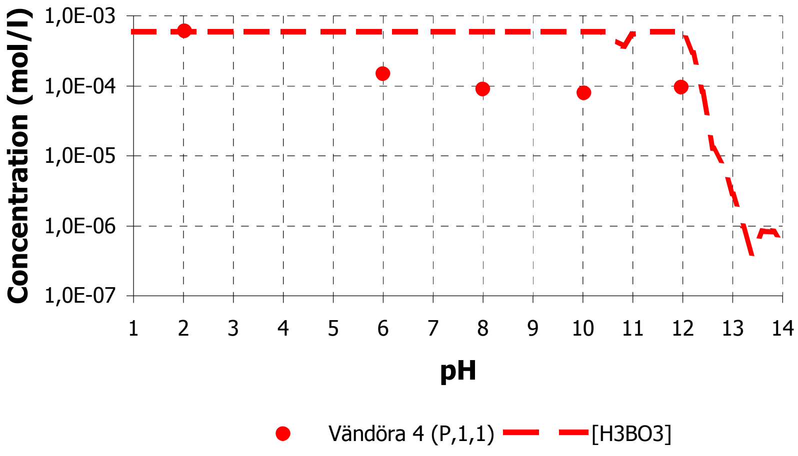

Partitioning liquid-solid, [H3BO3]

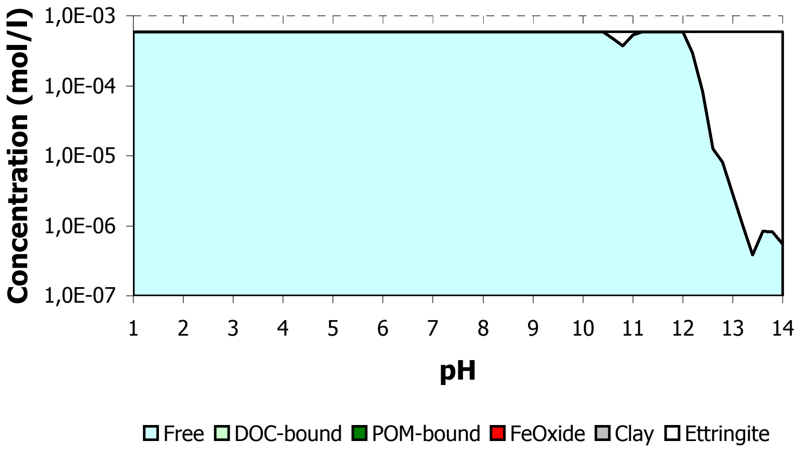

[MoO4-2] as function of pH

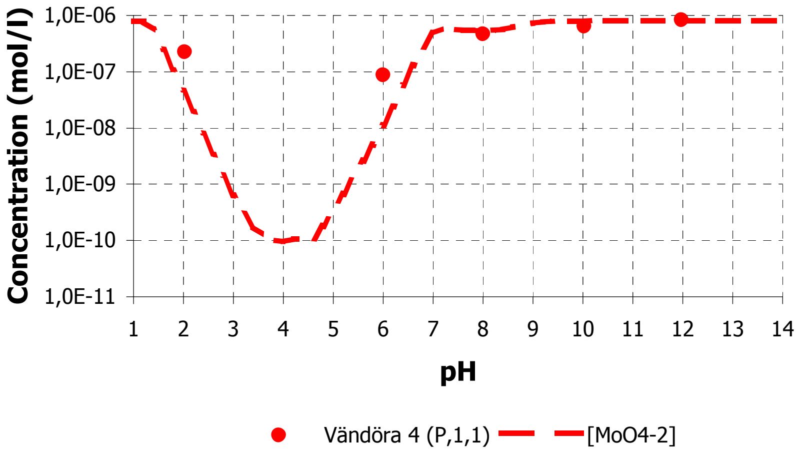

Partitioning liquid-solid, [MoO4-2]

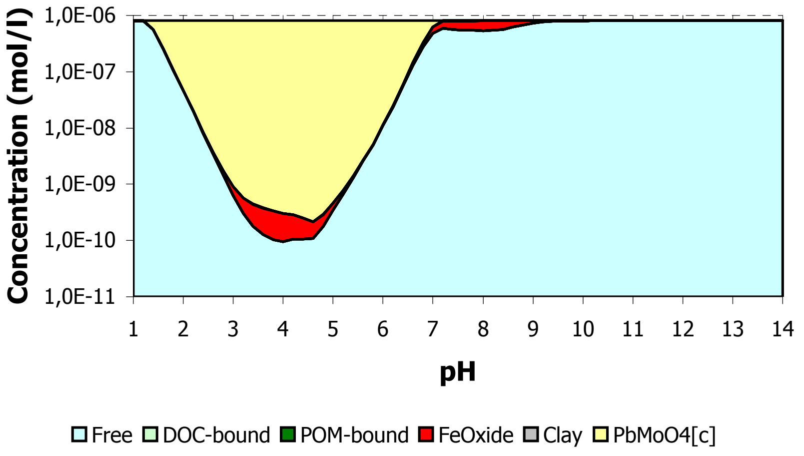

[Sb[OH]6-] as function of pH

Partitioning liquid-solid, [Sb[OH]6-]

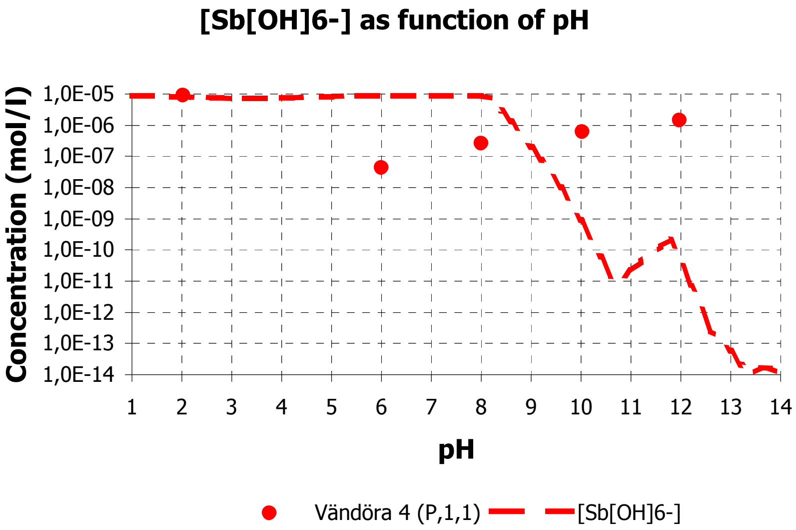
[Sb[OH]6-] as function of pH

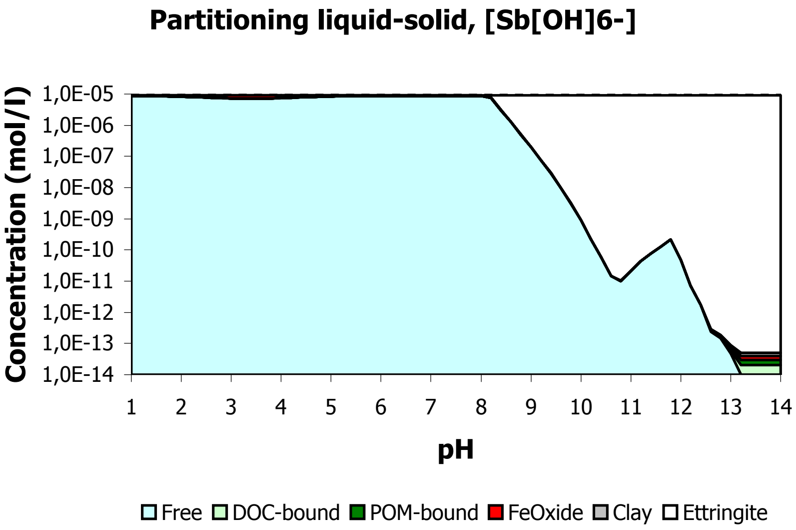
Partitioning liquid-solid, [Sb[OH]6-]

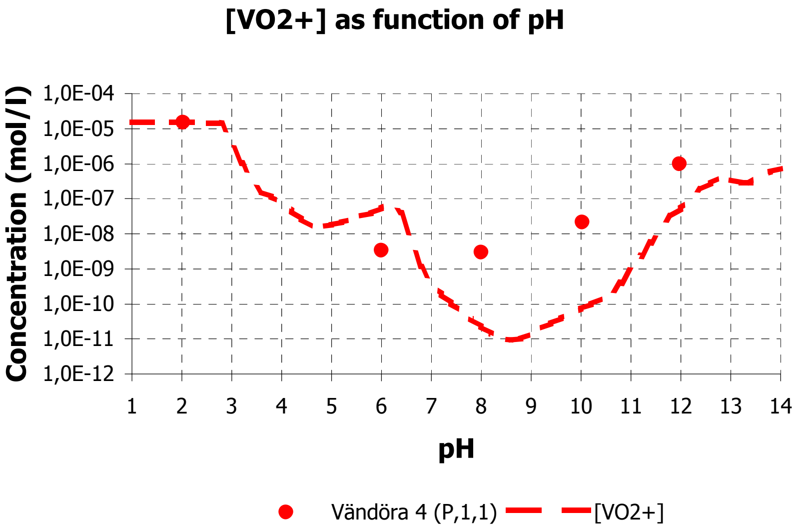
[VO2+] as function of pH

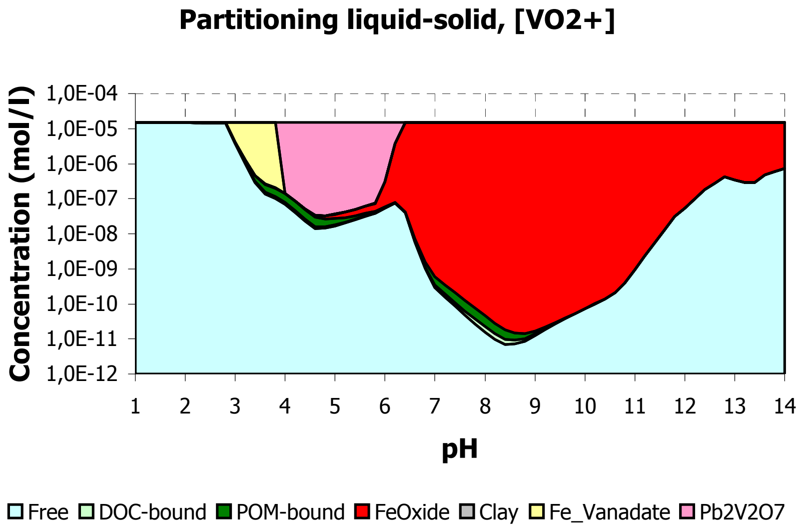
Partitioning liquid-solid, [VO2+]

[Br-] as function of pH

Partitioning liquid-solid, [Br-]

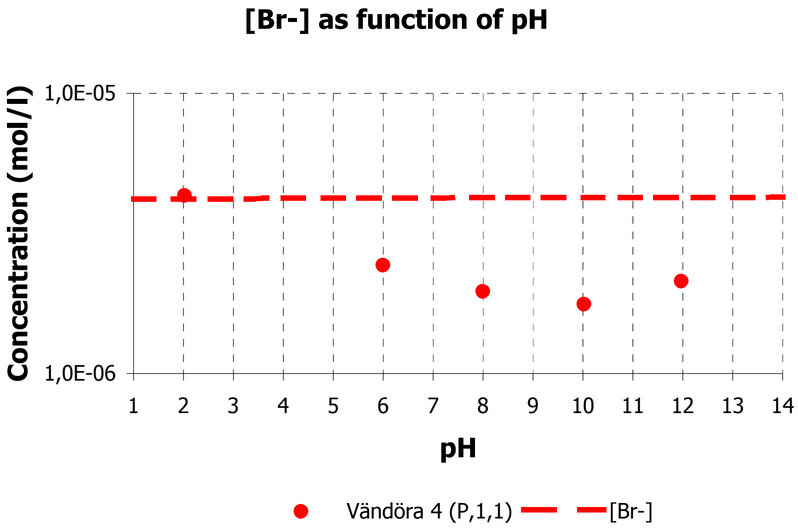
[Br-] as function of pH
Concentration (mol/l)
1,0E-05
1,0E-06
1 2 3 4 5 6 7 8 9 10 11 12 13 14
pH
● Vändöra 4 (P,1,1)
[Br-]

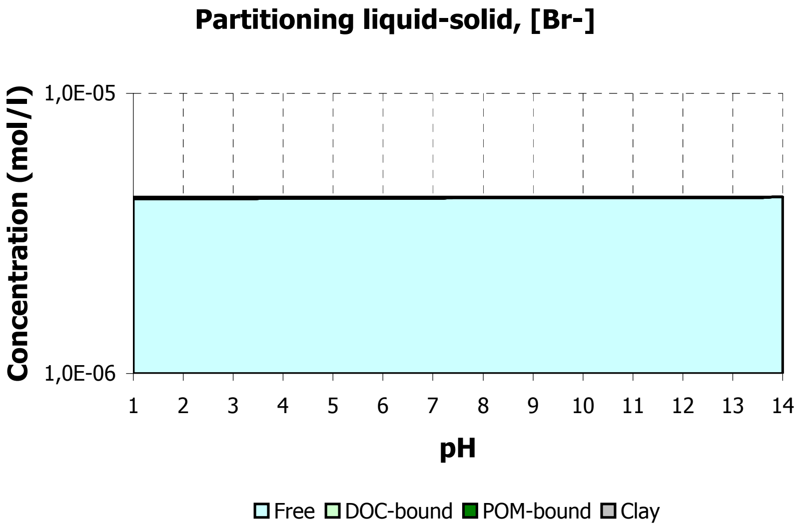
Partitioning liquid-solid, [Br-]
Concentration (mol/l)
1,0E-05
1,0E-06
1 2 3 4 5 6 7 8 9 10 11 12 13 14
pH
Free
DOC-bound
POM-bound
Clay

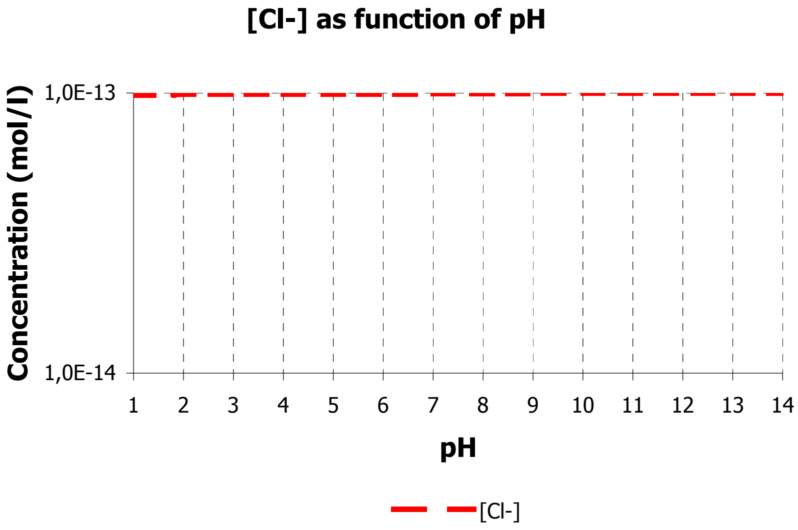
[Cl-] as function of pH
Concentration (mol/l)
1,0E-13
1,0E-14
1 2 3 4 5 6 7 8 9 10 11 12 13 14
pH
[Cl-]

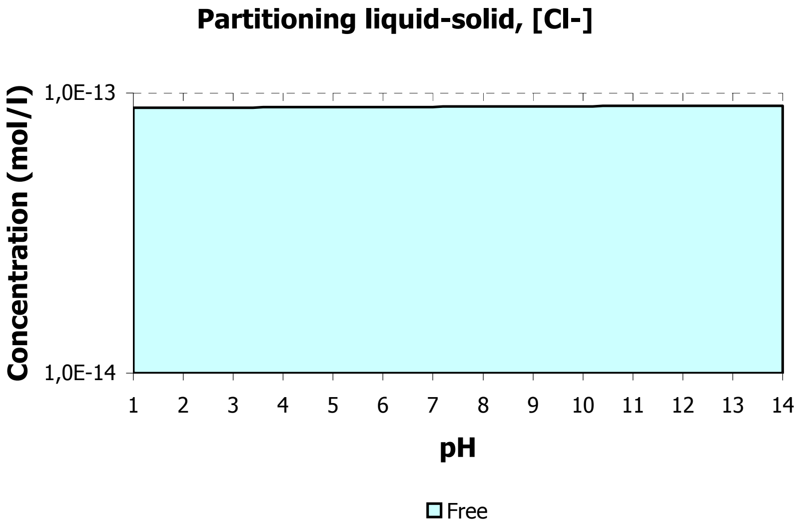
Partitioning liquid-solid, [Cl-]
Concentration (mol/l)
1,0E-13
1,0E-14
1 2 3 4 5 6 7 8 9 10 11 12 13 14
pH
Free

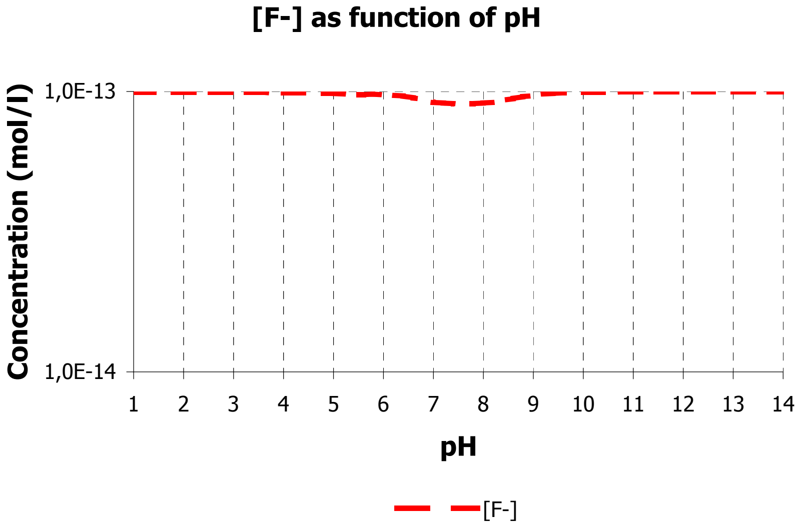

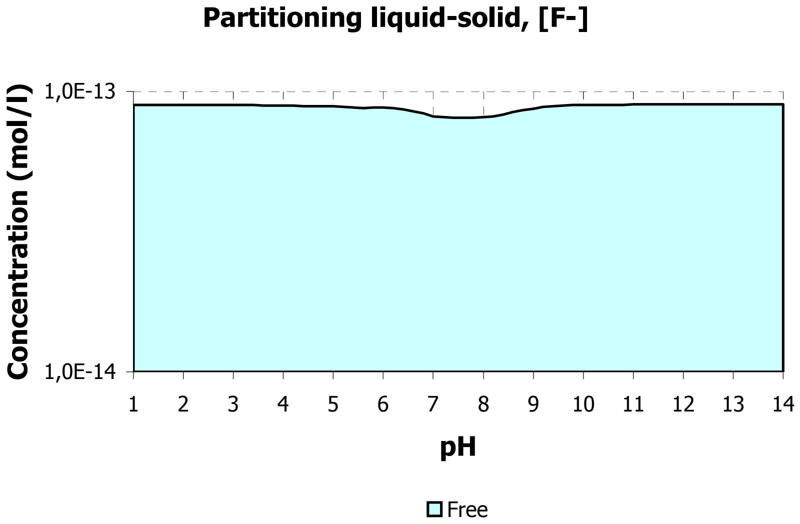

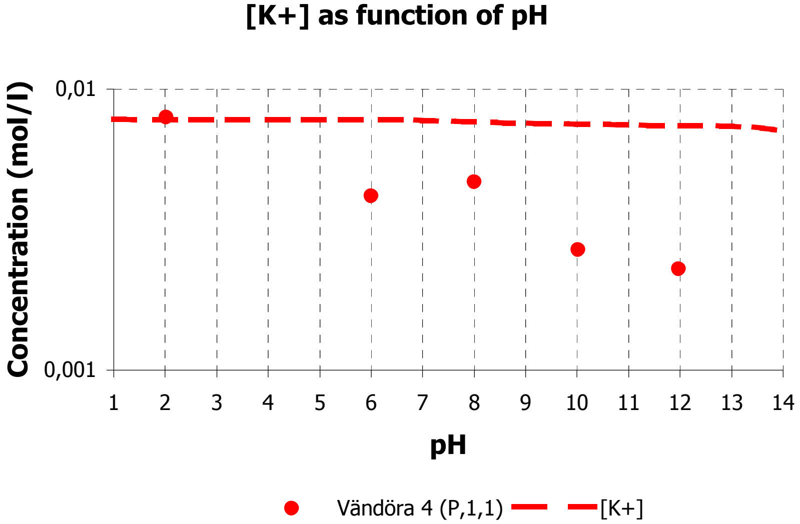

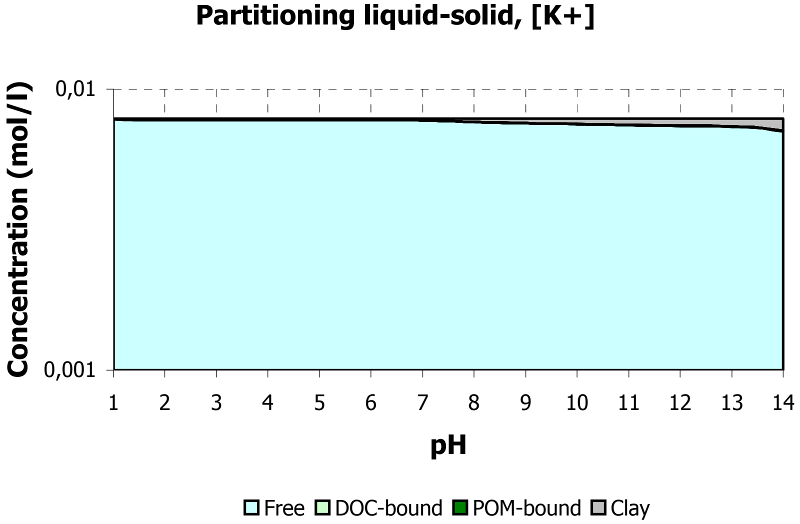

[Li+] as function of pH

Partitioning liquid-solid, [Li+]

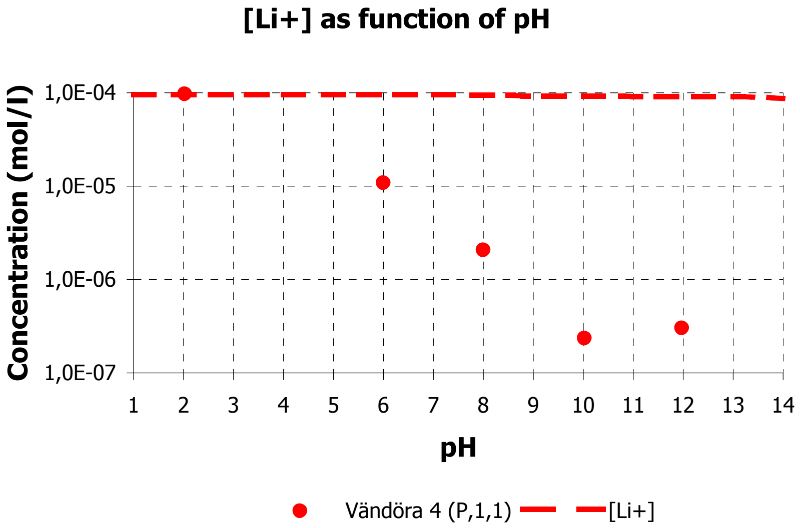
[Li+] as function of pH
Concentration (mol/l)
1,0E-04
1,0E-05
1,0E-06
1,0E-07
1
2
3
4
5
6
7
8
9
10
11
12
13
14
pH
● Vändöra 4 (P,1,1)
[Li+]

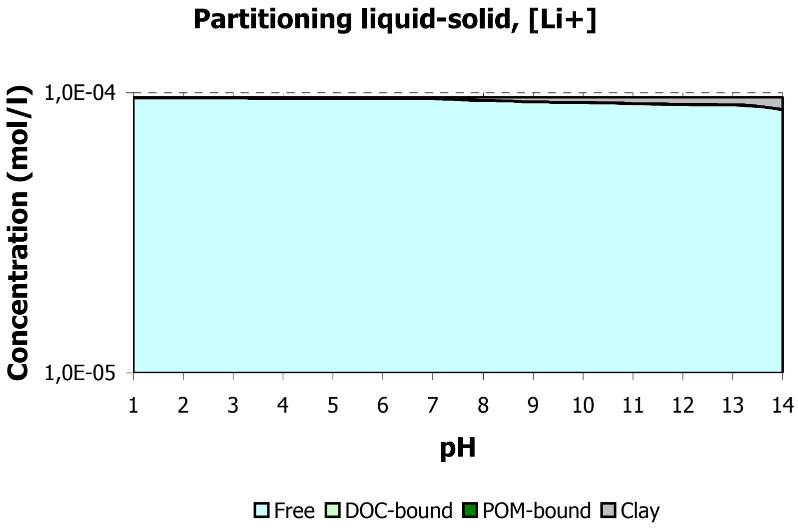
Partitioning liquid-solid, [Li+]
Concentration (mol/l)
1,0E-04
1,0E-05
1
2
3
4
5
6
7
8
9
10
11
12
13
14
pH
Free
DOC-bound
POM-bound
Clay

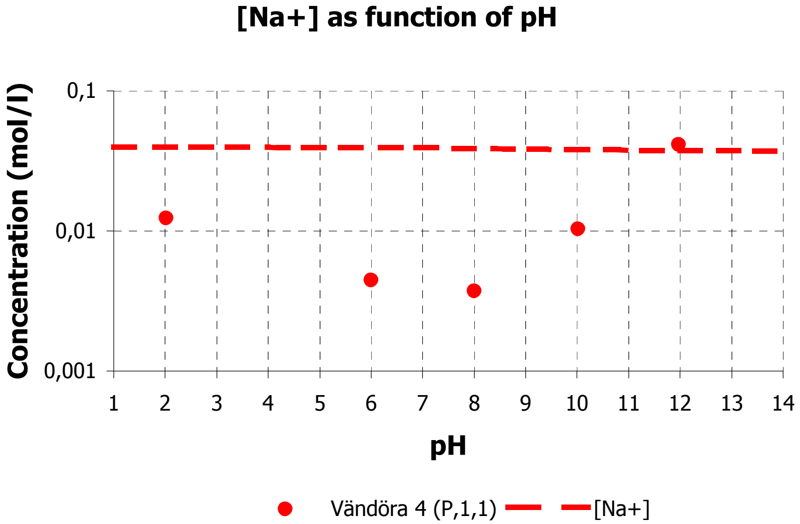
[Na+] as function of pH
Concentration (mol/l)
0,1
0,01
0,001
1
2
3
4
5
6
7
8
9
10
11
12
13
14
pH
● Vändöra 4 (P,1,1)
[Na+]

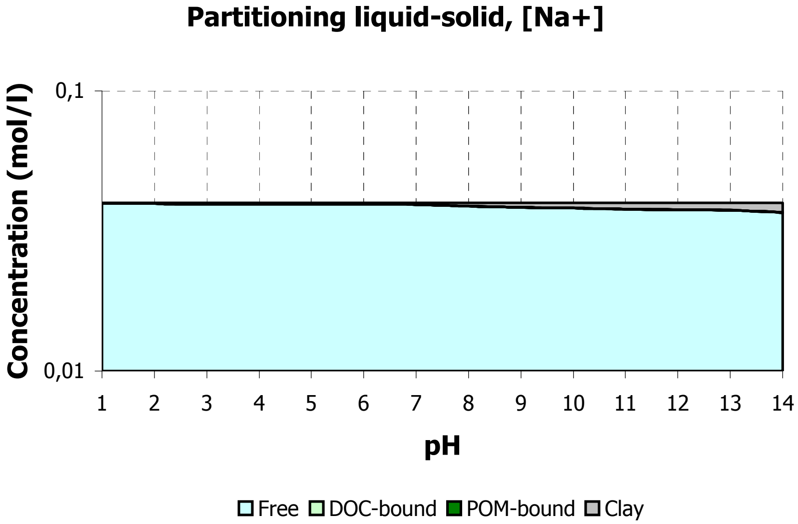
Partitioning liquid-solid, [Na+]
Concentration (mol/l)
0,1
0,01
1
2
3
4
5
6
7
8
9
10
11
12
13
14
pH
Free
DOC-bound
POM-bound
Clay

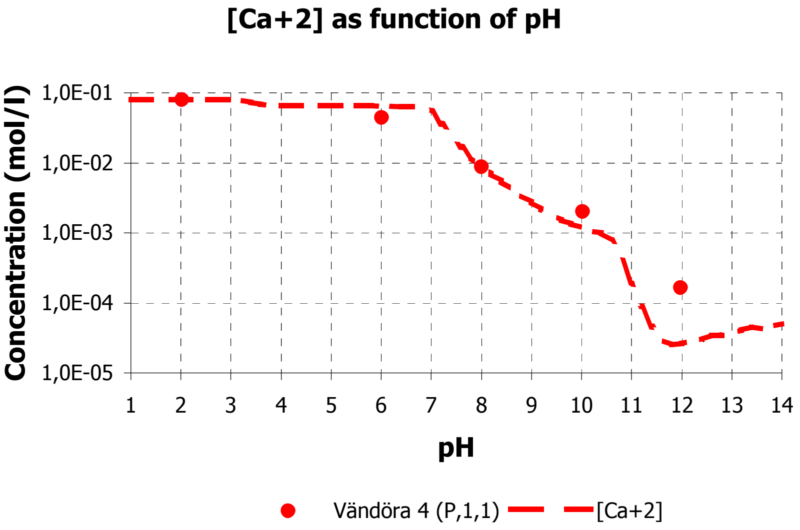
[Ca+2] as function of pH

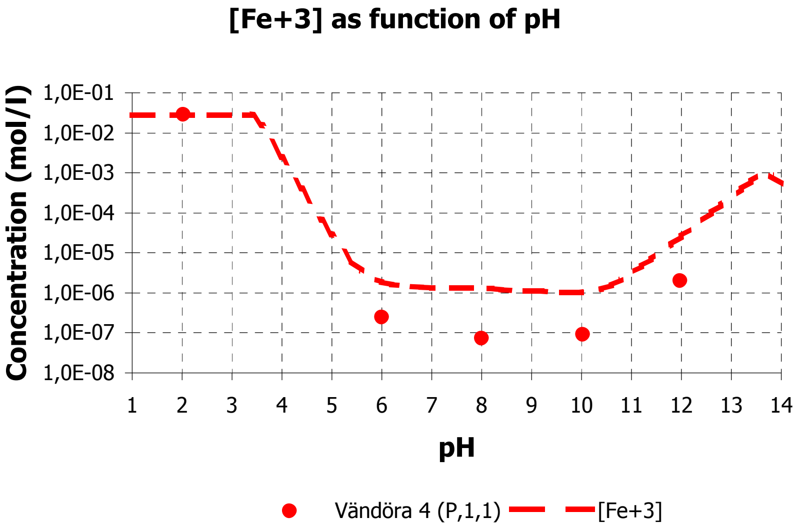
[Fe+3] as function of pH

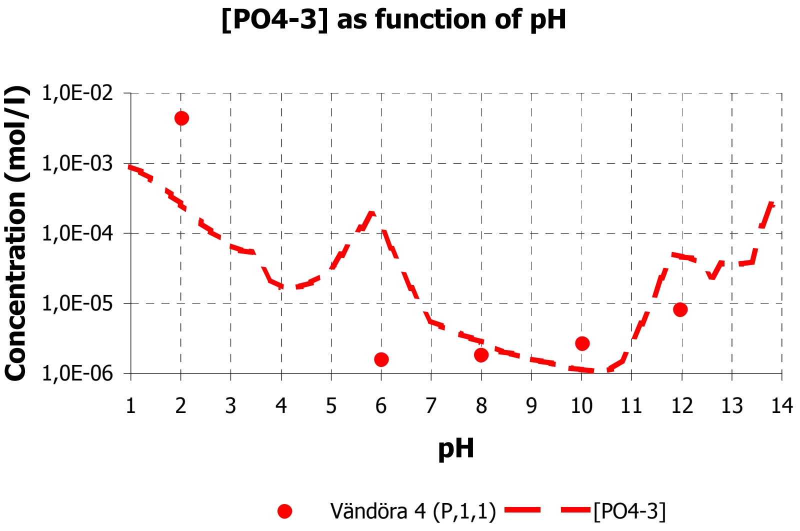
[PO4-3] as function of pH

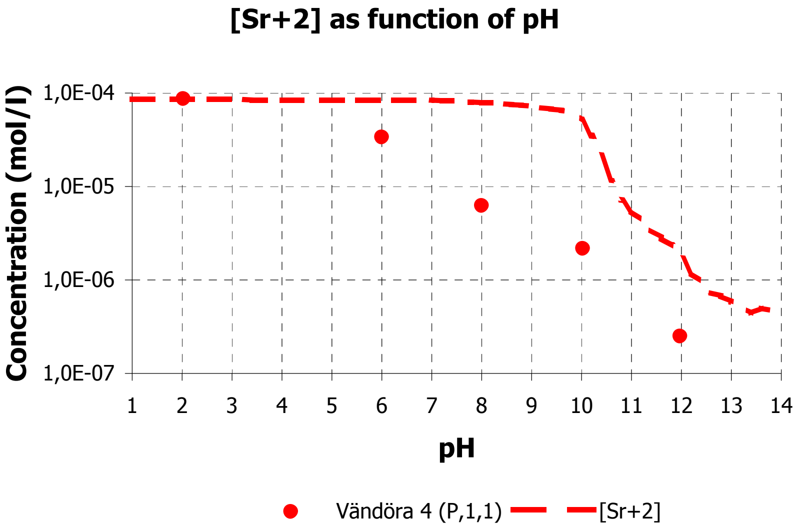
[Sr+2] as function of pH

[Mn+2] as function of pH

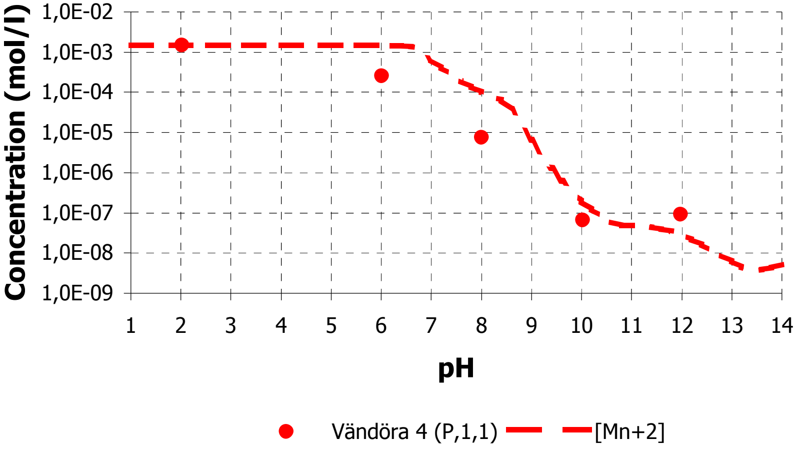

[Ni+2] as function of pH

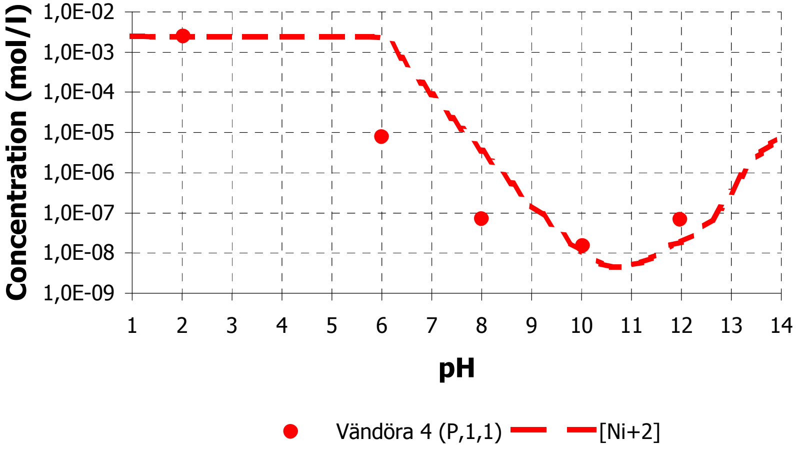

[H3BO3] as function of pH

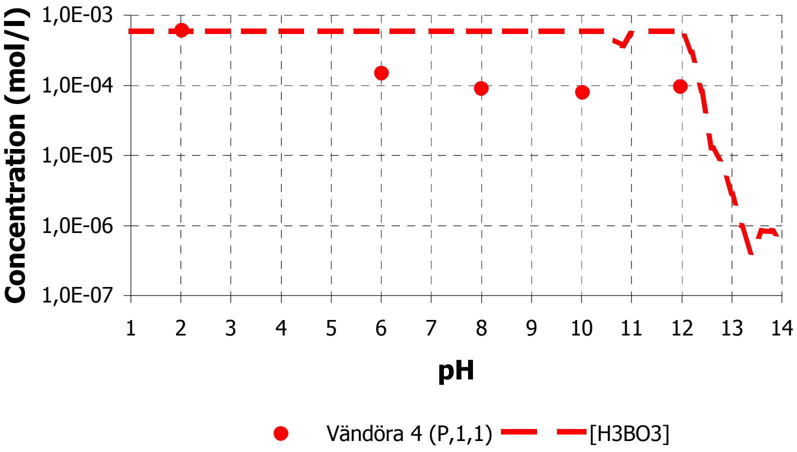

[MoO4-2] as function of pH

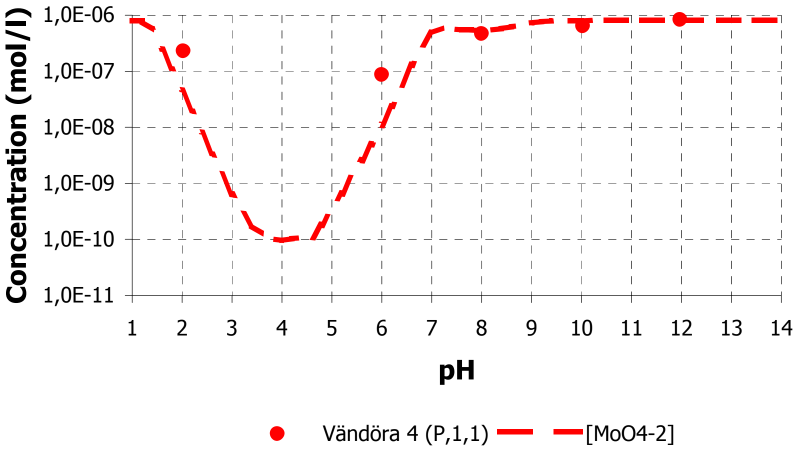

[F-] as function of pH

[K+] as function of pH

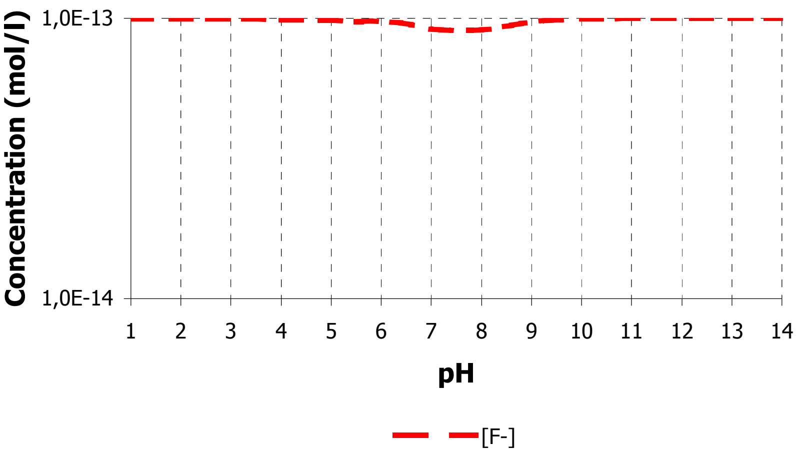
[F-] as function of pH

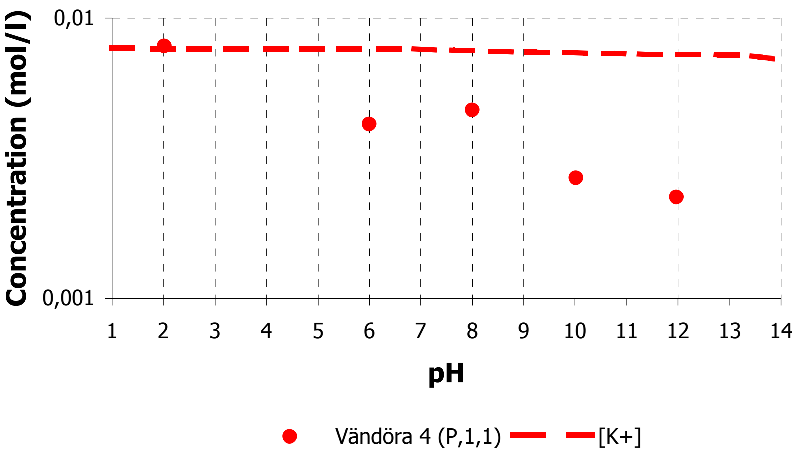
[K+] as function of pH

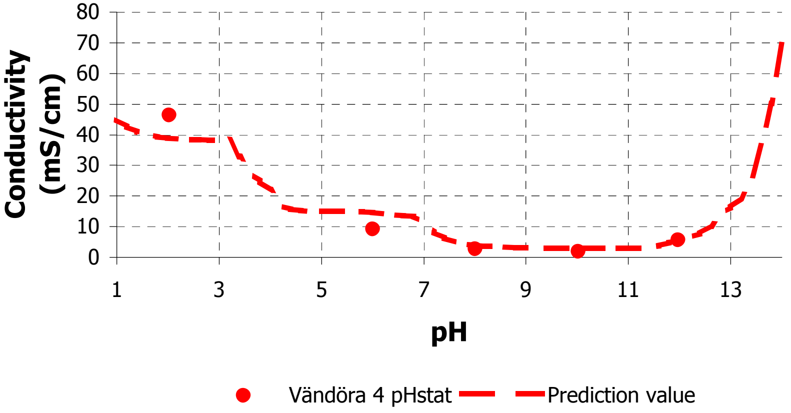
Vändöra 4 ecn-090406: Conductivity as function of pH

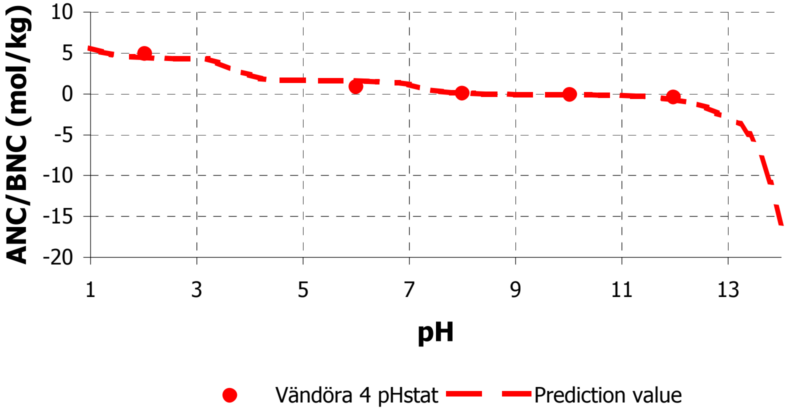
Vändöra 4 ecn-090406: ANC/BNC as function of pH

Al+3 fractionation in solution

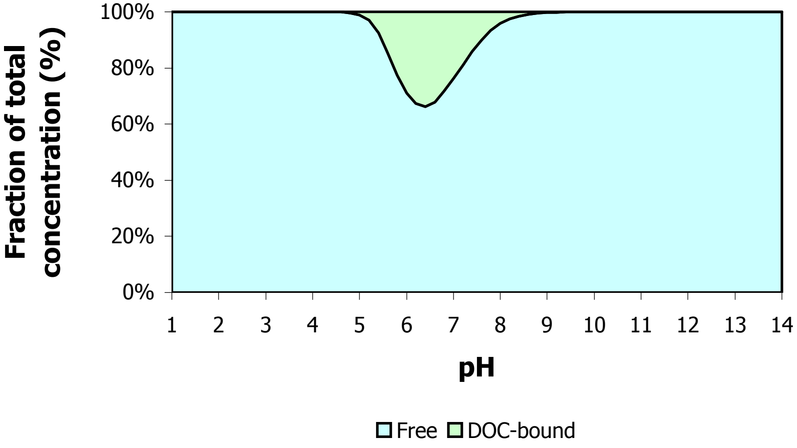

Al+3 fractionation in the solid phase

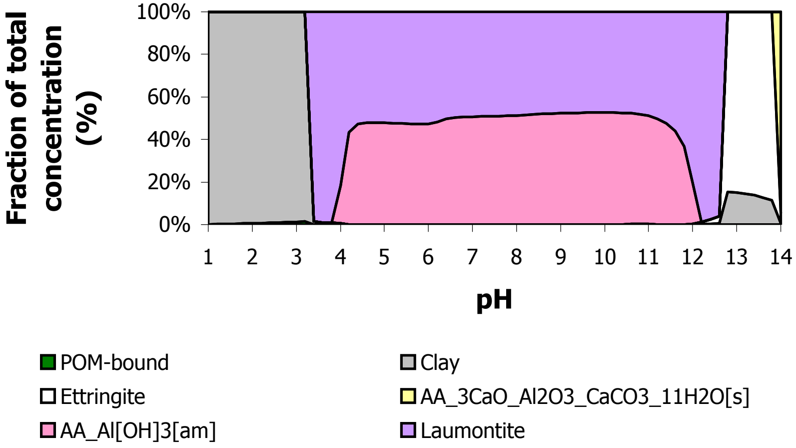

Ba+2 fractionation in solution

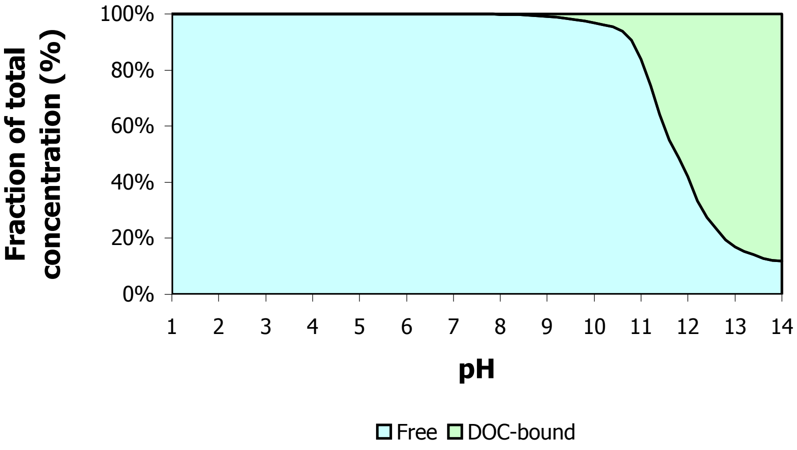

Ba+2 fractionation in the solid phase

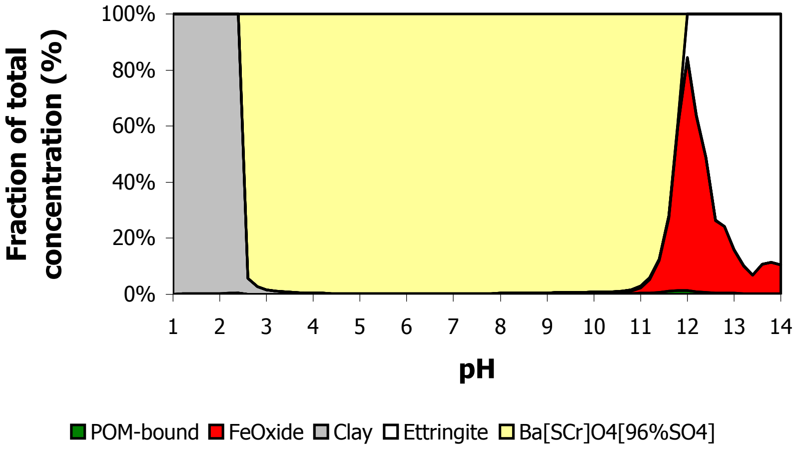

Ca+2 fractionation in solution

Ca+2 fractionation in the solid phase

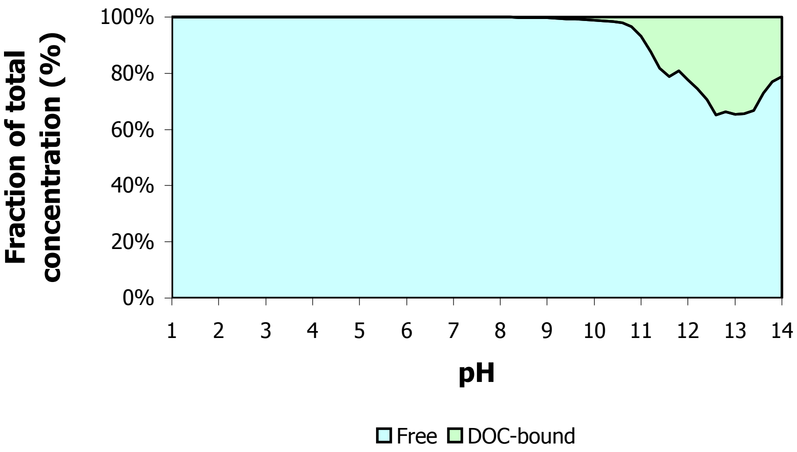
Ca+2 fractionation in solution

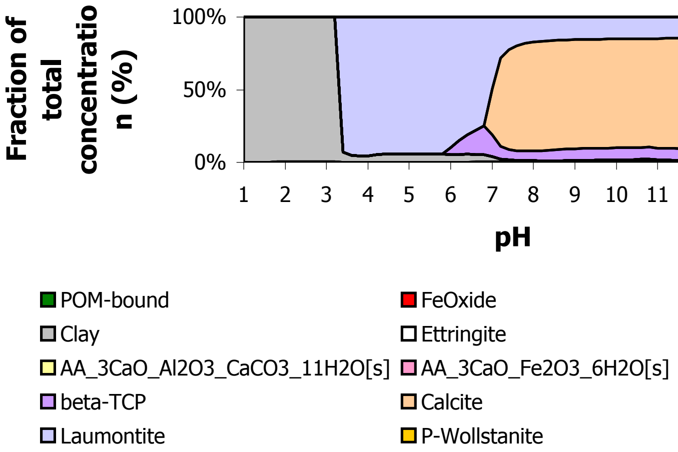
Ca+2 fractionation in the solid phase

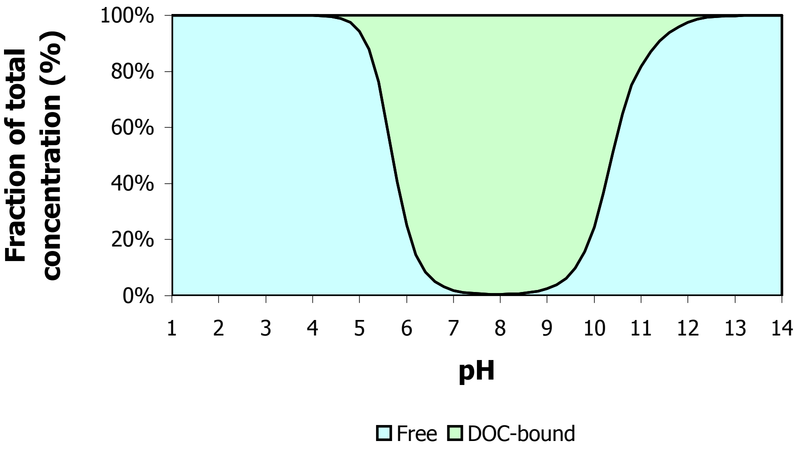
Fe+3 fractionation in solution

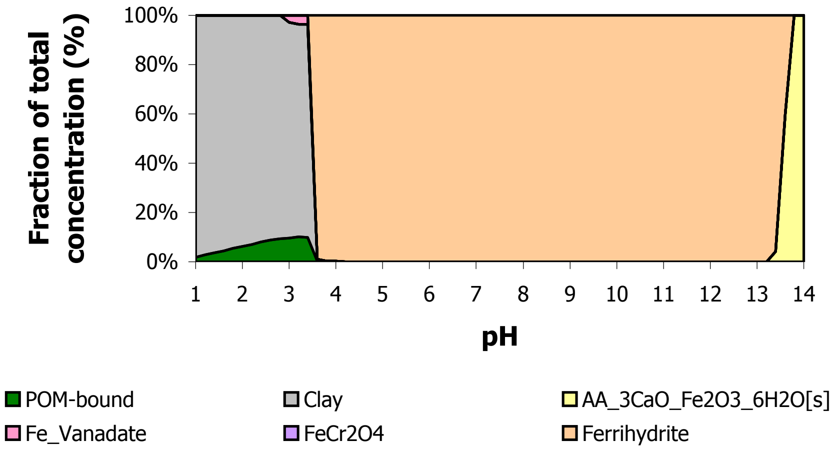
Fe+3 fractionation in the solid phase

H4SiO4 fractionation in solution

H4SiO4 fractionation in the solid phase

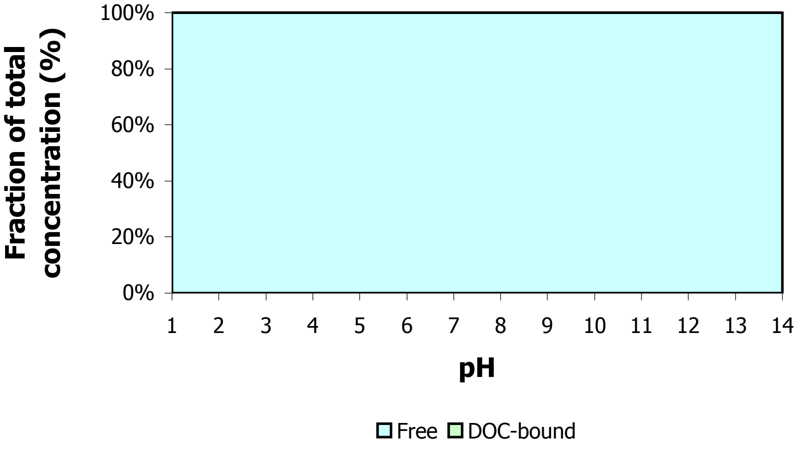
H4SiO4 fractionation in solution

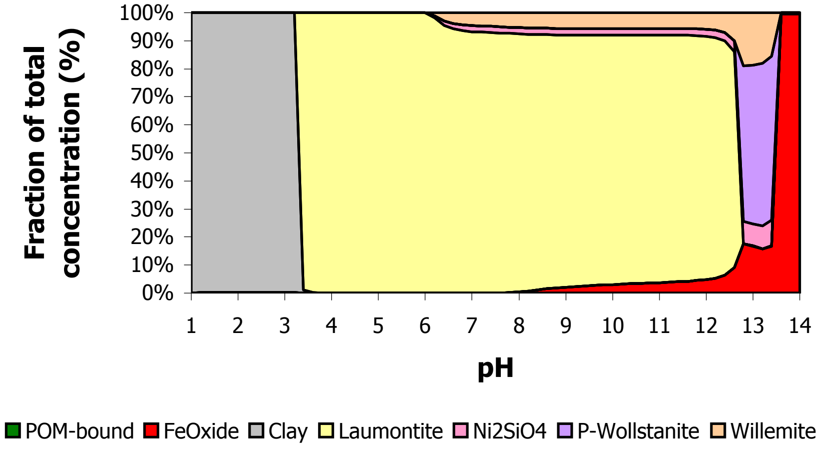
H4SiO4 fractionation in the solid phase

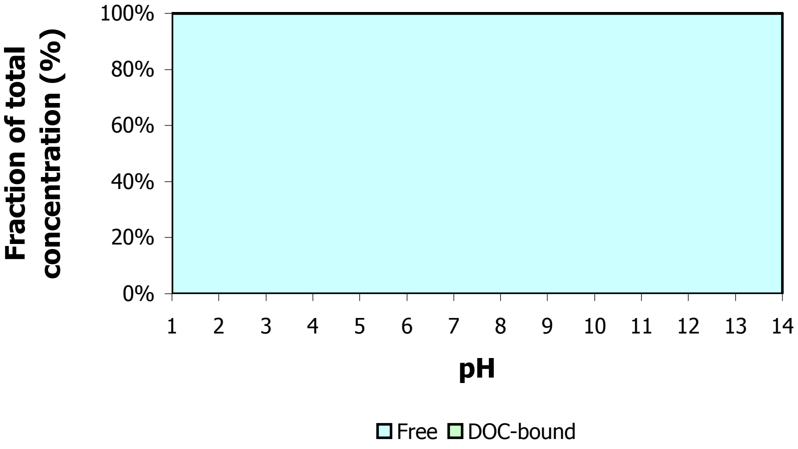
SO4-2 fractionation in solution

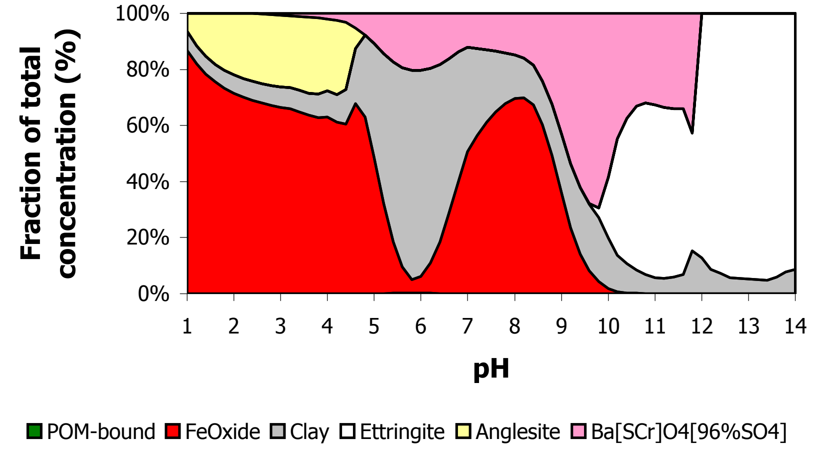
SO4-2 fractionation in the solid phase

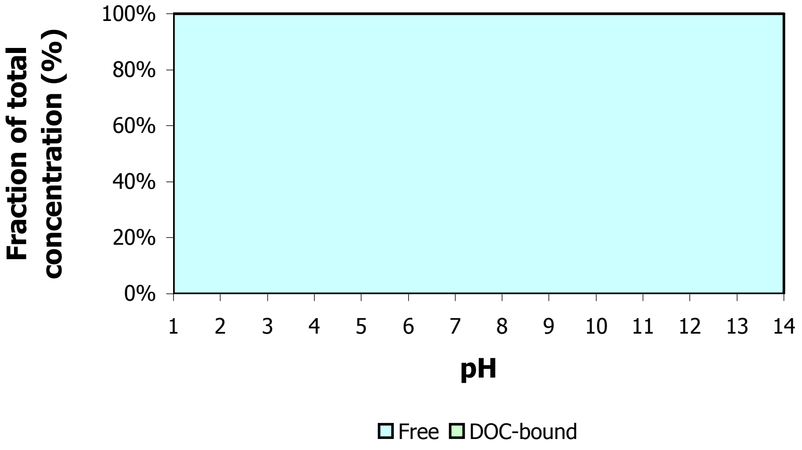

H2CO3 fractionation in solution

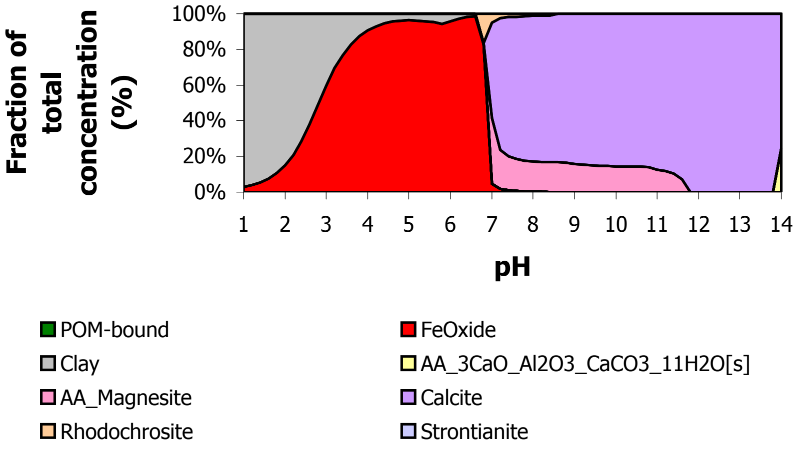

H2CO3 fractionation in the solid phase

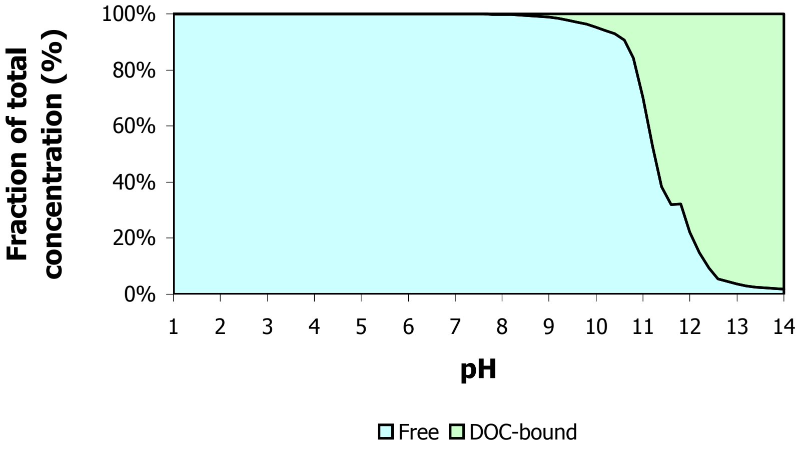

Mg+2 fractionation in solution

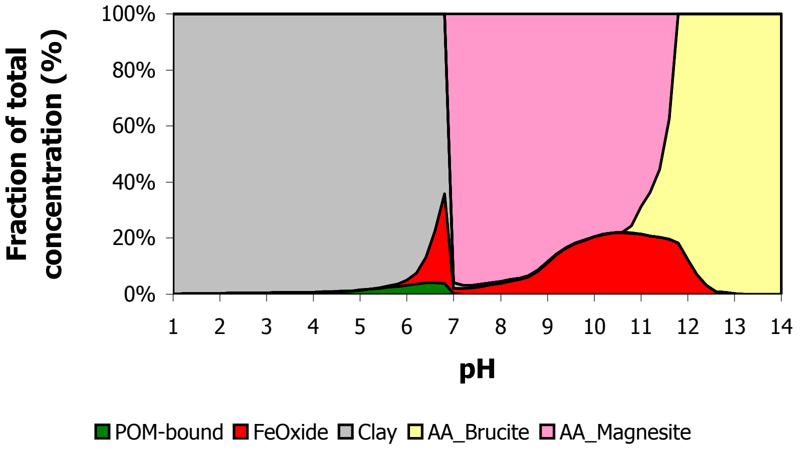

Mg+2 fractionation in the solid phase

PO4-3 fractionation in solution

PO4-3 fractionation in the solid phase

PO4-3 fractionation in solution

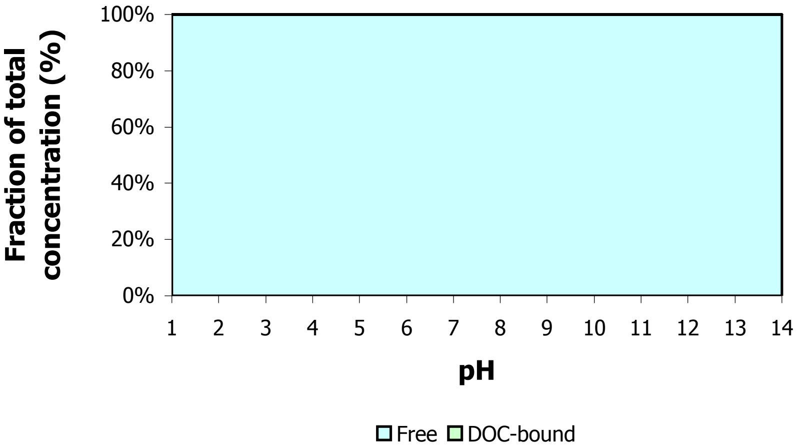

PO4-3 fractionation in the solid phase

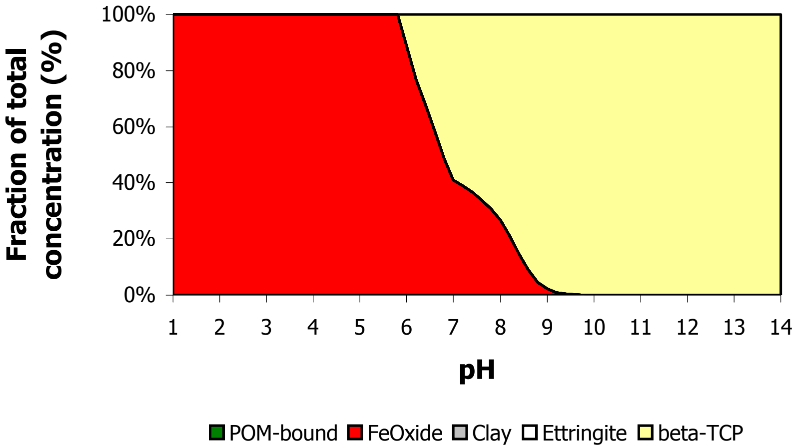

Sr+2 fractionation in solution

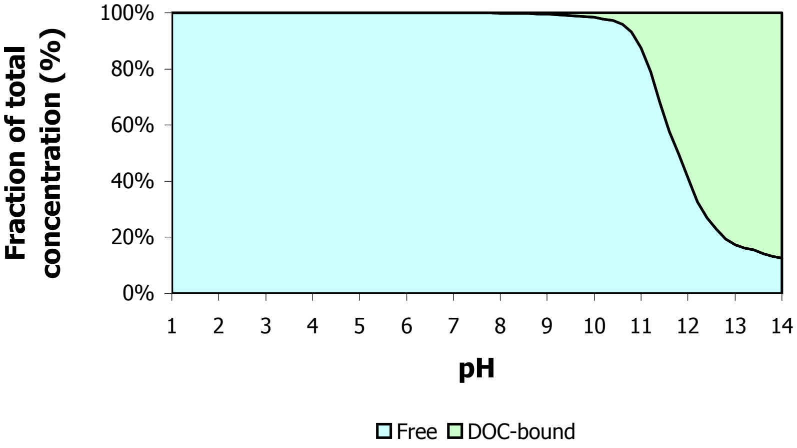

Sr+2 fractionation in the solid phase

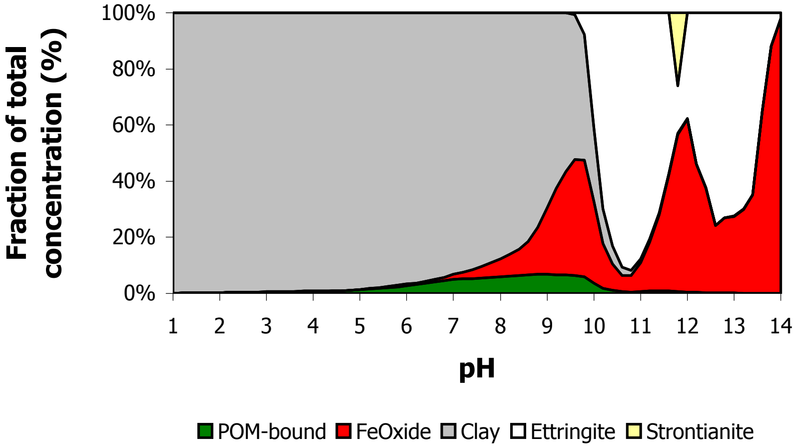

Cd+2 fractionation in solution

Cd+2 fractionation in the solid phase

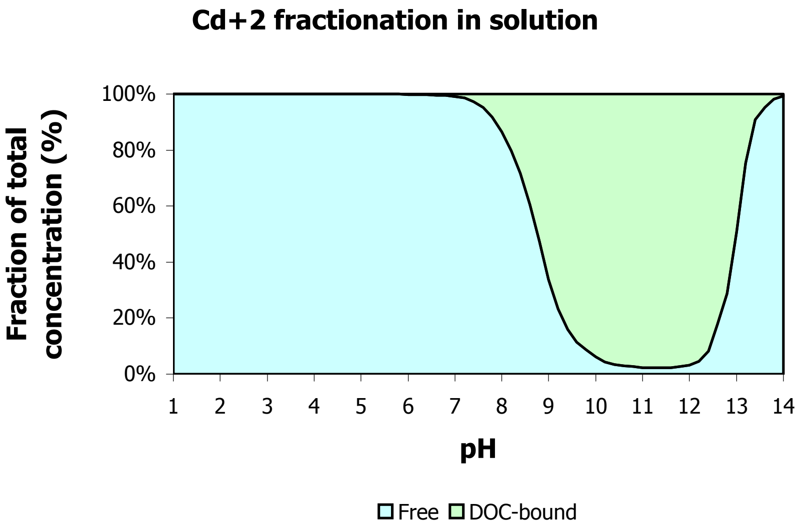

Cd+2 fractionation in solution

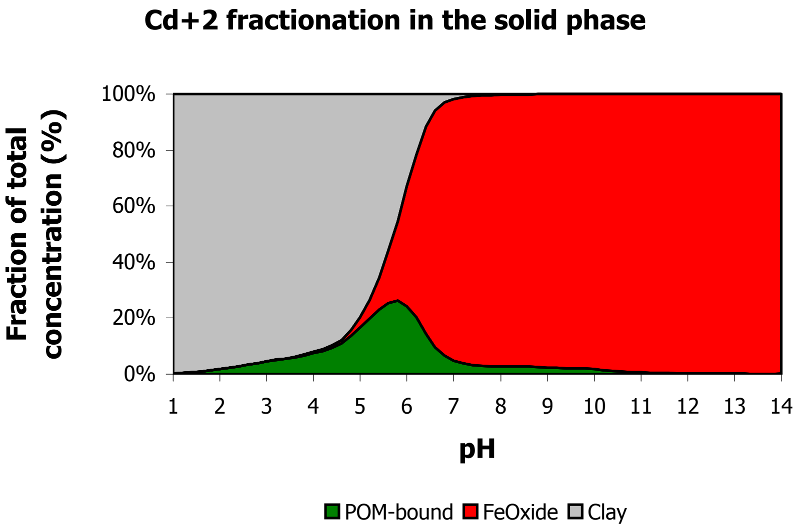

Cd+2 fractionation in the solid phase

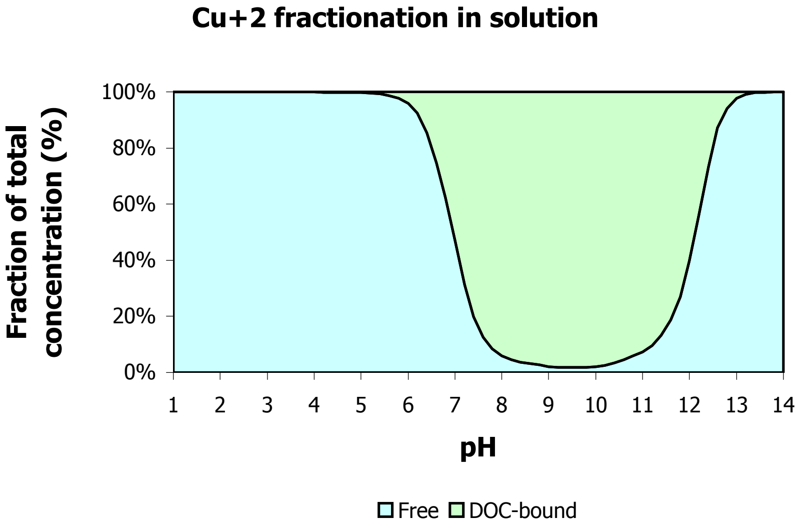

Cu+2 fractionation in solution

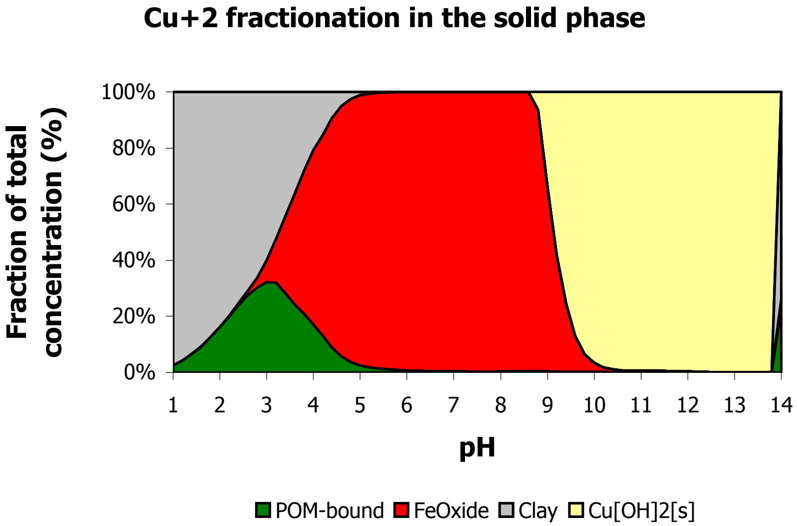

Cu+2 fractionation in the solid phase

Mn+2 fractionation in solution

Mn+2 fractionation in the solid phase

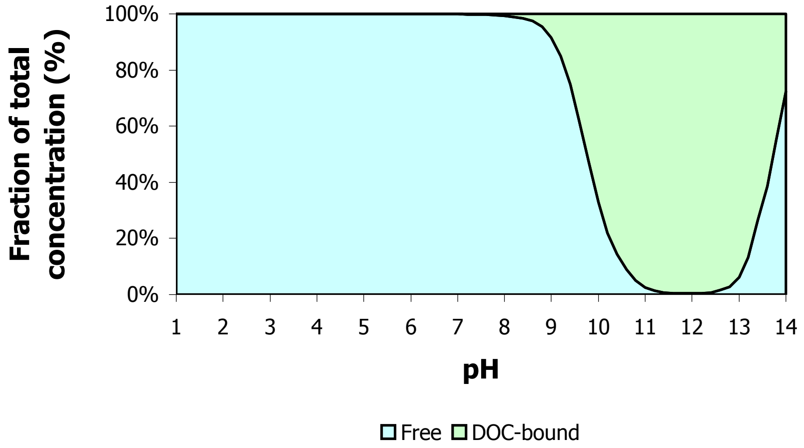
Mn+2 fractionation in solution

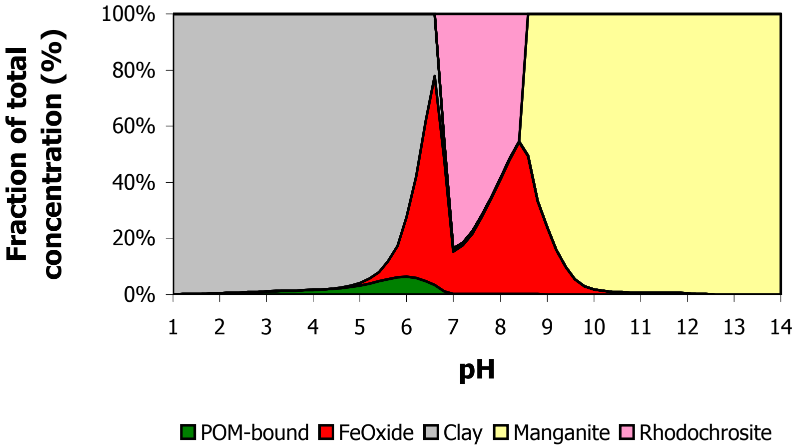
Mn+2 fractionation in the solid phase

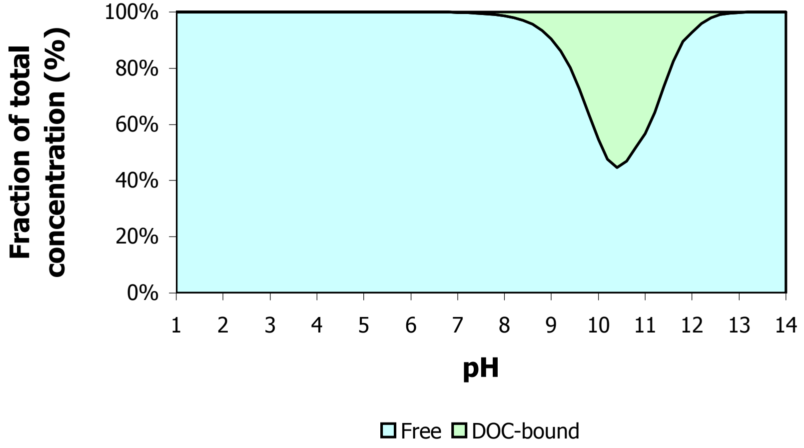
Ni+2 fractionation in solution

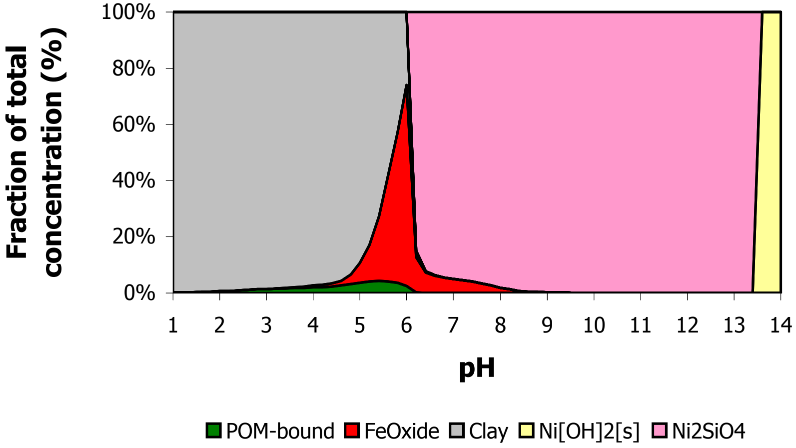
Ni+2 fractionation in the solid phase

Pb+2 fractionation in solution

Pb+2 fractionation in the solid phase

Pb+2 fractionation in solution

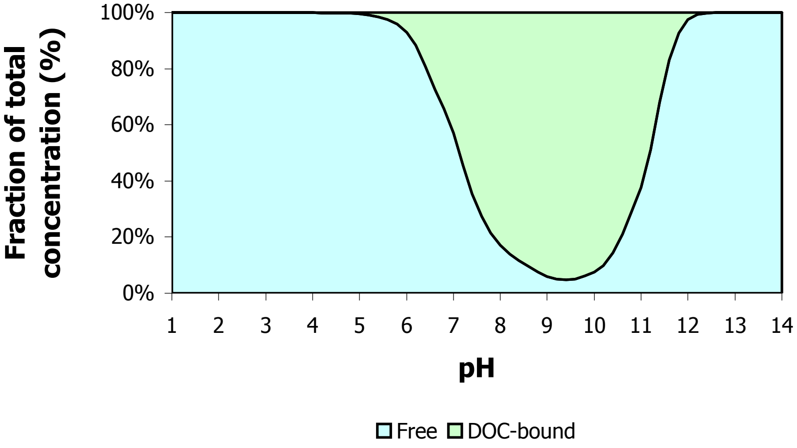

Pb+2 fractionation in the solid phase

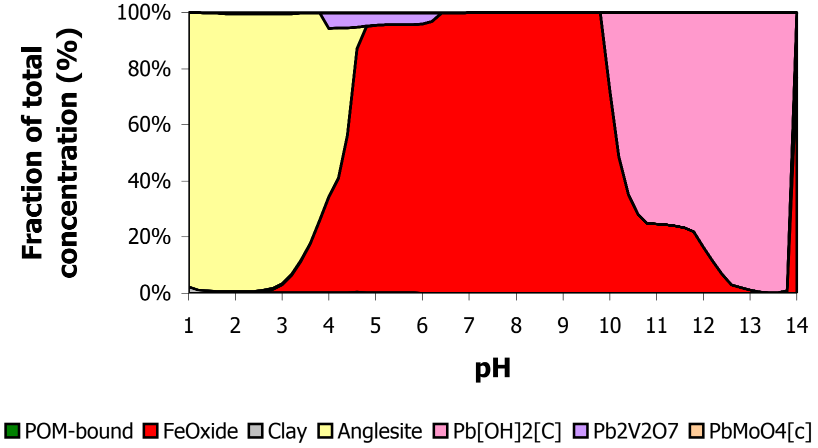

Zn+2 fractionation in solution

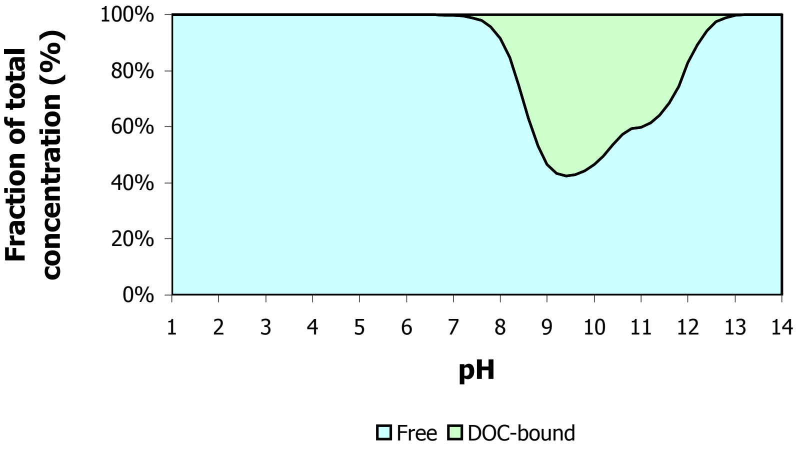

Zn+2 fractionation in the solid phase

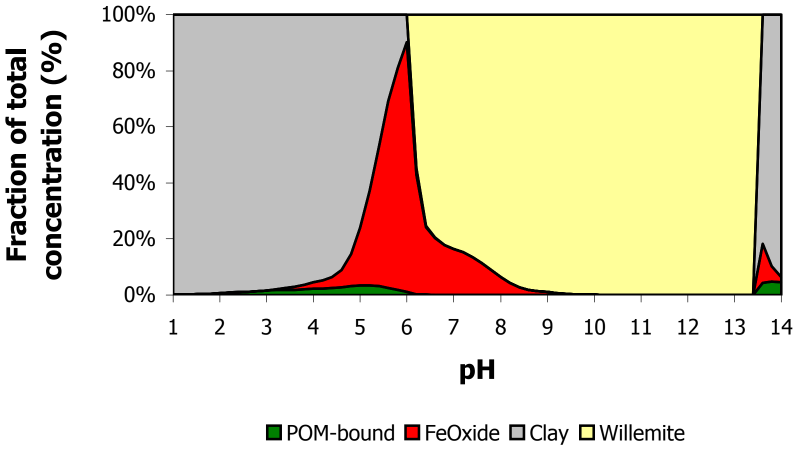

CrO4-2 fractionation in solution

CrO4-2 fractionation in the solid phase

CrO4-2 fractionation in solution

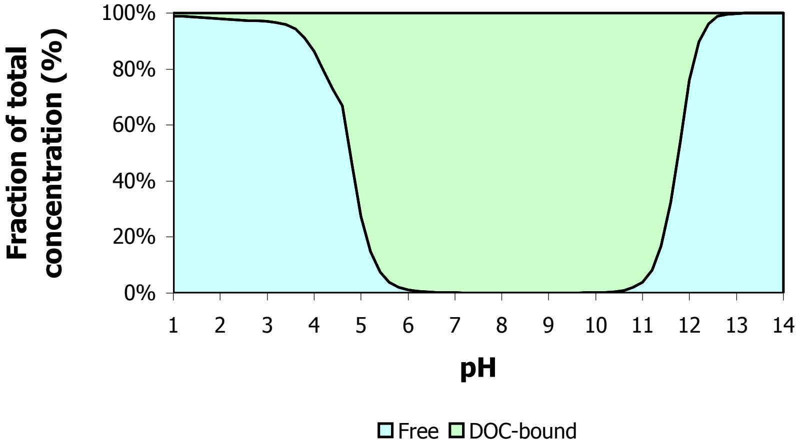

CrO4-2 fractionation in the solid phase

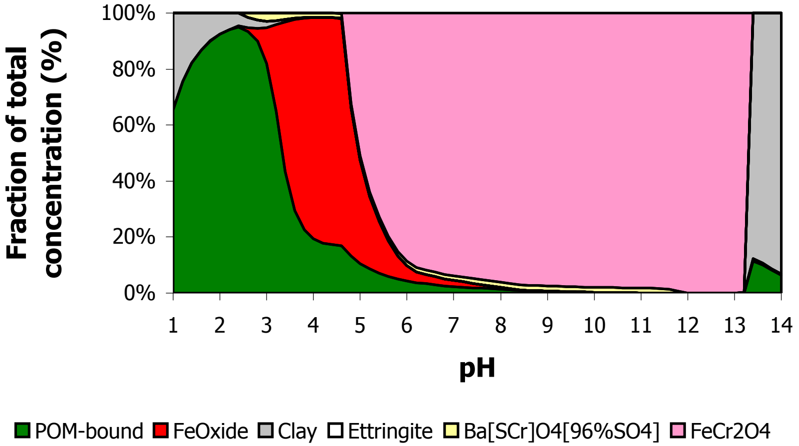

H3AsO4 fractionation in solution

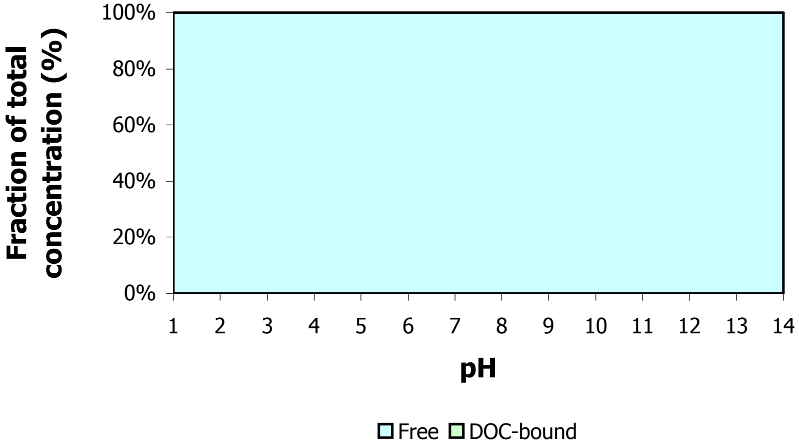

H3AsO4 fractionation in the solid phase

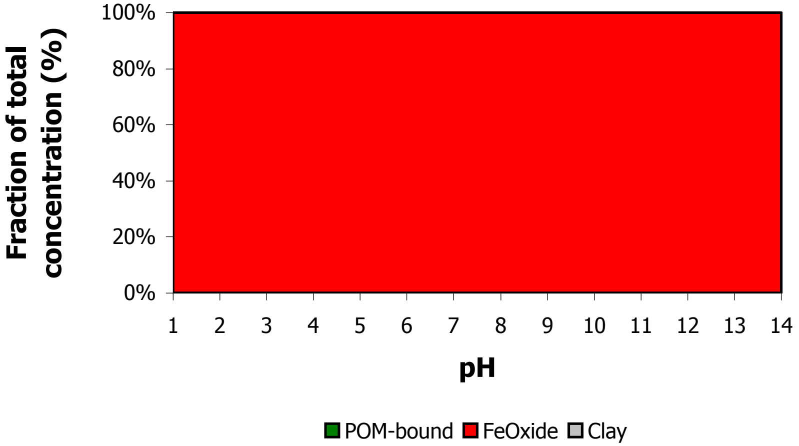

H3BO3 fractionation in solution

H3BO3 fractionation in the solid phase

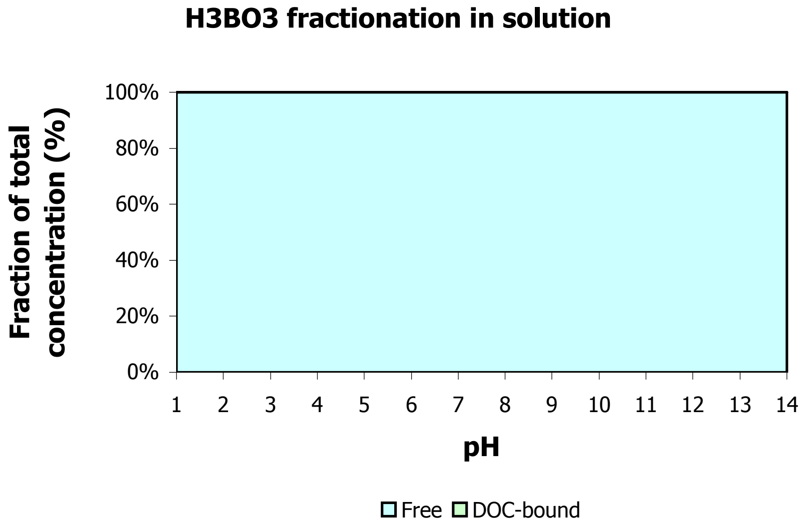
H3BO3 fractionation in solution

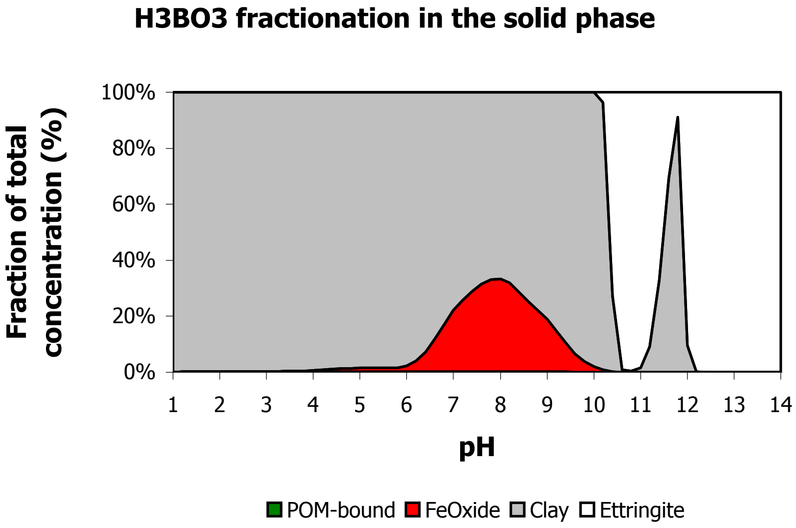
H3BO3 fractionation in the solid phase

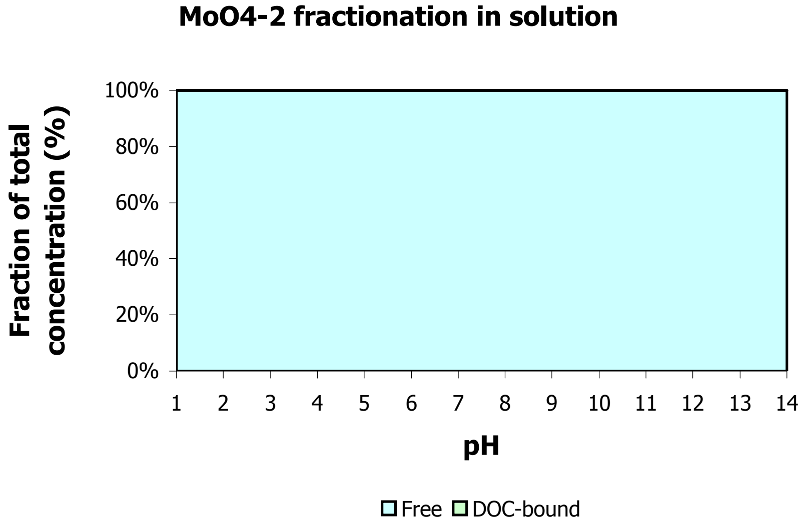
MoO4-2 fractionation in solution

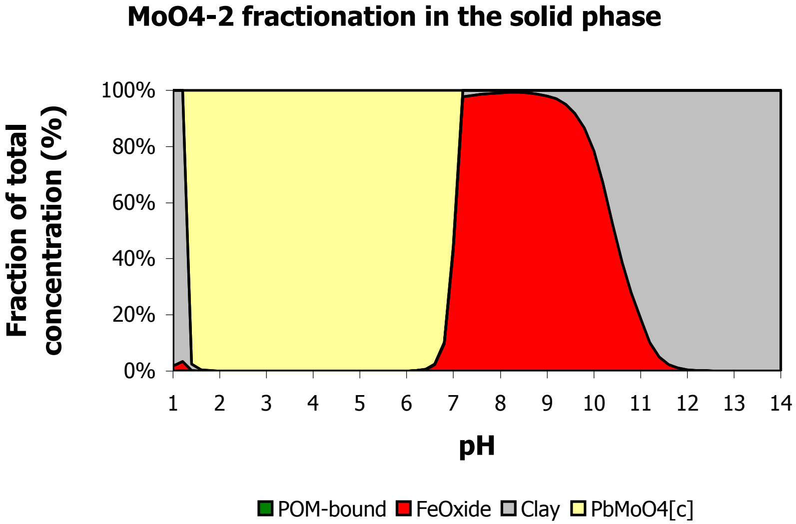
MoO4-2 fractionation in the solid phase

Sb[OH]6- fractionation in solution

Sb[OH]6- fractionation in the solid phase

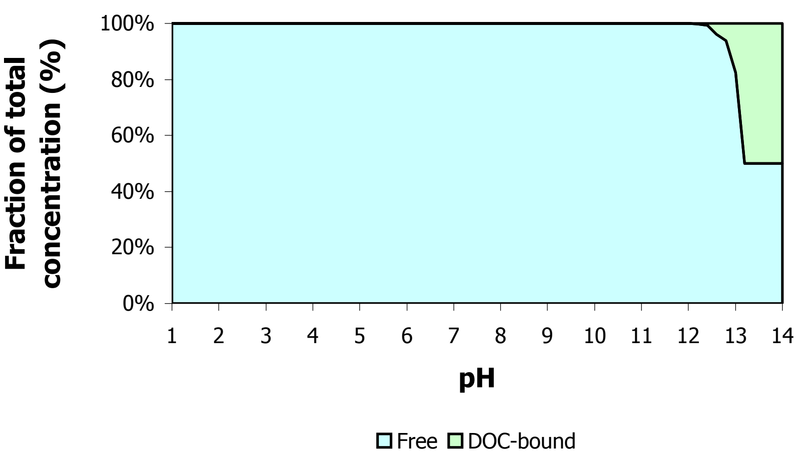
Sb[OH]6- fractionation in solution

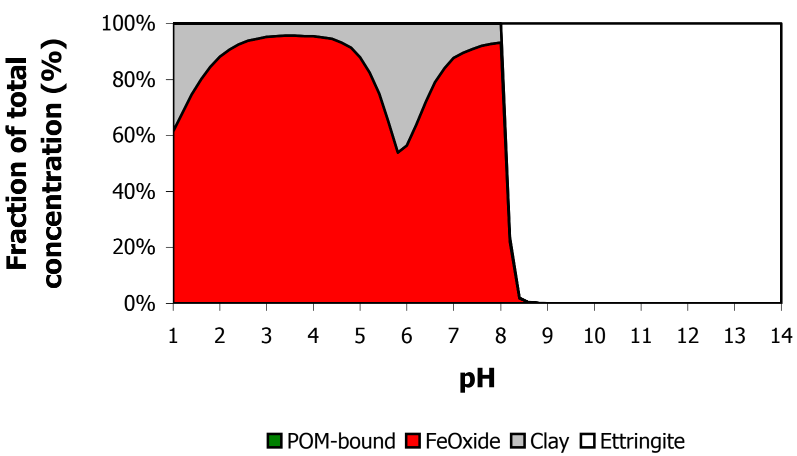
Sb[OH]6- fractionation in the solid phase

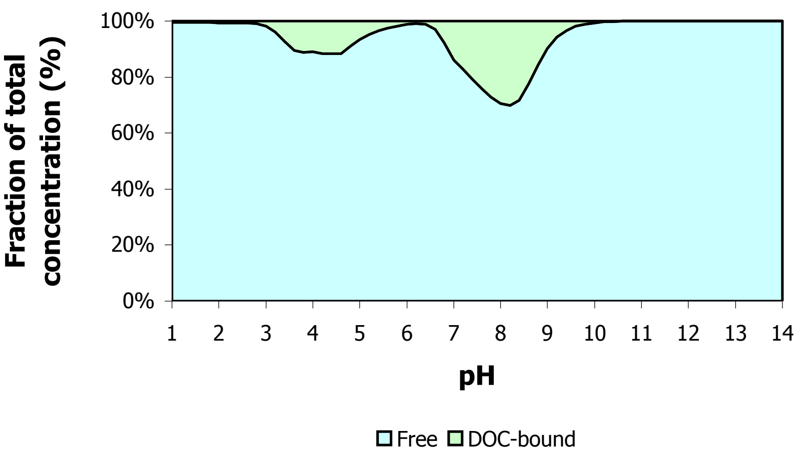
VO2+ fractionation in solution

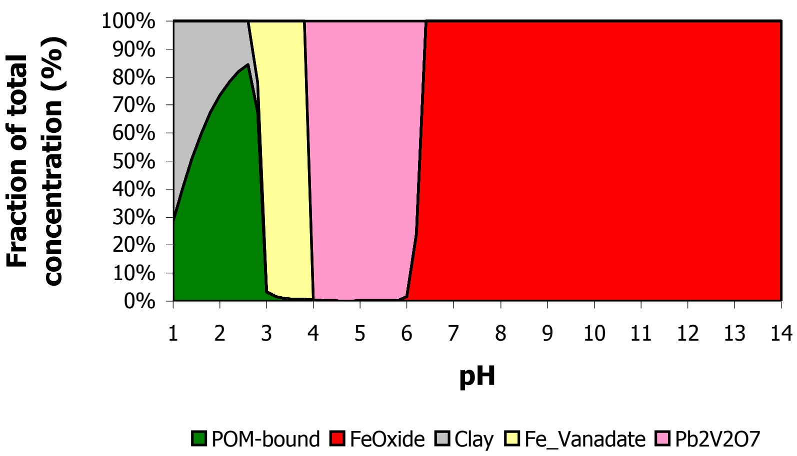
VO2+ fractionation in the solid phase

Br- fractionation in solution

Br- fractionation in the solid phase

Br- fractionation in solution

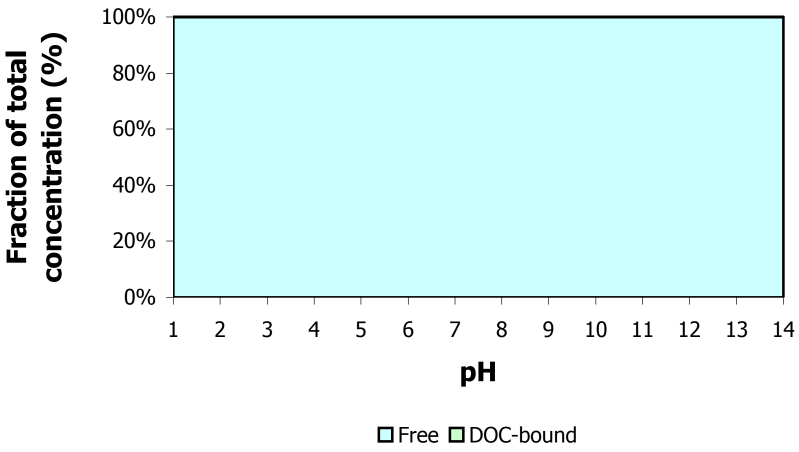

Br- fractionation in the solid phase

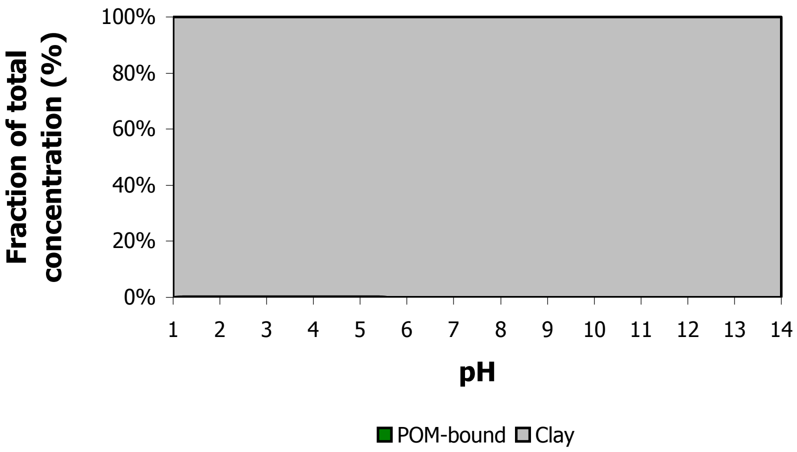

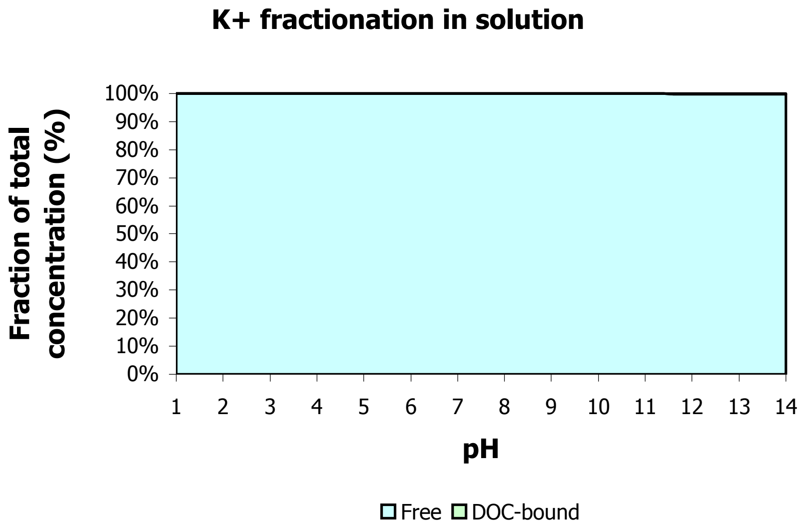

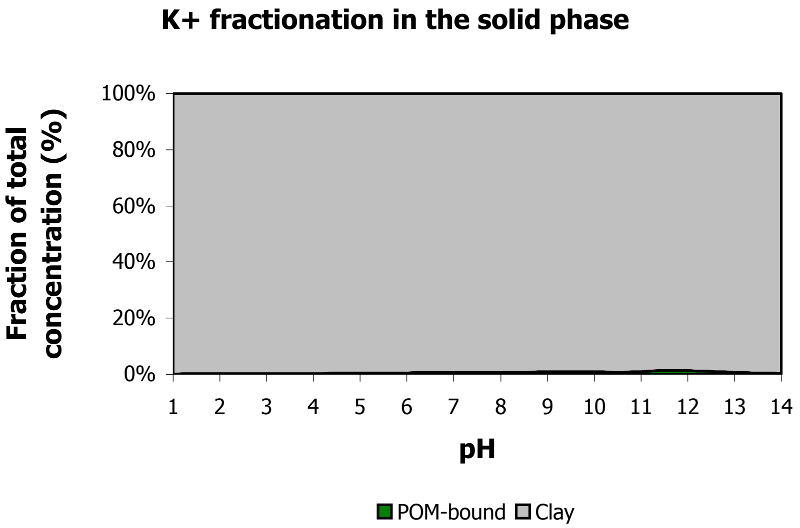

Li+ fractionation in solution

Li+ fractionation in the solid phase

Li+ fractionation in solution

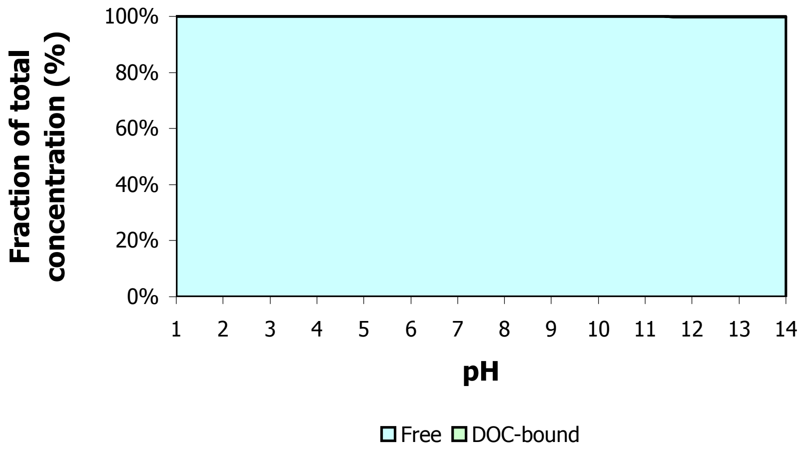

Li+ fractionation in the solid phase

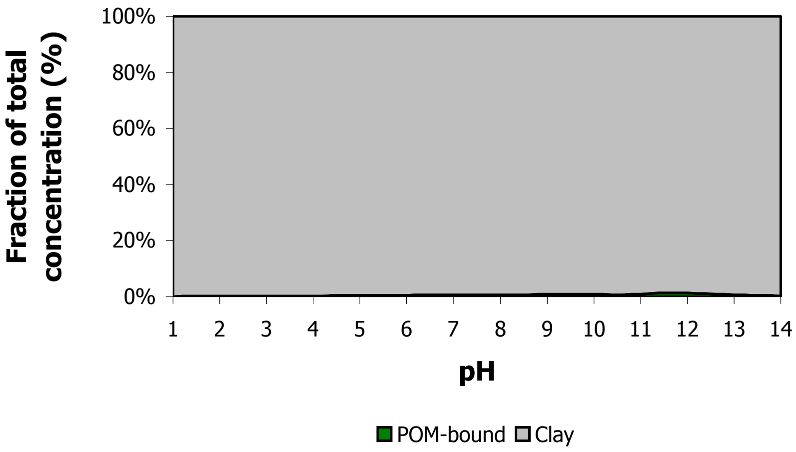

Na+ fractionation in solution

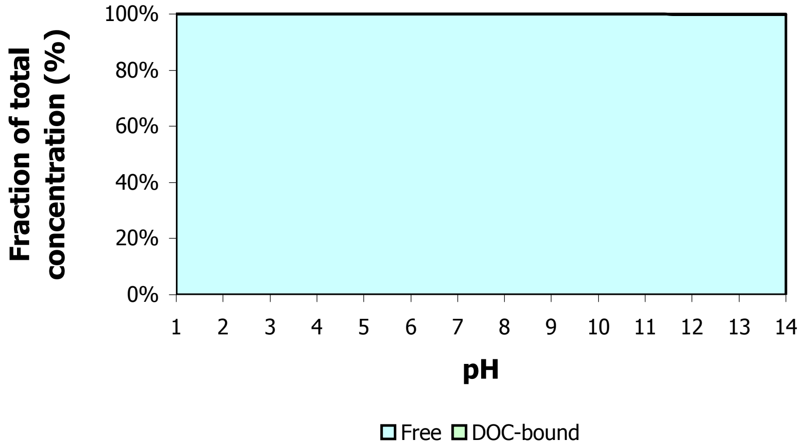

Na+ fractionation in the solid phase

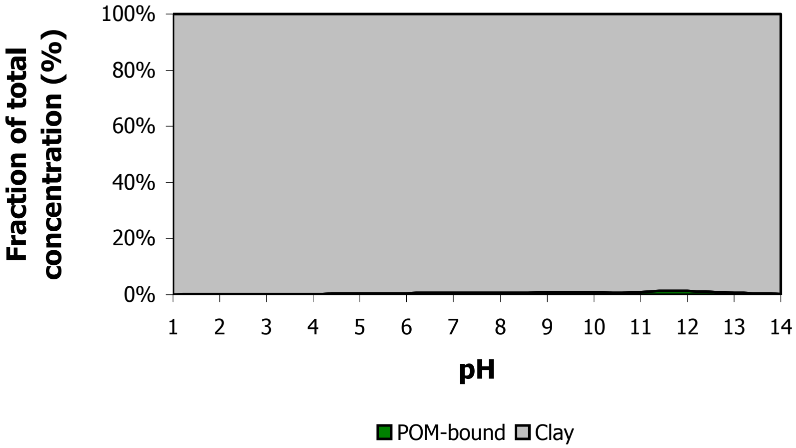

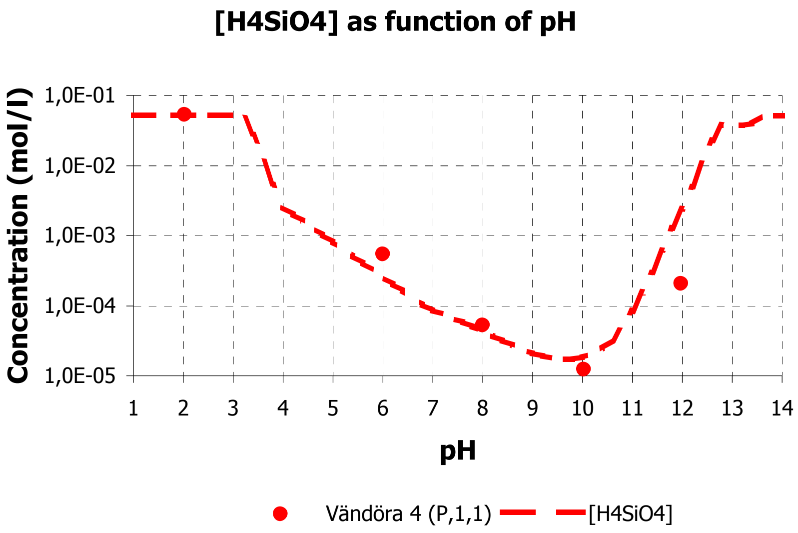
[H4SiO4] as function of pH
Concentration (mol/l)
1,0E-01
1,0E-02
1,0E-03
1,0E-04
1,0E-05
1
2
3
4
5
6
7
8
9
10
11
12
13
14
pH
Vändöra 4 (P,1,1)
[H4SiO4]

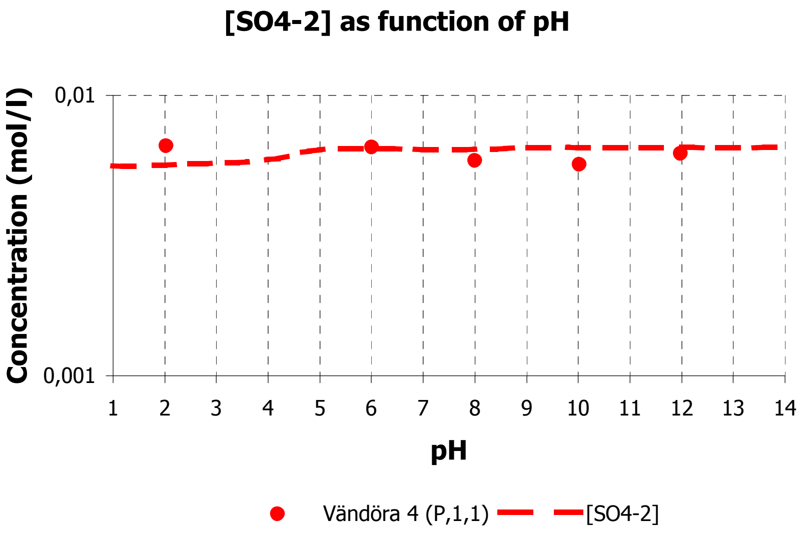
[SO4-2] as function of pH
Concentration (mol/l)
0,01
0,001
1
2
3
4
5
6
7
8
9
10
11
12
13
14
pH
Vändöra 4 (P,1,1)
[SO4-2]

[Pb+2] as function of pH

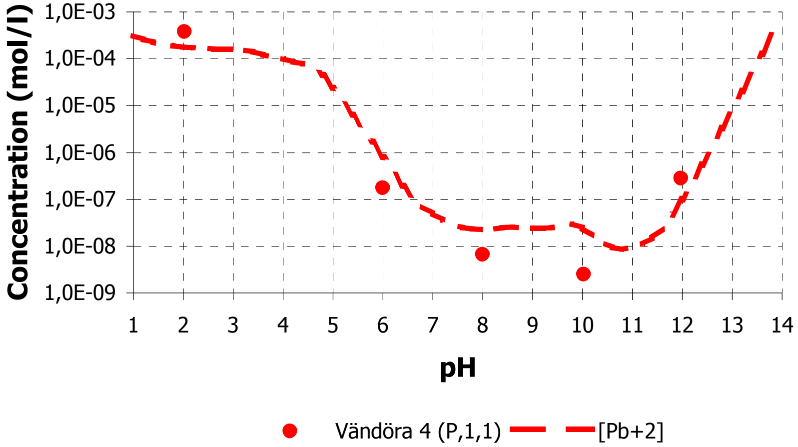

[Zn+2] as function of pH

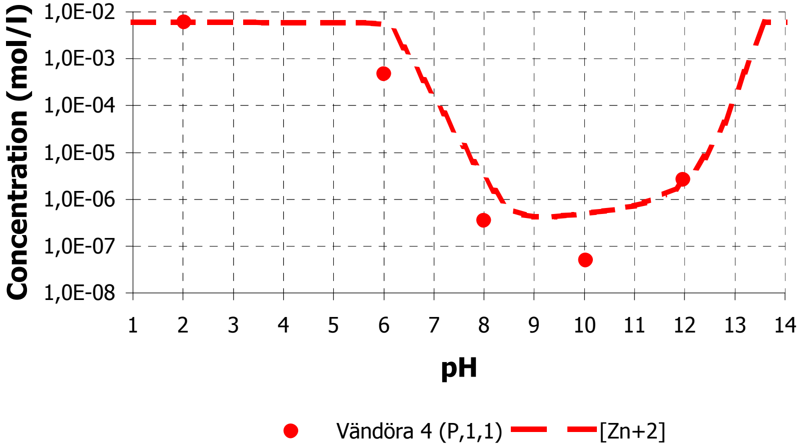

[Sb[OH]6-] as function of pH

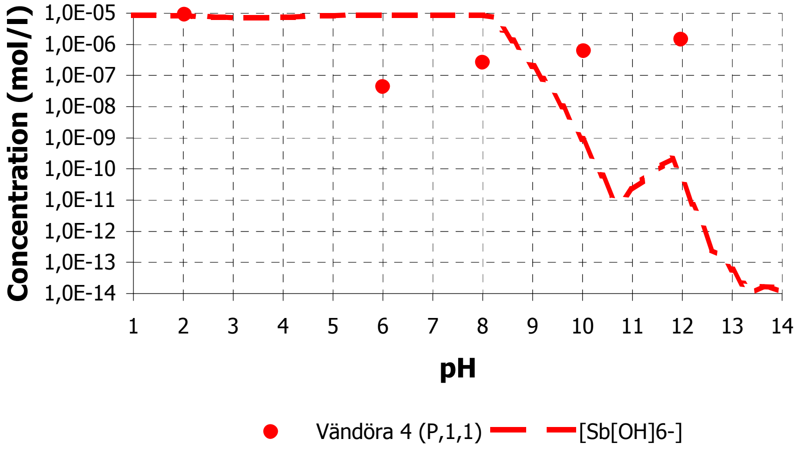

[VO2+] as function of pH

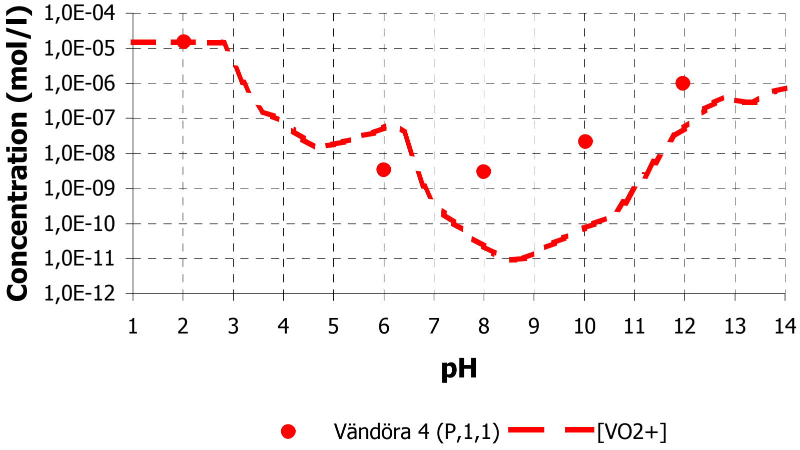

[Li+] as function of pH

[Na+] as function of pH

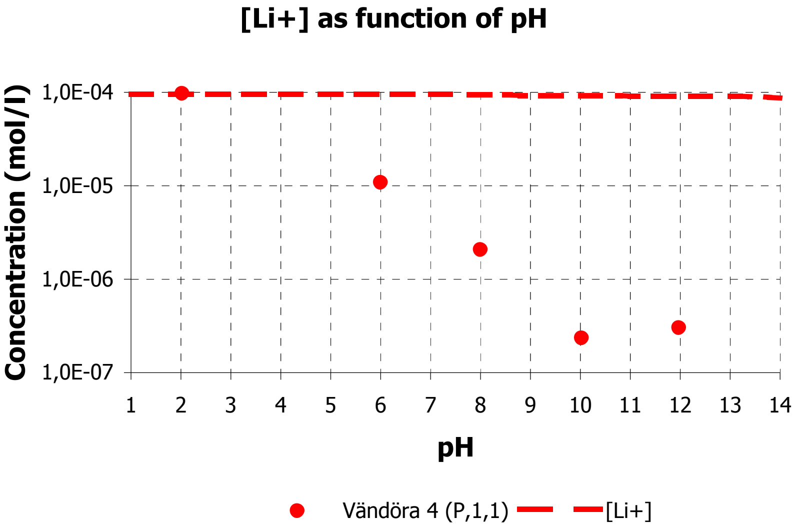
[Li+] as function of pH
Concentration (mol/l)
1,0E-04
1,0E-05
1,0E-06
1,0E-07
1
2
3
4
5
6
7
8
9
10
11
12
13
14
pH
Vändöra 4 (P,1,1)
[Li+]

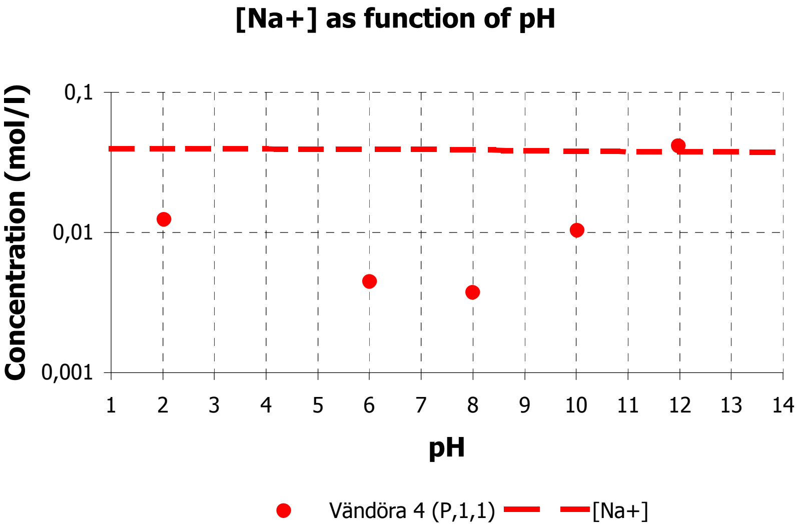
[Na+] as function of pH
Concentration (mol/l)
0,1
0,01
0,001
1
2
3
4
5
6
7
8
9
10
11
12
13
14
pH
Vändöra 4 (P,1,1)
[Na+]

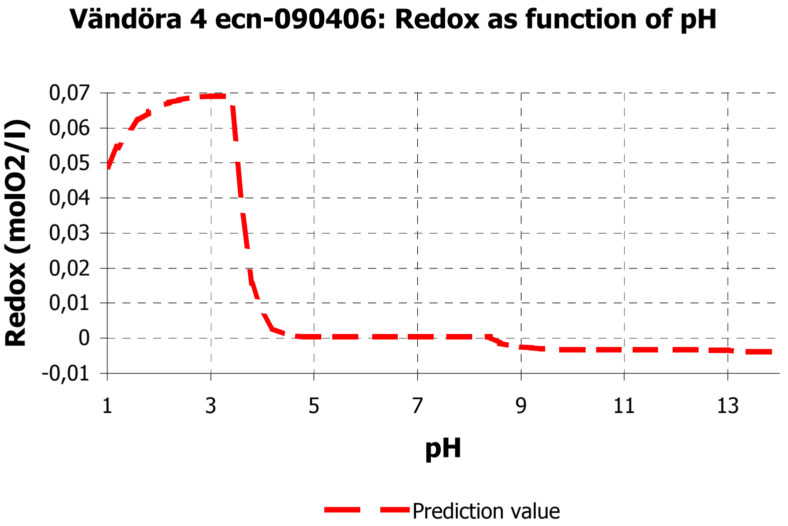
Vändöra 4 ecn-090406: Redox as function of pH
Redox (molO2/l)
0,07
0,06
0,05
0,04
0,03
0,02
0,01
0
-0,01
1
3
5
7
9
11
13
pH
Prediction value

Värmeforsk är ett organ för industrisamverkan inom värmeteknisk forskning och utveckling. Forskningsprogrammet är tillämpningsinriktat och fokuseras på energi- och processindustriernas behov och problem.

Bakom Värmeforsk står följande huvudmän:

- Elforsk
- Svenska Fjärrvärmeföreningen
- Skogsindustrin
- Övrig industri

VÄRMEFORSK SAMARBETAR MED
STATENS ENERGIMYNDIGHET

VÄRMEFORSK SERVICE AB
101 53 Stockholm
Tel 08-677 25 80